THE JOURNAL
OF
CHEMICAL PHYSICS

VOLUME 20, NUMBER 11 NOVEMBER, 1952

# Low Temperature Second Virial Coefficients for a 6–9 Potential

GLENN M. ROE, LEO F. EPSTEIN, AND MARION D. POWERS
*General Electric Company, Knolls Atomic Power Laboratory,* Schenectady, New York*
(Received April 28, 1952)

Alternate expressions for the second virial coefficient of a gas having a Lennard-Jones 6–9 potential are derived to cover the temperature range where the known power series expansion in $\theta=\epsilon/kT$ is inconvenient for numerical computations. For $\theta\geqslant 2$ the second virial coefficient can be expressed as a combination of Bessel functions of imaginary argument plus a small correction term. This formulation and an asymptotic expression derived from it are used to tabulate numerical values of the second virial coefficient in the range $2\leqslant\theta\leqslant 100$.

THE Lennard-Jones $6-s$ potential

$$U_s(r)=\{\epsilon/(s-6)\}[6(r_0/r)^s-s(r_0/r)^6], \qquad (1)$$

with $s=12$, has been widely applied to the computation of a great number of properties of gases and liquids.[1] The mathematical convenience of having the repulsive power $s$ exactly twice the attractive exponent results in particularly simple relations and is probably responsible, to some extent, for the fact that this, more than any other Lennard-Jones potential, has been extensively studied. Tables for computing the second virial coefficient, $B_{12}(T)$, for example, have now been computed[1,2,3] for the extremely wide range $0<\theta<100$, where $\theta=\epsilon/kT$.

There is, however, a considerable body of evidence that for some properties, the 6–9 potential gives a much better representation of the phenomena than the 6–12 potential. Thus, Kihara[4] found that improved agreement with the experimental values of the third virial coefficient of Ne, A, $CH_4$, and $N_2$ resulted when $s=9$ rather than $s=12$ was used. Hildebrand, Wakeham, and Boyd[5] concluded that their data on x-ray scattering in liquid mercury could best be represented by a 6–9 potential. Kerr and Lund,[6] working with the data of Hildebrand and Campbell,[7] deduced an even lower value, $s=8.3$. Also, in a very recent paper, Moelwyn-Hughes[8] has concluded, from the properties of liquid mercury, that the sum of the attractive and repulsive exponents is $15.0\pm0.8$, and their product is 53.8, i.e., $s=9$ in this case.

It thus seems worth while to explore the differences introduced by the use of the lower repulsive exponent. In a previous paper,[9] the function

$$G(\theta)=B(\theta)/(2/3)\pi N r_0^3 \qquad (2)$$

has been computed for the ranges $0<\theta(0.01)<1$, and $1<\theta(0.05)<2$ from the convergent power series[10]

$$G_9(\theta)=-(1/3)(2\theta)^{1/3}\sum_{n=0}^{\infty}\alpha_n\theta^{n/3}, \qquad (3a)$$

where

$$\alpha_n=\left(\frac{27}{4}\right)^{n/3}\frac{1}{n!}\left(\frac{2n-4}{3}\right)! \qquad (3b)$$

using punched-card machine techniques. The resulting tables are valid for high temperatures (small $\theta$), but because of the poor convergence properties of the series it is difficult to apply the same equations for large $\theta$ values. In a similar problem for the 6–12 potential, it was found possible[3] to express $G_{12}(\theta)$ in closed form

* The Knolls Atomic Power Laboratory is operated for the United States Atomic Energy Commission by the General Electric Company under Contract No. W-31-109 Eng-52.

[1] Hirschfelder, Curtis, Bird, and Spotz, *The Properties of Gases* (to be published). (Individual chapters, prepared under Navy Bureau of Ordnance contract, have been issued to a limited distribution list.)

[2] Hirschfelder, Bird, and Spotz, Trans. Am. Soc. Mech. Eng. **71**, 921 (1949).

[3] L. F. Epstein and G. M. Roe, J. Chem. Phys. **19**, 1320 (1951).

[4] T. Kihara, J. Phys. Soc. Japan **6**, 184 (1951).

[5] Hildebrand, Wakeham, and Boyd, J. Chem. Phys. **7**, 1094 (1939).

[6] R. R. Kerr and L. H. Lund, J. Chem. Phys. **19**, 50 (1951).

[7] J. A. Campbell and J. O. Hildebrand, J. Chem. Phys. **11**, 30 (1943).

[8] E. A. Moelwyn-Hughes, J. Phys. Colloid. Chem. **55**, 1246 (1951).

[9] L. F. Epstein and C. J. Hibbert, J. Chem. Phys. **20**, 752 (1952).

[10] R. H. Fowler and E. A. Guggenheim, *Statistical Thermodynamics* (Cambridge University Press, Cambridge, 1939), pp. 279 ff.

TABLE I. $G_9(\theta)$ for large values of $\theta$.[a]

| $\theta$ | $(\pi/3\theta)^{\frac{1}{2}}e^{+\theta}$ | $-G_9(\theta)$ | $-e^{-\theta}G_9(\theta)$ |
|---|---|---|---|
| 10 | $7.127\,859\times10^{3}$ | $8.04\times10^{3}$ | $0.364\ 9\pm0.000\ 2$ |
| 11 | $1.847\,384\times10^{4}$ | $2.054\times10^{4}$ | $0.343\ 08\pm0.000\ 08$ |
| 12 | $4.807\,905\times10^{4}$ | $5.288\ 6\times10^{4}$ | $0.324\ 94\pm0.000\ 03$ |
| 13 | $1.255\,657\times10^{5}$ | $1.369\ 10\times10^{5}$ | $0.309\ 46\pm0.000\ 01$ |
| 14 | $3.289\,069\times10^{5}$ | $3.560\ 20\times10^{5}$ | $0.296\,041\pm0.000\,004$ |
| 15 | $8.637\,457\times10^{5}$ | $9.292\ 59\times10^{5}$ | $0.284\,262\pm0.000\,002$ |
| 20 | $1.110\,169\times10^{8}$ | $1.170\,515\times10^{8}$ | 0.241 261 |
| 25 | $1.473\,691\times10^{10}$ | $1.536\,209\times10^{10}$ | 0.213 348 |
| 30 | $1.996\,587\times10^{12}$ | $2.066\,070\times10^{12}$ | 0.193 335 |
| 35 | $2.743\,387\times10^{14}$ | $2.824\,336\times10^{14}$ | 0.178 078 |
| 40 | $3.808\,584\times10^{16}$ | $3.906\,134\times10^{16}$ | 0.165 946 |
| 45 | $5.329\,172\times10^{18}$ | $5.449\,762\times10^{18}$ | 0.156 000 |
| 50 | $7.503\,319\times10^{20}$ | $7.655\,390\times10^{21}$ | 0.147 653 |
| 60 | $1.508\,716\times10^{25}$ | $1.534\,016\times10^{25}$ | 0.134 326 |
| 70 | $3.076\,657\times10^{29}$ | $3.120\,655\times10^{29}$ | 0.124 060 |
| 80 | $6.339\,104\times10^{33}$ | $6.418\,129\times10^{34}$ | 0.115 838 |
| 90 | $1.316\,426\times10^{38}$ | $1.330\,971\times10^{38}$ | 0.109 060 |
| 100 | $2.750\,822\times10^{42}$ | $2.778\,114\times10^{42}$ | 0.103 348 |

[a] The error in Table I, when stated, is taken as twice the first term neglected in the asymptotic series.

in terms of confluent hypergeometric functions. In the paragraphs below it will be shown that $G_9(\theta)$ can be written in terms of Bessel functions of a purely imaginary argument, plus a small correction term. For extremely large $\theta$ values, both $G_9(\theta)$ and $G_{12}(\theta)$ are expressible by asymptotic formulas with some interesting and curious points of similarity.

### $G_9(\theta)$ IN TERMS OF BESSEL FUNCTIONS

From the equation of definition[10]

$$B(T)=2\pi N\int_0^\infty r^2[1-\exp\{-U_s(r)/kT\}]dr, \quad (4)$$

introducing Eq. (1) with $s=9$ and $x=r/r_0$,

$$G_9(\theta)=3\int_0^\infty x^2[1-\exp\{\theta(3x^{-6}-2x^{-9})\}]dx. \quad (5)$$

Integrating by parts and making the substitution $x=(2\theta)^{1/9}z^{-1/3}$, Eq. (5) is readily transformed to

$$G_9(y)=2y\left[\int_0^y (z-\tfrac{2}{3}y)\exp(-z^3+yz^2)dz+\int_y^\infty (z-\tfrac{2}{3}y)\exp(-z^3+yz^2)dz\right], \quad (6)$$

where $y=(27\theta/4)^{1/3}$. Substituting

$$z=\tfrac{1}{3}y[2\cos\tfrac{1}{3}(\psi+\pi)+1] \quad (7a)$$

in the first integral of Eq. (6), and

$$z=\tfrac{1}{3}y[2\cosh(\xi/3)+1] \quad (7b)$$

in the second integral, and expressing $y$ in terms of $\theta$ again, a little algebraic and trigonometric manipulation leads to

$$G_9(\theta)=\theta e^{+(\theta/2)}\left[\int_{-\pi}^{+\pi} e^{+(\theta/2)\cos\psi}\times\left\{\sin\frac{2(\pi+\psi)}{3}-\sin\frac{(\pi+\psi)}{3}\right\}d\psi+\int_0^\infty \sinh\frac{\xi}{3}\left(2\cosh\frac{\xi}{3}-1\right)e^{-(\theta/2)\cosh\xi}d\xi\right]. \quad (8)$$

Now,

$$\sin\frac{2(\pi+\psi)}{3}-\sin\frac{(\pi+\psi)}{3}=+\sin\frac{2\psi}{3}\cos\frac{2\pi}{3}+\cos\frac{2\psi}{3}\sin\frac{2\pi}{3}-\cos\frac{\psi}{3}\sin\frac{\pi}{3}-\sin\frac{\psi}{3}\cos\frac{\pi}{3}.$$

The first of these terms leads to the integral,

$$\int_{-\pi}^{+\pi} e^{+(\theta/2)\cos\psi}\sin(2\psi/3)\cos(2\pi/3)d\psi,$$

which is identically zero because $\sin x$ is an odd function. Similarly, the third term vanishes on integration. Thus,

$$G_9(\theta)=\theta e^{+(\theta/2)}\left[\int_{-\pi}^{+\pi} e^{+(\theta/2)\cos\psi}\times\{\cos(2\psi/3)\sin(2\pi/3)-\cos(\psi/3)\sin(\pi/3)\}d\psi+\int_0^\infty e^{-(\theta/2)\cosh\xi}\{\sinh(2\xi/3)-\sinh(\xi/3)\}d\xi\right].$$

Because $\cos x$ is an even function, the first integral here can be doubled and taken over the limits zero to $+\pi$ rather than $(-\pi)$ to $(+\pi)$, leading to

$$G_9(\theta)=\theta e^{+\theta/2}\left\{\sqrt{3}\int_0^\pi e^{+(\theta/2)\cos\psi}\times[\cos(2\psi/3)-\cos(\psi/3)]d\psi+\int_0^\infty e^{-(\theta/2)\cosh\xi}[\sinh(2\xi/3)-\sinh(\xi/3)]d\xi\right\}. \quad (9)$$

From the relations involving Bessel functions with purely imaginary arguments of the first and second kinds,[11]

$$I_\nu(t)=\frac{1}{\pi}\int_0^\pi e^{+t\cos\psi}\cos\nu\psi d\psi-(\sin\nu\pi/\pi)\times\int_0^\infty e^{-t\cosh\xi-\nu\xi}d\xi, \quad (10a)$$

$$K_\nu(t)=\int_0^\infty e^{-t\cosh\xi}\cosh\nu\xi d\xi, \quad (10b)$$

[11] G. N. Watson, *Bessel Functions* (Cambridge University Press, Cambridge, 1945), second edition, p. 181.

it follows that

$$G_9(\theta)=\theta e^{+\theta/2}[\pi\sqrt{3}\{I_{2/3}(\theta/2)-I_{1/3}(\theta/2)\}+(3/2)\{K_{2/3}(\theta/2)-K_{1/3}(\theta/2)\}]-\tfrac{1}{3}T(\theta), \quad (11)$$

where the function $T(\theta)$ is given by

$$T(\theta)=\tfrac{3}{2}\theta e^{+\theta/2}\int_0^\infty e^{-(\theta/2)\cosh\xi}\times[\sinh(2\xi/3)-\sinh(\xi/3)]d\xi. \quad (12)$$

Using the definition (see reference 11, page 78),

$$K_\nu(t)\equiv(\pi/2\sin\nu\pi)[I_{-\nu}(t)-I_{+\nu}(t)], \quad (13)$$

the expression for $G_9(\theta)$ becomes

$$G_9(\theta)=(\pi\sqrt{3}/2)\theta e^{+\theta/2}[+\{I_{+2/3}(\theta/2)+I_{-2/3}(\theta/2)\}-\{I_{+1/3}(\theta/2)+I_{-1/3}(\theta/2)\}]-(1/3)T(\theta). \quad (14)$$

In the range where these equations are most useful, $\theta>2$, $T(\theta)\cong 1$, while $G_9(\theta)$ increases exponentially. Thus $(1/3)T(\theta)$ will, in general, be small compared with the term in square brackets in Eq. (14). $T(\theta)$ is not entirely negligible, however, for the range $2<\theta<10$, and methods of computing the function will be developed below.

## ASYMPTOTIC FORM FOR $G_9(\theta)$

For large $\theta$ values, the $T(\theta)$ term in Eq. (14) may be dropped for the reasons noted above. Then substituting the asymptotic form (see reference 11, page 203)

$$I_\nu(\theta/2)\cong e^{+\theta/2}/(\pi\theta)^{\frac{1}{2}}\sum_{m=0}(-1)^\nu(\nu,m)(1/\theta)^m, \quad (15)$$

where (see reference 11, page 198)

$$(\nu,m)=\frac{1}{m!}\cdot\frac{(\nu+m-1/2)!}{(\nu-m-1/2)!} \quad (16a)$$

$$=\frac{1}{m!4^m}(4\nu^2-1^2)(4\nu^2-3^2)(4\nu^2-5^2)\cdots\cdots(4\nu^2-[2m-1]^2) \quad (16b)$$

$$=(-\nu,m), \quad (16c)$$

in Eq. (14) gives

$$G_9(\theta)\cong+(3\pi\theta)^{\frac{1}{2}}e^{+\theta}\sum_{m=1}\{(\tfrac{2}{3},m)-(\tfrac{1}{3},m)\}(-1/\theta)^m. \quad (17)$$

The $m=0$ term vanishes since, from Eq. (16a), $(\nu,0)=1$. Using the relations,[12]

$$(+t)!(-t)!=\pi t/\sin\pi t \quad (18)$$

and

$$\sin(m\pi\pm\pi/6)=\pm(1/2)(-1)^m, \quad (19)$$

it follows that

$$\{(\tfrac{2}{3},m)-(\tfrac{1}{3},m)\}=\frac{(-1)^{m+1}}{\pi}\frac{(m-5/6)!(m-7/6)!}{(m-1)!}. \quad (20)$$

Substitute Eq. (20) in Eq. (17) and change the index by letting $n=m-1$, and the asymptotic formula for $G_9(\theta)$ becomes

$$G_9(\theta)\sim-(\pi/3\theta)^{\frac{1}{2}}e^{+\theta}\sum_{n=0}\beta_n(9)/\theta^n, \quad (21)$$

TABLE II. $T_n(\tau)$ and related functions.

| $n$ | $T_n(\tau)$ | $F(\tau)$ |
|---|---|---|
| 0 | $(3/4)+(1/2)\tau F_0$ | $F_0=(\sqrt{\pi}/2)e^{+\tau^2}[1-H(\tau)]$<br>$F_1=(1/2)-\tau F_0$ |
| 1 | $(1/4)F_3+(3/16\tau)F_4$ | $F_3=[1+\tau^2]F_1-(1/2)\tau F_0$<br>$F_4=(3/4)F_0-(3/2)\tau F_1-\tau F_3$ |
| 2 | $(1/64)(1/\tau)^2[\tau F_6+(3/4)F_7]$ | $F_6=[(5/2)+\tau^2]F_4-2\tau F_3$<br>$F_7=6F_3-3\tau F_4-\tau F_6$ |
| 3 | $(1/1536)(1/\tau)^3[\tau F_9+(3/4)F_{10}]$ | $F_9=[4+\tau^2]F_7-(7/2)\tau F_6$<br>$F_{10}=(63/4)F_6-(9/2)\tau F_7-\tau F_9$ |
| 4 | $(1/49{,}152)(1/\tau)^4[\tau F_{12}+(3/4)F_{13}]$ | $F_{12}=[(11/2)+\tau^2]F_{10}-5\tau F_9$<br>$F_{13}=30F_9-6\tau F_{10}-\tau F_{12}$ |
| 5 | $(1/1{,}966{,}080)(1/\tau)^5[\tau F_{15}+(3/4)F_{16}]$ | $F_{15}=[7+\tau^2]F_{13}-(13/2)\tau F_{12}$<br>$F_{16}=(195/4)F_{12}-(15/2)\tau F_{13}-\tau F_{15}$ |
| 6 | $(1/94{,}371{,}840)(1/\tau)^6[\tau F_{18}+(3/4)F_{19}]$ | $F_{18}=[(17/2)+\tau^2]F_{16}-8\tau F_{15}$<br>$F_{19}=72F_{15}-9\tau F_{16}-\tau F_{18}$ |

[12] E. Jahnke and F. Emde, *Tables of Functions* (Dover Publications, New York, 1945), fourth edition, p. 11.

TABLE III. $G_9(\theta)$ for $2<\theta<10$.

| $\theta$ | $\frac{1}{2}T(\theta)$ | $-G_9(\theta)$ | $-e^{-\theta}G_9(\theta)$ | $\delta$ | $(\pi/3\theta)^{\frac{1}{2}}e^{+\theta}$ |
|---|---|---|---|---|---|
| 2.0 | 0.315 031 | 7.463 959 | 1.010 137 | | 5.346 730 |
| 2.1 | 0.315 717 | 8.193 231 | 1.003 314 | 6 823 | 5.766 643 |
| 2.2 | 0.316 352[a] | 8.975 181 | 0.994 478 | 8 836 | 6.226 598 |
| 2.3 | 0.316 941 | 9.814 384 | 0.983 979 | 10 499 | 6.730 196 |
| 2.4 | 0.317 489[a] | 10.715 837 | 0.972 119 | 11 860 | 7.281 409 |
| 2.5 | 0.318 001 | 11.685 003 | 0.959 163 | 12 956 | 7.884 615 |
| 2.6 | 0.318 480 | 12.727 855 | 0.945 343 | 13 820 | 8.544 631 |
| 2.7 | 0.318 929[a] | 13.850 921 | 0.930 858 | 14 485 | 9.266 752 |
| 2.8 | 0.319 351[a] | 15.061 336 | 0.915 881 | 14 977 | 10.056 801 |
| 2.9 | 0.319 749[a] | 16.366 907 | 0.900 560 | 15 321 | 10.921 174 |
| 3.0 | 0.320 124 | 17.776 169 | 0.885 023 | 15 537 | 11.866 896 |
| 3.1 | 0.320 478[a] | 19.298 457 | 0.869 380 | 15 643 | 12.901 683 |
| 3.2 | 0.320 814[a] | 20.943 988 | 0.853 723 | 15 657 | 14.034 006 |
| 3.3 | 0.321 132[a] | 22.723 936 | 0.838 131 | 15 592 | 15.273 168 |
| 3.4 | 0.321 434[a] | 24.650 532 | 0.822 669 | 15 462 | 16.629 381 |
| 3.5 | 0.321 720$_6$ | 26.737 163 | 0.807 392 | 15 277 | 18.113 859 |
| 3.6 | 0.321 994[a] | 28.998 481 | 0.792 346 | 15 046 | 19.738 911 |
| 3.7 | 0.322 254[a] | 31.450 530 | 0.777 568 | 14 778 | 21.518 056 |
| 3.8 | 0.322 503[a] | 34.110 876 | 0.763 087 | 14 481 | 23.466 134 |
| 3.9 | 0.322 740[a] | 36.998 756 | 0.748 926 | 14 161 | 25.599 441 |
| 4.0 | 0.322 967 | 40.135 244 | 0.735 103 | 13 823 | 27.935 873 |
| 4.5 | 0.323 969 | 60.436 488 | 0.671 389 | 63 714 | 43.424 339 |
| 5.0 | 0.324 792 | 91.534 437 | 0.616 754 | 56 984 | 67.920 632 |
| 5.5 | 0.325 481 | 139.595 036 | 0.570 493 | 46 261 | 106.770 829 |
| 6.0 | 0.326 066 | 214.409 205 | 0.531 467 | 39 026 | 168.541 004 |
| 6.5 | 0.326 569 | 331.561 337 | 0.498 482 | 32 985 | 266.975 718 |
| 7.0 | 0.327 006$_5$ | 515.910 449 | 0.470 449 | 28 033 | 424.157 023 |
| 7.5 | 0.327 390 | 807.185 706 | 0.446 442 | 24 007 | 675.604 123 |
| 8.0 | 0.327 730 | 1268.990 763 | 0.425 699 | 20 743 | 1078.512 470 |
| 8.5 | 0.328 033 | 2003.308 716 | 0.407 610 | 18 089 | 1725.074 845 |
| 9.0 | 0.328 305 | 3173.890 955 | 0.391 689 | 15 921 | 2764.034 066 |
| 9.5 | 0.328 550 | 5044.004 249 | 0.377 553 | 14 136 | 4435.576 605 |
| 10.0 | 0.328 772 | 8037.401 863 | 0.364 897 | 12 656 | 7127.859 458 |

[a] Computed by Eq. (36).

where (see reference 12, page 12)

$$\beta_n(9)=\frac{1}{n!}\frac{(n+1/6)!(n-1/6)!}{(+1/6)!(-1/6)!} \tag{22}$$

$$=\left(\frac{1}{n!}\right)(1^2-1/36)(2^2-1/36)\cdots(n^2-1/36) \tag{23a}$$

$$=\left(n-\frac{1}{36n}\right)\beta_{n-1}(9) \tag{23b}$$

with $\beta_0(9)=1$. Equations (21) to (23) bear a close resemblance[13,3] to the corresponding asymptotic equations for $G_{12}(\theta)$. $G_9(\theta)$ for large $\theta$, computed using Eq. (21), is given in Table I. The function $e^{-\theta}G_9(\theta)$, which is also tabulated, is useful for interpolation.

## COMPUTATION OF $T(\theta)$ AND $G_9(\theta)$ FOR $\theta\leqslant 10$

From the definition [Eq. (14)] it follows that $T(\theta)$ satisfies the differential equation

$$2\theta T''-2\theta T'+[1+(4/9\theta)]T=1, \tag{24}$$

where primes signify derivatives of $T(\theta)$ with respect to $\theta$, a result which can most readily be proven by differentiating Eq. (12) and substituting in Eq. (24). The solution to this equation can be obtained as a semiconvergent power series in $1/\theta$:

$$T(\theta)=\sum_{n=0} a_n/\theta^n, \tag{25}$$

where

$$a_n=(-1)^n\frac{(3n)!}{(2n+1)!}\left(\frac{4}{27}\right)^n \tag{26a}$$

$$=(-1)^n\left(\frac{2}{9}\right)\frac{1}{3n+1}\prod_{k=1}^{n}\frac{(3k-1)(3k+1)}{2k+1}. \tag{26b}$$

But using these relations to compute $T(\theta)$, it will be found that the range of usefulness of the semiconvergent series is very small. Thus, if the sequence is terminated at the term just before the smallest one and the resulting error is taken to be twice the first term neglected, as is customary with series of this type,[14] the error in $T(\theta)$ thus computed is in the fourth decimal place for $\theta=7$; and the error increases rapidly for smaller values of $\theta$.

Although a large number of different methods of computing $T(\theta)$ were explored, only the following was found to be simple and convenient. Making the substitutions,†

$$\theta=32\tau^2/27, \tag{27a}$$

$$\zeta=(8/3)\tau[\cosh(\xi/3)-1], \tag{27b}$$

in the equation of definition [Eq. (12)],

$$T(\tau)=2\tau\int_0^\infty e^{-2\tau\zeta-\zeta^2}[1+(3\zeta/4\tau)]\exp(-\zeta^3/8\tau)d\zeta. \tag{28}$$

Expanding $\exp(-\zeta^3/8\tau)$ in a power series, it follows that

$$T(\theta)=\sum_{n=0}(-1)^nT_n(\tau), \tag{29}$$

where

$$T_n(\tau)=(2/n!)(1/8\tau)^n[\tau F_{3n}(\tau)+\tfrac{3}{4}F_{3n+1}(\tau)] \tag{30}$$

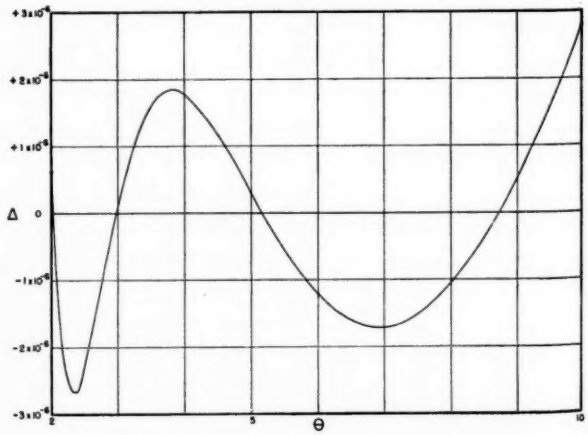


FIG. 1. Deviation function for Eq. (36).

[13] L. F. Epstein, J. Chem. Phys. **20**, 1670 (1952).

[14] J. B. Scarborough, *Numerical Mathematical Analysis* (Johns Hopkins Press, Baltimore, 1930), p. 140.

† The $\tau$ used here must not be confused with the $\tau$ symbol used by Hirschfelder and his associates (see references 1 and 2), which is defined as $1/\theta$.

and

$$F_i(\tau)\equiv\int_0^\infty t^i\exp(-2\tau t-t^2)dt. \tag{31}$$

From this definition,

$$F_0(\tau)=\exp(+\tau^2)\int_\tau^\infty \exp(-t^2)dt \tag{32a}$$

$$=(\pi/2)\exp(+\tau^2)[1-H(\tau)] \tag{32b}$$

and

$$F_1(\tau)=(1/2)-\tau F_0. \tag{33}$$

In Eq. (32b), $H(\tau)$ is the probability function

$$H(\tau)=[2/(\pi)^{\frac{1}{2}}]\int_0^\tau \exp(-t^2)dt, \tag{34}$$

which has been computed and tabulated with great accuracy over a wide range of the argument.[15] Also, integrating Eq. (31) by parts and juggling indices a little, the recursion formula

$$F_{i+1}=(i/2)F_{i-1}-\tau F_i \tag{35a}$$

is obtained, from which

$$F_{3n+3}=[\tfrac{1}{2}(3n+2)+\tau^2]F_{3n+1}-\tfrac{1}{2}(3n+1)\tau F_{3n} \tag{35b}$$

$$F_{3n+4}=\tfrac{3}{4}(3n+1)(n+1)F_{3n}-\tfrac{3}{2}(n+1)\tau F_{3n+1}-\tau F_{3n+3}. \tag{35c}$$

To compute $T(\theta)$ for the range $2<\theta<10$, it was necessary to carry the calculations of $T_n(\theta)$ out to $n=6$, and correspondingly, $F_n(\tau)$ values up to $n=19$ were required. The functions used are listed in Table II. Using the relations developed here, $T(\theta)$ was computed for $\theta=1.1$, 2.03, 2.1, 2.3, and 2.6, and $\theta=2.0$, 2.5, $3.0\cdots10.0$ to ten decimal places. The values of $(1/3)T(\theta)$ without asterisks given in Table III were obtained by rounding off the data derived in this way. The computations at $\theta=1.1$ and $\theta=2.0$ were made in order to compare the results of this paper with those obtained by the power series method;[9] the agreement is perfect at these two points.

The method for computing $T(\theta)$ outlined here is at best somewhat laborious. For values of $2<\theta<10$, the empirical formula

$$1-T(\theta)=A/\theta^{1/2}+B/\theta+C/\theta^{3/2}+D/\theta^2+\Delta, \tag{36}$$

with

$$A=-3.099\,828\times10^{-3} \tag{37a}$$

$$B=+1.775\,226\times10^{-1} \tag{37b}$$

$$C=-1.043\,212\times10^{-1} \tag{37c}$$

$$D=+2.088\,486\times10^{-2}, \tag{37d}$$

is recommended. This equation was obtained by fitting the data on $T(\theta)$ at $\theta=2.0$, 2.5, $3.0\cdots10.0$, by the method of least squares. The deviations $\Delta$ from this equation are less than three parts per million for this whole range, as can be seen from Fig. 1. The values of $T(\theta)$ computed at 2.03, 2.1, 2.3, and 2.6 were obtained in order to define the deviation plot accurately in this region, where it changes rather rapidly. The quantity $\sigma=\pm[\Sigma\Delta^2/(n-r)]^{\frac{1}{2}}$, where $n$ is the number of points (17 in this case) and $r$ is the number of arbitrary constants (4 in the equation above), is a measure of the fit of the equation, which reduces to the familiar standard deviation for $n\gg r$. In this case, $\sigma=\pm1.63\times10^{-6}$. The values of $(1/3)T(\theta)$ in Table III referred to in the footnote were obtained by the use of this empirical equation and the graphical deviation function.

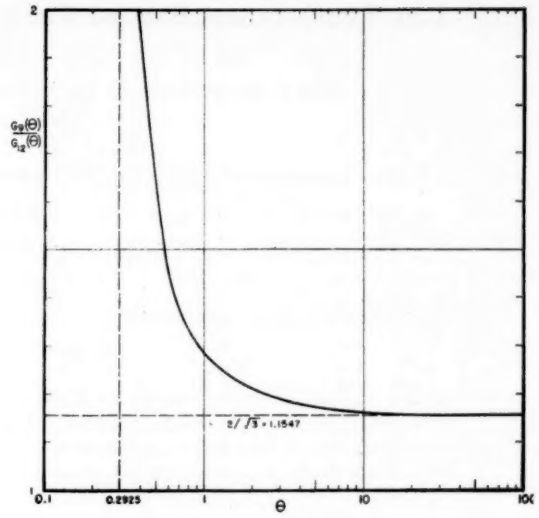


FIG. 2. The ratio $G_9(\theta)/G_{12}(\theta)$.

To find $G_9(\theta)$ for the range $2<\theta<10$, it is also necessary to compute the Bessel function term in square brackets in Eq. (14). This was done using the excellent National Bureau Standards tables.[16] The computation of these terms also was carried out with ten significant figures and subsequently rounded off to the values shown in Table III. The limiting form for very large $\theta$, $(\pi/3\theta)^{1/2}e^{+\theta}$, is included in the table for purposes of comparison, and the quantity $e^{-\theta}G_9(\theta)$ and its first differences for facilitating interpolation. Tables I and III are in excellent agreement in the region where they overlap. For $\theta>10$, Eq. (21) is satisfactory for most computations. In Fig. 2 the ratio $G_9(\theta)/G_{12}(\theta)$ is plotted to compare the behavior of the two functions. This ratio is infinite at the point where $G_{12}(\theta)=0$, and approaches the value $(12/9)^{\frac{1}{2}}$ for large values of $\theta$.

Physical conditions imposed by quantum-mechanical considerations[3] put a lower limit on the temperature to which Eq. (4) and the subsequent equations developed here may be used. These restrictions must not be ignored in the application of the results of the preceding paragraphs.

[15] A. N. Lowan, Editor, Computation Laboratory, National Bureau of Standards, *Tables of Probability Functions* (Columbia University Press, New York, 1941), Vol. I.

[16] A. N. Lowan, Editor, Computation Laboratory, National Bureau of Standards, *Tables of Bessel Functions of Fractional Order* (Columbia University Press, New York, 1949), Vol. II.

# Low Temperature Second Virial Coefficients for a Lennard-Jones Gas

LEO F. EPSTEIN
*General Electric Company, Knolls Atomic Power Laboratory,* Schenectady, New York*
(Received April 28, 1952)

For low temperatures, the second virial coefficient

$$B(\theta)=\tfrac{2}{3}\pi N r_0^3 G(\theta)$$

of a gas which follows a Lennard-Jones $6-s$ potential,

$$U_s(r)=\{\epsilon/(s-6)\}[6(r_0/r)^s-s(r_0/r)^6]$$

where $\theta=\epsilon/kT$, can be represented by

$$G_s(\theta)\sim-e^{+\theta}(3\pi/s\theta)^{\frac{1}{2}}\sum_{n=0}\beta_n(s)/\theta^n.$$

In two previous studies, formulas for $\beta_n(9)$ and $\beta_n(12)$ have been presented. In this paper, the relation for $G_s(\theta)$ is developed for the general case, using the method of steepest descents, and the first three coefficients $\beta_0(s)$, $\beta_1(s)$, and $\beta_2(s)$ are computed. The use of a Hooke's law potential and the quasi-ideal gas hypothesis yields the correct leading term in $G_s(\theta)$, but results in errors in $\beta_1(s)$ and $\beta_2(s)$.

## INTRODUCTION

IN two previous papers,[1,2] it has been shown that for a gas which follows a Lennard-Jones potential,

$$U_s(r)=\{\epsilon/(s-6)\}[6(r_0/r)^s-s(r_0/r)^6], \tag{1}$$

the second virial coefficient $B(\theta)$ can conveniently be expressed in terms of the function

$$G(\theta)=3B(\theta)/2\pi N r_0^3, \tag{2}$$

where $\theta=\epsilon/kT$. In a detailed analysis of the two cases, $s=9$ and $s=12$, it was found that for low temperatures (large $\theta$) asymptotic formulas for $G_s(\theta)$ could be obtained in the form

$$G_s(\theta)\sim-e^{+\theta}(3\pi/s\theta)^{\frac{1}{2}}\sum_{n=0}\beta_n(s)/\theta^n, \tag{3}$$

where

$$\beta_n(s)=\frac{1}{n!}\frac{\left[\left(n+\frac{s-6}{2s}\right)!\left(n-\frac{s-6}{2s}\right)\right]!}{\left[\left(+\frac{s-6}{2s}\right)!\left(-\frac{s-6}{2s}\right)\right]!}. \tag{4}$$

From this relation

$$\beta_0(s)=1, \tag{5a}$$

$$\beta_1(s)=(3/4s^2)(s+6)(s-2), \tag{5b}$$

$$\beta_2(s)=(9/32s^4)(5s-6)(s+6)(s-2)(s+2). \tag{5c}$$

The purpose of this study was to determine the asymptotic formula for $G_s(\theta)$ for values of $s$ other than 9 and 12. Anticipating the results of later paragraphs, it will be shown that Eq. (3) is valid for any value of $s>6$, but that Eq. (4) which is a convenient expression for the two important cases $s=9$ and $s=12$, does not apply to any other value of $s$.

## DERIVATION OF $G_s(\theta)$ FOR LARGE $\theta$

The relation[3]

$$B(T)=2\pi N\int_0^\infty r^2[1-\exp\{-U_s(r)/kT\}]dr \tag{6}$$

can be readily transformed into

$$G_s(T)=-(1/kT)\int_0^\infty x^3U_s'(x)\exp\{-U_s(x)/kT\}dr, \tag{7}$$

where $x=r/r_0$ and $U_s'(x)=dU_s(x)/dx$. Introducing Eq. (1), then

$$G_s(\theta)=+\{6s\theta/(s-6)\}[I_s(\theta)-I_6(\theta)], \tag{8}$$

where

$$I_j(\theta)=\int_0^\infty x^{-j+2}\exp\{-(\theta/s-6)[6x^{-s}-sx^{-6}]\}dx. \tag{9}$$

The saddle point in $U_s(x)$ occurs at $x=1$, so that the substitution $x=1+t$ is suggested.† With this,

$$I_j(\theta)=\int_{-1}^{+\infty}(1+t)^{-j+2}\exp\{-(\theta/s-6)\times[6(1+t)^{-s}-s(1+t)^{-6}]\}dt, \tag{10}$$

or asymptotically for large $\theta$, the lower limit of integration may be taken as $-\infty$. $I_j(\theta)$ can then be written as

$$I_j(\theta)\cong\int_{-\infty}^{+\infty}(1+t)^{-j+2}\exp[+\theta\sum_{k=0}A_kt^k]dt, \tag{11}$$

* The Knolls Atomic Power Laboratory is operated for the United States Atomic Energy Commission by the General Electric Company under Contract No. W-31-109 Eng-52.

[1] L. F. Epstein and G. M. Roe, J. Chem. Phys. **19**, 1320 (1951).

[2] Roe, Epstein, and Powers, J. Chem. Phys. **20**, 1665 (1952).

[3] R. H. Fowler and E. A. Guggenheim, *Statistical Thermodynamics* (Cambridge University Press, London, 1939), p. 279 ff.

† This method of evaluating the integral was suggested by G. M. Roe.

where the $A_k$'s are polynomials in $s$ of the order $(k-1)$ for $k \geqslant 1$, defined by

$$A_k(s)=\frac{1}{s-6}\frac{(-1)^n}{k!}\left[6\frac{(k+s-1)!}{(s-1)!}-s\frac{(k+5)!}{5!}\right] \quad (12)$$

and obtained by expanding the bracketted term in Eq. (10) by the binomial theorem. The first three values are $A_0=-1$, $A_1=0$, $A_2=3s$.

Letting $t=\alpha p$ where $\alpha=(1/3s\theta)^{1/2}$ and expanding $(1+t)^{-j+2}$ by the binomial theorem

$$I_j(\alpha)=\alpha\exp(+\tfrac{1}{3}s\alpha^2)\sum_{m=0}(-\alpha)^m\binom{j+m-3}{m} \times\int_{-\infty}^{+\infty}p^m\exp(-p^2)\exp\{(-\tfrac{1}{3}s\alpha^2)\sum_{k=3}A_k\alpha^k p^k\}dp. \quad (13)$$

The last exponential term in this expression can clearly be developed in a power series in $p$,

$$\sum_{n=m}C_{2n-m}p^n=p^m\exp\sum_{k=3}(-A_k/3s)\alpha^{k-2}p^k. \quad (14)$$

Substituting this in Eq. (13) and using the well-known expressions[4] for

$$\int_{-\infty}^{+\infty}p^{2n}\exp(-p^2)dp \quad \text{and} \quad \int_{-\infty}^{+\infty}\exp(-p^2)dp,$$

explicit formulas for $I_j(\alpha)$ can be obtained. Combining $I_s(\alpha)$ and $I_6(\alpha)$, the general expression for $G_s(\alpha)$ becomes

$$G_s(\alpha)\cong+(\pi)^{\frac{1}{2}}\exp(+1/3s\alpha^2) \times\sum_{m=1}\sum_{n=\left\{\substack{(1/2m)\\(1/2)(m+1)}\right\}}(-1)^m\alpha^{m-1} \times\left[\frac{1}{s-6}\left\{\binom{s+m-3}{m}-\binom{m+3}{m}\right\}\right] \times C_{2n-m}\frac{1\cdot3\cdot5\cdots(2n-1)}{2^{n-1}}. \quad (15)$$

The sum over $n$ is to be taken using integer values, the lowest being either $m/2$ or $(m+1)/2$. The quantity,

$$\left[\frac{1}{s-6}\left\{\binom{s+m-3}{m}-\binom{m+3}{m}\right\}\right],$$

is a readily evaluated polynomial in $s$ of the order $(m-1)$.

The most difficult part of this problem is the computation of the coefficients $C_j$. In order to obtain $\beta_2(s)$, it is necessary to compute all of the $C_j$'s up to $j=15$,

[4] B. O. Peirce, *A Short Table of Integrals* (Ginn and Company, New York, 1929), third edition, No. 492 and No. 494.

TABLE I. The coefficients $C_j$, correct to terms in $\alpha^5$.

| $j$ | $C_j$ |
|---|---|
| 0 | 1 |
| 1 | 0 |
| 2 | 0 |
| 3 | $+(1/3)(s+9)\alpha$ |
| 4 | $-(1/12)(s^2+12s+83)\alpha^2$ |
| 5 | $+(1/60)(s^3+16s^2+131s+836)\alpha^3$ |
| 6 | $-(1/360)(s^4+21s^3+211s^2+1491s+9220)\alpha^4$ $+(1/18)(s^2+18s+81)\alpha^2$ |
| 7 | $+(1/3\cdot840)(s^5+27s^4+337s^3+2757s^2+18{,}166s$ $+110{,}760)\alpha^5-(1/36)(s^3+21s^2+191s+747)\alpha^3$ |
| 8 | $+(1/18\cdot80)(13s^4+320s^3+3750s^2+26{,}080s+94{,}637)\alpha^4$ |
| 9 | $-(1/9\cdot240)(5s^5+144s^4+2018s^3+17{,}988s^2+107{,}993s$ $+374{,}124)\alpha^5+(1/6\cdot27)(s^3+27s^2+243s+729)\alpha^3$ |
| 10 | $-(1/8\cdot27)(s^4+30s^3+380s^2+2466s+6723)\alpha^4$ |
| 11 | $+(1/2\cdot27\cdot80)(9s^5+301s^4+4630s^3+41{,}870s^2$ $+226{,}721s+580{,}869)\alpha^5$ |
| 12 | $+(1/24\cdot81)(s^4+36s^3+486s^2+2916s+6561)\alpha^4$ |
| 13 | $-(1/4\cdot6\cdot81)(s^5+39s^4+650s^3+5886s^2+28{,}917s+60{,}507)\alpha^5$ |
| 14 | 0 |
| 15 | $+(1/120\cdot243)(s^5+45s^4+810s^3+7290s^2+32{,}805s+59{,}049)\alpha^5$ |

retaining terms of the order of $\alpha^5$ or less. The painful algebra involved yields the values given in Table I. Substituting these in Eq. (15), and carrying through the somewhat tedious arithmetic, results in a rather surprising amount of cancellation—only terms in $\alpha^2$ appear in the sum, for example. Finally in terms of $\theta$, rather than $\alpha$,

$$G_s(\theta)\sim-e^{+\theta}(3\pi/s\theta)^{\frac{1}{2}}[1+(1/72s)(s+6) \times(s+33)(1/\theta)+(1/10368s^2)(s+6) \times(s^3+360s^2+7101s+14310)(1/\theta)^2+\cdots]. \quad (16)$$

A comparison of this equation with Eqs. (3) and (5) will readily show that the two agree only for the special cases $s=9$ and $s=12$.

The method used to obtain $\beta_1(s)$ and $\beta_2(s)$ given here could in principle be used to obtain $\beta_3(s)$ and higher coefficients. Practically, the algebraic detail is enormous, perhaps prohibitive. In these equations for $G_s(\theta)$ at low temperatures, care must be exercised to restrict their use to regions where they are not invalidated by quantum restrictions, which have been omitted in the above derivations by treating the energy of the system as a continuum rather than being made up of discrete levels.[1]

## ALTERNATIVE DERIVATION OF LEADING TERM FOR $G_s(\theta)$ AT LOW TEMPERATURES

Professor Stockmayer[5] of the Massachusetts Institute of Technology has suggested the following alternative derivation of the leading term in the asymptotic form for $G_s(\theta)$, based on the facts that at low temperatures:

(1) The molecules will be close to the minimum in the potential well and thus will behave like dimeric species.

(2) Near the minimum, the vibrations of the mole-

[5] W. H. Stockmayer, private communication, May 22, 1951.

cule in the potential well can be approximated by the Hooke's law potential $U_s(r)=\epsilon[-1+(\mathbf{k}/2)(r-r_0)^2]$.

(3) The second virial coefficient of a gas can be obtained by assuming that it is made up of monomers and dimers, each species behaving like an ideal gas. The relative quantities of the two species present are determined by the mass action constant for the dimerization equilibrium, and this then can be computed from the partition functions of the two species (quasi-ideal gas hypothesis).

By expanding the potential function, Eq. (1), about the minimum $r_0$, the Hooke's law constant $\mathbf{k}$ is found to be

$$\mathbf{k}=6s\epsilon/r_0^2, \tag{17}$$

and the vibration frequency corresponding to this is

$$\nu=(1/\pi r_0)(3s\epsilon/m)^{1/2}. \tag{18}$$

Now the classical partition function for the dimeric molecule will be given by

$$Q_{II}=Q_{\rm tr}\cdot Q_{\rm rot}\cdot Q_{\rm vib}\cdot\exp(+\epsilon/kT), \tag{19}$$

where the factor $e^{+\epsilon/kT}$ is included because the energy is measured from an isolated atom as zero. Then

$$Q_{\rm tr}=\left[\frac{2\pi(2m)kT}{h^2}\right]^{\frac{3}{2}}V \quad \text{translation,} \tag{20a}$$

$$Q_{\rm rot}=\frac{8\pi^2(mr_0^2/2)kT}{2h^2} \quad \text{rotation-rigid rotator,} \tag{20b}$$

$$Q_{\rm vib}=kT/h\nu \quad \text{vibration-classical limiting form.} \tag{20c}$$

For the monomer, the partition function includes only translation

$$Q_I=(2\pi mkT/h^2)^{3/2}V. \tag{21}$$

The equilibrium constant for the dimerization reaction, expressing the concentrations of the species in moles per unit volume, is

$$K=NV(Q_{II}/Q_I^2), \tag{22}$$

and this is simply related[6] to the second virial coefficient, $B(T)=-K$. Combining Eqs. (17) to (21) and converting over to the $G_s(\theta)$ notation, this analysis leads at once to

$$G_s(\theta)\sim-e^{+\theta}(3\pi/s\theta)^{\frac{1}{2}}, \tag{23}$$

which is exactly the limiting law previously found. A more abstract treatment leads to the expression

$$G(T)\sim-(3/2\pi r_0^3)e^{+\epsilon/kT}[h^3/(\pi mkT)^{3/2}]Q_i, \tag{24}$$

where $Q_i$ refers to the internal degrees of freedom of the dimeric molecule. In the simple illustration above

$$Q_i=Q_{\rm rot}\cdot Q_{\rm vib}=[2\pi^3r_0^3m^{3/2}(kT)^2]/[h^3(3s\epsilon)^{1/2}]. \tag{25}$$

But if the molecule (a) is anharmonic and (b) shows vibration-rotation interaction, Eq. (25) is no longer a valid representation of the internal partition function, and it is necessary to go to a more complicated form for $Q_i$. Following the method outlined by Mayer and Mayer[7] it follows that, in general,

$$Q_i=2\pi r_0^2(\pi mkT/h^2)^{\frac{1}{2}}\int_{-\infty}^{+\infty}[1+(\xi/r_0)]^2e^{-U(\xi)/kT}d\xi. \tag{26}$$

The expression for $G_s(\theta)$ obtained by combining Eqs. (24) and (26) is rather like that obtained in the preceding section and can be integrated in a similar manner, although considerably more easily. The final result is that

$$\begin{aligned}G_s(\theta)\sim-e^{+\theta}(3\pi/s\theta)^{\frac{1}{2}}[1&+(1/72s)\\&\times\{(s+6)(s+33)+36\}(1/\theta)+(1/10368s^2)\\&\times\{(s+6)(s^3+360s^2+7101s+14310)\\&+360(2s^2+45s+159)\}(1/\theta)^2+\cdots].\end{aligned} \tag{27}$$

This equation agrees with the exact relation, Eq. (16), in the leading term but is in error in the higher coefficients. Thus $\beta_1(s)$ from Eq. (27) leads to a fairly small error, some 2–7 percent for $25>s>7$; and to a significantly larger error in $\beta_2(s)$, 8–19 percent for the same range of $s$ values. The differences between Eqs. (16) and (27) are probably due to the inadequacy of the basic assumption in this development that the individual species can be treated as ideal gases.[6]


## ACKNOWLEDGMENT

The writer wishes to express his deepest appreciation to Dr. G. M. Roe, whose suggestions and criticisms were invaluable, and to Mr. W. H. Howland and Miss M. D. Powers, who assisted in the checking of the mathematics and in the preparation of this paper.


[6] Hirschfelder, McClure, and Weeks, J. Chem. Phys. **10**, 201 (1942).

[7] J. E. Mayer and M. G. Mayer, *Statistical Mechanics* (John Wiley & Sons, Inc., New York, 1940), p. 167 ff.

# The Reaction of Hg($^3P_1$) with Ethylene†

B. deB. Darwent
*Division of Chemistry, National Research Laboratories, Ottawa, Canada*

(Received February 14, 1952)

The reaction of Hg($^3P_1$) with ethylene at room temperature has been re-investigated. Special attention was paid to the effects of the concentrations of ethylene and mercury on the reaction velocity. The results are in general agreement with a mechanism which requires the excited ethylene, produced initially, to decompose both in the gas phase and on the wall. The results are also compatible with the suggestion that a significant fraction of the quenching collisions between ethylene and Hg($^3P_1$) leads to the formation of metastable ($^3P_0$) atoms.

## INTRODUCTION

THERE have been several previous investigations of the reactions of Hg($^3P_1$) atoms with ethylene. The most recent of these was by LeRoy and Steacie,[1] who postulated that an excited ethylene molecule was produced in the initial act and that this could either decompose homogeneously or be deactivated by collision with an unexcited ethylene molecule. They also suggested that some $C_4$ hydrocarbons might have been formed at high pressures, since under those conditions the partial pressure of acetylene was no longer the same as the total pressure increase. This mechanism requires the reciprocal of the rate of hydrogen production to be a linear function of the concentration of ethylene when the concentration of ethylene is high enough for quenching to be complete. However, as mentioned in a previous communication,[2] the results of LeRoy and Steacie do not agree with their mechanism but appear to obey the relationship

$$I/R=A+Bp^2.$$

The present investigation was undertaken to study more carefully the effect of pressure and of the concentration of mercury on the rate of production of hydrogen, and also to examine the reactions responsible for the suggested formation of the $C_4$ hydrocarbons.

## EXPERIMENTAL

The reaction system consisted of a cylindrical quartz cell, with plane quartz windows, connected via a quartz-Pyrex graded seal to a McLeod gauge and a mercury cutoff. The apparatus was evacuated and filled through the mercury cutoff which was also used as a manometer. The quartz cell (10 cm×5-cm diam) was placed vertically and connected to the rest of the system near the bottom face. A low pressure mercury lamp with neon (3 mm) as a carrier gas was used as a source of unreversed λ2537. The radiation from the lamp was approximately collimated by a quartz lens and defined by a 2.5-cm stop. A drop of mercury in the bottom of the cell provided a constant and controllable concentration of mercury in the reaction volume. The lower 2 cm of the cell was surrounded by a large Dewar flask, which was used as a thermostat to control the concentration of mercury in the vapor phase. Water was used as the thermostat fluid, and the level was adjusted so that the top of the horizontal portion of the tube connecting the reaction flask to the rest of the system was always well covered by the liquid. Agitation of the thermostatic liquid by a slow stream of air ensured a constant temperature throughout the bath. The total volume of the system was 440 cc to which the reaction cell contributed 196 cc.

The reaction was followed by freezing out the unreacted ethylene and any condensable products with liquid nitrogen, and measuring the pressure of the permanent gas with the McLeod gauge. LeRoy and Steacie[1] have shown that hydrogen is the only detectable substance that is not removed at the temperature of liquid nitrogen. They have also shown that the rate of pressure increase decreases with continued illumination, and they ascribed this to increased quenching by hydrogen. Accordingly, in the present investigation the reaction was followed over very small conversions, the maximum pressure of hydrogen being less than $5\times10^{-2}$ mm, so that complications due to quenching by hydrogen should not have been significant. This was confirmed by preliminary experiments which established (a) that the pressure of hydrogen was, within the accuracy of the measurements, a linear function of time, (b) that there was no detectable change in the transparency of the incident window due to the deposition of polymer, and (c) that successive experiments could be carried out using the same sample of ethylene, without flaming the cell, with no detectable change in rate because of the accumulation of condensable products.

The intensity of λ2537 was estimated by using the mercury photosensitized decomposition of propane as an actinometer. The rate of production of hydrogen from propane (440 mm) was measured, and when 0.48 was used for the quantum efficiency,[3] the intensity was estimated to be $2.9\times10^{-7}$ einstein min$^{-1}$. This value was the average of several determinations, among which the

† Contribution No. 2845 from the National Research Laboratories, Ottawa, Canada.

[1] D. J. LeRoy and E. W. R. Steacie, J. Chem. Phys. **9**, 829 (1941).

[2] B. deB. Darwent, J. Chem. Phys. **19**, 258 (1951).

[3] S. Bywater and E. W. R. Steacie, J. Chem. Phys. **19**, 319 (1951).

TABLE I. The effect of pressure on the quantum yield.

| intensity≈$2\times10^{-7}$ einstein $min^{-1}$; beam diameter =2.5 cm volume of system =440 cc; Hg saturator =20.0°C | | | | |
|---|---|---|---|---|
| Expt. No. | Pressure mm Hg | Rate—mm $min^{-1}\times10^3$ Observed | Standard | $\phi_{H_2}$ |
| 54 | 9.80 | $3.27_5$ | 2.78 | 0.380 |
| 41 | $13.3_5$ | 3.02 | 2.76 | 0.351 |
| 52 | 29.0 | $2.37_5$ | 2.83 | 0.270 |
| 40 | 30.3 | 2.24 | 2.76 | 0.260 |
| 44 | 38.1 | 1.95 | 2.72 | 0.230 |
| 50 | 45.0 | 1.79 | 2.83 | 0.203 |
| 46 | 45.4 | 1.73 | 2.81 | 0.198 |
| 51 | 55.0 | 1.51 | 2.83 | 0.172 |
| 43 | 56.0 | $1.38_5$ | 2.72 | 0.164 |
| 47 | 66.0 | $1.21_5$ | 2.81 | 0.139 |
| 49 | 66.0 | 1.25 | 2.83 | 0.142 |
| 61 | 73.5 | 1.07 | 2.64 | 0.130 |
| 58 | 82.0 | $0.97_6$ | $2.76_5$ | 0.113 |
| 62 | 86.1 | 0.93 | 2.64 | 0.113 |
| 57 | 91.8 | 0.87 | $2.76_5$ | 0.101 |
| 63 | 96.0 | 0.80 | 2.64 | 0.097 |
| 56 | 99.5 | 0.76 | $2.76_5$ | 0.089 |

variation was less than ±5 percent. Experiments were carried out with ethylene and propane alternately, the temperature of the mercury supply being 20.0±0.1°C. The following values were obtained for the quantum yield of the hydrogen production from ethylene at various pressures:

| Pressure of $C_2H_4$ mm | $\phi_{H_2}$ |
|---|---|
| 10.65 | 0.375 |
| 39.8 | 0.222 |
| 48.5 | 0.186 |

The value of 0.375 for $\phi_{H_2}$ at 10.65 mm may be compared with that of 0.37 for 13 mm of ethylene, found by LeRoy and Steacie, who used uranyl oxalate as the actinometer.

Some difficulty was experienced in maintaining the light intensity constant over prolonged intervals, and this made the comparison of rates obtained several days apart somewhat uncertain. Hence the intensity was checked each day by carrying out experiments under standard conditions and referring all results to the standard rates obtained on that day. In practice, at least, two standard runs were made on each day, and the results showed that between these two runs the intensity remained constant. The standard conditions were 19.2±0.2 mm with the mercury supply at 20.0 ±0.1°C, and by interpolation of the results given above for $\phi_{H_2}$ at various pressures the value of $\phi$ under standard conditions ($\phi_s$) was found to be 0.321.

## RESULTS

The effect of pressure on the quantum yield with the mercury supply at 20.0°C is shown by the data given in Table I. The standard rates ($R_{H_2}{}^s$) used for calculating the quantum yields at the various pressures are given in column 4. These are the average results of two experiments done immediately before and after the experiments to which they are applied. The individual determinations of $R_{H_2}{}^s$ did not differ from the average by more than ±2 percent and were usually much closer to the average than ±1 percent. The reciprocal quantum yields are shown as a function of pressure ($p$) and ($p^2$) in Fig. 1. It is evident from Fig. 1 that neither the $p$ nor $p^2$ plot is linear and that they deviate from linearity in opposite directions. In the experiments at high mercury concentration (20°C), the plot of $1/\phi_{H_2}$ against $p^2$ appears to be linear at low pressures (up to about 40 mm) and to intersect the $1/\phi$ axis at about the point 2.65. The fact that the $p$ and $p^2$ curves deviate from linearity in opposite directions suggests that $1/\phi$ is actually a composite function of $p$ and $p^2$. This is consistent with $C_2H_4$* decomposing in the gas phase as well as on the wall.

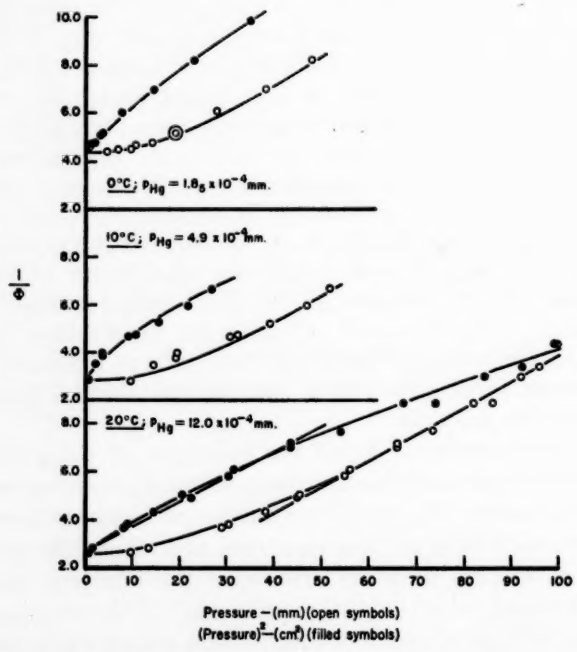


FIG. 1. The effect of ethylene pressure on the quantum yield. Mercury saturator temperature: top—0.0°C; middle—10.0°C; bottom—20.0°C.

TABLE II. Effect of mercury concentration on the quantum yield.

| Pressure of $C_2H_4$ =19.2(±0.1) mm | | |
|---|---|---|
| Saturator (°C) | $P_{Hg}$ mm $\times10^4$ | $\phi_{H_2}$ |
| 20.0 | 12.0 | 0.321 |
| 0.0 | $1.8_5$ | 0.197 |
| 16.0 | 8.5 | 0.297 |
| 10.0 | 4.9 | 0.266 |
| 4.0 | 2.8 | 0.230 |
| 23.5 | 16.1 | 0.335 |

Further indication that decomposition of $C_2H_4$* on the wall plays a significant part in the over-all process is provided by the effect of mercury pressure on $\phi_{H_2}$. These results (Table II) show that the quantum yield decreases progressively with decreasing concentration of

mercury vapor. By plotting $\phi$ against $\log p_{Hg}$ (Fig. 2) it becomes evident that the results are in good agreement with a linear relation between those two parameters. The linear relationship between $\phi$ and $\log p_{Hg}$ may be explained by assuming that the absorption of λ2537 by mercury was incomplete, since the amount of light absorbed is an exponential function of the concentration of mercury, so that a linear relationship exists between the absorbed intensity and $\log p_{Hg}$. However, calculations based on a reasonable value of the absorption coefficient[4] of mercury for λ2537, and independent experiments‡ both showed that the λ2537 should be almost completely absorbed in a 10-cm path even at the lowest concentration of mercury used. It may therefore be concluded that the decrease in rate with decreasing concentration of mercury was due to some factor other than the decrease in absorbed intensity.

The effect of pressure on the quantum yield of hydrogen production with the mercury supply at 10.0°C and 0.0°C are given in Table III, which is analogous to Table I. The reciprocal quantum yields are plotted against $p$(mm) and $p^2$(cm$^2$) in Fig. 1, and again we find that both plots deviate from straight lines.

In addition to the decomposition of $C_2H_4$*, the nature of the deactivation was investigated. A pressure of 196 mm of ethylene was taken into the reaction system (McLeod gauge excluded) and exposed to λ2537 for 6.0 hours with the mercury supply at 0°C. The hydrogen produced amounted to $14.4\times10^{-2}$ mm in the entire system. The condensable products were analyzed on the mass spectrometer and special attention was paid to the presence of $C_4$ hydrocarbons. No trace of $C_4$ hydrocarbons was found, indicating an upper limit of 0.03 percent $C_4$ in the condensable products.

Now at 0°C the initial quantum yield of hydrogen production, obtained by extrapolating to zero pressure, was 0.233. The intensity was about $2.0\times10^{-7}$ einstein min$^{-1}$, so that there should have been $2.0\times10^{-7}\times6\times60\times0.233=16.8\times10^{-6}$ mole of $C_2H_4$* produced in 6 hours. The hydrogen actually produced amounted to $3.5\times10^{-6}$ mole so that $13.8\times10^{-6}$ mole of $C_2H_4$* were deactivated. The total condensable products was $3.36\times10^{-3}$ mole, of which less than 0.03 percent were $C_4$ hydrocarbons. Hence, less than $1.01\times10^{-6}$ mole of $C_4$ hydrocarbons were produced by the deactivation of $13.8\times10^{-6}$ mole of $C_2H_4$*. Each deactivating collision involves one excited and one normal ethylene molecule and, if $C_4$ hydrocarbons were produced in the "deactivation" step, one mole of $C_4$ should be produced for each $C_2H_4$* that is deactivated. Hence, the result of this experiment shows that less than 8 percent of the deactivating collisions at room temperatures lead to the production of $C_4$ hydrocarbons.

[4] A. C. G. Mitchell and M. W. Zemansky, *Resonance Radiation and Excited Atoms* (Cambridge University Press, Cambridge, 1934).

‡ It was found that at least 96 percent of λ2537 was absorbed in a distance of 15 mm by mercury at a pressure of $20\times10^{-4}$ mm in the presence of 100 mm of hydrogen.

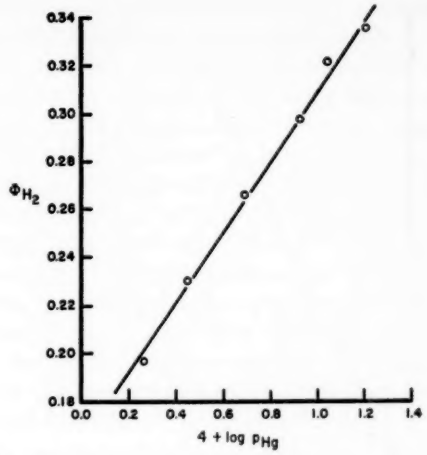


FIG. 2. The effect of mercury concentration on the quantum yield. Ethylene pressure—19.2 mm Hg.

## DISCUSSION

The following reactions,

$$C_2H_4+Hg(^3P_1)\rightarrow C_2H_4^*+Hg(^1S_0) \quad (1)$$

$$C_2H_4^*+C_2H_4\rightarrow 2C_2H_4 \quad (2)$$

$$C_2H_4^*\rightarrow C_2H_4+H_2, \quad (3)$$

were suggested[1] as a mechanism that would account for the nature of the products and for the effect of pressure on the rate of the mercury photosensitized reaction of ethylene. From this mechanism the relationship

$$1/R_3=\frac{1}{k_1[^3P_1]}\cdot\frac{1}{[C_2H_4]}+\frac{k_2}{k_1k_3[^3P_1]} \quad (A)$$

was derived, and it was concluded that "a plot of $1/R_3$ *vs* $1/C_2H_4$ should give a straight line for which the ratio of the intercept on the $1/R_3$ axis to the slope is $k_2/k_3$." By assuming a reasonable value for $k_2$, $\tau_3$ (or $1/k_3$), the average life of the excited ethylene molecule, was found to be about $10^{-7}$ sec. In a previous com-

TABLE III. Effect of pressure on the quantum yield at low mercury concentration. Conditions as in Table I except for mercury concentration.

| Hg saturator—10°C | | | Hg saturator—0°C | | |
|---|---|---|---|---|---|
| Pressure mm | Rate mm min$^{-1}\times10^3$ | $\phi_{H_2}$ | Pressure mm | Rate mm min$^{-1}\times10^3$ | $\phi_{H_2}$ |
| 19.1$_5$ | 2.11 | 0.266 | 27.9 | 1.33 | 0.166 |
| 9.8$_5$ | 2.88 | 0.362 | 9.9$_5$ | 1.77 | 0.220 |
| 14.4$_5$ | 2.28 | 0.287 | 14.2$_5$ | 1.70 | 0.212 |
| 33.0 | 1.67 | 0.210 | 4.78 | 1.82$_5$ | 0.227 |
| 18.9$_5$ | 1.82 | 0.254 | 6.98 | 1.79 | 0.223 |
| 30.6 | 1.69 | 0.216 | 2.54 | 1.76 | 0.219 |
| 51.6 | 1.18 | 0.151 | 18.9 | 1.56 | 0.194 |
| 39.0 | 1.49 | 0.191 | 18.8 | 1.56$_5$ | 0.194 |
| 46.9 | 1.31$_5$ | 0.168 | 38.3 | 1.14 | 0.143 |
| | | | 47.9 | 0.97 | 0.122 |
| | | | 59.0 | 0.807 | 0.101 |
| | | | 10.6$_5$ | 1.69 | 0.213 |

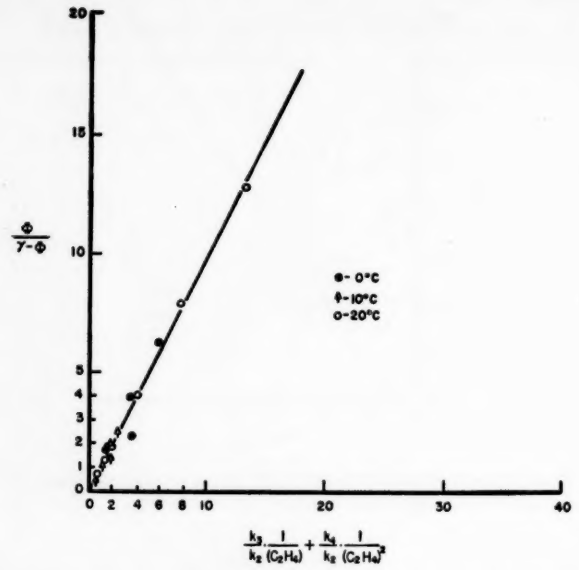


FIG. 3. The effect of the concentrations of mercury and ethylene on the quantum yield.

munication[2] it was pointed out that the foregoing mechanism does not agree with experiment and that the derivation of $\tau_3$ from Eq. (A) is not valid. We shall discuss this mechanism in the light of data obtained in the present investigation, the value of $\tau_3$, and the deactivation of excited ethylene.

## Mechanism of the Reaction

In any discussion about the mechanism of the mercury photosensitized reaction of ethylene, the processes

$$Hg(^1S_0)+h\nu \rightarrow Hg(^3P_1), \quad (a)$$

$$Hg(^3P_1) \rightarrow Hg(^1S_0)+h\nu \quad (b)$$

must, obviously, be considered in addition to reactions (1), (2), and (3). The usual stationary state treatment yields the following result:

$$[^3P_1]=I_a/(k_b+k_1[C_2H_4]). \quad (B)$$

This may be introduced into Eq. (A) to give

$$1/\phi=1+(k_2/k_3)[C_2H_4], \quad (C)$$

where $\phi=R_3/I_a$ is the quantum yield of the production of hydrogen. Hence, if the mechanism consisting of reactions (1), (2), and (3) is correct, the reciprocal quantum yield should be a linear function of the pressure, and the limiting extrapolated value at zero pressure should be unity. That such a relationship does not represent the experimental facts is obvious from Fig. 1. The results of LeRoy and Steacie[1] yield a straight line when $1/\phi$ is plotted against $[C_2H_4]^2$. For such a relationship to be valid it is necessary for the excited ethylene molecules to decompose on the wall,

$$C_2H_4^* \xrightarrow{\text{wall}} C_2H_2+H_2, \quad (4)$$

rather than homogeneously [as by reaction (3)], or for the deactivation process to occur only as the result of a triple collision,

$$C_2H_4^*+2C_2H_4 \rightarrow 3C_2H_4. \quad (5)$$

This latter process (5) appears to be most improbable and could hardly be reconciled with relatively low quantum yields since these require an efficient deactivation process. If we assume that the heterogeneous process (4) is responsible for the decomposition, we obtain, by the usual stationary state treatment, the relationship

$$1/\phi=1+(k_2/k_4)[C_2H_4]^2, \quad (C')$$

which agrees with the results of LeRoy and Steacie and, even if over only a limited range of conditions, with the results of the present experiments. Some support for reaction (4) is provided by the effect of mercury concentration on $\phi$ at constant pressure of ethylene (Fig. 2), which shows that $\phi$ decreases logarithmically with the concentration of mercury. This is understandable since $k_4$ must be assumed to be some function of the distance through which the excited ethylene molecules diffuse before they attain the wall, which is itself a logarithmic function of the concentration of mercury.

TABLE IV. Effect of mercury concentration on initial efficiency and rate constants.

| Saturator (0°C) | (Dimensions are mole, liter) $\gamma$ | $(k_3/k_2)\times10^3$ | $(k_4/k_3)\times10^6$ |
|---|---|---|---|
| 20.0 | 0.400 | 1.04 | 3.27 |
| 10.0 | 0.333 | 1.15 | 2.63 |
| 0.0 | 0.233 | 2.46 | 2.55 |

That neither Eq. (C) or (C') accurately describes the effect of concentration of ethylene on the quantum yield is obvious from the results plotted in Fig. 1. Since the plots deviate in opposite directions from the predicted straight lines we may conclude that processes (3) and (4) both occur and that their relative importance depends on the conditions of the experiment. This conclusion is supported by the fact that at high pressure the diffusion of excited ethylene molecules could become so slow that the average time taken for them to attain a wall would exceed their natural life.

If both reactions (3) and (4) are included, the following relationship is obtained:

$$\frac{\phi}{1-\phi}=\frac{k_3}{k_2}\cdot\frac{1}{[C_2H_4]}+\frac{k_4}{k_2}\cdot\frac{1}{[C_2H_4]^2}.$$

If we allow for the possibility of inefficiency in the initial act or in reaction (4), the above relationship may be shown to become

$$\frac{\phi}{\gamma-\phi}=\frac{k_3}{k_2}\cdot\frac{1}{[C_2H_4]}+\frac{k_4}{k_2}\cdot\frac{1}{[C_2H_4]^2}, \quad (D)$$

where $\gamma$ represents the product of the efficiencies of reactions (1) and (4). The value of $\gamma$ may be obtained by extrapolation to zero concentration of the $1/\phi$ *vs* $[C_2H_4]$ or $1/\phi$ *vs* $[C_2H_4]^2$ curves in Fig. 1. By using the value of $\gamma$ so obtained the best values of $k_3/k_2$ and $k_4/k_2$ (Table IV) were calculated by the method of least squares. The fact that $\phi/(\gamma-\phi)$ is a linear function of $1/[C_2H_4]+1/[C_2H_4]^2$, as demanded by Eq. (D), is shown in Fig. 3. Thus, the results are in reasonable agreement with the mechanism involving both the homogeneous and the heterogeneous decomposition of excited ethylene. The influence of the concentrations of ethylene and of mercury on the fraction of excited ethylene that decomposes on the wall is shown in Fig. 4. The fraction of the heterogeneous decomposition is given by the expression

$$\frac{(k_4/k_2)(1/[C_2H_4])^2}{(k_4/k_2)(1/[C_2H_4]^2)+(k_3/k_2)(1/[C_2H_4])}.$$

Although effects of changes in the concentrations of mercury and ethylene do indeed influence the rate of the reaction in the manner predicted by the mechanism, there are other effects which are not immediately predictable. These are as follows: (a) The value of $\gamma$ is seen (Table IV) to decrease with decreasing mercury concentration whereas the suggested mechanism does not predict that there should be any change. (b) The ratios $k_3/k_2$ and $k_4/k_2$ appear to be functions of the concentration of mercury vapor. (c) The results given in Tables I and III seem to indicate that the maximum rate occurs at progressively decreasing pressures as the mercury concentration is decreased. (d) No plausible explanation has been given for the fact[1] that the maximum rate is obtained only when the pressure of ethylene is as high as 9–10 mm when the pressure of mercury is $1\text{–}2\times10^{-3}$ mm.

Quenching measurements indicate that reaction (b) should be negligible at pressures higher than about 2 mm, and so it may be expected that the maximum rate would occur at about 1 or 2 mm. Some results obtained recently[5] in these laboratories suggest that at least part of the quenching of λ2537 by ethylene occurs by virtue of the reaction

$$C_2H_4+Hg(^3P_1)\rightarrow C_2H_4'+Hg(^3P_0), \qquad (c)$$

where $C_2H_4'$ represents ethylene with only a small amount (0.218 ev) of energy in excess of the thermal value. There are two reactions by which the metastable $(^3P_0)$ atoms can disappear:

deactivation to the ground state by collision with ethylene,

$$C_2H_4+Hg(^3P_0)\rightarrow C_2H_4^*+Hg(^1S_0); \qquad (d)$$

or by collision with the wall,

$$Hg(^3P_0)\xrightarrow{\text{wall}} Hg(^1S_0)+E. \qquad (e)$$

[5] B. deB. Darwent and F. G. Hurtubise, J. Chem. Phys. **20**, 1684 (1952).

There is no quantitative information about reaction (d), but Samson[6] found that with nitrogen the effective cross section for the transition $^3P_1\rightarrow{}^1S_0$ was very much greater than for $^3P_0\rightarrow{}^1S_0$. If a similar relationship holds for quenching by ethylene, it is obvious that deactivation of the metastable mercury atoms to the ground state by collision with ethylene may be complete only at a fairly high pressure. Hence without attempting a quantitative treatment of the problem, it is obvious that, if a significant fraction of the quenching occurs by the transition $^3P_1\rightarrow{}^3P_0$, the maximum rate may be reached at a pressure that is very much higher than that expected from the known quenching cross section. Also the maximum rate will occur when the rate of reaction (d) is small compared with that of (c). Since the rate of reaction (e) depends on the average distance through which the $(^3P_0)$ atoms diffuse before they strike the wall it is not difficult to see, qualitatively, that the maximum rate of reaction will occur at smaller pressures as the distance of diffusion is increased (i.e., as the concentration of mercury is decreased). Thus the foregoing points (c) and (d) may be explained reasonably on the basis of quenching to the metastable state. An explanation along similar lines could be suggested for the influence of mercury concentration on $\gamma$ and for the effect of [Hg] on $k_4/k_2$. However, the effect of concentration of mercury on the ratio $k_3/k_2$ appears to be quite inexplicable by a mechanism consisting of the reactions suggested above.

### Average Life of Excited Ethylene

The average life of the excited ethylene produced in reaction (1) was calculated[1] to be about $10^{-7}$ sec. The value of $k_2/k_3$ was derived from the ratio of intercept to slope of the straight line that resulted when $1/R_3$ was

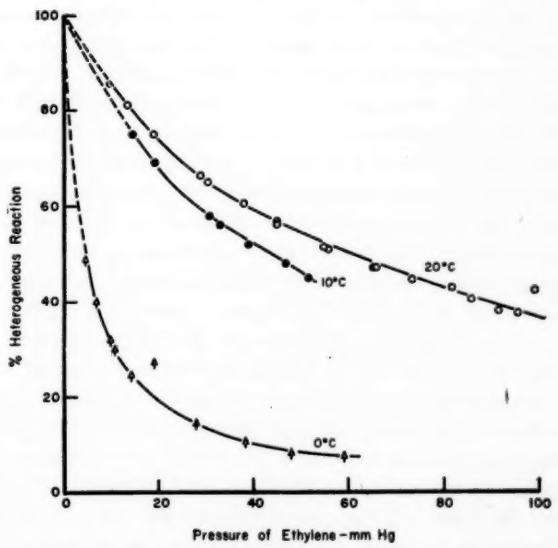


FIG. 4. The calculated effect of the concentrations of mercury and ethylene on the contribution of the wall reaction.

[6] E. W. Samson, Phys. Rev. **40**, 940 (1932).

plotted against $1/C_2H_4$ according to Eq. (A), and $1/k_3(=\tau_3)$ was obtained from this by using an assumed value for $k_2$. This procedure is not necessarily valid since, in general, the slope of the line is given by

$$\frac{d(1/R_3)}{d(1/C_2H_4)}=\frac{1}{k_1}\cdot\frac{1}{[^3P_1]}+\frac{1}{k_1}\cdot\frac{1}{[C_2H_4]}\cdot\frac{d(1/[^3P_1])}{d(1/[C_2H_4])}+\frac{k_2}{k_1k_3}\cdot\frac{d(1/[^3P_1])}{d(1/[C_2H_4])},$$

and it is only when $[^3P_1]$ is not a function of $[C_2H_4]$, i.e., when $d(1/[^3P_1])/d(1/[C_2H_4])=0$, that the slope will be equal to $1/k_1[^3P_1]$. The foregoing discussion has shown clearly that $[^3P_1]$ is, in fact, a function of $[C_2H_4]$, given by Eq. (B), and therefore the value of $\tau_3$ as calculated by LeRoy and Steacie is not necessarily correct. The usual stationary state treatment applied to reactions (a), (b), (1), (2), (3), and (4) gives the equation

$$1/\phi=\left(\frac{k_b}{k_1[C_2H_4]}+1\right)\left(1+\frac{k_2[C_2H_4]^2}{k_3[C_2H_4]+k_4}\right). \quad (E)$$

At low pressures the term $(k_2[C_2H_4]^2)/(k_3[C_2H_4]+k_4)$ may be neglected compared with unity, and the simple relationship

$$1/\phi=(k_b/k_1[C_2H_4])+1$$

is obtained. If allowance is made for possible inefficiency in the initial act, the equation then becomes

$$1/\phi=(k_b/k_1[C_2H_4])+\gamma. \quad (E')$$

It is now obvious why a straight line was obtained when $1/\phi$ (or $1/k_3$) was plotted against $1/[C_2H_4]$. However, it is evident that the ratio of intercept to slope of this line does not bear any relationship to the average life of excited ethylene but is related to the quenching process.

Some values of $k_3/k_2$ from which the magnitude of $\tau_3(=1/k_3)$ may be obtained are listed in Table IV. The values of $k_3/k_2$ appear to be between 1 and $2\times10^{-3}$ mole liter$^{-1}$. Taking an average value of $1.5\times10^{-3}$ mole liter$^{-1}$ for $k_3/k_2$ and assuming a value§ of $13\times10^{10}$ liter mole$^{-1}$ sec$^{-1}$ for $k_2$, we get $k_3=2\times10^8$ sec$^{-1}$ or $\tau_3=0.5\times10^{-8}$ sec. This value is quite different from those suggested earlier,[1,2] and it must be admitted that no great reliance should be placed on any of these estimates. The value given by LeRoy and Steacie[1] has been shown to have been based on a wrong premise. The value suggested in the author's previous note[3] was based on the assumption that no homogeneous decomposition occurs, and this is obviously wrong. The value calculated from $k_3/k_2$ may be considerably in error, since this ratio appears to be influenced by the concentration of mercury. However, if the trend (Table IV) of increasing value of $k_3/k_2$ with decreasing [Hg] is regarded as fictitious, the average life suggested above ($0.5\times10^{-8}$ sec) may have some validity, always provided that the assumptions about $k_2$ are correct.

§ Assuming that reaction (2) occurs on every collision.

### Nature of the Deactivating Reaction

An interesting result obtained in this investigation is the very small yield of $C_4$ hydrocarbons at high pressures, which allows an upper limit of about 10 percent to be placed on the percentage of "deactivating" collisions that lead to the formations of $C_4$ hydrocarbons. This result is interesting since Laidler[7] suggested that the excited ethylene produced in the initial step is actually a vibrationally excited triplet, which may be expected to undergo reactions similar to those of other free radicals. It is well known that methyl radicals are capable of adding to the double bond of ethylene, and therefore, it may be expected that the triplet ethylene (biradical), with its vibrational excitation, would add rather easily. The results of this investigation show quite clearly that the reaction is not fast and that at least 90 percent of the collisions between excited ethylene and ethylene, in which the excited molecules are deactivated, lead only to deactivation and not to addition.

LeRoy and Steacie[8] also investigated the effect of temperature on the mercury photosensitized reactions of ethylene. They found that the rate of hydrogen production was not affected significantly by changes in temperature, but that at high temperatures a rapid, free-radical, sensitized polymerization of ethylene occurred. They therefore suggested that the reaction

$$Hg(^3P_1)+C_2H_4\rightarrow C_2H_3+H+Hg \quad (1')$$

occurred, as well as reaction (1). The free radical sensitized polymerization may then take place by virtue of processes of the type

$$C_2H_3+C_2H_4\rightarrow C_4H_7,$$
$$H+C_2H_4\rightarrow C_2H_5.$$

However, their results appear to be equally well explained by the assumption of only a single initial step (1) if we then have competition between the deactivation reaction (2) and a reaction of the type

$$\cdot CH_2-CH_2\cdot+C_2H_4\rightarrow\cdot CH_2-CH_2-C_2H_4$$

between excited ethylene and ethylene. The foregoing addition probably requires some energy of activation, which is unlikely with the deactivation reaction (2). This suggestion is, of necessity, purely speculative, since there is little information available about reactions of this type.

#### ACKNOWLEDGMENT

The author expresses his cordial thanks to Mr. M. W. Thistle of these laboratories for his advice and assistance in the preparation of these manuscripts.

[7] K. J. Laidler, J. Chem. Phys. **10**, 43 (1942).
[8] D. J. LeRoy and E. W. R. Steacie, J. Chem. Phys. **10**, 676 (1942).

# The Reaction of Cd($^3P_1$) with Propane at Low Conversion*

P. AGIUS† AND B. DEB. DARWENT
*Division of Chemistry, National Research Council, Ottawa, Canada*

(Received February 14, 1952)

The reaction of Cd($^3P_1$) with propane has been investigated at 300°C under such conditions that the rates of production of hydrogen and methane are independent of time. The quantum yield of hydrogen production, when corrected for incomplete quenching, is close to unity and is approximately independent of the substrate pressure. The production of methane can be accounted for by the decomposition of propyl radicals. The ratio $CH_4/H_2$ increases with decreasing pressure of propane; if this ratio varies as $I_a^{-\frac{1}{2}}$ (as is the case when the methyl radicals are produced by the thermal decomposition of propyl radicals), the increase may be ascribed to the decreasing absorbed intensity at lower pressures.

## INTRODUCTION

THE mechanisms of the reactions of Hg($^3P_1$) with ethane[1] and propane[2] have been reasonably well established at room temperature. The products from propane consist almost exclusively of hydrogen and hexane down to low pressures. At low pressures the production of methane increases with decreasing pressure due to atomic cracking reactions. With ethane, atomic cracking sets in at higher pressures than with propane. This is probably due to the greater activation energy of

$$H+C_2H_6=C_2H_5+H_2$$

compared with

$$H+C_3H_8=C_3H_7+H_2,$$

which renders the atomic cracking process inherently more probable with ethane than with propane.

In an investigation of the reaction of Cd($^3P_1$) with propane Steacie, LeRoy, and Potvin[3] found that much more methane was produced than in the corresponding reaction of Hg($^3P_1$) at room temperature and tentatively suggested a reaction involving CdH molecules to account for these results. Their work was carried out at high propane conversions, and it is therefore possible that secondary reactions occurred, involving the products. The effect of accumulation of the reaction products can be judged from their quenching cross sections[4] in relation to that of propane, as follows:

| Substance | Quenching cross section (3261A) $cm^2\times10^{16}$ |
|---|---|
| $C_3H_8$ | 0.02 |
| $C_2H_4$ | 24.9 |
| $C_3H_6$ | 29.1 |
| $H_2$ | 3.54 |

Hence, it was decided to re-investigate the reaction of Cd($^3P_1$) with propane at very low conversions with emphasis on the effect of pressure (on which atomic cracking is known to be dependent) on the nature of the products.

## EXPERIMENTAL

The propane used for most of the experiments was obtained from the Phillips Petroleum Company. It was stated to be better than 99.9 mole percent propane by the National Bureau of Standards. Experiments carried out with a sample of less pure material, although carefully fractionated through a low temperature Stedman type column until no unsaturates could be detected on a mass spectrometer, gave low results.

The hydrogen used was taken from a commercial cylinder and was purified by passage through a heated palladium thimble followed by a liquid nitrogen trap.

The radiation source used was a low pressure cadmium discharge lamp. The central emitting portion was kept at about 350°C; the electrode ends were thermostatted to approximately 280°C. In this way self-absorption of the resonance radiation by cool cadmium vapor in the lamp was eliminated. The front and back of the oven were provided with double windows, which also served as filters, consisting of a plate of 1-mm Pyrex and a plate of 2-mm Red Purple Corex (Corning-9863). The forward radiation to the reaction cell was further filtered with 20 mm of 0.89 M $NiCl_2$ solution (iron free). The results of absorption experiments, which are described below, showed that 97 percent of the residual radiation was λ3261; this permitted a photocell system to be used to measure absorbed intensities. The lamp was operated from a 6000 v sign transformer at about 80 ma, the output being monitored with a photocell.

The radiation from the lamp was reduced to about 10 percent of its intensity by a chromel-quartz neutral density filter and focused from the rear window onto a screened IP 28 photomultiplier. The radiation from the forward window of the lamp was lightly converged through a quartz reaction vessel and also fell on a screened IP 28 photomultiplier. A stop between this photomultiplier and the cell ensured that only radiation which had passed through the cell fell on the photomultiplier.

* Contribution No. 2844 from the National Research Laboratories, Ottawa, Canada.

† National Research Council of Canada Postdoctorate Fellow, 1949–50. Present address: Esso European Laboratories, Esso House, Abingdon, Berkshire, England.

[1] B. deB. Darwent and E. W. R. Steacie, J. Chem. Phys. **16**, 381 (1948).

[2] B. deB. Darwent and E. W. R. Steacie, J. Chem. Phys. **13**, 563 (1945).

[3] Steacie, LeRoy, and Potvin, J. Chem. Phys. **9**, 306 (1941).

[4] E. W. R. Steacie and D. J. LeRoy, J. Chem. Phys. **11**, 164 (1943).

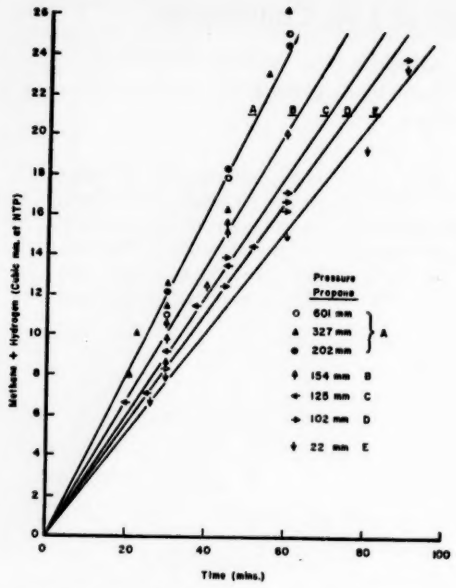


FIG. 1. The effect of time and propane pressure on the rate of production of $H_2+CH_4$.

The reaction vessel was a quartz cylinder 10 cm long and 5-cm diameter with plane quartz windows. It was placed in a horizontal furnace which was constructed to allow two 15-mm diameter quartz tubes, sealed to the top and bottom centers of the reaction cell to project outside the furnace casing. The lower tube contained about 1 g of outgassed and very pure cadmium. It was surrounded by a vertical furnace, the temperature of which could be controlled independently of that of the horizontal furnace to provide a known and constant pressure of cadmium. The upper tube was provided with a conical ground-quartz cutoff which was operated magnetically. This tube connected the reaction vessel to the rest of the apparatus and the cutoff, which was surrounded by an auxillary heater, prevented the cadmium from diffusing out of the heated reaction vessel and subsequently condensing on the cold connecting tubing. The cadmium saturator was maintained at 240°C, the reaction vessel at 300°C and the ground-quartz cutoff at a temperature slightly higher than that of the main body of the reaction cell. The faces of the reaction vessel were heated one or two degrees hotter than the center to prevent condensation of cadmium.

The reaction vessel was connected *via* mercury cutoffs, on the one hand, to a conventional high vacuum line and gas storage system, and on the other to a liquid nitrogen trap, mercury diffusion pump, and a combined Toepler pump and gas burette, a modification of a design by Halden and Luttrop.[5]

After irradiation for a measured time, the heated quartz cutoff to the reaction vessel was opened and the condensable gases held back in the liquid nitrogen trap. The uncondensable gases were pumped off with the diffusion and Toepler pumps and the volume measured in the gas burette. Methane-hydrogen analyses were carried out either by oxidation on copper oxide at 280°C or by mass spectrometric determination.

[5] W. L. Halden and E. S. Luttrop. Ind. Eng. Chem. Anal. Ed. **13**, 571 (1941).

### Absorption Experiments

To obtain information on the absorption of 3261A radiation and to check the purity of the radiation from the lamp, the percentage absorption of radiation passing through the reaction vessel for various saturator temperatures was determined. These experiments were carried out in the presence of 20 mm of hydrogen and with the reaction vessel at 300°C.

The absorption percentages were derived from the photocell readings, the latter having first been calibrated against standard chromel quartz neutral density filters. It was resolved to operate with the saturator at 240°C (corresponding to a cadmium vapor pressure of $3.0\times10^{-3}$ mm) giving an absorption of 85 percent and a large enough temperature differential between the reaction vessel and the saturator to ensure that the vapor pressure of the cadmium was effectively controlled by the latter.

### Actinometry

The quantum yield[6] of carbon monoxide production from acetone at 130°C and low radiation intensities was assumed to be unity at 3261A.

The reaction vessel was thoroughly freed from cadmium, and acetone (Mallinckrodt Chemical Works —Analytical Reagent Grade) was introduced at a suitable pressure. The acetone had been previously distilled at low pressure; only the middle third was retained, carefully outgassed, and stored in the dark at −80°C.

After irradiation, the gases uncondensable at liquid nitrogen temperatures were pumped off and measured. These consisted of methane and carbon monoxide, and were analyzed by combustion over copper oxide at 250°C. A separate series of experiments was carried out to measure the absorbed radiation using the calibrated photocells, and the absorbed intensity at the pressure

TABLE I. The effect of pressure on the rates of production of hydrogen and methane.

Reaction temperature = 300°C; Saturator = 240°C;
Absorbed intensity = $8.3\times10^{-7}$ einstein $\cdot hr^{-1}$
Uncondensable gas rate of production $mm^3\cdot hr^{-1}$

| Propane (mm Hg) | % $H_2$ | % $CH_4$ | Uncond. | $H_2$ | $CH_4$ | $\frac{CH_4}{H_2}$ |
|---|---|---|---|---|---|---|
| 601 | 61 | 39 | 24.2 | 14.8 | 9.4 | 0.64 |
| 327 | 62 | 38 | 24.2 | 15.0 | 9.1 | 0.60 |
| 202 | 51 | 49 | 24.2 | 12.4 | 11.8 | 0.95 |
| 154 | 47 | 53 | 20.4 | 9.6 | 10.8 | 1.12 |
| 125 | 38 | 62 | 18.1 | 6.9 | 11.2 | 1.62 |
| 102 | 42 | 58 | 16.8 | 7.1 | 9.8 | 1.38 |
| 22 | 45 | 55 | 15.2 | 6.8 | 8.4 | 1.25 |

[6] D. S. Herr and W. A. Noyes, Jr., J. Chem. Soc. **62**, 2052 (1940).

(214 mm) used during the actinometric runs was determined.

The maximum absorbed light intensity during the propane decomposition was taken as 85 percent of the output of the lamp. From an experiment with 214 mm acetone irradiated for 15.88 hours, 46.9 cu mm of CO and 68.9 cu mm $CH_4$ were obtained (at N.T.P.). This gave a value of $8.3\times10^{-7}$ einstein hour$^{-1}$ which has not been corrected for the possibly incomplete quenching of Cd($^3P_1$) by propane.

## RESULTS

The results of individual experiments demonstrating the effects of time on the production of uncondensable gas ($H_2+CH_4$) at different pressures are shown graphically in Fig. 1. At low conversions, the rates of production of hydrogen and methane are independent of time within the limits of accuracy of the measurements. Hence, it may be concluded that under such conditions, complications due to secondary reactions of the products (e.g., quenching of λ3261 by $C_2H_4$ and the removal of H atoms by $C_2H_4$) were not serious. However, it was found that when the same sample of propane was used in successive experiments the rate of production of hydrogen decreased with progressive irradiation even though the permanent gases ($H_2+CH_4$) were removed after each experiment. This is probably caused by the progressive accumulation of small amounts of ethylene which does not react readily[7] with Cd($^3P_1$) atoms but which quenches λ3261 very efficiently and reacts rapidly with hydrogen atoms. The reaction rate (Fig. 1) increased slowly but regularly with increasing pressure up to about 200 mm, above which no detectable increase in rate was noticed.

The basic results are summarized in Table I. The rates of production of uncondensable gas are derived from Fig. 1, and the analyses for $H_2$ and $CH_4$ are the averages of several individual measurements which were, on the whole, concordant. The rate of hydrogen formation decreases with decreasing pressure, whereas the rate of methane production appears to be independent of the pressure of propane.

The dependence of the rate of hydrogen production on the pressure of propane is illustrated in Fig. 2. On the same graph is shown the percentage of λ3261 quenched by propane at various pressures. These quenching results were obtained from the data of Steacie and LeRoy[4] who did not detect imprisonment of radiation in a 2 mm path up to cadmium pressures corresponding to saturation at 240°C. On this basis, the effective intensities and the effective quantum yields of hydrogen production were calculated for various pressures of propane used and the results recorded in Table II. These calculations were based on the assumption that imprisonment did not occur. However, the conditions of these experiments were far from ideal since no precautions were taken to adjust the dimensions of the reaction vessel so that imprisonment would be minimized. Hence, it is quite likely that imprisonment was serious. The effect of imprisonment would be negligible at high pressures where quenching was large but would be of increasing importance at lower pressures so that one cannot be at all certain of the magnitude of the quantum yield at pressures lower than about 100 mm.

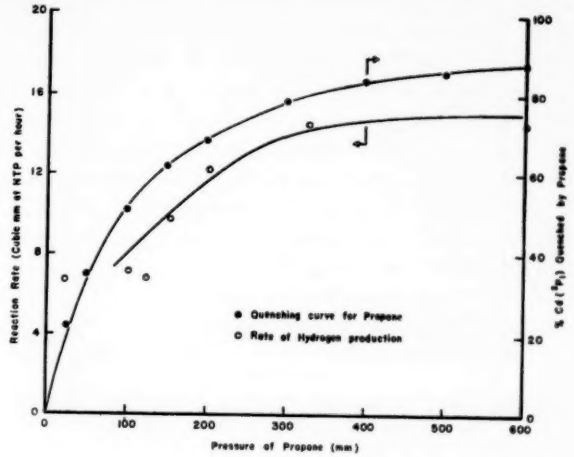


FIG. 2. The effect of pressure on the rate of production of hydrogen and on the quenching of λ3261.

The effect of pressure on the ratio $CH_4/H_2$ is shown by the last column of Table I and in Fig. 3 in which the experimentally determined points are shown in relation to a theoretical line. Although there appears to be a fairly large uncertainty attached to the value of this ratio, it seems that the ratio decreases with increasing pressure up to about 300 mm, beyond which further increase in the pressure has little or no effect on the value of the ratio.

Considerable amounts of methane were produced at all pressures, and it was of interest to find out how much $C_2$ hydrocarbons were formed compared to methane since this would provide some information about the mechanism of that process. The general nature of the heavier products of the reaction was established by Steacie, LeRoy, and Potvin[3] and it was not considered necessary to repeat that portion of the research, especially since the measurement of small quantities of $C_6$ and $C_4$ hydrocarbon, under the conditions of very small

TABLE II. The quantum yield of hydrogen production when corrections for incomplete quenching are applied.

| Pressure of $C_3H_8$ (mm) | Rate of $H_2$ production (c mm/hour) | [a]$I_{absorbed}\times10^7$ Einstein·hr$^{-1}$ | $\phi_{H_2}$ |
|---|---|---|---|
| 600 | 14.8 | 7.4 | 0.90 |
| 400 | 14.6 | 6.9 | 0.94 |
| 300 | 13.9 | 5.8 | 1.07 |
| 200 | 11.8 | 4.8 | 1.10 |
| 100 | 8.0 | 4.3 | 0.83 |

[a] Corrected for incomplete quenching.

[7] D. J. LeRoy and E. W. R. Steacie, J. Chem. Phys. **10**, 683 (1942).

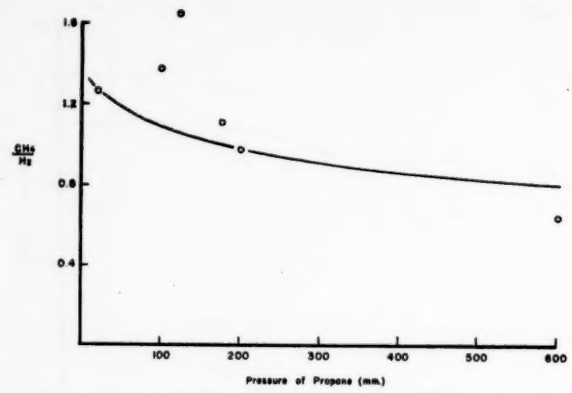


FIG. 3. The effect of pressure on the ratio $CH_4/H_2$. The points are experimental and the line theoretical.

conversion used in these experiments, would have been difficult and uncertain. A small amount of $C_4$ hydrocarbons, for example, would be lost in the large amount of propane in the products. This did not apply to the measurement of $CH_4$ and $C_2$ hydrocarbons which could be concentrated by a rough fractionation and subjected to mass spectrometric analysis. The products from several successive experiments of a total of 330 min duration were therefore collected and subjected to mass spectrographic analysis with the following results:

| Product | $CH_4$ | $C_2H_4$ | $C_2H_6$ |
|---|---|---|---|
| Rate ($mm^3\ hr^{-1}$) | 3.8 | 3.6 | 0.77. |

The rates of formation of methane and ethylene were approximately equal while that of ethane was considerably lower.

## DISCUSSION

The principal light products of the cadmium photosensitized reactions of propane at 300°C have been identified as hydrogen, methane, and ethylene. A previous investigation[3] of this reaction showed that hexane was produced in considerable amounts and that butane and other paraffins were also formed. The nature of the heavy products was not investigated in the experiments now reported, since only very small conversions were studied, and it has been assumed that hexanes, and possibly other higher hydrocarbons, were produced in addition to the hydrogen and ethylene. The reactions,

$$Cd(^3P_1)+C_3H_8\rightarrow C_3H_7+CdH \quad (1)$$

$$CdH\rightarrow Cd(^1S_0)+H \quad (2)$$

$$H+C_3H_8\rightarrow C_3H_7+H_2 \quad (3)$$

$$2C_3H_7\rightarrow C_6H_{14}, \quad (4)$$

which are similar to those suggested for the mercury photosensitized reactions of propane and which were proposed[3] previously to account for the products of the cadmium photosensitized reaction, explain adequately the production of hydrogen and hexane.

The fact that considerable amounts of methane are formed shows that some reaction occurs which leads to the breaking of a carbon to carbon bond. The most plausible processes for accomplishing this are "atomic cracking" reactions between H atoms and propyl radicals and the thermal decomposition of propyl radicals. The mechanisms associated with these processes are probably

A. *Atomic Cracking*

$$H+C_3H_7\rightarrow C_3H_8^* \quad (5)$$

$$C_3H_8^*\rightarrow CH_3+C_2H_5 \quad (6)$$

$$C_3H_8^*+M\rightarrow C_3H_8+M. \quad (7)$$

B. *Propyl Radical Decomposition*

$$C_3H_7\rightarrow CH_3+C_2H_4. \quad (8)$$

In both cases the methane would be produced by

$$CH_3+C_3H_8\rightarrow CH_4+C_3H_7. \quad (9)$$

The kinetics of Mechanism A are complicated and it is impossible, without making unwarranted assumptions about the magnitudes of the rate constants, to test the applicability of that mechanism to the experimental results. However, a choice between the two mechanisms may be made by considering the nature of the products, the quantum yield of hydrogen production, and some evidence provided by earlier experiments.

The products contained approximately equal quantities of methane and ethylene, whereas ethane amounted to only about $\frac{1}{5}$ of the methane. Of the two mechanisms only B contains a reaction by which ethylene is produced, and it therefore appears the more probable. The possibility that the ethyl radical, produced in reaction (6), decomposed to ethylene and a hydrogen atom,

$$C_2H_5\rightarrow C_2H_4+H, \quad (10)$$

must be discounted since, if the propyl radical does not decompose, it must be assumed that the ethyl radical is less stable than propyl and this is contrary to experience.[8]

The quantum yield of hydrogen production (Table II) is close to unity and approximately independent of pressure between about 100 and 600 mm. Since "atomic cracking" involves the loss of hydrogen atoms, the high quantum yield makes it appear unlikely that reaction 5 occurs to a significant extent.

In addition to the foregoing discussion, which provides some indication that the thermal decomposition of propyl radicals and not atomic cracking is responsible for the formation of methane, the following considerations may be mentioned as additional, and possibly more compelling evidence:

(a) Darwent and Steacie[2] have shown that only very small amounts of methane are produced in the mercury photosensitized reaction of propane at room tempera-

[8] S. Bywater and E. W. R. Steacie, J. Chem. Phys. **19**, 319, 326 (1951).

ture providing that the pressure was greater than 15 mm.

(b) Recent experiments in these laboratories[9] have shown that, in the mercury photosensitized reactions of ethane, the extent of "atomic cracking" decreases with increasing temperature and with decreasing intensity.

(c) Bywater and Steacie[8] found no methane in the mercury photosensitized reaction of propane up to 250°C. At 300°C methane was produced and this was ascribed to the thermal decomposition of propyl radicals and not to atomic cracking. The small amount of ethane may be ascribed to the recombination of methyl radicals or to the hydrogenation of ethylene.

It therefore appears probable, on the basis of the foregoing discussion, that the methane (and ethylene) arises from the thermal decomposition, and not the "atomic cracking," of the propyl radical.

In comparing the present results with those of Bywater and Steacie[8] we find that the ratio of the rates of production of methane to hydrogen is much higher with cadmium than with mercury:

$$\text{Cadmium } CH_4/H_2 \approx 1.0$$

$$\text{Mercury } CH_4/H_2 = 0.188 \text{ (at 300°C)}.$$

The discrepancy, a factor of about five, may be explained by a consideration of the kinetics of Mechanism B. The usual steady-state treatment yields the following identities:

$$R_{H_2} = k_3[H][C_3H_8] = k_1 \cdot I_a$$

$$R_{CH_4} = k_9[CH_3][C_3H_8] = k_8[C_3H_7] = k_8\left(\frac{2k_1 I_a}{k_4}\right)^{\frac{1}{2}}$$

$$R_{CH_4}/R_{H_2} = \frac{\sqrt{2} \cdot k_8}{(k_1 k_4 I_a)^{\frac{1}{2}}},$$

so that $R_{CH_4}/R_{H_2}$ should vary as $I_a^{-\frac{1}{2}}$. The intensities in question were $1.4\times10^{-5}$ (mercury) and $5.8\times10^{-7}$ (cadmium), both in einstein·hr$^{-1}$. Hence, the ratio in the cadmium experiments should be $0.188\times(1.4\times10^{-5})/(5.8\times10^{-7})^{\frac{1}{2}} = 0.93$. The ratios actually found (Table I) were 0.98 at 203 mm and 0.62 at 327 mm. This agreement is surprisingly good when the inaccuracy of the measurements is considered.

One other point that arises from the present results, and which merits some consideration, is the effect of propane pressure on the ratio $CH_4/H_2$, since it appears (Table I and Fig. 3) that this ratio increases with decreasing pressure of propane. One effect of decreasing the pressure is to reduce the extent of quenching and consequently $I_a$. The theoretical line in Fig. 3 is based on the estimated absorbed intensity (Table II, column 3) and on the relationship between $R_{CH_4}/R_{H_2}$ and $I_a$ given previously. It is obvious that the agreement between the theoretical line and the experimental points is not good, but there is a trend as predicted by theory and the results are not inconsistent with theory. The small accuracy of the measurements and of the estimation intensities at low pressures are probably responsible for the paucity of agreement.

An interesting result is that with very small conversions, the quantum yield of hydrogen production is constant and approximately unity over a 6-fold variation in pressure. This suggests

(a) that reaction (5) is not important under the experimental conditions;

(b) that if quenching occurs by some path, other than reaction (1), such as

$$Cd(^3P_1) + C_3H_8 \rightarrow Cd(^3P_0) + C_3H_8,$$

(and it is likely that a similar reaction occurs between ethane and $^3P_1$ mercury atoms),[10] the reverse process occurs so rapidly that the Cd($^3P_0$) atoms are all reelevated to the ($^3P_1$) state and do not lead an inefficiency in the over-all reaction. The process Cd($^3P_0$)→Cd($^3P_1$) requires only about 1.5 kcal mole$^{-1}$ and so should be rapid at 300°C.

## CONCLUSIONS

The results of the present investigation together with other pertinent information indicate that, contrary to previous suggestions,[3] "atomic cracking" is not serious in the cadmium photosensitized reactions of propane at fairly high pressures and temperatures and that there is no necessity to consider the improbable process

$$CdH + C_3H_8 \rightarrow CH_4 + C_2H_5 + Cd.$$

The results are not inconsistent with those obtained previously[2,8] from the mercury photosensitized reaction of propane at room temperature and at 300°C.

[9] B. deB. Darwent (unpublished results).

[10] B. deB. Darwent and F. G. Hurtubise, J. Chem. Phys. **20**, 1684 (1952).

# The Quenching of Mercury Resonance Radiation. II. The Production of Metastable ($^3P_0$) Atoms*

B. deB. Darwent and F. G. Hurtubise†
*National Research Laboratories, Ottawa, Canada*

(Received February 14, 1952)

The production of metastable ($^3P_0$) mercury atoms in the quenching of mercury resonance radiation has been investigated with $N_2$, $H_2$, $C_2H_4$, $C_2H_6$, $O_2$, and $CO_2$. Metastable atoms, by virtue of their ability to induce the emission of electrons from a nickel surface, were detected with the first four gases; none was detected with $O_2$ and $CO_2$.

## INTRODUCTION

THE effective cross sections of various substances in quenching mercury resonance radiation (λ2537) have been recorded[1,2] but differentiation has seldom been made between the effective cross sections for the two processes $(^3P_1)\xrightarrow{(1)}(^1S_0)$ and $(^3P_1)\xrightarrow{(2)}(^3P_0)$, either or both of which may be responsible for the over-all quenching process. Actually, the effective cross section ($\sigma_Q^2$) must be the sum of the cross sections for the above processes. It is well established[3–5] that nitrogen and water vapor quench λ2537 by the second process, and it has been suggested that other substances also effect the transition to the metastable state. Bates[6] has shown, qualitatively, that methane probably quenches λ2537 by deactivating $^3P_1$ to $^3P_0$, but he was unable to detect such a process with ethane. However, as he pointed out, the failure to detect metastable atoms with ethane was not conclusive since if ethane deactivates the metastable atoms $^3P_0\rightarrow{}^1S_0$ much more efficiently than it reactivates them by the endothermic process $^3P_0\rightarrow{}^3P_1$, the metastable atoms would not have been detected. Similarly, Samson's method of detecting $^3P_0$ mercury atoms, based on the effect of re-elevating $^3P_0$ and $^3P_1$ on the decay of λ2537, can be used only if the deactivating process is not very much faster.

The work of Messanger[7] and Coulliette[8] has shown that Hg($^3P_0$) atoms can be detected and their concentrations measured by the fact that they induce the emission of electrons when they strike a metal surface. That technique is not subject to the limitations of other methods based on the re-elevation of $^3P_0$ atoms to the $^3P_1$ state. Accordingly, it was adopted as a simple and sensitive method of detecting metastable mercury atoms in the presence of nitrogen, hydrogen, ethane, ethylene, carbon dioxide, and oxygen.

Table I. Effect of mercury concentration on the "zero reading."

| Temp. of side arm | Photocell reading—mv λ2537 present | λ2537 absent |
|---|---|---|
| 21°C | 0.23 | 0.08 |
| −196°C | 0.45 | 0.08 |

## EXPERIMENTAL

### Materials

The hydrogen and oxygen were taken from commercial cylinders. The hydrogen was purified by passage through a hot palladium tube and the oxygen by passage through a trap in liquid nitrogen. The carbon dioxide was a Matheson Company product. It was condensed in a trap cooled in liquid nitrogen and any uncondensable impurities were pumped off. The ethane and ethylene were Phillip's Petroleum Company's "Research Grade" products. They were stated to be 99.9 percent pure and were used after uncondensable gases had been removed by repeated evacuations at −195°C.

### Apparatus

The apparatus consisted of an exciting source, a focusing lens, and a photoelectric cell. The exciting source was a low pressure mercury lamp, with neon (3 mm) as a carrier gas, run off a Jefferson sign transformer at about 70 ma. The photoelectric cell consisted of a Pyrex envelope with a quartz window, attached by means of a thermosetting resin, and two nickel electrodes, about 3 mm apart, placed parallel to and about 30 mm from the front face of the cell. The internal resistance of the photoelectric cell was at least $10^{12}$ ohms, and the output was measured with the same dc amplifier that was used in the previous experiments.[2] A side tube, which was sealed to the photocell envelope, contained mercury at 21.0°C, thus providing a constant mercury pressure of about $1.3\times10^{-3}$ mm. A McLeod gauge connected to the cell was used for measuring low pressures. The cell was also connected to several gas storage bulbs and to a high vacuum system through a mercury "cutoff" which was used as a manometer.

* Contribution No. 2834 from the National Research Laboratories, Ottawa, Canada.

† Summer student (1950) from Carleton College, Ottawa.

[1] See A. G. Mitchell and M. W. Zemansky, *Resonance Radiation and Excited Atoms* (Cambridge University Press, Cambridge, 1934) for early references.

[2] B. deB. Darwent, J. Chem. Phys. **18**, 1532 (1950).

[3] R. W. Wood, Phil. Mag. **50**, 774 (1925); **4**, 446 (1927).

[4] E. W. Samson, Phys. Rev. **40**, 940 (1932).

[5] H. Klumb and P. Pringsheim, Z. Physik **52**, 610 (1929).

[6] J. R. Bates, J. Am. Chem. Soc. **52**, 3825 (1930).

[7] H. A. Messanger, Phys. Rev. **28**, 962 (1926).

[8] J. H. Coulliette, Phys. Rev. **32**, 636 (1928).

## Procedure

The foreign gas under study was admitted to the cell very slowly, and the reading of the photoelectric cell was noted when the concentration of mercury vapor had attained equilibrium. The pressure was reduced by slowly removing portions of the gas, and the photocell reading was taken at each pressure. The gas was irradiated for short periods so that the photosensitized decomposition was negligible. Good reproducibility was obtained when an interval of ten minutes was allowed to elapse between removing a portion of the gas and taking a reading. Essentially similar results were obtained when successive portions of the gas were admitted to, instead of removed from, the cell, provided that sufficient time was allowed for equilibrium to be established. The voltage across the nickel electrodes could be varied within quite wide limits (about fourfold) without affecting the reading.

## RESULTS

### Zero Reading

Preliminary experiments showed that a significant electron current was obtained when the cell was illuminated with only mercury vapor present. To investigate the cause of this zero reading, a λ2537 filter was placed between the cell and the lamp and the effect of varying the mercury vapor pressure on the reading was studied. The filter consisted of a quartz cell, 15 mm thick, containing hydrogen at 100-mm pressure and mercury vapor at room temperature. The results are given in Table I. When the λ2537 line was absent, a lower reading, which was independent of the mercury vapor pressure, was obtained. The absorption line of the filter was broader than that of mercury in a vacuum, so that the filter effectively removed most of the wings of the λ2537 line as well as the center of the line. On the other hand, in the absence of the filter, the "zero reading" increased with decreasing vapor pressure. This was due to the fact that, as the mercury vapor pressure was reduced, a larger portion of the resonance radiation, or its wings, reached the cathode. Thus the "zero reading" was mainly caused by a direct photoelectric effect, due to the broad line used, and not principally to impingement of Hg($^3P_1$) or ($^3P_0$) atoms on the nickel electrode.

### Effect of Intensity

When the electron current was plotted against the percent intensity, curves of the type shown in Fig. 1 were obtained. At low intensities the current varied linearly with the intensity, while at high intensities it was independent of the intensity. The type of curve obtained is reminiscent of photoelectric fatigue; obviously, only the linear part of the curves should be considered. Hence, subsequent measurements were made at low intensity, and the linearity of the "current *vs* intensity" curves was established before plotting the "current *vs* pressure" diagrams. Several runs were made with each gas, and the position of the maximum relative to the gas pressure was found to be fairly reproducible.

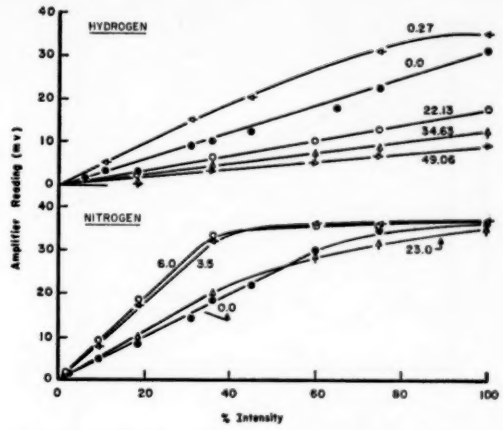


FIG. 1. The effect of intensity on photocell current for hydrogen (upper graph) and nitrogen (lower graph) at various pressures.

### Activation of the Electrode Surface

In this investigation, no attempt was made to obtain a quantitative measure of the effective cross sections for quenching to the metastable state. The fact that the sensitivity of the electron emission from a nickel surface varies considerably, depending on the nature of the foreign gas, would make such a determination uncertain. Sonkin[9] has investigated the variations in the sensitivity of metal surfaces due to the action of $^3P_0$ mercury atoms. He found that changes in the sensitivity of the surface were due to the state of the metal surface and not to the action of the metastable atoms themselves. He suggested that the surface has a definite equilibrium structure, consisting of mercury and oxygen atoms, and that a change in the sensitivity occurs if this arrangement is disturbed. During the present investigation, it was found that hydrogen activated the electrodes, causing the "zero reading" to increase by as much as thirtyfold; however, the sensitivity eventually became constant after several exposures, provided no other gas was admitted to the cell between runs; successive experiments (26, 27, and 28) with hydrogen were then fairly reproducible as shown in Fig. 2.

Comparatively good reproducibility was obtained with the two hydrocarbons, ethane and ethylene, and the surface was apparently unaffected by those gases. Oxygen, nitrogen, and carbon dioxide deactivated the nickel electrodes; the deactivation by nitrogen might have been caused by small amounts of oxygen present as an impurity.

### Production of Metastable Atoms

The validity of the method was first checked by studying nitrogen, since this gas is known to quench to

[9] S. Sonkin, Phys. Rev. **43**, 788 (1933).

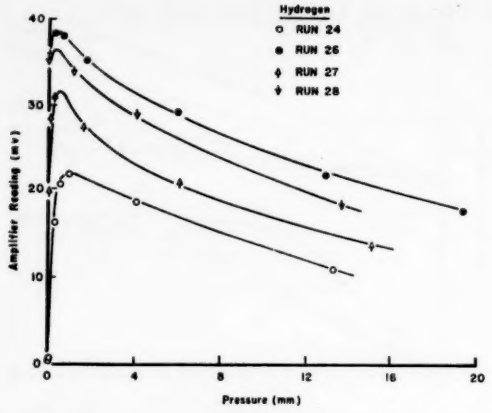


FIG. 2. The effect of repeated exposure with hydrogen on the sensitivity of the surface.

the ($^3P_0$) state. The type of "pressure *vs* current" curve obtained for nitrogen is shown in Fig. 3. The occurrence of a maximum at 6 mm agrees with the results of Klumb and Pringsheim,[5] Samson,[4] and others, which indicated that in the presence of nitrogen, the maximum concentration of Hg($^3P_0$) atoms occurs at about 7 mm.

The curve obtained for hydrogen (Fig. 3) also exhibits a maximum. The possibility that this maximum was due to H atom recombination on the nickel surface was investigated by observing the effect on the photocell current of a cylindrical piece of platinum gauze placed along the inside wall of the photocell between the front face and the nickel gauze. If the electron current were due to H atom recombination, the insertion of the platinum surface would have caused a decrease in current, since recombination occurs more efficiently on platinum than on glass. No such decrease was observed. Further indication that the maximum on the "pressure *vs* current" curve was not due to the recombination of hydrogen atoms was obtained from the effect of intensity on the current. The results, illustrated in Fig. 1, show that at high pressures and low intensity, the current varies linearly with the intensity.

The curves for ethane and ethylene exhibit maxima (Fig. 3) indicating that these two hydrocarbons also quench Hg($^3P_1$) to the metastable state, whereas those for oxygen and carbon dioxide, also shown in Fig. 3, show no such maxima.

## DISCUSSION

The general similarity between the curves of electron current *vs* pressure for nitrogen and those obtained previously by Klumb and Pringsheim[5] and Samson[4] for the effect of nitrogen pressure on the concentration of metastable atoms, and especially the fact that the maximum current occurred at about 7 mm, are strong indications that, in these experiments, the electron current is a measure of the concentration of Hg($^3P_0$) atoms.

An unexpected and surprising feature of our results is the well-defined maximum in the electron current *vs* pressure curve for hydrogen, since it has usually been assumed that hydrogen quenches λ2537 directly to the ground state. A possible alternative explanation is that the quenching actually occurs to the ground state, resulting in the production of H atoms, which combine on the nickel surface and so liberate enough energy to cause the emission of electrons. This would be also in agreement with the fact that the presence of hydrogen in the illuminated photocell increases the sensitivity of the surface. However, the results of the experiments with platinum gauze and the fact that at low intensities, where the cell does not exhibit photoelectric fatigue, the electron current is a linear function of the intensity, are strong indications that hydrogen atoms are not responsible for the electron emission, although they are produced and although they do probably attain the surface and so lead to an increased activity. Let us consider the reactions

$$\mathrm{Hg}(^3P_1)+\mathrm{H_2}\rightarrow 2\mathrm{H}+\mathrm{Hg}(^1S_0), \quad (1)$$

$$2\mathrm{H}+M\rightarrow \mathrm{H_2}+M, \quad (2)$$

$$\mathrm{H}\xrightarrow{w}1/2\mathrm{H_2}, \quad (3)$$

where $M$ is any molecule and $w$ the wall. Then

$$\frac{d}{dt}[\mathrm{H}]=0=2I_a-k_2[\mathrm{H}]^2[M]-k_3\frac{[\mathrm{H}]}{[M]}.$$

If the recombination is predominantly on the wall, we may ignore the term $k_2[\mathrm{H}]^2[M]$ compared with $k_3[\mathrm{H}]/[M]$. If the rate of electron emission is proportional to the rate with which $H$ atoms recombine on the nickel surface, we may write $E=\alpha k_3[\mathrm{H}]/[M]$, where $\alpha$ is a proportionality constant, representing the fraction of $H$ atoms that recombine on the nickel surface, and the fraction of these recombinations that lead to electron emission. Hence, under these conditions $E=2\alpha I_a$. This requires the electron current ($E$) to be a direct function of the intensity, in agreement with experiment, but to be independent of the pressure of hydrogen $[M]$, which is contrary to our findings. For $E$ to decrease with increasing pressure, hydrogen atoms must recombine homogeneously. At high pressures the homogeneous recombination will be much faster than the heterogeneous reaction, and we may then ignore $k_3[\mathrm{H}]/[M]$ and write

$$[\mathrm{H}]=\left(\frac{2I_a}{k_2[M]}\right)^{\frac{1}{2}},$$

which will give

$$E=\alpha k_3[\mathrm{H}]/[M]=\frac{\alpha k_3}{[M]}\left(\frac{2I_a}{k_2[M]}\right)^{\frac{1}{2}}.$$

This provides the required type of dependence of $E$ on $[M]$ (or pressure), but now requires $E$ to be proportional

to $I_a^{\frac{1}{2}}$ which is also contrary to experiment. We therefore have evidence that $H$ atoms do reach the nickel surface, where they presumably combine, but this does not lead to electron emission, although the energy liberated by the recombination (4.46 ev) is nearly as large as that possessed by $Hg(^3P_0)$ atoms (4.64 ev). This may be explained if the $H$ atoms are absorbed by fairly strong Ni—H bonds, since the energy available for electron emission, if only one Ni—H bond is broken in the recombination, i.e.,

$$Ni-H+H\rightarrow Ni+H_2,$$

will be less than 4.46 ev by an amount equivalent to the strength of the Ni—H bond. The strength of the Ni—H bond in nickel hydride is about 2.6 ev,[10] which would leave only about 1.86 ev for promoting the emission of the electron from the surface if the bonds formed on the surface are as strong as those in nickel hydride. This may well be lower than the photoelectric threshold of nickel. Hence it would seem logical to assume that, although reaction (1) does occur, the alternative process

$$Hg(^3P_1)+H_2\rightarrow H_2'+Hg(^3P_0) \qquad (1')$$

also takes place and that the ($^3P_0$) atoms disappear by the following two reactions:

$$Hg(^3P_0)+H_2\rightarrow Hg(^1S_0)+2H, \qquad (4)$$

$$Hg(^3P_0)\xrightarrow{W}Hg(^1S_0)+E. \qquad (5)$$

When the pressure is high enough for the spontaneous radiation of $Hg(^3P_1)$ atoms,

$$Hg(^3P_1)\rightarrow Hg(^1S_0)+h\gamma, \qquad (6)$$

to be not significant, we have

$$E=\left(\frac{k_1'}{k_1+k_1'}\right)\left(\frac{k_5 I_a}{k_4[H_2]^2+k_5}\right),$$

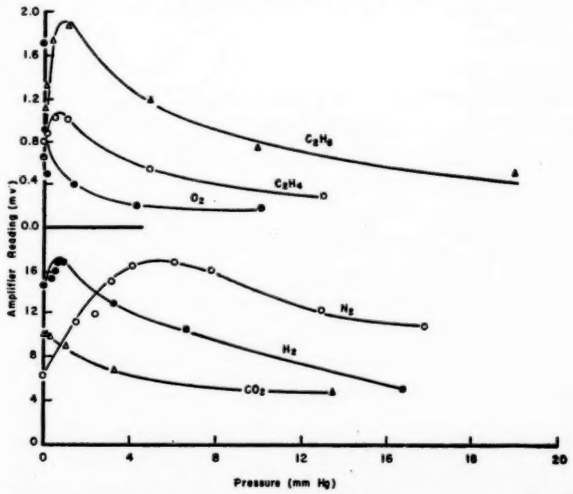


FIG. 3. The effect of pressure on the photocell current for $H_2$, $O_2$, $N_2$, $CO_2$, $C_2H_4$, and $C_2H_6$.

[10] Y. K. Syrkin and M. E. Dyatkina, *The Structure of Molecules* (Butterworth, London, 1950), p. 153.

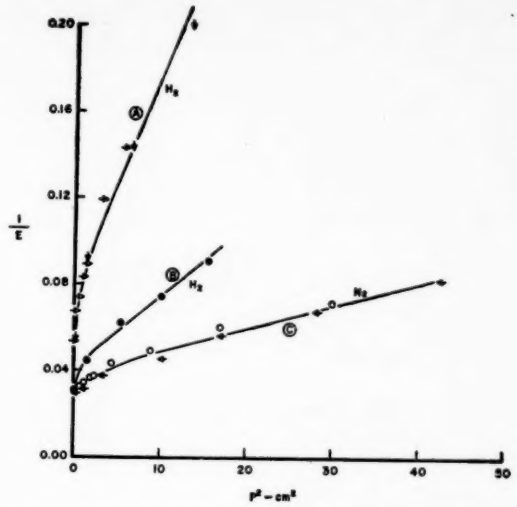


FIG. 4. The relationship between the reciprocal photocell reading and the square of the pressure. The two curves for hydrogen were obtained with surfaces of different sensitivities.

which requires $E$ to be a linear function of $I_a$ and to decrease with increasing pressure of hydrogen. The above expression may conveniently be inverted:

$$\frac{I}{E}=\frac{k_1+k_1'}{k_5'}\cdot\frac{1}{I_a}\left\{\frac{k_4}{k_5}[H_2]^2+1\right\},$$

whence $I/E$ should be a linear function of $[H_2]^2$. The results (Fig. 4) show that the above type of relationship is supported by the experimental results, and we may therefore assume that at least part of the process by which hydrogen quenches λ2537 is by reaction (1'). This result is in general agreement with the data of Thomas and Gwinn[11] who found that the effective cross section of hydrogen in quenching λ2537($\sigma_Q^2$) was about twice as large as the effective cross section for decomposing molecular hydrogen ($\sigma_R^2$) by the process

$$Hg(^3P_1)+H_2\rightarrow 2H+Hg(^1S_0). \qquad (1)$$

Our results indicate that reaction (1') also occurs. The cross section of this process ($\sigma_M^2$) may be quite large, since the maximum in the voltage *vs* pressure curve occurs at a low pressure, and, if $\sigma_M^2\approx\sigma_R^2\approx 0.5\sigma_Q^2$, our results to some extent confirm and explain the results of Thomas and Gwinn.

The energetics of reaction (1') are rather interesting since the process requires 0.218 ev to be transferred from the $Hg(^3P_1)$ to $H_2$. The first vibrational level of hydrogen is about 0.50 ev above the ground level, so that the energy must be taken up as rotation and translation. If these conclusions are valid, then the conversion of the electronic energy of the $Hg(^3P_1)$ atom into rotational energy of $H_2$, together with some translational energy of

[11] L. B. Thomas and W. D. Gwinn, J. Am. Chem. Soc. **70**, 2643 (1948).

separation of the particles, is not a very inefficient process, whereas it is generally assumed that the conversion of the energy of a free electron into rotational or translational energy of a molecule has a very low probability.

The same restrictions do not apply to ethane and ethylene, which also quench to the ($^3P_0$) level, since both of these molecules have many low-lying vibrational levels which could easily absorb most of the 0.218 ev involved.

The fact that no metastable atoms were detected with oxygen and carbon dioxide may be explained by assuming either that these substances quench entirely or almost entirely to the ground state, or that if they quench to the metastable state they are much more efficient in deactivating the metastable atoms.

THE JOURNAL OF CHEMICAL PHYSICS VOLUME 20, NUMBER 11 NOVEMBER, 1952

# The Dissociation of Ethyl Bromide and Iodide by Neutron Capture*

SOL WEXLER, *Argonne National Laboratories, Chicago, Illinois*

AND

T. H. DAVIES, *Institute for Nuclear Studies, University of Chicago, Chicago, Illinois*

(Received May 19, 1952)

A study has been made of recoil halogen species ejected from gaseous ethyl bromide and iodide after neutron capture. The results demonstrate that a fraction of the radio-halide fragments carry a positive charge. The fraction charged is 12 percent for the 4.4-hr $Br^{80m}$, 25 percent for the 36-hr $Br^{82}$, and 50 percent for the 25-min $I^{128}$. The corresponding estimate for the 18-min $Br^{80}$ is very approximately 18 percent. The positive charges are attributed to internal conversion processes in the stabilization of the compound nucleus formed by neutron capture. The fraction of positive recoil ions is interpreted as the minimum fraction of neutron capture processes which are followed by an internal conversion process. A comment is made upon the possible significance of the ions in the study of chemical reactions induced by radiative neutron capture.

A study of the 18-min $Rb^{88}$ from $\beta$-decay of the 2.8-hr $Kr^{88}$ was made using the procedures and equipment employed in the halogen experiments. The results show that all $Rb^{88}$ atoms are positively charged as expected.

## INTRODUCTION

IN slow neutron capture, the energies of the $\gamma$-rays promptly emitted by the capturing nuclide total from 5 to 10 Mev.[1] The recoil given the capturing nuclide, estimated by equating momenta of nucleus and photons, is of the order of one hundred electron volts.

A recoil impulse of this magnitude should dissociate molecules which contain the radiating atom[2] and release a molecular fragment or atom (often radioactive) which may itself be chemically very reactive. Indeed, a variety of chemical effects is observed to accompany neutron-capture oxidation-reduction reactions of inorganic ions in aqueous solution[3] and synthesis of new molecules containing particular radioactivities,[4] for example. The effects have been exploited to prepare samples of high specific radioactivity[5,6] and in other ways. Since dissociation processes of such high energy might conceivably yield products which are ions, several attempts have been made to collect the radioactive products on electrodes. However, as a result perhaps of the complications introduced by the necessary use of liquids or of gases at normal pressures, no information on the original character of the dissociation products could be obtained.[7]

In the present work, radioactive bromine and iodine species dissociated from gaseous ethyl halide by neutron capture are examined under nearly collision-free conditions. Sufficient radioactivity at such low pressure of target gas can be obtained only in the neutron flux of a chain reactor. The radioactivities studied were the 4.4-hr $Br^{80m}$, the 18-min $Br^{80}$, the 36-hr $Br^{82}$, and the 25-min $I^{128}$ from the corresponding stable halogen isotopes. In brief, the gases were neutron irradiated between concentric cylindrical collecting electrodes, the distribution of radioactivity among the two electrodes and the gas phase was determined, and the degree of

* This work is taken mainly from the thesis submitted by Sol Wexler in partial fulfillment of the requirements for the degree of Doctor of Philosophy in the Department of Chemistry, University of Chicago.

[1] S. Dancoff and H. Kubitschek, Phys. Rev. **76**, 531 (1949).

[2] L. Szilard and T. R. Chalmers, Nature **134**, 462 (1934).

[3] W. F. Libby, J. Am. Chem. Soc. **62**, 1930 (1940).

[4] E. G. Bohlman and J. E. Willard, J. Am. Chem. Soc. **64**, 1342 (1942).

[5] For example, see (a) O. Erbacher and K. Philipp, Z. physik. Chem. **A176**, 169 (1936). (b) C. S. Lu and S. Sugden, J. Chem. Soc. **1939**, 1273. (c) K. Starke, Naturwiss. **30**, 577 (1942). (d) J. Steigman, Phys. Rev. **59**, 498 (1941). (e) R. R. Williams, J. Phys. and Colloid Chem. **52**, 603 (1948). (f) Boyd, Cobble, and Wexler, J. Am. Chem. Soc. **74**, 237 (1952).

[6] For a review of chemical effects in nuclear transformations, see A. G. Maddock, Research **2**, 556 (1949).

[7] (a) E. Amaldi *et al.*, Proc. Roy. Soc. (London) **A149**, 522 (1935). (b) J. Fay and F. Paneth, J. Chem. Soc. **384**, **1936**; Nature **135**, 820 (1935). (c) Capron, Crèvecour, and Faes, J. Chem. Phys. **17**, 349 (1949).

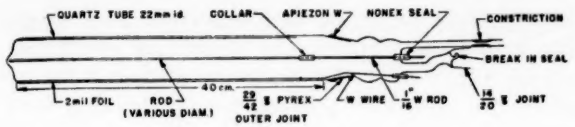


FIG. 1. Irradiation chamber.

dissociation and the charge carried were estimated from these observations.

## PROCEDURES AND RESULTS

The techniques employed resemble those used in the study of bromine dissociated from gaseous ethyl bromide by the nuclear process of isomeric transition with internal conversion.[8] Figure 1 shows the quartz irradiation chamber with Pyrex cap. The collecting surfaces of the two concentric cylinders were either copper foil reduced *in situ* by hydrogen, or copper amalgamated by dipping in dil $HNO_3$ containing mercuric ion. The washed foils were assembled as indicated in a chamber previously cleaned with hot $HNO_3$ and much water. Since as little as 0.1 $\mu$g of bromine deposited upon the electrodes from laboratory air or wash solutions will introduce an unmanageable blank correction, care must be taken throughout to avoid bromine contamination. The collecting electrodes were connected to a voltage source to give a potential difference (usually 4000 volts) or were connected to make the volume field-free. The effect of electric field was observed in successive experiments. In later runs, two electrode systems in tandem were present in the chamber. The upper was connected to the high voltage while the lower was made field-free.

The chamber was sealed to a vacuum line and flamed to drive off excess water and mercury and to outgas it. The chamber was filled to about three microns pressure of ethyl halide. The gas was condensed by immersing the chamber bottom in liquid nitrogen, and the filling tube sealed off at a previously outgassed point. The chamber, with electrical leads attached, was lowered into the thimble of the Argonne Heavy Water Reactor (or in the iodide experiments placed in a "stringer" of the graphite reactor) and exposed to a flux of *ca* $10^{12}$ neutrons/cm$^2$ sec for five to forty minutes. Hereafter, and until the intensely radioactive chamber and foils were stored, operations required heavy shielding and careful planning to protect the experimenter.

The irradiated chamber was reattached to the vacuum line if bromine activity in the gas phase was to be determined, and the gas was transferred via the break in seal to a sample of liquid ethyl bromide carrier. An aliquot of the latter was counted, using a calibrated liquid sample counter.

To determine the distribution of the radioactive dissociation products between the collectors, the chamber was opened and the collectors were removed and washed with carrier halide solutions. In the bromine experiments KBr solutions were used alone or followed with 1$M$ $HNO_3$ containing KBr and then by 2 percent ammonium carbonate solution. This procedure was found necessary to remove bromine species buried in the copper. The radio-bromine activity in the combined wash solutions was determined by oxidizing with $KMnO_4$, transferring to $CCl_4$, reducing with $NaHSO_3$, transferring to water, repeating the cycle once again, and precipitating AgBr, which was washed, dried, weighed, and counted under a thin end-window counter.

In the iodine experiments, the collectors were washed with 1$M$ $H_2SO_4$ containing carrier iodide and then with 2 percent ammonium carbonate solution. The combined solutions were analyzed for radio-iodine as with bromine, save that $KNO_2$ was the oxidizing agent.

In addition to more obvious checks of the procedure, such as the reproducibility of the chemical isolation of the radio-halide and the absence of adsorption of ethyl halide by the chemically active collecting surfaces, a number of tests were made of errors which might arise in working with low pressures of target gas and with extremely high radiation flux. The blank correction for radio-halide contamination on the collectors—obtained by carrying out the procedure with target gas omitted—was reduced, after persistent difficulties, to a level which, while variable from run to run, was small relative to the activities recovered in the primary experiments themselves. The acid and alkaline wash solutions were shown to be necessary and adequate for complete removal of radio-bromide from the electrode surfaces. The increase in pressure from outgassing of the chamber during irradiation was measured and found not to exceed 1 to 2 microns in the longest irradiations.

An especial cause for anxiety was the possibility that radiation destroyed the ethyl halide sample without nuclear activation early in the irradiation, with the result that the measurements had to do only with halide deposited upon the collectors before nuclear activation or with the nuclear activation of gas molecules other than ethyl halide. Some assurance to the contrary was obtained by the results of the following types of test. In one, the gaseous contents of an irradiated chamber were transferred to a second chamber and, after sufficient time for any gaseous radioactivity to decay, irradiated again. The yield of radio-halide recovered from the second chamber was the same within experimental error of that of the first chamber. In another experiment, the flux of neutrons and other pile radiations was increased thirty-fold without noticeable effect on the results. Irradiation time was varied eight-fold in other experiments without effect. Finally, the results will be shown to vary with the particular bromine isotopes under study—an outcome not to be expected if radiation decomposition is the decisive factor in determining distribution between the col-

[8] S. Wexler and T. H. Davies, J. Chem. Phys. **18**, 376 (1950).

TABLE I. Activities of 4.4-hr $Br^{80m}$ on opposed collectors where one collector is shiny Cu.

| Second collector | Activity ratio shiny Cu/second collector |
|---|---|
| Al | 3.1 |
| Al | 2.8 |
| Rough Cu | 0.96 |
| Ni | 3.2 |
| Sn | 1.7 |
| Pt | 2.1 |
| Ag | ~1 |
| Cu−Hg | 0.67 |

lectors. Ion pair formation in ethyl bromide as a result of high energy radiation should not vary detectably with the particular stable bromine isotope involved. Thus, radiation decomposition of ethyl bromide to give nonvolatile products or volatile species which react with the electrodes, such as HBr and $Br_2$, seems not to occur to an extent significant for the measurements.

Finally, interpretation of the experiments will presently be seen to rest upon the assumption that the radio-halide recoils stick to the collectors at first collision. Early experiments with ordinary copper and aluminum electrodes disclosed that radio-bromine was re-emitted, perhaps many times, from the foil surfaces. The distribution of radioactivity between inner and outer cylinders varied in repeat runs and deviated markedly from the distribution to be expected from geometrical considerations and an adsorption coefficient of unity (see *Calculations and Discussion*). Further, when the central rod was omitted and the outer single cylinder replaced by two symmetrically opposed hemicylindrical collectors, one of shiny copper and one of a second metal, the distribution of radio-bromine between the two was usually found very unequal—as if at least one surface reemitted the recoils. Table I gives these results. The low activity ratio with amalgamated copper indicates this to be the most efficient collecting surface. When central and outer collectors were of amalgamated or hydrogen-reduced copper, distribution coefficients close to those expected were observed. This suggests that with these surfaces, the adsorption coefficient is indeed close to unity. The assumption appears yet more certain for positively charged recoils colliding with a negative central rod, since in this case a relatively large fraction of the ions accelerated by the steep gradient of the electric field in the vicinity of the rod appears to be buried so deep as to require corrosive wash solutions to remove them.

TABLE II. Distribution of 4.4-hr $Br^{80m}$ in absence of an electric field.

| Expt. | Washing procedure[a] | $Br^{80m}$ (counts/min)[b] On rod | On wall | Ratio (wall/rod) ($R_3$) |
|---|---|---|---|---|
| 1 | *a* | 119 | 3007 | 26 |
| 2 | *a* | 96 | 2527 | 26 |
| 3 | *a* | 173 | 4707 | 27 |
| 4 | *a* | 120 | 2887 | 24 |
| | *b* | 155 | 3836 | 25 |
| 5 | *a* | 147 | 3969 | 27 |
| | *b* | 238 | 5685 | 24 |
| 6 | *a* | 156 | 2869 | 18 |
| | *b* | 186 | 5955 | 32 |
| | | | | Av. $R_3$=25 |

[a] The designation *a* refers to activity found in the $H_2O-Br^-$ washes only; *b* refers to the activity obtained in the complete washing procedure.
[b] In two blank runs (no $C_2H_5Br$), 26 and 15 counts/min were found on the rod, 177 and 186 on the wall using wash procedure *a*, and 72 and 415 on rod and wall using procedure *b*.

Table II and experiments 6, 7, and 8 of Table V present the distribution without electric field of 4.4-hr $Br^{80m}$ between a copper amalgam outer electrode of 1.1 cm radius and a central rod of 0.079 cm ("thin rod") or 0.55 cm ("thick rod"), respectively. Here and in later tables, the counting rates as presented are corrected for coincidence loss of the counter, variation in chemical yield of the carrier in individual runs, and for the contaminating radio-halide found in the blank runs described earlier. The distribution ratios of Table II and of experiments 6, 7, and 8 of Table V will be compared presently with theoretical values.

TABLE III. Distribution of 4.4-hr $Br^{80m}$ between rod and wall with wall at +4000 volts.

| Expt. | Washing procedure | $Br^{80m}$ (counts/min) On rod | On wall | Ratio (wall/rod) ($R_1$) |
|---|---|---|---|---|
| 1 | *a*[a] | 510 | 4307 | 8.5 |
| | *b* | 956 | 5828 | 6.1 |
| 2 | *a* | 189 | 2687 | 14 |
| | *b* | 750 | 4155 | 5.5 |
| 3[b] | *a* | 54 | 578 | 11 |
| | *b* | 205 | 1109 | 5.4 |
| | | | | Av.=5.7 (*b* results only) |

[a] Designations *a* and *b* as in Table II.
[b] Only one micron of $C_2H_5Br$ irradiated.

When an electric field is imposed, the distribution of activity changes sharply. Table III gives the results when the 0.079-cm radius central rod is 4000 volts negative to the outer collecting cylinder, and Table IV the results when the rod is positive.

Tables V and VI compare the distributions of 18-min $Br^{80}$, 36-hr $Br^{82}$, and 4.4-hr $Br^{80m}$. Corrections have been applied as before. The comparison is made possible by the disparate half-lives and neutron-capture cross sections of the target isotopes which cause the radiations of each of the three species to predominate successively at times of less than two hours, at five hours, and at two days after a short bombardment. Thus, a continuous decay curve furnishes the basis for determination of each component. While the counting efficiencies of the radioactivities differ, this does not affect the wall-rod ratio for a given activity. A pedagogic but not experimental difficulty appears in the necessary practice of measuring the decay of the 4.4-hr $Br^{80m}$, which emits very soft radiations, by means of the energetic $\beta$-par-

ticles from its 18-min $Br^{80}$ daughter.[9] However, it should be emphasized that the bombardment, cooling, and counting times were so arranged as to make the contribution of the 18-min $Br^{80}$ formed by isomeric transition during the irradiation period negligible with respect to the 18-min $Br^{80}$ formed directly by neutron capture or by isomeric transition after the irradiation period.

In experiments with ethyl iodide, chambers having a volume which is field-free and a volume subject to a field were used. Table VII gives the results and shows a yet larger field effect for radio-iodine *vs* bromine.

## CALCULATIONS AND DISCUSSION

The recoil energy spectrum of the halogens after neutron capture is perhaps in principle calculable from complete information on the numbers, energies, mutual orientations, and sequence in time of the capture $\gamma$-rays emitted. However, these features are only imperfectly known for even the most favorable cases. In brief review, the average number of $\gamma$-rays emitted per neutron capture varies with the capturing nuclide from 1.7 to 5.6. Capture by $Br^{79}$ to give 18-min $Br^{80}$ yields 3.4 $\gamma$-rays on the average, and no strong preferred mutual orientation of these is observed.[10] The approximate $\gamma$-ray energy spectrum in capture by Br has been reported by Hamermesh.[11] While most of the $\gamma$-rays recorded by Hamermesh must come from neutron capture by $Br^{79}$ to give 18-min $Br^{80}$ (from the argument of relative capture cross sections), nevertheless, it is not possible to attribute a given transition of minor intensity in the graph to capture by a given isotope. In considering the total binding energy available for $\gamma$-rays, we shall ignore the higher energy cutoff of this data at about 9.0 Mev in favor of transitions observed at 7.3 and 8.0 Mev. These are in good agreement with neutron binding energies of 7.3 and 7.8 Mev for $Br^{80}$ and $Br^{82}$, respectively, calculated from the Bohr-Wheeler theory and corrected for the errors of this calculation in this region of mass numbers.[12] If these are the most energetic $\gamma$-rays possible, then the transitions observed at energies greater than, say, 5.3 Mev must decide the approximate value of the bromine recoil energies. This follows from the consideration that the 2.4 $\gamma$-rays which on the average accompany the $\gamma$-ray of $E>5.3$ Mev must share 8.0–5.3 or 2.7 Mev. or less. The associated recoil energies of the radiating bromine atom will then range from about 45 ev to 428 ev. The corresponding minimum internal energy of the ethyl bromide molecule will be 12 ev.[13] This should dissociate it. Unfortunately, however, in the absence of data on the capture $\gamma$-ray spectrum below 3 Mev, it is not entirely certain that the energetic $\gamma$-rays observed by Hamermesh accompany the major fraction of the capture processes. If there is a strong tendency for $\gamma$-rays of nearly equal energy to be emitted, then these would lie below Hamermesh's 3-Mev detection limit and, depending upon the mutual orientation of the quanta, the corresponding recoil atom energies could run from 428-ev to zero energy. Survival of ethyl bromide molecules would then be determined by the value of the "net" recoil energy and by the rapidity with which the successive $\gamma$-rays were emitted.

In the present studies, less than 1 percent of the total 4.4-hr $Br^{80m}$ was found in the gas phase. Survival of the target molecules would be expected if opposed $\gamma$-rays giving a "net $\gamma$-ray" of less than about 1.4 Mev were emitted in less than about $10^{-14}$ seconds. The

TABLE IV. Distribution of 4.4-hr $Br^{80m}$ between rod and wall with rod at +4000 volts.

| Exptl. | Washing procedure | $Br^{80m}$ (counts/min) On rod | On wall | Ratio (wall/rod) ($R_2$) |
|---|---|---|---|---|
| 1 | *a*[a] | 79 | 3547 | 45 |
| 2 | *a* | 63 | 2147 | 34 |
| 3 | *a* | 170 | 6079 | 36 |
| 4 | *a* | 77 | 3337 | 43 |
| | *b* | 120 | 4749 | 40 |
| | | | | — |
| | | | | Av. $R_2=40$ |

[a] Designations *a* and *b* as in Table II.

TABLE V. Comparison of bromine recoils from three different nuclear processes (thick rod assembly).

| Exptl. | +4000 V on | Activity (counts/min) $Br^{80}$ Rod | $Br^{80}$ Wall | $Br^{80m}$ Rod | $Br^{80m}$ Wall | $Br^{82}$ Rod | $Br^{82}$ Wall | Ratio (wall/rod) $Br^{80}$ | $Br^{80m}$ | $Br^{82}$ |
|---|---|---|---|---|---|---|---|---|---|---|
| 1 | Wall | 4615 | 6090 | 1423 | 2151 | 130 | 149 | 1.3 | 1.5 | 1.1 |
| 2 | Wall | 6475 | 7670 | 1945 | 3023 | 153 | 185 | 1.2 | 1.6 | 1.2 |
| 3 | Wall | 4615 | 6025 | 1543 | 2346 | 123 | 163 | 1.3 | 1.5 | 1.3 |
| 4 | Rod | 2545 | 6880 | 1892 | 4428 | 127 | 364 | 2.7 | 2.3 | 2.9 |
| 5 | Rod | 3295 | 10360 | 1381 | 3430 | 82 | 283 | 3.1 | 2.5 | 3.5 |
| 6 | No field | 5935 | 10550 | 1579 | 3148 | 114 | 201 | 1.8 | 2.0 | 1.8 |
| 7 | No field | 3620 | 6820 | 998 | 1906 | 70 | 134 | 1.9 | 1.9 | 1.9 |
| 8 | No field | 4005 | 7760 | 988 | 1934 | 64 | 145 | 1.9 | 2.0 | 2.3 |
| 9 | Blank | 885 | 1450 | 189 | 379 | 11 | 23 | | | |

TABLE VI. Distribution ratios of bromine recoils from three different nuclear processes (thin rod assembly).

| Exptl. | +4000 V on | Activity (counts/min)[a] $Br^{80}$ Rod | $Br^{80}$ Wall | $Br^{80m}$ Rod | $Br^{80m}$ Wall | $Br^{82}$ Rod | $Br^{82}$ Wall | Ratio (wall/rod) $Br^{80}$ | $Br^{80m}$ | $Br^{82}$ |
|---|---|---|---|---|---|---|---|---|---|---|
| 1 | No field | | | 209 | 4929 | 49 | 1265 | | 24 | 26 |
| 2 | No field | | | 154 | 5016 | 49 | 1444 | | 33 | 30 |
| 3 | No field[b] | | | 128 | 2448 | 8 | 175 | | 19 | 22 |
| 4 | No field | | | 239 | 4390 | 86 | 1700 | | 18 | 20 |
| 5 | Wall | | | 681 | 3805 | 335 | 1069 | | 5.6 | 3.2 |
| 6 | Wall[c] | | | 183 | 1025 | 69 | 201 | | 5.6 | 2.9 |
| 7 | Wall | 3035 | 11670 | 611 | 3235 | 320 | 754 | 3.9 | 5.3 | 2.4 |

[a] The $Br^{80}$ and $Br^{80m}$ counting rates were in general measured with a counting geometry of about 10 percent, while the $Br^{82}$ activities were taken at ~30 percent geometry. The blanks subtracted were as follows: $Br^{80}$, 285 and 1760 counts/min on the rod and wall, respectively; $Br^{80m}$, 72 and 415 counts/min; $Br^{82}$, 22 and 141 counts/min. Washing procedure *b* was used throughout.

[b] The bombardment time in this experiment was 5 minutes. The counter geometry was approximately 30 percent.

[c] One rather than three microns of $C_2H_5Br$ was irradiated.

[9] See E. Segrè and A. C. Helmholz, Revs. Modern Phys. **21**, 291 (1949) for the detailed decay scheme of $Br^{80m}$.

[10] C. O. Muehlhause, Phys. Rev. **79**, 277 (1950).

[11] B. Hamermesh, Phys. Rev. **80**, 415 (1950).

[12] J. A. Harvey, Phys. Rev. **81**, 353 (1950).

[13] H. Suess, Z. physik. Chem. **B45**, 297 (1939).

TABLE VII. Distribution of $I^{128}$ recoils from ethyl iodide.

| Exptl. | Radius of rod (mm) | Voltage on wall | $I^{128}$ activity (cts/min) Rod | Wall | Ratio (wall/rod) |
|---|---|---|---|---|---|
| 1[a] | 0.79 | 0 | 38 | 996 | 26 |
| | | +3500 | 409 | 498 | 1.2 |
| 2[a] | 0.79 | 0 | 32 | 1240 | 39 |
| | | −3500 | 23 | 1710 | 74 |
| 3[a] | 1.3 | 0 | 110 | 1334 | 12 |
| | | −3500 | 68 | 1978 | 29 |
| 4[a] | 1.3 | 0 | 103 | 1338 | 13 |
| | | −3500 | 52 | 1706 | 33 |
| 5[a] | 1.3 | 0 | 45 | 687 | 15 |
| | | +3500 | 377 | 474 | 1.3 |
| 6[b] | 0.79 | 0 | 56 | 1020 | 18 |
| | | +3000 | 351 | 844 | 2.4 |
| 7[b] | 1.3 | 0 | 67 | 1208 | 18 |
| | | +3500 | 588 | 600 | 1.0 |
| 8[b] | 1.3 | 0 | 19 | 308 | 16 |
| | | +3500 | 112 | 205 | 1.8 |
| 9[b] | 1.3 | 0 | 67 | 769 | 11 |
| | | +3500 | 446 | 319 | 0.72 |
| 10[b,c] | 1.3 | 0 | 762 | 15800 | 21 |
| | | +3500 | 7160 | 4970 | 0.69 |

[a] $H_2$-reduced copper electrodes used.
[b] Cu-amalgam electrodes used.
[c] Chamber irradiated in central thimble of heavy water reactor for 5 min.

experiment suggests that cancellation to this degree occurs infrequently. Suess[13] found 3 percent of the 18-min $Br^{80}$ in the gas fraction after neutron irradiation of gaseous ethyl bromide, and Libby[14] found 5 percent of the 4.4-hr $Br^{80m}$. The contrast with our results appears to be real but may be attributable to the following. In these investigators' experiments at normal gas pressure, any ethyl bromide molecules surviving neutron capture will be brought to thermal velocities before reaching the container walls. In our experiments, any molecules which survive the nuclear process will generally strike the chamber wall without an intervening gas space collision and with high velocity. The molecule may then penetrate the wall, dissociate because of the impact, or because of its high energy react with the wall. In all three events, this radio-bromine would be classed by the analytical procedure with bromine directly dissociated in neutron capture. When the character of the wall was altered by substituting aluminum collectors, the level of bromine activity in the gas phase was again less than 1.0 percent of the total.

The distribution of recoil atoms between central rod and outer cylinder can be readily calculated provided the cylinders are very long relative to the width of the annular gas space and provided gas space collisions and re-emission of the recoil from the struck surfaces do not occur. From purely geometrical considerations, the fraction $F$ of the recoil atoms which will strike the central rod first is given by

$$F=\frac{2}{\pi(r_w^2-r_c^2)}\int_0^{\pi/2}\int_0^{\sin^{-1} r_c/r}\int_{r_c}^{r_w} r\cos\phi\, d\theta\, d\phi\, dr, \quad (1)$$

where $r_c$ and $r_w$ are rod and wall radii, $r$ the distance from the locus of the neutron capture to the axis of the rod, and $\cos\phi d\theta d\phi$ the increment of solid angle subtended by the rod. On integrating,

$$F=\frac{r_c}{\pi(r_w^2-r_c^2)}\left[\frac{r_w^2}{r_c}\sin^{-1}\frac{r_c}{r_w}+(r_w^2-r_c^2)^{\frac{1}{2}}-\frac{\pi r_c}{2}\right]. \quad (5)$$

Table VIII compares calculated and observed $F$ values for field-free experiments employing central cylinders of several sizes. The observed values represent the average of a number of runs in some cases. No systematic discrepancy between the two columns is evident, although the variation is larger than that expected from repeat runs. Some comment is now in order on the assumptions used to derive Eq. (1). The length to radius ratio of the irradiation chambers used is either 15 or 30 to 1. The "end effect" for the shorter assembly has been calculated for us by Dr. M. Hamermesh of the Argonne National Laboratory and found to affect the value of $F$ by a few percent only. Using estimated van der Waal radii for Br and $C_2H_5Br$, we find that at 3 microns pressure approximately one-half of the recoils should collide with a gas molecule before striking a wall. No direct evidence on re-emission of recoils from the amalgamated or reduced copper surfaces is available, but the general conformity of the observed $F$ values to those predicted suggests that re-emission is slight.

Since an electric field alters the recoil distribution, charged particles must result from the neutron capture. Since the distribution ratio $R$ decreases when the wall is positive with respect to the rod and increases when the wall is negative, positive recoils must predominate over negative recoils. An estimate of the fractions of neutral, positive, and negative recoils can be obtained from the three types of experiment, provided the collection efficiencies of the electrodes for oppositely charged recoils are known. Calculations disclose, however, that the collection efficiency of the central rod cannot be estimated from theory for the case of the central rod. The recoil energy spectrum and indeed the magnitude of the charge carried by the recoils are both too uncertain. However, in a series of experiments with $C_2H_5Br$ and with the central rod at varying negative potential to the wall, the distribution of radioactivity was found to change progressively with increasing voltage until about 1500 volts was reached, after which the distribution remained constant to the usual potential of 4000 volts. This behavior is taken as evidence that above 1500 volts the collection efficiency of each

[14] W. F. Libby, Science 93, 283 (1941).

electrode has approached unity. At 4000 volts potential difference, then, the distribution of neutral recoils on the electrodes should be the same as that for all recoils in the field-free experiments, the negative electrode should have all positive recoils and none of the negative, and conversely for the positive electrode. Thus,

$$R_1=\frac{N_0(R_3/R_3+1)+N_-}{(N_0/R_3+1)+N_+}, \quad (2)$$

$$R_2=\frac{N_0(R_3/R_3+1)+N_+}{(N_0/R_3+1)+N_-}, \quad (3)$$

and

$$N_0+N_++N_-=1. \quad (4)$$

Here $N_0$, $N_+$, $N_-$ are the fractions of recoils which are neutral, positive, and negative, respectively. $R_1$ is the wall-to-rod activity ratio when the wall is 4000 volts positive, and $R_2$ is the experimental ratio with the electric field reversed. $R_3$ is the activity ratio in the absence of a field.

When the average $R$ values of Tables II, III, and IV are introduced in the equations, the values $N_+=0.12$, $N_-=-0.01$, and $N_0=0.89$ are found for the distribution of 4.4-hr $Br^{80m}$ recoils with respect to charge. The small negative value observed here for $N_-$ reappears constantly in other runs and undoubtedly reflects some systematic error in the procedure. In further calculations, we have assumed $N_-=0$. This permits independent solution of Eqs. (3) and (4). Then, for the wall positive, $N_+=0.12$, but for wall negative, $N_+=0.37$. The latter experiments with thin central rod and wall negative are weak, however, since the total activity on the rod is very low and very sensitive to error in assigning a contamination correction, while the positive recoils on the wall must be counted against a high background of neutral recoils. Neither of these objections applies to the thin rod negative experiments, however. Accordingly, we consider the lower value for $N_+$ much the more reliable. The thicker rod experiments of Table V give $N_+=0.10$ and $N_+=0.12$ for the fraction of positive $Br^{80m}$ when the wall is, respectively, positive and negative.

In Table VI, the distribution of 36-hr $Br^{82}$ recoils in an electric field is compared with that of 4.4-hr $Br^{80m}$. The data for comparison come from the same experiment, the activity levels of the two isotopes being determined by analysis of gross decay curves. The thin rod experiments with rod negative here again demonstrate the absence of negative recoils of both isotopes and yield $N_+=0.23$ for $Br^{82}$. In the thick rod experiments of Table V, $N_+=0.18$ and 0.28 for $Br^{82}$ when the wall is respectively positive and negative.

Table V represents a more extensive effort to establish conclusively whether charge differences exist among the three Br isotopes. Despite the scatter of $R$ values among different experiments, the fraction of positive $Br^{82}$ recoils definitely exceeds that of $Br^{80m}$. The isotope effect is more convincingly seen if attention is focused upon corresponding results within single experiments. Here many of the factors leading to variation among different experiments must have cancelled. In summary about 12 percent of the 4.4-hr $Br^{80m}$ recoils and 25 percent of the 36-hr $Br^{82}$ recoils are positively charged, while the positive fraction of 18-min $Br^{80}$ appears to have an intermediate value.

When Eqs. (3), (4), and (5) are solved with the averaged results of Table VII for 25-min $I^{128}$ recoils, $N_-$ is again very small and negative. The values of $N_+$ using $H_2$-reduced copper surfaces are 0.44 and 0.40 for thin and thick rods respectively. The corresponding $N_+$ values using amalgamated copper are 0.25, in one run, and 0.46, the average of several experiments. The iodine contamination correction averaged from several blank runs proved negligible. In summary, approximately half of the iodine recoils from neutron capture reach the collecting electrodes as positive ions.

If charge exchange between the recoils and bulk gas molecules occurs during the flight of the former to the collector, the fraction of recoils collected as positive ions will be smaller than the fraction of radio-halide species originally dissociated as positive ions. No information on cross sections for reactions similar to the exchange of charge between $Br^+$ and $C_2H_5Br$ is available. Hasted[15] has determined the exchange cross section for a number of projectile ions moving through various simple gases at velocities comparable to our recoils. The cross sections are substantially smaller than van der Waal's cross sections. In view of this and since several successive exchange steps may be required to neutralize the multiple charge of radio-halide ions created by internal conversion (see below), we suppose that the error in the present measurements from this source is not important.

We attribute the positive ions observed in neutron capture by bromine and iodine to processes of internal conversion which occur during the stabilization of the compound nucleus. Hamermesh and Hummel[16] have noted $\gamma$-rays of about 200-kev energy from $n$-capture by Br. Such transitions may readily proceed via internal

TABLE VIII. Comparison of calculated and observed average $F$ values for field-free systems.

| Radio-nuclide | Electrode surface | Rod radius (mm) | $F$ calc | $F$ obs |
|---|---|---|---|---|
| $Br^{80m}$ | Cu-amalgam | 0.79 | 0.043 | 0.039 |
| $Br^{80m}$ | Cu-amalgam | 5.5 | 0.26 | 0.35 |
| $Br^{82}$ | Cu-amalgam | 0.79 | 0.043 | 0.039 |
| $Br^{82}$ | Cu-amalgam | 5.5 | 0.26 | 0.33 |
| $I^{128}$ | Cu-amalgam | 0.79 | 0.043 | 0.053 |
| $I^{128}$ | Cu-amalgam | 1.3 | 0.077 | 0.057 |
| $I^{128}$ | $H_2$-reduced Cu | 1.3 | 0.077 | 0.070 |
| $I^{128}$ | $H_2$-reduced Cu | 0.79 | 0.043 | 0.031 |

[15] J. B. Hasted, Proc. Roy. Soc. (London) **A205**, 421 (1951).
[16] Private communication. For low energy capture $\gamma$-ray spectra of several other nuclides, see B. Hamermesh and V. Hummel, Phys. Rev. **83**, 663 (1951).

TABLE IX. Fraction of positive Rb atoms from $Kr^{88}$ decay.

| Exptl. | +3000 V on | $Rb^{88}$ activity (cts/min) Rod | Wall | Total | Ratio (wall/rod) | Fraction $Rb^+$ |
|---|---|---|---|---|---|---|
| 1 | Wall | 976 | 26 | 1002 | 0.027 | 0.97 |
| | No field | 31 | 1090 | 1121 | 36 | |
| | Rod | 12 | 1232 | 1244 | 103 | 0.65 |
| 2 | Wall | 6690 | 930 | 7620 | 0.14 | 0.87 |
| | No field | 366 | 6930 | 7296 | 19 | |
| | Rod | 0 | 8560 | 8560 | ∞ | 1.00 |
| 3 | No field | 124 | 2455 | 2579 | 20 | |
| 4 | Wall | 4560 | 290 | 4850 | 0.064 | 0.94 |

conversion if the corresponding spin and parity charges are favorable.[17] Amaldi and Rasetti[18] reported conversion electrons in neutron capture by gadolinium. Hibdon and Muehlhause[19] have found mono-energetic electrons in neutron capture by all of five elements studied by them. The electron energies correspond to transitions of 50 to 500 kev. Unfortunately, the method of Hibdon and Muehlhause is not sufficiently sensitive to detect conversion in elements of only average neutron capture cross section, so that direct information on bromine and iodine could not be obtained in this way. Recently, Yosim and Davies[20] observed that the majority of Au and In recoil atoms from neutron capture in Au and In films was positively charged. The charges were attributed to internal conversion. Thus, internal conversion appears to accompany neutron capture throughout the Periodic Table.

Internal conversion following neutron capture should produce halogen ions which carry positive charges as large as those which are believed to result from internal conversion of the 4.4-hr $Br^{80m}$ isomeric state to the 18-min $Br^{80}$ state. Several investigators have predicted the loss of four or five electrons in this transition,[21,22,23] and positive $Br^{80}$ ions from gaseous $C_2H_5Br^{80m}$ have been demonstrated.[8] The spread in kinetic energies of the neutron-capture recoils of the present study frustrated the attempts to determine the charge distribution by experiments with varying collection voltages.

The ubiquity of conversion in neutron capture adds a further complication to the discussions of chemical reactions induced in condensed media by nuclear recoil.[24] If recoil atoms from neutron capture are stopped by collisions before the internal conversion step shall have occurred, the latter by producing ions of high charge will set in train a new series of chemical reactions which must be considered in addition to the billiard-ball and free-radical processes already under discussion.

## APPENDIX: THE FRACTION OF POSITIVE $Rb^{88}$ IONS FROM $Kr^{88}$ DECAY

As an over-all test of the procedures and equipment employed in the halogen recoil studies, a determination of the positive ion yield was made for the reaction 2.8-hr $Kr^{88} \rightarrow$ 18-min $Rb^{88} + \beta^-$. In this case, all $Rb^{88}$ atoms should carry at least one positive charge and have been observed to do so.[25] In our experiments, the $Kr^{88}$ was obtained from uranium fission, and the $Rb^{88}$ recoil atoms were collected at about 3 microns pressure, probably of air. Three Cu amalgam electrode systems were used to permit simultaneous determination of $R_1$, $R_2$, and $R_3$, and the $Rb^{88}$ extracted from the collectors by $1M$ $HNO_3$ was precipitated with Rb carrier as chloroplatinate. The results appear in Table IX. The data obtained with positive central rod are judged unreliable because of very low counting rates for the rod relative to background. The other experiments give the expected result that all $Rb^{88}$ atoms are positive ions and confirm the observations of Jacobsen and Kofoed-Hansen.[25]

[17] M. Goldhaber and A. W. Sunyar, Phys. Rev. **83**, 906 (1951).
[18] E. Amaldi and F. Rasetti, Ricerca sci. **10**, 115 (1939).
[19] C. T. Hibdon and C. O. Muehlhause, Phys. Rev. (to be published).
[20] S. Yosim and T. H. Davies, J. Phys. Chem. **56**, 599 (1952).
[21] D. C. DeVault and W. F. Libby, J. Am. Chem. Soc. **63**, 3216 (1941).
[22] E. P. Cooper, Phys. Rev. **61**, 1 (1942).
[23] J. L. Magee and E. F. Gurnee, J. Chem. Phys. **20**, 894 (1952).
[24] W. F. Libby, J. Am. Chem. Soc. **69**, 2523 (1947); Miller, Gryder, and Dodson, J. Chem. Phys. **18**, 579 (1950); S. Goldhaber and J. E. Willard, J. Am. Chem. Soc. **74**, 318 (1952).
[25] J. C. Jacobsen and O. Kofoed-Hansen, Phys. Rev. **73**, 675 (1948).

THE JOURNAL OF CHEMICAL PHYSICS VOLUME 20, NUMBER 11 NOVEMBER, 1952

# Microwave Spectra and Structures of $XYH_3$ Molecules

JOHN M. MAYS* AND BENJAMIN P. DAILEY
*Chemistry Department, Columbia University, New York, New York*
(Received May 5, 1952)

Work on the microwave spectra of $CH_3Cl$, $SiH_3Cl$, $GeH_3Cl$, $CH_3Br$, $SiH_3Br$, and $GeH_3Br$, performed at this laboratory and others, is summarized, and preliminary reports of work at this laboratory are expanded. Structural parameters, dipole moments, and quadrupole coupling constants obtained from analysis of these spectra are tabulated and discussed, and a unified picture of the bonding in these series of molecules, based on the derived quantities, is presented.

## I. INTRODUCTION

THROUGH the work of several groups of investigators, the pure rotation spectra of a number of molecules of the $XYH_3$ type have been observed and analyzed. From the spectral data for each molecule values of the structural parameters, the molecular dipole moments, and the nuclear quadrupole coupling constants have been derived. From the point of view of valence theory, it should be of considerable interest to attempt to account for this large mass of data in terms of a simple and consistent set of valence bonds for molecules having this symmetry. In this paper two related series of molecules are considered: $CH_3Cl$, $SiH_3Cl$, and $GeH_3Cl$; $CH_3Br$, $SiH_3Br$, and $GeH_3Br$. The derived data are summarized, preliminary reports of work done at this laboratory are expanded, and information concerning the type of chemical bonding present in the molecules is presented.

## II. EXPERIMENTAL

### A. Materials

The samples used in this laboratory were obtained as follows. Isotopically unenriched $CH_3Cl$ was obtained from the Matheson Company. An enriched sample was prepared by the action of $HgCl_2$ on $CH_3I$ containing 50 percent $C^{13}$, obtained from the Eastman Kodak Company $SiH_3Cl$, $GeH_3Cl$, and $GeH_3Br$ were all prepared by the following procedure. First, the hydride, $SiH_4$ or $GeH_4$, was prepared by the reaction of $LiAlH_4$ with the tetrachloride in ether solution.[1] Second, the hydride was allowed to react with HCl or HBr over $AlCl_3$ or $AlBr_3$.[2] The resulting mixture was fractionated at low temperatures to give samples of adequate purity. A sample of $SiH_3Br$ was very kindly provided by Dr. A. H. Sharbaugh of the General Electric Research Laboratory.

Because of the high resolution possible with the microwave spectrometer, there is little probability of difficulty from the superposition of spectral lines due to the small amounts of impurities present in some of these samples. Since the molecules studied were symmetric rotors, their spectral lines could easily be distinguished from those due to such impurities as dichloro-silane by observation of the Stark effects in the spectra.

### B. Apparatus and Procedure

The instrument used at the Columbia Radiation Laboratory was a Stark-modulation microwave spectrometer.[3] Frequency measurements were made by comparing the spectral frequencies with harmonic frequencies of a 7.5-mc quartz crystal. The absolute frequencies were determined by measuring the frequency of some spectral line whose frequency was accurately known and applying the correction factor so obtained to the measured frequencies.

The technique used in measuring dipole moments has been described by Shulman and Townes.[3]

## III. THEORY AND RESULTS

### A. Structural Determinations

All of the molecules discussed in this paper are symmetric top molecules. The frequencies of pure rotational absorption lines of a hypothetical rigid molecule of this sort are given by the formula[4]

$$\nu = 2BJ/h, \tag{1}$$

where

$$B = h^2/2I_b$$

($I_b$ = the principal moment of inertia perpendicular to the figure axis) and the transition is $J-1$ to $J$.

Correction terms for centrifugal distortion have been derived[5] but are negligible for spectra considered in this work, in which molecules are in the lower rotational energy states. Much more important is the effect of vibration of the molecule. This effect is most easily illustrated for the diatomic molecule, where the vibration may be represented by the motion of one nucleus. The rotational constant $B$ is proportional to $1/I$ or $1/r^2$. Even for simple harmonic oscillation $\langle 1/r^2 \rangle_{Av}$ is greater than $1/r_e^2$, where $r_e$ is the equilibrium bond distance,

* Eastman Kodak Fellow, 1949–50. Present address, Bell Telephone Laboratories, Murray Hill, New Jersey.

[1] Finholt, Bond, Wilzbach, and Schlesinger, J. Am. Chem. Soc. **69**, 2692 (1947).

[2] A. Stock and C. Somieski, Ber. **52**, 695 (1919); L. M. Dennis and P. R. Judy, J. Am. Chem. Soc. **51**, 2321 (1929).

[3] R. G. Shulman and C. H. Townes, Phys. Rev. **77**, 500 (1950).

[4] See G. Herzberg, *Molecular Spectra and Molecular Structure. II. Infrared and Raman Spectra of Polyatomic Molecules* (D. Van Nostrand Co., Inc., New York, 1945).

[5] Z. I. Slawsky and D. M. Dennison, J. Chem. Phys. **7**, 509 (1939).

TABLE I. Values of structural parameters, dipole moments, and nuclear quadrupole coupling constants obtained from microwave spectra and by other methods.

| Molecule | | $CH_3Cl$ | $SiH_3Cl$ | $GeH_3Cl$ | $CH_3Br$ | $SiH_3Br$ | $GeH_3Br$ |
|---|---|---|---|---|---|---|---|
| $D_{YX}$ | Microwave | 1.781 ±0.005 | 2.048 ±0.004 | 2.148 ±0.003 | 1.939[j] | 2.209[l] | 2.298 ±0.003[m] |
| (A) | Electron Diffraction[a] | 1.77 ±0.01 | 2.06 ±0.05 | | 1.91 ±0.06 | | |
| Sum of Covalent Radii[b] (A) | Single bond | 1.76 | 2.16 | 2.21 | 1.93 | 2.31 | 2.36 |
| | Double bond | | 1.96 | 2.01 | | 2.11 | 2.16 |
| $D_{YH}$ (A) | | 1.101 ±0.01[c] | 1.50 ±0.03 | 1.52 ±0.03 | 1.100 ±0.01[c] | 1.57[l] | 1.44 ±0.10[m] |
| ∠HYH | | 110°13′ ±30′ [c] | 110°57′ ±90′ | 110°54′ ±90′ | 111°0′ ±30′ [c] | 111°20′[l] | 109°25′ ±4° [m] |
| $\mu$ (Debye) | Microwave | 1.869[d] | 1.303 ±0.01 | 2.124 ±0.02 | 1.797 ±0.015[d] | 1.32 ±0.03 | |
| | Classical | 1.86 ±0.05[e] | 1.284 ±0.005[g] | 2.03[i] | 1.79 ±0.01[k] | | |
| $(eqQ)_X$ (Mc/sec) | $Cl^{35}$ or $Br^{79}$ | −75.13[f] | −40.0[h] | −46 | 577.0[f] | 336[l] | 380[m] |

[a] P. W. Allen and L. E. Sutton, Acta Cryst., 3(I), 46 (1950).
[b] See reference 27.
[c] See reference 7.
[d] Shulman, Dailey, and Townes, Phys. Rev. **78**, 145 (1950).
[e] Sänger, Steiger, and Gächter, Helv. Phys. Acta **5**, 200 (1932).
[f] Gordy, Simmons, and Smith, Phys. Rev. **74**, 243 (1948).
[g] See reference 20.
[h] See reference 8.
[i] See reference 21.
[j] J. W. Simmons and W. O. Swan, Phys. Rev. **80**, 289 (1950).
[k] L. G. Groves and S. Sugden, J. Chem. Soc. 158 (1937).
[l] Sharbaugh, Bragg, Madison, and Thomas, Phys. Rev. **76**, 1419 (1949).
[m] See reference 11.

and thus $B$ varies with the vibrational state. For a polyatomic molecule $B_v$ can be represented to a first approximation as

$$B_{v_1v_2}\cdots = B_e - \alpha_1(v_1+\tfrac{1}{2}) - \alpha_2(v_2+\tfrac{1}{2}) - \cdots, \quad (2)$$

where $v_i$ is the vibrational quantum number of the $i$th mode, the $\alpha$'s are small constants, and $B_e$ is the hypothetical equilibrium value of $B$. The $\alpha$'s corresponding to simple harmonic motion can be calculated for simple molecules,[6] but the calculation for actual molecules, whose vibrations are anharmonic, requires a greater knowledge of the potentials than is usually available. Inasmuch as each nondegenerate mode and each group of degenerate modes has a half-quantum of energy in the ground state, the vibrational correction is always necessary.

If a molecule has $n$ independent modes of vibration, the measurement of $n$ lines due to the same $J$ transition of molecules in different vibrational states suffices to determine the $n$ $\alpha$'s and thus $B_e$. In practice temperatures high enough to excite sufficient molecules to the higher energy modes reduce the intensity of the rotational lines so much that the excited state transitions cannot be observed. In no polyatomic molecule has it been possible to determine all the $\alpha$'s. Therefore, one generally obtains from microwave spectra only $B_0$, the rotational constant in the ground vibrational state, and the moment of inertia $I_0$ derived from it will differ from the equilibrium value $I_e$ by a small amount.

In order to obtain the moments of inertia from the observed frequencies, it is also necessary to consider the hyperfine splitting of lines due to nuclear quadrupole coupling. This effect is discussed below.

A formula for the moment of inertia $I_b$ of axial $XYH_3$ molecules is

$$I_b = X(1-X/M)D_{XY} + (6XH/M)aD_{XY} + (3H(X+Y)/M)a^2 + 2HD_{YH}\sin^2(\beta/2), \quad (3)$$

where $Y, X, H, M$ = masses of the central atom, halogen, hydrogen and entire molecule, respectively; $D_{XY}$, $D_{YH}$ = $C-Y$ and $Y-H$ bond distances; $\beta = \angle HYH$; and $a$ = distance from the plane of the hydrogens to central atom. The additional relation $\sin^2(\beta/2) = \frac{3}{4}(1-a^2/D_{YH}^2)$ is easily obtained. Three experimental values of $I_b$ obtained for three isotopic species of the molecule suffice to determine the three structural parameters $D_{XY}$, $D_{YH}$, and $\beta$. The isotopic masses used are shown in Table III.

The structural parameters determined from microwave spectra are assembled in Table I. Values of the internuclear distances of the heavy atoms obtained from electron-diffraction measurements are given when available. The microwave and electron-diffraction values for these distances are consistent within the

[6] H. H. Nielsen, Phys. Rev. **60**, 794 (1941).

limits of error assigned. The microwave measurements give considerably more precise values of this parameter.

### 1. Accuracy of Structural Determinations

The errors in structural parameters determined from microwave measurements may be divided into two classes. The first class depends upon the precision with which the frequencies of the spectral lines for the different isotopic species can be measured. The second class arises from the presence of zero-point vibrations. The magnitude of errors of the first type can be minimized and is easily estimated. Errors of the second type are fixed and can be estimated only very roughly for molecules of the sort with which we are dealing.

The limiting error in measuring the frequency of a single spectral line is the precision with which the frequency marker can be placed visually on the maximum point of the line. When quadrupole coupling is present, it is necessary to measure the frequency of two identifiable quadrupole components in order to determine the undisplaced frequency of the rotational line. If the hyperfine pattern is at all complex, it is often not possible to observe two components undistorted by adjoining components. Sometimes it happens that spectra due to different isotopic species overlap. In cases of this sort, uncertainties as to what point on the theoretical pattern corresponds to the maximum of the observed complex line may result in considerable error.

The effect of a given error in frequency upon the accuracy of a derived structural parameter depends upon both the molecule and the parameter in question. The error depends much more strongly upon the accuracy of the isotopic shift measurements than upon the absolute frequency measurements. Thus when a choice is possible, widely spaced isotopic species are measured. For a given accuracy of isotopic shift measurement, the sensitivity of $I_b$ to small changes in the magnitude of a structural parameter determines the accuracy with which the parameter is obtained. Clearly, in the case of $XYH_3$ molecules, small changes in the distance of the plane of the hydrogens from the central atom will have a much smaller effect on $I_b$ than will a small change in the $Y-X$ distance. Much smaller even than this will be the difference in $I_b$ for two sets of values of the $Y-H$ distance and $HYH$ angle that give the same component along the figure axis.

The effect of zero-point vibrations can be conveniently discussed in terms of the $\alpha$'s (see Eq. (2)). There are five $\alpha$'s, all unknown, for the molecules in which we are interested. These $\alpha$'s vary appreciably from one isotopic species to another. Thus, not only the absolute frequencies but also the isotopic shifts of observed rotational lines differ from those for the hypothetical nonvibrating molecules.

The probable magnitude of these errors has been discussed by Miller, Aamodt, Dousmanis, Townes, and Kraitchman in their careful structural determination of the methyl halides.[7] In their experiments observation of the $1_1 \rightarrow 2_0$ transition, with a frequency equal to $3B+C$, and the $1_0 \rightarrow 2_{-1}$ transition with a frequency of $3C+B$ for the slightly asymmetric, doubly deuterated methyl halides helped determine the methyl halide structures. The difference in frequency of the two lines $2(B-C)$ is very sensitive to the hydrogen bond angle and to distance.

As a result, the structures of the methyl halides are known with greater accuracy than those of the similar silicon and germanium compounds. Miller *et al.* estimate the errors in the methyl halide parameters as approximately 0.01 A for the C−H distance, 30′ for the H−C−H angle, and 0.003 A in the C−X distance. The errors in the hydrogen parameters for the silicon and germanium compounds must be at least twice as great. The order of magnitude of the errors involved in use of symmetric rotor frequencies alone is seen by comparing the parameters for $CH_3Cl$ obtained in this manner† $D_{C-H}=1.12$ A, $\angle HCH=110°48'$ with those obtained by Miller *et al.* $D_{C-H}=1.101\pm0.01$ A, $\angle HCH=110°13'\pm30'$.

### 2. Experimental Determinations

$SiH_3Cl$: Sharbaugh[8] had previously obtained values for the Si−Cl distance and HCH angle by combining microwave measurements of the $J=1\rightarrow2$ transition of

TABLE II. Frequencies (Mc/sec) of pure rotational transitions used in structural determinations at Columbia.

| $CH_3Cl$ mass numbers CCl | $J=0\rightarrow1$ | $GeH_3Cl$ | $J=2\rightarrow3$ |
|---|---|---|---|
| 12–35 | 26,585.77[a] | 70–35 | 26,410.26 |
| 12–37 | 26,176.37[a] | 74–35 | 26,003.46 |
| 13–35 | 25,592.4 | 74–37 | 25,067.4 |
| 13–37 | 25,180.0 | 76–37 | 24,879.0 |
| $SiH_3Cl$ | $J=1\rightarrow2$ | $GeH_3Br$[c] | $J=4\rightarrow5$ |
| 28–35 | 26,695.2[b] | 70–79 | 24,385.54 |
| 28–37 | 26,049.6[b] | 70–81 | 24,101.61 |
| 30–35 | 25,943.2 | 74–81 | 23,474.75 |

[a] Gordy, Simmons, and Smith, Phys. Rev. **74**, 243 (1948).
[b] See reference 8.
[c] See reference 11.

TABLE III. Values of atomic masses and constant used in structural determinations at Columbia.

| | |
|---|---|
| $H^1=1.008123$ m.u. | $Cl^{35}=34.97867$ |
| $H^2=2.014708$ | $Cl^{37}=36.97750$ |
| $C^{12}=12.00382$ | $Ge^{70}=69.9531$ |
| $C^{13}=13.00751$ | $Ge^{74}=73.9504$ |
| $Si^{28}=27.9866$ | $Br^{79}=78.9444$ |
| $Si^{29}=28.9866$ | $Br^{80}=80.9423$ |
| $Si^{30}=29.9832$ | |

$$B=\frac{\hbar^2}{2I_b}=5.054_{268}\times10^5/I_b \text{ (amu) Mc/sec}$$

[7] Miller, Aamodt, Dousmanis, Townes, and Kraitchman, J. Chem. Phys. **20**, 1112 (1952).
† Using frequencies of lines for $C^{12}H_3Cl^{35}$, $C^{12}H_3Cl^{37}$, and $C^{13}H_3Cl^{35}$.
[8] A. H. Sharbaugh, Phys. Rev. **74**, 1870 (1948).

$Si^{28}H_3Cl^{35}$ and $Si^{28}H_3Cl^{37}$ with a value of the Si−H distance obtained from infrared measurements on $SiH_4$. At the CRL the $J=1\rightarrow2$ lines of $Si^{29}H_3Cl^{35}$, $Si^{29}H_3Cl^{37}$, and $Si^{30}H_3Cl^{35}$ (natural abundances: $Si^{28}=89.6$ percent, $Si^{29}=6.2$ percent, $Si^{30}=4.2$ percent) were observed with an unenriched sample.[9] The wave guide was cooled with dry ice to give greater intensity and to inhibit decomposition of the sample, which is relatively unstable. The quadrupole pattern was not sufficiently complex to interfere with frequency measurements, which were made with an accuracy of 0.1 Mc/sec. The error due to zero-point vibrations is therefore predominant. The parameters were obtained on the basis of the $Si^{28}H_3Cl^{35}$, $Si^{28}H_3Cl^{37}$, and $Si^{30}H_3Cl^{35}$ lines.

$GeH_3Cl$: Germanium has five stable isotopes with mass numbers and natural abundances 70 (21.2 percent), 72 (27.3 percent), 73 (7.9 percent), 74 (37.1 percent), and 76 (6.5 percent). All of the ten lines arising from the $J=2\rightarrow3$ transition of $GeH_3Cl^{35,37}$ were observed with an unenriched sample.[9] Dry ice was used to increase intensity and inhibit decomposition. The hyperfine pattern was very much compressed and thus essentially unresolved. The highest point of the line, which should correspond to the undisplaced position, was measured. Owing to the width of the line, the accuracy assigned is 0.5 mc. Direct calculation shows that this introduced an uncertainty of 0.0004A in $D_{GeCl}$, 0.015A in $D_{GeH}$, and 20′ in ∠HGeH. The masses of the Ge isotopes are not known exactly. The masses used were calculated using a reasonable packing fraction $-6.7\times10^{-4}$ mass units.[10] The error from this source should be very small. The major source of uncertainty is thus the zero-point vibrations. The parameters were obtained from the frequencies of the $Ge^{70}H_3Cl^{35}$, $Ge^{74}H_3Cl^{35}$, and $Ge^{74}H_3Cl^{37}$ lines.

$GeH_3Br$: The work on this molecule was done jointly with Dr. A. H. Sharbaugh's group (General Electric Research Laboratory).[11] All of the ten lines arising from the $J=3\rightarrow4$, $J=4\rightarrow5$, and $J=5\rightarrow6$ transitions of $GeH_3Br^{79,81}$ were observed (natural abundances $Br^{79}=50.6$ percent, $Br^{81}=49.4$ percent). Decomposition was so rapid at room temperature that dry-ice cooling was essential. The uncertainty in measurement of isotopic shifts in frequency is estimated as 0.1 Mc/sec. The errors due to zero-point vibrations thus predominate. The parameters were obtained on the basis of the frequencies of the $Ge^{70}H_3Br^{79}$, $Ge^{70}H_3Br^{81}$, and $Ge^{74}H_3Br^{81}$ lines, using the same Ge masses as for $GeH_3Cl$.

### B. Nuclear Quadrupole Coupling

The rotational lines of all the molecules under discussion are split into hyperfine components by interaction of the nuclear quadrupole moment of the halogen atom with the field produced by the other charges in the molecule. The shift in energy due to a quadrupole coupling of a single nucleus on the axis of a symmetric top molecule is[12,13]

$$W=-eqQ\frac{\frac{3}{4}C(C+1)-I(I+1)J(J+1)}{2I(2I-1)(2J-1)(2J+3)}\times(1-3K^2/J(J+1)), \quad (4)$$

where $e$ = the charge of the proton; $Q$ = the quadrupole moment of the nucleus; $q=\partial^2V/\partial z^2$, $V$ = electrostatic potential due to all molecular charges outside a small sphere surrounding the nucleus; $z$ = the coordinate along the molecular axis; $F$ = the quantum number for the total angular momentum $\mathbf{F}=\mathbf{I}+\mathbf{J}$, where $\mathbf{I}$ and $\mathbf{J}$ are the nuclear spin and molecular rotation angular momenta, respectively; $C=F(F+1)-I(I+1)-J(J+1)$. Bardeen and Townes[13] provide tables useful for computation of $W$. In rotational transitions the additional selection rule $\Delta F=0, \pm1$ is operative. The relative intensities of components with the same value of $K$ can be found in tables constructed for $LS$ coupling.[14] Correlation for different values of $K$ is obtained by multiplying by $g_{KJ}[(J+1)^2-K^2/(J+1)(2J+1)]$, where $J$ and the statistical weight factor refer to the lower state.[15] Relative values of $g_{KJ}$ for molecules treated in this work are 1 for $K\neq3n$ and 2 for $K=3n(n\neq0)$.

The values of $eqQ$ (see Table I) for the halogen atom in the six compounds, and hence the frequency of the hypothetical unsplit line, were obtained by comparison of observed and theoretically predicted quadrupole coupling patterns. Only in the case of $Ge^{73}$ was evidence of a nuclear quadrupole moment for the central atom found. Determination of the spin of $Ge^{73}$ as 9/2 has been reported in an earlier paper.[16]

The quantity $q$ is essentially a measure of the departure of the molecular field at the nucleus from spherical symmetry and thus of the variation of nuclear quadrupole energy with angular orientation. Since closed electronic shells and $s$ electrons give spherically symmetrical charge distributions, they make no contribution to $q$. It has been shown by Townes and Dailey[17] that the value of $q$ depends almost entirely upon the distribution of electrons in $p$ orbitals of the valence shell. Hybridization of a $p$ orbital with other types of orbitals alters its contribution to $q$ only in so far as its importance is lowered by renormalization. For symmetric top molecules with an atom having $Q\neq0$ on the figure axis, the effect on $q$ of the distribution of electrons in $p$ orbitals is proportional to the number of "un-

[9] Dailey, Mays, and Townes, Phys. Rev. **76**, 136 (1949).
[10] J. Mattauch, *Nuclear Physics Tables* (Interscience Publishers, Inc., New York, 1940), p. 113.
[11] Sharbaugh, Pritchard, Thomas, Mays, and Dailey, Phys. Rev. **79**, 189 (1950).
[12] H. B. G. Casimir, *On the Interaction between Atomic Nuclei and Electrons* (Teyler's Tweede Genootschap, E. F. Bohn, Haarlem, 1936); J. H. Van Vleck, Phys. Rev. **71**, 468 (1947).
[13] J. Bardeen and C. H. Townes, Phys. Rev. **73**, 97 (1948).
[14] H. E. White, *Introduction to Atomic Spectra* (McGraw-Hill Book Company, Inc., New York, 1934), first edition, p. 439.
[15] Reference 4, p. 422.
[16] J. M. Mays and C. H. Townes, Phys. Rev. **81**, 940 (1951).
[17] C. H. Townes and B. P. Dailey, J. Chem. Phys. **17**, 782 (1949).

balanced" $p$ electrons along the figure axis. Deductions concerning chemical bonding from experimental values of $eqQ$ are presented below.

### C. Dipole Moments

Dipole moments were obtained by observation of the Stark effect. In the presence of an external electric field, the $M$ degeneracy in symmetric rotor energy states is destroyed. States with different $M$ have different average values of the orientation energy of the molecular dipole in the field. The Hamiltonian corresponding to the orientation of a dipole $\boldsymbol{\mu}$ in an electric field $\mathbf{E}$ is $\boldsymbol{\mu}\cdot\mathbf{E}$. If the effect of the electric field is taken as a perturbation, the usual treatment gives[18]

$$W_s=-\frac{\mu EMK}{J(J+1)}+\frac{4\mu^2E^2}{B}(F_{JMK}-F_{J+1,M,K}), \quad (5)$$

where

$$F_{JMK}=\frac{(J^2-M^2)(J^2-K^2)}{(2J-1)(2J)^2(2J+1)}.$$

In the instrument used in this work the external field is applied parallel to the direction of the electric vector of the radiation. Under these circumstances the selection rule on $M$ is $\Delta M=0$. Thus, rotational absorption lines are split into a number of Stark components by application of an electric field. The intensities of the various components are proportional to $(J^2-M^2)(J^2-K^2)$, where $J$ refers to the upper state.

The Stark effect of symmetric tops exhibiting quadrupole coupling due to a single nucleus has been worked out by Low and Townes.[19] We shall be concerned with cases where the effect of the electric field is of the same order of magnitude as the quadrupole coupling effects but very small compared with the energy separation of levels with different $J$. In this case $J, I, K$, and $M_F$ continue to be good quantum numbers while $F$ does not. The number of Stark components of a level originally characterized by $J$, $I$, $K$, and $F$ is determined by the possible values of $M_F$. A complete solution involves a secular equation with off-diagonal elements connecting states of the same $M_F$ but different $F$. Transitions are determined by the additional selection rule $\Delta M_F=0$. If the Stark perturbation is large compared with the quadrupole coupling, the Stark components behave essentially as if no quadrupole coupling were present.

By measuring the displacement of a given Stark component with field, one can determine the dipole moment of the molecule.

[18] Mannebeck, Physik. Z. **28**, 72 (1927); R. Kronig and I. Rabi, Phys. Rev. **29**, 262 (1927); and D. M. Dennison, Revs. Modern Phys. **3**, 280 (1931).

[19] W. Low and C. H. Townes, Phys. Rev. **76**, 1295 (1949). In this paper, the right-hand side of Eq. (7) should contain the factor $M$. The next to last equation of the appendix should read

$$W_2=\frac{W(Q_1)+W(Q_2)+a+b}{2}\pm\tfrac{1}{2}\{[W(Q_1)-W(Q_2)+a-b]^2+4C^2\}^{\frac{1}{2}}.$$

TABLE IV. Dipole moment of $SiH_3Cl$. Displacement of $M_F=5/2$ component of $J=1\rightarrow2$, $K=1$, $F=5/2\rightarrow7/2$ component for various field strengths and values of $\mu$ derived therefrom.

| | Displacement (Mc/sec) | Potentiometer reading (volts) | $E$ (Mc/sec Debye) | $\mu E$ (Mc/sec) | $\mu$ Debye |
|---|---|---|---|---|---|
| (1) | 14.8 | 0.0339 | 38.95 | 48.90 | 1.255 |
| (2) | 30.76 | 0.0660 | 75.83 | 97.65 | 1.288 |
| (3) | 45.00 | 0.0937 | 107.66 | 140.68 | 1.307 |
| (4) | 55.51 | 0.1151 | 132.25 | 172.34 | 1.303 |
| (5) | 56.38 | 0.1164 | 133.76 | 174.96 | 1.308 |
| (6) | 66.58 | 0.1377 | 158.24 | 205.65 | 1.300 |
| (7) | 115.22 | 0.2360 | 271.16 | 351.77 | 1.297 |

#### *1. Experimental Determinations*

The dipole moments determined in these experiments will be found in Table I. Previous values obtained by polarization measurements are given when available. The microwave values are considered more reliable, both because the techniques of measurement are more sensitive and because the results obtained are virtually independent of sample purity and partial decomposition of the sample during the course of the measurement. Work at this laboratory that has not been fully described previously is discussed below. The experimental technique and the errors involved in microwave determinations of dipole moments have been treated in detail by Shulman and Townes.[3]

$SiH_3Cl$: The $M_F=5/2$ component of the $J=1\rightarrow2$, $K=1$, $F=5/2\rightarrow7/2$ transition was used to determine the dipole moment of this molecule. The $F=5/2\rightarrow7/2$ transition gives the strongest hyperfine component, and the region to higher frequency is relatively free of other components. The lower state ($J=1$, $K=1$, $M_F=5/2$) can be formed only from the $F=5/2$ state since $F_{\max}=5/2$. Its displacement is $-\mu E/2$. In the case of the upper state ($J=2$, $K=1$, $M_F=5/2$), perturbation by the applied field mixes the states $F=7/2$ and $F=5/2$, both of which can have $M_F=5/2$. Solution of the resulting secular equation gives the following expression for the displacement:

$$-2.500+0.2500\mu E+(6.250+0.05951\mu E+0.006944\mu^2E^2)^{\frac{1}{2}} \text{ mc.}$$

An expression for the displacement of the observed component was obtained and inverted to give the theoretical $\mu E$ for a given displacement.

The experimental data and intermediate quantities are shown in Table IV. $E$ is obtained from the potentiometer reading and $\mu E$ from the theoretical equation. The root-mean-square deviation of values 3–7 is 0.004 Debye units. Values 1 and 2 are not used because of their large deviations and the fact that they are more sensitive to errors in measurement of the undisplaced position. The component followed was not interfered with by other components and thus could be measured quite accurately, as is evidenced by the consistency of

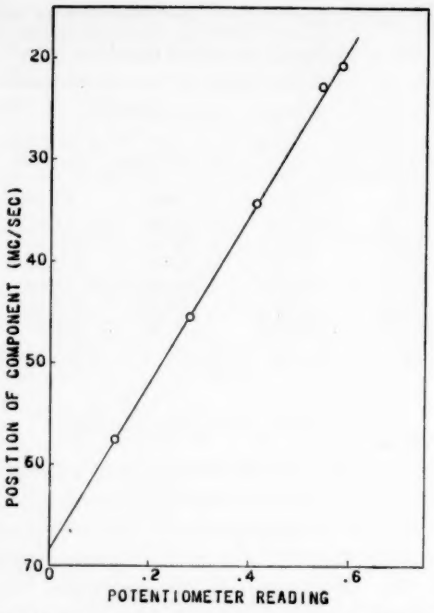


FIG. 1. Experimental points used in determination of $GeH_3Cl$ dipole moment. $E$ (Mc/sec. Debye) = 495.1 pot.

data for large displacements. The value determined and estimated uncertainty are

$$\mu = 1.303 \pm 0.01 \text{ Debye units.}$$

This value is to be compared with that obtained from polarization methods,[20] $\mu = 1.284 \pm 0.005$ Debye units.

$GeH_3Cl$: The quadrupole coupling pattern in this molecule is so compressed that the strong field solution, in which $m_J$ is a good quantum number, is applicable. Viewed experimentally, the hyperfine structure is essentially unresolved and the Stark components for the various possible combinations of $m_J$ and $K$ move out in the same manner as if there were no quadrupole coupling. In the present case each component is made up of two components corresponding to $m_I = \pm\frac{3}{2}$ and $\pm\frac{1}{2}$. The broadening of the component due to this effect is smaller than that produced by the quadrupole coupling.

The measurement was made with the $m_J = \pm 1$, $K = \mp 1$ component of the $J = 2 \rightarrow 3$ transition of $Ge^{74}H_3Cl^{37}$. The formula for displacements is $-\mu E/12$. A graph of experimentally determined displacements is shown in Fig. 1. Since the displacement varies linearly with field, the dipole moment is determined from the slope and is thus independent of the zero reading. The best slope gives $\mu = 2.124$. On the basis of variations in the data and considering the limitations on measuring accurately, the frequency of a relatively wide line the uncertainty is given as

$$\mu = 2.124 \pm 0.02 \text{ Debye units.}$$

This value is to be compared with that obtained from polarization measurements,[21] $\mu = 2.03$ Debye units. It is interesting to note that these investigators obtained higher dipole moments, lying between this value and the microwave value, at lower temperatures. This would seem to indicate that their low value is a result of sample decomposition.

$SiH_3Br$: The $J = 2 \rightarrow 3$ transition of this molecule, lying at about 25,750 mc, was the only one whose Stark effect could be conveniently measured. The Stark effect of this transition is complicated by the fact that all the strong hyperfine components correspond to the superposition of two or more lines each of whose Stark components moves differently with field. For $J = 3$ and $K = \pm 2$, the factor $(1 - 3K^2/J(J+1))$ in the expression for quadrupole coupling energy (see Eq. (4)) is zero, and there is therefore effectively no quadrupole splitting. The best hyperfine component for measurement was the $(J = 2,\ K = \pm 2,\ F = 7/2) \rightarrow (J = 3,\ K = \pm 2)$ transition. Owing to the degeneracy of the upper level, the selection rule becomes $\Delta m_J = 0$. The lower level exhibits normal quadrupole coupling, and its Stark splitting is therefore most easily described in terms of the $J, I, F, M_F$ representation. However, in order to determine the transitions and intensities, the $J, I, m_J, m_I$ representation must be used. The transformation coefficients $(JIm_Jm_I|JIFM_F)$ are available in Condon and Shortley.[22] The decomposition is as follows:

| $F = 7/2$ | $M_F$ | $(m_J, m_I)$ |
|---|---|---|
| | $\pm 7/2$ | $(2, \frac{3}{2})$ |
| | $\pm 5/2$ | $(2, \frac{1}{2}), (1, \frac{3}{2})$ |
| | $\pm\frac{3}{2}$ | $(2, -\frac{1}{2}), (1, \frac{1}{2}), (0, \frac{3}{2})$ |
| | $\pm\frac{1}{2}$ | $(2, -\frac{3}{2}), (1, -\frac{1}{2}), (0, \frac{1}{2}), (-1, \frac{3}{2}),$ |

where only the upper sign of $m_J$ and $m_I$ is given. The displacement of Stark components is represented to the first order by $\mu EK(m_J/12 - 2M_F/21)$. The relative intensities and displacements of the ten Stark components that move to lower frequency are shown in Fig. 2. The relative intensities were determined by multiplying the usual factor $(J_{\text{upper}}^2 - m_J^2)$ by the square of the appropriate transformation coefficient.

It will be noted that the components fall into two rather well-defined groups. The more widely split group was used in the measurement. The frequency of the highest point was measured for various applied fields. It is quite difficult to correlate these readings with the theoretical pattern. From the appearance of the line on the oscilloscope, the maximum was estimated to be somewhere between the center of gravity of the two lowest frequency components (Case I) and the center of gravity of the three lowest (Case II). Experimental data and the dipole moments determined assuming Case I and Case II are shown in Table V. The theoretical $\mu E$ values for the two cases were determined from graphs prepared from the theoretical equations. The extreme right component is a transition between pure states. For

[20] L. O. Brockway and I. E. Coop, Trans. Faraday Soc. **34**, 1429 (1938).

[21] Smyth, Grossman, and Ginsburg, J. Am. Chem. Soc. **62**, 192 (1940).

[22] E. U. Condon and G. H. Shortley, *The Theory of Atomic Spectra* (The Macmillan Company, 1951), p. 76.

the next component a second-order secular equation was solved to take into account mixing of the lower state wave functions. First-order approximations were used for the position of the third component and the intensities of the second and third, since it was felt that in view of the experimental uncertainties more accurate treatment was not warranted. The value assigned, the mean of values obtained for Cases I and II is

$$\mu = 1.32 \pm 0.03 \text{ Debye units.}$$

## IV. CONCLUSIONS

Microwave measurements have now been made on the spectra of two related series of molecules: $CH_3Cl$, $SiH_3Cl$, and $GeH_3Cl$ and $CH_3Br$, $SiH_3Br$, and $GeH_3Br$. These measurements provide, for each molecule, the value of $eqQ$ for the halogen atom, an accurate value of the internuclear distance of the two heavy atoms, and, except in the case of $GeH_3Br$, the magnitude of the dipole moment of the molecule (see Table I). On the basis of these data, a fairly complete picture of the bonding in the molecules can be obtained.

The methyl halides can be thought of as resonance hybrids of the single bond and ionic structures $H_3C-X$ and $H_3C^+Cl^-$. As Pauling[23] has pointed out, for the silane and germane derivatives the double bond structure of the type $H_3Si^- = Cl^+$, involving use of a $d$ orbital to form five Si bonds, would be expected to contribute. The considerable shortening of the $Si-X$ and $Ge-X$ bonds from the predicted single bond distances fits in well with this hypothesis, as does the fact that the $GeH_3Cl$ dipole moment is considerably larger than the $SiH_3Cl$, in spite of the fact that Ge and Si have almost the same electronegativity. Pauling[24] has shown that approximate values of the percent double bond character can be obtained by assuming the force constant for a double bond is three times that for a single bond, adding the two potential functions, and finding their minimum. The resulting formula for the fraction double bond

TABLE V. Dipole moment of $SiH_3Br$. Displacement of unresolved Stark components for various field strengths and resulting values of $\mu$ for two cases described in text.

| Displacement (Mc/sec) | $E$ Mc/sec Debye | $\mu E$—Case I (Mc/sec) | $\mu E$—Case II (Mc/sec) | $\mu$—Case I (Debye) | $\mu$—Case II (Debye) |
|---|---|---|---|---|---|
| 8.84 | 21.09 | 27.7 | 27.0 | 1.313 | 1.280 |
| 10.94 | 26.08 | 34.0 | 33.1 | 1.304 | 1.269 |
| 12.58 | 30.10 | 39.3 | 38.4 | 1.306 | 1.276 |
| 14.80 | 34.67 | 45.9 | 44.7 | 1.324 | 1.289 |
| 17.52 | 40.63 | 54.2 | 52.9 | 1.334 | 1.302 |
| 18.97 | 44.03 | 58.6 | 57.0 | 1.331 | 1.295 |
| 21.47 | 49.05 | 66.0 | 64.2 | 1.346 | 1.309 |
| 24.08 | 54.80 | 74.1 | 72.1 | 1.352 | 1.316 |
| 26.69 | 60.76 | 81.8 | 79.3 | 1.346 | 1.305 |
| 30.50 | 69.85 | 92.9 | 90.0 | 1.330 | 1.288 |
| 35.54 | 80.39 | 107.7 | 104.2 | 1.340 | 1.296 |

[23] L. C. Pauling, *The Nature of the Chemical Bond* (Cornell University Press, Ithaca, 1940), Chapter VII.
[24] Reference 23, p. 175.

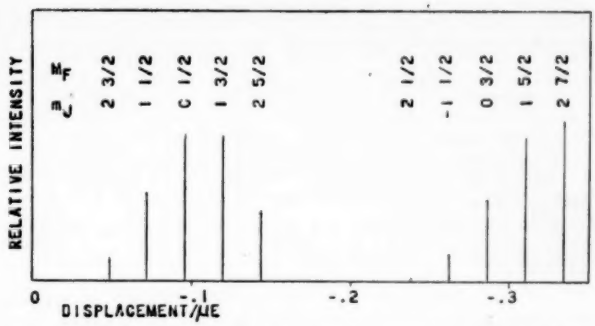


FIG. 2. Stark components of the $(J=2, K=-2, F=7/2) \rightarrow (J=3, K=-2)$ transition of $SiH_3Br$.

character $y$ in terms of the single bond distance $r_1$, the double bond distance $r_2$, and the observed bond distance $r_0$ is

$$y = (r_1 - r_0)/(r_1 + 2r_0 - 3r_2). \quad (6)$$

This formula is used with sums of covalent radii to obtain the double bond characters shown in Table VI.

The number of unbalanced $p$ electrons along the figure axis for the halogen atoms in these molecules is obtained as follows:[17]

Ionic structure, e.g., $H_3Si^+X^-$. The halogen is essentially an ion with a closed valence shell and thus has a spherically symmetrical electron distribution and makes no contribution to $q$.

Single bond structure, e.g., $H_3Si-X$. If the halogen atom contributes a pure $p_z$ orbital to the bond, its $p_x$ and $p_y$ valence orbitals each contain two electrons while the $p_z$ orbital contains only one. Thus this structure results in a deficiency of one electron along the bond axis. Townes and Dailey,[17,25] in their analysis of quadrupole coupling data, have found it necessary to assume that halogen bonds are $s-p$ hybrids, with the amount of $s$ character varying with the ionicity of the bonds. The amount of $s$ character reaches a constant maximum value, however, for bonds whose ionicity exceeds a certain quantity. Therefore, in this discussion it will be assumed that all of the Cl bonds are $s-p$ hybrids with 18 percent $s$ character and that all of the Br bonds have 8 percent $s$ character. The presence of $d$ character in the hybrid halogen bonds is rather arbitrarily excluded.

Double bond structure, e.g., $H_3Si^- = Br^+$. In this structure it is assumed that the halogen contributes an $s-p$ hybrid orbital with 8 percent $s$ character to the sigma component of the double bond, and a pure $p$ orbital to the pi-component of the double bond. As a partial justification of this assumption, it should be noted that the promotional energy necessary for the hybrid sigma-bond is regained to some extent in greater bond strength due to an increase in the bond's overlap integral. This would not occur for the pi-component of the bond. If all three $p$ orbitals were filled equally, there would be no unbalanced electrons. Thus, if we represent

[25] C. H. Townes and B. P. Dailey, J. Chem. Phys. (to be published).

TABLE VI. Characters of $Y-X$ bonds on basis of nuclear quadrupole coupling.

| Structure | $eqQ$ (Mc/sec) | $CH_3Cl^{35}$ % weight | $eqQ$ | $SiH_3Cl^{35}$ % weight | $eqQ$ | $GeH_3Cl^{35}$ % weight | $eqQ$ |
|---|---|---|---|---|---|---|---|
| double bond | −44 | 0 | 0 | 29% | −13 | 15% | −6 |
| single bond | −92 | 82% | −75 | 34% | −27 | 44% | −40 |
| ionic bond | 0 | 18% | 0 | 37% | 0 | 43% | 0 |
| Total $eqQ$ (Mc/sec) | | | −75 | | −40 | | −46 |
| Dipole moment (Debye) | | 1.88 | | 1.30 | | 2.12 | |
| Electronegativity difference[27] | | 0.5 | | 1.2 | | 1.3 | |

| Structure | $eqQ$ (Mc/sec) | $CH_3Br^{79}$ % weight | $eqQ$ | $SiH_3Br^{79}$ % weight | $eqQ$ | $GeH_3Br^{79}$ % weight | $eqQ$ |
|---|---|---|---|---|---|---|---|
| double bond | 401 | 0 | 0 | 25% | 100 | 15% | 60 |
| single bond | 704 | 82% | 577 | 34% | 236 | 46% | 320 |
| ionic bond | 0 | 18% | 0 | 41% | 0 | 39% | 0 |
| Total $eqQ$ (Mc/sec) | | | 577 | | 336 | | 380 |
| Dipole moment | | 1.80 | | 1.32 | | | |
| Electronegativity difference | | 0.3 | | 1.0 | | 1.1 | |

the contribution of the three $p$ orbitals by $x$, $y$, and $z$, $x+y+z=0$. Since the two orbitals perpendicular to the bond give identical contributions, $x=y=-z/2$, so that a deficiency of one electron in a perpendicular orbital is equivalent to an excess of $\frac{1}{2}$ an electron along the bond axis. For the double bond with the hybrid sigma-component, the deficiency of electrons along the bond axis is therefore, for bromine, $(0.92-0.5=0.42)$. This must be multiplied by 1.25 to take into account the formal positive charge, which pulls the electrons closer to the nucleus.[17] Therefore, the correct figure for the hybrid bromine bond is 0.525. For the chlorine double bond whose sigma-component has 18 percent $s$ character, the correct figure is 0.40.

The analysis of the quadrupole coupling data is carried out as follows:

1. The value of $eqQ$ per unbalanced electron is taken as $-110.4$ Mc/sec[17] for $Cl^{35}$, and 765 Mc/sec[26] for $Br^{79}$. The values were determined from measurements on atomic chlorine and molecular bromine. In the case of bromine it was assumed that, as opposed to the case of iodine, the neighboring molecules in the solid have little effect on the value of $eqQ$.

2. The percent double bond character is obtained by use of Eq. (6), and the double bond contribution to $eqQ$ is determined.

3. The figure obtained in (2) is subtracted from the observed $eqQ$. This difference gives the contribution of the single bond structure to $eqQ$, since the ionic structure does not contribute. In this way the percent single covalent bond and ionic characters are obtained.

The results of this analysis are compared in Table VI with the dipole moments and electronegativity differences. The covalent radii and electronegativities used were taken from the work of Schomaker and Stevenson.[27] Some of the assumptions involved in this discussion are rather arbitrary so that the uncertainty of the values in Table VI is at least 5 percent.

In spite of this uncertainty certain conclusions seem to be definitely established by the data of Table VI. The double bond structure seems to play an important role in the silicon compounds, to be present to a considerably smaller extent in the germanium compounds, and to be completely absent in the methyl compounds. These results are in good agreement with Pauling's ideas[23] on the role of partial double bond character for the halogen compounds of elements beyond the first row of the periodic table. Carbon has no $d$ orbitals in its valence shell available for double bond formation. Germanium, as a third row element, would be expected to form double bonds with greater difficulty than silicon, a second row element. Sheridan and Gordy[28] have found similar effects in their study of trifluorosilane derivatives.

The reason for the failure to find a larger change in double bond and ionic character in going from Cl to Br compounds is not clear. It may be that the greater tendency of Cl to form double bonds is counter-balanced by the greater difficulty in removing an electron from Cl, due to its larger electronegativity. This electronegativity effect would favor greater double bond character for the Si than for the Ge compounds.

The bond distances of the central atoms to hydrogen are known accurately only for the methyl halides. However, for the methyl halides, and for the other molecules as well, these distances correspond, within the limits of experimental error, to the sum of the appropriate single bond covalent radii. The H−Y−H angles which are known with any semblance of accuracy are all approximately 111°. It would seem that this structural parameter is little affected by the use of $d$ orbitals for the bond to the halogen atoms or to changes in the ionicity or hybridization of this bond.

It is difficult to make deductions concerning bond

[26] J. Sheridan and W. Gordy, J. Chem. Phys. **19**, 965 (1951).
[27] V. Schomaker and D. P. Stevenson, J. Am. Chem. Soc. **63**, 37 (1941).
[28] J. Sheridan and W. Gordy, Phys. Rev. **77**, 719 (1950).

character from the observed value of the dipole moment. It has been shown by Robinson[29] that even in so simple a molecule as HCl the large contribution to the dipole moment by purely covalent structures and the sensitivity of this contribution to hybridization of bonding orbitals renders attempts at simple correlation of dipole moment and ionic character of doubtful value. *A fortiori*, attempts at detailed correlation of the dipole moment of a polyatomic molecule with properties of a bond in the molecule must be viewed with great scepticism. However, it seems likely that in a rough, qualitative fashion, the marked reduction in the dipole moment observed for the silicon compounds is a result of the importance of double bond structures for these molecules.

The authors are indebted to the Columbia Radiation Laboratory of the Physics Department for the use of the microwave spectrometer and other facilities, and to the members of that laboratory for much assistance. They wish especially to express their gratitude to Professor C. H. Townes for his valuable advice. One of the authors (J.M.M.) was aided in carrying out this work by a fellowship provided by the Eastman Kodak Company.

[29] D. Z. Robinson, J. Chem. Phys. **17**, 1022 (1949).

THE JOURNAL OF CHEMICAL PHYSICS VOLUME 20, NUMBER 11 NOVEMBER, 1952

# The Molecular Structure of Cyclobutane

J. D. DUNITZ* AND VERNER SCHOMAKER
*Gates and Crellin Laboratories of Chemistry,† California Institute of Technology, Pasadena, California*

(Received May 9, 1952)

The cyclobutane molecule has been found by electron diffraction to have the following bond distances and bond angles: C−C, $1.56_8 \pm 0.02$A; C−H, $1.09_6 \pm 0.04$A; ∠HCH, $114 \pm 8°$. On the average the ring is nonplanar, with dihedral angle 20° (+10°, −20°), but the equilibrium symmetry may be either $D_{2d}$ (puckered ring) or $D_{4h}$ (planar ring with low rigidity leading to large amplitude of out-of-plane bending). This point is discussed in connection with earlier spectroscopic work. The long bond distances found in four-membered rings are contrasted against the short distances in three-membered rings, and the strain energies, bond distances, and HCH angles of cycloalkanes are discussed in terms of modern valence concepts. It is suggested that the potential energy arising from a repulsion of the nonbonded carbon atoms may contribute significantly to the apparently anomalously high strain energy of cyclobutane. The repulsive force associated with such a potential is shown to account satisfactorily for the long C−C distances.

RECENT structure analyses of cyclobutane derivatives provide evidence that the carbon-carbon single bonds in 4-membered rings are longer than 1.54A, the standard distance. Reported values are 1.55 ±0.02A and 1.56±0.03A for methylenecyclobutane,[1,2] 1.56±0.05A for dimethyl ketene dimer,[3] 1.555 and 1.585 (both ±0.02A) for tetraphenylcyclobutane,[4] 1.60A for octafluorocyclobutane,[5] and 1.59A for octachlorocyclobutane;[6] in dinaphthylenecyclobutane[7] the distances projected onto a crystal plane are 1.56A and 1.60A. In tetraphenylcyclobutane and dinaphthylenecyclobutane the 4-membered ring is centrosymmetric and therefore planar, but in the octafluoro and octachloro derivatives the ring appears to be definitely puckered. We have undertaken the present electron diffraction investigation in order to determine the structure of the parent hydrocarbon cyclobutane.

## EXPERIMENTAL

Our sample was kindly supplied from the Chemical Laboratories of the University of California by Professor K. S. Pitzer, and the electron diffraction photographs were taken using the apparatus described by Brockway.[8] Visual examinations of the photographs were made by both of us, independently and also in consort, and we believe that the reduced intensity curve is represented by Fig. 1 (*V*) subject to certain modifications.[9]

The radical distribution curve (Fig. 1, *R*), calculated

* Present address: Laboratory of Chemical Crystallography, University Museum, Oxford, England.

† Contribution No. 1691.

[1] Shand, Schomaker, and Fischer, J. Am. Chem. Soc. **66**, 636 (1944).

[2] S. H. Bauer and J. Y. Beach, J. Am. Chem. Soc. **64**, 1142 (1942).

[3] W. N. Lipscomb and V. Schomaker, J. Chem. Phys. **14**, 475 (1946).

[4] J. D. Dunitz, Acta Cryst. **2**, 1 (1949).

[5] H. P. Lemaire and R. L. Livingston, J. Chem. Phys. **18**, 569 (1950).

[6] T. B. Owen and J. L. Hoard, Acta Cryst. **4**, 172 (1951).

[7] J. D. Dunitz, XIIth International Congress of Pure and Applied Chemistry, New York, 1951.

[8] L. O. Brockway, Revs. Modern Phys. **8**, 231 (1936). Camera distance, 10.95 cm. Wavelength, 0.06082 A, determined from ZnO photographs (C. S. Lu and E. W. Malmberg, Rev. Sci. Instr. **14**, 271 (1943): $a = 3.2492$ A, $c = 5.20353$ A). Corrections were made for film expansion.

[9] The curve is based on J. D. D.'s original interpretation of the photographs and was used for the radial distribution calculation. In showing the 3rd, 4th, 6th, and 7th maxima equally intense, it differs slightly from V. S.'s interpretation, which makes the 4th maximum slightly stronger and the 6th slightly weaker than the average of these features. It happens, also, that the nature of the fifth ring (shoulder) as indicated by both our original sketches is better represented by theoretical curves *B* and *D* than by *V*.

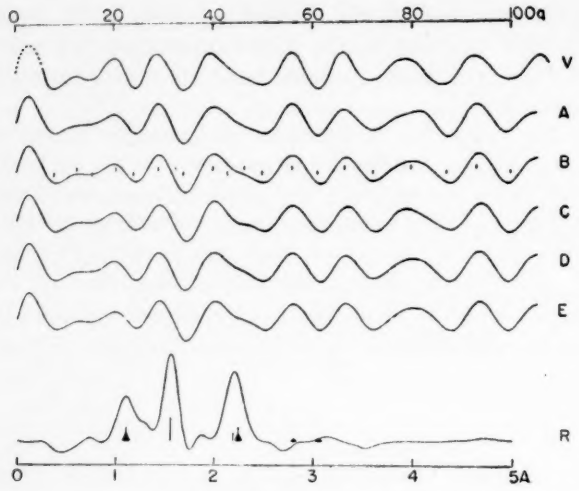


FIG. 1. Electron diffraction curves for cyclobutane, $C_4H_8$. *V*, visual curve. (The dotted portion is drawn in accordance with the theoretical curves.) *A–E*, theoretical curves.

| Model | C−C (A) | C−H (A) | ∠HCH (°) | Dihedral angle (°) |
|---|---|---|---|---|
| *A* | 1.56 | 1.10 | 116 | 0 |
| *B* | 1.56 | 1.10 | 116½ | 22 |
| *C* | 1.56 | 1.10 | 117 | 33 |
| *D* | 1.56 | 1.10 | 112 | 22 |
| *E* | 1.56 | 1.08 | 113½ | 22 |

*R*. Radial distribution curve from *V*.

with the equation[10,11]

$$rD(r)=\sum_{q=1,2\cdots}^{q\,\max} I(q)\exp(-aq^2)\sin\frac{\pi}{10}qr$$

with $\exp[-a(100)^2]=0.1$, has maxima at 1.11 A (C−H), 1.56 A (C−C), and 2.21 A (nonbonded C···C and shorter nonbonded C···H). No peaks corresponding to longer C···H distances appear.

The theoretical intensity curves were calculated with the simplified scattering formula[10]

$$I(q)=\sum_{i,j}\frac{Z_iZ_j}{r_{ij}}\exp(-b_{ij}q^2)\sin\left(\frac{\pi}{10}r_{ij}q\right)$$

with $b_{ij}$ equal to 0.00016 for bonded C−H, 0.0003 for unbonded C···H,[12] and zero for C−C and C···C terms. An effective value, 1.25, was taken for $Z_H$. All $H\cdots H$ terms were omitted.

Models of symmetry $D_{4h}$ were first examined over a reasonable range of the shape parameters, $\rho=1.56$ C−H/C−C and ∠HCH, but none was found completely satisfactory. Closest agreement with our observations is given by the model with $\rho=1.10$ and ∠HCH=116° (Curve *A*), which was chosen as starting point for models of the lower symmetry $D_{2d}$. For these, the local $C_{2v}$ symmetry of the $>CH_2$ groups was retained. A 22° dihedral angle between opposite triads of carbon atoms then leads to almost complete accord with our observations (Curve *B*); increase of the angle to 33° (Curve *C*) introduces certain disagreements, perhaps worse than those with angle 0°. Finally, the values of $\rho$ and ∠HCH were readjusted somewhat in accordance with a strict adherence to the fine details of our interpretation of the appearance of the photographs. Quantitative comparison of measured and calculated *q* values for three models which agree almost equally well with our observations leads (Table I) to the final parameter values and limits of error, $C-C=1.56_8\pm0.02$A, $C-H=1.09_6\pm0.04$A, ∠HCH=114±8°, and dihedral angle =20°(+10°, −20°).

Consideration of the frequency of the totally symmetric C−H stretching vibration in cyclobutane[13] (2937 $cm^{-1}$) together with the C−H distances and corresponding frequencies in methane[14] (1.093A, 2914 $cm^{-1}$) and ethane (1.102A,[15] 2899 $cm^{-1}$)[16] makes it unlikely that our estimate of the C−H distance in cyclobutane is actually in error by more than 0.01A. The assumption of this limit of error would reduce the uncertainty of the ∠HCH determination by about 2°.

Our result shows that the cyclobutane ring is nonplanar, but we are unable to distinguish between static nonplanarity (symmetry $D_{2d}$) and dynamic nonplanarity (symmetry $D_{4h}$ with large amplitude of out-of-plane ring bending.) Wilson,[13] on spectroscopic evidence, has assigned the symmetry $D_{4h}$ to the molecule and a frequency 145 $cm^{-1}$ to the out-of-plane bending vibration. With this frequency and the assumption of harmonicity we expect[17] a measurement of the root-mean-square dihedral angle to give a value of about 15°. Wilson, however, considered an incorrect point group ($C_{2v}$) for the nonplanar model so that his conclusions, although not inconsistent with the electron diffraction evidence, are questionable; the reported infrared and Raman frequencies appear to agree at least as well with $D_{2d}$ as with $D_{4h}$ selection rules. Further spectroscopic work is obviously required for the establishment of the correct molecular symmetry.

## DISCUSSION

The present analysis provides a further example of the lengthening of carbon-carbon bonds in four-mem-

[10] R. Spurr and V. Schomaker, J. Am. Chem. Soc. **64**, 2693 (1942).

[11] Shaffer, Schomaker, and Pauling, J. Chem. Phys. **14**, 659 (1946).

[12] Some additional curves were calculated with a larger value of $b_{ij}$ for the longer unbonded C···H terms, but the resulting changes were insignificant.

[13] T. P. Wilson, J. Chem. Phys. **11**, 369 (1943).

[14] D. M. Dennison, Revs. Modern Phys. **12**, 175 (1940).

[15] G. E. Hansen and D. M. Dennison, J. Chem. Phys. **20**, 313 (1952).

[16] G. Herzberg, *Molecular Spectra and Molecular Structure*, (D. Van Nostrand Company, Inc., New York, 1945), Vol. II, p. 345.

[17] In the expression $\overline{x^2}=h\coth(h\nu/2kT)/8\pi^2\mu\nu$ for the mean-square displacement of a harmonic oscillator, we have taken $\mu=17$ rather than $\mu=14$ for the system, composed of two pairs of $CH_2$ groups, to allow for the greater amplitude of the hydrogen atoms compared with carbon.

bered rings. The lengthening is all the more striking if these bond distances are compared not only with the standard value 1.54A but also with the short distances reported for three-membered rings. In cyclopropane, the C−C distance has been reported as 1.53±0.03A,[18] 1.54A,[19] and 1.515±0.02A;[20] in the highly strained spiropentane molecule[21] the average distance is 1.49 ±0.01A, the central bonds, subject to the greatest strain, being somewhat shorter than the peripheral bonds; 1.473A has been found for the C−C distance in ethylene oxide;[22] and in cyclopropene[23] the distances are 1.286±0.04A for the double bond, also shorter than normal, and 1.525±0.02A for the single bonds. The experimental evidence thus indicates that the C−C distance is lengthened in four-membered rings, but is shortened in three-membered rings. The HCH angles in these strained molecules are significantly larger than tetrahedral, the reported values being 114° for cyclobutane, 118°[19] and 116°[20] for cyclopropane, 117° for ethylene oxide, and 120° for spiropentane. (We shall not attempt to discuss the notably lesser widening, in corresponding substituted molecules, of peripheral bond angles HCX and XCX, with X not equal to H, from their normal values.) The empirical strain energies are, of course, also of interest, and recent values for theh eats of combustion of cyclopropane[24] (499.9 kcal mole$^{-1}$), cyclobutane[25] (655.8 kcal mole$^{-1}$), and cyclopentane and cyclohexane[26] (793.6 and 944.5 kcal mole$^{-1}$) lead to strain energies per $CH_2$ group (9.2, 6.5, 1.3, and zero kcal, respectively) somewhat different from those which have previously been discussed.

These and other effects of angle strain can be discussed in terms of modern valence theory, although mainly from a semi-empirical and often speculative, rather than fundamental, viewpoint. We shall now review this discussion briefly, adding some new elements and consciously emphasizing those which appear to be most directly pertinent to the C−C distances, HCH angles, and strain energies.

Kilpatrick and Spitzer[27] have treated the cycloalkanes, taking the C−C bond strength proportional to the product of the angular parts of the bonding orbitals in the bond direction (whether or not the orbitals point in this direction) and varying the hybridization ratio to maximize the product for the bond angle required by the geometry of the molecule, and Förster[28] and Coulson and Moffitt[29,30] have made related but much more elaborate quantum-mechanical considerations. And we have made calculations following the procedure described by Kilpatrick and Spitzer, except that simultaneous variation of the energy contributions $E_{CC}$ and $E_{CH}$ has been taken into account[31] on the assumption that they are given by $E_{ij}=S_iS_jE_{ij}^0/(S_iS_j)_{max}$, with $S_i$ the value of the angular part of the bonding orbital in the internuclear direction. For $E_{CC}^0$ and $E_{CH}^0$ we have rather arbitrarily used the values 57.6 and 87.3 kcal mole$^{-1}$.[32] These treatments lead to strain energies and HCH bond angles in rough agreement with the experimental values (Table II). Coulson and Moffitt,[30] furthermore, argue that the bond "bendings" which are involved may well lead to shortening of the C−C internuclear distances, but they have given no quantitative estimates of the effect. It appears that this argument might be expressed in terms of the significant existence of a bond line, to be distinguished from the internuclear (straight) line, which more or less follows a line of maximum density of the bonding electron dis-

TABLE I. Measured and calculated $q$ values.

| Max | Min | Curve $q_0$ | $B$ $q/q_0$ | $D$ $q/q_0$ | $E$ $q/q_0$ |
|---|---|---|---|---|---|
| | 1 | 7.60 | (1.039) | (1.053) | (1.053) |
| 1 | | 12.34 | (1.029) | (1.054) | (1.048) |
| | 2 | 15.31 | (0.980) | (0.947) | (0.947) |
| 2 | | 20.19 | (0.981) | (0.976) | (0.981) |
| | 3 | 23.75 | (1.021) | (1.019) | (1.021) |
| 3 | | 28.79 | 1.007 | 1.006 | 1.006 |
| | 4 | 33.89 | 1.012 | 1.008 | 1.009 |
| 4 | | 39.81 | 1.006 | 1.005 | 1.007 |
| | 5 | 42.78 | (1.017) | (1.028) | (1.028) |
| 5 | | 46.10 | (1.009) | (1.009) | (1.009) |
| | 6 | 49.74 | 1.005 | 1.003 | 1.008 |
| 6 | | 55.72 | 1.004 | 1.000 | 1.005 |
| | 7 | 60.91 | 1.009 | 1.008 | 1.006 |
| 7 | | 66.36 | 1.007 | 1.002 | 1.002 |
| | 8 | 72.05 | 1.001 | 0.999 | 0.999 |
| 8 | | 79.60 | 1.005 | 1.005 | 1.007 |
| | 9 | 86.84 | 1.008 | 1.005 | 1.008 |
| 9 | | 92.84 | 1.006 | 1.005 | 1.001 |
| | 10 | 99.59 | (0.996) | (0.995) | (0.994) |
| 10 | | 105.18 | (0.997) | (0.997) | (0.996) |
| Average, 11 features | | | 1.0064 | 1.0042 | 1.0053 |
| Average deviation | | | 0.0020 | 0.0023 | 0.0026 |

Scale factor: $\frac{1}{3}(1.0064+1.0042+1.0053)=1.0053$.

$C-C=1.56\times1.0053=1.568$A
$C-H=1.09\times1.0053=1.096$A

[18] L. Pauling and L. O. Brockway, J. Am. Chem. Soc. **59**, 1223 (1937).

[19] O. Bastiansen and O. Hassel, Tidsskr. Kemi Bergv. Met. **6**, 71 (1946). Dr. Bastiansen has informed us that 1.525 A is a more likely value on the basis of their work, in view of the exact position (1.535 A) of their radial distribution maximum and of a probable error of +0.6 percent in wavelength calibration.

[20] H. Pfeiffer, Ph.D. thesis, California Institute of Technology, 1948.

[21] Donohue, Humphrey, and Schomaker, J. Am. Chem. Soc. **67**, 332 (1945).

[22] Cunningham, Boyd, Gwinn, and LeVan, J. Chem. Phys. **17**, 211 (1949).

[23] Dunitz, Feldman, and Schomaker, J. Chem. Phys. **20**, 1708 (1952).

[24] J. W. Knowlton and F. D. Rossini, J. Research Natl. Bur. Standards **43**, 113 (1949).

[25] J. Coops and S. J. Kaarsemaker, Rec. trav. chim. **69**, 1364 (1950).

[26] R. Spitzer and H. M. Huffman, J. Am. Chem. Soc. **69**, 211 (1947).

[27] J. E. Kilpatrick and R. Spitzer, J. Chem. Phys. **14**, 463 (1946).

[28] T. Förster, Z. physik. Chem. (*B*) **43**, 58 (1939).

[29] C. A. Coulson and W. E. Moffitt, J. Chem. Phys. **15**, 151 (1947).

[30] C. A. Coulson and W. E. Moffitt, Phil. Mag. **40**, 7th series, 1 (1949).

[31] We are indebted to Professor Pauling for having drawn our attention to the improvement that can be obtained in this way.

[32] L. Pauling, *The Nature of the Chemical Bond* (Cornell University Press, Ithaca, New York 1939).

TABLE II. Observed and calculated values of HCH angles and strain energies (in kcal $(CH_2\ mole)^{-1}$) for cyclopropane and cyclobutane.

| | Cyclopropane | | Cyclobutane | |
|---|---|---|---|---|
| | ∠HCH | Strain energy | ∠HCH | Strain energy |
| Observed | 118° (reference 19)<br>116° (reference 20) | 9.2 | 114° | 6.5 |
| Kilpatrick and Spitzer | 122° | 8 | 115½° | 2 |
| Coulson and Moffitt (reference 29) | 113° | ... | ... | ... |
| Coulson and Moffitt (reference 30) | 116° | ~12 | 111° | ... |
| Förster | 119½° | ~35 | 113½° | 6.4 |
| Dunitz and Schomaker | 117° | 7.0 | 113° | 1.1 |

tribution, and which, in the bent bond, tends to retain a fixed length, thereby possibly causing the internuclear distance to be shortened in spite of the resulting increased internuclear repulsion. The ends of this line would presumably be tangent to the directions of the two bonding orbitals. Indeed, Copley[33] and Bernstein[34] have drawn attention to the remarkable fact that if the central bonds of ethylene and acetylene are regarded as extreme cases of bent bonds (formed by two and three $sp^3$ bonds, respectively), the internuclear distances are related to the ethane value as chord and arc of a circle ($d=d_0 \sin\theta/\theta$, where $\theta$ is the half-angle of strain). The agreement obtained for these extreme cases is surprising, but one could expect the relationship to hold for the comparatively small strain angles of the ring compounds, and Copley was able to show that it does hold for cyclopropane. Values obtained with this relationship, especially in slightly modified form, are in fact in good agreement (Table III) with the present experimental values, except, of course, for cyclobutane.

For Table III we have taken no account of any change in covalent radius which might occur purely as a result of rehybridization. Coulson's values of atomic radius as function of hybridization ratio[35] and Coulson and Moffitt's hybridization ratios[30] predict increases in C—C distance of about 0.01A for cyclobutane and 0.04A for cyclopropane. It is not clear whether this effect is really to be expected, and we shall ignore it in the remaining discussion. It may be noted, however, that the predicted magnitude is small enough to be essentially immaterial for cyclobutane and not out of the question for cyclopropane, since Table III need not be regarded as limiting for the amount of the characteristic bent bond shortening. For spiropentane, moreover, necessary retention of $sp^3$ hybridization at the central atom may well account for the shorter central bonds, by way of the absence of rehybridization change of radius or greater bent-bond shortening or both, while the forces due directly to the unequal effective bond angle strains must also contribute.

We believe that most of the lengthening of C—C bonds in four-membered rings, contrasted with the slight shortening to be expected from the bent bond concept, may well be an altogether different kind of effect, due to repulsion of nonbonded carbon atoms. The cross-ring distance in cyclobutane is only 2.22A and interaction of the non-bonded atoms may therefore be expected to be of some significance. In cyclopropane, on the other hand, each carbon atom is bonded to both others so that no interaction of this type exists; in cyclopentane, with the C—C—C angle close to tetrahedral, the interactions would be comparatively small although there are twice as many per $CH_2$ group as in cyclobutane.

Support for the existence of such a potential is given by the strain energies of the cycloalkanes if the magnitudes of the valence deformation energies are correctly indicated by Kilpatrick and Spitzer's, Coulson and Moffitt's, and our calculations, rather than by Förster's. This is illustrated by Fig. 2 (based on our calculation, which, we feel, may provide the best working formula in spite of its obvious deficiencies); with suitable corrections for torsional strain, good agreement is obtained for cyclopentane and cyclopropane but cyclobutane is 3.4 kcal $(CH_2\ mole)^{-1}$ more unstable than expected. Attributing this difference to repulsion of nonbonded carbon atoms we obtain $V_{C\cdots C}=6.8$ kcal mole$^{-1}$. Moreover, the force constant for CCC bond bending (dotted curve) is very much greater than would follow from valence deformation (full curve) alone and the difference can be attributed to a C···C repulsion representable by a quadratic potential with minimum at 109½° and amounting to about 5.4 kcal mole$^{-1}$ at 90°, in good agreement with the previous estimate.[36]

These values for the nonbond potential are in

TABLE III. Bond distances calculated with the relationship $d=1.542 \sin\theta/\theta$.[a]

| | $\theta$ | $d$ | $\theta'$ | $d'$ |
|---|---|---|---|---|
| Ethylene | 54°44′ | 1.318 | 50° | 1.353 |
| Acetylene | 70°32′ | 1.181 | ... | ... |
| Cyclopropane | 24°44′ | 1.495 | 22° | 1.504 |
| Cyclobutane | 9°44′ | 1.535 | 9° | 1.535 |

[a] The effective half-angle of strain $\theta'$ is given as corrected for rehybridization by Coulson and Moffitt (see reference 30).

[33] C. N. Copley, Chem. and Ind. 663 (1941).
[34] H. J. Bernstein, J. Chem. Phys. 15, 284 (1947).
[35] C. A. Coulson, Victor Henri Commemorative volume, *Contribution à l'Étude de la Structure Moléculaire* (Desoer, Liège, 1948), p. 15.

[36] That repulsive forces between nonbonded heavy atoms are not negligible compared with bond stretching or bond bending forces has been demonstrated by T. Simanouti, J. Chem. Phys. 17, 245, 734, 858 (1949). See also J. W. Linnett and D. F. Heath J. Chem. Phys. 19, 801 (1940); Trans. Faraday Soc. 44, 873, 878, 884 (1948); 45, 264 (1949). Although it has been inferred that the nonbonded H···H force constants in methane are negligibly small, Mulliken, in his recent treatment (reference 38) of bond energies, is led to expect them to be considerable. Moreover, a Kilpatrick, Spitzer, and Pauling calculation of the contribution of valence deformation to the force constants for methane leads to a very much too small value of the HCH bending constant, even though the observed vibrational potential function can be nicely represented as a pure-stretching, pure-bending function without interaction terms.

rough accordance with Pauling's relationship[37] $-\Delta R(n)=0.353 \log n$, which may be assumed to apply, at least for order of magnitude, to antibonding as well as bonding; for $\Delta R \sim 0.34$ (i.e., $(2.22-1.54)/2$) the relationship gives a bond number $n$ of about 0.1, as would correspond in the case of bonding to an energy of about 6 kcal mole$^{-1}$. For $\Delta R(n) \sim 0.5$ (tetrahedral CCC angle), the corresponding $n$ is about 0.04. Examination of the variation of Mulliken's overlap integrals[38] with interatomic distance shows that they also would lead to the same order of magnitude for the nonbond interaction.

We now estimate the stretching of the C—C bonds in cyclobutane due to C···C repulsion, by expressing the energy of the symmetrical molecule as

$$V(r_{CC})=V_0+k_1(R^0_{C\cdots C}-\sqrt{2}r_{CC})^2+2k_2(r_{CC}-r_{CC}{}^0)^2.$$

Here $R^0_{C\cdots C}$ is the C···C distance for tetrahedral angle (2.52A), $r_{CC}{}^0$ is 1.54A, and $k_1$ and $k_2$ are respectively the force constants for C···C repulsion and C—C stretching. The equilibrium condition is then

$$(r_{CC}-r_{CC}{}^0)=\frac{R^0_{C\cdots C}-\sqrt{2}r_{CC}{}^0}{\sqrt{2}}\cdot\frac{k_1}{k_1+k_2}=\frac{0.34}{\sqrt{2}}\cdot\frac{k_1}{k_1+k_2},$$

which on the assumption of $k_1=133$ kcal mole$^{-1}$ $A^{-2}$ (from $2V_1=12=k_1(0.30)^2$) and $k_2=5\times10^5$ erg cm$^{-2}$ $=715$ kcal mole$^{-1}$ $A^{-2}$ gives $(r_{CC}-r_{CC}{}^0)=0.038$ A, in pleasing agreement with the observed lengthening.

Following the above discussion the potential energy per $CH_2$ group as function of the dihedral angle of puckering can be expressed as

$$V'=V_0'-2V_1'(1-\cos 3\phi)+4V_2'(\theta)+k_1[R^0_{C\cdots C}-R_{C\cdots C}]^2,$$

where $V_1'$ is the torsional potential barrier,[39] $\phi$ the torsional angle, $4V_2'(\theta)$ the valence deformation energy corresponding to the CCC angle strain, and $k_1$ the repulsion force constant previously introduced. We find that the balance of these terms is so delicate at small dihedral angles as to make it impossible to predict whether the equilibrium configuration of the ring is planar or slightly nonplanar, and we await the results of future spectroscopic work with great interest. It may be noted that the total potential energy associated with the C—C torsions would presumably be a decreasing function of $r_{CC}$, at least for the opposed orientation, and so might contribute to the apparent stretching of C—C as discussed above, especially in the preceding paragraph. This effect is probably negligible, however, since cyclopentane, with its quite small bond-angle strains, shows normal or possibly even slightly shortened C—C distances, in spite of the predominantly opposed orientations[39] (see also the reference in the legend to Fig. 2) about the C—C bonds.

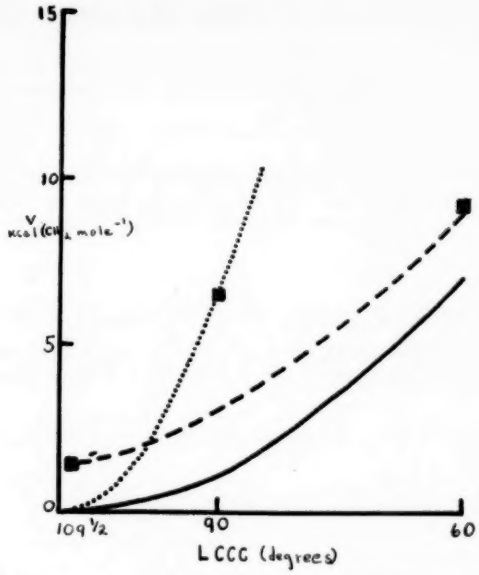


FIG. 2. Observed strain energies (in kcal ($CH_2$ mole)$^{-1}$) for cyclopropane, cyclobutane, and cyclopentane. Full curve: calculated valence deformation energy as function of CCC angle. Dashed curve: calculated valence deformation energy (full curve) plus estimated correction for torsional strain energy caused by opposition of adjacent $CH_2$ groups (see reference 39), of 2 kcal mole$^{-1}$ for cyclopropane and cyclobutane and 1.3 kcal mole$^{-1}$ (the total strain energy) for cyclopentane. The lower value for cyclopentane is appropriate because of ring puckering. Dotted curve: the quadratic potential $V=\frac{1}{2}k(\Delta\theta)^2$ with $k=8\times10^{-12}$ radian$^{-2}=35$ cal mole$^{-1}$ degree$^{-2}$ (Kilpatrick, Pitzer, and Spitzer, J. Am. Chem. Soc. **69**, 2683 (1947)).

[37] L. Pauling, J. Am. Chem. Soc. **69**, 542 (1947).
[38] R. S. Mulliken, J. Am. Chem. Soc. **72**, 4493 (1950).
[39] See K. S. Pitzer, Science **101**, 672 (1945).

# The Molecular Structure of Cyclopropene, $C_3C_4$

J. D. DUNITZ,* H. G. FELDMAN, AND VERNER SCHOMAKER
*Gates and Crellin Laboratories of Chemistry,† California Institute of Technology, Pasadena, California*
(Received May 9, 1952)

Cyclopropene, $C_3H_4$, has been investigated by the electron diffraction method. The cyclic structure is confirmed and the following interatomic distances and angles are found: C−C, $1.52_5$±0.02 A; C=C, $1.28_6$±0.04 A; ⟨C−H⟩, $1.08_7$±0.04 A; ∠H−C−H, 118° (assumed); ∠C=C−H, 152±12°.

SOME years ago, Dr. E. R. Buchman and Dr. M. J. Schlatter suggested that the structure of the unusual hydrocarbon cyclopropene,[1] $C_3H_4$, might be confirmed by electron diffraction investigation. We wish to report here on the interpretation of a set of electron diffraction photographs, prepared in 1940, of a sample of cyclopropene provided by them (see Table I).

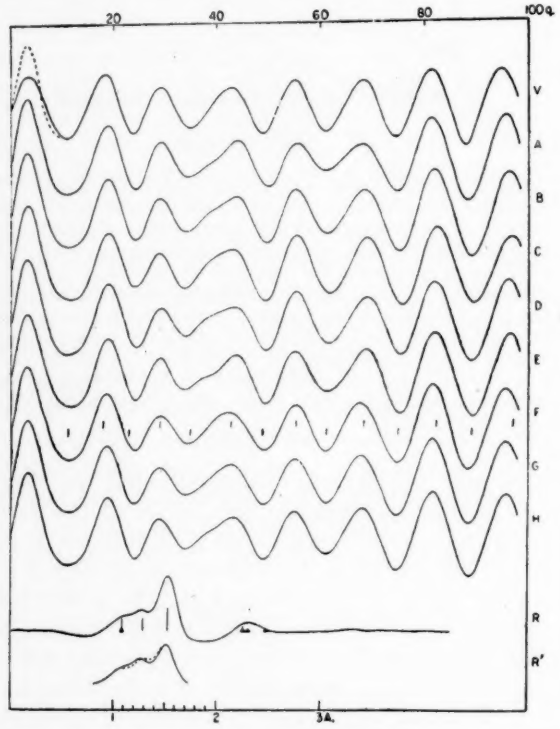


FIG. 1. Electron diffraction curves for cyclopropene, $C_3H_4$. *V*. Visual curve. (The full curve was used for calculation of *R*. The broken curve shows the first feature as given by the theoretical curves.) *A–H*. Theoretical curves.

| Model | C−C | C=C | ⟨C−H⟩ | ⟨C···H⟩ | ∠HCH° | ∠C=C−H° |
|---|---|---|---|---|---|---|
| *A* | 1.52 | 1.31 | 1.08 | 2.29 | | |
| *B* | 1.52 | 1.28 | 1.08 | 2.29 | | |
| *C* | 1.52 | 1.25 | 1.08 | 2.29 | | |
| *D* | 1.52 | 1.28 | 1.11 | 2.29 | | |
| *E* | 1.52 | 1.28 | 1.08 | 2.32 | | |
| *F* | 1.53 | 1.29 | 1.09 | | 118 | 147.5 |
| *G* | 1.53 | 1.29 | 1.09 | | 118 | 157.5 |
| *H* | 1.53 | 1.29 | 1.09 | | 118 | 167.5 |

*R*. Radial distribution curve from *V*. *R'*. Synthesis of portion of *R* as sum of Gaussian curves. C−C, 1.52 A, ⟨C−H⟩, 1.08 A, C=C, 1.28 A (full line). C−C, 1.52 A, ⟨C−H⟩, 1.08 A, C=C, 1.30 A (broken line).

The structure is confirmed by the radial distribution curve[2] of Fig. 1, particularly by the absence of any strong peak past 2.5 A. The peak extending from 0.9 to 1.7 A is, moreover, evidently composed of C−C, C=C, and C−H interactions in about the correct proportions. The C−C distance is obviously close to 1.53 A, but the other two interactions are not resolved. On the assumption of C−C=1.52 A and C−H=1.08 A, analysis of the composite peak in terms of three Gaussian curves of appropriate heights and widths leads to C=C=1.29 A.

For the correlation treatment the molecule was assumed to have symmetry $C_{2v}$, with all bonded C−H distances equal. For the initial models, further, the three nonbonded C···H distances were represented by a single suitably temperature-factored term. Systematic variation of the remaining shape parameters (⟨C−H⟩/C−C, C=C/C−C, and ⟨C···H⟩/C−C) showed curve *B* to be the best of this type. Splitting the

TABLE I. Observed and calculated *q* values.

| Model Max | Model Min | $q_0$ | *F* $q/q_0$ | *G* $q/q_0$ |
|---|---|---|---|---|
| | 1 | 10.95 | (1.050) | (1.050) |
| 1 | | 17.9 | (1.039) | (1.045) |
| | 2 | 22.8 | (1.053) | (1.053) |
| 2 | | 28.95 | 1.002 | 0.998 |
| | 3 | 34.8 | 0.991 | 0.980 |
| 3 | | 42.6 | 0.986 | 1.000 |
| | 4 | 48.7 | 1.010 | 1.006 |
| 4 | | 55.2 | 1.002 | 0.996 |
| | 5 | 61.0 | 1.000 | 1.002 |
| 5 | | 68.2 | 0.990 | 0.991 |
| | 6 | 74.8 | 0.999 | 0.997 |
| 6 | | 82.15 | (0.992) | (0.992) |
| | 7 | 88.95 | (0.994) | (0.995) |
| 7 | | 96.95 | (0.985) | (0.985) |
| Mean, 8 features | | | 0.9975 | 0.9962 |
| Mean deviation | | | 0.006 | 0.006 |

C−C, 1.52 ×0.9968 = 1.525
C=C, 1.29 ×0.9968 = 1.286
C−H, 1.09 ×0.9968 = 1.087

* Present address: Laboratory of Chemical Crystallography, University Museum, Oxford, England.
† Contribution No. 1690.
[1] For method of preparation and earlier references see M. J. Schlatter, J. Am. Chem. Soc. **63**, 1733 (1941).
[2] For experimental procedures and methods of calculation see J. D. Dunitz and V. Schomaker, J. Chem. Phys. **20**, 1703 (1952).

nonbonded C···H distances then led to completely satisfactory agreement (curves $F$ and $G$). Our final parameter values and limits of error are: C−C, $1.52_5 \pm 0.02$ A; C=C, $1.28_6 \pm 0.04$ A; (∠C−C−C, 49.9°); ⟨C−H⟩, $1.08_7 \pm 0.04$ A; ∠H−C−H, 118° (assumed: ∠C−C−H = ∠H−C−H); and ∠C=C−H, $152 \pm 12$°.

The single bonds appear to be shortened, as in other three-membered rings,[3,4,5] and it is interesting that the double bond is even more shortened.

[3] H. G. Pfeiffer, Ph.D. thesis, California Institute of Technology, 1948.
[4] Cunningham, Boyd, Gwinn, and LeVan, J. Chem. Phys. **17**, 211 (1949).
[5] Donohue, Humphrey, and Schomaker, J. Am. Chem. Soc. **67**, 332 (1945).

THE JOURNAL OF CHEMICAL PHYSICS VOLUME 20, NUMBER 11 NOVEMBER, 1952

# The Asymmetric Rotor. X. The Hydrogen Sulfide Spectrum in the 5150 cm$^{-1}$ Region*

HARRY C. ALLEN, JR.,† AND PAUL C. CROSS
*Department of Chemistry and Chemical Engineering, University of Washington, Seattle, Washington*

AND

M. K. WILSON
*Department of Chemistry, Harvard University, Cambridge, Massachusetts*

(Received June 3, 1952)

The absorption spectrum of hydrogen sulfide in the region from 5000 to 5250 cm$^{-1}$ has been measured and the rotational fine structure analyzed. The structure can be accounted for as arising from two vibrational transitions yielding a type $A$ band centered at 5147 cm$^{-1}$ and a type $B$ band centered at 5145 cm$^{-1}$. The excited state constants giving the best fit are type $A$ band, $A^*=10.04$, $B^*=8.68$, $C^*=4.61$ cm$^{-1}$; type $B$ band, $A^*=10.08$, $B^*=8.68$, $C^*=4.59$ cm$^{-1}$.

The frequencies and rotational band types indicate that these bands are the $(n_\sigma, n_\pi, n_\delta)=(110)$ (type $A$) and the lower component of the resonating pair (020) (200) (type $B$).

## INTRODUCTION

THE infrared band system of hydrogen sulfide has recently been fitted to a self-consistent scheme,[1] a clue to the nature of which was the recognition of the absorption in the 5150 cm$^{-1}$ region as too complex to be assigned to a single vibrational transition. The analysis of the rotational fine structure of this region was undertaken to provide precise values of the frequencies of the two vibrational transitions assumed to be present and to obtain the inertial parameters of the excited states.

The experimental data presented in Fig. 1 and Table I were obtained under the same conditions used for recording the absorption in the 6290 cm$^{-1}$ region.[2] The

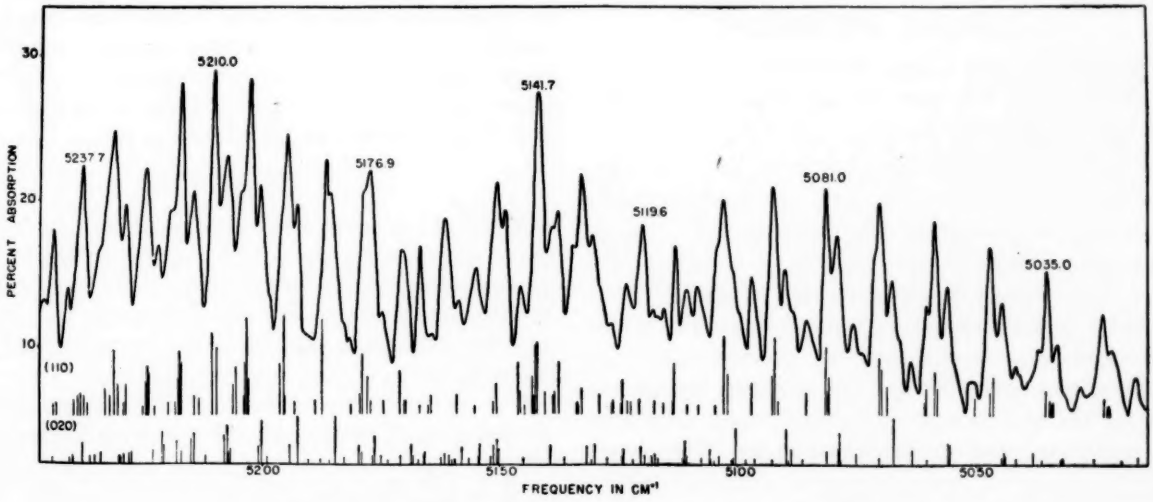


FIG. 1. Calculated and observed spectrum in the 5146 cm$^{-1}$ region.

* The work reported herein was supported in part by the ONR under Contract N8onr 52010.
† Now at the Chemistry Department, Harvard University.
[1] Allen, Cross, and King, J. Chem. Phys. **18**, 1412 (1950).
[2] Allen, Cross, and Wilson, J. Chem. Phys. **18**, 691 (1950).

TABLE I. Absorption frequencies of the $H_2S$ spectrum in the 5150 $cm^{-1}$ region. Frequencies labeled *S* are unresolved shoulders.

| Frequency $cm^{-1}$ | Frequency $cm^{-1}$ | Frequency $cm^{-1}$ | Frequency $cm^{-1}$ |
|---|---|---|---|
| 5268.8 | 5194.5 | 5123.0 | 5058.2 |
| 5263.6 | 5192.3 | 5119.6 | 5055.6 |
| 5260.0 | 5186.3 | 5117.2 | 5050.8 |
| 5257.3 | 5185.3 | 5114.9 | 5046.6 |
| 5255.3 | 5182.5 *S* | 5112.6 | 5044.2 |
| 5251.6 *S* | 5181.2 | 5110.2 | 5041.3 |
| 5249.6 | 5178.3 *S* | 5108.0 | 5036.8 *S* |
| 5245.9 | 5176.9 | 5103.6 *S* | 5035.0 |
| 5243.9 | 5174.2 | 5102.5 | 5032.6 |
| 5240.7 | 5170.1 | 5100.6 *S* | 5027.7 |
| 5237.7 | 5166.3 | 5099.0 *S* | 5023.3 |
| 5233.8 *S* | 5163.8 | 5096.6 | 5021.3 |
| 5231.2 | 5161.0 | 5092.1 | 5016.5 |
| 5228.6 | 5158.0 | 5089.6 | 5011.0 |
| 5224.3 | 5154.4 | 5087.9 *S* | 5007.6 |
| 5221.6 | 5150.2 | 5085.0 | 5004.1 |
| 5218.9 *S* | 5148.4 | 5081.0 | 4995.8 |
| 5217.0 | 5145.1 | 5078.6 | 4992.4 |
| 5214.2 | 5141.7 | 5075.1 | 4988.5 |
| 5210.0 | 5138.4 *S* | 5073.0 *S* | 4985.4 |
| 5207.0 | 5137.3 | 5070.7 *S* | 4980.4 |
| 5203.9 *S* | 5134.2 | 5069.7 | 4972.0 |
| 5202.4 | 5132.5 | 5067.1 | 4964.2 |
| 5200.1 | 5130.0 | 5065.7 *S* | |
| 5198.1 *S* | 5128.5 *S* | 5063.2 | |
| | 5125.9 | 5060.0 | |

absorption shows what appear to be well-defined *P*, *Q*, and *R* branches. A closer examination reveals that each strong peak in the *P* and *R* branches is accompanied by a satellite displaced about 3 $cm^{-1}$ to its low frequency side. This spacing is fairly constant throughout the *P* and *R* branches. Such a pattern is not compatible with the type of rotational fine structure possible for one band of an asymmetric rotor such as $H_2S$. The satellites were therefore interpreted as the *P* and *R* branches of a second, weaker band.

## VIBRATIONAL ASSIGNMENTS

The appearance of a collected *Q* branch indicates that one of the bands is a type *A* band. This fact, together with the magnitude of the frequency, indicates that the most likely vibrational assignment is $(n_\sigma, n_\pi, n_\delta) = (110)$.

There is no other combination which would normally be centered in this region. However, the pair of bands (020) and (200) were estimated to be at about 5200 $cm^{-1}$. These bands fit the condition for the Darling-Dennison type of resonance; and the magnitude of the interaction parameter $|\gamma| \simeq 47$ $cm^{-1}$, as estimated from the resonating pair (130) (310),[3,4] provided an explanation for the presence of the second band. It will be convenient to refer to this band as the (020) band, although it must be remembered that this is not strictly true. Both bands of this pair are type *B*.

## ANALYSIS

As in the cases of the 6290 and 1183 $cm^{-1}$ bands[2,5] the resolution was not adequate to enable the assignment of specific transitions through the use of known ground-state energies;[3] hence, the previously described method of analysis was used.[2]

An initial estimate of the excited state inertial constants was required. This was readily obtained through use of the expressions for the linear expansions of the moments of inertia in terms of the vibrational quantum numbers.[6] The inertial constants for the (020) band derived in this manner were averaged as described by Darling and Dennison[7] to allow for the effect of the resonance interaction. The effect of a possible Coriolis interaction on the inertial parameters was shown to be negligible.[6]

The values of $C^*$ for the two bands as deduced in this manner were found, with but slight change, to fix the band centers and to give an excellent fit to the main wings of the *P* and *R* branches of both bands.

It was necessary to modify the predicted value of $A^*$ for the (110) band in order to account for the collected *Q* branch. It was possible to vary the other three inertial constants, i.e., $B^*$ of the (110) band and $A^*$ and $B^*$ of the (020) band, over a considerable range without materially affecting the fit. Thus, in the final calculations the predicted values of these constants were used. The constants giving the fit shown in Fig. 1 are

(110) band
$A^* = 10.04$ $cm^{-1}$ $B^* = 8.68$ $C^* = 4.61$ $\nu_0 = 5147$ $cm^{-1}$,
(020) band
$A^* = 10.08$ $cm^{-1}$ $B^* = 8.68$ $C^* = 4.59$ $\nu_0 = 5145$ $cm^{-1}$.

In presenting the calculated bands the previously described intensity scale was used.[2] In order to include a rough estimate of the relative importance of the two bands the intensities of the transitions of the (020) band have been scaled down by a factor of two.

## CONCLUSION

Three of the six excited state constants ($A_{110}^*$, $C_{110}^*$, $C_{020}^*$) were determined with a fair degree of precision. The remaining inertial parameters could be varied by as much as 0.03 $cm^{-1}$ without destroying the general agreement between the calculated spectrum and that observed.

The authors wish to express their appreciation to Professor R. M. Badger for the use of his spectrograph.

[3] P. C. Cross, Phys. Rev. **47**, 7 (1935).
[4] Grady, Cross, and King, Phys. Rev. **75**, 1450 (1949).
[5] H. C. Allen and P. C. Cross, J. Chem. Phys. **19**, 140 (1951).
[6] H. C. Allen, thesis, University of Washington, 1951.
[7] B. T. Darling and D. M. Dennison, Phys. Rev. **57**, 128 (1940).

# Diffusion of Acetone into Polyvinyl Acetate above and below the Second-Order Transition

R. J. KOKES, F. A. LONG, AND J. L. HOARD
*Department of Chemistry, Cornell University, Ithaca, New York*

(Received March 17, 1952)

The sorption kinetics for the system polyvinyl acetate-acetone have been investigated both above and below 30°C, the second-order transition temperature for the pure polymer. At 30, 40, and 50°C, the diffusion obeys Fick's law with a concentration-dependent diffusion coefficient. With increasing acetone concentration the value of the diffusion coefficient increases strongly, and the energy of activation for diffusion decreases. At each temperature below 30°C, diffusion is Fickian only for sorption and desorption experiments where the solvent concentration is above a certain critical value. It was found, by comparison with the results of volume-temperature measurements on the system polyvinyl acetate-acetonyl acetone, that the temperature corresponding to a given critical concentration is the second-order transition temperature for this polymer-solvent mixture. Evidently, the changes which occur at the second-order transition have a pronounced influence on the diffusion process.

SEVERAL investigations of kinetics of vapor sorption by polymer films have been carried out recently.[1–4] Usually, it is assumed that diffusion is the rate controlling process and that the sorption kinetics can be represented by Fick's law,

$$\frac{\partial c}{\partial t}=\frac{\partial}{\partial x}\left\{D\frac{\partial c}{\partial x}\right\}, \tag{1}$$

where $D$ is the diffusion coefficient and $c$ is the concentration at a time $t$, a distance $x$ from the film surface. For sorption into a film of thickness $l$ the boundary conditions are

$$c(0, t)=c(l, t)=c_f, \qquad c(x, 0)=c_i, \tag{2}$$

where $c_i$ and $c_f$ are the initial and final equilibrium concentrations of vapor in polymer.

In general, for polymer-small molecule systems the diffusion coefficient is a strong function of concentration. Under these conditions Eq. (1) has not been solved analytically. However, for the initial sorption, i.e., until the concentration at the film center changes appreciably, the "infinite solid" approximation is appropriate. For an infinite solid Boltzmann's substitution yields an explicit equation for the amount of vapor taken up by the film,

$$\Delta Q_t/\Delta Q_\infty=K(c_i, c_f)t^{\frac{1}{2}}/l, \tag{3}$$

where $\Delta Q_t$ is the weight of vapor sorbed (or desorbed) from time $t=0$ to $t$, $\Delta Q_\infty$ is the equilibrium weight change, and $K(c_i, c_f)$ is a constant for fixed values of $c_i$ and $c_f$, i.e., for a given experiment. It will be seen later that $K(c_i, c_f)$ represents an *effective* diffusion coefficient, and if its concentration dependence is known $D$ may be evaluated.

It follows from Eq. (3) that $Q_t$ must be initially linear in $t^{\frac{1}{2}}$ unless $D$ is a function of variables other than $c$. It may also be shown from Eqs. (1) and (2) that $Q$ *vs* $t$ plots must have no inflection points at any time if $D(c)$ is always positive.[5] In the subsequent discussion sorption kinetics which do not satisfy both the above conditions will be denoted as non-Fickian. It is obvious that such kinetics will be observed only if $D$ is a function of variables other than $c$ or if the above boundary conditions are not appropriate.

The complexity of the sorption kinetics observed with polymers depends to a large extent on the systems chosen for examination. For example, Prager and Long[4] have shown that for polyisobutylene-hydrocarbon systems, $Q$ *vs* $t$ plots show no inflection and $Q$ *vs* $t^{\frac{1}{2}}$ plots are initially linear; consequently, the diffusion processes are Fickian. However, this is not always the case. $Q$ *vs* $t$ plots for the sorption of acetone by cellulose nitrate[6] or cellulose acetate[3] have inflection points, and $Q$ *vs* $t^{\frac{1}{2}}$ plots for the system polystyrene-methylene chloride[2] have initially increasing slopes. Therefore, sorption kinetics for these systems are non-Fickian. Many suggestions have been made regarding the nature of diffusion processes which would give rise to a diffusion coefficient which is a function of variables other than $c$; these suggestions, however, are for the most part speculative.

It appears from the available data, that non-Fickian diffusion is observed only when investigations are carried out below the second-order transition temperature $T_g{}^0$ of the pure polymer. For this reason and since many physical properties of polymers are strikingly different above and below $T_g$, it is of interest to investigate the effect of the second-order transition on diffusion processes. In this paper the sorption kinetics for the system polyvinyl acetate-acetone have been investigated both above and below the second-order transition temperature of the pure polymer (30°C). Furthermore, in order to interpret the data observed below 30°C, the concentration dependence of the second-order transition temperature for the system polyvinyl acetate-acetonyl acetone has been determined dilatometrically.

[1] G. S. Park, Trans. Faraday Soc. **46**, 684 (1950).
[2] (a) G. S. Park, Trans. Faraday Soc. **48**, 11 (1952); (b) J. Crank and G. S. Park, Trans. Faraday Soc. **47**, 1072 (1951).
[3] Leo Mandelkern and F. A. Long, J. Polymer Sci. **6**, 457 (1951).
[4] S. Prager and F. A. Long, J. Am. Chem. Soc. **73**, 4072 (1951).
[5] S. Prager, doctoral thesis, Cornell University, 1951.
[6] P. D. Drechsel (unpublished data).

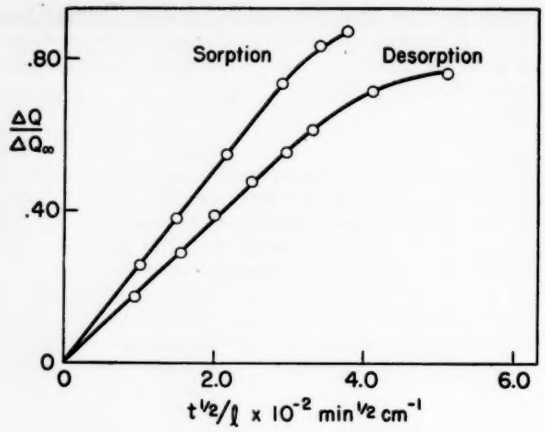


FIG. 1. Interval sorption and desorption results at 40°C; $P_i = 151$ mm, $P_f = 189$ mm.

## EXPERIMENTAL

Polyvinyl acetate of commercial grade, AYAT, was obtained from Carbide and Carbon Chemicals Corporation. The unfractionated material had a viscosity average molecular weight, using the formula of Wagner,[7] of 170,000. Both acetone and acetonyl acetone were of reagent grade and were dried over Drierite. The acetonyl acetone was vacuum distilled prior to use.

Polymer films were cast from acetone solutions on a mercury surface in a vacuum desiccator. The films were air dried and then leached with water or methanol vapor. It was found that after removal of the leaching vapor no detectable amount of casting solvent remained. For sorption experiments a segment of known area was cut from the film prepared as above. The thickness of the films, as calculated from the weight and the density, varied from 0.001 to 0.015 cm depending on their intended use. Sorption experiments were carried out in an apparatus similar to that described by Prager and Long.[4]

Two different experimental procedures were employed. These will be designated as *integral* and *interval* experiments. In *integral* sorption experiments the pure dried polymer film was suspended from a quartz spring in an evacuated chamber; then acetone was admitted at a given pressure, and the increase in weight due to vapor sorption was measured by observing the spring extension as a function of time; when equilibrium was attained, the chamber was evacuated and the kinetics of desorption back to zero pressure were observed. In *interval* experiments the film was initially equilibrated with the vapor at a pressure $P_i$. The pressure was then suddenly increased to $P_f$, and sorption kinetics were measured. After equilibrium was attained, the pressure $P_f$ was suddenly reduced to $P_i$, and the resulting desorption process was observed.

The specific volume for the system polyvinyl acetate-acetonyl acetone was determined as a function of temperature using the dilatometric techniques described by Mandelkern and Flory.[8] Absolute values of the specific volume as well as the volume fractions were computed assuming no volume change on mixing. Above 5°C all measurements were made in a constant temperature bath regulated to ±0.1°C. At 5°C and below, temperatures were constant to ±0.5°C. Homogeneous polymer-diluent samples were obtained by a procedure similar to that used by Flory, Mandelkern, and Hall.[9] In the present investigation the prolonged heating (at 200°C) during the sample preparation resulted in a weight loss even for pure polyvinyl acetate; consequently, a correction was required in calculating the composition of polymer-diluent mixtures. Since the weight loss for pure polymer was only about 1 percent of the initial weight, this correction was quite small.

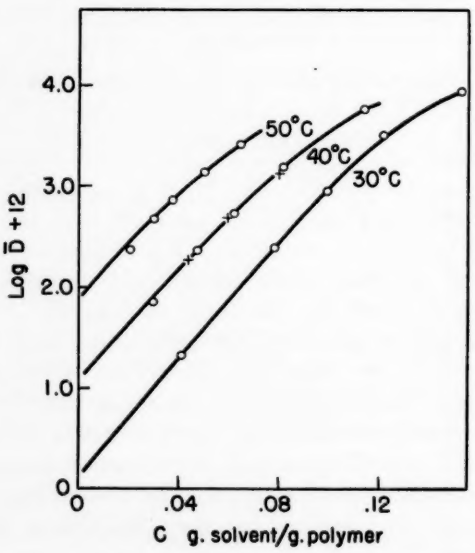


FIG. 2. Integral diffusion coefficient as a function of concentration and temperature. ○—from Eq. 6; + from Eq. 5.

[7] R. H. Wagner, J. Polymer Sci. **2**, 21 (1947).

## CALCULATIONS

If the sorption kinetics satisfy both conditions for Fickian diffusion, $D$ may be determined from the experimental data even if it is a function of concentration. If $D$ is independent of concentration, then for *integral* sorption measurements

$$D = \pi/16K_s^2(0, c) = \pi/16K_d^2(c, 0), \tag{4}$$

where $K$ is defined by Eq. (3) and the subscripts $s$ and $d$ indicate sorption and desorption. The calculations when $D$ is a function of $c$ are more complicated. Numerical solutions for calculating $D$ from Eq. (1) are available,[10,11] but since they are rather tedious we have made use of an empirical equation suggested by Crank and co-workers.[11] Their equation reduces to

$$\bar{D} = \pi/32[K_s^2(0, c) + K_d^2(c, 0)], \tag{5}$$

where $\bar{D}$, the integral diffusion coefficient is defined by

$$\bar{D} \equiv \frac{1}{c}\int_0^c D dc. \tag{5a}$$

It is obvious from (4) that Eq. (5) becomes exact for $D$ constant. Consequently, when $D$ is a function of $c$, Eq. (5) should hold best over concentration intervals where $D$ varies little. On this basis, a better approximation to $\bar{D}$ should be obtained from sorption experiments over small intervals. For such *interval* experiments the following modification of Eq. (5) can be employed:

$$\bar{D}(c_f) = \frac{c_i\bar{D}(c_i) + (c_f - c_i)\pi/32[K_s^2(c_i, c_f) + K_d^2(c_f, c_i)]}{c_f}. \tag{6}$$

[8] L. Mandelkern and P. J. Flory, J. Am. Chem. Soc. **73**, 3206 (1951).

[9] Flory, Mandelkern, and Hall, J. Am. Chem. Soc. **73**, 2352 (1951).

[10] S. Prager, J. Chem. Phys. **19**, 537 (1951).

[11] J. Crank and G. S. Park, Trans. Faraday Soc. **45**, 240 (1949).

We have used both Eqs. (5) and (6), the former for *integral* experiments and the latter for *interval* experiments. Values of $\bar{D}$ evaluated by either procedure agree within experimental error, indicating that for this system both equations are equally good.

Equations (5) and (6) are independent of concentration units, and we have actually employed the units grams solvent per gram of polymer. Actually these equations include an assumption implicit in Eq. (2), namely, that there is negligible swelling during sorption. At higher concentrations this is a poor approximation, and a correction must be made to obtain accurate values for the diffusion coefficients. Hartley and Crank[12] have derived a quantitative relation between the $D$ calculated assuming no swelling occurs (i.e., from Eq. (5) and (6)) and the true diffusion coefficients. For comparison with other data their relation is extremely useful; however, since this correction does not alter the results in a qualitative fashion, we have ignored it in our calculations. Furthermore, since $D$ may be easily evaluated from $\bar{D}$ by the use of the definition in Eq. (5a), we have only reported values of $\bar{D}$.

## RESULTS AND DISCUSSION

Sorption and desorption experiments have been made at six temperatures, 50°, 40°, 30°, 20°, 13°, and 8°C. The first three of these are above $T_g^0$, the second-order transition temperature for the pure polymer (30°C), and the last three are below. Data for a typical *interval* experiment in the higher temperature range are shown in Fig. 1 which gives plots of $\Delta Q_t/\Delta Q_\infty$ *versus* $t^{\frac{1}{2}}/l$ for both sorption and desorption at 40°C. In this case, and for all similar interval experiments made at temperatures of 30° or higher, the initial slopes of $t^{\frac{1}{2}}$ plots are linear. Similar results are obtained for all *integral* experiments, i.e., where $P_i$ is zero, again if the temperature is 30° or higher. This linearity of the $Q_t$ *versus* $t^{\frac{1}{2}}$ plots, and the further fact that in no cases do the $Q$ *versus* $t$ plots show inflections, indicates that the diffusion at these temperatures is Fickian. Since this is so, values of $\bar{D}$ can be calculated using either Eqs. (5) or (6). The results of such calculations are shown in Fig. 2 where values of $\log\bar{D}$ are given as a function of solvent concentration for the temperatures 30°, 40°, and 50°. Values of $\bar{D}$ calculated by Eqs. (5) and (6) agree closely, and reproducibility from film to film is good.

For each temperature, $\bar{D}$ is a strong function of concentration; at 30° it increases by a factor of almost $10^4$ for a change in solvent concentration from zero to 15 grams per 100 grams of polymer. For small solvent concentrations the plots of Fig. 2 are linear. Hence, for low concentrations we can write

$$\bar{D}=\bar{D}_0 e^{\alpha c}, \tag{7}$$

where $c$ is the weight ratio of solvent to polymer and $\alpha$ is a constant. This relation has been observed to hold for other polymer-small molecule systems,[1,4] and attempts have been made to place it on a semiquantitative basis by application of the hole theory of diffusion.[4]

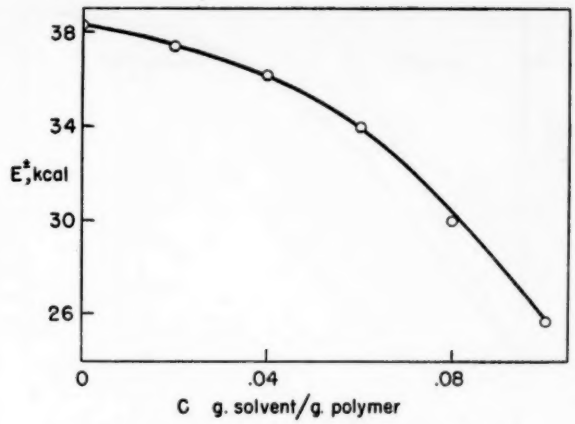


FIG. 3. Activation energy for diffusion as a function of concentration.

For the sake of comparison with other diffusion data it is occasionally useful to evaluate $D$ from the data of Fig. 2. This may be done by the use of the equation

$$d(c\bar{D})/dc=D, \tag{8}$$

or when (7) holds,

$$D=\bar{D}(1+\alpha c). \tag{9}$$

Thus $D$ has the same value as $\bar{D}$ for diffusion into pure polymer, but increases more rapidly with concentration. Experimentally, plots of $\log D$ *vs* $c$ are not linear even at low concentrations.

For a given concentration the values of $\bar{D}$ at the three temperatures, 30°, 40°, and 50°, are well fitted by an Arrhenius equation of the type

$$\bar{D}=Ae^{-E^{\pm}/RT}, \tag{10}$$

in which $A$ and $E^{\pm}$ are functions of $c$ alone. The experimental values of $E^{\pm}$ decrease considerably with concentration as may be seen in Fig. 3. The value of $E^{\pm}$ is 38.3 kcal for the pure polymer and 25.6 kcal at $c=0.10$. This

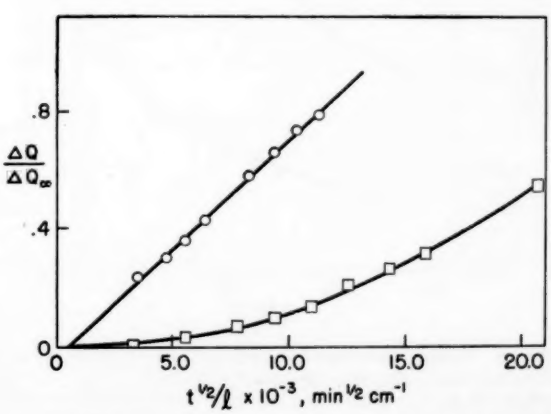


FIG. 4. Interval sorption experiments at 13°C. ○—$P_i=28$ mm, $P_f=41$ mm; □—$P_i=21$ mm, $P_f=35$ mm.

[12] G. S. Hartley and J. Crank, Trans. Faraday Soc. **45**, 801 (1949).

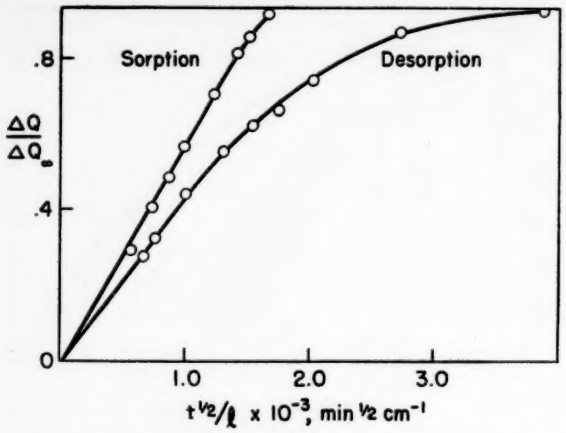


FIG. 5. Interval sorption and desorption results above critical concentration at 20°C. $P_i = 60$ mm, $P_f = 74$ mm.

decrease of $E^{\pm}$ with concentration is in agreement with the notion that $E^{\pm}$ corresponds to the energy required for hole formation in the polymer. As might be expected, the values of $E^{\pm}$ for this polar system are considerably greater than those found for the nonpolar polyisobutylene-hydrocarbon systems.[13]

Below 30°, the second-order transition temperature for the pure polymer, the sorption kinetics are no longer always Fickian. Illustrative $\Delta Q_t/\Delta Q_\infty$ *vs* $t^{\frac{1}{2}}/l$ plots for *interval* sorption experiments at 13°C are shown in Fig. 4. The sorption plot for the lower initial pressure shows an increasing slope with time, whereas that for the higher initial pressure is linear with time. More detailed investigations at each temperature (20°, 13°, and 8°C) show that for interval experiments where $P_i$, the initial pressure, is less than a certain critical pressure $P_c$, the $\Delta Q_t/\Delta Q_\infty$ *vs* $t^{\frac{1}{2}}/l$ plots have initially increasing slopes, indicating that non-Fickian diffusion is taking place. On the other hand, if experiments are carried out over pressure intervals wholly above $P_c$, initially linear plots characteristic of Fickian diffusion are obtained for both sorption and desorption (Fig. 5).* This critical pressure $P_c$, which determines whether the diffusion is Fickian or not, has been evaluated as a function of temperature by a detailed investigation of sorption kinetics in overlapping pressure intervals. These results are summarized in Table I, which shows $P_c$ and also $\mathcal{V}_c$ at several temperatures. The value of $\mathcal{V}_c$, the equilibrium volume fraction of acetone in the polymer which corresponds to the pressure $P_c$, is obtained from the equilibrium isotherm for the particular temperature. From Table I it is apparent that the values of $\mathcal{V}_c$ increase considerably with decreasing temperature. The last column of Table I will be discussed shortly.

A plausible explanation for the existence of a temperature-dependent critical concentration is that Fickian diffusion occurs only above $T_g$, the apparent second-order transition temperature of the polymer-acetone mixture. For a polymer-solvent system, $T_g$, of course, decreases with increasing volume fraction of solvent; hence, any given temperature below 30° represents a value of $T_g$ for a particular mixture of solvent volume fraction, $\mathcal{V}_g$. If the second-order transition does affect diffusion as postulated, $\mathcal{V}_g$ should be identical with $\mathcal{V}_c$.

TABLE I. Critical concentration and pressure as a function of temperature.

| T°C | $P_c$, mm | $\mathcal{V}_c$, vol. frac. of solvent | $\mathcal{V}_g$, vol. frac. for $T_g$ |
|---|---|---|---|
| 30 | 0 | 0 | 0 |
| 20 | 23 | 0.036 | 0.039 |
| 13 | 27 | 0.065 | 0.068 |
| 8 | 26 | 0.080 | 0.088 |

This hypothesis can be tested by determining the values of $\mathcal{V}_g$ at the temperatures 20°, 13°, and 8°, and comparing the results with the values of $\mathcal{V}_c$ in Table I. Actually, for this evaluation of $\mathcal{V}_g$ it is more convenient to measure $T_g$ as a function of volume fraction of solvent and then read off the values of $\mathcal{V}_g$ at the desired temperatures. Also because of the high volatility of the solvent, it is experimentally difficult to determine $T_g$ for the system polyvinyl acetate-acetone. Fortunately, $T_g$ of a polymer-diluent mixture is usually the same function of volume fraction for all solvents provided the

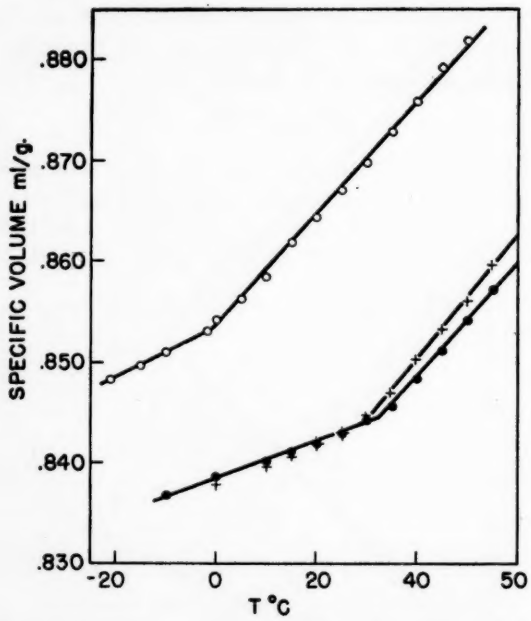


FIG. 6. Volume-temperature plots for the system polyvinyl acetate-acetonyl acetone. ●—pure polymer (film), +—pure polymer (slug), ○—plasticized polymer (solvent volume fraction of $0.14_5$).

[13] Prager, Long, and Bagley (unpublished data).

* The pressure interval must be fairly small for these effects to be observed. Even for integral sorption experiments where $P_i$ is zero, linear plots of $Q_t$ *versus* $t^{\frac{1}{2}}$ are observed provided $P_f$ is considerably higher than $P_c$. This means that over such intervals diffusion at higher concentrations is dominant, which is, of course, a logical consequence of the observed concentration dependence of $D$.

polymer is noncrystalline.[8,14] This should be especially true for the systems polyvinyl acetate-acetone and polyvinyl acetate-acetonyl acetone since the latter solvent is essentially a dimer of acetone. Therefore, we have determined by dilatometric methods the relation between $T_g$ and solvent volume fraction for the nonvolatile system polyvinyl acetate-acetonyl acetone; we have then assumed that the same relation holds for the system polyvinyl acetate-acetone and have used these results to determine values of $v_g$.

Typical plots of specific volume as a function of temperature are shown in Fig. 6. In each case the characteristic break in the volume-temperature plot is sufficiently sharp to determine $T_g$ to 1° or 2°C. To investigate the effects of prolonged heating during sample preparation, two samples of unplasticized polymer were prepared, one by heating to 200°C and the other by casting techniques used to prepare films for sorption experiments. Volume-temperature plots for both samples are shown in Fig. 6. Below $T_g$, these data are well represented by a single straight line; above $T_g$, this is not the case, and the break for the film sample occurs at a higher temperature. Fox and Flory[15] have observed similar results for fractionated samples of polystyrene. In the light of their data, it appears that degradation does occur in the preparation of our samples at elevated temperatures; nevertheless, the effect of this degradation on $T_g$ is small enough to be considered negligible. Both values of $T_g^0$ for the pure polymer (i.e., 32°C for the film and 30°C for the plug) are slightly higher than those reported by other investigators,[16] but in view of the fact that $T_g^0$ varies with both molecular weight and the type of chain ends on the polymer,[14,15] the agreement with previous results is satisfactory. On the basis of the combined data, it seems that the best value for $T_g^0$ of polyvinyl acetate is 30°±2°C.

A typical volume-temperature plot for a mixture of polyvinyl acetate and acetonyl acetone is also shown in Fig. 6 and is similar in form to that for pure polymer.

The apparent second-order transition temperature for the system polyvinyl acetate-acetonyl acetone is shown in Fig. 7 as a function of the volume fraction of solvent. As anticipated from similar data for other systems,[14] $T_g$ *vs* $v_g$ is adequately represented by a straight line.

The last column of Table I gives values of $v_g$ for those temperatures for which the critical volume fraction, $v_c$, was determined. The agreement between the two volume fractions is excellent and clearly substantiates the hypothesis that the shift from Fickian to non-Fickian diffusion occurs at the second-order transition temperature.

On the basis of this picture of the dependence of diffusion properties on $T_g$, one could expect that, at

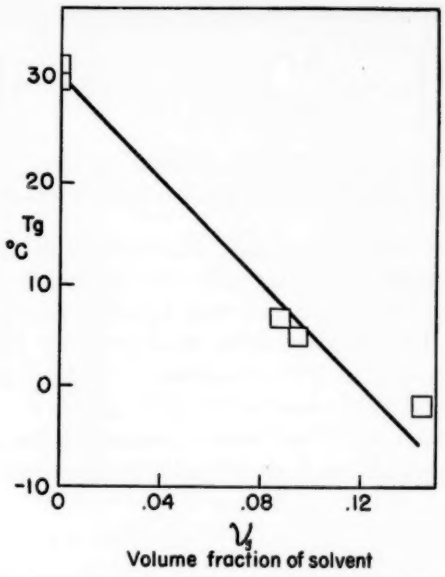


FIG. 7. Concentration dependence of the second-order transition temperature for the system polyvinyl acetate-acetonyl acetone.

temperatures below $T_g^0$ for the pure polymer but at solvent concentrations *above* $v_c$, the diffusion coefficient would be the same function of temperature as found at temperatures above 30°. This can be confirmed by comparing values of $D$ at a temperature of 20°C obtained (a) by applying Eq. (10) and (8) to obtain "extrapolated" values of $D$, and (b) by determining $D$ experimentally at volume fractions above 0.04. (Note that at temperatures below $T_g^0$, $\bar{D}$ is not a useful function to use for this comparison since it implies a knowledge of $D$ below $v_c$.) From *interval* experiments made at 20° and at concentrations above $v_c$, we have

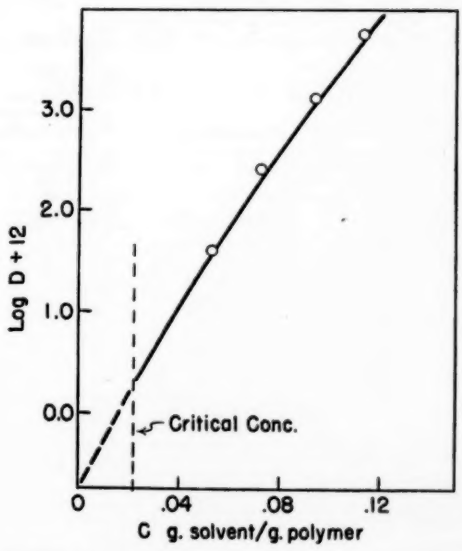


FIG. 8. Diffusion coefficient as a function of concentration at 20°C. Solid line represents extrapolated values; circles are experimental values.

[14] Thomas G. Fox, Phys. Rev. 86, 652 (1952).
[15] Thomas G. Fox and Paul J. Flory, J. Appl. Phys. 21, 581 (1950).
[16] R. H. Wiley and G. M. Brauer, J. Polymer Sci. 4, 351 (1950).

calculated values of $D$ using the equation,

$$D_{cf}=\frac{d}{dc_f}\left[(c_f-c_i^0)\frac{\pi}{32}\left\{\overline{K_s(c_i^0,c_f)^2}+\overline{K_d(c_f,c_i^0)^2}\right\}\right], \quad (11)$$

where $c_i^0$ is a fixed lower concentration, larger than $v_c$, and $c_f$ is variable. This equation follows directly from Eq. (6).

Figure 8 shows the comparison between extrapolated and experimental values of $D$. The agreement is excellent, and one can conclude that for temperatures above $T_g$ the diffusion coefficients show a similar functional dependence even if the temperature of the experiment is below $T_g^0$, the value for the pure polymer.

Although we do not have a complete explanation of the marked change in the diffusion process which occurs at $T_g$, it is not at all surprising that a change does occur. Below $T_g$ the mobility of polymer segments is strongly restricted, and this should considerably modify the process of hole formation. Furthermore, with low segment mobility, it is plausible that the diffusion process will frequently cause orientation of the polymer chains, and it is known that orientation strongly influences the diffusion.[6,17] In this connection we have some evidence that with polyvinyl acetate successive sorption-desorption experiments at temperatures below $T_g$ result in orientation of the polymer chains in the direction of the diffusion, just as has been observed with cellulose nitrate and acetate.[6,17]

This work was carried out as part of a research project sponsored by Army Ordnance.

[17] G. S. Hartley, Trans. Faraday Soc. **45**, 820 (1949).

THE JOURNAL OF CHEMICAL PHYSICS VOLUME 20, NUMBER 11 NOVEMBER, 1952

# The Infrared Spectra of $NF_3$ and $PF_3$

M. KENT WILSON AND SANTIAGO R. POLO*
*Mallinckrodt Chemical Laboratory, Harvard University, Cambridge, Massachusetts*

(Received May 20, 1952)

The infrared spectra of $NF_3$ and $PF_3$ have been investigated with a prism instrument in the range 250 $cm^{-1}$ to 5000 $cm^{-1}$. The fundamental frequencies are for $NF_3$, $\nu_1(A_1)=1032$ $cm^{-1}$, $\nu_2(A_1)=647$ $cm^{-1}$, $\nu_3(E)=905$ $cm^{-1}$, and $\nu_4(E)=493$ $cm^{-1}$; and for $PF_3$, $\nu_1(A_1)=892$ $cm^{-1}$, $\nu_2(A_1)=487$ $cm^{-1}$, $\nu_3(E)=860$ $cm^{-1}$, and $\nu_4(E)=344$ $cm^{-1}$. Force constants as well as thermodynamic functions are calculated for both molecules.

## INTRODUCTION

THERE is a striking dissimilarity in the ability of $NF_3$ and $PF_3$ to form addition compounds. $PF_3$ forms a complex with ferrohaemoglobin, $HbPF_3$, while $NF_3$ does not.[1] The compound $Ni(PF_3)_4$, analogous to $Ni(CO)_4$, is known, but no similar compound of $NF_3$ has been prepared.[2] The low value of the $NF_3$ dipole moment, $0.2D$,[3] is additional evidence that the electronic structure of $NF_3$ is significantly different from that of $PF_3$.

TABLE I. Observed frequencies and band assignments for $NF_3$.

| Present work ($cm^{-1}$) | Relative intensity ($a$)[a] | Assignment | Bailey, Hale, and Thompson[b] ($cm^{-1}$) | Assignment |
|---|---|---|---|---|
| 493 | 0.06 | $\nu_4(E)$ | (420)[d] | $\nu_4$ |
| 647 | 0.07 | $\nu_2(A_1)$ | 505 | $\nu_2$ |
| 905 | 7.5 | $\nu_3(E)$ | 908 | $\nu_1$ |
| 985 | 0.09 | $2\nu_4(A_1+E)$ | 1004 | $\nu_3$ |
| 1032 | 1.2 | $\nu_1(A_1)$ | | |
| 1136 | [c] | $\nu_4+\nu_2(E)$ | | |
| 1523 | 0.06 | $\nu_4+\nu_1(E)$ | | |
| 1809 | 0.13 | $2\nu_3(A_1+E)$ | | |
| 1929 | 0.6 | $\nu_3+\nu_1(E)$ | | |
| 2180 | 0.01 | $2\nu_2+\nu_3(E)$ | | |
| 2680 | 0.01 | $3\nu_3(A_1+A_2+E)$ | | |

[a] The figure given is the apparent absorption coefficient at the maximum of the band defined by the equation $a=(1/pL)\log_{10}T_0/T$. The equivalent path, $pL$, is expressed in cm atmos at 0°C.
[b] See reference 4.
[c] Overlaid by $\nu_1$.
[d] Estimated.

TABLE II. Observed frequencies and band assignments for $PF_3$.

| Present work ($cm^{-1}$) | Relative intensity ($a$)[a] | Assignment | Yost and Anderson[b] Raman shifts Gas ($cm^{-1}$) | Liquid ($cm^{-1}$) | Assignment |
|---|---|---|---|---|---|
| 344 | 0.8 | $\nu_4(E)$ | 487 | 486 | $\nu_4$ |
| 487 | 2.0 | $\nu_2(A_1)$ | ··· | 531 | $\nu_2$ |
| 693 | 0.02 | $2\nu_4(A_1+E)$ | 851 | 840 | $\nu_3$ |
| 831 | [c] | $\nu_4+\nu_2(E)$ | 893 | 890 | $\nu_1$ |
| 860 | 11.0[c] | $\nu_3(E)$ | | | |
| 892 | 10.0 | $\nu_1(A_1)$ | | | |
| 1196 | 0.05 | $\nu_4+\nu_3(A_1+A_2+E)$ | | | |
| 1238 | 0.02 | $\nu_4+\nu_1(E)$ | | | |
| 1375 | 0.004 | $\nu_2+\nu_1(A_1)$ | | | |
| 1713 | 0.1 | $2\nu_3(E_1+E)$ | | | |
| (1752) | [c] | $\nu_1+\nu_3(E)$ | | | |
| 1781 | 0.02 | $2\nu_1(A_1)$ | | | |

[a] The figure given is the apparent absorption coefficient at the maximum of the band defined by the equation $a=(1/pL)\log_{10}T_0/T$. The equivalent path, $pL$, is expressed in cm atmos at 0°C.
[b] See reference 5.
[c] Overlaid by other bands.

* Research Fellow of the Spanish National Council for Scientific Research.

[1] Wilkinson, Nature **168**, 514 (1951).

[2] Wilkinson, J. Am. Chem. Soc. **73**, 5501 (1951).

[3] Watson, Kane, and Ramasmamy, Proc. Roy. Soc. (London) **A156**, 130 (1936).

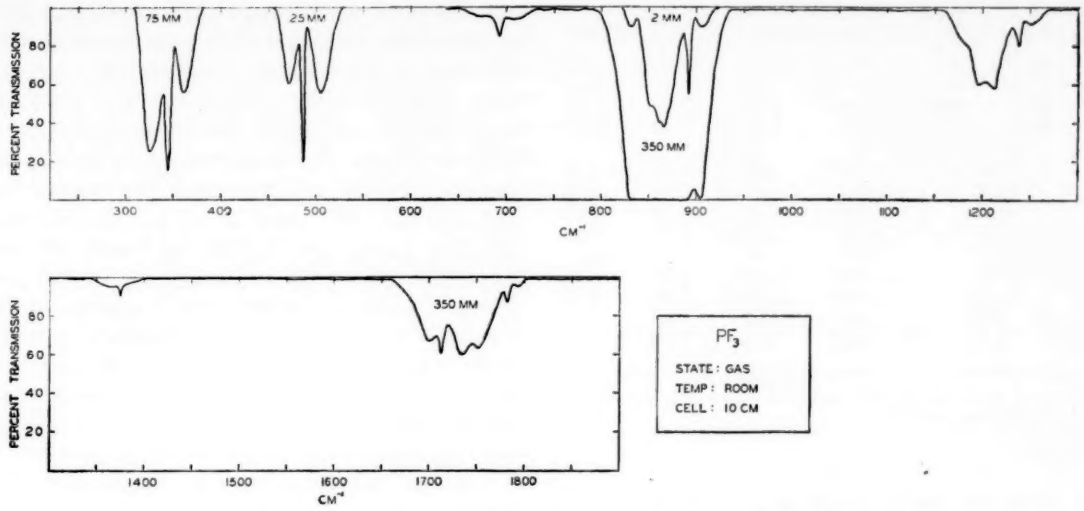


FIG. 1. The infrared absorption spectrum of nitrogen trifluoride.

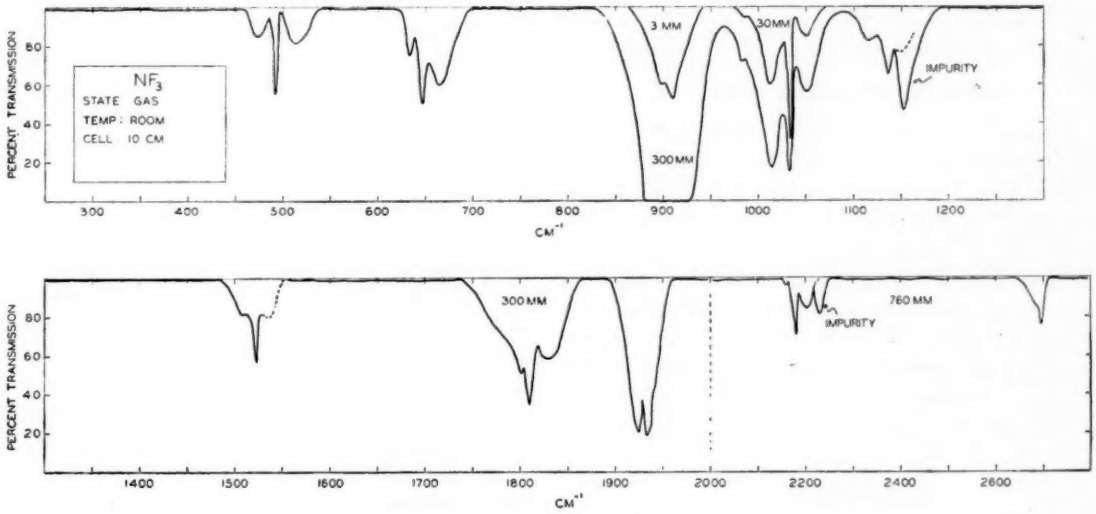


FIG. 2. The infrared absorption spectrum of phosphorous trifluoride.

An investigation of the absolute intensities of the vibration bands of these molecules would yield information concerning the change in dipole moment with normal coordinate and, perhaps, to the electronic structure itself. The infrared spectrum of $NF_3$ has been reported only briefly by Bailey, Hale, and Thompson,[4] the Raman spectrum of $PF_3$ was investigated by Yost and Anderson,[5] and the microwave spectra of both molecules have been determined by Gordy and coworkers.[6,7] Since, to the authors' knowledge, no other work on the vibration spectrum of either molecule is in the literature, and an assignment of the fundamental frequencies is necessary for the intensity investigation, the present paper is a report of the infrared spectra of $NF_3$ and $PF_3$.

## EXPERIMENTAL TECHNIQUES

The infrared spectra of $NF_3$ and $PF_3$ were measured with a Perkin-Elmer Model 12C equipped with $CaF_2$, NaCl, and KBr prisms, a modified Perkin-Elmer Model 12B[8] equipped with a KRS-5 prism, and a Baird Associates spectrophotometer equipped with NaCl optics. Gas cells 5 or 10 cm in length with KBr or polythene windows were used in the appropriate regions. The polythene windows cut from a commercial polythene washbottle were of sufficient thickness to permit the cell to be evacuated and yet transmit about 60 percent throughout the KRS-5 region.

Two samples of $NF_3$ gas prepared by different methods were used in this investigation. One sample was prepared by electrolyzing molten ammonium bifluoride,[9]

[4] Bailey, Hale, and Thompson, J. Chem. Phys. **5**, 274 (1937).
[5] D. M. Yost and T. F. Anderson, J. Chem. Phys. **2**, 624 (1934).
[6] John Sheridan and Walter Gordy, Phys. Rev. **79**, 513 (1950).
[7] Gilliam, Edwards, and Gordy, Phys. Rev. **75**, 1014 (1949).
[8] Lord, MacDonald, and Miller, J. Opt. Soc. Am. **42**, 149 (1952).
[9] Ruff, Fischer, and Luft, Z. anorg. u. allgem. Chem. **172**, 417 (1928).

TABLE III. Potential constants for $NF_3$ and $PF_3$.[a]

| | $F_{12}$ | $F_{34}$ | $F_{11}$ | $F_{33}$ | $F_{22}$ | $F_{44}$ |
|---|---|---|---|---|---|---|
| $HCF_3$ | 0.62 | 0.64 | 8.00 | 5.37 | 3.27 | 1.62[b] |
| | 0.63 | 0.63 | 8.18 | 5.28 | 3.20 | 1.61[c] |
| $NF_3$ | 0.75 | | 5.25 | 3.80 | 2.80 | 1.59 |
| | 0.90 | | 6.31 | 3.97 | 2.36 | 1.58 |
| | 1.00 | | 6.60 | 4.07 | 2.28 | 1.59 |
| | 1.25 | | 7.20 | 4.31 | 2.17 | 1.63 |
| $PF_3$ | 0 | | 5.70 | 4.55 | 2.17 | 1.15 |
| | 0.25 | | 6.07 | 4.85 | 2.05 | 1.12 |
| | 0.50 | | 6.37 | 5.02 | 1.98 | 1.12 |
| | 0.75 | | 6.62 | 5.15 | 1.95 | 1.15 |

[a] $F_{11}$ and $F_{33}$ are given in millidynes/angstrom, $F_{12}$ and $F_{34}$ in millidynes, $F_{22}$ and $F_{44}$ in millidynes·angstrom.
[b] See reference 21.
[c] See reference 20.

and the crude gas was purified by a series of bulb-to-bulb distillations at −165°C. The second sample was obtained through the courtesy of the Minnesota Mining and Manufacturing Corporation. This sample was known to contain about ten percent $CF_4$ as an impurity.

## EXPERIMENTAL RESULTS

The observed frequencies, band assignments, and relative intensities for $NF_3$ as well as the data given by Bailey, Hale, and Thompson[4] are listed in Table I. The observed spectrum replotted on a linear frequency scale is shown in Fig. 1. Similar data for $PF_3$ are contained in Table II and Fig. 2. Since the spectra were taken at various pressures and path lengths the equivalent pressure for a pathlength of 10 cm is indicated in the figures. As the absorption coefficients listed in Tables I and II are not "true" absorption coefficients, the values serve only to indicate the relative intensities of the various bands.

## DISCUSSION

Both $NF_3$[6,10] and $PF_3$[7,11,12] have been shown to have the expected $C_{3v}$ symmetry of ammonia.

For a pyramidal $XY_3$ molecule the six normal modes of vibration may be described as a totally symmetric stretching vibration, $\nu_1(A_1)$, a totally symmetric bending vibration $\nu_2(A_1)$, a doubly degenerate stretching frequency $\nu_3(E)$, and a doubly degenerate bending vibration $\nu_4(E)$. All fundamentals, overtones, and combinations are allowed both in Raman and infrared. Since no polarization data are available for either $NF_3$ or $PF_3$ the frequency assignments were made by considering, band shapes and the relative magnitude of similar vibrational frequencies of related molecules.

From the magnitude of the four frequencies in both molecules which must be assigned to the fundamental vibrations it is clear that the two lowest are bending frequencies, while the higher frequencies are to be ascribed to stretching vibrations. The problem that remains is the assignment to symmetric and degenerate modes within each pair of frequencies. This decision in the case of the bending modes is clear cut. In $PCl_3$, $PBr_3$, $AsCl_3$,[13] $OPF_3$, $OPCl_3$, $OPBr_3$,[14] $CHF_3$,[15,16] and other related molecules the degenerate $(E)$ bending mode is always the lowest frequency in the molecule. Thus, in $NF_3$ we assign the band at 493 $cm^{-1}$ as $\nu_4(E)$ and the 647 $cm^{-1}$ band as $\nu_2(A_1)$. In $PF_3$ the corresponding bands are at 344 $cm^{-1}$ and 487 $cm^{-1}$, respectively. That both of these bands exhibit prominent $Q$ branches and generally similar appearance in $PF_3$ and $NF_3$ is in agreement with the behavior of other symmetric top molecules, e.g., $BF_3$.[17] In fluoroform both of these bands exhibit prominent $Q$ branches, but in the Raman effect the lowest frequency band is depolarized and, therefore, must be an $(E)$ vibration.

The two high frequency fundamentals may be assigned on the basis of their band contours. In both molecules the highest frequency band has a clearly defined $PQR$ structure and is assigned as $\nu_1(A_1)$, the symmetric valence vibration. The remaining fundamental is comparatively narrow and has no well-defined structure. Its appearance in both molecules resembles very closely a perpendicular band for a symmetric top with a series of unresolved $Q$ branches and, accordingly, is assigned as $\nu_3$.

The spectrum of neither molecule is rich in overtones and combination bands; accordingly, for the most part their assignment is straightforward. Indeed, it is only the band at 1929 $cm^{-1}$ in $NF_3$ that is in doubt, but the appearance of this band is most troublesome. Its half-width is smaller than any other band in the $NF_3$ spectrum and the contour of the band clearly resembles a doublet. It is difficult to see how a symmetric top like $NF_3$ could have a doublet band. At the same time it seems improbable that it is due to an impurity. This band occurred in both samples of $NF_3$ with the same relative intensity and showed no tendency to diminish in intensity during the purification process. Furthermore, this is the most intense combination band in the

TABLE IV. Thermodynamic functions for $NF_3$ (cal/deg mole).

| T (°K) | $C°_p$ | $S^0$ | $\frac{(H-H_0)}{T}$ | $\frac{(F-H_0)}{T}$ |
|---|---|---|---|---|
| 200 | 10.21 | 57.71 | 8.50 | 49.21 |
| 273.15 | 12.14 | 61.18 | 9.22 | 51.96 |
| 298.15 | 12.74 | 62.27 | 9.49 | 52.78 |
| 400 | 14.77 | 67.32 | 10.59 | 56.72 |
| 600 | 17.06 | 72.80 | 12.42 | 60.38 |
| 800 | 18.23 | 77.88 | 13.73 | 64.15 |
| 1000 | 18.72 | 81.99 | 14.68 | 67.32 |
| 1200 | 19.05 | 85.47 | 15.38 | 70.09 |
| 1500 | 19.34 | 89.72 | 16.15 | 73.58 |

[10] Schomaker and Lu, J. Am. Chem. Soc. **72**, 1182 (1950).
[11] Brockway and Wall, J. Am. Chem. Soc. **56**, 2373 (1934).
[12] Pauling and Brockway, J. Am. Chem. Soc. **57**, 2684 (1935).
[13] Cabannes and Rousset, Ann. phys. **19**, 229 (1933).
[14] Delwaulle and Francois, Compt. rend. **222**, 550 (1946).
[15] Plyler and Benedict, J. Research Natl. Bur. Standards **47**, 202 (1951).
[16] Rank, Shull, and Pace, J. Chem. Phys. **18**, 885 (1950).
[17] Gage and Barker, J. Chem. Phys. **7**, 455 (1939).

spectrum, and the calculated position of the combination band involving the two most intense fundamentals is 1937 $cm^{-1}$ as compared to the observed value of 1929 $cm^{-1}$. If this band is an impurity present in minor amounts, its true intensity must be tremendous. A comparison with $PF_3$ is of little aid in this problem, since the corresponding combination band is overlapped by $2\nu_3$ and $2\nu_1$.

Excluding bands resulting from $CF_4$ in the $NF_3$ samples, five bands were observed which clearly were not caused by $NF_3$. These were at 740, 990, 1152, 1380, and 1535 $cm^{-1}$. The first two bands were not present in the material obtained from the Minnesota Mining and Manufacturing Company, while the last three were observed in both samples, but with diminished intensity in the product from ammonium bifluoride. None of these bands appear to be connected with the band at 1929 $cm^{-1}$ with respect to position or relative intensity in either sample.

It is seen that the fundamental assignment advanced here for both molecules differs in one respect from the conclusions of the previous workers. Bailey, Hale, and Thompson[4] gave 420 $cm^{-1}$ as an estimated value for the lowest fundamental in $NF_3$ as compared to the value of 493 $cm^{-1}$ observed in the present investigation. For $PF_3$ Yost and Anderson[5] assigned as $\nu_2$ a Raman shift of 531 $cm^{-1}$ which they observed in the liquid but not in the vapor phase. In the present work infrared bands were observed at 344 and 487 $cm^{-1}$, while no absorption was detected near 530 $cm^{-1}$. Although no definite explanation can be given for this discrepancy, it may be suggestive that the difference between the lowest frequency observed in the infrared, and the 890 $cm^{-1}$ Raman shift is 546 $cm^{-1}$ which is near the reported value of 531 $cm^{-1}$.

## NORMAL COORDINATE TREATMENT

The symmetry coordinates used are, for the $A_1$ vibrations,

$$s_1=(\Delta d_1+\Delta d_2+\Delta d_3)/\sqrt{3},$$
$$s_2=(\Delta\alpha_{12}+\Delta\alpha_{13}+\Delta\alpha_{23})/\sqrt{3},$$

and for the $E$ vibrations

$$s_3=(\Delta d_2-\Delta d_3)/\sqrt{2}, \qquad s_3'=(2\Delta d_1-\Delta d_2-\Delta d_3)/6^{\frac{1}{2}},$$
$$s_4=(\Delta\alpha_{12}-\Delta\alpha_{13})/\sqrt{2}, \qquad s_4'=(2\Delta\alpha_{23}-\Delta\alpha_{12}-\Delta\alpha_{13})/6^{\frac{1}{2}}.$$

$d$ is the N–F (or P–F) distance and $\alpha$ the FNF (or FPF) angle.

The corresponding F matrix elements[18] are the following:

$$F_{11}=f_d+2f_{dd} \qquad F_{12}=2f_{d\alpha}+f_{d\alpha}'$$
$$F_{22}=f_\alpha+2f_{\alpha\alpha},$$
$$F_{33}=f_d-f_{dd} \qquad F_{34}=f_{d\alpha}-f_{d\alpha}'$$
$$F_{44}=f_\alpha-f_{\alpha\alpha}.$$

The values of the interatomic distances and angles used in the calculations were

$$d_{NF}=1.37A, \qquad FNF=102°9'^{6}$$
$$d_{PF}=1.53_5A, \qquad FPF=100°.^{19}$$

Since these molecules have only four fundamental vibrations, the six potential constants cannot be uniquely determined without further assumptions.

Under this condition, it seems to us that a reasonable approximation would be to set $F_{12}=F_{34}$, suggested by the analogy with $HCF_3$, iso-electronic with $NF_3$. The potential constants for $HCF_3$, treated with the CH group as a unit, are included in Table III. Their values have been deduced[20,21] by suitable transformation to account for the different coordinates used.

Several sets for $NF_3$ and $PF_3$ obtained for different values of $F_{12}=F_{34}$ within a reasonable range are listed in Table III.

There is no further criterion to decide which set near this range is the correct one. It can be seen that the values for $NF_3$ compare well with those of $HCF_3$. It would be interesting to compare the values for $PF_3$ with those for $HSiF_3$, but spectral data for this molecule are not yet available.

TABLE V. Thermodynamic functions for $PF_3$ (cal/deg mole).

| $T$ (°K) | $C°_p$ | $S°$ | $\frac{(H-H_0)}{T}$ | $\frac{(F-H_0)}{T}$ |
|---|---|---|---|---|
| 200 | 11.62 | 60.07 | 9.13 | 50.94 |
| 273.15 | 13.48 | 63.98 | 10.06 | 53.92 |
| 298.15 | 14.03 | 65.19 | 10.37 | 54.82 |
| 400 | 15.79 | 69.57 | 11.54 | 58.03 |
| 600 | 17.67 | 76.39 | 13.31 | 63.07 |
| 800 | 18.54 | 81.60 | 14.52 | 67.08 |
| 1000 | 18.99 | 85.79 | 15.38 | 70.42 |
| 1200 | 19.24 | 89.28 | 16.00 | 73.28 |
| 1500 | 19.46 | 93.56 | 16.64 | 76.92 |

## THERMODYNAMIC FUNCTIONS

Thermodynamic functions for $NF_3$ and $PF_3$ within a convenient range of temperatures are given in Tables IV and V. These values have been calculated for the ideal gaseous state at 1 atmos pressure, in a rigid-rotator, harmonic-oscillator approximation.

## ACKNOWLEDGMENTS

The authors wish to thank Professor Richard C. Lord for many helpful discussions, Mr. Earl Muetterties for preparing a sample of $NF_3$, Mr. H. G. Bryce of the Minnesota Mining and Manufacturing Company for a sample of $NF_3$, and Professor Geoffrey Wilkinson for the sample of $PF_3$. This work was partially supported by a grant-in-aid from the American Academy of Arts and Science.

[18] E. B. Wilson, Jr., J. Chem. Phys. 7, 1047 (1939); 9, 76 (1941).

[19] Williams, Sheridan, and Gordy, J. Chem. Phys. 20, 164 (1952).

[20] Decker, Meister, and Cleveland, J. Chem. Phys. 19, 784 (1951).

[21] E. L. Pace, J. Chem. Phys. 18, 881 (1950).

THE JOURNAL OF CHEMICAL PHYSICS VOLUME 20, NUMBER 11 NOVEMBER, 1952

# Rotational Isomers of Chloroacetyl Chloride, Bromoacetyl Chloride, and Bromoacetyl Bromide

ICHIRO NAKAGAWA, ISAO ICHISHIMA, KENJI KURATANI, TATSUO MIYAZAWA, TAKEHIKO SHIMANOUCHI, AND SAN-ICHIRO MIZUSHIMA
*Chemical Laboratory, Faculty of Science, Tokyo University, Hongo, Tokyo, Japan*
(Received May 9, 1952)

The Raman spectra of chloroacetyl chloride, bromoacetyl chloride, and bromoacetyl bromide have been measured in the solid and liquid states. The infrared absorption spectra of these substances have also been measured in the liquid and the gaseous states. From the experimental results it has been concluded that there are two rotational isomers in the liquid and gaseous states and only one of them persists in the solid state. The temperature dependence of the intensity of the infrared absorption in the gaseous state has also been studied, and the energy difference between these two isomers has been found as $1.0\pm0.1$ kcal/mol for bromoacetyl chloride and $1.9\pm0.3$ kcal/mol for bromoacetyl bromide.

The calculation of the normal vibrations and of the product rule has been made for various configurations of rotational isomers, and it has been shown that the more stable form is the *trans* form (or nearly this one) with regard to the two halogen atoms. The less stable form is considered to have an azimuthal angle between the two carbon-halogen bonds of about 150°.

IN a series of researches[1] we have studied the internal rotation of molecules that can be regarded as basic units of a polypeptide chain. As a continuation of these researches we shall report in the present communication the experimental results obtained for chloroacetyl chloride, bromoacetyl chloride, and bromoacetyl bromide, all of which have a $-CO-CH_2-$ bond, which is one of the internal rotation axes contained in a polypeptide chain.

## EXPERIMENTAL

Chloroacetyl chloride was prepared by the reaction[2] of thionyl chloride with monochloroacetic acid and was distilled several times (b.p. 105°C).

Bromoacetyl chloride was prepared[3] from monobromoacetic acid and thionyl chloride. The product was distilled several times (b.p. $127°\pm0.5°C$).

Bromoacetyl bromide was prepared by the reaction[4] of glacial acetic acid with bromine and red phosphorus and was distilled several times (b.p. $149°\pm0.5°C$). The sample was further purified by redistillation in vacuum.

The Raman spectra were observed in the liquid and the solid states with the apparatus described previously.[5] For bromoacetyl bromide and bromoacetyl chloride, saturated aqueous solution of sodium nitrite was used as a filter in order to avoid decomposition by ultraviolet radiation. As to the spectra in the liquid state the measurements were made not only at room temperature but also at higher temperatures: at 80–85°C for chloroacetyl chloride, at 95–100°C for bromoacetyl chloride, and at 60–65°C for bromoacetyl bromide, the last one being observed at a lower temperature than the other two in order to avoid thermal decomposition. The Raman spectra in the solid state were observed by cooling the sample with a mixture of dry ice and ethanol. The results obtained are shown in Table I.

Infrared spectra were observed in the region from 550 $cm^{-1}$ to 3000 $cm^{-1}$ in the liquid state, and in the region from 550 $cm^{-1}$ to 800 $cm^{-1}$ in the gaseous state (see Table I). The apparatus and the method of measurement were similar to those described previously,[6] except that a sylvine prism prepared in our laboratory[7] was used for the measurements in the region from 550 $cm^{-1}$ to 650 $cm^{-1}$. Baird automatic recording infrared spectrometer was also used in the measurements.

## DISCUSSION

Since the molecules $ClCH_2COCl$, $BrCH_2COCl$, and $BrCH_2COBr$ all contain seven atoms, the maximum number of observable fundamental Raman frequencies for one configuration is fifteen, including one C=O stretching and two carbon-halogen stretching frequencies. However, the number of Raman lines actually observed in the liquid state is much larger than this value, and it is worthy of note that we have observed two Raman lines at about 1800 $cm^{-1}$ corresponding to the C=O stretching vibrations and four Raman lines in the region from 600 $cm^{-1}$ to 800 $cm^{-1}$, where carbon-halogen stretching vibrations are expected to appear. It is, therefore, probable that there are rotational isomers in the liquid state, as in the case of 1,2-dihalogenoethanes,[8] although Sanyal and Majumdar[9] denied the existence of such isomers from a similar study of Raman spectra. The fact that we have found two groups of Raman lines, of which one group shows a different behavior of temperature dependence of the intensity from the other, provides us with other evidence of the existence of rotational isomers, since this fact could be

[1] Last communication, Mizushima, Shimanouchi, Tsuboi, Sugita, Kao, atnd Kondo, J. Am. Chem. Soc. **73**, 1330 (1951).
[2] E. de B. Barnett, Chem. News **122**, 220 (1920).
[3] H. Meyer, Monatsh. Chem. **22**, 415 (1901).
[4] K. Anwers, Ber. deut. chem. Ges. **24**, 2218 (1891).
[5] S. Mizushima and Y. Morino, Proc. Ind. Acad. Sci. **8**, 351 (1938).
[6] Shimanouchi, Tsuruta, and Mizushima, Sci. Pap. Inst. Phys. Chem. Research (Tokyo) **42**, 165 (1946).
[7] T. Miyazawa, Annual Meeting, Chemical Society, Japan (1951).
[8] See, e.g., Mizushima, Morino, Watanabe, Shimanouchi, and Yamaguchi, J. Chem. Phys. **17**, 591 (1949).
[9] S. B. Sanyal and M. M. Majumdar, Indian J. Phys. **23**, 1 (1949).

TABLE I. Raman and infrared spectra of $ClCH_2COCl$, $BrCH_2COCl$, and $BrCH_2COBr$.

| $ClCH_2COCl$ | | | | $BrCH_2COCl$ | | | | $BrCH_2COBr$ | | | |
|---|---|---|---|---|---|---|---|---|---|---|---|
| Solid R | Liquid R[a] | IR | Vibrational mode[b] | Solid R | Liquid R[a] | IR | Vibrational mode[b] | Solid R | Liquid R[a] | IR | Vibrational mode[b] |
| | *187(2) | | $\delta_1'$ | | *157(4) | | $\delta_1'$ | | *148(1) | | $\delta_1'$ |
| 218(0) | 214(4) | | $\delta_1$ | 190(0) | 181(7) | | $\delta_1$ | | 181(3) | | $\delta_1$ |
| 248(0) | 242(3) | | | 254(7) | 252(10*b*) | | $\delta_2$ | 193(4) | 197(9*b*) | | $\delta_2$ |
| 300(6) | 301(10b) | | $\delta_2$ | | *344(4) | | $\delta_2'$ | | *311(5) | | $\delta_2'$ |
| | *362(2) | | $\delta_2'$ | 451(9) | 444(10*b*) | | $\delta_3$ | 357(3) | 360(9*b*) | | $\delta_3$ |
| | 421(2) | | | 475(0) | 477(2) | | ($\pi$) | | 459(2) | | ($\pi$) |
| 454(10) | 448(10*b*) | | $\delta_3$ | | *525(9) | | $\delta_3'$ | | *501(6*b*) | | $\delta_3'$ |
| 485(0) | 484(2) | | ($\pi$) | | *617(5*b*) | 613(*m*) | $\nu_a'$(C−X) | | *588(4) | 579(*m*) | $\nu_a'$(C−X) |
| | *559(6) | 562(*m*) | $\delta_3'$ | 668(5) | 667(6) | 660(*s*) | $\nu_a$(C−X) | | 631(5) | 629(*s*) | $\nu_a$(C−X) |
| | 675(1) | | $\nu_a'$(C−X) | 700(0) | 700(0) | | | | *695(5) | | $\nu_s'$(C−X) |
| | | 712(*m*) | | | *719(5) | 712(*w*) | $\nu_s'$(C−X) | 716(4) | 720(10*b*) | 714(*m*) | $\nu_s$(C−X) |
| 725(4) | 715(8*b*) | 722(*m*) | $\nu_a$(C−X) | 732(10) | 731(10) | 731(*m*) | $\nu_s$(C−X) | | | 723(*vw*, *sh*) | |
| | | 752(*vw*) | | | 859(2) | 858(*w*) | | | 850(3) | | |
| 781(9) | 778(10*b*) | 779(*m*) | $\nu_s$(C−X) | | 901(2) | 902(*w*) | | | 905(4) | 904(*m*) | |
| 902(0) | 900(3) | 898(*w*) | $\nu_s'$(C−X) | 954(2) | 949(3) | 946(*s*) | | 952(1) | 952(6) | 949(*vs*) | |
| | 922(0) | | | 973(3) | 980(4) | 974(*vs*) | | | 1002(1) | 999(*vs*) | |
| 960(1) | 962(5) | 957(*m*) | | | 1018(2) | 1014(*s*) | | | 1147(4*b*) | 1151(*m*) | |
| 979(1) | 987(5) | 977(*vs*) | | | | 1110(*vw*) | | | | 1193(*vw*) | |
| 1048(0) | 1030(0) | 1036(*m*) | | 1155(0) | 1153(4*b*) | 1160(*m*) | | | *1215(2) | 1212(*vw*) | |
| | 1130(0) | | | | *1217(4) | 1214(*vw*) | | | 1236(6) | 1231(*w*) | |
| 1182(3) | 1178(5) | 1182(*w*) | | 1253(4) | 1247(7) | 1244(*vw*) | | | 1383(5) | 1389(*s*) | |
| 1221(0) | | 1218(*vw*) | | | | 1289(*w*) | | | 1408(2) | 1415(*w*) | |
| | *1270(0) | 1268(*w*) | | | 1330(0) | 1330(*vw*) | | | *1790(2) | 1783(*sh*) | $\nu'$(C=O) |
| 1290(0) | 1292(5) | 1287(*w*) | | 1388(5) | 1391(7) | 1395(*s*) | | | 1810(4) | 1807(*vs*) | $\nu$(C=O) |
| | 1343(0) | | | 1421(1) | 1423(2) | 1421(*w*) | | | | 1882(*w*) | |
| 1370(0) | 1373(3) | 1376(*w*) | | | *1779(3) | 1773(*sh*) | $\nu'$(C=O) | | 2947(7) | 2955(*m*) | $\nu$(C−H) |
| 1391(4) | 1400(8) | 1401(*s*) | | 1797(3) | 1804(7*b*) | 1802(*vs*) | $\nu$(C=O) | | 2964(1) | | and |
| 1590(1) | | | | | | 1898(*w*) | | | 3003(4) | 3008(*m*) | $\nu'$(C−H) |
| | *1780(3) | 1779(*w*, *sh*) | $\nu'$(C=O) | 2951(7) | 2956(8) | 2958(*m*) | $\nu$(C−H) | | | | |
| 1799(2) | 1814(8*b*) | 1809(*vs*) | $\nu$(C=O) | | 2977(2) | | and | | | | |
| | | 1912(*w*) | | 3000(3) | 3014(4) | 3006(*m*) | $\nu'$(C−H) | | | | |
| 2950(10) | 2950(10) | 2955(*m*) | $\nu$(C−H) | | | | | | | | |
| 2990(1) | 3004(5) | 3000(*m*) | and $\nu'$(C−H) | | | | | | | | |

[a] The intensity of Raman lines marked with asterisk was found to increase unambiguously with temperature. There may be other lines which behave similarly to these lines, but because of their weak intensity we could not see this behavior definitely.
[b] $\delta$ is a deformation vibration, $\nu$ a stretching vibration, and $\pi$ a out-of-plane vibration of the more stable isomer. $\delta'$ and $\nu'$ are the corresponding vibrations of the less stable isomer.

explained most easily by considering different population ratios of two rotational isomers at different temperatures. In each of the following pairs of lines: (214, 187) (301, 362) (448, 559) (1814, 1780) for chloroacetyl chloride, (181, 157) (252, 344) (444, 525) (667, 617) (731, 719) (1804, 1779) for bromoacetyl chloride, and (181, 148) (197, 311) (360, 501) (631, 588) (720, 695) (1810, 1790) for bromoacetyl bromide, the latter increased its relative intensity at higher temperature as compared with the former. From the similarity of frequency values, the two lines of each pair would be assigned to similar normal vibrations of the two rotational isomers.

All the Raman lines which become relatively stronger at higher temperatures in the liquid state disappear completely on solidification, and the number of Raman lines in the solid state becomes small enough to be explained by assuming a single configuration. Therefore, we can consider that only the isomer that is more stable in the liquid state persists in the solid state, just as in the case of 1,2-dihalogenoethanes.[8]

In the frequency region of carbon-halogen stretching vibrations, we have observed several infrared absorption peaks in the liquid and gaseous states which have almost the same frequencies as the corresponding Raman lines. The temperature dependence of the intensity of each of these bands was found to be exactly the same as that of the corresponding Raman lines. There is, therefore, hardly any doubt that there are two rotational isomers in the liquid and the gaseous states, and only the more stable one of them persists in the solid state.

Let us now discuss the spectra more in detail, utilizing the idea of rotational isomerism (see Table I). There is no doubt that the two Raman lines observed around 1800 $cm^{-1}$ for each of these three substances can be assigned to the C=O stretching vibrations of the two isomers.

In bromoacetyl bromide, four C−Br stretching frequencies were observed. From the temperature dependence of the intensity of infrared and Raman spectra we can group them into two pairs, and one pair which contains the two frequencies 720 $cm^{-1}$ and 631 $cm^{-1}$ can be assigned to the more stable isomer. Of these two frequencies the intensity of the former was found stronger in the Raman effect and weaker in the infrared absorption than the latter. This can be explained in the following way. Although this molecule, in any configuration, has no twofold axes, the two vibrations may behave similarly to the symmetric and antisymmetric vibrations of this symmetry just as in the case of 1,2-dibromoethane. Therefore, the stronger Raman line at 720 $cm^{-1}$ and the weaker one at 631 $cm^{-1}$ may be considered, respectively, as the symmetric and antisymmetric C−Br stretching vibrations of the more stable isomer, from which we can understand the observed intensity relations stated above. Similarly, the two lines at 695 $cm^{-1}$ and at 588 $cm^{-1}$ may be considered as the symmetric and antisymmetric C−Br stretching vibrations of the less stable isomer.

The carbon-halogen stretching vibrations of chloroacetyl chloride and bromoacetyl chloride can be assigned in a similar way, if we can consider that the Raman line

TABLE II. Calculated and observed skeletal frequencies of $ClCH_2COCl$ and $BrCH_2COCl$.

| $ClCH_2COCl$ Calculated frequencies | | | | | Observed frequencies | |
|---|---|---|---|---|---|---|
| 0° (*trans*) | 90° | 120° | 150° | 180° (*cis*) | More stable form ($\nu$) | Less stable form ($\nu'$) |
| 192 | 318 | 280 | 198 | 143 | 214 | 187 |
| 288 | 402 | 402 | 376 | 364 | 301 | 362 |
| 486 | 492 | 497 | 501 | 501 | 448 | 559 |
| 715 | 637 | 609 | 601 | 600 | 715 | (675) |
| 726 | 726 | 753 | 780 | 791 | 778 | 778 |
| 1080 | 1064 | 1064 | 1067 | 1068 | ( )[a] | ( ) |
| 1739 | 1735 | 1740 | 1745 | 1747 | 1814 | 1780 |

| $BrCH_2COCl$ | | | | | |
|---|---|---|---|---|---|
| 0° (*trans*) | 120° | 150° | 180° (*cis*) | More stable form ($\nu$) | Less stable form ($\nu'$) |
| 164 | 260 | 177 | 115 | 181 | 157 |
| 250 | 386 | 346 | 329 | 252 | 344 |
| 486 | 490 | 494 | 494 | 444 | 525 |
| 658 | 565 | 572 | 574 | 667 | 617 |
| 704 | 715 | 738 | 748 | 731 | 719 |
| 1085 | 1063 | 1063 | 1064 | ( )[a] | ( ) |
| 1738 | 1742 | 1748 | 1751 | 1804 | 1779 |

[a] The C−C stretching frequency would be considerably coupled with hydrogen bending frequencies, so that the comparison between the observed value and the theoretical one (calculated as a pure skeletal motion) has not much significance.

In our calculation of the product rule we have assumed the same frequency for the C−C stretching vibrations of the two isomers. This would be reasonable, because these frequencies cannot differ much from each other. Even a difference of 100 $cm^{-1}$ which would be almost inconceivably large does not affect our conclusion.

corresponding to the symmetric C−Cl vibration of the less stable isomer of chloroacetyl chloride is covered by the broad line (778 $cm^{-1}$) of the more stable isomer.

As to the skeletal deformation vibrations of

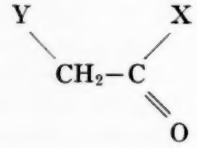

which are expected to appear in the frequency region from 150 $cm^{-1}$ to 550 $cm^{-1}$, there are three such ones, $\delta_1$, $\delta_2$, and $\delta_3$, of which

$\delta_1$, corresponds mainly to the deformation of the bond angle Y−$CH_2$−C,

$\delta_2$, to that of the bond angle $CH_2$−C−X and

$\delta_3$, to the rocking of C=O bond in the plane of

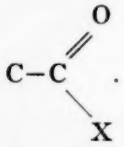

From the nature of these vibrations it will be seen that $\delta_1$ of bromoacetyl chloride and bromoacetyl bromide has almost the same frequency, which is slightly lower than that of chloroacetyl chloride, and that $\delta_3$ of chloroacetyl chloride and bromoacetyl chloride has the same frequency, which is higher than that of bromoacetyl bromide. Moreover, the frequency of $\delta_3$ of these substances will not be much different from that of the corresponding vibration of acetyl chloride (435 $cm^{-1}$) or acetyl bromide (338 $cm^{-1}$). These are all taken into account in making the assignments shown in Table I, where we differentiate by prime the frequencies of the less stable isomer from those of the more stable one. It will be seen that the corresponding vibrations of the two rotational isomers have frequencies not much different from each other, but they behave quite differently in the temperature dependence of intensity.

To the C−C stretching vibration and the four C−H bending vibrations ($CH_2$ deformation, wagging, rocking, and twisting), we can assign the Raman lines observed in the region from 800 $cm^{-1}$ to 1400 $cm^{-1}$ (see Table I). The line corresponding to the torsional oscillation ($\tau$) which would have a frequency of about 100 $cm^{-1}$ could not be observed.

The Raman lines observed at 484 $cm^{-1}$ (chloroacetyl chloride), at 477 $cm^{-1}$ (bromoacetyl chloride), and at 459 $cm^{-1}$ (bromoacetyl bromide) that have not so far been assigned would correspond to the out-of-plane vibration

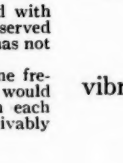

Let us now discuss the molecular configuration of these rotational isomers. According to electron diffraction experiments[10] recently carried out in our laboratory, the more stable isomer which persists in the solid state was shown to be in the *trans* configuration with respect to the two halogen atoms. In other words, the two halogen atoms are at the farthest distance apart in this configuration (see Fig. 1). This conclusion is in agreement with the result of the normal vibration calculation shown in next section in which we have chosen the force constants of chloroacetyl chloride and of bromoacetyl chloride from those of the more simple molecules having the similar structures (see Table II).

As to the configuration of the less stable isomer, it is not very easy to derive a final conclusion, but so far as the normal vibration calculation is concerned the observed frequencies agree well with the calculated frequencies for the configuration with an azimuthal angle between the two carbon-halogen bonds of 150° (see Table II and Fig. 1).

FIG. 1. The two stable forms of chloroacetyl chloride as viewed along the C−C axis.

[10] Y. Morito *et al* (to be published).

This conclusion is also in agreement with the product rule for the rotational isomers derived in our previous paper.[11]

If we neglect the interaction between heavy atoms of the two rotating groups, the $F$-matrix[12] in the normal vibration calculation does not include the azimuthal angle $\theta$ of internal rotation, and the product of the normal frequencies can be determined from the configuration of rotational isomers according to the following formula:

$$\frac{\Pi\nu'\,(\text{less stable isomer})}{\Pi\nu\,(\text{more stable isomer})}=\left(\frac{|G(\theta)|}{|G\,(trans)|}\right)^{\frac{1}{2}}, \quad (1)$$

where $G$ is the $G$-matrix, which depends in this case only on the azimuthal angle $\theta$. Table III shows that among the calculated values of the right-hand side of Eq. (1), that for $\theta=150°$ is in agreement with the observed ratio of the left-hand side.

We have also made a preliminary determination of the energy difference between the rotational isomers of bromoacetyl chloride and bromoacetyl bromide according to the method described in our previous paper.[6] We have chosen two absorption bands observed in the gaseous state for each of these two substances, one band being assigned to the more stable isomer, and the other band to the less stable isomer. Their absorption peaks appeared at 608 $cm^{-1}$ and 654 $cm^{-1}$ for bromoacetyl chloride and at 567 $cm^{-1}$ and 622 $cm^{-1}$ for bromoacetyl bromide, where the peaks at 654 $cm^{-1}$ and 622 $cm^{-1}$ were assigned to the more stable isomers. From the temperature dependence of the intensity of the two pairs of bands, we have obtained the energy difference between the rotational isomers as $1.0\pm0.1$ kcal/mol for bromoacetyl chloride and $1.9\pm0.3$ kcal/mol for bromoacetyl bromide.

## CALCULATIONS OF THE NORMAL VIBRATIONS

Normal vibrations were calculated according to Wilson's method[12] based on a potential function of the

TABLE III. Product rule.

| Calculated values of $(\lvert G(\theta)\rvert/\lvert G\,(trans)\rvert)^{\frac{1}{2}}$ | | |
|---|---|---|
| | $ClCH_2COCl$ | $BrCH_2COCl$ |
| 0° (*trans*) | 1.00 | 1.00 |
| 90° | 2.06 | 2.43 |
| 120° | 1.81 | 2.11 |
| 135° | 1.55 | 1.76 |
| 150° | 1.25 | 1.35 |
| 180° (*cis*) | 0.88 | 0.86 |

| Values of $\Pi\nu'$ (less stable form)/$\Pi\nu$ (more stable form) | |
|---|---|
| $ClCH_2COCl$ | $BrCH_2COCl$ |
| 1.25 | 1.27 |

[11] Mizushima, Morino, and Shimanouchi, Sci. Pap. Inst. Phys. Chem. Research, Tokyo **40**, 87 (1942); J. Chem. Phys. **17**, 663 (1949); T. Shimanouchi, Bull. Inst. Phys. Chem. Research (Tokyo) **23**, 371 (1944).

[12] E. B. Wilson, J. Chem. Phys. **7**, 1047 (1939); **9**, 76 (1941).

TABLE IV. Force constants[a] and molecular parameters used in calculation.

Force constants (in $10^5$ dyne/cm)

| | |
|---|---|
| $K(C-Cl)$ | = 1.75 |
| $K(C=O)$ | = 11.0 |
| $K(C-CH_2)$ | = 3.4[b] |
| $K(CH_2-Cl)$ | = 2.6 |
| $K(CH_2-Br)$ | = 2.35[c] |
| $H(O=C-CH_2)$ | = 0.4 |
| $H(Cl-C-CH_2)$ | = 0.1 |
| $H(O=C-Cl)$ | = 0.3 |
| $H(Cl-CH_2-C)$ | = 0.2 |
| $H(Br-CH_2-C)$ | = 0.1[c] |
| $F(O\cdots CH_2)$ | = 0.4 |
| $F(Cl\cdots CH_2)$ | = 0.6 |
| $F(Cl\cdots O)$ | = 1.0 |
| $F(Cl\cdots C)$ | = 0.5 |
| $F(Br\cdots C)$ | = 0.7[c] |

$F'=-(1/10)F$

Molecular parameters

| Bond distances (A | | Bond angles | |
|---|---|---|---|
| $r(C-Cl)$ | = 1.76 | $\angle(O=C-CH_2)$ | = 125° |
| $r(C=O)$ | = 1.22 | $\angle(Cl-C-CH_2)$ | = 110° |
| $r(C-C)$ | = 1.54 | $\angle(O=C-Cl)$ | = 125° |
| $r(CH_2-Cl)$ | = 1.76 | $\angle(Cl-CH_2-C)$ | = 112° |
| $r(CH_2-Br)$ | = 1.92 | $\angle(Br-CH_2-C)$ | = 112° |

[a] See references 8, 11, and 13.
[b] The value of $K(C-CH_2)$ is obtained by interpolation of $K(-C-C-)$ and $K(-CH_2-CH_2-)$.
[c] These values are those which give the best fit with the frequencies of $CH_3-CH_2-Br$, $Br-CH_2-Br$, and $Br-CH_2-CH_2-Br$, the details of which will be published shortly.

Urey-Bradley type:[13]

$$V=\sum_r\{K'r_0(\Delta r)+\tfrac{1}{2}K(\Delta r)^2\}+\sum_\alpha\{H'r_0^2(\Delta\alpha)+\tfrac{1}{2}Hr_0^2(\Delta\alpha)^2\}+\sum_q\{F'q_0(\Delta q)+\tfrac{1}{2}F(\Delta q)^2\}, \quad (2)$$

where $r$'s are the bond lengths, $\alpha$' sthe bond angles, and $q$'s the distances between atoms not bonded directly. $K$, $K'$, $H$, $H'$, $F$, and $F'$ are force constants, of which $F$ and $F'$ are concerned with the repulsion terms and $K'$ and $H'$ can be expressed in terms of $F'$ by the equilibrium conditions.[13] Here the interactions between the two halogen atoms and between halogen (Y) and oxygen atoms contained in different movable groups are neglected.

The values of force constants used in this calculation are the same as those of $Cl-CH_2-Cl$, $CH_3-CH_2-Cl$, $Br-CH_2-Br$, $CH_3-CH_2-Br$, and $CH_3-CO-Cl$, which gave the best fit with the spectral frequencies of these simple molecules. Moreover, these force constants have been shown to give calculated frequencies of $Cl-CO-CO-Cl$, $Cl-CH_2-CH_2-Cl$, and $Br-CH_2-CH_2-Br$,[14] which are in good agreement with the observed ones.

Table IV shows the values of these force constants

[13] T. Shimanouchi, J. Chem. Phys. **17**, 245, 734, 848 (1949).

[14] Mizushima, Morino, and Shimanouchi, Sci. Pap. Inst. Phys. Chem. Research (Tokyo) **40**, 87 (1942).

together with the molecular parameters used in this calculation. Although we believe these values of molecular parameters are quite reasonable, we would like to point out that small changes in these values do not affect our conclusion at all. By solving the seventh-order secular equation, $|GF-E\lambda|=0$, the seven skeletal frequencies other than the out-of-plane ($\pi$) and torsional ($\tau$) frequencies can be calculated. Table II shows the result of this calculation made for various molecular configurations with different values of the azimuthal angle $\theta$ where the origin of $\theta$ has been taken, as stated above, at the *trans* position for two halogen atoms. The calculated frequencies vary considerably with $\theta$, and those for $\theta=0°$ (*trans* form or the more stable form) and for $\theta=150°$ (the less stable form) agree most satisfactorily with the observed frequencies.

THE JOURNAL OF CHEMICAL PHYSICS VOLUME 20, NUMBER 11 NOVEMBER, 1952

# Kinetics of Decomposition of Nitric Oxide at Elevated Temperatures. II. The Effect of Reaction Products and the Mechanism of Decomposition*

HENRY WISE AND MAURICE F. FRECH
*Jet Propulsion Laboratory, California Institute of Technology, Pasadena, California*
(Received June 9, 1952)

The effects of nitrogen and oxygen on the kinetics of decomposition of nitric oxide have been investigated. In the temperature region in which the heterogeneous mechanism prevails (at $T<1000°K$) the presence of nitrogen has a marked retarding influence on the reaction rate of nitric oxide due to poisoning of the surface. On the other hand, the addition of oxygen results in a marked increase in the rate of decomposition of nitric oxide over the entire temperature range studied. At high concentrations of oxygen the following empirical rate expression obtains,

$$-\frac{d[NO]}{dt}=k_a[NO]^2+k_b[NO][O_2]^{\frac{1}{2}},$$

with an activation energy of 78.2 kcal for the rate-determining step. It is apparent therefore that the decomposition of nitric oxide is autocatalytic. On the basis of these experimental observations a mechanism is proposed involving a chain propagated by the atomic species formed in the reaction.

IN a recent publication[1] the kinetics of decomposition of nitric oxide in a quartz vessel were shown to exhibit the predominance of a heterogeneous mechanism at temperatures below 1000°K and of a homogeneous mechanism at temperatures above 1600°K. Although the over-all kinetics of this reaction appear to follow a second-order rate law, the mechanism of this chemical transformation is more complex than indicated by a simple bimolecular process. In order to investigate this mechanism in more detail the present study of the effect of the reaction products on the kinetics of decomposition was undertaken.

TABLE I. Effect of oxygen on rate of thermal decomposition of nitric oxide at 980 and 1150°K.

| Temp $T$ (°K) | Concentration (mole $\times cc^{-1}$) $\times 10^6$ NO | $O_2$ | Decomposition rate (mole $\times cc^{-1} \times sec^{-1}$) $\times 10^{12}$ With $O_2$ | Without $O_2$ |
|---|---|---|---|---|
| 980 | 7.841 | 0.309 | 123.3 | 15.9 |
| | 5.485 | 0.216 | 74.0 | 7.7 |
| | 7.233 | 0.083 | 26.1 | 13.3 |
| | 5.884 | 0.061 | 25.4 | 8.8 |
| | 4.789 | 0.050 | 16.1 | 5.8 |
| | 3.958 | 0.041 | 14.2 | 4.0 |
| 1150 | 5.619 | 0.220 | 475.0 | 89.0 |
| | 3.914 | 0.154 | 354.0 | 43.2 |
| | 3.298 | 0.130 | 277 | 30.6 |
| | 2.770 | 0.109 | 217.5 | 21.6 |
| | 2.839 | 0.030 | 42.4 | 22.8 |
| | 2.382 | 0.025 | 43.6 | 16.0 |
| | 1.989 | 0.021 | 26.9 | 11.2 |
| | 1.642 | 0.017 | 20.5 | 7.6 |

## EXPERIMENTAL MEASUREMENTS

The apparatus and procedures used in the experimental measurements are similar to those previously described.[1] Uniform gas mixtures of known composition with respect to NO and the additive ($N_2$ or $O_2$) were prepared, aliquots of which were subjected to the decomposition studies in the quartz reactor. Although at room temperature the preparation of such gas mixtures by the addition of the desired partial pressure of $O_2$ to a given quantity of NO leads to the formation of an equilibrium concentration of $NO_2$ and $N_2O_4$ in the storage vessel, the rate of the reverse reaction[2] is very rapid compared with the rate of decomposition of NO at the experimental temperatures employed in these studies. The extent of reaction[1] is determined quantitatively by manometric analysis for $N_2$ and spectrometric analysis for $NO_2$.

* This paper presents the results of one phase of research carried out at the Jet Propulsion Laboratory, California Institute of Technology, under contract No. DA-04-495-ORD18 sponsored by the Department of the Army Ordnance Corps.

[1] H. Wise and M. F. Frech, J. Chem. Phys. **20**, 22 (1952).

[2] Bodenstein and Ramstetter, Z. physik. Chem. **100**, 106 (1922).

TABLE II. Thermal decomposition of nitric oxide in presence of oxygen.

| Temp °K | Specific reaction rate constants[a] $k_a$ (mole/cc)$^{-1}$ sec$^{-1}$ | $k_b$ (mole/cc)$^{-\frac{1}{2}}$ sec$^{-1}$ |
|---|---|---|
| 1525 | $1.4\times10^{3}$ | 0.9 |
| 1690 | $1.2\times10^{4}$ | 16 |
| 1840 | $9.6\times10^{4}$ | 99 |
| 1912 | $4.6\times10^{5}$ | 262 |

[a] See Eq. (1). Values based on data given in reference 4.

## EFFECT OF OXYGEN

It is apparent from the results shown in Table I that the decomposition rate of nitric oxide is markedly increased in the presence of even small concentrations of oxygen. A more detailed analysis of the experimental data shows that the rate of transformation in the presence of added oxygen is given by

$$-\frac{d[NO]}{dt}=k_a[NO]^2+k_b[NO][O_2]^{\frac{1}{2}}/([NO]+[O_2]). \quad (1)$$

The autocatalytic nature of the reaction is clearly indicated. Consequently only in the initial stage of the decomposition when the concentration of oxygen is vanishingly small does the reaction follow a second-order rate law as has previously been found to apply.[1,3] Also, for low concentrations of $O_2$ with respect to NO, the rate of decomposition of NO may be approximated by

$$-\frac{d[NO]}{dt}\simeq k_a[NO]^2+k_b[O_2]^{\frac{1}{2}}. \quad (2)$$

Thus, the difference in rate between pure NO and a gas mixture containing NO and $O_2$ is proportional to the concentration of oxygen raised to the $\frac{3}{2}$th power, as borne out by the empirical results.

Conversely, for high concentrations of oxygen relative to NO, Eq. (1) reduces to

$$-\frac{d[NO]}{dt}\cong k_a[NO]^2+k_b[NO][O_2]^{\frac{1}{2}}. \quad (3)$$

Experimental measurements have recently been published[4] which apply to the region of relatively high concentrations of oxygen in the reactant mixture and which may be interpreted on the basis of the rate equation just presented. These determinations are of interest not only because they involve partial pressures of $O_2$ as high as 90 mole percent but also because they have been extended to temperatures as high as 1900°K. Graphical analysis of the reported data shows that Eq. (3) is valid over the entire temperature and concentration range studied. Thus the rate constants in (3) may be evaluated from the straight lines obtained in a plot of $\{-(d[NO]/dt)/[NO]^2\}$ *vs* $\{[O_2]^{\frac{1}{2}}/[NO]\}$ (Table II).

[3] K. Jellinek, Z. anorg. u. allgem. Chem. **49**, 229 (1906).
[4] K. Vetter, Z. Elektrochem. **53**, 369 (1949).

## EFFECT OF NITROGEN

The experimental measurements of the rates of decomposition of nitric oxide in the presence of nitrogen are summarized in Table III. A definite decrease in the rate of transformation of the reactant is noted in the presence of nitrogen. However, in spite of the more than tenfold variation in the initial concentration of nitrogen in the gas mixture the measured reaction rates appear to be insensitive to the partial pressure of the additive. At the same time it is to be noted that over the range of nitrogen concentration studied the difference in reaction rates for the two systems is relatively constant (Fig. 1). Thus the kinetics still follow a second-order rate law, but the new curve extrapolates to a point of intersection corresponding to a concentration of nitric oxide of about $2.8\times10^{-6}$ mole $\times$cc$^{-1}$ (Fig. 1). Since at the temperature of these experimental measurements the heterogeneous kinetics are predominant,[1] the observed results suggest partial poisoning of the surface by nitrogen. Even at the lowest concentrations of nitrogen employed in these measurements the number of nitrogen molecules are in excess of the minimum amount required to cover the surface of the reactor. In addition, there is evidence that the surface plays an active role not only in initiating the reaction but also in the termination of the process. As previously shown[1] an increase in the surface-to-volume ratio by a factor of 2.2 yields a proportional increase in decomposition rate only at relatively high pressures of NO (Table IV). However, the addition of nitrogen to the "packed" reactor results in a marked increase in rate as compared to that observed in the vessel with lower surface-to-volume ratio containing excess nitrogen. Thus the adsorption of nitrogen on the walls of the container plays the dual role of poisoning

TABLE III. Effect of nitrogen on rate of thermal decomposition of nitric oxide.

| Temp °K | $N_{N_2}$ | [NO] mole $\times$cc$^{-1}\times10^{8}$ | [$N_2$] | Decomposition rate mole $\times$cc$^{-1}\times$sec$^{-1}\times10^{12}$ With $N_2$ | Without $N_2$ |
|---|---|---|---|---|---|
| 980 | 0.0142 | 8.492 | 0.122 | 16.20 | 18.31 |
| | | 6.918 | 0.100 | 9.87 | 12.14 |
| | 0.0254 | 5.655 | 0.147 | 5.44 | 8.16 |
| | | 4.586 | 0.119 | 2.97 | 5.31 |
| | | 3.750 | 0.098 | 1.63 | 3.58 |
| | 0.105 | 7.824 | 0.934 | 13.79 | 15.50 |
| | | 6.366 | 0.760 | 7.37 | 10.30 |
| | | 5.185 | 0.619 | 4.44 | 6.81 |
| | | 4.221 | 0.504 | 2.99 | 4.52 |
| | | 3.424 | 0.409 | 1.45 | 2.97 |
| | 0.153 | 8.395 | 1.516 | 16.21 | 17.97 |
| | | 6.844 | 1.236 | 9.20 | 11.91 |
| | | 5.574 | 1.007 | 5.46 | 7.89 |
| | | 4.551 | 0.822 | 3.32 | 5.26 |
| | | 3.721 | 0.672 | 2.11 | 3.52 |
| | | 3.015 | 0.545 | 1.13 | 2.31 |

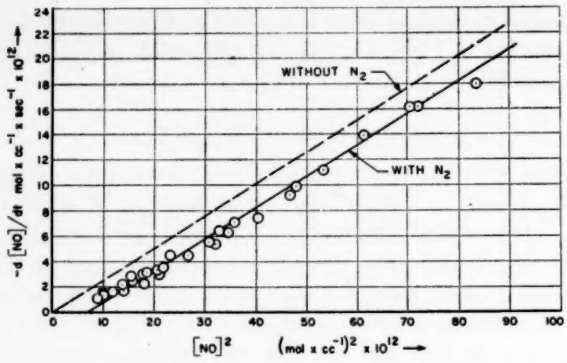


FIG. 1. Effect of $N_2$ on rate of thermal decomposition of NO.

the surface for the initiation process as well as for the termination reaction. Some contribution may of course also be made by the decrease in the rate of diffusion of active species to the surface in the presence of nitrogen.

As the temperature of the system is raised into the region of the homogeneous mechanism[1] the effect of nitrogen on the reaction kinetics of NO diminishes (Table V). The results show that in the presence of $N_2$ in concentrations as high as 46 mole percent the reaction still follows a second-order rate law, although the value of the specific reaction rate constant is decreased by about 10 percent at 1150°K from that measured for pure NO at the same temperature. These observations substantiate the effect of nitrogen as a surface poison which becomes of less importance in the homogeneous temperature region. It is not surprising, therefore, that at 1150°K a three-component system containing NO, $O_2$, and $N_2$ essentially exhibits a decomposition rate (Table V) calculated for the binary mixture NO and $O_2$ as given by Eq. (1). On the other hand, at 980°K the influence of $N_2$ is definitely apparent for such a multicomponent mixture.

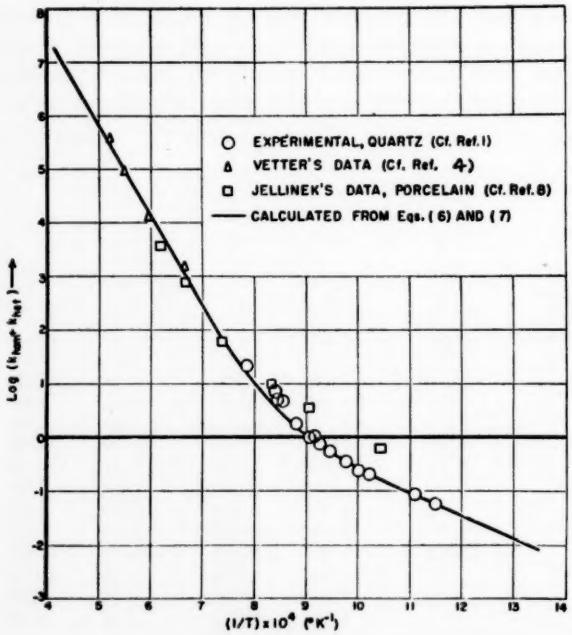
EXPERIMENTAL, QUARTZ (Cf. Ref. 1)
VETTER'S DATA (Cf. Ref. 4)
JELLINEK'S DATA, PORCELAIN (Cf. Ref. 8)
CALCULATED FROM Eqs. (6) AND (7)
Log ($k_{bimol}$/$k_{tot}$)
(1/T) x $10^4$ (°K$^{-1}$)

FIG. 2. Variation of specific reaction rate constant with temperature.

## MECHANISM OF THERMAL DECOMPOSITION

Based on the experimental results the following mechanism is proposed for the thermal degradation of nitric oxide:

$$\text{I. } 2NO \xrightarrow{k_1} N_2O+O \qquad \Delta H_0^0 = +35.2 \text{ kcal}$$

$$\text{II. } O+NO \xrightarrow{k_2} O_2+N \qquad \Delta H_0^0 = +4.6$$

$$\text{III. } N+NO \xrightarrow{k_3} N_2+O \qquad \Delta H_0^0 = -47.6$$

$$\text{IV, V. } O+O(+M) \underset{k_5}{\overset{k_4}{\rightleftarrows}} O_2(+M) \qquad \Delta H_0^0 = -117.3$$

The formation of nitrous oxide in the decomposition of nitric oxide has been reported.[5] In the present investigation this compound has not been isolated among the reaction products. However, its absence may be due to the rapid rate of decomposition of $N_2O$ at the temperatures studied[6] particularly in the presence of nitric oxide. Experimental measurements indicate that the rate of formation of $N_2$ for the binary mixture NO—$N_2O$ is far in excess of the rate observed for pure nitric oxide[1] or nitrous oxide[7] (Table VI). The exact mechanism of this reaction has not been fully investigated, however it appears that the decomposition of $N_2O$ is accelerated in the presence of NO as postulated by Musgrave and Hinshelwood.[6]

TABLE IV. Effect of surface and nitrogen on rate of thermal decomposition of nitric oxide.

| Concentration [(mole x cc$^{-1}$) x $10^8$] | | Decomposition rate [(mole x cc$^{-1}$ x sec$^{-1}$) x $10^{12}$] | |
|---|---|---|---|
| NO | $N_2$ | Surface/volume = 0.49 cm$^{-1}$ | Surface/volume = 1.12 cm$^{-1}$ |
| 9.49 | 0 | 24.3 | 36.2 |
| 3.66 | 0 | 3.6 | 4.3 |
| 2.98 | 0 | 2.4 | 2.8 |
| 9.49 | 0.51 | 22.6 | 42.5 |
| 3.66 | 0.21 | 1.8 | 3.2 |
| 2.98 | 0.18 | 0.8 | 1.6 |

The chain reaction represented by steps II and III of the proposed mechanism have been considered by Zeldovich[8] and Frank-Kamenetzky[9] in the interpretation of the kinetics of formation of NO from the elements.

[5] J. Y. McDonald, J. Chem. Soc. **1928**, 1.
[6] Musgrave and Hinshelwood, Proc. Roy. Soc. (London) **A135**, 23 (1932).
[7] Hinshelwood and Burk, Proc. Roy. Soc. (London) **A106**, 284 (1924).
[8] Ya. B. Zeldovich, Acta Physicochim. U.R.S.S. **21**, 577 (1946).
[9] D. Frank-Kamenetzky, Acta Physicochim. U.R.S.S. **23**, 27 (1947).

Since reaction II is endothermic to the extent of 4.6 kcal (based on the heat of dissociation of nitrogen of 169.5 kcal/mole), the energy of activation for this reaction must be in excess of this value. This fact is borne out by the experimental data presented which permits an evaluation of the energy barrier for this process.

On the basis of the proposed mechanism and with the assumption of the steady-state concentration of atomic species the rate of disappearance of nitric oxide is given by

$$-d(\mathrm{NO})/dt = 2k_1(\mathrm{NO})^2 + 2k_2(\mathrm{NO})^2 \times \left\{ \frac{k_1}{2k_4(M)} + K_e \frac{(\mathrm{O_2})}{(\mathrm{NO})^2} \right\}^{\frac{1}{2}}, \quad (4)$$

where $K_e$ is the equilibrium constant for the reaction $O_2 = 2O$.

TABLE V. Combined effects of nitrogen and oxygen on rate of thermal decomposition of nitric oxide.

| Temp $T$ (°K) | Concentration [(mole $\times$cc$^{-1}$) $\times 10^6$] NO | $N_2$ | $O_2$ | Decomposition rate [(mole $\times$cc$^{-1}$ $\times$sec$^{-1}$) $\times 10^{12}$] Without additive[a] Calculated | With additive Experimental | With additive Calculated |
|---|---|---|---|---|---|---|
| 1150 | 4.677 | 0.120 | 0.113 | 61.5 | 274.2 | 271.0 |
| | 3.221 | 0.083 | 0.078 | 28.6 | 155.5 | 141.7 |
| | 2.200 | 0.056 | 0.053 | 13.7 | 84.6 | 84.0 |
| 980 | 4.476 | 0.114 | 0.108 | 5.3 | 16.1 | 28.1 |
| | 3.080 | 0.079 | 0.074 | 2.6 | 9.8 | 15.6 |

[a] Based on data from reference 1.

If at high concentrations of oxygen, the first term under the square-root sign of Eq. (4) is small compared with the second, then

$$-d(\mathrm{NO})/dt = 2k_1(\mathrm{NO})^2 + 2K_e^{\frac{1}{2}}k_2(\mathrm{O_2})^{\frac{1}{2}}(\mathrm{NO}), \quad (5)$$

which is of the same functional form as the empirical rate expression previously found to apply at high concentrations of $O_2$.

It is thus possible to evaluate the activation energies for step I and II of the mechanism from the temperature coefficients of the specific reaction rate constants presented in Table VII. Thus the following rate expression obtains for the homogeneous decomposition of nitric oxide, i.e., at temperatures above 1600°K

$$k_{\mathrm{homog}} = 2.2 \times 10^{14} e^{-78200/RT}. \quad (6)$$

Combined with the rate expression for the heterogeneous reaction observed in quartz,[1]

$$k_{\mathrm{heterog}} = 1.4 \times 10^{4} e^{-21400/RT}, \quad (7)$$

TABLE VI. Effect of nitrous oxide on rate of thermal decomposition of nitric oxide.

| Temp °K | [NO] mole $\times$cc$^{-1}$ $\times 10^6$ | [$N_2O$] | $N_{N_2O}$ % | Rate of formation of $N_2$ mole $\times$cc$^{-1}$ $\times$sec$^{-1}$ $\times 10^{12}$ With $N_2O$ | Without $N_2O$ |
|---|---|---|---|---|---|
| 1151 | 3.64 | 0.044 | 1.2 | 362.5 | 40.0 |
| | 3.04 | 0.037 | 1.2 | 216.7 | 27.8 |
| | 2.54 | 0.031 | 1.2 | 130.8 | 19.4 |
| | 3.44 | 0.018 | 0.53 | 126.0 | 35.4 |
| | 2.91 | 0.016 | 0.53 | 58.3 | 25.4 |
| | 2.46 | 0.013 | 0.53 | 27.0 | 18.1 |
| 981 | 7.66 | 0.093 | 1.2 | 87.5 | 14.9 |
| | 6.19 | 0.075 | 1.2 | 50.3 | 9.8 |
| | 5.11 | 0.062 | 1.2 | 50.8 | 6.6 |
| | 7.31 | 0.039 | 0.53 | 21.1 | 13.6 |
| | 5.97 | 0.032 | 0.53 | 16.4 | 9.0 |
| | 4.84 | 0.026 | 0.53 | 13.3 | 6.0 |

the composite curve results as shown in Fig. 2. Of particular interest is the agreement observed between the calculated and measured rates[3,4] at temperatures above 1500°K where the homogeneous gas-phase reaction predominates. At lower temperatures the divergence between the data obtained in quartz[1] and porcelain[3] is to be expected because of the differences in surface activity.

Based on the data presented in Table VII the temperature coefficient for reaction II involves an activation energy of 22.9±3 kcal. It is evident therefore that the occurrence of step II by a bimolecular process as written becomes less probable if the heat of dissociation of nitrogen is in excess of 7.38 ev.[10] Consequently this step may involve the formation of an electronically excited intermediate $NO_2$*[11] by a three-body collision

TABLE VII. Specific reaction rate constants for thermal decomposition of nitric oxide[a]

| Temp °K | $k_1$ (mole/cc)$^{-1}$ $\times$sec$^{-1}$ $\times 10^{-4}$ | $k_2$ (mole/cc)$^{-\frac{1}{2}}$ sec$^{-1}$ $\times 10^{-3}$ |
|---|---|---|
| 1525 | 0.14 | 0.26 |
| 1690 | 1.2 | 0.71 |
| 1840 | 9.6 | 1.0 |
| 1912 | 46 | 1.5 |

[a] Data based on analysis of the experimental results published in reference 4.

at high temperatures and/or a surface reaction at temperatures below 1500°K. Similarly in the temperature region in which the heterogeneous mechanism applies, step I represents a surface reaction involving an activation energy of only 21.4 kcal.

[10] A. G. Gaydon, *Dissociation Energies and Spectra of Diatomic Molecules* (John Wiley and Sons, Inc., New York, 1947).
[11] Spealman and Rodebush, J. Am. Chem. Soc. **57**, 1474 (1935).

# On the New Absorption Bands of the Oxygen Molecule in the Far Ultraviolet Region

YOSHIO TANAKA*
*Optical Institute, Tokyo University of Education, Tokyo, Japan*
(Received April 16, 1952)

The absorption bands of the oxygen molecule in the extreme ultraviolet region were studied using a 3-meter grazing incidence vacuum spectrograph. Two new progressions of bands were found in the region between 1200A and 1290A (one of which is considered to be a member of the Rydberg series converging to the first ionization potential of the oxygen molecule). There were also observed a few short continua near the short wavelength end of the Schumann-Runge absorption continuum. The behavior of three strong and diffuse bands, at 1200~1290A, were studied at pressures ranging from 0.01 to several mm of Hg. Assuming the diffuseness of these bands as being due to predissociation, the existence of oxygen atoms in $^1S$ metastable states in the upper atmosphere is briefly discussed.

## INTRODUCTION

TO study the highly excited states of the oxygen molecule, as well as in connection with the study of the phenomena in the upper atmosphere, it is interesting to investigate the absorption bands in the extreme ultraviolet region. Price and Collins[1] have observed many absorption bands in the region $\lambda<1250$A; in particular, they found four Rydberg type series in the region $\lambda<1000$A: $(H, I, \cdots)$, $(H', I', \cdots)$, $(M, N, \cdots)$, $(P, Q, \cdots)$, each of which converges to some excited states of the ionized oxygen molecule. Tanaka and Takamine[2,3] have repeated Price and Collins' work, and from the vibrational structure of the bands and the assignment of the higher bands to a $^3\Sigma_g^- \rightarrow {}^4\Sigma_g^-$ Rydberg series ($P, Q, \cdots$, series) they obtained a value of the fourth ionization potential of $O_2$ which agreed well with the value obtained by a combination of electron impact data and band spectra data.

In the wavelength region $\lambda>1000$A, Price and Collins tried to find without success the Rydberg series converging to the first ionization potential of $O_2$. They suggested as reason why such a series was not observed that, as in the case of $N_2$, such a series would have a much smaller intensity than the band series converging to the higher ionization potentials. In fact, the bands appearing in this region ($\lambda\sim1000$A) have no apparent regularities in either their spacings or their intensities, so that it is difficult to arrange these bands in progressions or series.

In the present work, restricted to 1000A–1300A, we varied the pressure from 0.01 to a few mm of Hg in order to observe (1) what kind of variations will occur in the intensity and width of these bands, and (2) whether other bands which have not been observed in previous studies should appear at comparatively high pressures.

## EXPERIMENTS

Though the apparatus and the method used in the present experiment are exactly the same as those which have been reported in our previous work on $H_2$ absorption,[4] we will briefly mention the main features. A 3-meter grazing incidence grating spectrograph was used with a dispersion of 1.9 A/mm in the first order in the wavelength region 1000–1300A. A Lyman continuum light source was employed operating with the same kind of gas as that in the body of the spectrograph. A system of differential pumping maintained the pressure difference between the discharge tube and the spectrograph. The gas pressure was controlled by regulating the gas influx into the spectrograph and the discharge tube, and it was measured by a McLeod gauge.

Oxygen gas, prepared by the electrolysis of a weak aqueous solution of KOH, was dried by passing first through concentrated $H_2SO_4$ and then $P_2O_5$, and was stored in a reservoir until use.

As we emphasized in our previous notes,[5] the $H_2O$ absorption conceals much of the region below 1200A because of the enormous intensities of these bands and their complicated structure. We were able to remove these bands almost completely by leaving several small trays of $P_2O_5$ powder in the spectrograph overnight and by passing the entering $O_2$ through a trap immersed in liquid air.

The absorptions of the atomic lines, SiI, SiII, and OI always appear and sometimes, when the discharge tube is contaminated with stopcock grease vapor, the fourth positive bands of CO also appear weakly. The absorption of the Lyman series of hydrogen could not be removed, possibly because the hydrogen was adsorbed or occluded in the capillary or in the aluminum electrodes.

The Schumann plates used were prepared by myself according to the method of Hopfield and Appleyard[6] with a slight modification.

* Present address: Physics Department, University of Chicago, Chicago 37, Illinois.
[1] W. C. Price and G. Collins, Phys. Rev. **48**, 714 (1935).
[2] Y. Tanaka and T. Takamine, Phys. Rev. **59**, 771 (1941).
[3] Y. Tanaka and T. Takamine, Sci. Papers Inst. Phys. Chem. Research (Tokyo) **39**, 437 (1942).
[4] Y. Tanaka, Sci. Papers Inst. Phys. Chem. Research (Tokyo) **42**, 49 (1944).
[5] Y. Tanaka, Sci. Papers Inst. Phys. Chem. Research (Tokyo) **42**, 49 (1944).
[6] J. J. Hopfield and E. T. S. Appleyard, J. Opt. Soc. Am. **22**, 488 (1932).

## RESULTS AND DISCUSSION

### (A) General Aspect

Spectrograms were taken covering the region from 800 to 2000A. In the case of high pressures (a few mm Hg), the Schumann-Runge absorption bands are well developed, extending from 1750–2000A, and followed by the well-known Schumann-Runge continuous absorption which extends to around 1300A. In gross appearance, there are three strong, very broad bands near the end of this continuum. These are followed by many broad bands, some of which are diffuse and others are sharp, becoming more and more confused with each other until they finally merge into a continuum around 1040A. Probably, this is not a true continuum, but only an apparent one composed of many bands lying close together.

In the case of low pressures (~0.01 mm Hg), the S−R absorption bands have completely disappeared, but the S−R continuum still remains around 1450A with a narrow extension. In this case, the bands in question ($\lambda<1300$A) appear weakly and, as was pointed out by Price and Collins, some have clear shadings, but others have such a compact structure that they look like an atomic line. Beyond this region ($\lambda<1000$A), the $H, H', M, M', \cdots$, progressions appear clearly with strong intensity.

### (B) The Continua Near the End of the S-R Continuum

Ladenburg and van Voorhis[7] pointed out that the intensity distribution of the S−R continuum has a maximum value around 1450A, and decreases more rapidly on the shorter wavelength side. It has been observed in the present study that near the short wavelength end of this continuum ($\lambda\sim1300$A), the intensity does not decrease monotonously but has several weak though distinct maxima (these are at 1349A, 1334A, and 1290A). Upon gradually increasing the pressure, the continuum extends step by step quite abruptly to 1349A, 1334A, and 1290A. Finally, at a pressure of a few mm Hg, the tail of this last continuum merges into the tail of the next band which is called by Price and Collins, "the longest band." At such high pressure, there appears another weak continuum which fills up the region between the head of the "longest band" and the Lyman $\alpha$-line (1216A). As will be described more fully below, at high pressures, the band (1206A), which we shall call the "second band" tentatively, has been much broadened, with its long wavelength side reaching the Lyman $\alpha$-line. Therefore, under such conditions, the spectrogram looks as if the S−R continuum extends to around 1190A, and is crossed by narrow emission continua at 1240A and 1216A.

Of these three absorption maxima described above, the longest one (1349A) lies situated energetically very near the dissociation limit 9.00 ev ($^1D+^1D$), and the remaining two (1334A and 1290A) are very near to but slightly higher than the dissociation limit 9.25 ev ($^3P+^1S$). From the dissociation products in the two cases, many molecular states are derivable using Wigner and Witmer's rules, but on account of the ordinary selection rules, only the transition to the $^3\Pi_u$ state is allowed from the $^3\Sigma_g^-$ ground state. Consequently, we can ascribe at least one of the last two continua to this transition. The energy difference between the dissociation limit 9.25 ev ($^3P+^1S$) and the corresponding energy of the maximum intensity of the 1290A continuum is only 0.35 ev. If we assume that the upper state $^3\Pi_u$ is a genuinely unstable state, and that the Franck-Condon principle can be applied, the upper potential curve must be very flat even in the region $r=1.2$A. Of course, it is also possible to suppose that the upper state has a shallow minimum.

The other continua lying at 1349A and 1334A are probably due to transitions forbidden by the ordinary selection rules from the ground state to some of the excited states expected from the same products. These are also unstable.

The existence of atomic oxygen in the metastable state $^1S$ in the upper atmosphere is an interesting problem. Though the continua mentioned above that would dissociate into the metastable $^1S$ atomic state are weaker and narrower than those of the S−R continuum, it may safely be said that there are definite possibilities of the existence of the metastable $^1S$ state of atomic oxygen in the upper atmosphere. This idea will be strengthened by the consideration of other diffuse bands later in the paper.

### (C) Characteristic Diffuse Bands

The so-called "longest band" (1244A) has a strong intensity comparable with those of the members of the $H, I, \cdots$, progressions. At the lowest pressure we tried (~0.001 mm Hg), it appears as a close doublet (1244.3A and 1243.5A measured at their centers), and with a gradual increase in pressure, it extends considerably but only towards the longer wavelength side. Finally, at a pressure of about 1.0 mm Hg, it merges into the 1290A continuum. This band has quite a sharp head at the shorter wavelength side, whose position is not influenced by the variation in pressure. We tried to find the rotational structure using a narrower slit and better definition, but we failed even in resolving its tail. Price and Collins have described the upper state of this transition as somewhat predissociated, and this is clearly confirmed in the present study. We might consider a possible alternative explanation. A weak continuous absorption might overlie the band so that it might have the appearance of a very broad and diffuse band at high pressures. As will be described later, there appear two other bands and a few unclassified atomic

[7] R. Ladenburg and C. C. van Voorhis, Phys. Rev. 43, 315 (1933).

TABLE I.

| λ(A) in vacuum | ν(cm⁻¹) | I | Designation | Remarks |
|---|---|---|---|---|
| 1349 | 74130 | 9 | continuous maximum | dissociation products: $^3P+^1S$ or $^1D+^1D$ |
| 1334 | 74960 | 7 | continuous maximum | dissociation products: $^3P+^1S$ or $^1D+^1D$ |
| 1290 | 77520 | 6 | continuous maximum | dissociation products: $^3P+^1S$ |
| 1293.31 | 77321.0 | 2 | progression (I), 1 | obscured by 1290A continuum |
| 1292.52 | 77368.2 | 2 | | |
| 1268.81 | 78814.0 | 1 | | band due to transition from $v''=1$ of the ground state to the same upper state of "the longest band" |
| 1268.08 | 78859.4 | 1 | | |
| 1262.97 | 79189.7 | 3 | progression (I), 2 | |
| 1262.14 | 79230.5 | 3 | | |
| 1258.88 | 79435.7 | 3 | atomic abs. line | obscured by "longest band" |
| 1256.52 | 79584.9 | 4 | atomic abs. line | obscured by "longest band" |
| 1255.33 | 79660.3 | 3 | atomic abs. line | obscured by "longest band" |
| 1250.51 | 79967.7 | 2 | progression (II), 1 | obscured by "longest band" |
| 1250.21 | 79998.7 | 2 | | |
| 1244.26 | 80369.2 | 10 | "longest band" | at high pressure, it extends to around 1269A, but its head is not influenced |
| 1243.49 | 80419.0 | 10 | | |
| 1234.09 | 81031.4 | 4 | progression (I), 3 | at high pressure, it is obscured by continuum appearing around 1227A |
| 1233.43 | 81074.7 | 4 | | |
| 1229.34 | 81344.5 | 2 | atomic line | unclassified |
| 1228.64 | 81390.8 | 2 | atomic line | unclassified |
| 1227.51 | 81465.7 | 2 | atomic line | unclassified |
| 1226.96 | 81502.2 | 2 | atomic line | unclassified |
| 1226.75 | 81516.2 | 2 | atomic line | unclassified |
| 1224.93 | 81637.3 | 2 | atomic line | unclassified |
| 1224.21 | 81685.3 | 2 | atomic line | unclassified |
| 1223.83 | 81710.7 | 2 | atomic line | unclassified |
| 1222.58 | 81794.2 | 2 | progression (II), 2 | |
| 1222.01 | 81832.4 | 2 | | |
| 1217.65 | 82125.4 | 5 | OI | used as a reference line |
| 1215.66 | 82259.8 | 8 | H, Lyman "α" | |
| 1207.50 | 82815.7 | 9 | "second band" | at high pressure, it extends to around 1214A, and for shorter wavelength, extends to around 1190A |
| 1206.75 | 82867.2 | 9 | | |
| 1205.38 | 82961.4 | 9 | | |
| 1204.54 | 83019.2 | 9 | may be progression (I), 4 | |
| 1200.71 | 83284.1 | 4 | NI | used as a reference line |
| 1200.22 | 83318.1 | 4 | NI | used as a reference line |
| 1199.55 | 83364.6 | 4 | NI | used as a reference line |
| 1169.14 | 83602.3 | 3 | progression (II), 3 | |
| 1194.50 | 83717.0 | 3 | Si II | used as a reference line |
| 1193.31 | 83800.5 | 3 | Si II | used as a reference line |
| 1190.42 | 84004.0 | 3 | Si II | used as a reference line |
| 1182.32 | 84579.5 | 2 | progression (I), 5 | |
| 1181.64 | 84628.1 | 2 | | |
| 1172.08 | 85318.4 | 7 | "third band" | very diffuse |
| 1171.35 | 85371.6 | 7 | progression (II), 4? | |
| 1164.23 | 85893.7 | 9 | group "a" | line-like appearance at low pressure |
| 1163.87 | 85920.2 | 10 | | line-like appearance at low pressure |
| 1162.98 | 85986.0 | 8 | | line-like appearance at low pressure |
| 1162.44 | 86025.9 | 8 | | |
| 1161.72 | 86079.3 | 9 | | line-like appearance (very sharp) |
| 1161.47 | 86097.8 | 5 | | |
| 1154.36 | 86628.1 | 6 | group "a" | line-like appearance |
| 1154.06 | 86650.6 | 10 | | |
| 1153.20 | 86715.2 | 8 | | |
| 1152.98 | 86731.8 | 6 | | |
| 1152.14 | 86795.0 | 8 | OI | |
| 1151.67 | 86830.4 | 7 | | |
| 1151.46 | 86846.3 | 6 | | |
| 1148.62 | 87061.0 | 2 | progression (II), 5? | at high pressure, it shows rotational structure |
| 1137.28 | 87929.1 | 8 | atomic line? | at high pressure, it is obscured by very diffuse band |

absorption lines overlying this band; therefore, without a detailed measurement of the intensity distribution within this band, we cannot decide between the two alternatives. In any case, the strong diffuse appearance of this band, even in the case of very low pressures, is strong support for the idea of predissociation occurring in the upper electronic state of this band.

The next conspicuous band, which we shall tentatively call the "second band," is situated at 1206A. Close inspection of the plates taken at low pressures

TABLE I.—*Continued.*

| λ(A) in vacuum | ν(cm⁻¹) | I | Designation | Remarks |
|---|---|---|---|---|
| 1136.41 | 87996.4 | 5 | | |
| 1136.09 | 88021.2 | 5 | group "b" | shading to shorter wavelengths |
| 1135.13 | 88095.6 | 5 | | |
| 1134.74 | 88125.9 | 5 | | shading to shorter wavelengths |
| 1125.60 | 88841.5 | 4 | | shading to shorter wavelengths and shows rotational structure |
| 1125.34 | 88862.0 | 5 | | shading to shorter wavelengths and shows rotational structure |
| 1124.68 | 88914.2 | 4 | group "c" | shading to shorter wavelengths and shows rotational structure |
| 1123.62 | 88998.1 | 3 | | shading to shorter wavelengths and shows rotational structure |
| 1123.08 | 89040.9 | 6 | | line-like appearance |
| 1122.78 | 89064.6 | 3 | | line-like appearance |
| 1122.34 | 89099.6 | 5 | | shading to shorter wavelengths |
| 1121.94 | 89131.3 | 5 | | shading to shorter wavelengths |
| 1120.98 | 89207.7 | 5 | group "b" | shading to shorter wavelengths |
| 1120.76 | 89225.2 | 5 | | shading to shorter wavelengths |
| 1116.78 | 89543.2 | 3 | | shading to shorter wavelengths |
| 1115.87 | 89616.2 | 4 | | shading to shorter wavelengths |
| 1115.10 | 89678.1 | 5 | | line-like appearance |
| 1113.89 | 89775.5 | 3 | | shading to longer wavelengths |
| 1112.98 | 89848.9 | 3 | | shading to longer wavelengths |
| 1112.29 | 89904.6 | 2 | | shading to longer wavelengths |
| 1106.36 | 90386.5 | 4 | | shading to shorter wavelengths |
| 1106.13 | 90405.3 | 5 | | shading to shorter wavelengths |
| 1105.00 | 90497.7 | 3 | | shading to shorter wavelengths |
| 1104.41 | 90546.1 | 4 | group "c" | shading to shorter wavelengths |
| 1103.95 | 90583.8 | 5 | | shading to shorter wavelengths |
| 1103.64 | 90609.3 | 4 | | shading to shorter wavelengths |
| 1102.59 | 90695.5 | 4 | | shading to shorter wavelengths |
| 1102.37 | 90713.6 | 5 | | shading to shorter wavelengths |
| 1101.74 | 90765.5 | 4 | group "d" | shading to shorter wavelengths |
| 1100.34 | 90881.0 | 4 | | shading to shorter wavelengths |
| 1090.63 | 91690.1 | 5 | | line-like appearance |
| 1089.82 | 91758.3 | 3 | | shading to shorter wavelengths |
| 1089.46 | 91788.6 | 4 | | shading to shorter wavelengths |
| 1088.68 | 91854.4 | 4 | group "c" | shading to shorter wavelengths |
| 1088.38 | 91879.7 | 5 | | shading to shorter wavelengths |
| 1084.51 | 92207.5 | 4 | | shading to shorter wavelengths |
| 1083.67 | 92279.0 | 4 | | shading to shorter wavelengths |
| 1083.44 | 92298.6 | 5 | group "d" | shading to shorter wavelengths |
| 1082.29 | 92396.7 | 6 | | shading to shorter wavelengths |
| 1067.22 | 93701.4 | 8 | | shading to shorter wavelengths |
| 1066.85 | 93733.9 | 8 | | shading to shorter wavelengths |
| 1066.09 | 93800.7 | 8 | | shading to shorter wavelengths |
| 1065.78 | 93828.0 | 8 | group "d" | shading to shorter wavelengths |
| 1064.93 | 93902.9 | 8 | | shading to shorter wavelengths |
| 1064.68 | 93924.9 | 8 | | shading to shorter wavelengths |
| 1050.17 | 95222.7 | 6 | | shading to shorter wavelengths |
| 1049.86 | 95250.8 | 8 | | shading to shorter wavelengths |
| 1048.91 | 95337.1 | 7 | | shading to shorter wavelengths |
| 1048.64 | 95361.6 | 6 | group "d" | shading to shorter wavelengths |
| 1047.60 | 95456.3 | 6 | | shading to shorter wavelengths |
| 1047.41 | 95473.6 | 6 | | shading to shorter wavelengths |
| 1032.70 | 96833.5 | 5 | | shading to shorter wavelengths |
| 1031.35 | 96960.3 | 5 | group "d"? | shading to shorter wavelengths |

shows that this band consists of two bands, each of which apparently has two branches. They are 1207.5A, 1206.8A and 1205.4A, 1204.5A. The latter band belongs to what we will later call progression I. Both bands are diffuse and at high pressure; they broaden on both sides, with a much greater extension toward the shorter wavelength side. At the highest pressures we tried, the long wavelength side extends to a position about 2A from the Lyman $\alpha$-line where it is terminated abruptly. The absorption decreases slowly on the short wavelength side while simultaneously weak, but distinct absorption bands appear in this region along with some SiII and NI absorption lines. Like in the "longest band" described above, the upper state of the "second band" may also be strongly predissociated.

The band located at 1172A which we shall tentatively call the "third band" has a diffuse appearance like the other two bands discussed above. It is weak at low pressures, but at higher pressures it becomes as strong as the other two bands. The behavior of extension of

this band is opposite to that of the "second band," namely, it extends greatly toward longer wavelengths and in a portion of its tail some rotational fine structure is slightly observable.

The three bands described above are characterized by their strength, their diffuseness, and their abnormal behavior of changing in width with variation of the pressure in the tank. Even at such very low pressures that the S−R continuum completely disappears, the first two bands remain with an intensity comparable to that of the $H, I, \cdots$, progressions. Therefore, if the diffuseness is ascribed to predissociation in their upper states, the probability of photodissociation of the oxygen molecule due to the absorption of the corresponding radiations should be considerable.

It seems likely that the predissociation should be due to the perturbation by the repulsive states derived from the dissociation products $(^1S+^3P)$ and $(^1D+^1D)$. The strong diffuseness shown in these bands suggests that both states (the dissociable one and the perturbing one) must have the same multiplicity, and the strong intensity suggests that this multiplicity must be the same as that of the ground state (for detailed discussion, of course, we must consider all of the selection rules). Consequently, the perturbing states which cause predissociation should be the ones derived from the dissociation products $(^1S+^3P)$ as the other possibility cannot give rise to a triplet state. Thus, we can consider the existence of the $^1S$ metastable atomic oxygen in the upper atmosphere with a certain confidence.

### (D) New Band Progressions

Two new progressions of bands were observed in the same region as the three bands described above. In general, they are weak and not all appear in the case of low pressures, but with increased pressure, they acquire a strong intensity. As described above, since the strong diffuse bands occur superimposed on them, it is difficult to pick out all of them on any one plate taken at some specific condition. The results of their measurement are shown in Table I, along with that of the other bands.

The bands belonging to progression I have doublet features and the averaged separation of them is about $\Delta\nu=45$ cm$^{-1}$. They are shaded toward the shorter wavelength side and some show clear rotational structure. Except for the fourth member, the intensity distribution in this progression seems to be normal. The first member is weak, and since it appears at just the position of the 1290A continuum, it is difficult to find this band under any conditions. In a few cases, we observed it due to the favorable contrast of the plates used.

The $Q$ heads of these bands can be arranged in the following formula:

$$\nu=77204.2+1906.97(v'+\tfrac{1}{2})-18.22(v'+\tfrac{1}{2})^2 -1580.32(v''+\tfrac{1}{2})+11.99(v''+\tfrac{1}{2})^2.$$

In the calculation, we assigned $v'=0$ to the lowest member (1292.52A). Using the empirical formula, we obtained $D=6.19$ ev (49900 cm$^{-1}$) as the dissociation energy of the upper state. Combining this with the dissociation energy of the normal state $D=5.08$ ev the excitation energy of the dissociation products comes out to be 10.58 ev. There are three levels in the oxygen atom near this energy, $2p^3 3s^5S$ (9.1 ev), $2p^3 3s^3S$ (9.5 ev), and $2p^3 3p^5P$ (10.7 ev). The value of $\omega_e$ obtained is by 30.6 cm$^{-1}$ greater than that of the ground state $^2\Pi_g$ of the ionized molecule, and the coefficient of anharmonicity $\omega_e\chi_e$ is also very similar in these two states; thus it can be assumed that this progression is the first member of a Rydberg series of bands converging to the first ionization potential of the $O_2$ molecule.

The fourth member of this progression coincides with the component band (1205.4/1204.5A) of the "second characteristic band" described above, and since this band is very diffuse and strong, there will be a strong predissociation near $v'=3$ in the upper electronic state. The fifth member is weak and has somewhat diffuse appearance.

In the same wavelength region, there appears another progression II. The bands belonging to this progression have the doublet feature too and shade distinctly towards the shorter wavelength side. The average value of the doublet separation is $\Delta\nu=29$ cm$^{-1}$. All of the bands show clear rotational structure, but as in the case of progression I, the diffuse characteristic bands overlap them, and hence it is difficult to see them on any one plate. At high pressures, the first member of this progression is completely hidden by the "longest band," and the third member joins the tail of the "second band." The fourth one seems to be part of the "third" characteristic diffuse band. The $Q$-heads of these bands can be arranged in the following formula:

$$\nu=78274.1+1890.50(v'+\tfrac{1}{2})-29.41(v'+\tfrac{1}{2})^2 -1580.32(v''+\tfrac{1}{2})+11.99(v''+\tfrac{1}{2})^2.$$

In this case, too, we have assigned $v'=0$ to the lowest member (1250.21A).

Rough extrapolation of $\Delta G$ values gives $D=3.77$ ev (30370 cm) as the dissociation energy of the upper electronic state of this progression. Combining this with $D=5.08$ ev for the normal state, we obtain 8.48 ev as excitation energy of the dissociation products which is very near 8.34 ev for the dissociation products $(^1S+^1S)$. The only type of molecular state derivable from these states is $a^1\Sigma$, and according to the ordinary selection rules, the transition from the ground state to such a state is generally forbidden. Without more detailed investigation we cannot say anything more about the character of the upper state. The anharmonicity of this state is large compared with the other states so far known.

There remains a clear but unclassified band at 1269.0A which is very weak except at high pressures

and which appears as a doublet ($\Delta\nu=45.37$ cm$^{-1}$) similar to those of progression I above. Its shading is not clear. Perhaps it is due to the transition from $v''=1$ to the same vibrational level of the upper state of the "longest band."

### (E) Other Bands Between 1160A and 1000A

There appear many bands from 1000A to 1160A with an irregular spacing. Some have clear heads and shading, while others have a somewhat headless appearance. Some bands show rotational structure while others are diffuse. With the exception of a few bands, most of them shade towards shorter wavelengths; that is, roughly speaking, the upper states of the bands are more stable than the ground state.

The results of the measurements are shown in Table I. Because of the irregularities of the bands, both in their spacing and their intensities, a complete grouping is difficult.

Because of similarities in their appearance, four groups (a, b, c, and d) of bands are tentatively classified. Group "a" includes two bands, each of which is composed of three components. The component on the long wavelength side has two heads, each with a compact structure, so that at low pressures they look like two atomic lines. But at higher pressures, they shade towards the longer wavelength side and show a close lying rotational structure in the tail. The middle component also has two heads, but they shade oppositely to each other. The component on the short wavelength has two subcomponents, both of them shading towards the shorter wavelength side. As in the case of the first mentioned component, the last one has a $P$-branch that appears very much like an atomic line. At high pressures, these six components merge into each other and appear as a broad band having a rectangular distribution of intensity.

Group "b" includes two bands, each of which is composed of two components. Each component has apparently two heads and both shade towards the shorter wavelength side.

The bands forming the group "c" are apparently single and degrade towards the shorter wavelength side, but a closer inspection shows that each of them is composed of two heads. The lower members show rotational structure.

The last group "d" is the longest progression among the groups now picked out, and each member is seen to consist of three bands, each of which has two heads which shade towards shorter wavelengths.

Near 1112A there appears a group of bands, each of which shades to the long wavelength side. Price and Collins observed a weak continuum near 1105A extending towards shorter wavelengths. In the present investigation, there appeared in this region some of the discrete bands belonging to the groups "c" and "d" while the continuum observed by Price and Collins was scarcely observable. Since this region corresponds to the dissociation limit ($^1D+^1S$, $\lambda=1100$A), there is a certain possibility that this group of bands is a progression which converges to this limit, and the weak continuum found by Price and Collins may be the dissociation continuum. In fact, the intensity distribution in this group is normal and the interval between successive bands decreases quite normally. If the suggestion is right, the upper state of this group of bands has a very shallow minimum, because there is no extension of the bands observed in this group toward the longer wavelength side.

### (F) Rydberg Series of Bands Converging to the First Ionization Potential

Some efforts were made to find the Rydberg series of absorption bands which converges to the first ionization potential of $O_2$, but we have not yet succeeded. Using the values obtained by electron impact experiments and band spectra, we can expect the first ionization potential with confidence to be $12.3\pm0.1$ ev. There appear many absorption bands in the region between 1000A and 1020A mostly showing a line-like appearance and a close doublet feature. The line-like appearance resembles those of the bands appearing in the end of the Worley and Jenkins[8] series of $N_2$. The doublet feature also resembles that of the bands of progression I which we considered as being the first member of the Rydberg but series, unfortunately, we cannot pick out the bands which can be arranged in a series formula principally on account of the crowded appearance of many bands. When the pressure is increased a little more, there appear some diffuse bands in this region, so that the line-like bands are almost completely masked out. The work is being continued in an attempt to find this series.

[8] R. E. Worley and F. A. Jenkins, Phys. Rev. **54**, 305 (1938); R. E. Worley, Phys. Rev. **64**, 207 (1943).

# The Dissociation of Cyclopropane under Electron Impact

F. H. FIELD*
*Department of Chemistry, University of Texas, Austin, Texas*
(Received February 21, 1952)

The electron-impact-induced dissociations of cyclopropane are determined from the appearance of potentials of the several ions formed. In general, the dissociations involve a considerable amount of atomic rearrangement, and the evidence points to the opening of the carbon ring in the formation of the $C_3$ ions. The energy required to convert cyclopropane to ethylene and methylene is found to 77 kcal/mole, from which it is estimated that the C—C bond dissociation energy in cyclopropane is at least 50 kcal/mole. The unexpectedly good agreement of the values of the heat of formation of an ion formed by electron impact from several different sources is noted, and a question is raised as to the role of activation energies in the electron-impact dissociations of polyatomic molecules.

## EXPERIMENTAL

THIS paper reports the results of a study of the dissociation of cyclopropane under electron impact. Except for some work[1] on benzene, cyclohexane, and pyridine, no cyclic molecules have been studied by electron impact methods, and it was thought that cyclopropane would provide an interesting subject, particularly because of the presence in the molecule of large amounts of ring strain. Further, it was hoped that the results would permit the calculation of the C—C bond strength in the molecule, but unfortunately, the hope was only partially realized.

The appearance potentials were determined with a Westinghouse Type LV mass spectrometer using the vanishing current method.[2] The minimum ion current which gave a signal distinguishable from the background "noise" in the electrometer amplifier was less than $2\times10^{-15}$ amp. The electron accelerating voltages were measured with a Leeds and Northrup Type K-2 potentiometer used in conjunction with a suitable voltage divider. No external heat was applied to either the gas inlet system or the mass spectrometer tube, but the heat from the filament raised the ion-source temperature during the measurements to about 75°C as measured at the gas supply block (Plate 7).

Krypton was used as the electron voltage calibration standard for all of the measurements except those on the mass 13 fragment from cyclopropane, in which case neon was used. The proportions of the gases introduced were such that at an electron accelerating voltage of 75 volts, equal ion currents of $Kr^+$ (or $Ne^+$) and the ion from cyclopropane were obtained.

For the ions of greatest interest, replicate measurements of the appearance potentials were made, and the sequence of the measurements was such as to spread the several measurements on a given ion over a period of about three months. Thus, the effects of any short-term instrumental vagaries were minimized. The continuing adequacy of the apparatus and method was checked by interspersing among the cyclopropane measurements determinations of the ionization potentials of compounds for which this quantity is known. In general, the ratio of the determinations of unknowns to knowns was 5 to 1. The compounds used were propylene, ethylene, ethane, carbon dioxide, nitrogen, argon, and neon. In all cases the agreement with previously published values was satisfactory and is given in Table I.

The cyclopropane used was of medical grade and was subjected to a distillation through a five-foot column at a high reflux ratio. The cut boiling over a 0.4°C range at about −33°C was collected for the measurements. Since difficulty was encountered in achieving thermal equilibrium with the temperature measuring device of the distillation apparatus, the temperatures given are somewhat uncertain; however, there is no doubt that the cyclopropane collected did not contain significant amounts of propylene, the most serious possible contaminator.

The appearance potentials obtained are listed in Table II. The uncertainties given are estimates, and in those cases where replicate determinations were made, the uncertainties are always at least as large as the average deviation of the individual determinations from the average. It is felt that the consistent checking of known ionization potentials markedly decreases the possibility of the presence of systematic errors.

## DISCUSSION

Given the process $R_1R_2+e\rightarrow R_1^++R_2\cdot+2e$, the appearance potential $A$ of $R_1^+$ may be considered as the endothermicity of the ionization reaction, and if the heats of formation of $R_2\cdot$ and $R_1R_2$ are known, $A$ may be utilized to calculate an energetic quantity which shall be called the heat of formation[3] of the gaseous ion $R_1^+$, i.e., $\Delta H_f(R_1^+)=A-\Delta H_f(R_2\cdot)+\Delta H_f(R_1R_2)$. The ionic heat of formation thus defined might be

[1] Hustrulid, Kusch, and Tate, Phys. Rev. **54**, 1037 (1938); Kambara, J. Phys. Soc. Japan **2**, 25 (1947).

[2] For a general discussion of the significance of the various methods of determining appearance potentials see T. Mariner and W. Bleakney, Phys. Rev. **72**, 807 (1947).

[3] The use of ionic heats of formation was suggested to the author by Dr. J. L. Franklin of the Humble Oil and Refining Company, Baytown, Texas. See J. L. Franklin and H. E. Lumpkin, J. Am. Chem. Soc. **74**, 1023 (1952).

expected to depend strongly on the reaction path and the state of excitation of the fragments, but it would appear (see below) that the heat of formation of an ion is independent of the source of the ion and the mechanism by which the ion is formed to such an extent that it can be used as a means of characterizing the ion. This will be the chief use made of the quantity, and while the ionic characterizations will not be unique, the method serves at least as well as those used heretofore, from which, of course, it is not conceptually different. In this work, as a matter of expediency, the appearance potentials are combined with molecular heats of formation at 298°K rather than those at 0°K, as is strictly proper. The errors entailed are largely negligible for the ions of interest here.

The molecular heats of formation needed were taken from the A.P.I.-N.B.S. compilation,[4] and free radical heats of formation were taken from the list given by Roberts and Skinner.[5] Knowlton and Rossini's[6] value of 12.74 kcal/mole at 298°K was taken as the heat of formation of cyclopropane. In this work 1 ev=23.06 kcal/mole.

### $C_3H_6^+$, A = 10.2$_3$±0.1 ev = 235.$_9$±2.$_3$ kcal/mole

A value of 10.14±0.05 ev for the ionization potential of cyclopropane has been previously published,[7] but the measurements were made with the ionization chamber of the mass spectrometer at 213°C. This procedure has been criticized[8] because of the possibility of the isomerization of the cyclopropane to propylene at the relatively high temperature; consequently, the present measurements at an appreciably lower temperature were made. The difference in the two values is within the limit of the quoted uncertainties, and the ionization potential of cyclopropane is without doubt of the order of 10.2 ev.

There appears to be a possibility that the ionization of cyclopropane by electron impact brings about an opening of the carbon ring. Such ring opening is indicated for some of the other $C_3$ ions from cyclopropane, and further, the use of Franklin's method of group equivalents[9] as extended to ions and radicals[10] allows one to estimate the heat of formation of the $^+CH_2CH_2\dot{C}H_2$ ion-radical to be 241 kcal/mole. This is close enough to the experimental cyclopropane $C_3H_6^+$ heat of formation of 249 kcal/mole to warrant at least mention of the possibility of ring opening, although no definite postulate can be made. The alternative possibility, the formation of the propylene molecule-ion, is less likely, for its heat of formation is 232 kcal/mole.[11]

[4] American Petroleum Institute Research Project 44 at the National Bureau of Standards. Selected Values of Properties of Hydrocarbons.

[5] J. S. Roberts and H. A. Skinner, Trans. Faraday Soc. **45**, 339 (1949).

[6] J. W. Knowlton and F. D. Rossini, J. Research Natl. Bur. Standards **43**, 113 (1949).

[7] F. H. Field and E. A. Hinkle, J. Chem. Phys. **18**, 1122 (1950).

[8] P. J. Dyne, private communication.

[9] J. L. Franklin, Ind. Eng. Chem. **41**, 1070 (1949).

[10] J. L. Franklin, paper presented at the Seventh Southwest Regional Meeting of the American Chemical Society (unpublished).

TABLE I. Ionization potentials of standard compounds.

| Compound | Mass | Ionization potential (volts) This work | Reported values |
|---|---|---|---|
| Krypton | 84 | primary standard | 14.01[a] |
| Propylene | 42 | 9.84 | 9.84[b], 9.77[c] |
| Ethylene | 28 | 10.68 | 10.62[b], 10.51[d], 10.87[e] |
| Ethane | 30 | 11.78 | 11.76[b], 11.66[f] |
| Carbon dioxide | 44 | 13.88 | 13.85[b], 13.79[g] |
| Nitrogen | 28 | 15.52 | 15.60[b], 15.58[h] |
| Argon | 40 | 15.79 | 15.76[a] |
| Neon | 20 | 21.67 | 21.54[a] |

[a] R. F. Bacher and S. Goudsmit, *Atomic Energy States* (McGraw-Hill Book Company, Inc., New York, 1932). Values corrected for change in $cm^{-1}$/volt conversion factor.
[b] R. E. Honig, J. Chem. Phys. **16**, 105 (1948).
[c] D. P. Stevenson and J. A. Hipple, J. Am. Chem. Soc. **64**, 2769 (1942).
[d] W. C. Price and W. T. Tutte, Proc. Roy. Soc. (London) **A174**, 207 (1940). Spectroscopic value.
[e] Kusch, Hustrulid, and Tate, Phys. Rev. **52**, 843 (1937).
[f] See reference c, p. 1588.
[g] W. C. Price and D. M. Simpson, Proc. Roy. Soc. (London) **A169**, 501 (1939).
[h] G. Herzberg, *Molecular Spectra and Molecular Structure. I. Spectra of Diatomic Molecules* (D. Van Nostrand Company, Inc., New York, 1950), second edition.

### $C_3H_5^+$, A = 12.1$_0$±0.1 ev = 279.$_0$±2.$_3$ kcal/mole

The only ionization process possible is $C_3H_6 \rightarrow C_3H_5^+ + H$,[12] $\Delta H_f(C_3H_5^+) = 240$ kcal/mole. In regard to the structure of the ion, the heat of formation of the $\overset{+}{C}H_2CH_2CH$ ion can be estimated from Franklin's group equivalent method to be 224 kcal/mole, assuming the ring strain in the ion to be the same as that in the cyclopropane molecule. The group equivalent method when applied to noncyclic ions gives values in good agreement with those found experimentally, and while the uncertainty in the $\overset{+}{C}H_2CH_2CH$ estimate is larger because of the necessity of guessing the amount of

TABLE II. Appearance potentials of ions formed from cyclopropane.

| Ion | Mass | Number determinations | Appearance potential ev | kcal |
|---|---|---|---|---|
| $C_3H_6^+$ | 42 | 9 | 10.2$_3$±0.1 | 235.$_9$±2.$_3$ |
| $C_3H_5^+$ | 41 | 7 | 12.1$_0$±0.1 | 279.$_0$±2.$_3$ |
| $C_3H_4^+$ | 40 | 6 | 12.2$_6$±0.1 | 282.$_7$±2.$_3$ |
| $C_3H_3^+$ | 39 | 2 | 14.0$_9$±0.1 | 324.$_9$±2.$_3$ |
| $C_3H_2^+$ | 38 | 1 | 13.8 ±0.2 | 318 ±5 |
| $C_3H^+$ | 37 | 1 | 15.0 ±0.5 | 346 ±12 |
| $C_3^+$ | 36 | 1 | 12.4 ±0.5 | 286 ±12 |
| $C_2H_3^+$ | 27 | 3 | 13.3$_7$±0.1 | 308.$_3$±2.$_3$ |
| $C_2H_2^+$ | 26 | 4 | 13.6$_2$±0.1 | 314.$_1$±2.$_3$ |
| $CH_3^+$ | 15 | 3 | 16.9 ±0.2 | 390 ±5 |
| $CH_2^+$ | 14 | 5 | 18.5 ±0.2 | 427 ±5 |
| $CH^+$ | 13 | 3 | 25.5 ±0.6 | 588 ±14 |

[11] Calculated from R. E. Honig, J. Chem. Phys. **16**, 105 (1948).
[12] In this and subsequent ionization equations, for simplicity the electrons involved will not be represented.

ring strain, it is felt that the 16 kcal/mole discrepancy between the estimated and experimental heats of formation indicates that the $C_3H_5^+$ ion does not have a cyclic structure.

The heats of formation and structures of noncyclic $C_3H_5^+$ ions can be calculated from published appearance potential data if assumptions are made concerning the ionization reactions. Usually only one of the several conceivable reactions for the formation of a given ion will give a reasonable value for its heat of formation. Thus, from allyl chloride,[13] $C_3H_5Cl \rightarrow CH_2=CHCH_2^+ + Cl\cdot$, $\Delta H_f(C_3H_5^+)=227$ kcal/mole, where the heat of formation of allyl chloride is taken as zero as estimated by the group equivalent method. From 1-butene,[14] $C_4H_8 \rightarrow CH_2=CHCH_2^+ + CH_3\cdot$, $\Delta H_f(C_3H_5^+)=237$ kcal/mole, but Stevenson postulates a 9 kcal/mole "excess" activation energy in the formation of the ion, which when taken into account would give a heat of formation value in agreement with that found from allyl chloride.[15] From isobutene,[16] $C_4H_8 \rightarrow CH_3\dot{C}=CH_2 + CH_3\cdot$, $\Delta H_f(C_3H_5^+)=230$ kcal/mole, and from 2-butene,[17] $C_4H_8 \rightarrow CH_3CH=\overset{+}{C}H + CH_3\cdot$, $\Delta H_f(C_3H_5^+)=237$ kcal/mole (average of values from *cis*- and *trans*-2-butene). The differences between the heats of formation of the three $C_3H_5^+$ ions are small, but since in all cases the quoted uncertainties in the corresponding appearance potentials are 0.1 ev (2 kcal/mole), it is felt that they are significant.

The cyclopropane $C_3H_5^+$ ion heat of formation corresponds reasonably closely to that of $CH_3CH=\overset{+}{C}H$, and it is postulated that the cyclopropane ion has this structure. The formation of this ion requires what might appear to be an unlikely amount of atomic rearrangement, but on the other hand, a ring opening is indicated in the formation of the $C_3H_4^+$ and $C_3H_3^+$ ions; and indeed, cyclopropane is notable for the amount of rearrangement that seems to occur in its ionization processes. Further, the possibility of the occurrence of a $CH_3CH=\overset{+}{C}H$ ion with a heat of formation of about 240 kcal/mole is bolstered by considering the ionization of *n*-butane,[18] $C_4H_{10} \rightarrow C_3H_5^+ + CH_3\cdot + H_2$, $\Delta H_f(C_3H_5^+)=240$ kcal/mole. This mechanism and the $CH_3CH=\overset{+}{C}H$ structure are at least as likely as any others that might be postulated.

As a matter of interest, the $C_3H_5^+$ heats of formation at 0°K were calculated. If it is assumed that the heats of formation at 0°K for cyclopropane and allyl chloride are 3 kcal/mole larger than the values at 298°K, then the heats of formation of the ions from allyl chloride, isobutene, 2-butene, cyclopropane, and *n*-butane are 230, 235, 242, 243, and 247 kcal/mole. The relationship between the values for the ions of different structure is essentially unchanged.

### $C_3H_4^+$, $A = 12.2_6 \pm 0.1$ ev $= 282._7 \pm 2._3$ kcal/mole

Two ionization processes are possible: $C_3H_6 \rightarrow C_3H_4^+ + 2H$, $\Delta H_f(C_3H_4^+)=192$ kcal/mole, and $C_3H_6 \rightarrow C_3H_4^+ + H_2$, $\Delta H_f(C_3H_4^+)=296$ kcal/mole. The ionization potential of allene is 10.0 ev from electron impact experiments[19] or 10.19 ev from Rydberg series in allene,[20] and the corresponding heats of formation of the $CH_2=\overset{+}{C}-\dot{C}H_2$ ion are 277 or 281 kcal/mole. From isobutene,[16] $C_4H_8 \rightarrow CH_2=\overset{+}{C}-\dot{C}H_2 + CH_4$, $\Delta H_f(C_3H_4^+)=283$ kcal/mole; and from propylene,[19] $C_3H_6 \rightarrow CH_2=\overset{+}{C}-\dot{C}H_2 + H_2$, $\Delta H_f(C_3H_4^+)=283$ kcal/mole. There does not seem to be any question that the heat of formation of the allene molecule-ion is about 280 kcal/mole. On the other hand, the ionization potential of methyl acetylene is 11.30 ev,[21] from which the heat of formation of the $CH_3C^+=\dot{C}H$ molecule-ion is 304 kcal/mole. From 2-butene,[17] $C_4H_8 \rightarrow CH_3\dot{C}=\overset{+}{C}H + CH_4$, $\Delta H_f(C_3H_4^+)=304$ kcal/mole (average of values from *cis*- and *trans*-2-butene).

The ionization process for the formation of the $C_3H_4^+$ ion from cyclopropane is clearly the second listed above, and it is also fairly clear that the ion is not the allene molecule-ion. It is postulated that the ion has the methyl acetylene molecule-ion structure, although the correspondence of the ionic heat of formation values is admittedly not as good as might be desired.

### $C_3H_3^+$, $A = 14.0_9 \pm 0.1$ ev $= 324._9 \pm 2._3$ kcal/mole

The heats of formation of the $C_3H_3^+$ ions (assumed to have the $CH_2=C=\overset{+}{C}H$ structure) formed from several sources are from allene,[19] $C_3H_4 \rightarrow C_3H_3^+ + H$, $\Delta H_f(C_3H_3^+)=284$ kcal/mole; from propylene,[19] $C_3H_6 \rightarrow C_3H_3^+ + H_2 + H$, $\Delta H_f(C_3H_3^+)=280$ kcal/mole; from 2-butene,[17] $C_4H_8 \rightarrow C_3H_3^+ + CH_4 + H$, $\Delta H_f(C_3H_3^+)=287$ kcal/mole (average of values from *cis*- and *trans*-2-butene); from isobutene,[16] $C_4H_8 \rightarrow C_3H_3^+ + CH_4 + H$,

[13] J. L. Franklin and H. E. Lumpkin, J. Chem. Phys. **19**, 1073 (1951).

[14] D. P. Stevenson, J. Am. Chem. Soc. **65**, 209 (1943).

[15] M. G. Evans and M. Szwarc in a recent publication [J. Chem. Phys. **19**, 1322 (1951)] dispute this assignment of activation energy to the 1-butene dissociation on the basis of the assumption that the $C_3H_5^+$ ion from propylene has the $CH_3C^+=CH_2$ structure and, further, that this ion is more stable than the allyl ion. The heat of formation of the ion from propylene is 230 kcal/mole (see reference 16), which, when compared with that of the ion from isobutene, indicates that the isoallyl structure is correct. However, from the work on allyl chloride it seems that the assumption concerning the relative stabilities of the $C_3H_5^+$ ions is not correct and that the ion from 1-butene does contain about 10 kcal/mole extra energy. If the heat of formation of the allyl ion is taken to be 227 kcal/mole and that of the allyl radical to be 28 kcal/mole (as calculated from the data given by Evans and Szwarc), the ionization potential of the allyl radical is 199 kcal/mole = 8.6 ev rather than 9.05 ev as given by Evans and Szwarc.

[16] D. P. Stevenson and J. A. Hipple, J. Am. Chem. Soc. **64**, 2769 (1942).

[17] V. H. Dibeler, J. Research Natl. Bur. Standards **38**, 329 (1947).

[18] See reference 16, p. 1588.

[19] J. Delfosse and W. Bleakney, Phys. Rev. **56**, 256 (1939).

[20] L. H. Sutcliffe and A. D. Walsh, J. Chem. Soc. **1952**, 899.

[21] W. C. Price and A. D. Walsh, Trans. Faraday Soc. **41**, 381 (1945).

$\Delta H_f(C_3H_3^+)=290$ kcal/mole; average $\Delta H_f(C_3H_3^+)=285$ kcal/mole. The use in the cases of 2-butene and isobutene of the alternate ionization processes involving the formation of a methyl radical and a hydrogen molecule would increase the ionic heats of formation by only two kcal/mole. The heat of formation of the $C_3H_3^+$ ion from cyclopropane assuming the process $C_3H_6 \rightarrow C_3H_3^+ + H_2 + H$ is $\Delta H_f(C_3H_3^+)=286$ kcal/mole. The agreement indicates strongly the correctness of the process and $CH_2=C=\dot{C}H$ as the ionic structure.

**$C_2H_3^+$, $A=13.3_7\pm0.1$ ev $=308._3\pm2._3$ kcal/mole**

It is most reasonable to assume that the vinyl ion is formed. The heats of formation of the $C_2H_3^+$ ions (assumed to have the vinyl structure) formed from several sources are as follows:

from ethylene,[22] $C_2H_4 \rightarrow C_2H_3^+ + H$,
$\Delta H_f(C_2H_3^+)=288$ kcal/mole;
from *n*-butane,[18] $n-C_4H_{10} \rightarrow C_2H_3^+ + CH_3\cdot + CH_4$,
$\Delta H_f(C_2H_3^+)=283$ kcal/mole;
from *i*-butane,[18] $i-C_4H_{10} \rightarrow C_2H_3^+ + CH_3\cdot + CH_4$,
$\Delta H_f(C_2H_3^+)=292$ kcal/mole;
from ethane,[18] $C_2H_6 \rightarrow C_2H_3^+ + H_2 + H$,
$\Delta H_f(C_2H_3^+)=278$ kcal/mole;
from propylene,[19] $C_3H_6 \rightarrow C_2H_3^+ + CH_3\cdot$,
$\Delta H_f(C_2H_3^+)=310$ kcal/mole;
and from isobutene,[16] $C_4H_8 \rightarrow C_2H_3^+ + C_2H_4 + H$,
$\Delta H_f(C_2H_3^+)=282$ kcal/mole,

giving an average value of 284 kcal/mole (propylene value omitted). The only reaction for the formation of the $C_2H_3^+$ ion from cyclopropane which gives an ionic heat of formation at all close to this value is $C_3H_6 \rightarrow C_2H_3^+ + CH_3\cdot$, $\Delta H_f(C_2H_3^+)=288$ kcal/mole.

By means of the following thermochemical cycle an energy value to be associated with the C−C bond dissociation energy in cyclopropane can be calculated:

| | |
|---|---|
| $C_3H_6 \rightarrow C_2H_3^+ + CH_3$ | $\Delta H=308$ kcal/mole |
| $C_2H_3^+ \rightarrow C_2H_3$ | $\Delta H=-232$[23] |
| $CH_3 \rightarrow CH_2 + H$ | $\Delta H=92$[24] |
| $C_2H_3 + H \rightarrow C_2H_4$ | $\Delta H=-91$[23] |
| $C_3H_6 \rightarrow C_2H_4 + CH_2$ | $\Delta H=77$ kcal/mole |

Bond dissociation energy is usually defined as the endothermicity of a process wherein one bond in a molecule is broken. However, as an extension of the idea, half of the endothermicity of the reaction producing ethylene and methylene from cyclopropane may be considered as the average C−C bond dissociation energy of two C−C bonds in cyclopropane, i.e., $D(C-C)=38.5$ kcal/mole.

The C−C bond dissociation energy in cyclopropane is usually considered to be the endothermicity of the reaction of $C_3H_6 \rightarrow \cdot CH_2CH_2CH_2\cdot$, and several values for the quantity have been reported. Ogg and Priest[25] give 32.9 kcal/mole based on studies of the reactions of iodine with cyclopropane, although in a later private communication[26] Ogg estimates that the value may be about 50 kcal/mole. Presumably the second value is obtained using newer values of the C−I bond energy. Corner and Pease[27] have found that the activation energy for the thermal isomerization of cyclopropane to propylene is 65.2 kcal/mole, and they more or less tentatively identify this with the energy required to open the cyclopropane ring. Franklin,[10] using his method of group equivalents, estimates the heat of formation of the trimethylene biradical and from it calculates a cyclopropane bond energy of 50 kcal/mole.

The C−C bond dissociation energy calculated from the electron impact data is really not comparable with these values, for it is the average of the energy required to open the cyclopropane ring and that required to break a C−C bond in the resulting trimethylene biradical to form ethylene and methylene. One can make a crude calculation of the energy for the second process by estimating the C−C bond strength in the trimethylene biradical and the strengths of the $\sigma$- and $\pi$-portions of the C−C double bond, from which the energy of the first reaction can be calculated from the electron impact data by difference. One thus obtains $D(C-C)\text{cyclo}=44+3R$ kcal/mole,[28] where $R$ represents the energy of reorganization in producing $CH_2$ from ethylene and trimethylene biradical. The value of $R$ is not known with any certainty,[29] but if it is at all different from zero, the electron impact results appear to be compatible with a cyclopropane C−C bond dissociation energy of at least 50 kcal/mole.

[22] Kusch, Hustrulid, and Tate, Phys. Rev. **52**, 843 (1937).

[23] Stevenson (reference 14) gives $I(C_2H_3)=9.9$ ev $=228$ kcal/mole and $D(C_2H_3-H)=3.95$ ev $=91.1$ kcal/mole. These values depend on the assumption of a 0.4 ev activation energy in the combinations of an ethyl radical or a hydrogen atom with the vinyl ion. The assumption is based on a thermochemical calculation stemming from the appearance potential of the vinyl ion in the mass spectrum of ethane (reference 18). In view of the spread of the vinyl ion heats of formation listed above, it seems preferable to base the calculation of the ionization potential and dissociation energy on the average value of the vinyl ion heat of formation (284 kcal/mole). Thus, taking $\Delta H_f(C_2H_3)=52$ kcal/mole (calculated from Stevenson), $I(C_2H_3)=232$ kcal/mole and $D(C_2H_3-H)=91$ kcal/mole. It should be pointed out that as calculated above the value of the heat of the reaction $C_3H_6 \rightarrow C_2H_4+CH_2$ is independent of the value of $\Delta H_f(C_2H_3)$ used.

[24] H. H. Voge, J. Chem. Phys. **16**, 984 (1948). See also F. H. Field, J. Chem. Phys. **19**, 793 (1951).

[25] R. A. Ogg and W. J. Priest, J. Chem. Phys. **7**, 736 (1939).

[26] See H. E. Gunning and E. W. R. Steacie, J. Chem. Phys. **17**, 351 (1949).

[27] E. S. Corner and R. N. Pease, J. Am. Chem. Soc. **67**, 2067 (1945).

[28] $C_2H_4 \rightarrow 2CH_2$, $\Delta H=2\times72-13=131$ kcal/mole $=D(C-C)_\sigma+D(C-C)_\pi-2R$, where $\Delta H_f(CH_2)=72$ kcal/mole as calculated from $A(CH_2^+)$ in the mass spectrum of methane. Assume $D(C-C)_\sigma \cong D(C-C)_{C_2H_6}=83$ kcal/mole (reference 14), from which $D(C-C)_\pi \cong 48+2R$ kcal/mole. $D(\cdot CH_2CH_2-CH_2\cdot)=D(C-C)_\sigma-D(C-C)_\pi-R$. Assume $D(C-C)_\sigma \cong D(C-C)_{C_3H_8}=81$ kcal/mole (reference 14), from which $D(\cdot CH_2CH_2-CH_2\cdot) \cong 33-3R$. Then $D(C-C)\text{cyclo} \cong 77-(33-3R)=44+3R$ kcal/mole.

[29] For several views see K. J. Laidler and E. S. Casey, J. Chem. Phys. **17**, 213, 1087 (1949); L. H. Long and R. G. W. Norrish, Proc. Roy. Soc. (London) **187A**, 337 (1946); and A. D. Walsh, Disc. Faraday Soc. **2**, 18 (1947).

**$C_2H_2^+$, $A=13.6_2\pm0.1$ ev $=314._1\pm2._3$ kcal/mole**

The ionization potential of acetylene is 11.43 ev,[11] from which the heat of formation of the $C_2H_2^+$ ion is 317 kcal/mole. The cyclopropane ionization process which gives an acetylene ion heat of formation closest to this value is $C_3H_6\rightarrow C_2H_2^+ + CH_4$, $\Delta H_f(C_2H_2^+)=344$ kcal/mole. The energy agreement is not good, but other conceivable processes give heat of formation values so far different from 317 kcal/mole as to leave little doubt that the above process is correct.

**$CH_3^+$, $A=16.9\pm0.2$ ev $=390\pm5$ kcal/mole**

It should be noted that this is a rearrangement ion. The heats of formation of the methyl ion as calculated from the appearance potential of the ion in the methane mass spectrum[30] and from the ionization potential of the methyl radical[31] are 264 and 265 kcal/mole, respectively. The cyclopropane ionization process which gives a methyl ion heat of formation closest to this value is $C_3H_6\rightarrow CH_3^+ + C_2H_2 + H$, $\Delta H_f(CH_3^+)=295$ kcal/mole. As in the case of the acetylene ion, the agreement is not good, but other processes are far worse.

**$CH^+$, $A=25.5\pm0.6$ ev $=588\pm14$ kcal/mole**

The heat of formation of the $CH^+$ ion as calculated from the appearance potential of the ion in the methane mass spectrum is 366 kcal/mole[30] or 344 kcal/mole.[32] The cyclopropane ionization process which gives a methine ion heat of formation closest to these values is $C_3H_6\rightarrow CH^+ + C_2H_2 + 3H$, $\Delta H_f(CH^+)=391$ kcal/mole. As with the previous two ions, other processes give poorer agreement.

In the above three ions the discrepancies between the heats of formation of the ions as formed from cyclopropane and from other sources are roughly the same, i.e., 27, 30, and 25 (or 47) kcal/mole. Further, in each case the fragment $C_2H_2$ is formed, either as an ion or a molecule, and it is possible that the observed excess energies correspond to the formation of the $C_2H_2$ fragment in an excited state.

**$CH_2^+$, $A=18.5\pm0.2$ ev $=427\pm5$ kcal/mole**

The heat of formation of the methylene ion as calculated from the appearance potential of the ion in the mass spectrum of methane[30] is 348 kcal/mole. The best cyclopropane ionization process is $C_3H_6\rightarrow CH_2^+ + C_2H_3 + H$, $\Delta H_f(CH_2^+)=335$ kcal/mole. It is of interest that some measurements of the appearance potential of the $C_2H_4^+$ ion from cyclopropane gave an ionic heat of formation which is about 50 kcal/mole too low. The phenomenon is tentatively attributed to the ionization of molecular ethylene formed by the decomposition of the cyclopropane on the wolfram filament of the mass spectrometer, and since $CH_2$ might also be a product of the decomposition, the low $CH_2^+$ heat of formation can be explained in the same way. Stevenson[33] has recently observed a similar pyrolytic formation of olefins from alkanes.

It is felt that the extent of the pyrolysis is not so great as to require rejection of the postulated ionization process and, further, that the results indicate the absence of excess energy such as that found associated with the formation of the mass 26, 15, and 13 ions. However, more elaborate energetic considerations are not warranted.

In considering the ionization and dissociation processes in cyclopropane, and, indeed, such processes in polyatomic molecules in general, one cannot but be impressed by the extent to which the heat of formation of an ion formed by a relatively complicated mechanism involving appreciable amounts of atomic rearrangement agrees with the value for the ion as formed from a different substance and by a different mechanism, which in turn may be simple or complex. In many cases it would appear that the appearance potential gives nearly the true endothermicity of a reaction, regardless of the number of intermediate "processes"—bond breakings, bond makings, atomic rearrangements, etc.—which might be thought necessary to accomplish the reaction.

If the ionization and dissociation of a molecule be considered as a Franck-Condon type process, the appearance potential of an ion should be a measure of the difference in energy between the ground state of the molecule and the highest point of the largest activation energy barrier involved in the decomposition of the parent molecule-ion to form the reaction products. However, in a number of ionization processes the activation energies which might be expected on the basis of the usual concepts of reaction processes do not seem to be present to any appreciable degree. For instance, the heat of formation of $C_2H_4^+$ from ethane is 260 kcal/mole,[18] which is to be compared with the value of 255 kcal/mole as calculated from the spectroscopic ionization potential of ethylene. Molecular hydrogen is produced along with the formation of the ion from ethane, and it seems reasonable to think that the reaction mechanism is $C_2H_6\rightarrow C_2H_6^{+*}\rightarrow C_2H_4^+ + H_2$, where $C_2H_6^{+*}$ represents an excited ethane molecule-ion with energy equal to that of $C_2H_4^+ + H_2$. Further, one might expect that the decomposition of the $C_2H_6^{+*}$ molecule-ion would involve an activation energy, and the 5 kcal/mole difference in the $C_2H_4^+$ heats of formation observed experimentally shall, for the sake of argument, be considered as such.

To estimate theoretically the activation energy it shall be assumed, for lack of a better method, that as

[30] L. G. Smith, Phys. Rev. **63**, 121 (1943).
[31] J. A. Hipple and D. P. Stevenson, Phys. Rev. **63**, 121 (1943).
[32] Average of values from C. A. McDowell and J. W. Warren, Disc. Faraday Soc. **10**, 53 (1951), and J. Geerk and H. Neuert, Z. Naturforsch. **5A**, 502 (1950).
[33] D. P. Stevenson, Disc. Faraday Soc. **10**, 35 (1951).

an approximation the activated state of the decomposition involves a four-center type of interaction and that it is valid to apply Hirschfelder's[34] rule that the energy of such an activated complex is 28 percent of the sum of the energies of the bonds broken in the reaction. One thus calculates an activation energy of about 30 kcal/mole.[35] Even granting that the calculation may be wrong in detail, the discrepancy between the calculated and experimental value seems large enough to raise a question about the adequacy of ordinary reaction concepts in explaining these electron-impact-induced reactions.

Perhaps even more striking is the fact that, as has been shown, the heat of formation of the vinyl ion formed from ethane is 10 kcal/mole less than that of the vinyl ion formed from ethylene. Not even a crude quantitative estimate of the activation energies can be made in this case, but in view of the fact that $H_2$ accompanies the formation of the vinyl ion from ethane (and thus an appreciable activation energy might be expected), whereas the ion is formed from ethylene by fission of one bond, the lower heat of formation in the ethane case is somewhat mystifying.

It will be observed from the heat of formation values quoted previously that, in general, the values for a given ion as formed from several compounds differ amongst themselves to a certain extent. This might be attributed to the presence of different activation energies in the processes by which the ions are formed, but in a number of cases, as in the example above, the differences are contrary to what one might expect. On the other hand, the variations might be attributed to experimental errors in the appearance potential values, but some new determinations in this laboratory of the heats of formation of the vinyl ions formed from a number of different compounds give values which differ from each other in the same manner (although to a smaller extent) as those calculated from earlier work. It seems fairly certain that at least not all the observed variations are the result of experimental error.

The author wishes to acknowledge the financial aid given this work by the University of Texas Research Institute and the help of Mr. J. M. Goff and Mr. T. W. Becker in making the measurements.

[34] J. O. Hirschfelder, J. Chem. Phys. **9**, 645 (1941).

[35] From the heats of formation of $C_2H_6^+$, $C_2H_5^+$, and $C_2H_4^+$ it follows that for $C_2H_6^+ \rightarrow C_2H_5^+ + H$, $\Delta H = D(C_2H_5^+ - H) = 20$ kcal/mole and for $C_2H_5^+ \rightarrow C_2H_4^+ + H$, $\Delta H = D(C_2H_4^+ - H) = 88$ kcal/mole. Taking these as the energies of the bonds broken in the reaction $C_2H_6^{+*} \rightarrow C_2H_4^+ + H_2$, activation energy $= 0.28(20+88) = 30$ kcal/mole. Alternatively, the calculation may be based on the reverse reaction $C_2H_4^+ + H_2 \rightarrow C_2H_6^{+*}$, activation energy $= 0.28(D(H_2) + D(C-C)_\pi)$, where $D(C-C)_\pi$ = difference in carbon-carbon bond energy in $C_2H_6^+$ and $C_2H_4^+$. Then activation energy $= 0.28(104 + D(C-C)_\pi) = 29 + D(C-C)_\pi \cong 30$ kcal/mole.

THE JOURNAL OF CHEMICAL PHYSICS VOLUME 20, NUMBER 11 NOVEMBER, 1952

# Heat Capacity, Gas Imperfection, Infrared Spectra, and Internal Rotation Barriers of Ethyl Alcohol

GORDON M. BARROW
*Department of Chemistry, Northwestern University, Evanston, Illinois*

(Received May 14, 1952)

The vapor heat capacities of ethyl alcohol have been measured, as a function of pressure, at 368, 422, and 476°K. From the variation of the heat capacity with pressure, together with vapor densities calculated by the Clapeyron equation, an equation of state for ethyl alcohol has been obtained. This equation has been used to extrapolate the measured heat capacities to the ideal gas state and likewise to correct the observed entropy.

The infrared spectra of vapor $C_2H_5OH$, $C_2H_5OD$, and liquid $C_2H_5OD$ are presented and a vibrational assignment is obtained which is sufficiently reliable for the statistical calculation of the thermodynamic properties.

Comparison of the observed and statistically calculated heat capacities and entropies shows that, with a barrier to internal rotation of the $CH_3$ group of 3000 calories, the rotation of the OH group is hindered by a barrier between 0 and 1200 calories. Most satisfactory agreement is obtained for $CH_3$ and OH barriers of 3300 and 800 calories, respectively. Furthermore, comparison of the observed and calculated equilibrium constants for the reaction

$$C_2H_4(g) + H_2O(g) \rightleftarrows C_2H_5OH(g)$$

supports the selection of fundamental frequencies and internal rotation barriers.

THE subject of internal rotation in alcohols has frequently been investigated. Most of the earlier work on methyl and ethyl alcohol has been discussed by Halford.[1,2]

Weltner and Pitzer[3] have recently reported vapor heat capacity results for methyl alcohol and have shown that the observed vapor heat capacities and entropy are consistent with an internal rotation barrier of about 1000

[1] J. O. Halford, J. Chem. Phys. **18**, 361, 1051 (1950).
[2] J. O. Halford, J. Chem. Phys. **17**, 111 (1949).

[3] W. Weltner and K. S. Pitzer, J. Am. Chem. Soc. **73**, 2606 (1951).

calories, as is indicated spectroscopically. Furthermore, they show that much of the difficulty in treating the thermodynamics of this compound has arisen from the unexpectedly large gas imperfection corrections occurring in a hydrogen bound compound of this type. As a result of this work, the inconsistencies regarding the barrier to internal rotation in methyl alcohol have been essentially removed.

Ethyl alcohol has also been considerably studied. The third law entropy has been measured by Kelley.[4] Heats of vaporization, vapor pressures, and heat capacities of the liquid have been determined by Fiock, Ginnings and Holton[5] at temperatures from 0 to 130°C. Several investigations[6,7,8] of the equilibrium

$$C_2H_4(g)+H_2O(g)\rightleftarrows C_2H_5OH(g)$$

have given consistent and reliable equilibrium constants. Some vapor heat capacities have also been reported.[9] On the basis of certain of these data, various estimates of the barriers to internal rotation of the $CH_3$ and OH groups have been made, but no set of entirely consistent and satisfactory values has been obtained. The principal difficulties have been concerned with the correction of the thermal data to the ideal gas state and uncertainties in the assignment of frequencies to the fundamental vibrations.

The infrared spectra of vapor $C_2H_5OH$ and $C_2H_5OD$ aid in selecting the frequencies of the fundamentals, and the new heat capacity measurements provide additional thermal data and, together with results from the Clapeyron equation, permit a satisfactory equation of state to be derived. As a result, fairly definite values for the barriers hindering internal rotation in ethyl alcohol can now be obtained.

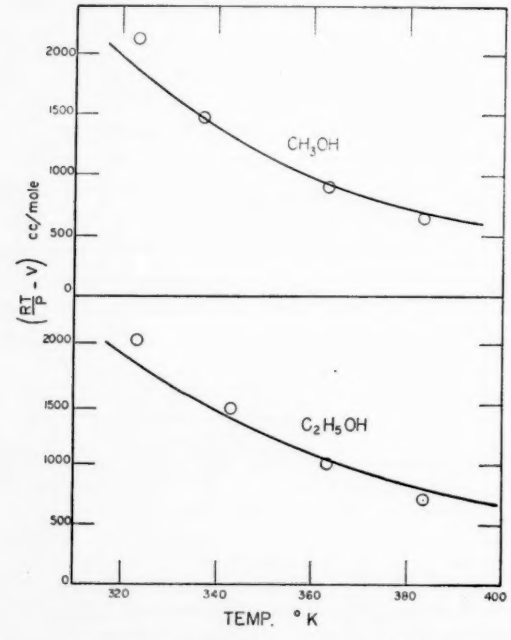


FIG. 1. $(RT/P-V)$ of methyl and ethyl alcohol vapor. Circles are calculated from the Clapeyron equation. Solid lines are obtained from the equation of state.

## EXPERIMENTAL*

The vapor heat capacities were measured with the flow calorimeter previously used by Weltner and Pitzer.[3] They have discussed the modifications of this particular calorimeter and give references to more detailed discussions of flow calorimeters. The thermometer calibration was also that used for the methyl alcohol work and was shown to give heat capacity results for benzene in reasonable agreement with the results of other workers.

The usual procedure for measuring heat capacities by the flow calorimeter method was followed. This has been discussed in detail by Waddington, Todd, and Huffman.[10]

The ethyl alcohol used for the heat capacity determinations was dried with sodium and distilled in a slow stream of dry nitrogen through a 30-plate all-glass column.

The infrared measurements were made with a Beckman IR-2T spectrometer equipped with rock salt and lithium fluoride monochromators.

The deuterated ethyl alcohol was prepared by the method of Beersmans and Jungers[11] from diethylglyoxal, sodium carbonate, and $D_2O$. The product was fractionated through a 30-cm column of glass helices. From the intensity of the infrared absorption band of the O—H stretching vibration, it was estimated that the product contained about 5 percent ordinary alcohol. Ordinary ethyl alcohol prepared by this method and similarly fractionated gave an infrared spectrum identical with the published curve,[12] thus indicating the absence of other impurities.

## EQUATION OF STATE

Although it has been recognized[1,2,13] that the gas imperfection corrections to the thermodynamic properties of alcohols were probably more important than for molecules incapable of hydrogen bonding, the only

[4] K. K. Kelley, J. Am. Chem. Soc. **51**, 779 (1929).
[5] Fiock, Ginnings and Holton, J. Research Natl. Bur. Standards **6**, 881 (1931).
[6] Stanley, Youell and Dymock, J. Soc. Chem. Ind. **53**, 205T (1934).
[7] R. H. Bliss and B. F. Dodge, Ind. Eng. Chem. **29**, 19 (1937).
[8] Applebey, Glass, and Horsely, J. Soc. Chem. Ind. **56**, 279T (1937).
[9] A. Eucken and E. U. F. Franck, Z. Electrochem. **52**, 195 (1948); they also give the results of earlier workers.

* The heat capacity measurements were made at the Department of Chemistry, University of California, Berkeley, while the author was doing graduate studies under the direction of Professor K. S. Pitzer and Professor William D. Gwinn.
[10] Waddington, Todd, and Huffman, J. Am. Chem. Soc. **69**, 22 (1947).
[11] J. Beersmans and J. C. Jungers, Bull. soc. chim. Belg. **56**, 72 (1947).
[12] American Petroleum Institute Research Project 44, Carnegie Institute of Technology, Catalog of Infrared Spectral Data. Serial No. 748, Ethanol, contributed by the National Bureau of Standards, Radiometry Lab. Washington, D. C.
[13] K. Ito, J. Chem. Phys. **19**, 1313 (1951); **20**, 531 (1952).

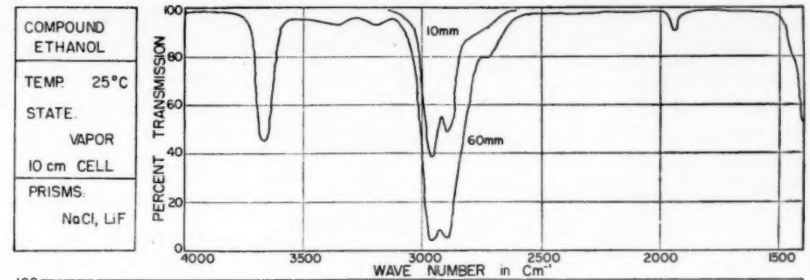


FIG. 2. Infrared spectrum of vapor $C_2H_5OH$ at pressures of 60, 30, and 10 mm of Hg.

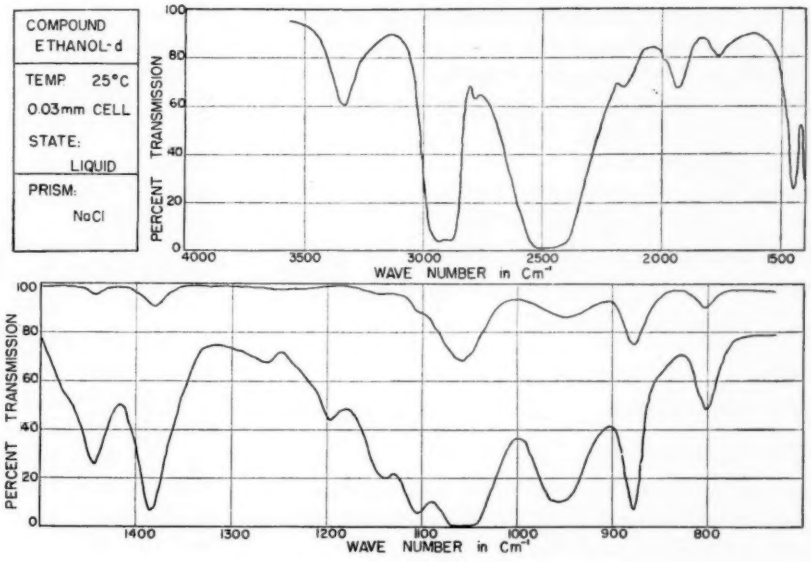


FIG. 3. Infrared spectrum of liquid $C_2H_5OD$, 0.03 mm and thin film path lengths.

successful treatment has been that recently given by Weltner and Pitzer.[3] They found that for methyl alcohol they could best fit the available data, i.e., the vapor density results and the variation of $C_p$ with pressure, by assuming that association in the vapor state led to dimers and tetramers. For ethyl alcohol a similar situation should exist, and furthermore, it is reasonable to expect that the values of the heats and entropies of formation of the dimers and tetramers for the two compounds will not differ greatly. We have therefore taken the form of the gas imperfection equations found for methyl alcohol and have obtained, after adjusting the values of the energy terms, suitable agreement with the available data for ethyl alcohol.

No useful directly measured vapor densities are available for ethyl alcohol. The work of Ramsay and Young,[14] as with methyl alcohol, does not seem to be sufficiently accurate. Fairly reliable vapor densities for the saturated vapor can, however, be obtained from the accurate vapor pressures and heats of vaporization of Fiock, Ginnings, and Holton[5] by application of the Clapeyron equation. It is necessary to recognize that a higher virial coefficient than the second is important in this region and that the quantity $[V-(RT/P)]$ is a function of pressure. This dependence on pressure explains the discrepancy found by Curtiss and Hirschfelder[15] for methyl alcohol in comparing the values of $[V-(RT/P)]$ calculated for the vapor in equilibrium with the liquid with those measured by Eucken and Meyer[16] at approximately one atmosphere.

An equation of state for ethyl alcohol has been obtained which reproduces the observed change of heat capacity with pressure and also the vapor densities

[14] W. Ramsay and S. Young, Roy. Soc. London, Phil. Trans. **177**, 123 (1886).

[15] C. F. Curtiss and J. O. Hirschfelder, J. Chem. Phys. **10**, 491 (1942).

[16] A. Eucken and L. Meyer, Z. physik. Chem. **5B**, 452 (1929).

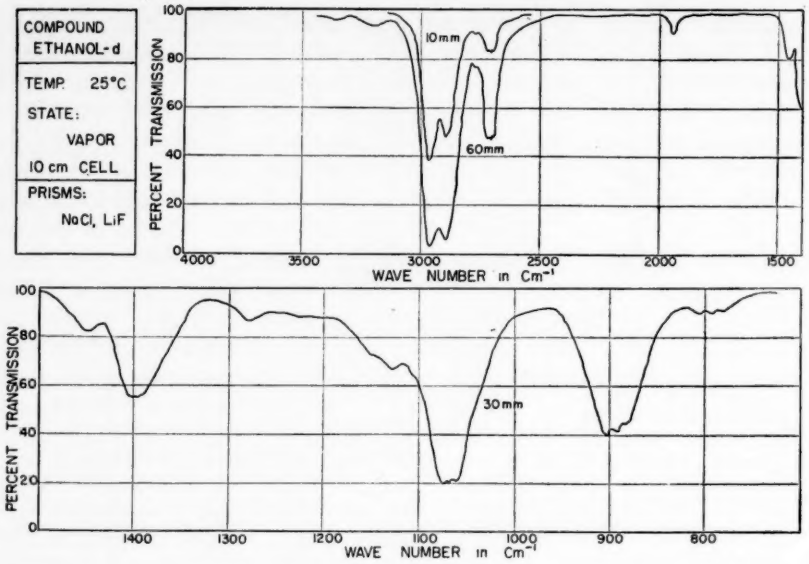


FIG. 4. Infrared spectrum of vapor $C_2H_5OD$ at pressures of 60, 30, and 10 mm of Hg.

obtained by application of the Clapeyron equation. As a check on the reliability of this latter procedure, a comparison of the Clapeyron gas imperfections for methyl alcohol with those given by the equations of Weltner and Pitzer has been made. Figure 1 gives the results for both the alcohols.

On the basis of the model chosen by Weltner and Pitzer,[3] i.e., $\Delta Cp$ of polymerization equal to zero, the terms of the virial equation $PV=RT+BP+DP^3$ are

$$B=b-RTe^{-\Delta S_2/R}e^{\Delta H_2/RT}=100-0.02023Te^{1710/T},$$

$$D=-3RTe^{-\Delta S_4/R}e^{\Delta H_4/RT}=-4.27\times10^{-16}e^{12460/T},$$

in which

$$\Delta H_2=3400 \text{ cal/mole}, \quad \Delta S_2=16.57 \text{ cal/deg mole},$$

$$\Delta H_4=24{,}800 \text{ cal/mole}, \quad \Delta S_4=81.45 \text{ cal/deg mole}.$$

The variations of heat capacity and entropy with pressure are given by the use of these terms in equations reported by Weltner and Pitzer.[3]

## VIBRATIONAL ASSIGNMENT

The vapor phase infrared spectra of ethyl alcohol and deuteroethyl alcohol and the liquid phase spectrum of the deutero compound are shown in Figs. 2, 3, and 4.

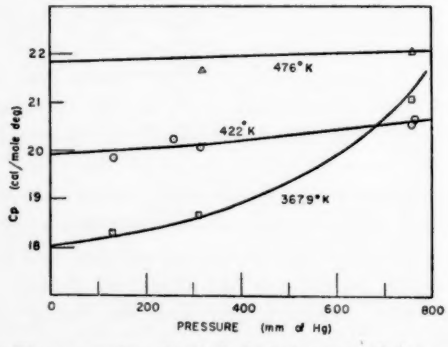


FIG. 5. Heat capacity of ethyl alcohol vapor. Points are measured values; slopes of the curves calculated from the equation of state.

Much of the difficulty in selecting the fundamental vibrational frequencies for ethyl alcohol arises because of uncertainty regarding the position and coupling of the O—H bending vibration. Previous statistical calculations[9,17,18] of the entropy of ethyl alcohol have relied on some rather arbitrary average frequency for the six bending vibrations of doubtful assignment. With the present data, an attempt is made to select a complete set of fundamental frequencies, but it cannot be claimed that the choice is entirely unambiguous.

Of the twenty-one internal degrees of freedom, two are the internal rotations of the $CH_3$ and OH groups which are not assigned to spectroscopic bands. Thirteen are vibrations for which fairly certain assignments can immediately be made. These include the O—H stretching vibration at 3660 $cm^{-1}$, the five C—H stretching modes at about 2940 $cm^{-1}$, three C—H bending motions at 1450 $cm^{-1}$, the $CH_3$ symmetric bending at 1398 $cm^{-1}$, and the three skeletal vibrations at 433,[19] 885, and 1070 $cm^{-1}$.

The remaining six vibrations are essentially C—H and O—H bending motions. Three of these will be vibrations symmetric with respect to the plane of the molecule (assuming the O—H bond is in the plane of the C—C—O bonds) and will have a component parallel to the small moment of inertia axis of the molecule. These can be expected to give rise to bands having contours of $P$, $Q$, and $R$ branches of approximately equal prominence, as is observed for the assigned in-plane bands at 3660, 1398, 1070, and 885 $cm^{-1}$. The band at 1242 $cm^{-1}$ which apparently shifts to 1140 $cm^{-1}$ on deuteration is such a band. Furthermore, the band at 803 $cm^{-1}$ in the spectrum of the deuterated compound has this contour, and the product rule applied to the in-plane vibrations predicts a corresponding band at about 1050 $cm^{-1}$ in the

[17] S. C. Schumann and J. G. Aston, J. Chem. Phys. **6**, 480 (1938).
[18] Aston, Isserow, Szasz, and Kennedy, J. Chem. Phys. **12**, 336 (1944).
[19] G. Bolla, Z. Physik **89**, 513 (1934), **90**, 607 (1934).

undeuterated compound. This is observed as a definite shoulder on the strong 1070 $cm^{-1}$ band. If these two bands, at 1050 and 1242 $cm^{-1}$, are assigned, as seems most likely, to vibrations involving the $CH_3$ and OH groups, then the remaining in plane mode will be a $CH_2$ wagging motion. No band can be readily assigned to this vibration, and a value of 1300 $cm^{-1}$ has been arbitrarily taken as a reasonable estimate.[20,21,22]

The three remaining out-of-plane rocking vibrations are then assigned to the bands at 805 and 1104 $cm^{-1}$ observed in the spectrum of $C_2H_5OH$ and 1270 $cm^{-1}$ occurring in the spectrum of $C_2H_5OD$. These bands are expected to have a prominent $Q$ branch, and this contour is shown by the band at 805 $cm^{-1}$ in the higher vapor pressure spectrum.

The frequencies chosen for the fundamental vibrations of ethyl alcohol are 3660, 2940(5), 1450(3), 1398, 1300, 1270, 1242, 1104, 1070, 1040, 895, 805, and 433 $cm^{-1}$.

Comparison of the statistically calculated and observed heat capacities shows that assignment of appreciably lower frequencies to the fundamental vibrations than that made here is not permissable since then the calculated heat capacities would be too large for any reasonable internal rotation potential functions for the $CH_3$ and OH groups.

## THERMODYNAMIC DATA

The experimental vapor heat capacities are plotted in Fig 5. The slopes of the curves are obtained from the gas imperfection equations previously referred to. The resulting value of $C_p^0$ at 367.9, 422, and 476°K are 18.05, 19.93, and 21.8 cal/deg mole. These $C_p^0$ results, along with those of earlier workers,[9] are shown in Fig. 6. The agreement of the different sets of data is quite satisfactory.

TABLE I. Entropy of ethyl alcohol.

| | 298.2°K | 351.5°K | 403.2°K |
|---|---|---|---|
| $S$ liquid | 38.5±0.3 | 43.3±0.3 | 48.4±0.3 |
| $\Delta S$ vaporization | 33.97 | 26.33 | 19.93 |
| Gas imperfection | 0.15 | 0.54 | 1.12 |
| $R \ln P$ | −5.10 | 0.00 | 3.45 |
| $S^0$ observed | 67.5±0.3 | 70.2±0.3 | 72.9±0.3 |
| $S^0$ calculated | 67.58 | 70.26 | 72.85 |

The third law entropy has been measured by Kelley, who reports the value 38.4±0.3 cal/deg mole for the liquid at 298.1°C. When this result is combined with the heats of vaporization and heat capacities of the liquid of Fiock, Ginnings, and Holton, the entropy of the real gas at the vapor pressure for that temperature is obtained. From the equation of state, this is corrected to the entropy of the ideal gas at one atmosphere. Table I shows the terms in this calculation at three temperatures.

The equilibrium constants for the reaction

$$C_2H_4(g)+H_2O(g) \rightleftarrows C_2H_5OH(g)$$

between 150 and 380°C as obtained by three different sets of workers are shown in Fig. 7. The results have

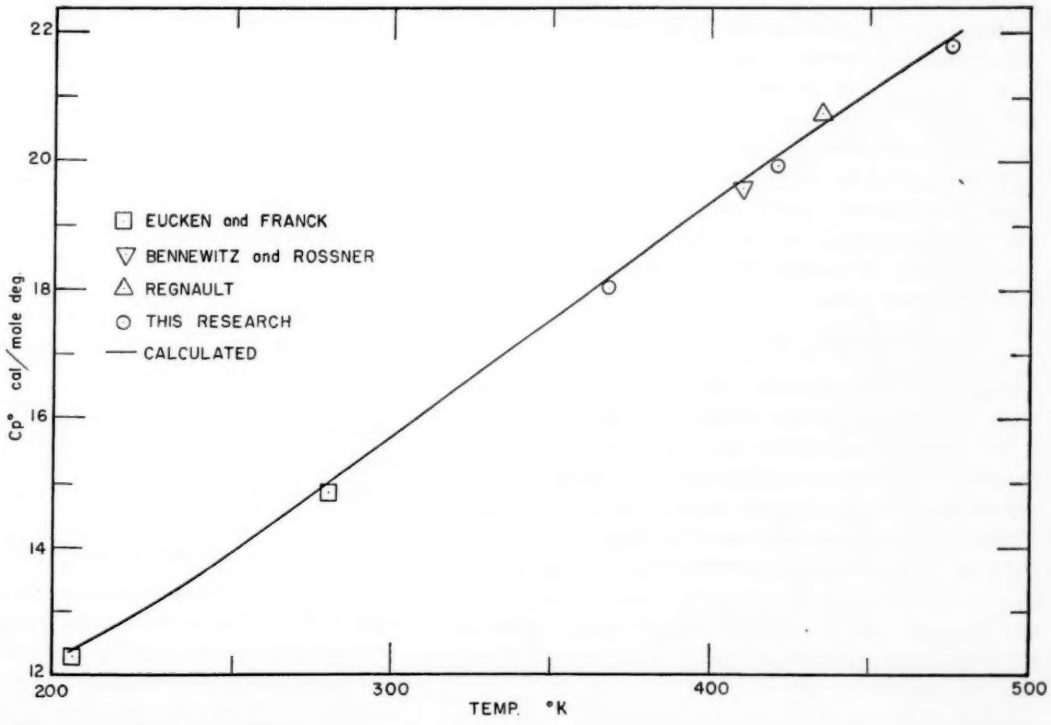


FIG. 6. Heat capacity of ethyl alcohol in the ideal gas state.

[20] R. S. Rasmussen, J. Chem. Phys. **16**, 712 (1948).
[21] N. Sheppard, J. Chem. Phys. **17**, 79 (1949).
[22] G. M. Barrow, J. Chem. Phys. **19**, 345 (1951).

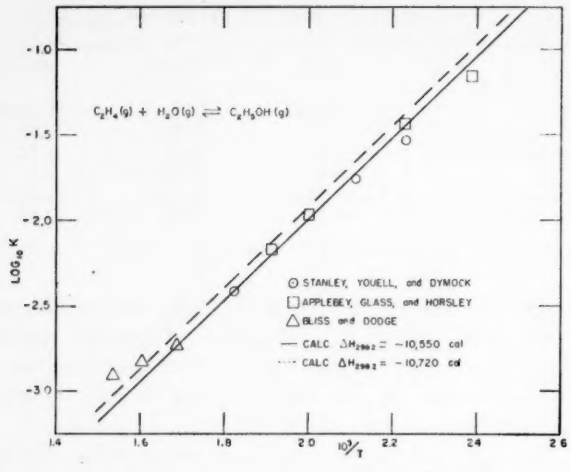


FIG. 7. Calculated and observed constants for the equilibrium of $C_2H_4H_2O$, and $C_2H_5OH$ as a function of temperature.

previously been treated by Aston[23] and by Schumann and Aston[17] who used them for comparison with a statistical calculation. In addition to the measured equilibrium constants, it is necessary to have also a value for the heat of reaction. As shown by Aston, this can be obtained from the known heats of formation of the three compounds. It is necessary, however, to use a reliable gas imperfection correction in calculating the heat content of ethyl alcohol in the ideal gas state from the observed heat of formation of the liquid. Using our equation of state, this term is calculated as 250 cal as compared to the Berthelot term of 5 cal. This leads to a heat of reaction, $\Delta H^\circ_{298.2} = -10,720 \pm 300$ cal.

Correction of the observed equilibrium constants to fugacities has not been made since a satisfactory treatment is impossible. However, since the results of Bliss and Dodge,[7] which were determined at a total pressure of 7 and 11 atmospheres, agree with the other two sets of data both of which were determined at a total pressure of one atmosphere, it seems likely that no great error is introduced by using the equilibrium constants in terms of pressures for comparison with those calculated statistically.

## INTERNAL ROTATION BARRIERS

Previous calculations of barriers to the rotation of the $CH_3$ and OH groups have been discussed by Halford.[2]

The recent confirmation of a barrier of about 1000 cal for internal rotation in methyl alcohol[3] makes the higher values reported for the OH rotation appear less likely. Furthermore, choice of a potential function for internal rotation of the OH group which has unequal minima, i.e., a trans form of lower energy than the skew forms, can be ruled out, if only reasonable energy differences are considered, because of its too large contribution to the heat capacity.

Detailed calculations have therefore been made using symmetric threefold potential functions for both the $CH_3$ and OH groups. Contributions to the thermodynamic properties of the internal rotations were obtained from the tables of Pitzer and Gwinn.[24] For the heat capacities at 200 and 280°K, these tables are not applicable, and this internal rotation contribution has been estimated by comparison with Halford's[1] results for methyl alcohol in this region. The reduced moments of inertia used for the $CH_3$ group was $4.6\times10^{-40}$ g cm$^2$ and for the OH group $1.35\times10^{-40}$ g cm$^2$. With a $CH_3$ barrier of 3000 cal, both the calculated entropy and heat capacity give satisfactory agreement with the observed values for barriers up to about 1200 cal for the OH rotation. Best agreement is obtained for the $CH_3$ barrier equal to 3300 cal and an OH barrier of 800 cal. The heat capacity curve of Fig. 6 and the calculated entropies of Table I are based on these barriers. The dashed curve of Fig. 7 gives the calculated equilibrium constants based on these barriers and the observed value of $\Delta H^\circ_{298.2} = -10,720$ cal. The solid curve is based on $\Delta H^\circ_{298.2} = -10,550$ cal, a value which gives best agreement with the experimental data. The difference is well within the experimental error of the thermal data.

## CONCLUSIONS

Barriers hindering internal rotation of the $CH_3$ and OH groups of about 3000 and 1000 cal, respectively, are in agreement with the observed heat capacities, entropies, and constants for the equilibrium of water, ethylene, and ethyl alcohol.

Use has been made of a new vibrational assignment deduced from infrared spectra of $C_2H_5OH$ and $C_2H_5OD$. Comparison of the calculated and observed thermodynamic properties shows that choice of an appreciably lower set of frequencies would not be admissible. Likewise, an unsymmetrical potential function for the OH rotation is not allowed.

An important factor in treating the observed thermodynamic data, as in the case of methyl alcohol, is the correction of these data to the ideal gas state. When vapor density measurements are not available, use can be made of the Clapeyron equation if the important virial coefficients are recognized.

The agreement of the calculated entropy with that observed, using a statistical calculation which fits the heat capacities and equilibrium constants, indicates the absence of zero-point entropy in ethyl alcohol.

## ACKNOWLEDGMENT

The author wishes to express his appreciation for the help of Dr. William Weltner, who made available some of the heat capacity results reported here and aided in the calculations and vibrational assignment.

[23] J. G. Aston, Ind. Eng. Chem. **34**, 514 (1942).

[24] K. S. Pitzer and W. D. Gwinn, J. Chem. Phys. **10**, 428 (1942).

# Separation of the Absorption Spectra of $NO_2$ and $N_2O_4$ in the Range of 2400-5000A

T. C. HALL, JR., AND F. E. BLACET
*Department of Chemistry, University of California, Los Angeles, California*
(Received May 19, 1952)

The individual absorption coefficient curves of $NO_2$ and $N_2O_4$, separated by means of a mechanical analog differential analyzer are presented. Beer's law is assumed to be applicable to the system. The range 2400–5000A is covered. A discussion of the apparently continuous nature of the $N_2O_4$ absorption is included.

## INTRODUCTION

INCIDENTAL to researches in the photochemistry of $NO_2$ it became necessary to know quantitatively the relative probabilities of absorption of a photon in the range 2400–5000A by each of the species $NO_2$ and $N_2O_4$ present in the equilibrium mixture. A better postulation could then be made of the probable primary processes in the photochemical reactions of systems containing $N_2O_4 \rightleftarrows 2NO_2$. This entailed the calculation of the absorption coefficients of $NO_2$ and $N_2O_4$ from the optical density curves ($\log I_0/I$) of the mixture under conditions of different total pressure where the ratios of $NO_2$ and $N_2O_4$ are different. A continuous calculation of the absorption coefficients over the range of wavelengths was made by means of a differential analyzer. The input spectrophotometer optical density curves yielded the complete absorption coefficient curves of $NO_2$ and $N_2O_4$ separately in the output.

## EXPERIMENTAL

The $NO_2$ used in these experiments was obtained from the Mathieson Company and was purified by passing $O_2$ through the liquid at 0°C until a pure white solid could be obtained on cooling the sample to −78°C. Reduced oxides of nitrogen could be detected by the blue and brown colors which they imparted to the frozen solid. The white solid was then repeatedly distilled, frozen, and pumped at −78°C to rid the material of $N_2$, $O_2$, $CO_2$, etc. The white crystalline solid obtained in this manner was then stored over $P_2O_5$ in a Pyrex vessel. This reservoir was connected to the gas handling system through a stopcock.

Pressure measurements in excess of 40 mm were made by balancing air pressure, read on a mercury manometer by means of cathetometer, against the total $NO_2-N_2O_4$ pressure through a separating manometer filled with Dow Corning Silicone Fluid No. 200 (viscosity = 100 centistokes). Small gas pressures (0–40 mm Hg) were read directly on this silicone manometer with zero pressure maintained on the mercury manometer side by means of a high vacuum pumping system.

The negligible vapor pressure of the Dow Corning Silicone Fluid used as well as its chemical inertness in the presence of $NO_2-N_2O_4$ made it ideally suitable for the use cited above. The fluid showed a slight tendency to dissolve the $NO_2$ over extended periods of time but this introduced negligible errors into the pressure measurements if they were made with reasonable rapidity. High vacuum silicone stopcock grease was used throughout on all ground joints and stopcocks.

The silica absorption cells were filled at 25°C to the required pressures by warming the $NO_2-N_2O_4$ reservoir to room temperature and allowing the vapor to escape into the attached evacuated absorption cell until the approximate required pressure was obtained. The connecting stopcock was then closed and the total pressure ($Pi$) measured accurately as described above. After filling, the cell was removed from the gas handling apparatus and thermostated at 25°C in the exit beam of a Cary recording ultraviolet spectrophotometer. Optical density ($\log I_0/I$) curves were obtained over the range 2400–5000A. Over this range the spectral band width varied between 2 and 5A and averaged approximately 4A.

Three absorption curves were run at 25°C and at three total pressures: $P_A = 32.72$ mm, $P_B = 126.2$ mm, and $P_C = 306.9$ mm. The total pressure was selected so as to be approximately inversely proportional to the path length. This insured that the optical density values at all wavelengths would not vary beyond the range of the spectrophotometer.

## CALCULATIONS AND ERRORS

The additivity of optical densities ($d$) is based on the validity of Beer's law, which was assumed to apply under the conditions which prevailed in this work. Considerable support for this assumption derives from the fact cited below that relatively large pressures of a third gas ($N_2$) caused no observable effect on the optical density of the $NO_2-N_2O_4$ mixture in the wavelength range covered. A pair of simultaneous linear algebraic equations with the absorption coefficients as the two unknowns may therefore be set up and solved for a given wavelength and two different total pressures.

At total pressure $Pi$, $(d/l) = k_1p_1 + k_2p_2$, where $d$ = observed optical density of mixture at the given wavelength ($\log I_0/I$), $l$ = path length used (cm), $p_1$ and

TABLE I.

| Case | (cm) | $Pi$ (mm Hg) | $K_{eq}^{25°}$ (atmos) | $p_1$ (mm Hg) | $p_2$ (mm Hg) | $p_2/p_1$ |
|---|---|---|---|---|---|---|
| *A* | 10.00 | 32.72 | 0.1415 | 26.29 | 6.43 | 0.245 |
| *B* | 2.500 | 126.2 | 0.1387 | 74.10 | 52.10 | 0.703 |
| *C* | 1.000 | 306.9 | 0.1319 | 132.2 | 147.7 | 1.321 |

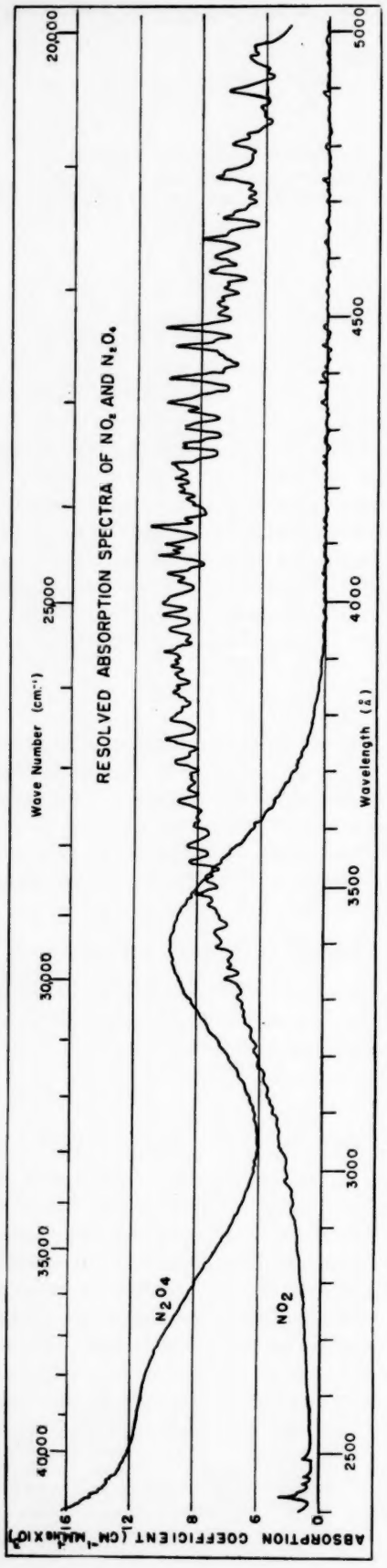


FIG. 1. Absorption coefficients ($1/pl \log_{10} I_0/I$) of $NO_2$ and $N_2O_4$ *vs* wavelength and wave number, measured at 25°C.

$p_2$=partial pressures of $NO_2$ and $N_2O_4$, respectively (mm Hg), and $k_1$ and $k_2$=absorption coefficients of $NO_2$ and $N_2O_4$, respectively ($cm^{-1}$ $mm^{-1}$ Hg).

For two such equations obtained at two different total pressures and thus at two different ratios of partial pressures ($p_2/p_1$), a simultaneous solution for $k_1$ and $k_2$ is possible at any given wavelength. The condition for least amplification of the errors inherent in the experimental method is obviously the one in which the greatest possible difference in the values of the total pressure is obtained. The pressure dependence of the equilibrium $N_2O_4 \rightleftarrows 2NO_2$ consequently produces the required divergence in the values of ($p_2/p_1$). It can easily be shown that for small differences in the total pressure the uncertainties introduced in the solution of the simultaneous equations become very large. Within the limits of experimental practicality then, the most widely separated values of the total pressure should be selected.

The perfect gas assumption of proportionality of concentration and pressure was made in this work. This is undoubtedly not strictly correct for $NO_2$ and $N_2O_4$; however, over the pressure range employed here, the linear relation is true to a good approximation. In view of these and other practical considerations, the values of $P_i$ and the corresponding parameters listed in Table I were used.

The curves shown together in Fig. 1 represent solutions to the linear equations corresponding to $P_A$ and $P_C$ (combination $A-C$). For purposes of checking the method and observing any possible pressure dependent deviations from Beer's law for the various combinations of pressures used, a third intermediate pressure $P_B$ is included in Table I. The solutions obtained for this pressure in combination with $P_A$ or $P_C$ deviate only slightly from the solutions given in Fig. 1.

The values of $p_1$ and $p_2$ were calculated from $P_i$ and the equilibrium constant expression of Verhoek and Daniels.[1] By a method of successive approximations an accurate numerical value of $K_{eq}^{25°}$ was obtained for each pressure used for the equilibrium $N_2O_4 \rightleftarrows 2NO_2$, which was assumed to be the only significant one. At 25°C the equilibrium constant is given by

$$K_{eq}^{25°}\ (\text{atmos}) = 0.1426 - 0.7588 C_2^0,$$

from which the $K_{eq}^{25°}$ values in Table I were calculated. $C_2^0$ is the concentration of $N_2O_4$ in moles per liter which would exist if all the substances were present as $N_2O_4$. This equilibrium constant has a high temperature coefficient, and therefore, it was necessary to thermostat the apparatus. The temperature was kept at 25±0.1°C during the filling operations and absorption spectrum runs.

The construction of a graph of solutions of $k_1$ and $k_2$ *vs* wavelength would require a point-by-point solution

[1] F. H. Verhoek and F. Daniels, J. Am. Chem. Soc. **53**, 1250 (1931).

of a pair of simultaneous equations at every wavelength if full advantage were to be taken of the resolution of the data from the spectrophotometer. This individual solution method would require an inordinate quantity of calculating, and much of the fine structure might be missed since the method could not be continuous. This difficulty was overcome by the use of the mechanical analog differential analyzer of the Department of Engineering, University of California at Los Angeles. The differential analyzer was set up with the appropriate parameters from Table I to solve in a continuous fashion the pair of simultaneous equations over the range of wavelength covered in the optical density traces.

At each wavelength a pair of simultaneous equations was solved by the machine, continuously and directly, from the absorption data curves over the range 2400–5000A. The two optical density curves from the spectrophotometer were traced semiautomatically and simultaneously by two machine operators. From this process of curve fitting, values of the absorption coefficients $k_1$ and $k_2$ of $NO_2$ and $N_2O_4$, respectively, were obtained continuously at the output of the machine. The uncertainty introduced by the time lag of the observers in following the input curves is reflected as small erratic fluctuations in the output curves of $k_1$ and $k_2$, which are shown together in Fig. 1. Large sharp peaks in the $NO_2$ trace are reflected as "noise" in the $N_2O_4$ trace. This is most apparent above 4000A where $N_2O_4$ is transparent.

## DISCUSSION OF RESULTS

The results shown in Fig. 1 are those obtained for the two most divergent values of total pressure $P_i$ (combination $A-C$). Check runs of $P_A$ and $P_C$ against the intermediate pressure $P_B$ yielded $k_1$ and $k_2$ curves of the same general shape with slightly different percentage deviations at different wavelengths. Good correspondence was obtained in the $NO_2$ curves over all pressure ranges. The high pressure combination, $B-C$, gave slight negative deviations, and the low pressure combination, $A-B$, yielded slight positive deviations at certain wavelengths in the $N_2O_4$ curve. These deviations never exceeded $\pm 4$ percent and averaged less than $\pm 1$ percent over the entire wavelength range. They are possibly real since a systematic experimental error would be expected to yield a constant percentage error over the whole wavelength range. The deviations cannot be attributed to simple pressure effects, since the absorption of 30 mm of $NO_2-N_2O_4$ remained essentially unchanged in intensity and structure when a pressure of 1 atmosphere of dry nitrogen was allowed into the absorption cell. This fact provides further support for the conclusions of Verhoek and Daniels[1] that the constant for the $N_2O_4 \rightleftarrows 2NO_2$ equilibrium and consequently the forward and reverse rates are essentially independent of foreign gas pressure.

The maximum in the absorption of $N_2O_4$ at 3400A corroborates the work of others.[2–4] The value of the absorption coefficient in the visible range must be zero, contrary to the results of Lambrey and Corbiere[3] who reported significant absorption by $N_2O_4$ at 4105A. The validity of Beer's law, when it is assumed that only $NO_2$ absorbs above 4000A, reported by Dixon[5] is in agreement with our results. The values of the absorption coefficients reported by Holmes and Daniels[4] for eight different lines of the mercury arc are in good agreement with our data.

No fine structure appears in the spectrum of $N_2O_4$. Probably this is due not to its absence but rather to extreme fineness which may prove almost impossible to resolve. The presence of gross structure is good reason for suspecting fine structure.

The dissociation energy of $N_2O_4$ is about 14 kcal,[6] corresponding to absorption near 5000 $cm^{-1}$ or 20,000A. The absorption in Fig. 1, therefore, probably represents excitation to one or more electronic levels. The sharp, well-defined structure which appears in the $NO_2$ spectrum does not appear in the $N_2O_4$ spectrum, probably because of the large number of closely spaced energy levels introduced into the molecule by the formation of the weak $N-N$ bond assumed in the symmetrical planar $N_2O_4$ model of Sutherland.[7] The energy of the $N-N$ linkage in this molecule is small as compared with the energy of the $N-O$ bonds ($\sim$120 kcal). This low energy of formation of the $N-N$ bond together with the large effective masses at either end of the bond reduce the energy level spacings for the various vibrations of this bond. The narrow spacing and large number of energy levels apparently is sufficient to obliterate the well-defined, comparatively simple structure which is characteristic of the $NO_2$ spectrum. The low energy of the $N-N$ bond stretching as well as its possible low energy torsional vibration probably gives rise to a fine structure resulting in further broadening. Finally the rotational energy level spacings for the $N_2O_4$ molecule are reduced due to its larger moment of inertia as compared with $NO_2$. In view of all these factors, the apparent continuous nature of the $N_2O_4$ absorption is to be expected.

Figure 2 shows the effect of a thermal equilibrium shift on the $N_2O_4 \rightleftarrows 2NO_2$ absorption. The increase of $NO_2$ and decrease of $N_2O_4$ concentrations as the temperature is raised is evident in the range 2400–2900A. The continuous absorption of $N_2O_4$ at the shorter wavelengths has decreased, and the superimposed banded absorption of $NO_2$ has increased. This is in qualitative agreement with the quantitative results shown in

[2] L. Harris, Proc. Natl. Acad. Sci. **14**, 690 (1928).
[3] M. Lambrey and C. Corbiere, Compt. rend. **201**, 1334 (1935).
[4] H. H. Holmes and F. Daniels, J. Am. Chem. Soc. **56**, 630 (1934).
[5] J. K. Dixon, J. Chem. Phys. **8**, 157 (1940).
[6] W. F. Giauque and J. D. Kemp, J. Chem. Phys. **6**, 40 (1938).
[7] G. B. B. M. Sutherland, Proc. Roy. Soc. (London) **141**, 343 (1933).

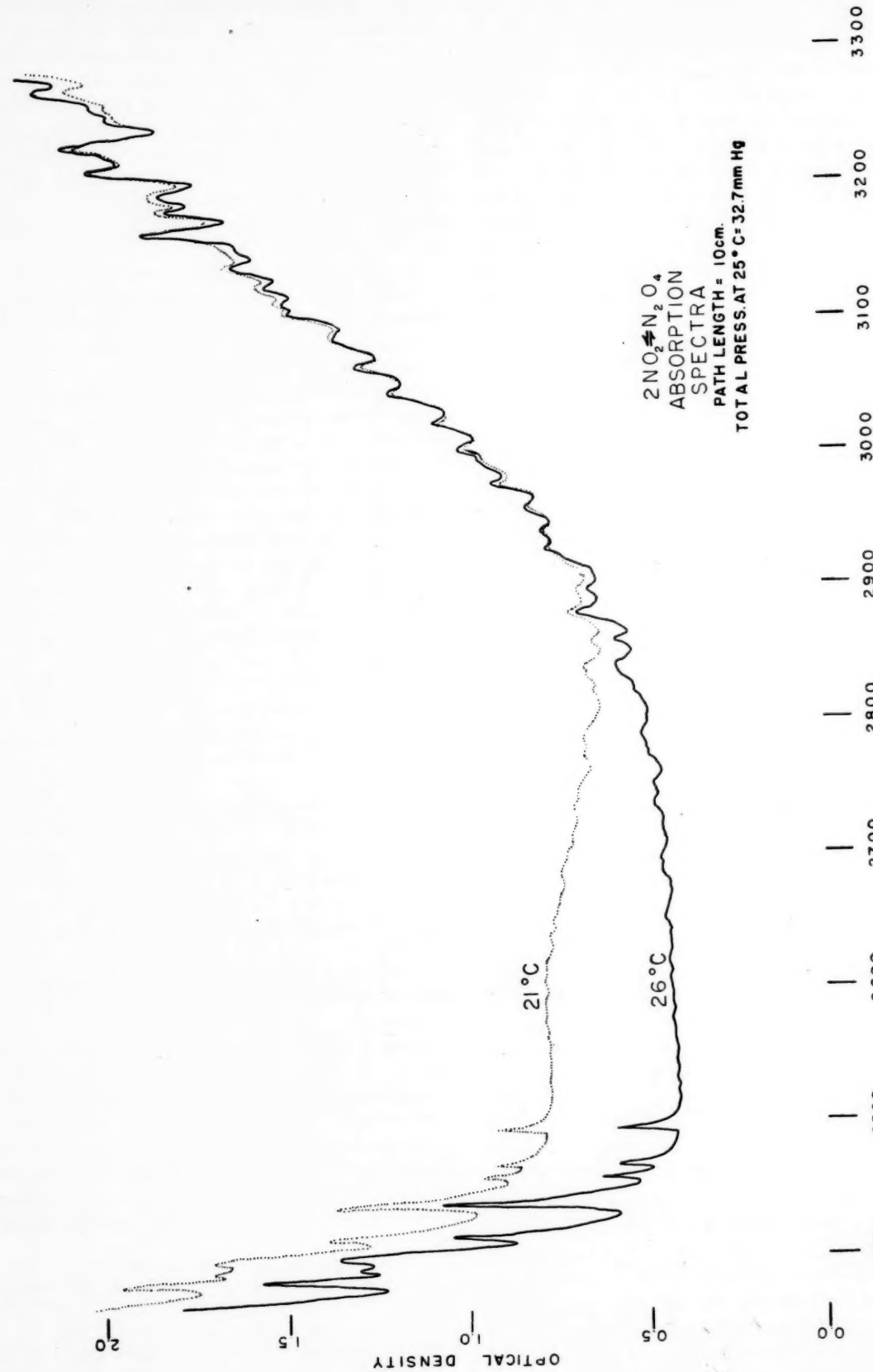


FIG. 2. Effect of temperature on total absorption of equilibrium mixture of $NO_2$ and $N_2O_4$.

Fig. 1. If the total absorption curves shown in Fig. 2 had been extended to longer wavelengths, the predominance of the $NO_2$ absorption at that end of the spectrum would be evident. The condition for coincidence of the two optical density traces can be shown to be $k_2/k_1=2$. This value is approximated in the interval 2950–3400A, resulting in a range rather than a point of crossover of the two curves as shown in Fig. 2 above 2950A. The fact that the curves do not deviate greatly from each other in this range, despite considerable variation in $k_2/k_1$, derives from the fact that the optical density is not a very sensitive function of this ratio. This is seen at 2600A where $k_2/k_1=10$. At that wavelength the optical density curves of Fig. 2 differ by a factor of only 2.

The increased probability of the $N_2O_4$ rather than the $NO_2$ absorbing incident radiation as the wavelength is decreased is of photochemical interest. The postulation of a given primary process depends upon the species which absorbs the incident light. Thus, quantum yield data for systems containing $N_2O_4 \rightleftarrows 2NO_2$ should be a function of the ratio $p_2/p_1$ and hence the total pressure $P_i$. In addition, reduction of the wavelength of incident light over a sufficient range could change the primary absorber from $NO_2$ to $N_2O_4$ and thus alter the photochemistry of the system.

The authors wish to express their appreciation to the Los Angeles County Air Pollution Control District for funds made available for this research.

Fig. 2. Effect of temperature on total absorption of equilibrium mixture of $NO_2$ and $N_2O_4$.

THE JOURNAL OF CHEMICAL PHYSICS VOLUME 20, NUMBER 11 NOVEMBER, 1952

# A Note on the Vibrational Frequencies and the Entropy of Decaborane*

W. E. KELLER AND H. L. JOHNSTON
*The Cryogenic Laboratory, Department of Chemistry, The Ohio State University, Columbus, Ohio*

(Received May 12, 1952)

The infrared spectra of solid decaborane and of decaborane in a solution of carbon disulfide as well as the Raman spectrum of the solution have been recorded. A rough selection of fundamental frequencies is made; this, together with the molecular parameters from x-ray data, is used for calculating $S^0_{298.16}$ of the gas, for which a value of 83.85 eu is obtained. This figure compares with that derived from thermodynamic measurements, namely, 87.36 eu.

KASPER, Lucht, and Harker[1] by x-ray diffraction studies of single crystals, have elucidated the crystal and molecular structure of decaborane, including the determination of the positions of all the hydrogen atoms. Although the infrared and Raman spectra for so large a molecule as $B_{10}H_{14}$ would not be expected to add significantly to knowledge of the structure once this had been carefully determined by other means, it was thought that the spectra would be of interest primarily because the structure was known: a comparison of the structure and spectra of this molecule might aid in clarifying structural problems of members of the boron hydride series. There was also the possibility that thermodynamic quantities for gaseous decaborane might be computed. It is the object of this note to present the spectroscopic data obtained in this laboratory and to consider these implications.

## EXPERIMENTAL

The infrared spectrum of solid decaborane was obtained with a model 12-B Perkin Elmer instrument, employing for the regions 3 to 5$\mu$, 5 to 15$\mu$, and 15 to 25$\mu$ a LiF, a NaCl, and a KBr prism, respectively. The solid specimen, part of the material used in calorimetric work at this laboratory,[2] was prepared by melting crystalline $B_{10}H_{14}$ (mp 99.7°C) between two AgCl plates and allowing the "sandwich" to cool. The infrared spectrum from 2 to 15$\mu$ of $B_{10}H_{14}$ in $CS_2$ solution was obtained with a Baird Associates double-beam spectrometer. For direct comparison, the spectrum of the solid also was recorded on the Baird instrument.

Raman spectra of a solution of 4 g $B_{10}H_{14}$ in 25 cc of cp $CS_2$ were recorded on a Lane Wells spectrograph using two water-cooled Hg arcs as a source of exciting line $\lambda$4358A. Although first films were taken with a Wratten 2-A gelatin filter, and later ones with a rhodamine 5GDN Extra gelatin filter added, all the records showed considerable background. This was traced to decomposition of decaborane, during exposure to Hg radiation, into compounds[3] not soluble in $CS_2$. The solid particles not only acted as secondary scatterers, but also settled to the bottom of the Raman tube, thereby diminishing the intensity of all scattered light reaching the spectrograph slit. Several times between exposures the solution was filtered; and after the last filtration a sample of the soultion was examined with the Baird instrument. No trace of compounds other than

* This work was supported in part by the ONR under contract with The Ohio State University Research Foundation.

[1] Kasper, Lucht, and Harker, Acta Cryst. **3**, 436 (1950). The authors wish to thank Dr. Kasper for supplying them with the structural data prior to publication.

[2] Kerr, Hallett, and Johnston, J. Am. Chem. Soc. **73**, 1117 (1951).

[3] A. Stock and E. Pohland, Ber. deut. chem. Ges. **62B**, 90 (1929).

TABLE I. Infrared and Raman frequencies in $cm^{-1}$ of decaborane.[a]

| | I.R. (solid) | I.R. ($CS_2$ sol'n.) | Raman ($CS_2$ sol'n.) | | I.R. (solid) | I.R. ($CS_2$ sol'n.) | Raman ($CS_2$ sol'n.) |
|---|---|---|---|---|---|---|---|
| 1. | | | 230 (m) | 39. | 1250 (vw) | 1250 (vw) | |
| 2. | | | 295 (w) | 40. | 1265 (vw) | 1265 (vw) | |
| 3. | | | 350 (s) | 41. | 1300 (vw) | | |
| 4. | | | 424 (vw) | 42. | 1360 (m) | 1355 (w) | |
| 5. | 446 (w) | | | 43. | 1390 (m) | | |
| 6. | 461 (w) | | 456 (m) | 44. | 1415 (m) | 1415 (w) | |
| 7. | | | 508 (w) | 45. | 1450 (m) | ↑ | |
| 8. | | | 588 (w) | 46. | 1490 (m) | strong $CS_2$ | |
| 9. | 623 (m) | | | 47. | 1550 (s) | ↓ | |
| 10. | 635 (m) | | | 48. | 1570 (vs) | absorption | |
| 11. | 649 (m) | 643 (w) | | 49. | 1590 (s) | | |
| 12. | 690 (m) | | | 50. | 1625 (m) | 1625 (w) | |
| 13. | 701 (m) | 701 (m) | | 51. | 1665 (m) | 1675 (w) | |
| 14. | 712 (vs) | | 709 (s) | 52. | 1700 (vw) | 1700 (vw) | |
| 15. | 718 (s) | 716 (vs) | | 53. | 1720 (vw) | | |
| 16. | 744 (m) | 740 (w) | | 54. | | 1745 (vw) | |
| 17. | 752 (s) | | | 55. | 1795 (m) | 1790 (vw) | |
| 18. | 765 (shoulder) | 766 (s) | 763 (w) | 56. | | 1820 (w) | |
| 19. | 773 (m) | | | 57. | 1875 (s) | 1890 (m) | 1880 (w) |
| 20. | 816 (vs) | 808 (s) | | 58. | 1900 (m) | | |
| 21. | 823 (s) | 817 (m) | | 59. | | 1925 (m) | |
| 22. | 858 (vs) | 856 (m) | 858 (s) | 60. | 1950 (w) | 1950 (w) | 1946 (w) |
| 23. | 901 (m) | 896 (m) | 901 (w) | 61. | 1990 (vw) | 2000 (vw) | |
| 24. | 915 (s) | | | 62. | 2020 (vw) | | |
| 25. | 920 (vs) | 918 (s) | 921 (w) | 63. | | 2040 (vw) | |
| 26. | 938 (s) | 932 (s) | | 64. | 2085 (vw) | 2080 (vw) | |
| 27. | 943 (m) | | | 65. | 2140 (vw) | 2145 (vw) | |
| 28. | 954 (m) | 955 (w) | | 66. | 2190 (vw) | 2200 (vw) | |
| 29. | 961 (m) | 960 (m) | 960 (w) | 67. | 2245 (vw) | | |
| 30. | 968 (m) | | | 68. | 2280 (vw) | 2290 (vw) | |
| 31. | 1003 (m) | 1009 (vs) | 1005 (w) | 69. | 2532 (vs) | 2500 | 2550 |
| 32. | 1035 (m) | 1042 (vw) | 1040 (vw) | 70. | 2544 (s) | ↑ | ↑ |
| 33. | 1058 (vw) | 1065 (w) | 1060 (vw) | 71. | 2566 (vs) | One | One |
| 34. | 1100 (m) | 1110 (w) | | 72. | 2578 (s). | strong | strong |
| 35. | 1145 (vw) | 1152 (vw) | | 73. | 2594 shoulder | band | band |
| 36. | 1160 (vw) | 1170 (vw) | | 74. | 2613 (vs) | ↓ | ↓ |
| 37. | 1190 (vw) | | | 75. | 2624 (s) | 2650 | 2600 |
| 38. | 1210 (vw) | 1210 (vw) | | | | | |

[a] Relative intensity: vs = very strong; s = strong; m = medium; w = weak; vw = very weak.

decaborane was found. Finally, in order to distinguish between decaborane lines and carbon disulfide lines, a Raman spectrum was taken of a portion of $CS_2$ distilled from the decaborane solution. Films were measured both visually and with a Leeds and Northrup microphotometer. No polarization measurements were obtained because of the aforementioned decomposition.

## RESULTS AND DISCUSSION

The infrared and Raman data are presented in Table I. Decaborane has $C_{2v}$ symmetry and with 24 atoms has 66 fundamental frequencies, which may be classed roughly as shown in Table II. For each type of vibration the expected frequency range is given. It should be noted that the structure[1] of $B_{10}H_{14}$ indicates 21 B—B bonds and therefore only $3\times10-6-21=3$ frequencies which are primarily boron skeleton bending modes. These would be the lowest frequencies of the molecule and could be represented by the Raman lines at 230, 295, and 350 $cm^{-1}$. A comparison of Tables I and II would indicate that while the listed frequencies cannot be individually assigned, the observed spectra may account for the vibrational modes expected.

The spectroscopic data for decaborane, though complex, do lend qualitative support to the refined structure of Kasper *et al.*, rather than to the structure reported earlier.[4] The main difference between the two configurations concerns the placement of hydrogen atoms. The preliminary structure has two $BH_2$ groups and two B···H—B bridges, while the latest configuration has no $BH_2$ groups but instead has four B···H—B bridges. The decaborane spectrum has no strong infrared bands or Raman lines in the region 1100 to 1200 $cm^{-1}$ as would be expected were there $BH_2$ groups present (compare spectrum of $B_2H_6$). Furthermore, the large number of rather intense bands in the 1750 to 1950 $cm^{-1}$ range indicated more than two B···H—B bridges.

Both x-ray[5] and electron diffraction[6] data on pentaborane, $B_5H_9$, presented recently indicate that the structure is as shown in Fig. 1a, while a study by Duffey[7] shows the bonding to be as given in Fig. 1b. A

[4] Kasper, Lucht, and Harker, J. Am. Chem. Soc. **70**, 881 (1948).
[5] W. J. Dulmage and W. N. Lipscomb, J. Am. Chem. Soc. **73**, 3539 (1951).
[6] Hedberg, Jones, and Schomaker, J. Am. Chem. Soc. **73**, 3538 (1951).
[7] G. H. Duffey, J. Chem. Phys. **20**, 194 (1952).

TABLE II. Classification of expected fundamental frequencies of $B_{10}H_{14}$.

| Type of mode | Number | Region expected ($cm^{-1}$) |
|---|---|---|
| B—B skeletal stretching | 21 | 400–1100 |
| B—B skeletal bending | 3 | 200–400 |
| B—H stretching | 10 | 2500–2650 |
| B—H bending $\perp C_2$ axis | 10 | 1100–1400[a] |
| B—H bending $\parallel C_2$ axis | 10 | 600–800[a] |
| B—H···B bridge | 12 | 1400–2000[b] |

[a] Compare B—H bending vibrations of $B_3N_3H_6$, J. T. Crawford and B. L. Edsall, J. Chem. Phys. **7**, 223 (1939).
[b] Compare bridge frequencies in $B_2H_6$, Webb, Neu, and Pitzer, J. Chem. Phys. **17**, 1007 (1949); this article contains other references to $B_2H_6$ spectra.

comparison of the spectroscopic data obtained in this laboratory for $B_5H_9$[8] and for $B_{10}H_{14}$ with the diffraction data for these molecules presents a consistent picture with respect to the positions of the hydrogen atoms: above 600 $cm^{-1}$ the distributions of the observed frequencies for the two compounds are remarkably similar, indicating, in accordance with the diffraction information, that in $B_5H_9$ there are no $BH_2$ groups, but only BH groups and H bridges. As for distinguishing between the two possibilities of Fig. 1, the spectral data are ambiguous. If the structure were that of 1a, there should be one low, active, essentially B—B bending frequency, whereas a careful search of the Raman spectrum of liquid pentaborane did not satisfy this expectation. On the other hand, the structure of 1b, in which adjacent basal B atoms are not formally bonded as in the structure of 1a and of $B_{10}H_{14}$, should have no fundamental frequency below about 450 wave numbers. However, it is often fruitless to speculate on the absence of expected frequencies.

TABLE III. Calculated and experimental entropy of gaseous decaborane at 298.16°K and 1 atmos.

| | | |
|---|---|---|
| *Calculated* | | |
| Vibration | | |
| $34\nu$'s, 230 to 1100 $cm^{-1}$ | 13.24 eu | |
| $10\nu$'s, average 1250 $cm^{-1}$ | 0.34 | |
| $10\nu$'s, average 2550 $cm^{-1}$ | 0.00 | |
| $8\nu$'s, average 1450 $cm^{-1}$ | 0.12 | |
| $4\nu$'s, average 1900 $cm^{-1}$ | 0.01 | |
| Total | | 13.71 |
| Rotation+translation[a] | | 70.14 |
| $S^0_{calc}$ | | 83.85 eu |
| *Experimental* | | |
| $S^0_{298.16}$ of the solid | | 42.48[b] |
| $(\Delta H^0_{sub}-\Delta F^0)/T$ | | 44.88[c] |
| $S^0_{expt}$ | | 87.36 eu |

[a] Calculated from standard formulas, nuclear spin entropy not included: $ABC=2.240\times10^{-7}$ in A. W. and angstrom units; $\sigma=2$; M. W. = 122.3.
[b] See reference 2.
[c] See references 3 and 9.

[8] Taylor, Beckett, Tung, Holden, and Johnston, Phys. Rev. **79**, 234 (1950).

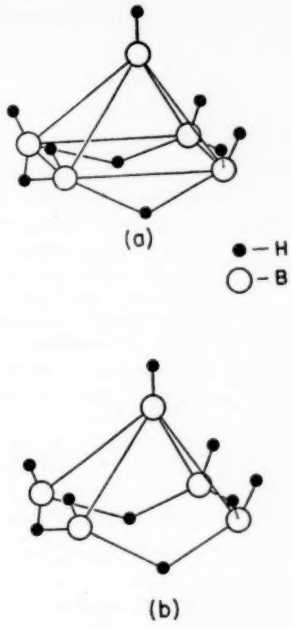


FIG. 1. Structure of pentaborane.

Although intensity considerations may indicate that most bands below 1100 $cm^{-1}$ are fundamentals, such a conclusion is difficult to substantiate for so large a molecule. Nevertheless, for thermodynamic calculations these bands are considered as fundamentals, especially since the frequency distribution satisfies our expectation. Many of the weaker bands above 1100 $cm^{-1}$ are undoubtedly overtones and combinations. At 298.16°K the contribution to the thermodynamic quantities made by frequencies above 1100 $cm^{-1}$ is small; consequently, the 32 fundamentals expected in that region also are not assigned separately but are considered in three groups, with an average frequency for each group. The choice of frequencies is made with reference to both the observed spectra and the information collected in Table II. Utilizing these selections for the fundamental frequencies in conjunction with the values of the molecular parameters obtained from the x-ray work, we can compute the hypothetical but useful entropy of gaseous decaborane at 298.16°K and 1 atmos. Table III lists the contributions to $S^0$ and compares the calculated value with that derived from the existing experimental data. The values of the heat of sublimation, $\Delta H^0_{sub}$, and of the standard change of free energy, $\Delta F^0$, were obtained by Kelley[9] from the vapor pressure data of Stock and Pohland[3] for the solid between 55°C and the melting point. Considering the uncertainty in the value for the slope of the vapor pressure curve (about ±15 percent) as well as in the choice of fundamental frequencies, the agreement between the two figures for $S^0$ is quite satisfactory.

[9] K. K. Kelley, U. S. Bur. of Mines Bull. 383 (1935).

THE JOURNAL OF CHEMICAL PHYSICS VOLUME 20, NUMBER 11 NOVEMBER, 1952

# The Franck-Condon Principle and Its Application to Crystals*

MELVIN LAX
*Physics Department, Syracuse University, Syracuse, New York*
(Received May 5, 1952)

The semiclassical Franck-Condon principle is shown to be related to the more rigorous ("exact") quantum-mechanical perturbation formula in the following ways: (1) the Franck-Condon formula can be derived from the "exact" formula by using a mean value approximation or by neglecting certain commutators; (2) if the electric dipole moments are treated as approximately independent of position, the Franck-Condon and the "exact" absorption (or emission) spectrum have the same zeroth, first, and second moments, i.e., the same integrated spectrum, mean absorption frequency, and breadth; (3) the errors in higher moments than the second become relatively unimportant at high temperatures. If the electron-nuclear interaction is sufficiently strong the errors are unimportant even at absolute zero.

The use of a quasi-molecular description in a many particle problem is found to be possible only if the masses or stiffnesses are allowed to be temperature dependent.

A detailed analysis is made of the case in which the energy difference between the two electronic states is a linear function of the vibrational coordinates—and the latter are describable by normal modes. "Exact" formulas for the absorption and emission spectrum are obtained.

## I. INTRODUCTION

THE Franck-Condon principle has been applied with considerable success to the calculation of the broadening of emission and absorption lines in simple molecules.[1,2] Useful qualitative interpretations of luminescence phenomena in crystals have been obtained by using a single schematic coordinate.[3–6] Williams[7] set up an absolute (quantitative) theory of luminescence using a single real coordinate and a semiclassical treatment. Williams and Hebb[8] extended the latter result by treating the one-coordinate problem in an all quantum-mechanical fashion. Huang and Rhys,[9] in treating $F$ centers, made the quantum-mechanical treatment of a many coordinate problem. Their technique is restricted, however, by the assumption that the vibrational modes are optical, i.e., all have the same frequency.

The author has made a quantitative calculation of the broadening of impurity center levels in homopolar semiconductors (to be published elsewhere). The trapped electron orbit in this case is sufficiently large that a treatment of the Williams type based on a single real coordinate is inadequate. Furthermore, acoustical modes make a significant contribution to the broadening so that the Huang-Rhys treatment is inadequate. The author was forced, therefore, to investigate the validity of the Franck-Condon principle in its various forms with particular reference to crystalline problems. The results of this investigation are reported in the present paper.

It may be of interest to list here the most frequently used approximations in rough order of decreasing validity:

(1) A first-order perturbation treatment of the light absorption or emission using Born-Oppenheimer wave-functions. For our purposes this treatment is "exact."

(2) Same as (1) except that the dependence of the electric dipole matrix elements on nuclear positions is neglected. This approximation may be referred to as the "Condon" approximation. It is a fairly good approximation and is often used as the standard of comparison for more severe approximations. The Huang-Rhys paper[9] uses this approximation.

(3) The semiclassical Franck-Condon principle: the nuclei are regarded as standing still during the optical transition. The probability of a given initial configuration is based on quantum statistical mechanics.

(4) The classical Franck-Condon principle: same as (3) but the initial configuration is treated by classical statistical mechanics.

(5) The quasi-molecular viewpoint: a complex system is simplified by neglecting all but a small number of coordinates—or by introducing a suitable small number of parameters.

The order chosen above is based on the following results to be demonstrated in the paper: the semiclassical principle (3) can be derived from the exact formula (1), (without necessarily using (2)). The order (4) and (5) could possibly be interchanged since the quasi-molecular viewpoint (5) can be derived from the semiclassical principle (3) without using (4). On the other hand, unless the coordinates used are truly normal

* This research was carried out under the auspices of the Crystal Branch of the Naval Research Laboratory during the summer of 1951, while the author was on summer leave from Syracuse University. The author wishes to thank Mr. E. Burstein and P. Egli for their stimulation, interest, and hospitality during the course of this research. This work was also supported in part by the ONR.

[1] A. G. Gaydon, *Dissociation Energies* (Dover Publications, New York, 1950).
[2] G. Herzberg, *Molecular Spectra* (Prentice-Hall, Inc., New York, 1939), see p. 217 ff, and p. 412 ff.
[3] F. Seitz, J. Chem. Phys. **6**, 150, 454 (1938); Trans. Faraday Soc. **35**, 74 (1939).
[4] R. W. Gurney and N. F. Mott, Trans. Faraday Soc. **35**, 69 (1939).
[5] P. Pringsheim, Revs. Modern Phys. **14**, 132 (1942).
[6] F. E. Williams and H. Eyring, J. Chem. Phys. **15**, 289 (1947).
[7] F. E. Williams, J. Chem. Phys. **19**, 457 (1951); Phys. Rev. **82**, 281 (1951).
[8] F. E. Williams and M. H. Hebb, Phys. Rev. **84**, 1181 (1951).
[9] K. Huang and A. Rhys, Proc. Roy. Soc. (London), **204A**, 406 (1950).

coordinates, it does not seem possible to derive the quasi-molecular viewpoint (5) from the "exact" treatment (1). Thus it is not necessarily consistent to attempt an all quantum-mechanical treatment of an effective one-parameter system (e.g., reference 8). In this notation, the Williams' papers[7] use the respective approximations (5) and (4), and then (5) and (3) in addition to (2).

The quasi-molecular viewpoint developed in this paper from the semiclassical principle is somewhat more general than the use of a simplified physical system and is equivalent to the latter only if we endow the stiffnesses or masses of the simple system with temperature dependence. Conversely, the use of a simple system is not strictly valid in conjunction with the semiclassical principle unless temperature dependent coefficients are allowed.

It was found possible to calculate the exact moments of the quantum-mechanical spectrum as well as the corresponding semiclassical moments. A comparison of these moments affords a test of the accuracy of the semiclassical procedure. The zeroth moments (integrated spectrum) are found to agree precisely. The first and second moments (mean absorption frequency and breadth) are also found to agree if the Condon approximation (2) is made. All higher moments in general disagree.

*Finally, it has been found possible to generalize the Huang-Rhys procedure and make an all quantum-mechanical calculation of the broadening regardless of the nature of the vibration spectrum.* The Condon approximation is made, but the methods used are easily extended if the electric dipole moments are not constants but, say, linear functions of the nuclear displacements.

## II. THE QUANTUM-MECHANICAL TRANSITION PROBABILITY

Let $x$ denote a set of nuclear coordinates and $M_{ba}(x)$ the transition electric dipole matrix element between the initial and final electronic states $\Phi_a(r, x)$ and $\Phi_b(r, x)$. The vibrational state $X_{am}(x)$ is associated with electronic state $a$. The usual formulas for the absorption cross section $\sigma$ and total emission probability per unit time $w$ corrected for the presence of a medium can be written

$$\sigma(\nu)=\left[\frac{n}{\epsilon}\left(\frac{E_e}{E}\right)^2\right]\frac{8\pi^3\nu}{3c}I_{ba}(\nu), \tag{2.1}$$

$$w=\int\left[\frac{n^3}{\epsilon}\left(\frac{E_e}{E}\right)^2\right]\frac{64\pi^4\nu^3}{hc^3}I_{ab}(\nu)d(h\nu), \tag{2.2}$$

$$I_{ba}(\nu)=\mathrm{Av}_m\sum_n\left|\int X_{bn}^*(x)M_{ba}(x)X_{am}(x)dx\right|^2 \times\delta(E_{bn}-E_{am}-h\nu). \tag{2.3}$$

The average $\mathrm{Av}_m$ is understood to be an average over the initial vibrational states weighting each with the customary Boltzmann factor $\exp[-E_{am}/kT]$. If, both on absorption and emission, we regard state $a$ as the lower electronic state, and state $b$ as the higher energy electronic state, then $I_{ab}(\nu)$ for the emission transition, $a\leftarrow b$, is obtained from $I_{ba}(\nu)$ simply by interchanging the operations of summation and averaging. (In each case, the average is over initial vibrational states, and the sum over final vibrational states.)

(An expression similar to (2.3) applies to nonradiative transitions if $M_{ba}$, the electric dipole moment is replaced by the usual perturbing operator for the latter case. Methods similar to those used here have been applied to the latter problem. Results will be discussed in another paper.)

If broadening is unimportant, $I_{ba}(\nu)$ is simply a delta-function: $I_{ba}(\nu)\simeq\langle|M_{ba}|^2\rangle\delta(E_b-E_a-h\nu)$, and the integrated cross section $\int\sigma(\nu)d(h\nu)$, aside from the factors in brackets, reduces to the usual atomic absorption formula.[10] Similar remarks apply to the emission case. Thus, Eqs. (2.1) and (2.2) are absolute formulas containing the necessary normalization constants.

The factors in brackets represent correction factors because the absorption and emission processes take place in a medium (a crystal). The factor $1/\epsilon$ (where $\epsilon$ = dielectric constant at the optical frequency involved) appears because the transition probability is of the form $|M\cdot E|^2$ and the electric field whose energy corresponds to one photon per unit volume obeys $\epsilon E^2/4\pi=h\nu$.

To obtain an absorption cross section, a transition probability must be divided by the incident flux associated with one photon per unit volume, i.e., by the velocity of light $v$ in the medium. This accounts for the factor $n$, the index of refraction, in (2.4).

To obtain the total emission probability, the emission into one photon state must be summed over the possible photon states. The number of such states is proportional to the cube of the photon momentum $(h\nu/v)^3$ which yields a factor $n^3$ when compared with the corresponding vacuum quantity $(h\nu/c)^3$.

The factor $(E_e/E)^2$ describes the fact that the electron in question is located at a center in a crystal at which the effective field $E_e$ may differ from the average macroscopic electric field $E$.

It will be convenient for us to re-express (2.3) as an invariant expression—a trace over the initial states. *If $M_{ba}$ is regarded as an arbitrary operator, the procedure used here is applicable to all perturbation calculations since the latter have the same form as (2.3).*

Introducing, therefore, the integral representation

$$\delta(E_{bn}-E_{am}-h\nu)=h^{-1}\int_{-\infty}^{+\infty}\exp[i(E_{bn}-E_{am}-h\nu)t/\hbar]dt, \tag{2.4}$$

[10] See, for example, H. Bethe, *Handbuch der Physik*, 24/1, Kap. 3, Eqs. (47.3) and (38.11).

the absorption spectrum can be re-written in the form

$$I_{ba}(\nu)=h^{-1}\int \exp(-i2\pi\nu t)dt I_{ba}(t), \tag{2.5}$$

$$I_{ba}(t)=\mathrm{Av}_m\sum_n(am|M_{ba}{}^{+}|bn)\times(bn|e^{iH_bt/\hbar}M_{ba}e^{-iH_at/\hbar}|am), \tag{2.6}$$

where $E_{am}$ and $E_{bn}$ have been replaced by the corresponding Hamiltonian operators $H_a$ and $H_b$ in order to permit the closure sum over $n$:

$$I_{ba}(t)=\mathrm{Av}_m(am|M_{ba}{}^{+}e^{iH_bt/\hbar}M_{ba}e^{-iH_at/\hbar}|am), \tag{2.7}$$

where $M_{ba}{}^{+}=M_{ba}{}^{*}(x)$ for purely space operators.

The Boltzmann average can be facilitated by inserting a factor $\exp[-\beta H_a]$ where $\beta=(kT)^{-1}$. Thus we can without ambiguity express the result in terms of traces:

$$I_{ba}(t)=tr[M_{ba}{}^{*}e^{iH_bt/\hbar}M_{ba}e^{-iH_at/\hbar}e^{-\beta H_a}]/tr[e^{-\beta H_a}]. \tag{2.8}$$

In a similar fashion, corresponding formula for emission $I_{ab}(t)$ can be written

$$I_{ab}(t)=\mathrm{Av}_n[M_{ba}e^{-iH_at/\hbar}M_{ba}{}^{*}e^{iH_bt/\hbar}] \tag{2.9}$$

$$=tr[M_{ba}e^{-iH_at/\hbar}\times M_{ba}{}^{*}e^{iH_bt/\hbar}e^{-\beta H_b}]/tr[e^{-\beta H_b}]. \tag{2.10}$$

The result for emission (2.10) can be obtained from the corresponding result for absorption (2.8) by interchanging $H_a$ and $H_b$ and taking the complex conjugate, or somewhat symbolically

$$I_{ab}(t)=I_{ba}{}'(t)^{*}. \tag{2.11}$$

To save repetition, we shall hereafter state formulas only for the absorption case and omit subscripts for simplicity. For example, (2.7) can be written

$$I(t)=\mathrm{Av}[M^{+}e^{iH_bt/\hbar}Me^{-iH_at/\hbar}]. \tag{2.12}$$

## III. THE SEMICLASSICAL FRANCK-CONDON PRINCIPLE

After an optical transition, the heavy particles, subject to a new potential, will not be in equilibrium with the latter. Hence, the important final states for the transition will be excited states with large quantum numbers which, according to the Bohr correspondence principle, can be treated as approximately classical. Thus the final vibrational state $X_{bn}(x)$ will oscillate rapidly except near the classical turning points, i.e., the points $x$ for which $E_b(x)=E_{bn}$. A good approximation to the sum over $n$ in (2.3) can therefore be obtained by replacing $E_{bn}$ in the delta-function by a mean value independent of $n$:

$$\bar{E}_{bn}=E_b(x). \tag{3.1}$$

The sum over $n$ can now be performed with the help of the closure relationship

$$\sum_n X_{bn}{}^{*}(x')X_{bn}(x)=\delta(x-x'), \tag{3.2}$$

and (2.3) simplifies to the value

$$I_{ba}(\nu)=\mathrm{Av}_m\int |M_{ba}(x)|^2|X_{am}(x)|^2\times\delta(E_b(x)-E_{am}-h\nu)dx. \tag{3.3}$$

If many initial states $m$ are involved, it is convenient to use a corresponding mean-value approximation $\bar{E}_{am}=E_a(x)$, with the result

$$I_{ba}(\nu)=\int |M_{ba}(x)|^2P_a(x)\delta(\Delta E(x)-h\nu)dx, \tag{3.4}$$

$$\Delta E(x)=E_b(x)-E_a(x), \tag{3.5}$$

$$P_a(x)=\mathrm{Av}_m[|X_{am}(x)|^2]. \tag{3.6}$$

Here $E_a(x)$ and $E_b(x)$ are the effective Born-Oppenheimer potentials for the heavy particles when the electron is in state $a$ and $b$, respectively; $P_a(x)$ is the quantum-statistical mechanical probability distribution for the heavy particles. The emission spectrum $I_{ab}(\nu)$ may be obtained simply by replacing $P_a(x)$ by $P_b(x)$, i.e., in each case the probability distribution associated with the *initial* state is used.

Equation (3.4) is the semiclassical Franck-Condon principle. If $P_a(x)$ is calculated using classical statistics, (3.4) reduces to the classical Franck-Condon principle. In words, (3.4) states that the probability of absorbing $h\nu$ in $d(h\nu)$ is to be obtained from the probability of a transition $|M_{ba}(x)|^2$ at configuration $x$ times the probability $P_a(x)$ of this configuration occurring times the requirement that the configurational energy difference $\Delta E(x)$ will equal $h\nu$. The delta-function $\delta(\Delta E(x)-h\nu)$ also takes care of the Jacobian $dx/d(h\nu)$ necessary to convert $x$ intervals into $h\nu$ intervals. Ferd Williams has, in fact, used the Franck-Condon principle in essentially this form without supplying a formal justification.[7]

Although the "derivation" presented above for the semiclassical principle is intuitively appealing, it provides no hint as to how the semiclassical approach can be improved. An alternative derivation, more suggestive of improvements, will therefore be presented.

*The semiclassical approximation can also be obtained from (2.7) or (2.12) by judiciously neglecting a few commutators:*

$$I_{ba}(t)\overset{\text{S.C.}}{\longrightarrow}\mathrm{Av}_m\{|M_{ba}(x)|^2\exp[i\Delta E(x)t/h]\}, \tag{3.7}$$

where

$$\Delta E(x)=H_b-H_a=E_b(x)-E_a(x) \tag{3.8}$$

because the kinetic energies cancel. Inserting (3.7) into (2.5) the semiclassical spectrum becomes

$$I_{ba}(\nu)\overset{\text{S.C.}}{\longrightarrow}\mathrm{Av}_m[|M_{ba}(x)|^2\delta(\Delta E(x)-h\nu)], \tag{3.9}$$

which is identical to (3.4).

## IV. MOMENTS OF THE SPECTRUM, EXACT AND SEMICLASSICAL

The Fourier relation (2.5) between the distribution function $I(\nu)$ and the corresponding characteristic function $I(t)$ can be inverted:

$$I(t)=\int I(\nu)\exp(i2\pi\nu t)d(h\nu). \tag{4.1}$$

Expanding the exponential in powers of $t$, we learn that the coefficients are simply the (unnormalized) moments of the spectrum:

$$\int(h\nu)^r I(\nu)d(h\nu)=[d/d(it/\hbar)]^r I(t)|_{t=0}. \tag{4.2}$$

The moments from zero to four, using (2.12) are given by

$$\int I(\nu)d(h\nu)=\mathrm{Av}[|M_{ba}|^2], \tag{4.3}$$

$$\int h\nu I(\nu)d(h\nu)=\mathrm{Av}[M_{ba}{}^*H_bM_{ba}-|M_{ba}|^2H_a], \tag{4.4}$$

$$\int(h\nu)^2 I(\nu)d(h\nu)=\mathrm{Av}[M_{ba}{}^*H_b{}^2M_{ba}-2M_{ba}{}^*H_bM_{ba}H_a+|M_{ba}|^2H_a{}^2], \tag{4.5}$$

$$\int(h\nu)^3 I(\nu)d(h\nu)=\mathrm{Av}[M_{ba}{}^*H_b{}^3M_{ba}-3M_{ba}{}^*H_b{}^2M_{ba}H_a+3M_{ba}{}^*H_bM_{ba}H_a{}^2-|M_{ba}|^2H_a{}^3], \tag{4.6}$$

$$\int(h\nu)^4 I(\nu)d(h\nu)=\mathrm{Av}[M_{ba}{}^*H_b{}^4M_{ba}-4M_{ba}{}^*H_b{}^3M_{ba}H_a+6M_{ba}{}^*H_b{}^2M_{ba}H_a{}^2-4M_{ba}{}^*H_bM_{ba}H_a{}^3+|M_{ba}|^2H_a{}^4]. \tag{4.7}$$

The corresponding moments of the semiclassical spectrum are

$$\int(h\nu)^r I_{ba}(\nu)d(h\nu)=\mathrm{Av}[|M_{ba}|^2(\Delta E)^r], \tag{4.8}$$

where $\Delta E=H_b-H_a$ is a space function. The following comparisons may be made between the quantum-mechanical and semiclassical formulas:

(1) The semiclassical zeroth moment agrees exactly with the quantum-mechanical zeroth moment. Note that the thermal vibrations affect the integrated absorption (or emission) spectrum only to the extent that they change the mean-square electric dipole moment.

(2) Expressions for the higher moments differ only in the order of certain operators.

(3) If the "Condon" approximation is made ($M_{ba}$ is approximately a constant) then the first and second moments are given correctly by the semiclassical formula. (For the second moment we make use of $\mathrm{Av}[(H_a, H_b)]=0$.)

(4) The difference between the semiclassical and quantum-mechanical higher moments does not vanish as $T\to\infty$, but this difference becomes relatively less important. For example, the difference between the quantum-mechanical and semiclassical third moments becomes small compared to the three-halves power of the second moment. In fact, the latter statement can be used as a measure of the region of validity of the semiclassical procedure. This region is approximately the region in which

$$\mathrm{Av}[(H_a, H_b)\Delta E]\ll[\mathrm{Av}(\Delta E)^2]^{\frac{3}{2}}. \tag{4.9}$$

This criterion will always be satisfied at sufficiently high temperatures. If $\Delta E$ is sufficiently large, however, it may be satisfied for all temperatures including absolute zero. The latter possibility is, in fact, not at all unusual, as we shall see in Sec. VIII, so that the semiclassical procedure will be a completely valid approximation for many problems.

## V. THE QUASI-MOLECULAR VIEWPOINT

Since the semiclassical principle has an important region of validity, we consider next methods that can be used to simplify its application to complex systems. One of the most commonly adopted procedures[3-6] is to describe the system in terms of a single schematic coordinate, or in terms of one or two real coordinates.[7,8] In this section, therefore, we shall investigate the conditions under which a description involving a small number of parameters is feasible. We shall show that such a description is always possible in principle, and usually possible in practice, but that the parameters involved will usually not be real coordinates. For example, a one-parameter description will not be precisely equivalent to a one-coordinate physical system unless the latter is endowed with say a temperature dependent mass.

Using (3.4) and (4.3) the normalized spectrum

$$G_{ba}(\nu)=I_{ba}(\nu)/\mathrm{Av}[|M_{ba}|^2], \tag{5.1}$$

$$\int G_{ba}(\nu)d(h\nu)=1 \tag{5.2}$$

is given by

$$G_{ba}(\nu)=\int P_a'(q_1,\cdots q_N)\times\delta(\Delta E(q_1\cdots q_N)-h\nu)dq_1\cdots dq_N, \tag{5.3}$$

where

$$P_a'(q_j)=|M_{ba}(q_j)|^2P_a(q_j)/\mathrm{Av}[|M_{ba}|^2] \tag{5.4}$$

and $q_1 \cdots q_N$ are the normal coordinates of the complex system. In the Condon approximation $P_a'$ is identical with $P_a$.

It is always possible to regard $\Delta E$ as a function of a single parameter $\xi$:

$$\Delta E(q_1 \cdots q_N) = \Delta E(\xi), \tag{5.5}$$

$$\xi = \xi(q_1 \cdots q_N). \tag{5.6}$$

(If necessary, $\xi$ can be set equal to $\Delta E$!) Equation (5.3) can then be rewritten in the form of a one-parameter description:

$$G_{ba}(\nu) = \int P_a(\xi)\delta(\Delta E(\xi) - h\nu)d\xi, \tag{5.7}$$

$$G_{ba}(\nu) = [P_a(\xi)d\xi/d\Delta E(\xi)]_{\Delta E(\xi)=h\nu}, \tag{5.8}$$

where the normalized probability $P_a(\xi)$ must be obtained from an $N$ dimensional integral:

$$P_a(\xi) = \int P_a'(q_1 \cdots q_N)\delta(\xi - \xi(q_1 \cdots q_N))dq_1 \cdots dq_N. \tag{5.9}$$

*It is highly unlikely* (unless $\xi$ is itself one of the normal coordinates $q_j$) *that the $P_a(\xi)$ obtained in this way could also be obtained from a real one-coordinate physical system.*

The use of a single-parameter description in practice depends on the feasibility of evaluating (5.9). Since $P_a$ for a crystal is an exponential of a quadratic form, (5.9) can be evaluated easily if $\xi$ is a linear function of the $q$'s. But $\Delta E$ cannot always be expressed as a function (even a nonlinear one) of a single linear parameter. For a trapped electron, however, $\Delta E$ will usually depend strongly, i.e., nonlinearly, on only a small number of nearest neighbor coordinates. It may depend weakly, i.e., linearly, on a large number of coordinates. The latter dependence, however, can be represented by a single parameter: the appropriate linear combination of the distant coordinates. Thus there will be an important class of problems for which $\Delta E$ can be represented as a (possibly nonlinear) function of several linear parameters.

For this case

$$\Delta E(q_1 \cdots q_N) = \Delta E(\xi^1 \cdots \xi^s), \tag{5.10}$$

$$\xi^r = N^{-\frac{1}{2}} \sum_1^N a_j{}^r q_j, \tag{5.11}$$

$$G_{ba}(\nu) = \int P_a(\xi^1 \cdots \xi^s) \times \delta(\Delta E(\xi^1 \cdots \xi^s) - h\nu)d\xi^1 \cdots d\xi^s, \tag{5.12}$$

$$P_a(\xi^1 \cdots \xi^s) = \int P_a'(q_2 \cdots q_N) \times \prod_{r=1}^{s} \delta(\xi^r - \xi^r(q_1 \cdots q_N))dq_1 \cdots dq_N. \tag{5.13}$$

If we make the Condon approximation (so that $P_a' = P_a$), then for a crystal describable in terms of normal modes

$$P_a(q_1 \cdots q_N) = \prod_{j=1}^{N} [2\pi\langle q_j{}^2\rangle]^{-\frac{1}{2}} \exp[-\tfrac{1}{2}q_j{}^2/\langle q_j{}^2\rangle], \tag{5.14}$$

$$\langle q_j{}^2\rangle = (\hbar/M\omega_j)[\bar{n}(\omega_j) + \tfrac{1}{2}], \tag{5.15}$$

$$\bar{n}(\omega_j) = [\exp(\hbar\omega_j/kT) - 1]^{-1}, \tag{5.16}$$

and we have made use of the fact that the quantum-mechanical, thermal average, distribution function of a harmonic oscillator is a Gaussian function.[11]

After inserting (5.11) and (5.14), the integrations in (5.13) can be performed explicitly with the result

$$P_a(\xi^1 \cdots \xi^s) = (2\pi)^{-s/2}[det\langle \xi^r \xi^{r'}\rangle]^{-\frac{1}{2}} \times \exp[-\tfrac{1}{2}\sum D_{rr'}\xi^r\xi^{r'}], \tag{5.17}$$

where $D_{rr'}$ is a matrix whose reciprocal is the matrix $\langle \xi^r \xi^{r'}\rangle$:

$$(D^{-1})_{rr'} = \langle \xi^r \xi^{r'}\rangle = N^{-1}\sum_j a_j{}^r a_j{}^{r'}\langle q_j{}^2\rangle. \tag{5.18}$$

If only one parameter $\xi$ enters, (5.17) reduces to

$$P_a(\xi) = [2\pi\langle \xi^2\rangle]^{-\frac{1}{2}} \exp[-\tfrac{1}{2}\xi^2/\langle \xi^2\rangle], \tag{5.19}$$

$$\langle \xi^2\rangle = N^{-1}\sum_j a_j{}^2(\hbar/M\omega_j)[\bar{n}(\omega_j) + \tfrac{1}{2}], = \langle a_j{}^2(\hbar/M\omega_j)[\bar{n}(\omega_j) + \tfrac{1}{2}]\rangle, \tag{5.20}$$

where the last average in (5.20) is an average over modes $j$ in the sense

$$\langle f(a_j, \omega_j)\rangle = N^{-1}\sum_{j=1}^{N} f(a_j, \omega_j). \tag{5.21}$$

The procedure adopted in this section is more general than the usual quasi-molecular viewpoint since the distribution function $P_a(\xi^1 \cdots \xi^s)$ *is not obtained from the statistical mechanics of an s particle system, but is obtained from (5.13) which considers the contribution of all degrees of freedom.* For example, $\xi$ cannot be regarded in (5.19) as the coordinate of a "real" harmonic oscillator with an effective mass $M_e$ and frequency $\omega_e$ since the temperature dependence of $\langle \xi^2\rangle$ differs from that of any single oscillator of fixed mass and frequency. However, $\langle \xi^2\rangle$ does approach a constant at low temperatures (zero-point oscillations) and a linear function of the temperature at high temperatures.

An effective mass $M_e$ and effective frequency $\omega_e$ can be so chosen for a simple harmonic oscillator that the mean square displacement of the oscillator agrees with $\langle \xi^2\rangle$ for these two limiting cases. The low and high temperature conditions are, respectively:

$$(M_e\omega_e)^{-1} = \langle a_j{}^2/M\omega_j\rangle, \tag{5.22}$$

$$(M_e\omega_e{}^2)^{-1} = \langle a_j{}^2/M\omega_j{}^2\rangle, \tag{5.23}$$

[11] M. Born, Reports on Progress in Physics **9**, 294 (1942-3) Appendix 1. Also, H. Ott, Ann. Physik **23**, 169 (1935).

where the average over modes are in the sense (5.21). The condition for a perfect fit in the intermediate region

$$\langle \xi^2 \rangle = (\hbar/M_e\omega_e)[\bar{n}(\omega_e)+\tfrac{1}{2}] \tag{5.24}$$

can only be satisfied if $M_e$ (or $\omega_e$) is allowed to become temperature dependent.

A conventional quasi-molecular viewpoint such as the one adopted by Williams[7] uses several real coordinates, e.g., the first and second nearest neighbor distances. But the probability distribution $P(\xi^1\xi^2)$ was not obtained by evaluating (5.13) but rather by considering $\xi^1$ and $\xi^2$ as real coordinates of a two particle physical system and using the result $\exp[-V(\xi^1, \xi^2)/kT]$ of classical statistical mechanics. The potential energy $V(\xi^1, \xi^2)$ as a function of the first and second nearest neighbors is evaluated by holding *all other atoms fixed*. Such a "static" procedure yields effective stiffnesses that are greater than the "dynamic" stiffnesses obtained from (5.13) in which all atoms are allowed to move.

## VI. TRAPPED ELECTRON

For an electron trapped in a crystal, the energy shift of the trapped electron due to its interaction with the lattice *motion* can to a first approximation be represented as a linear function of the lattice displacements (particularly if the electron orbit is large so that the interaction with any one atom is weak):

$$\begin{aligned} \Delta E_b &= N^{-\frac{1}{2}} \sum A_j{}^b q_j, \\ \Delta E_a &= N^{-\frac{1}{2}} \sum A_j{}^a q_j, \end{aligned} \tag{6.1}$$

where $N$ is the number of normal modes. The energy difference,

$$\Delta E(x) = E_b(x) - E_a(x),$$

is then

$$\Delta E(x) = E_b(0) - E_a(0) + N^{-\frac{1}{2}} \sum A_j q_j \tag{6.2}$$

$$A_j = A_j{}^b - A_j{}^a, \tag{6.3}$$

where $E_b(0)-E_a(0)$ is the energy difference for the nuclei constrained to the perfect lattice positions $q_j=0$. The linear energies (6.1) will shift the equilibrium positions in states $a$ and $b$ from $q_j=0$ to

$$\bar{q}_j{}^a = -N^{-\frac{1}{2}} A_j{}^a/(M\omega_j{}^2); \quad \bar{q}_j{}^b = -N^{-\frac{1}{2}} A_j{}^b/(M\omega_j{}^2). \tag{6.4}$$

The mean absorption and emission energies may be obtained according to (4.8) by taking the thermal average of $\Delta E(x)$ in states $a$ and $b$, respectively:

$$\begin{aligned} h\bar{\nu}_a &= E_b - E_a - \langle A_j A_j{}^a/(M\omega_j{}^2)\rangle, \\ h\bar{\nu}_e &= E_b - E_a - \langle A_j A_j{}^b/(M\omega_j{}^2)\rangle, \end{aligned} \tag{6.5}$$

or

$$\begin{matrix} h\bar{\nu}_a \\ h\bar{\nu}_e \end{matrix} = h\nu_0 \pm \langle A_j{}^2/(2M\omega_j{}^2)\rangle, \tag{6.6}$$

where

$$h\nu_0 = E_b - E_a + \langle [(A_j{}^a)^2 - (A_j{}^b)^2]/(2M\omega_j{}^2)\rangle, \tag{6.7}$$

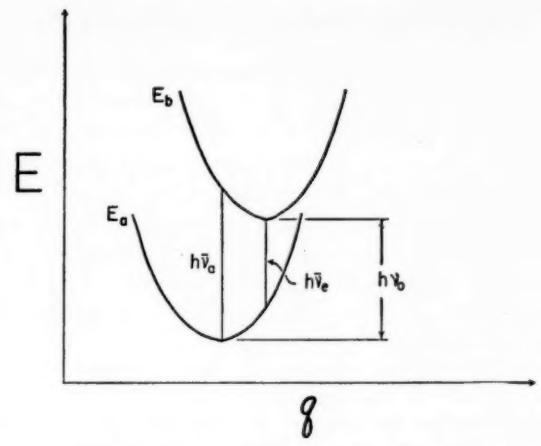


FIG. 1. Configurational coordinate curves $E_b(q)$ and $E_a(q)$ are shown for the excited and ground electronic states, respectively. The mean absorption energy $h\bar{\nu}_a$, the mean emission energy $h\bar{\nu}_e$, and the energy separation between minima $h\nu_0$ are indicated.

is the energy separation between the shifted equilibrium positions in the presence of the electron lattice, i.e., the energy separation between the minimum points of two parabolas (see Fig. 1).

According to (4.8) the mean square broadening $\langle (h\nu - h\bar{\nu})^2\rangle$ in the Condon approximation is given by

$$\begin{aligned} \mathrm{Av}[\Delta E(x)]^2 - [\mathrm{Av}\Delta E(x)]^2 &= N^{-1} \sum A_j{}^2 \langle (q_j - \bar{q}_j{}^a)^2\rangle \\ &= \langle A_j{}^2 (\hbar/M\omega_j)[\bar{n}(\omega_j)+\tfrac{1}{2}]\rangle, \end{aligned} \tag{6.8}$$

where the last average is over modes in the sense (5.21).

For the case of a linear energy difference (6.2) it is always possible to introduce $\xi = \Delta E(x)$ as a one-parameter description. Comparison with (5.7) and (5.19) indicates that for this case, the *spectral distribution* on absorption (or emission) is Gaussian. Thus this distribution is completely characterized (in semiclassical approximation) by the mean energy (6.6) and the broadening (6.8).

## VII. THE USE OF ORDERED OPERATORS

From this point on, we shall assume the validity of the "Condon approximation": $M_{ba}(x) \simeq$ constant. This assumption is made for the following reasons: (1) the Condon approximation is valid in most applications; (2) usually one does not have more information about $M_{ba}$ than a rough measure of its value; (3) the arguments to be presented below will be unobscured by an attempt to keep small correction terms; (4) if $M_{ba}(x)$ is an approximately linear or quadratic function of the displacements, the methods to be presented below can readily be generalized to take into account these corrections.

Using (2.12) and the Condon approximation, the characteristic function can be written

$$I(t) = |M_{ba}|^2 G(t), \tag{7.1}$$

$$G(t) = \mathrm{Av}[\exp(iH_b t/\hbar)\exp(-iH_a t/\hbar)]. \tag{7.2}$$

The corresponding semiclassical expression for $G(t)$,

$$G_{sc}(t)=\mathrm{Av}[\exp(i\Delta Et/\hbar)] \tag{7.3}$$

where

$$\Delta E=H_b-H_a=\Delta E(x), \tag{7.4}$$

can be obtained by neglecting a few commutators. Since (7.2) and (7.3) differ only in the order of appearance of certain operators, an interesting comparison between the two formulas can be obtained by using the notation of ordered operators introduced by Dyson[12] and exploited by Feynman[13] and Goldberger and Adams.[14] In particular we need the theorem[15]

$$\exp(a+b)=\exp_{[-]}\left\{\int_0^1 b(s)ds\right\}\exp(a), \tag{7.5}$$

where

$$b(s)=\exp(as)b\exp(-as). \tag{7.6}$$

If we choose $a=iH_at/\hbar$, $b=i\Delta Et/\hbar$, Eq. (7.2) can be rewritten in the suggestive form

$$G(t)=\mathrm{Av}\exp_{[-]}\left\{i\int_0^t \Delta E(x(s))ds/\hbar\right\}, \tag{7.7}$$

where

$$x(s)=\exp(iH_as/\hbar)x(0)\exp(-iH_as/\hbar) \tag{7.8}$$

is the position operator at time $s$, i.e., the position operator in the Heisenberg representation, where $x(0)$ is the usual position operator $x$ in the Schrödinger representation.

The negatively ordered exponential is to be interpreted in the following sense: (1) Expand the exponential in a power series; (2) write each factor $\int\Delta E(s)ds$ using a different integration variable; (3) a product of factors of the form $\Delta E(s_1)\Delta E(s_2)\cdots\Delta E(s_n)$ is understood to act in reverse time order, regardless of the way in which the factors are written, i.e., the factor acting on the extreme right is the one whose value $s_j$ is the largest of all the values $s_1, s_2\cdots s_j, \cdots s_n$. For example, to terms of second order,

$$\exp_{[-]}\left\{i\int_0^t \Delta E(s)ds/\hbar\right\}=1+(i/\hbar)\int_0^t \Delta E(s)ds$$
$$-\tfrac{1}{2}(\hbar)^{-2}\int_0^t ds\int_0^s ds'\Delta E(s')\Delta E(s)$$
$$-\tfrac{1}{2}(\hbar)^{-2}\int_0^t ds\int_s^t ds'\Delta E(s)\Delta E(s'). \tag{7.9}$$

The last two terms are in fact equal, as may be verified by interchanging dummy indices $s$ and $s'$. Thus to second order,

$$G(t)\simeq 1+(i/\hbar)\int_0^t ds\,\mathrm{Av}[\Delta E(s)]$$
$$-(\hbar)^{-2}\int_0^t ds\int_0^s ds'\,\mathrm{Av}[\Delta E(s')\Delta E(s)]. \tag{7.10}$$

## VIII. QUANTUM TREATMENT OF COMPLEX SYSTEMS

Let us consider a system describable by normal modes in accord with the assumptions of Sec. VI. The energy difference between the two electronic states is assumed to be a linear form (6.2):

$$\Delta E=E_b(0)-E_a(0)+N^{-\frac{1}{2}}\sum A_jq_j \tag{8.1}$$

or

$$\Delta E=h\bar{\nu}_a+N^{-\frac{1}{2}}\sum A_j(q_j-\bar{q}_j{}^a), \tag{8.2}$$

where $h\bar{\nu}_a$ is the mean absorption energy (6.5a). Thus (7.7) can be rewritten in the form

$$G(t)=\exp(i2\pi\bar{\nu}_at)$$
$$\times\prod_j \mathrm{Av}\exp_{[-]}\left\{iN^{-\frac{1}{2}}A_j\int_0^t q_j(s)ds/\hbar\right\}, \tag{8.3}$$

where we have written $q_j(s)$ briefly, in place of $q_j(s)-\bar{q}_j{}^a$ and according to (7.8),

$$q_j(s)=q_j(0)\cos\omega_js+[p_j(0)/M\omega_j]\sin\omega_js, \tag{8.4}$$

where $q_j(0)$ and $p_j(0)$ are the usual Schrodinger position and momentum operators (using $\bar{q}_j{}^a=0$ as origin).

Let us consider a single harmonic oscillator, and omit the subscript $j$ for simplicity. Because of the factor $N^{-\frac{1}{2}}$, it will be sufficient to expand to terms of second order. Since $\mathrm{Av}q(s)=0$, comparison with (7.10) indicates that

$$\mathrm{Av}\exp_{[-]}\left\{iN^{-\frac{1}{2}}A\int_0^t q(s)ds/\hbar\right\}\simeq 1$$
$$-N^{-1}\hbar^{-2}A^2\int_0^t ds\int_0^s ds'\,\mathrm{Av}[q(s')q(s)]. \tag{8.5}$$

Introducing (8.4) we obtain

$$\mathrm{Av}[q(s')q(s)]=\mathrm{Av}[q^2(0)]\cos\omega s\cos\omega s'$$
$$+\mathrm{Av}[(p(0)/\omega M)^2]\sin\omega s\sin\omega s'$$
$$+\mathrm{Av}[q(0)p(0)/\omega M]\sin\omega s\cos\omega s'$$
$$+\mathrm{Av}[p(0)q(0)/\omega M]\cos\omega s\sin\omega s'. \tag{8.6}$$

Because of the equality of potential and kinetic energies,

$$\mathrm{Av}[q^2(0)]=\mathrm{Av}[(p(0)/\omega M)^2]=h(\bar{n}+\tfrac{1}{2})/M\omega, \tag{8.7}$$

where $\bar{n}$, the average quantum number is given by (5.16). With the help of the commutation value $(q,p)=i\hbar$ we find

$$\mathrm{Av}(qp)=-\mathrm{Av}(pq)=i\hbar/2. \tag{8.8}$$

[12] F. Dyson, Phys. Rev. **75**, 486, 1736 (1949).
[13] R. P. Feynman, Phys. Rev. **84**, 108 (1951).
[14] M. L. Goldberger and E. N. Adams, J. Chem. Phys. **20**, 240 (1952).
[15] See reference 14, Eq. (1.13a); reference 13, Sec. 3, and Appendix A, last paragraph.

The integrations over $s$ and $s'$ in (8.5) can now be performed and the result rewritten (correct to order $1/N$) in exponential form:

$$\text{Av}\exp_{[-]}\left\{iN^{-\frac{1}{2}}A_j\int_0^t q_j(s)ds/h\right\}$$
$$=\exp\{N^{-1}C_j^2[i(\sin\omega_j t-\omega_j t)-(2\bar{n}_j+1)(1-\cos\omega_j t)]\} \quad (8.9)$$

where

$$C_j^2=A_j^2/(2hM\omega_j^3). \quad (8.10)$$

Inserting (8.9) into (8.3) and using (6.5), (6.7) the characteristic function for absorption is given by

$$G_{ba}(t)=\exp[i2\pi\nu_0 t+f(t)], \quad (8.11)$$
$$f(t)=\langle C_j^2[i\sin\omega_j t-(2\bar{n}_j+1)(1-\cos\omega_j t)]\rangle. \quad (8.12)$$

The average over modes $j$ is taken as in (5.21). The corresponding emission spectrum according to (2.11) may be obtained by interchanging $a$ and $b$ and taking the complex conjugate:

$$G_{ab}(t)=\exp[i2\pi\nu_0 t+f^*(t)]. \quad (8.13)$$

The normalized moments $\langle(h\nu)^r\rangle$ can be obtained from (4.2) with $I(t)$ replaced by $G(t)$. For moments beyond the first it is convenient to shift the origin to the mean energy $h\bar{\nu}=\langle h\nu\rangle$ and calculate the moments relative to the center of gravity of the spectrum:

$$\langle(h\nu-h\bar{\nu})^r\rangle=(-ihd/dt)^r\exp[f(t)-f'(0)t]|_{t=0}. \quad (8.14)$$

The most important absorption moments are then given by

$$\begin{aligned}\langle(h\nu)^0\rangle&=\exp[f(0)]=1\\ \langle h\nu\rangle&=h\bar{\nu}=h\nu_0-ihf'(0)\\ \langle(h\nu-h\bar{\nu})^2\rangle&=-h^2f''(0)\\ \langle(h\nu-h\bar{\nu})^3\rangle&=ih^3f'''(0)\\ \langle(h\nu-h\bar{\nu})^4\rangle&=3[h^2f''(0)]^2+h^4f^{(4)}(0).\end{aligned} \quad (8.15)$$

The corresponding moments for emission are obtained by replacing $f(t)$ by $f^*(t)$. Making use of (8.12) the explicit forms of these moments for absorption (upper sign) and emission (lower sign) are given by

$$\begin{aligned}h\bar{\nu}&=h\nu_0\pm\langle C_j^2h\omega_j\rangle\\ \langle(h\nu-h\bar{\nu})^2\rangle&=\langle C_j^2(2\bar{n}_j+1)(h\omega_j)^2\rangle\\ \langle(h\nu-h\bar{\nu})^3\rangle&=\pm\langle C_j^2(h\omega_j)^3\rangle\\ \langle(h\nu-h\bar{\nu})^4\rangle&=3|\langle(h\nu-h\bar{\nu})^2\rangle|^2+\langle C_j^2(2\bar{n}_j+1)(h\omega_j)^4\rangle.\end{aligned} \quad (8.16)$$

The averages on the right-hand side of (8.16) are averages over the modes $j$ in the sense of (5.21).

In accord with the general arguments presented in Sec. IV, moments one and two of (8.16) are in agreement with the corresponding semiclassical results (6.5) and (6.8). The reason for the agreement to second order and no higher is that the semiclassical formula (7.3) replaces (8.9) by

$$\text{Av}[\exp(iN^{-\frac{1}{2}}A_jq_j(0)t/h)]\simeq\exp[-N^{-1}C_j^2(2\bar{n}_j+1)(\omega_j t)^2/2], \quad (8.17)$$

which agrees with (8.9) to terms of order $t^2$ but no higher. Using (8.17), the semiclassical expression for $G(t)$ is a Gaussian in $t$, and the corresponding spectrum $G(\nu)$ is a Gaussian in $\nu$. Thus the semiclassical result is strictly symmetric: the skewness (third moment) and all higher odd moments vanish.

On the other hand, the quantum-mechanical distribution possesses skewness (nonvanishing third moment). This skewness is positive for absorption and negative for emission, i.e., on absorption the high energy tail of the distribution is dominant. The physical origin of this skewness lies in the Stokes rule that it is easier to emit a phonon than to absorb one (in the ratio $(\bar{n}+1)/\bar{n}$). On absorption of light this permits the absorption of a higher energy photon. On emission of light, however, this requires the emission of a lower energy photon. This remark explains the signs in both the first and third moments of (8.16).

Since the fourth moment (kurtosis) of a Gaussian distribution is three times the square of the second moment, (8.16) indicates that the quantum-mechanical fourth moment always exceeds the semiclassical fourth moment. The relative importance of the skewness and kurtosis can be ascertained from the coefficient of skewness and the coefficient of excess:[16]

$$\gamma_1=\langle(h\nu-h\bar{\nu})^3\rangle/[\langle(h\nu-h\bar{\nu})^2\rangle]^{\frac{3}{2}}, \quad (8.18)$$
$$\gamma_2=\{\langle(h\nu-h\bar{\nu})^4\rangle/[\langle(h\nu-h\bar{\nu})^2\rangle]^2\}-3. \quad (8.19)$$

If $2\bar{n}_j+1$ and $C_j$ are replaced by mean values, the coefficients of skewness and excess are $[(2\bar{n}+1)C]^{-1}$ and $[(2\bar{n}+1)C^2]^{-1}$. Thus the semiclassical procedure will be valid at all temperatures if $C\gg1$, and will usually be valid above the Debye temperature where $\bar{n}>1$. If $h\bar{\nu}_a-h\bar{\nu}_e$ and the broadening are large compared to the Debye energy $k\theta$, then (8.16) indicates that $C\gg1$. Thus, the conditions for validity of the semiclassical procedure can be determined directly from the experimental data.

In any case the normalized quantum-mechanical spectral distribution can be obtained from

$$G(\nu)=h^{-1}\int_{-\infty}^{\infty}\exp[i2\pi(\nu_0-\nu)t+f(t)]dt. \quad (8.20)$$

## IX. COMPARISON WITH HUANG AND RHYS: OPTICAL MODES ONLY

In this section we shall make the specializing assumption that all modes have a single frequency $\omega_j=\omega$. Our results should then reduce to those of Huang and Rhys[9] who used this assumption from the start. Formula (8.12) reduces to

$$f(t)=S[i\sin\omega t-(2\bar{n}+1)(1-\cos\omega t)], \quad (9.1)$$
$$=-(2\bar{n}+1)S+z\cos(\omega t-\varphi),$$

where

$$\tan\varphi=i/(2\bar{n}+1);\quad z=2S[(\bar{n}+1)\bar{n}]^{\frac{1}{2}} \quad (9.2)$$

[16] H. Cramer, *Mathematical Methods of Statistics* (Princeton University Press, Princeton, 1946), Sec. 15.8.

and

$$S=\langle C_j^2\rangle=(2hM\omega^3)^{-1}\langle A_j^2\rangle. \tag{9.3}$$

The symbol $S$ has been chosen to agree with Huang's notation.

It is convenient to introduce into (8.20) a new variable,

$$y=(h\nu-h\nu_0)/h\omega, \tag{9.4}$$

equal to the (possibly fractional) number of phonons that must be emitted to conserve energy. Then (8.20) together with (9.1) takes the form

$$h\omega G(\nu)=\exp[-(2\bar{n}+1)S-iy\varphi]J(-y), \tag{9.5}$$

$$\exp(-iy\varphi)=[(\bar{n}+1)/\bar{n}]^{\frac{1}{2}y}, \tag{9.6}$$

$$J(y)=(2\pi)^{-1}\int_{-\infty}^{\infty}\exp[iyx+z\cos x]dx. \tag{9.7}$$

But $J(-y)=J(y)$ can be simplified by breaking the integral up into the region from $2\pi r$ to $2\pi(r+1)$ and summing over all integral $r$:

$$J(y)=[\sum_{r=-\infty}^{+\infty}\exp(i2\pi ry)]I_y(z), \tag{9.8}$$

$$=[\sum_{p=-\infty}^{+\infty}\delta(y-p)]I_y(z), \tag{9.9}$$

where

$$I_y(z)=(2\pi)^{-1}\int_0^{2\pi}\exp[iyx+z\cos x]dx \tag{9.10}$$

is simply the modified Bessel function of order $y$. Relation (9.9) through the Dirac delta-function $\delta(y-p)$ indicates that the variable $y$ can only take on the integral values $p$. In other words, the absorption spectrum is discrete because phonons can be produced only with the discrete energies $ph\omega$.

The emission spectrum in accord with (8.13) is obtained by using $f^*(t)$ in place of $f(t)$. This is equivalent to changing the sign of $\varphi$ in (9.2), hence of $y$ on the right-hand side of (9.6).

Our results can be summarized in terms of the integrated spectrum:

$$\int G(\nu)d(h\nu)=\sum_p\exp\{-(2\bar{n}+1)S \pm\tfrac{1}{2}p\ln[(\bar{n}+1)/\bar{n}]\}I_p(2S[(\bar{n}+1)\bar{n}]^{\frac{1}{2}}), \tag{9.11}$$

where the upper sign applies to absorption, the lower to emission, and each term in the sum represents the strength of the absorption or emission line at $h\nu=h\nu_0+ph\omega$. These results are in precise agreement with those of Huang and Rhys.[9]

Huang and Rhys find that agreement with $F$ center absorption will be produced only if $S$ is given the large value of 22. They also state that suitable tabulations of the modified Bessel functions do not exist and obtain the values of these functions by "laborious computation."

They also note that all the factors in $G(\nu)$ depend on the temperature through $\bar{n}$. But they find upon computation that the maximum of the $G(\nu)$ curve "occurs practically at the same value of $p(=22)$ for all the temperatures considered." This last result may be obtained rather easily with no computation, by specializing Eqs. (8.15) or (8.16) to the case $\omega_j=\omega$. Using $p=(h\nu-h\nu_0)/h\omega$, these equations can be written in the form

$$\begin{aligned}&\langle p\rangle=\bar{p}=\pm S,\\ &\langle(p-\bar{p})^2\rangle=(2\bar{n}+1)S,\\ &\langle(p-\bar{p})^3\rangle=\pm S,\\ &\langle(p-\bar{p})^4\rangle=3[(2\bar{n}+1)S]^2+(2\bar{n}+1)S.\end{aligned} \tag{9.12}$$

Thus, $\langle p\rangle=S=22$ at all temperatures. Furthermore, because of the large value of $S$, the coefficients of skewness and excess of Eqs. (8.18) and (8.19) are small.[17] Thus the spectrum can be adequately approximated by a Gaussian whose peak and width are given by (9.12), i.e., by the semiclassical spectrum. The discreteness of the spectrum indicated by (9.9) is in fact an idealization arising from the Huang-Rhys assumption $\omega_j=\omega$. (A discrete spectrum can be observed if the broadening is mainly produced by optical vibrations in a narrow optical band.)

## X. A CONCLUDING SUGGESTION

Most of the experimentally observed emission or absorption spectra are sufficiently close to Gaussian in form that they can be adequately fitted by any curve whose first few moments are correct. There are various ways of approximating a distribution in terms of its moments. One of the simplest, due to Edgeworth,[18] yields for the spectrum:

$$I(\nu)=\sigma^{-1}\,\mathrm{Av}(M_{ba}^2)\Big[\phi(x)-\frac{\gamma_1}{3!}\phi^{(3)}(x)+\frac{\gamma_2}{4!}\phi^{(4)}(x)+\frac{10\gamma_1^2}{6!}\phi^{(6)}(x)\cdots\Big], \tag{10.1}$$

where

$$\sigma^2=\langle(h\nu-h\bar{\nu})^2\rangle,$$

$$x=(h\nu-h\bar{\nu})/\sigma,$$

$$\phi(x)=(2\pi)^{-\frac{1}{2}}\exp(-\tfrac{1}{2}x^2),$$

where $\gamma_1$ and $\gamma_2$ are the coefficients of skewness and excess defined by (8.18) and (8.19). These coefficients can be readily calculated from the exact moments (4.3)–(4.7). The normal curve $\varphi(x)$ and its derivatives are available in tabulated form.

[17] There will, of course, be some skewness present because of nonlinear terms in $\Delta E$.

[18] Reference 8, Sec. 17.7.

# A Note on Rotational Line Strengths in Slightly Asymmetric Rotors*

DAVID R. LIDE, JR.†
*Mallinckrodt Chemical Laboratory, Harvard University, Cambridge, Massachussets*
(Received June 27, 1952)

Direction-cosine matrix elements for slightly asymmetric rotors are calculated by a second-order perturbation treatment around the limiting symmetric rotor. This permits evaluation of the line strengths which are involved in calculations of absorption intensities, Stark effects, and nuclear-quadrupole couplings in rotational spectra. Explicit formulas are derived for the first-order terms.

CROSS, Hainer, and King[1] have published a useful table of rotational line strengths for all asymmetric-rotor transitions of $J<13$. Unfortunately, this table includes entries only at $\kappa=0$, $\pm0.5$, and $\pm1$. For many transitions whose strengths change rapidly with asymmetry, interpolation for intermediate values of $\kappa$ is a rather uncertain process. This uncertainty is particularly noticeable in the calculation of Stark effects[2] and nuclear-quadrupole couplings[3] in microwave spectra, since these effects are quite sensitive to the line strengths between interacting levels. Exact calculations of asymmetric-rotor line strengths may be carried out by evaluating the elements of the transformation matrix which diagonalizes the asymmetric-rotor energy, as given by King, Hainer, and Cross[4] (Eq. 54). This process is rather tedious, however, particularly for transitions involving high-$J$ levels. If the Mathieu-equation approximation is valid for the levels involved, approximate wave functions, and hence line strengths, may be calculated by an extension of the procedure used by Golden[5] for the calculation of energies. In this paper a perturbation technique is developed which is convenient for calculating line strengths in slightly asymmetric rotors ($|\kappa|\gtrsim0.90$).

The Hamiltonian of a prolate symmetric rotor may be written[4]

$$H_0=[aP_a^2+c(P_b^2+P_c^2)]/\hbar^2.$$

The introduction of asymmetry may be considered as a perturbation $H'$ given by

$$H'=(b-c)P_b^2/\hbar^2=(a-c)\delta P_b^2/\hbar^2,$$

where $\delta=(b-c)/(a-c)$. The asymmetric-rotor Hamiltonian is then given by

$$H=H_0+H'=(aP_a^2+bP_b^2+cP_c^2)/\hbar^2.$$

If we identify $P_b$ with $P_x$ and $P_a$ with $P_z$ (type $I^r$ representation), the matrix elements of $H'$ in the usual symmetric rotor representation become

$$(H')_{J,K;\,J,K}=(a-c)\delta[J(J+1)-K^2]/2,$$

$$(H')_{J,K;\,J,K+2}=-(a-c)\delta[f(J,K+1)]^{\frac{1}{2}}/2.$$

The transformation of $H'$ to a basis of Wang functions, which are correct zeroth-order functions for the degenerate levels in the symmetric rotor, may be accomplished by using the results of King, Hainer, and Cross for the reduced energy matrix; i.e., $H'$ will factor into four submatrices whose elements may be obtained from Eqs. (35) through (38) of KHC. With the aid of these elements, conventional perturbation theory gives the wave function of any asymmetric-rotor level as a linear combination of Wang functions, all of which must come from the same submatrix. Each asymmetric-rotor level may be specified, in the KHC notation, by the quantities $J$, $K_{-1}$, $K_1$ (except that $K_{-1}$ will henceforth be abbreviated as $K$); or, alternatively, by $J$, $K$, $\gamma$, where $\gamma=0$ if $J+K+K_1$ is even and $\gamma=1$ if $J+K+K_1$ is odd. Omitting the $J$ and $\gamma$ labels we have, to second order,

$$\psi_K^{(2)}=[1-(\alpha^2+\beta^2)/2]S_K+\alpha S_{K-2}+\beta S_{K+2}+\mu S_{K-4}+\nu S_{K+4},$$

where

$$\alpha=\alpha(J,K,\gamma)=\frac{H'_{K,K-2}}{W_K-W_{K-2}}=\frac{D^{\frac{1}{2}}_{K,K-2}}{E_{K-2}-E_K}\sim\delta,$$

$$\beta=\beta(J,K,\gamma)=\frac{H'_{K,K+2}}{W_K-W_{K+2}}=\frac{D^{\frac{1}{2}}_{K+2,K}}{E_{K+2}-E_K}\sim\delta,$$

$$\mu=\frac{H'_{K-4,K-2}H'_{K-2,K}}{(W_K-W_{K-4})(W_K-W_{K-2})}\sim\delta^2,$$

$$\nu=\frac{H'_{K+4,K+2}H'_{K+2,K}}{(W_K-W_{K+4})(W_K-W_{K+2})}\sim\delta^2.$$

Here $D_{K,K-2}$ is an element of the appropriate submatrix in KHC, Eqs. (37) and (38), and $E_K$ is the reduced energy $E_\tau^J(\kappa)$, to first order, of the level $J$, $K$, $\gamma$. The

* The research reported in this paper was made possible by support extended Harvard University by the Office of Naval Research under ONR Contract N5ori-76, Task Order V.
† Standard Oil of California Predoctoral Fellow.
[1] Cross, Hainer, and King, J. Chem. Phys. **12**, 210 (1944) (hereafter authors referred to as CHK).
[2] S. Golden and E. B. Wilson, Jr., J. Chem. Phys. **16**, 669 (1948).
[3] J. K. Bragg, Phys. Rev. **74**, 533 (1948).
[4] King, Hainer, and Cross, J. Chem. Phys. **11**, 27 (1943). The notation used here will follow this reference (hereafter authors referred to as KHC).
[5] S. Golden, J. Chem. Phys. **16**, 78 (1948).

functions $S_K=S(J, K, \gamma)$ are the Wang linear combinations of symmetric rotor functions.

In order to calculate asymmetric-rotor line strengths, the above expansion for $\psi^{(2)}$ must be substituted into the direction-cosine integral $\int\psi_{J\tau}{}^*\Phi_{Fg}\psi_{J'\tau'}dV$. For the case of perpendicular transitions ($\Delta K=\pm1$), the only nonvanishing integrals remaining are of the type

$$\int S(J, K, \gamma)^*\Phi_{Fg}S(J', K\pm1, \gamma')dV=(\Phi_{Fg}{}^0)_{J, K; J', K\pm1},$$

where $(\Phi_{Fg}{}^0)_{J, K; J', K\pm1}$ is the symmetric-rotor direction-cosine element as given in Table I of CHK. (Note, however, that the expression for $(\Phi_{Fg}{}^0)_{J, 0; J', 1}$ must be multiplied by $\sqrt{2}$.) If $\alpha$ and $\beta$ refer to the asymmetric-rotor level $J$, $K$, $K_1$ and $\alpha'$, $\beta'$ to the level $J'$, $K+1$, $K_1'$, we find

$$\begin{aligned}(\Phi_{Fg}{}^{(2)})_{J, K, K_1; J', K+1, K_1'}&=[1-(\alpha^2+\beta^2+\alpha'^2+\beta'^2)/2](\Phi_{Fg}{}^0)_{J, K; J', K+1}\\&\quad+\alpha'(\Phi_{Fg}{}^0)_{J, K; J', K-1}+\beta(\Phi_{Fg}{}^0)_{J, K+2; J', K+1}\\&\quad+\alpha\alpha'(\Phi_{Fg}{}^0)_{J, K-2; J', K-1}+\beta\beta'(\Phi_{Fg}{}^0)_{J, K+2; J', K+3}.\end{aligned}$$

For parallel transitions the first-order perturbation vanishes, and we have

$$\begin{aligned}(\Phi_{Fg}{}^{(2)})_{J, K, K_1; J', K, K_1'}&=[1-(\alpha^2+\beta^2+\alpha'^2+\beta'^2)/2](\Phi_{Fg}{}^0)_{J, K; J', K'}\\&\quad+\alpha\alpha'(\Phi_{Fg}{}^0)_{J, K-2; J', K-2}+\beta\beta'(\Phi_{Fg}{}^0)_{J, K+2; J', K+2}.\end{aligned}$$

In order to calculate the direction-cosine elements to second order, therefore, it is only necessary to evaluate an $\alpha$ and $\beta$ for each level of the transition. Explicit formulas for $\alpha$ and $\beta$ for the various possible cases are given in Table I. The $(\Phi_{Fg}{}^0)$ elements are repeated for convenience in Table II. The line strength $\lambda$, which is the quantity tabulated in the appendix of CHK, is defined by

$$\lambda_{J, \tau; J'\tau'}=\sum_{F, M, M'}|\Phi_{Fg}|^2{}_{J, \tau, M; J', \tau', M'}.$$

This may be calculated immediately, since the remaining direction-cosine factors are invariant to the transformation to an asymmetric-rotor basis. It is found that

$$\lambda^{(2)}=A\,|\Phi_{Fg}{}^{(2)}|^2{}_{J, K, K_1; J', K', K_1'},$$

where $A$ has the value $1/4(J+1)$, $(2J+1)/4J(J+1)$, or $1/4J$ for $J'=J+1$, $J$, or $J-1$, respectively. The product of $\lambda$ with the Boltzmann factor and any nuclear-spin weights provides a relative measure of the intensity of a spectral line.

When a definite selection rule is specified and the above formulas are expressed explicitly in terms of $J$ and $K$, a certain amount of algebraic simplification is possible in the first-order term. For dipole moment parallel to the axis of intermediate moment of inertia ($g=b=x$), or to the axis of greatest moment of inertia ($g=c=y$), the line strength of the transition $J$, $K$, $K_1\rightarrow$ $J'$, $K+1$, $K_1'$ may be written $\lambda/\lambda^0=1+k\delta$, where $k$ is given in Table III. The symmetric-rotor line strength $\lambda^0$ may be read from the $\kappa=-1$ column of the CHK tables, or it may be calculated from the explicit formulas given here in Table IV. For dipole moment parallel to the axis of least moment of inertia, the first-order term vanishes, since $\Delta K=0$.

The above formulation has been developed in a near-prolate representation. Transitions in a near-oblate rotor are treated most conveniently by calculating the

TABLE I. Coefficients in the second-order expansion of asymmetric-rotor wave functions. $\gamma$ refers to the parity of $J+K+K_1$, and $f(J, n)=(J-n)(J-n+1)(J+n)(J+n+1)/4$.

| | $\alpha$ | $\beta$ |
|---|---|---|
| $K=0$ | 0 | $(2^{\frac{1}{2}}/8)f^{\frac{1}{2}}(J, 1)(\delta+\delta^2/2)$ |
| $K=1$, $\gamma=0$ | 0 | $(1/16)f^{\frac{1}{2}}(J, 2)\{\delta+[16\pm J(J+1)]\delta^2/32\}$ |
| $K=1$, $\gamma=1$ | 0 | ditto, lower sign |
| $K=2$, $\gamma=0$ | $-(2^{\frac{1}{2}}/8)f^{\frac{1}{2}}(J, 1)(\delta+\delta^2/2)$ | $(1/24)f^{\frac{1}{2}}(J, 3)(\delta+\delta^2/2)$ |
| $K=2$, $\gamma=1$ | 0 | ditto |
| $K=3$, $\gamma=0$ | $-(1/16)f^{\frac{1}{2}}(J, 2)\{\delta+[16\pm J(J+1)]\delta^2/32\}$ | $(1/32)f^{\frac{1}{2}}(J, 4)(\delta+\delta^2/2)$ |
| $K=3$, $\gamma=1$ | ditto, lower sign | ditto |
| $K>3$ | $-\dfrac{f^{\frac{1}{2}}(J, K-1)}{8(K-1)}(\delta+\delta^2/2)$ | $\dfrac{f^{\frac{1}{2}}(J, K+1)}{8(K+1)}(\delta+\delta^2/2)$ |

TABLE II. Values of direction-cosine elements in a symmetric-rotor representation. Line one applies to $K>0$; line two to all $K$.

| | $J'=J+1$ | $J'=J$ | $J'=J-1$ |
|---|---|---|---|
| $(\Phi_{Fy}{}^0)_{J, K; J', K\pm1}=\mp i(\Phi_{Fx}{}^0)_{J, K; J', K\pm1}$ | $\mp[(J\pm K+1)(J\pm K+2)]^{\frac{1}{2}}$ | $[(J\mp K)(J\pm K+1)]^{\frac{1}{2}}$ | $\mp[(J\mp K)(J\mp K-1)]^{\frac{1}{2}}$ |
| $(\Phi_{Fz}{}^0)_{J, K; J', K}$ | $2[(J+K+1)(J-K+1)]^{\frac{1}{2}}$ | $2K$ | $-2[J^2-K^2]^{\frac{1}{2}}$ |
| $(\Phi_{Fy}{}^0)_{J, 0; J', 1}=-i(\Phi_{Fx}{}^0)_{J, 0; J', 1}$ | $-[2(J+1)(J+2)]^{\frac{1}{2}}$ | $[2J(J+1)]^{\frac{1}{2}}$ | $-[2J(J-1)]^{\frac{1}{2}}$ |

TABLE III. Value of $k$ in $\lambda/\lambda^0=1+k\delta$ for the transition $J, K, K_1 \rightarrow J', K+1, K_1'$ (near-prolate case). The upper sign refers to dipole moment in $b$ axis; the lower sign to dipole moment in $c$ axis. $\gamma$ is the parity of $J+K+K_1$.

| | $J'=J+1$ | $J'=J$ | $J'=J-1$ |
|---|---|---|---|
| $K=0$ | $\pm J(J-1)/8$ | $\mp(J-1)(J+2)/8$ | $\pm(J+1)(J+2)/8$ |
| $K=1, \gamma=0$ | $\pm(J-1)(J-2)/16$ | $\pm 3(J^2+J+2)/16$ | $\pm(J+2)(J+3)/16$ |
| $K=1, \gamma=1$ | $\mp(3J^2+7J-2)/16$ | $\mp(J-2)(J+3)/16$ | $\mp(3J^2-J-6)/16$ |
| $K\geqq 2$ | $\pm\frac{1}{8}\left[3-\frac{(J+1)(2K+J+2)}{K(K+1)}\right]$ | $\pm\frac{1}{8}\left[3+\frac{J(J+1)}{K(K+1)}\right]$ | $\pm\frac{1}{8}\left[3+\frac{J(2K-J+1)}{K(K+1)}\right]$ |

TABLE IV. Symmetric-rotor line strengths. Line one applies to $K>0$; line two to all $K$. The statistical-weight factor of two which enters the intensity formula in an exact symmetric rotor for levels of $K\neq 0$ is not included in this table.

| | $J'=J+1$ | $J'=J$ | $J'=J-1$ |
|---|---|---|---|
| $\lambda^0_{J,K;\,J',K+1}$ | $\frac{(J+K+2)(J+K+1)}{4(J+1)}$ | $\frac{(2J+1)(J+K+1)(J-K)}{4J(J+1)}$ | $\frac{(J-K-1)(J-K)}{4J}$ |
| $\lambda^0_{J,K;\,J',K}$ | $\frac{(J+K+1)(J-K+1)}{J+1}$ | $\frac{K^2(2J+1)}{J(J+1)}$ | $\frac{J^2-K^2}{J}$ |
| $\lambda^0_{J,0;\,J',1}$ | $(J+2)/2$ | $(2J+1)/2$ | $(J-1)/2$ |

strength of the "inverse" transition, as defined in Sec. VI of CHK, for the corresponding near-prolate rotor. This requires that $\delta$ be replaced by $1-\delta$.

An estimate of the accuracy of this treatment may be obtained by calculating $\lambda$ at $\delta=0.25(\kappa=-0.5)$ and comparing with the tabulated value at this point. For transitions which are permitted at both the prolate and oblate limits, the first-order formula is generally good to at least 10 percent at $\delta=0.25$, while including second-order terms brings the agreement to 1 percent or better. Even for transitions which have dropped to essentially zero strength by $\delta=0.25$ (such as the ${}^bR_{\bar{1}3}$ branch), the trend of the numbers indicates that the second-order expression should be off by no more than 20 percent at $\delta=0.10$ (for $J<12$); at greater asymmetries a perturbation treatment is obviously meaningless. While the procedure must be used with care, it should prove adequate for present experimental data when applied to the majority of transitions in molecules of $|\kappa|>0.90$; in some cases it is useful for even greater asymmetries.

The author is indebted to Professor E. Bright Wilson, Jr., for the suggestion of this problem.

# Reactions of Free Radicals with Aldehydes. The Reactions of Methyl and *t*-Butoxy Radicals with Acetaldehyde and Acrolein

DAVID H. VOLMAN AND ROBERT K. BRINTON
*Department of Chemistry, University of California, Davis, California*

(Received May 29, 1952)

The reaction in the gas phase of radicals derived from the thermal decomposition of *di-t*-butyl peroxide with acetaldehyde and acrolein has been studied. The activation energy for H atom abstraction from acetaldehyde by methyl was found to be 7.5±0.3 kcal/mole. The steric factor was about $3.7\times10^{-3}$, in agreement with many similar reactions. Evidence for chain ending steps other than the recombination of methyl radicals is given. Acrolein polymerizes as well as decomposes in the presence of radicals. The polymerization follows the kinetics to be expected from chain propagation by radical-monomer interaction and chain termination by radical combination. Evidence that the decomposition may be the splitting off of carbon monoxide from the polymerizing chain is presented.

## INTRODUCTION

STUDIES on the thermal[1] and photochemical[2] decomposition of mixtures of azomethane and acetaldehyde and on the thermal decomposition of *di-t*-butyl peroxide-acetaldehyde mixtures[3,4] have shown that the gas phase decomposition of acetaldehyde may be induced at temperatures far below the ordinary thermal decomposition temperature. Similarly the decomposition of acrolein has been induced by radicals derived from the thermal decomposition of ethylene oxide.[5]

Using *di-t*-butyl peroxide as a radical source as in our previous work,[6,7] we have been able to obtain additional quantitative and qualitative information bearing on the problem of aldehyde decomposition and polymerization. The decomposition of *di-t*-butyl peroxide yields *t*-butoxy radicals in the initial step,[8]

$$(CH_3)_3COOC(CH_3)_3 \rightarrow 2(CH_3)_3CO. \quad (1)$$

*T*-butoxy radical may react in a bimolecular step or may decompose unimolecularly:

$$(CH_3)_3CO \rightarrow CH_3+CH_3COCH_3. \quad (2)$$

Thus, both *t*-butoxy and methyl radicals are formed.

## EXPERIMENTAL METHOD

The experimental procedure was similar to that described previously.[6] Measured pressures of aldehyde and peroxide were mixed in a one-liter flask at room temperature. The mixture was expanded into the one-liter reaction chamber immersed in an oil-bath thermostat. The reaction was terminated by expanding the reaction mixture into a receiver at room temperature. This aliquot sample was separated by use of a toepler pump into a volatile fraction, not condensable at −120°C, and a nonvolatile sample, the remainder. The volume of the volatile fraction was determined by a gas microburet. Analyses of both fractions were made by a Consolidated mass spectrometer. Reaction rates were taken as $\Delta c/\Delta t$ over the time interval of each experiment. The runs were stopped at small percentage completion so that $\Delta c/\Delta t$ closely approximated the initial reaction rates.

*Di-t*-butyl peroxide was kindly supplied by the Shell Development Company; it was further purified by bulb-to-bulb distillation. Acetaldehyde was prepared by the acid depolymerization of paraldehyde and purified by fractional distillation. Acrolein, a commercial product, was fractionally distilled.

### 1. Acetaldehyde

The results of the experiments with acetaldehyde are shown in Table I. The only decomposition products positively identified were methane, ethane, carbon monoxide, *t*-butyl alcohol, and acetone.

#### *Discussion*

The nature of the products and the generally accepted features of acetaldehyde decomposition leads to the following mechanism:

$$CH_3+CH_3CHO \rightarrow CH_4+CH_3CO, \quad (3)$$

$$(CH_3)_3CO+CH_3CHO \rightarrow (CH_3)_3COH+CH_3CO, \quad (4)$$

$$CH_3CO \rightarrow CH_3+CO, \quad (5)$$

$$CH_3+CH_3 \rightarrow C_2H_6, \quad (6)$$

$$CH_3+CH_3CO \rightarrow CH_3COCH_3. \quad (7)$$

If (3) and (6) are the only reactions producing methane and ethane, then

$$\frac{d[CH_4]/dt}{(d[C_2H_6]/dt)^{\frac{1}{2}}}=\frac{R_{CH_4}}{R_{C_2H_6}^{\frac{1}{2}}}=\frac{k_3}{k_6^{\frac{1}{2}}}[CH_3CHO] \quad (8)$$

[1] A. O. Allen and D. V. Sickman, J. Am. Chem. Soc. **6**, 2031 (1934).
[2] F. E. Blacet and A. Taurog, J. Am. Chem. Soc. **61**, 3024 (1939).
[3] Bayer, Niclause, and Letort. Compt. rend. **231**, 475 (1950).
[4] R. K. Brinton and D. H. Volman, J. Chem. Phys. **26**, 1053 1(952).
[5] C. J. M. Fletcher and G. K. Rollefson, J. Am. Chem. Soc. **58**, 2135 (1936).
[6] D. H. Volman, J. Chem. Phys. **19**, 668 (1951).
[7] R. K. Brinton and D. H. Volman, J. Chem. Phys. **20**, 25 (1952).
[8] Raley, Rust, and Vaughan, J. Am. Chem. Soc. **70**, 88 (1948).

TABLE I. Reaction of acetaldehyde with *di-t*-butyl peroxide.

| Temp. °C | Initial pressure, mm Peroxide | Aldehyde | Initial rates, moles cc$^{-1}$ sec$^{-1}$ ×10$^{10}$ CO | $CH_4$ | $C_2H_6$ | $CH_3COCH_3$ | $(CH_3)_3COH$ |
|---|---|---|---|---|---|---|---|
| 124.4 | 15.1 | 0 | 0 | 0.0051 | 0.0511 | 0.113 | 0 |
| 124.4 | 15.1 | 31.5 | 0.228 | 0.206 | 0.0402 | 0.0886 | 0.0388 |
| 124.4 | 15.1 | 89.8 | 0.630 | 0.595 | 0.0352 | 0.0713 | 0.0561 |
| 124.4 | 15.1 | 212.5 | 1.185 | 1.143 | 0.0235 | 0.055 | 0.059 |
| 134.1 | 15.1 | 0 | 0 | 0.0094 | 0.159 | 0.309 | 0 |
| 134.1 | 15.1 | 12.2 | 0.248 | 0.226 | 0.153 | 0.327 | 0.067 |
| 134.1 | 15.1 | 23.2 | 0.441 | 0.382 | 0.135 | 0.319 | 0.088 |
| 134.1 | 15.1 | 50.7 | 0.945 | 0.864 | 0.131 | 0.307 | 0.141 |
| 134.1 | 15.1 | 116.0 | 1.869 | 1.759 | 0.102 | 0.312 | 0.194 |
| 134.1 | 15.1 | 226.0 | 3.00 | 2.885 | 0.071 | 0.202 | 0.202 |
| 155.8 | 16.5 | 0 | 0 | 0.056 | 1.825 | 4.05 | 0 |
| 155.8 | 16.5 | 33.8 | 3.29 | 2.94 | 1.62 | 3.29 | 0.656 |
| 155.8 | 16.5 | 79.0 | 6.76 | 6.17 | 1.34 | 3.52 | 1.12 |
| 155.8 | 16.5 | 206.5 | 14.44 | 13.32 | 0.98 | 2.34 | 1.25 |

for a steady state of methyl radicals. The plot of $R_{CH_4}/R_{C_2H_6}^{\frac{1}{2}}$ as a function of acetaldehyde concentration, Fig. 1, shows that this relationship holds very well over the entire range studied and that the proposed reactions must be the only ones yielding methane and ethane. The Arrhenius plot, Fig. 2, gives $E_3-\frac{1}{2}E_6=7.5\pm0.3$ kcal/mole. The use of Gomer and Kistiakowsky's value of $k_6=2.1\times10^{12}T^{\frac{1}{2}}$ (moles/cc)$^{-1}$ sec$^{-1}$ and $E_6=0$ for methyl radical combination[9] gives

$$k_3=4.2\times10^{10}T^{\frac{1}{2}}e^{-7.5/RT}\ (\text{moles/cc})^{-1}\ \text{sec}^{-1}.$$

Assignment of a collisional diameter of 3.7A for the reaction of methyl radical and acetaldehyde molecule, a value similar to that used by Gomer and Kistiakowsky for the analogous reaction with acetone, gives a steric factor for reaction (3) of about $3.7\times10^{-3}$. This is in good agreement with the steric factors of a large number of other hydrogen abstraction reactions reported by Trotman-Dickenson and Steacie.[10] It is interesting to note that these authors predicted a steric factor of about unity for the abstraction reaction in the case of acetaldehyde on the basis of rate data, the over-all photolysis activation energy of about 10 kcal/mole, and a photolysis mechanism entailing reactions (3), (5), and (6). However, the lower experimentally determined activation energy gives a steric factor for this reaction in line with other hydrogen abstraction reactions.

Recently it has been shown that a relationship analogous to (8) holds for the rates of formation of methane and ethane in the high temperature photolysis of acetaldehyde.[11] It seems evident that the same chain generating and chain ending steps are taking place in both the high temperature photolysis and the induced decomposition. Leermakers,[12] Akeroyd and Norrish,[13] and Grahame and Rollefson[14] have determined the activation energy for the over-all photodecomposition of acetaldehyde at elevated temperatures. This energy should in each case be a minimum value for $E_3$. Leermakers reports 10 kcal, Akeroyd and Norrish 9.8, and Grahame and Rollefson $8.3\pm0.5$. Considering the inherent difficulties in precise quantum yield determinations and the necessary assumption of a temperature independent primary quantum yield of radical formation, we believe the latter value is in reasonable agreement with the value reported in this study.

The mechanism given by Grahame and Rollefson corresponds to the one we have given with the exception that our Eq. (7) assumes a chain breaking step involving acetyl radical. It is obvious that at temperatures lower than those used by Grahame and Rollefson, chain breaking steps involving acetyl radical might become important. Under these conditions the activation energy for acetyl decomposition (5) would contribute to the over-all activation energy. For example, Blacet and

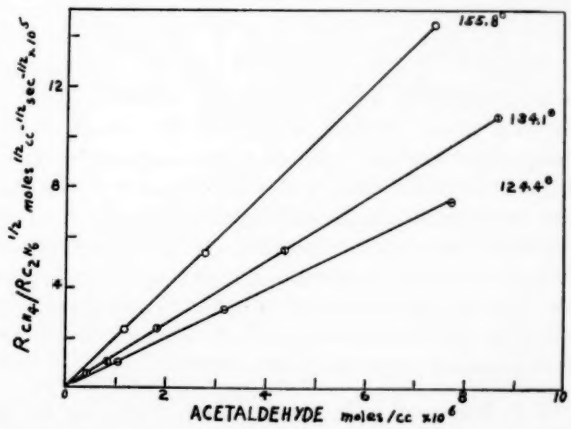


FIG. 1. Ratio of rate of methane production to square root of rate of ethane production *vs* acetaldehyde concentration at various temperatures.

[9] R. Gomer and G. B. Kistiakowsky, J. Chem. Phys. **19**, 85 (1951).
[10] A. F. Trotman-Dickenson and E. W. R. Steacie, J. Chem. Phys. **19**, 329 (1951).
[11] Danby, Buchanan, and Henderson, J. Chem. Soc. **1951**, 1426.
[12] J. A. Leermakers, J. Am. Chem. Soc. **56**, 1537 (1934).
[13] E. I. Akeroyd and R. G. W. Norrish, J. Chem. Soc. **1936**, 890.
[14] D. C. Grahame and G. K. Rollefson, J. Chem. Phys. **8**, 98 (1940).

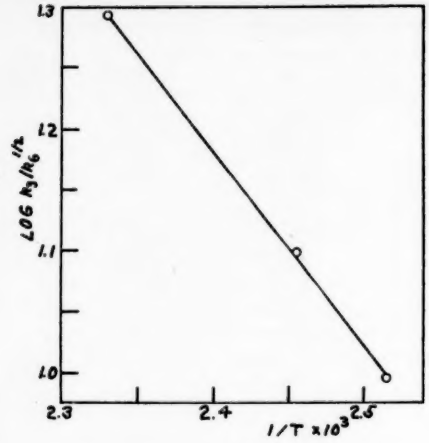


FIG. 2. Effect of temperature on the rate constant ratio $k_3/k_6$.

Loeffler[15] attribute all of the over-all activation of 9.6 kcal found for the photochemical reaction in the temperature range 100–150° to $E_5$. Since $E_5$ is probably in the range 13–16 kcal per mole,[16,17] it is possible that the value of Blacet and Loeffler is between $E_3$ and $E_5$ and cannot be attributed to either exclusively. Blacet and Blaedel[18] have found considerable biacetyl in the reaction products at low temperatures. Since the radical combinations at high temperatures appear to be solely methyl plus methyl, it is evident that in an intermediate range methyl plus acetyl [Eq. (7)] should occur.

Some experimental evidence for reaction (7) was obtained in this study. Acetone may be formed either by (7) or by (2). If (2) is the only reaction leading to acetone formation, the usual treatment gives

$$\frac{R_{(CH_3)_3COH}}{R_{CH_3COCH_3}} = \frac{k_4}{k_2}[CH_3CHO]. \quad (9)$$

A plot of $R_{(CH_3)_3COH}/R_{CH_3COCH_3}$ as a function of acetaldehyde concentration under these conditions should yield a straight line. Formation of acetone by radical combination (7) would cause this plot to curve towards the concentration axis. The higher concentrations of aldehyde favor acetone formation by (7) since the steady-state concentration of acetyl radicals increases with acetaldehyde concentrations. Figure 3 shows that these conditions are, indeed, fulfilled. Also if the only chain breaking step were reaction (6), the rate of ethane production should be independent of acetaldehyde pressure. The steady falling off of ethane production with increasing aldehyde pressure, Table I, shows that other chain breaking steps must be operating.

[15] F. E. Blacet and D. E. Loeffler, J. Am. Chem. Soc. **64**, 893 (1942).
[16] D. H. Volman and W. M. Graven, J. Chem. Phys. **26**, 000 (1952).
[17] F. B. Marcotte and W. A. Noyes, Jr., J. Am. Chem. Soc. **74**, 783 (1952).
[18] F. E. Blacet and W. J. Blaedel, J. Am. Chem. Soc. **62**, 3374 (1940).

## 2. Acrolein

The original objective in the investigation of acrolein-peroxide mixtures was to compare the induced polymerization of acrolein to the butadiene polymerization previously reported.[6] However, the appreciable quantities of carbon monoxide produced in the initial experiments indicated that the interaction of radicals with acrolein induced both decomposition and polymerization, and both aspects must be considered.

### *Experimental Results and Discussion*

The analytical results obtained with acrolein are shown in Table II and Figs. 4 and 5. The only products positively identified are shown in Table II.

In accordance with the mechanism of induced acetaldehyde decomposition, methane and *t*-butyl alcohol are formed by abstraction of a hydrogen atom,

$$CH_3+CH_2=CHCHO \rightarrow CH_4+CH_2CHCO, \quad (10)$$

$$(CH_3)_3CO+CH_2=CHCHO \rightarrow (CH_3)_3COH+CH_2CHCO. \quad (11)$$

If CO were then formed by a mechanism analogous to reaction (5) for acetaldehyde,

$$CH_2CHCO \rightarrow CH_2=CH+CO, \quad (12)$$

followed by

$$CH_2=CH+CH_2=CHCHO \rightarrow CH_2=CH_2+CH_2CHCO \quad (13)$$

to give a chain decomposition yielding carbon monoxide, the carbon monoxide yield should equal the sum of methane, *t*-butyl alcohol, and ethylene. For acetaldehyde, the sum of methane and *t*-butyl alcohol yield is actually about equal to the carbon monoxide yield. For acrolein, however, the methane plus *t*-butyl alcohol is far less than the amount of carbon monoxide and no ethylene was formed. Although experimentally it would be difficult to detect small amounts of ethylene, Eqs. (12) and (13) and the large amounts of carbon monoxide relative to methane plus alcohol would lead to appreciable amounts of ethylene. These considerations

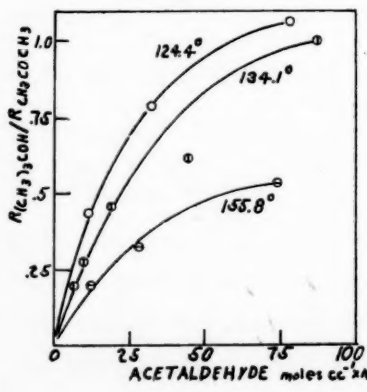


FIG. 3. Ratio of rate of *t*-butyl alcohol production to rate of acetone production *vs* acetaldehyde concentration at various temperatures.

TABLE II. Reaction of acrolein with *di-t*-butyl peroxide.

| Temp. °C | Initial pressure, mm | | Initial rates, moles $cc^{-1}$ $sec^{-1}$ $\times 10^{10}$ | | | | |
|---|---|---|---|---|---|---|---|
| | Peroxide | Aldehyde | CO | $CH_4$ | $C_2H_6$ | $(CH_3)_2CO$ | $(CH_3)_3COH$ |
| 134.1 | 14.5 | 0 | 0 | 0.0048 | 0.127 | 0.249 | 0.00 |
| 134.1 | 14.5 | 13.9 | 0.115 | 0.019 | 0.0020 | 0.244 | 0.035 |
| 134.1 | 14.5 | 37.7 | 0.231 | 0.012 | 0.000 | 0.226 | 0.067 |
| 134.1 | 14.5 | 101.3 | 0.378 | 0.0087 | 0.000 | 0.173 | 0.113 |
| 168.7 | 14.5 | 0 | 0 | 0.113 | 5.45 | 12.0 | 0.00 |
| 168.7 | 14.5 | 21.1 | 2.40 | 0.705 | 0.275 | 13.1 | 1.58 |
| 168.7 | 14.5 | 44.5 | 4.73 | 0.730 | 0.100 | 12.1 | 1.82 |
| 168.7 | 14.5 | 67.5 | 6.27 | 0.697 | 0.052 | 11.8 | 2.00 |
| 168.7 | 14.5 | 113.5 | 8.38 | 0.492 | 0.013 | | |

make it unlikely that the carbon monoxide production is linked to a hydrogen atom abstraction mechanism.

The polymerization of acrolein is undoubtedly initiated by radical addition to acrolein,

$$R+CH_2=CHCHO \rightarrow RCH_2CHCHO. \qquad (14)$$

A radical such as formed in (14) might be expected to break down to give carbon monoxide by a mechanism analogous to (5). It may be observed that the acrylyl radical can resonate in the forms

$$H-C=C-C=O \quad \text{and} \quad H-C-C=C=O,$$

which would tend to render it stable. This mode of resonance is not available to the radical produced in (14), and its stability would be less for this reason. It is also possible that a formyl radical would result from a decomposition of this radical, but the absence of hydrogen in the reaction products makes this unlikely. The actual mechanism may be a concerted process involving the simultaneous shift of a hydrogen atom and elimination of carbon monoxide.

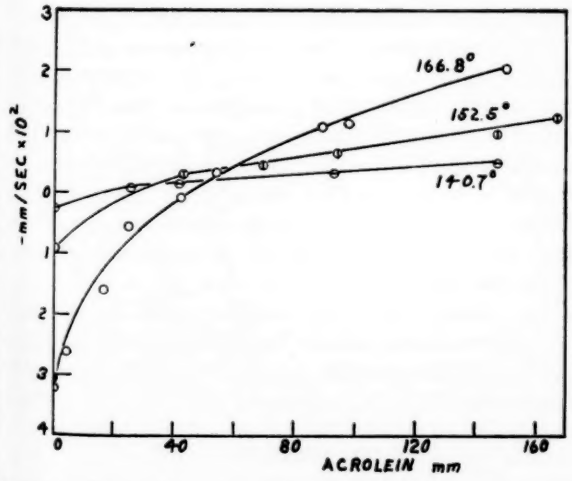


FIG. 4. Initial rate of pressure change *vs* initial acrolein pressure for an initial *di-t*-butyl peroxide pressure of 20.8 mm.

That radical induced polymerization follows the kinetics expected for formation of radicals by (1), initiation and propagation of the chain by (14), and termination by radical combination may be seen from Figs. 4 and 5. The ordinary steady-state considerations lead to the rate equation[6]

$$-d[M]/dt=k_p(k_i/k_t)^{\frac{1}{2}}[M][C]^{\frac{1}{2}}, \qquad (15)$$

where $M$ refers to monomeric acrolein, $C$ to the peroxide initiator, and $k_p$, $k_i$, $k_t$, to the rate constants for propagation, initiation, and termination. An Arrhenius plot of the slopes of Fig. 5 leads to an over-all activation energy of about 22 kcal/mole,

$$E=E_p+\tfrac{1}{2}E_i-\tfrac{1}{2}E_t\cong 22.$$

This compares well with the value found for the polymerization of butadiene initiated by *di-t*-butyl peroxide.[6] Since $E_t$ is probably about zero, the value of $E_p$ must be about the same as for butadiene. Using our recently determined value of $E_i=36.0$ kcal/mole[7], the value of $E_p\cong 4$ kcal is found.

The data of Table II indicate that *t*-butoxy radical does not add to acrolein, nor does it enter into chain ending steps. The approximate constancy in the alcohol plus acetone yields show that all of the *t*-butoxy radicals formed lead to acetone or *t*-butyl alcohol. Since the yield of methyl radicals must be about equivalent to the yield of acetone, the small amounts of methane formed show

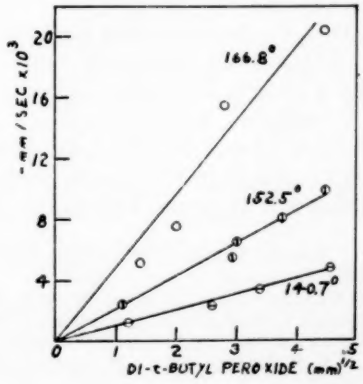


FIG. 5. Initial polymerization rate *vs* square root of the initial *di-t*-butyl peroxide pressure for an initial acrolein pressure of 148 mm.

that methyl addition to acrolein occurs much more readily than hydrogen atom abstraction. This is contrary to the reactions of *t*-butoxy radical since *t*-butyl alcohol seems to be readily formed and no addition occurs.

We wish to express our appreciation to the Research Corporation for financial aid and to Dr. Amos Newton of the Radiation Laboratory of the University of California for assistance with the mass spectrometric analyses.

---

THE JOURNAL OF CHEMICAL PHYSICS VOLUME 20, NUMBER 11 NOVEMBER, 1952

# The Infrared and Raman Spectra of $CF_3OF$†

R. T. LAGEMANN,* E. A. JONES,* AND P. J. H. WOLTZ
*K-25 Laboratories, Carbide and Carbon Chemicals Division, Union Carbide and Carbon Corporation, Oak Ridge, Tennessee*
(Received June 25, 1952)

The infrared spectrum has been obtained for gaseous $CF_3OF$ from 2 to 25$\mu$. The Raman shifts have been measured for the liquid. Nine of the twelve fundamental vibration frequencies have been assigned and an interpretation made of the observed spectra on the basis that $CF_3OF$ belongs to point group $C_s$.

THIS report gives the results of a vibrational analysis of the infrared and Raman spectra of the fluorocarbon derivative fluoroxymethforane $CF_3OF$, for which no previous studies of the vibrational spectra exist. This molecule is not only of interest because of the recent studies on the structures of fluorine containing molecules but also because it is an analog of methyl alcohol on whose spectra and their analysis considerable effort has been expended.

## EXPERIMENTAL

The sample of $CF_3OF$ was prepared in this laboratory. Carbon monoxide and fluorine at atmospheric pressure were passed simultaneously over silver fluoride to form $F_2CO$. The $F_2CO$ was then further fluorinated in the presence of $AgF_2$ to form the $CF_3OF$. Various flow rates were tried. The method is not the same as that described by Kellogg and Cady,[1] the only others to report the preparation of $CF_3OF$, but they do mention this procedure. $CF_4$, $F_2CO$, and HF were present as impurities, as could be noted from the spectrum. $F_2CO$ was present to the extent of about 5 inches Hg per atmosphere pressure of the sample studied. A good knowledge of the spectra of these impurities exists, so that for the most part it was possible to eliminate bands due to them from the spectra.

The infrared absorption spectrum of $CF_3OF$ in the gas state was investigated over the range from 2 to 25$\mu$ by means of two Perkin-Elmer prism spectrometers. A double-beam Model 21 was used for the NaCl region. The region from 15–25$\mu$ was studied with a Model 12-C using a KBr prism. The entire spectrum was recorded at a pressure of 24 inches Hg, and regions of strong and weak absorption at lower and higher pressures, respectively. The cell length was 10 cm.

When using NaCl and KBr windows on the cell, there was noted the formation of "window bands," mostly in the region 2–10$\mu$, presumably due to the reaction of the gas with the window material. This absorption persisted when the cell was evacuated. It was possible, nevertheless, to observe in these regions by using $CaF_2$ windows. Also, the presence of such bands could be determined by noting that they remained constant in intensity (allowing time for them to form) as the gas pressure was varied.

The Raman spectrum of the liquid was photographed by means of a Lane-Wells spectrograph. The standard Lane-Wells mercury arc excitation unit was used. Appropriate filters were used to eliminate the background and excitation from mercury lines other than from the desired parent line. The Raman shift at 250 $cm^{-1}$ was found using 5460A as the parent; all others were found as shifts from 4358A.

The liquid sample, which boils at about minus 94°C, was contained in a glass Raman tube about one-half inch in diameter inserted in a Dewar. The Dewar was equipped with a plane window to permit exit of the Raman light and was so made that liquid filters could be poured in to surround the sample. The sample was maintained in the liquid state by a stream of cold, dried nitrogen that had passed through coils placed in liquid nitrogen.

The Raman spectrum was recorded on Eastman Tri-X Panchromatic film. A slit width of 150 microns was used with exposures varied from $\frac{1}{2}$ to 3 hours. No polarization data were secured.

## RESULTS

The infrared absorption spectrum of gaseous $CF_3OF$ between 2 and 25$\mu$ is shown in Fig. 1, which gives per-

---

* Now at Physics Department, Vanderbilt University, Nashville, Tennessee.

† This document is based on work performed for the Atomic Energy Commission by Carbide and Carbon Chemicals Division, Union Carbide and Carbon Corporation at Oak Ridge, Tennessee.

[1] K. B. Kellogg and G. H. Cady, J. Am. Chem. Soc. **70**, 3986 (1948).

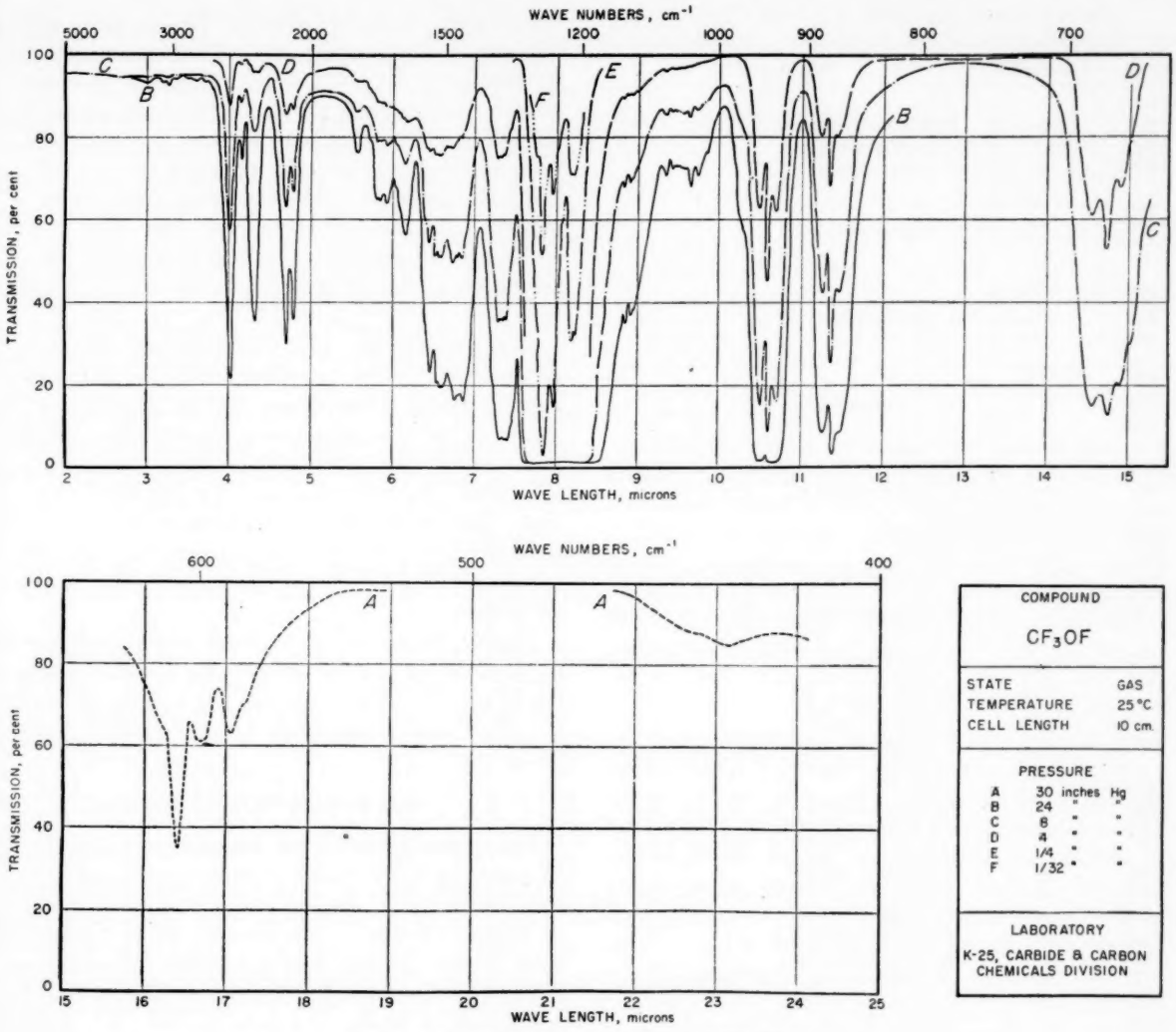


FIG. 1. Infrared absorption spectrum of $CF_3OF$ gas.

cent transmission curves for a variety of pressures. The measured frequencies are listed in the first column of Table I, and, in the second column, the relative intensities are indicated by means of the following abbreviations: *vs* very strong, *s* strong, *m* medium, *w* weak, etc.

Bands found at 3788 and 4032 $cm^{-1}$, believed due to HF, and at 631, 650, 2179, and 2545 $cm^{-1}$, thought caused by $CF_4$, and at 774, 1927, and 1953 $cm^{-1}$ from $F_2CO$ are not included in Fig. 1. It was impossible, however, to subtract the absorption due to $F_2CO$ at 583, 960, and 1235 $cm^{-1}$ and that due to $CF_4$ at 1282 $cm^{-1}$ so that, at least at high pressures, part of the intensity at these points in the spectrum must be enhanced by the impurities. The band at 432 $cm^{-1}$ cannot be confused with the 437 one of $CF_4$, which is infrared inactive. The band at 586 $cm^{-1}$ is believed, after a careful examination of intensities, making use of a sample of pure $F_2CO$ available, to be real and attributable in part to $CF_3OF$. The absorption peak at 1282 $cm^{-1}$ is believed caused in part by $CF_4$ (we consistently find it near 1280 rather than at 1265 $cm^{-1}$).[2]

The Raman results are listed in Table II. Except for the 250 $cm^{-1}$ shift, all have been noted on more than one exposure.

## INTERPRETATION

The fact that the $F_2O$ molecule is bent suggests that the C—O—F chain in $CF_3OF$ is bent also. The remainder of the molecule is no doubt of a tetrahedral nature, the whole resembling methyl alcohol. If the F atom of the OF group is located in one of the planes of symmetry of the $CF_3$ group, as one might expect, the molecule would have just one plane of symmetry, the C—O—F plane, and belong to point group $C_s$. Accordingly, there would be eight vibrations symmetric with respect to this plane and four antisymmetric.

If the C—O—F unit were linear, four doubly degenerate vibrations would result, with the components of each coincident, in addition to four nondegenerate ones. If the molecule were strongly asymmetric, twelve

[2] E. L. Pace, J. Chem. Phys. **16**, 74 (1950).

TABLE I. Infrared spectrum of gaseous $CF_3OF$.

| Frequency ($cm^{-1}$) | Description | Interpretation |
|---|---|---|
| 432 | *w* | $A''$ fundamental |
| 586 | *w* | $A''$ fundamental |
| 609 | *m* | $A'$ fundamental |
| 670 | | |
| 679 | *s* | $A'$ fundamental |
| 687 | | |
| 872 | | |
| 880 | *s* | $A'$ fundamental |
| 889 | | |
| 936 | | |
| 945 | *s* | $A'$ fundamental |
| 954 | | |
| 1028 | *w* | $432+586=1018A'$ |
| 1037 | *w* | $432+609=1041A''$ |
| 1044 | *vvw* | |
| 1064 | *vw* | |
| 1071 | *vw* | |
| 1117 | *vw* | $432+679=1111A''$ |
| 1125 | *vw* | |
| 1133 | *vw* | $(250)+880=1130A'$ |
| 1217 | *vs* | $A'$ fundamental |
| 1223 | *vs* | |
| 1259 | *vs* | $A'$ fundamental |
| 1282 | *vs* | $A''$ fundamental |
| 1355 | *s* | |
| 1362 | *s* | $2(679)=1358A'$ |
| 1374 | *s* | $432+945=1377A''$ |
| 1462 | *m* | $586+880=1466A''$ |
| 1475 | *m* | $(250)+1220=1470A'$ |
| 1488 | *m* | $609+880=1489A'$ |
| 1522 | *w* | $(250)+1259=1509A'$ |
| 1536 | *w* | $586+945=1531A''$ |
| 1553 | *w* | $609+945=1554A'$; $679+880=1559A'$ |
| 1629 | *w* | $679+945=1624A'$ |
| 1688 | *w* | $432+1259=1691A''$ |
| 1712 | *vw* | $432+1282=1714A'$ |
| 1724 | *vw* | |
| 1799 | *w* | $586+1220=1806A''$ |
| 2092 | *m* | $880+1220=2100A'$ |
| 2137 | *m* | $880+1259=2139A'$ |
| 2326 | *m* | $CO_2$ impurity? |
| 2415 | *w* | $2(1220)=2440A'$ |
| 2500 | *m* | $1220+1282=2502A''$; $2(1259)=2518A'$ |
| 3067 | *vw* | |
| 3155 | *vw* | |
| 3401 | *vw* | |

nondegenerate vibrations would appear in the spectrum, and we have interpreted the spectrum on the basis that $CF_3OF$ belongs to the point group $C_s$. If the molecule is only slightly asymmetric, the splitting should be small, if detectable, for the internal vibrations of the $CF_3$ group. For the deformation vibrations of the $(F_3)-C-O-F$ chain, on the other hand, considerable splitting might occur.

It is convenient to consider the $CF_3OF$ molecule, so far as certain of its vibrations are concerned, as essentially a five-atom system, assuming the OF group as one particle. The use of such a scheme introduces the assumption that the asymmetry caused by the position of the hypofluorite fluorine atom will have but small effect upon the vibrations which belong essentially to the trifluoromethyl and trifluoromethoxy groups. In this case, six of the expected vibrations for $CF_3OF$ would be similar to those of the methyl halides, keeping in mind that the presence of the OF group splits the three twofold degenerate frequencies of the methyl halide model. One can then note the three additional vibrations which are introduced by a consideration of the OF group so as to arrive at the total expected.

Considering first the vibrations of the five-atom approximate model, one would expect to find six fundamental modes, three being doubly degenerate. There would be three nondegenerate bands corresponding to the symmetrical $CF_3$ deformation, the symmetrical $CF_3$ stretching vibration, and the CO stretching vibration. The three doubly degenerate bands would be associated with the $CF_3$ unsymmetrical stretching, the unsymmetrical $CF_3$ deformation, and the $CF_3$ rocking vibrations.

Finally, there would be three vibrations associated primarily with the OF group. One of these would consist of an OF valence stretch, one a deformation of the C—O—F angle, and lastly a torsion oscillation of the OF group.

## THE FUNDAMENTAL MODES

Upon examination of the infrared spectrum, one notes at once the three strong parallel type bands, showing well resolved *P*, *Q*, and *R* branches. Two of these, those at 880 and 945 $cm^{-1}$, coincide with the two most intense lines of the Raman spectrum. The infrared band at 679 $cm^{-1}$ is found in the Raman at 676 $cm^{-1}$, although not strong or sharp. The band at 880 $cm^{-1}$ is assigned to the CO stretch. Generally, the CO stretch is found at higher frequencies, but support for this assignment is noted in methyl alcohol where the characteristic CO frequency changes from 1034 $cm^{-1}$ in the ordinary molecule to 989 $cm^{-1}$ in the completely deuterated one.[3] The substitution of the heavier fluorine atoms ought to lower the CO frequency still further. The band at 945 $cm^{-1}$ should be associated with the OF stretch, which in $F_2O$[4] is found at 928 $cm^{-1}$. These assignments and the others to follow are found in Table II.

Comparison with the methyl halides is very helpful in making the assignments of the $CF_3$ unsymmetrical deformation modes. They and the symmetrical deformation should be of about equal value and should be roughly half the CF stretching frequencies. They should also be weaker than most of the fundamentals and the unsymmetrical deformation should be the lowest of those associated primarily with the perfluoromethyl group. We therefore assign 609 and 586 $cm^{-1}$ to the unsymmetrical deformation modes of species $A'$ and $A''$,

[3] H. Noether, J. Chem. Phys. **10**, 693 (1942).
[4] Jones, Kirby-Smith, Woltz, and Nielsen, J. Chem. Phys. **19**, 337 (1951).

respectively. The symmetrical $CF_3$ deformation of species $A'$ should be found near the unsymmetrical deformation, and to it is assigned the band at 679 $cm^{-1}$. In $CF_3H$[5] the unsymmetrical and symmetrical $CF_3$ deformations are found at 508 and 697 $cm^{-1}$.

The high intensity of the 1259 $cm^{-1}$ band in the infrared and its absence in the Raman indicate that it must be associated with CF stretching. Probably it is an unsymmetrical $CF_3$ stretching of species $A'$. The strong infrared band at 1282 $cm^{-1}$ is probably the corresponding $A''$ vibration. The band at 1220 $cm^{-1}$ is best assigned as essentially a symmetrical $CF_3$ stretching of species $A'$. Evidence for these three assignments is seen in the fact that the valence vibrations of the $CF_3$ group in $CF_3COOH$ and $CF_3COOD$[6] are included in the range 1244–1182 $cm^{-1}$. Further support is noted in the assignments[7] for $CF_3CH_3$.

The infrared absorption between 400 and 450 $cm^{-1}$ is wide and poorly resolved. Similarly the Raman line at 432 $cm^{-1}$ is diffuse. It is likely that this region includes the two frequencies of species $A'$ and $A''$ associated with the rocking and the wagging of the $CF_3$ group. We attribute the band at 432 $cm^{-1}$ to the wagging mode, although it might be the rocking mode. Perhaps some of the bands in Table I explained as combinations involving 432 $cm^{-1}$ are in reality combinations involving the other frequency which likely falls in this region. The rocking frequency of $CH_3-CF_3$ is found at 365 $cm^{-1}$.

Experimental conditions, due in part to the low boiling point of the compound, and the unavailability of a spectrometer, prevented confirmatory runs on a Raman line at 250 $cm^{-1}$ found on one plate. If real, this band is to be associated with the COF bending. Invoking its use, three bands may then be explained as binary combinations in Table I.

[5] Rank, Shull, and Pace, J. Chem. Phys. **18**, 885 (1950).
[6] Josien, Fuson, Lawson, and Jones, Compt. rend. **234**, 1163 (1952).
[7] Nielsen, Classen, and Smith, J. Chem. Phys. **18**, 1471 (1950).

TABLE II. The fundamental vibration frequencies of $CF_3OF$.

| Infrared (gas) | | Raman (liquid) | | | |
|---|---|---|---|---|---|
| Wave number | Description | Wave number | Description | Species | Approximate character[a] |
| 1259 | *vs* | | | $A'$ | $CF_3$ unsymmetrical stretch |
| 1220 | *vs* | | | $A'$ | $CF_3$ symmetrical stretch |
| 945 | *s* | 939 | *s* | $A'$ | OF stretch |
| 880 | *s* | 879 | *vs* | $A'$ | CO stretch |
| 679 | *s* | 673 | *w* | $A'$ | $CF_3$ symmetrical deformation |
| 609 | *m* | | | $A'$ | $CF_3$ unsymmetrical deformation |
| | | | | $A'$ | $CF_2$ rocking |
| | | (250?) | *w* | $A'$ | COF bending |
| 1282 | *vs* | | | $A''$ | $CF_3$ unsymmetrical stretch |
| 586 | *w* | 583 | *vw* | $A''$ | $CF_3$ unsymmetrical deformation |
| 432 | *w* | 431 | *w* | $A''$ | $CF_3$ wagging |
| | | | | $A''$ | OF torsion |

[a] The designations in this column have only rough meaning.

There remains to be assigned a frequency to the OF torsion of species $A''$. At present we have no evidence which indicates the position of this frequency.

The interpretation of the infrared spectrum is given in the last column of Table I. The explanations are presented on the basis that $CF_3OF$ is an asymmetric molecule belonging to the point group $C_s$ and that, therefore, all combination bands are permitted.

## CONCLUSIONS

Nine of the twelve fundamental frequencies of $CF_3OF$ have been identified in a plausible manner, while a tenth is put forward tentatively. All but seven of the infrared bands have been interpreted as fundamentals or binary combinations of ten fundamentals. Since two of the fundamental frequencies have not been identified, it seems best not to invoke ternary combinations although several of the seven bands for which no assignment is given could be fitted by ternary combinations.

It is a pleasure to acknowledge the kind assistance of various persons in the Physics Department of the K-25 Laboratories, in particular Dr. A. E. Cameron, Dr. J. S. Kirby-Smith, and T. G. Burke. We also wish to extend our thanks to A. V. Faloon and W. B. Kenna, who prepared the compound.

# Velocity Distribution of Electrons in Field Emission. Resolution in the Projection Microscope

ROBERT GOMER
*Institute for the Study of Metals, University of Chicago, Chicago, Illinois*
(Received April 21, 1952)

The velocity distribution of electrons in field emission has been calculated on the basis of a simple free electron or one-band model. It is found that the component of velocity transverse to the direction of emission varies approximately as the square root of the applied field. This leads to the result that resolution in the field emission microscope is practically independent of applied voltage, since transit times vary as $V^{-\frac{1}{2}}$; resolution turns out to be of the order of 30A. Image formation in the case of molecules and the resolution obtainable with the proton microscope are briefly discussed.

THE phenomenon of cold emission from metal surfaces under the action of high external fields has been given new emphasis by the advent of the field emission projection microscope of E. W. Müller.[1] In order to understand the mechanism of image formation by this device it is necessary to understand the factors governing its resolution. This necessitates a determination or calculation of the distribution of electron velocities transverse to the direction of emission. The first section of this paper performs this calculation for an assumed free electron model obeying Fermi-Dirac statistics. The results of this section are then applied to the field emission microscope. It will turn out that only electrons near the top of the Fermi sea are involved in field emission, so that the value of the work function but not of the depth of the sea is important. It is felt that this fact justifies, admittedly *a posteriori*, the use of the free electron model. Although it is quite probable that electronic surface states play a role in field emission, their chief noticeable effect should be a change in the effective band width, i.e., depth of the sea. Since the work functions used are determined experimentally in any case, their values will be automatically correct. It would be interesting to check the derived velocity distributions experimentally.

## ELECTRONIC VELOCITY DISTRIBUTION IN FIELD EMISSION

We calculate first the number of electrons in unit volume with a given $x$ component of velocity regardless of $y$ and $z$ components. It is assumed that motion in the positive $x$ direction leads to penetration of the barrier or reflection by it. The barrier is assumed infinite in the $y$ and $z$ directions. Then

$$N(\dot{x},\dot{y},\dot{z})d\dot{x}d\dot{y}d\dot{z} = \frac{2m^3}{h^3}\frac{d\dot{x}d\dot{y}d\dot{z}}{\exp([(m/2)(\dot{x}^2+\dot{y}^2+\dot{z}^2)-\mu]/kT)+1}. \quad (1)$$

$\dot{x}$, $\dot{y}$, $\dot{z}$ are velocity components along the Cartesian directions, $m$ is the effective electron mass, $h$, Planck's constant, and $\mu$ the chemical potential of the electrons in the sea.

Hence, switching to polar coordinates in two dimensions and integrating over the angular distribution

$$N(\dot{x})d\dot{x} = \frac{4\pi m^2 d\dot{x}}{h^3}\int_0^\infty \frac{d\epsilon}{e^{(E_x+\epsilon-\mu)/kT}+1}, \quad (2)$$

where $\epsilon$ is the variable of integration and $E_x=\frac{1}{2}m\dot{x}^2$. This integral must be evaluated separately for the two cases $E_x<\mu$ and $E_x\gtrsim\mu$.

For $E_x<\mu$ the integral in Eq. (2) is very nearly equal to

$$\int_0^\infty \frac{d\epsilon}{e^{(E_x+\epsilon-\mu)/kT}+1} \approx \int_0^{(\mu-E)} d\epsilon = \mu-E \quad (3)$$

at ordinary temperatures when $kT\ll\mu-E$. This condition holds well at room temperature up to $\mu-E\sim0.05$ ev. Hence,

$$N(\dot{x})d\dot{x} = (4\pi m^2/h^3)(\mu-E_x)d\dot{x} \quad (E_x<\mu). \quad (4)$$

For the case $E\gtrsim\mu$ the value of the exponent in the integral of (2) is never less than zero, so that we can expand in powers of $\exp-(E-\mu+\epsilon)/kT$, leading to

$$\int_0^\infty \frac{d\epsilon}{e^{(E_x+\epsilon-\mu)/kT}+1} = \int_0^\infty e^{-(E-\mu)/kT}e^{-\epsilon/kT} \times(1-e^{-(E_x-\mu)/kT}e^{-\epsilon/kT}+e^{-2(E_x-\mu)/kT}e^{-2\epsilon/kT}+\cdots)d\epsilon, \quad (5)$$

so that

$$N(\dot{x})d\dot{x} = \frac{4\pi m^2 kT}{h^3}e^{-(E_x-\mu)/kT} \times\left(1+\sum_{n=2}^{\infty}(-1)^{n-1}(1/n)e^{-n(E_x-\mu)/kT}\right) \quad (E_x\gtrsim\mu). \quad (6)$$

For the special case $E=\mu$ this reduces to

$$N(\dot{x}_\mu)d\dot{x} = (4\pi m^2 kT/h^3)\ln 2 \quad (E_x=\mu), \quad (7)$$

and for values of $E_x$ appreciably larger than $\mu$ the series converges extremely rapidly.

[1] J. A. Becker, Bell System Tech. J. **XXX**, 907 (1951), gives references to the work of Müller and other pertinent work.

We calculate next the average transverse velocity, regardless of orientation, possessed by an electron in the range of $\dot{x}$ velocities between $\dot{x}$ and $\dot{x}+d\dot{x}$. This is the average scalar value of the vector sums of $\dot{y}$ and $\dot{z}$ for a given range of $\dot{x}$. We denote this quantity by $\langle yz\rangle(\dot{x})$. Then

$$\langle yz\rangle(\dot{x})=\left[d\dot{x}\int_{-\infty}^{\infty}\int_{-\infty}^{\infty}(\dot{y}^2+\dot{z}^2)^{\frac{1}{2}}N(\dot{x},\dot{y},\dot{z})d\dot{y}d\dot{z}\right]\Big/ [N(\dot{x})d\dot{x}]. \quad (8)$$

On transforming to polar coordinates and integrating over the angular distribution the integral in the numerator becomes

$$\langle yz\rangle\cdot N(\dot{x})=\frac{4\pi m^3}{h^3}\times\int_0^{\infty}\frac{r^2dr}{\exp[m/2(\dot{x}^2+r^2)-\mu]/kT+1}. \quad (9)$$

By making the substitution $\epsilon=\frac{1}{2}mr^2$ the integral becomes

$$\langle yz\rangle\cdot N(\dot{x})=\frac{2\pi(2m)^{\frac{3}{2}}}{h^3}\cdot\int_0^{\infty}\frac{\epsilon^{\frac{1}{2}}d\epsilon}{e^{(E_x+\epsilon-\mu)/kT}+1}. \quad (10)$$

This is of the form of the usual Fermi-Dirac integral, but must again be solved separately for the region $E_x<\mu$ and $E_x\gtrsim\mu$. For the first region the method of Bethe and Sommerfeld[2] can be used, the approximation being in this case that $(E_x-\mu)/kT\approx-\infty$. This gives for $\langle yz\rangle$:

$$\langle yz\rangle\cdot N(\dot{x})=\left(\frac{4\pi(2m)}{3h^3}\right)^{\frac{3}{2}}\times\left[(\mu-E)^{\frac{3}{2}}+\frac{(\pi kT)^2}{8}(\mu-E)^{-\frac{1}{2}}\right]. \quad (11)$$

For $E_x\gtrsim\mu$ we may again expand the integrand in powers of $e^{-(E_x-\mu+\epsilon)/kT}$ leading to

$$\langle yz\rangle N(\dot{x})=\left(\frac{\pi 2mkT}{h^2}\right)^{\frac{3}{2}}e^{-(E_x-\mu)/kT}\times\left(1+\sum_{n=2}^{\infty}(-1)^{n-1}\cdot\frac{1}{n^{\frac{3}{2}}}\cdot e^{-n(E_x-\mu)/kT}\right). \quad (12)$$

The series converges very quickly except at $E_x=\mu$; at $E_x=\mu$ Eq. (12) reduces to

$$\langle yz\rangle N(\mu)=0.765\left(\frac{2\pi mkT}{h^2}\right)^{\frac{3}{2}}. \quad (13)$$

[2] A Sommerfeld and H. Bethe, Handbuch d. Physik XXIV/2 (1934).

We are now able to find $\langle yz\rangle(\dot{x})$ from Eqs. (3) to (12). For $E_x<\mu$,

$$\langle yz\rangle(\dot{x})=\tfrac{2}{3}\left(\frac{1}{m}\right)^{\frac{1}{2}}\left((\mu-E_x)^{\frac{3}{2}}+\frac{(\pi kT)^2}{8}(\mu-E_x)^{-\frac{1}{2}}\right) \quad (14)$$

and

$$E_{\langle yz\rangle}=\frac{4}{9}\left((\mu-E_x)^{\frac{3}{2}}+\frac{(\pi kT)^2}{8}(\mu-E_x)^{-\frac{1}{2}}\right)^2\approx\frac{4}{9}(\mu-E_x), \quad (15)$$

where $E_{\langle yz\rangle}$ is defined as $E_{\langle yz\rangle}(\dot{x})=(m/2)\langle yz\rangle^2$. For $E_x=\mu$,

$$E_{\langle yz\rangle}=0.956kT, \quad (16)$$

and for $E_x>\mu$,

$$E_{\langle yz\rangle}=\frac{\pi kT}{4}\left(\left[1+\sum_2^{\infty}(-1)^{n-1}\left(\frac{1}{n}\right)^{\frac{3}{2}}e^{-n(E_x-\mu)/kT}\right]\Big/\left[1+\sum_2^{\infty}(-1)^{n-1}(1/n)e^{-n(E_x-\mu)/kT}\right]\right)^2\approx\frac{\pi kT}{4}. \quad (17)$$

It is seen that $E_{\langle yz\rangle}\approx 4/9(\mu-E_x)$ for $E_x<\mu$ and $E_{\langle yz\rangle}\approx kT$ for all other values of $E_x$. At ordinary temperatures it is furthermore safe to replace $\mu$ by $\mu_0$, the chemical potential at $T=0°$K, since

$$\mu=\mu_0(1-(\pi^2/12)(kT/\mu_0)^2+\cdots)\approx\mu_0. \quad (18)$$

We must now find the actual current per unit area, $I(\dot{x})d\dot{x}$, penetrating the barrier as a function of $E_x$ and $\dot{x}$:

$$I(\dot{x})d\dot{x}=N(\dot{x})\cdot\dot{x}\cdot D(\dot{x})d\dot{x}. \quad (19)$$

$D(\dot{x})$ is the transmission coefficient and gives the chance that an electron of given momentum in the direction of the potential barrier will penetrate it. $D(E_x)$ has been calculated by Fowler and Nordheim[3] and corrected for image potential by Nordheim:[4]

$$D(E_x)=\frac{4(E_x(\chi+\mu-E_x))^{\frac{1}{2}}}{(\chi+\mu)}\cdot\exp-\frac{4}{3}\left(\frac{8\pi^2m}{h^2}\right)^{\frac{1}{2}}(\chi+\mu-E_x)^{\frac{3}{2}}/(Fe/\alpha). \quad (20)$$

$\chi$ is the *thermionic* work function, $F$ the surface field, and $e$ the electronic charge. $(\alpha)$ is a correction factor for image field so that $F/\alpha$ represents the effective field. $(\alpha)$ may be determined from Nordheim's formula[4] and is given as a function of $F^{\frac{1}{2}}/\chi$ by him. $\alpha$ has values of

[3] R. H. Fowler and L. W. Nordheim, Proc. Roy. Soc. (London) **A111**, 173 (1928).

[4] L. W. Nordheim, Proc. Roy. Soc. (London) **A121**, 628 (1928).

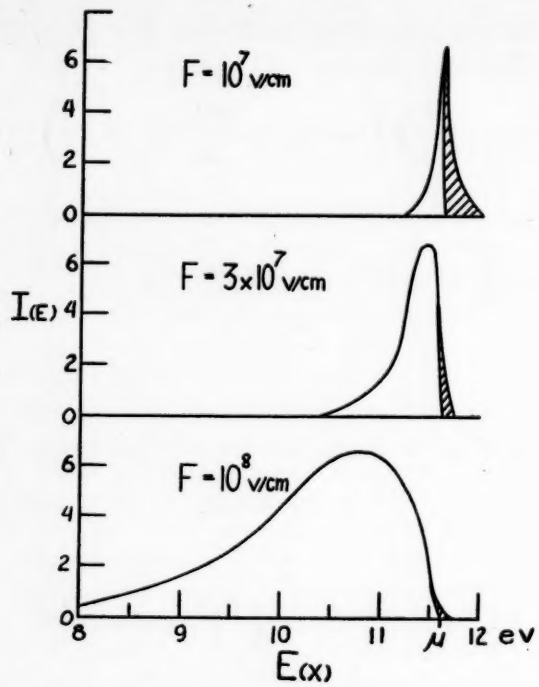


FIG. 1. $I(E_x)$ *vs* $E_x$ for various applied fields. Ordinates have been adjusted to make comparison possible. To convert to (amperes/cm²/sec)/electron-volt multiply ordinates by $3.7\times10^{-3}$ for $F=10^8$; $2.1\times10^{-11}$ for $F=3\times10^7$; $1.1\times10^{-33}$ for $F=10^7$.

0.9—0.4 in the range of fields of interest ($10^7-10^8$ v/cm). $I(E_x)dE_x$ therefore becomes, for $\mu>E_x$,

$$I(E_x)dE_x=\frac{16\pi m(\mu-E_x)}{h^3(\chi+\mu)}\cdot(E_x(\chi+\mu-E_x))^{\frac{1}{2}}\times\exp-\frac{6.84\times10^7(\chi+\mu-E_x)^{\frac{3}{2}}}{F/\alpha}dE_x. \quad (21)$$

If $\chi$, $\mu$, and $E_x$ are expressed in electron volts and $F$ in volts/cm, this becomes

$$I(E_x)dE_x=2.04\times10^{10}\frac{E_x^{\frac{1}{2}}(\chi+\Delta)^{\frac{1}{2}}\cdot\Delta}{(\chi+\mu)}\cdot\exp\left[-\frac{6.84\times10^7}{F/\alpha}(\chi+\Delta)^{\frac{3}{2}}\right], \quad (22)$$

where $\mu-E_x=\Delta$. For $\mu=E_x$ the current is

$$I(\mu)dE_x=1.41\times10^{10}\frac{kT(\chi\mu)^{\frac{1}{2}}}{(\chi+\mu)}\cdot\exp-\frac{6.84\times10^7}{F/\alpha}\chi^{\frac{3}{2}}, \quad (23)$$

if $kT$ is expressed in electron volts. For $E_x>\mu$ the expression becomes

$$I(E_x)dE_x=2.04\times10^{10}\frac{kT}{\chi+\mu}\times e^{\Delta/kT}\left(1+\sum_2^\infty(-1)^{n-1}\frac{1}{n}e^{+n\Delta/kT}\right)-\exp-\frac{6.84\times10^7}{F/\alpha}\cdot(\chi+\Delta)^{\frac{3}{2}}. \quad (24)$$

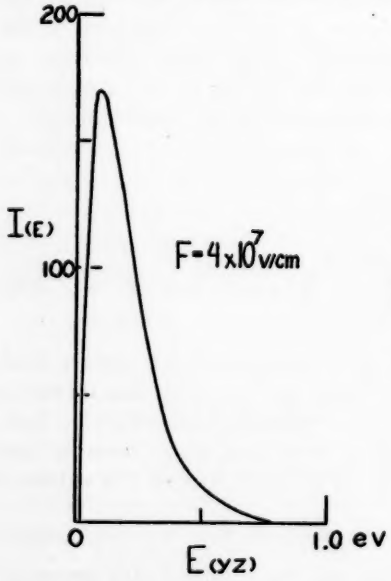


FIG. 2. $I(E_x)$ *vs* $E_{(yz)}$ for an applied field of $F=4\times10^7$ volts/cm. Ordinate should be multiplied by $10^{-9}$ to convert to (amperes/cm²/sec)/electron-volt.

Figure 1 shows plots of $I(E_x)$ *vs* $E_x$ for nickel at various values of $F$. The values $\chi=5$ ev, $\mu=11.6$ ev have been used. The latter is undoubtedly high. It should be noted, however, that these curves are relatively insensitive to the actual values of $E_x$ and $\mu$, but are sensitive to the values of $\chi$ and $\Delta$. This is a consequence, of course, of the inability of slow electrons to penetrate the barrier, so that only electrons near the top of the Fermi sea contribute appreciably to the current. It should be noted that the shaded regions in the curves of Fig. 1 represent the difference between the current at $T=300°K$ and $T=0$, i.e., the "Boltzmann tail." This shaded area is also a measure of the error in the Fowler-Nordheim equation.[3] It is seen that this error becomes more appreciable the weaker the applied field, but is practically negligible for reasonable values of $F(\sim3\times10^7$ v/cm). It should also be mentioned that the distribution of energies in the current broadens appreciably as the field is increased, the maximum shifting to the left.

Figure 2 shows a typical distribution of velocities transverse to the direction of propagation. It will be seen from these figures that the region of importance is that for which $E_x<\mu$, so that Eqs. (15) and (22) apply. It becomes an easy matter, therefore, to determine the relation between the applied field and the maximum of the $I(E_x)$ *vs* $E_x$ and $I(E_x)$ *vs* $E_{(yz)}$ curves.

We note first of all that the factor $(E_x(\chi+\mu-E_x))^{\frac{1}{2}}$ in Eq. (21) is practically invariant with $E_x$ over the regions of interest, so that we can neglect it in differentiating Eq. (21). Equating the result to 0, we obtain

$$F/\alpha=1.025\times10^8\Delta(\chi+\Delta)^{\frac{1}{2}}\approx1.03\times10^8\Delta\cdot\chi^{\frac{1}{2}}. \quad (25)$$

Combining this result with that of Eq. (16) we find, on making the approximation $(\chi+\Delta)^{\frac{1}{2}}\approx\chi^{\frac{1}{2}}$, which is certainly a good one at reasonably low field strengths (see Figs. 1 and 2),

$$E_{\langle yz\rangle_{\max}}=4.33\times10^{-9}\chi^{-\frac{1}{2}}(F/\alpha). \tag{26}$$

In other words, there is an approximately linear relation between the applied effective field and the transverse energy of escaping electrons.

## APPLICATION TO THE FIELD EMISSION MICROSCOPE

These results will now be applied to the projection microscope. First, however, we shall calculate the resolution obtainable if the electrons had no transverse momentum other than that required by the uncertainty principle. This amounts to a diffraction calculation.

We consider electrons emerging from a region of width $\delta$ on the tip. The image of the region $\delta$ would appear as a spot of width $D_0$ on the screen:

$$D_0=\delta x/r\beta. \tag{27}$$

$x$ is the distance from screen to tip, $r$ the radius of curvature of the tip, and $\beta$ a numerical factor of the order of 1.2. $\beta$ arises because the tip is not a free hemisphere but joined to a cylindrical or conical section of wire which tends to "compress" the pattern slightly, preserving, however, its axial symmetry. ($\beta$ can easily be determined by comparing the observed angles at which principal crystallographic planes (identifiable from symmetry) appear with the theoretical ones.)

By the uncertainty principle the electrons emerging from $\delta$ must have a minimum average transverse velocity of the order of

$$v\cong(1/4\pi)(h/m\delta), \tag{28}$$

so that the image $D_0$ will appear enlarged by an added amount $D=2vt$.

The time of transit of the electrons is given by

$$t=\left(\frac{m}{2Ve}\right)^{\frac{1}{2}}\left(x+\frac{r}{2}\ln x/r\right)\approx x\left(\frac{m}{2Ve}\right)^{\frac{1}{2}}, \tag{29}$$

so that

$$D=\frac{x}{2\pi\delta}\left(\frac{h^2}{2mVe}\right)^{\frac{1}{2}}=\frac{x}{2\pi\delta}\frac{12.5}{(V)^{\frac{1}{2}}} \tag{30}$$

for $x$ in cm and $\delta$ in A. It will be noticed that $12.5V^{-\frac{1}{2}}=\lambda$, the final de Broglie wavelength of the electrons. Strictly this wavelength is too small by the factor $(1+(r/2x)\ln x/r)$, which is negligible. The result of Eq. (30) could have been obtained[5] by expressing $t$ in terms of an average velocity of transit $\bar{v}$, $t=x/\bar{v}$, so that from Eq. (28),

$$D=\frac{hx}{2\pi\delta m\bar{v}}=\frac{x}{2\pi\delta}\bar{\lambda}. \tag{31}$$

[5] The author wishes to thank Professor Gregor Wentzel, to whom the following proof is due.

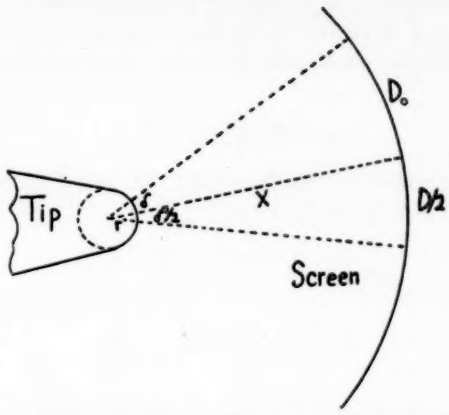


FIG. 3. Schematic diagram of projection microscope. $D_0$ is geometric magnification for a compression factor $\beta$ of unity. $D/2$ represents additional magnification due to diffraction.

The deviation of $\bar{\lambda}$ from the final wavelength is negligible as shown. Equation (31) could have been written down immediately on the basis of diffraction; however, it seems to be intuitively difficult to accept the fact that the final rather than initial electron wavelength is involved here. The total spot size on the screen caused by an emitter $\delta$ on the tip is then

$$D+D_0=(x/r\beta)[\delta+(r\beta/2\pi\delta)\lambda]. \tag{32}$$

Two regions of width $\delta$ will be resolved if their distance from each other on the tip $\delta'$ just corresponds to an apparent separation $D$ on the screen. Therefore,

$$\delta'=r\beta\lambda/2\pi\delta. \tag{33}$$

It is seen that the resolution here depends on the quantity $\delta\delta'$. For $r=3\times10^{-5}$ cm, $\beta=1.2$, and $\lambda=0.12$A, $\delta\delta'=68.8$A$^2$. This means that two regions 8.3A wide and 8.3A apart will be resolved.

We must now see whether the mean transverse velocity of the electrons due to their statistical distribution as calculated in the first part of this paper exceeds that required by uncertainty considerations. If this is the case, Eq. (33) is not applicable. We therefore calculate $\delta$ using for the lateral velocity of the electrons the value $\langle yz\rangle=((2/m)E_{\langle yz\rangle_{\max}})^{\frac{1}{2}}$. The diameter of a scattering disk $D$, caused by electrons emerging from a point on the tip, is therefore

$$D=2x\left(\frac{E_{\langle yz\rangle_{\max}}}{V}\right)^{\frac{1}{2}} \tag{34}$$

(for $E$ and $V$ in electron volts), so that the resolution becomes

$$\delta=2\beta r\left(\frac{E_{\langle yz\rangle_{\max}}}{V}\right)^{\frac{1}{2}}. \tag{35}$$

The resolution calculated for a field of $4\times10^7$ v/cm and a tip size of $3\times10^{-5}$ cm turns out to be $\sim$30A. The formula

$$F=kV/r \tag{36}$$

has been used. The value of $k$ is in most cases $k\sim\frac{1}{5}$, and is not very sensitive to the precise formula used. Here the following, due to W. P. Dyke[6] and associates, was used:

$$k=1/[0.4\ln(x/0.4r)]. \tag{37}$$

It is instructive to combine Eqs. (35) and (26). We first write $F/\alpha$ in terms of $V/\alpha$:

$$F/\alpha=kV/r\alpha, \tag{38}$$

so that

$$\delta=1.31\times10^{-4}\beta\left(\frac{kr}{\alpha\chi^{\frac{1}{2}}}\right)^{\frac{1}{2}}. \tag{39}$$

For a field of $4\times10^7$ v/cm, $r=3\times10^{-5}$ and $\alpha=0.8$, a resolution of 30A is calculated from (39) in agreement with the previous calculation.

It will be seen that Eq. (39) places a lower limit of *ca* 30A on the resolution for statistical reasons. However, uncertainty considerations (or diffraction) may indicate a poorer resolution as shown by Eq. (33).

Equation (39) implies that resolution should be nearly independent of applied voltage for a given tip. This explains satisfactorily why tungsten patterns obtained by W. P. Dyke[6] by means of pulse techniques at field strengths considerably above those used by other workers lead to patterns indistinguishable from the latter. It will be seen that a choice of $E_{\langle yz\rangle}$ larger than $E_{\langle yz\rangle\max}$, for instance $aE_{\langle yz\rangle\max}$, will lead to a resolution worse by a factor of $\sqrt{a}$. Thus, a choice of $2E_{\langle yz\rangle\max}$ leads to resolution of the order of 40A.

## RESOLUTION OF THE PROTON MICROSCOPE

E. W. Müller has recently developed an ingenious modification of the field emission microscope based on the ionization of adsorbed hydrogen.[7] The device consists of an ordinary field emission microscope containing $H_2$ at a pressure of *ca* $10^{-4}$ mm of Hg. When the tip is made the anode, adsorbed hydrogen can be pulled off as protons at fields of the order of $2\times10^8$ volts/cm.

The resolution is now given by Eq. (34) with $E_{\langle yz\rangle}$ replaced by $E_{\text{proton}}$. The zero point energy of the proton bending vibration on the metal surface must be of the order of 1000 wave numbers ($C-H$ bending vibration 1450 wave numbers, $B-H$, 1100) which leads to $E_{\text{proton}}=0.03$ ev. Since this is of the order of $kT$ at room temperature, it is permissible to set $E_{\text{proton}}=kT$ as was done by Müller, who found resolutions of $\sim$3A could be obtained.[7] No increase in resolution is to be expected by cooling, but by an increase in applied potential.

In the case of the proton microscope, the fundamental identity of the statistical and diffraction (uncertainty principle) points of view can be seen very clearly. At low temperatures the statistical energy is essentially the zero point energy. But the existence and even the order of magnitude of zero point energies in general can be derived from the uncertainty principle in a very direct manner,[8] so that the diffraction picture leads back to statistics.

## IMAGE OF SINGLE MOLECULES

There is considerable evidence to show that single molecules of such substances as phthalocyanine give rise to individual "images" or patterns showing the symmetry of the molecule. It seems contradictory to the conclusions of this paper that 10A molecules should give rise to patterns showing structure other than that due to diffraction if the electrons responsible are not capable of resolving distances less than 30A. However, it seems quite reasonable to assume that the electrons responsible for the molecular patterns originate in the molecules themselves, ($\pi$-electrons) and hence do not belong to the Fermi sea of the substrate. Furthermore, there is undoubtedly considerable field enhancement in the vicinity of these molecules, giving rise to electron optical effects. Thus electrons will be emitted most readily outward from the four "corners" (benzene rings) of phthalocyanine where the field is highest. The emerging electrons will therefore acquire considerable velocity components directed away from the molecule's center.

Thus the four-leaf-clover patterns of phthalocyanine will result. The size of these patterns corresponds to an additional 10–20 fold enlargement over that of the tip. This is accounted for by the large gain in lateral velocity of the emitted electrons, due to the field distortion. This hypothesis is essentially that advanced by E. W. Müller.[9] Detailed evidence in its favor will be presented soon.

## ACKNOWLEDGMENT

It is a pleasure to acknowledge most stimulating and helpful discussions with Dr. T. H. Walnut on many aspects of this work. This work was supported in part by Contract AF 33(038)-6534 with the United States Air Force.

[6] Private communication from Dr. W. P. Dyke, Department of Physics, Linfield College, McMinnville, Oregon. See also reference, 1, p. 912.

[7] E. W. Müller, Z. Physik **131**, 136 (1951).

[8] F. O. Rice and E. Teller, *The Structure of Matter* (John Wiley and Sons, Inc., New York, 1949), p. 7. This book applies the method to the H atom. The application to the harmonic oscillator or particle in a box is obvious.

[9] E. W. Müller, Z. Physik **131**, 136 (1951).

# Ultrasonic Propagation in Xenon in the Region of Its Critical Temperature

A. G. CHYNOWETH* AND W. G. SCHNEIDER
*National Research Laboratories, Ottawa, Canada*
(Received May 12, 1952)

The velocity of ultrasonic waves has been measured in xenon through its critical region. Only the limited frequency range from 250 kc/sec to 1250 kc/sec could be used close to the critical temperature and over this interval a velocity dispersion of as much as 6 percent was observed. The dispersion was accompanied by an abnormally high attenuation of the sound wave confirming in this respect the previously observed behavior of other systems near their critical point. From an analysis of the dispersion measurements it is concluded that structural relaxation processes play a dominant role in the mechanical behavior of the system. The results also indicated the presence of a very wide spectrum of relaxation times.

## INTRODUCTION

INVESTIGATIONS on the nature of ultrasonic propagation in the vicinity of the liquid-vapor critical temperature of sulfur hexafluoride and the critical solution temperatures of binary liquid systems have been reported previously.[1–3] A very high attenuation of sound was observed in both cases. This phenomenon, which is apparently characteristic of these transition points, was explained on the basis of a structural relaxation mechanism. If this explanation is correct, a measurable dispersion in the sound velocity may be expected. A dispersion in the sound velocity near the liquid vapor critical point of xenon has now been observed and is described in the present paper.

In the previous measurements a fixed frequency of 600 kc/sec was employed. For the present experiments a frequency range from 250 kc/sec to 2250 kc/sec was obtained by driving a 250-kc quartz crystal at its fundamental resonant frequency as well as at its third, fifth, seventh, and ninth harmonics.

Xenon was chosen for the present measurements in order to avoid possible complications due to relaxing vibrational modes which may occur in polyatomic molecules.

## EXPERIMENTAL TECHNIQUE

The double crystal acoustic interferometer used for these experiments has been described in detail in an earlier paper.[2] The crystals used had a fundamental frequency of 250 kc/sec, and the output from the lower crystal, which acted as the receiver, was fed via a low loss, doubly screened lead to a pre-amplifier mounted as close as possible to the interferometer. The pre-amplifier output was fed into a tuned amplifier possessing a selector control whereby any one of the five frequency bands could be chosen. The band width in each case was about $\pm 10$ percent of the actual frequency to allow some freedom in finding the exact frequencies which gave the most suitable response curves. The rectified output from the amplifier was recorded by an Esterline-Angus paper recorder. The frequency of the driving signal was measured by means of a General Radio frequency meter, Type 620-A. The driving signal was never more than a few volts so as to avoid overheating, such precautions being particularly necessary in the highly sensitive critical region.

The method of filling the interferometer was exactly as that described previously. It should be pointed out, however, that forcing the xenon in under external pressure has been found to introduce a trace of impurity from the packing used in the metal valves in the gas handling system.[4] Nothing could be done to avoid this happening when filling the interferometer. It is certain, however, that the trace of impurity present cannot seriously alter the behavior of the system as regards ultrasonic propagation.

## PHENOMENOLOGICAL BEHAVIOR

At a temperature sufficiently below the critical temperature, the properties of the denser phase can be regarded as approximating to those of a normal, unassociated, monatomic liquid. Under these conditions it is to be expected that the structural relaxation (involving a change in the site of the atom in the liquid matrix) will only be appreciable at the extremely high frequencies corresponding to the frequency of vibration of the atom (or, more generally, the molecule) about its equilibrium site. These frequencies are beyond the range of ultrasonic techniques in most cases. However, as the critical point is approached, the properties of the medium undergo considerable changes owing to the large increase in the free volume. The liquid-phase gradually loses its liquid-like structure and becomes inhomogeneous, the atoms showing a slight tendency to cluster with the result that the density fluctuates through the medium. The clusters, that is, the slightly denser regions, can be regarded as being mobile to a certain extent by means of the process of condensing atoms on to one part of their "surface" and evaporating at another. Consequently, the boundaries of the clusters are ill-defined and constantly changing as the atoms attach and detach themselves, only extremely low

* National Research Laboratories Postdoctorate Fellow.
[1] W. G. Schneider, J. Chem. Phys. **18**, 1300 (1950).
[2] W. G. Schneider, Can. J. Chem. **29**, 243 (1951).
[3] A. G. Chynoweth and W. G. Schneider, J. Chem. Phys. **19**, 1566 (1951).
[4] M. A. Weinberger and W. G. Schneider Can. J. Chem. **30**, 422 (1952).

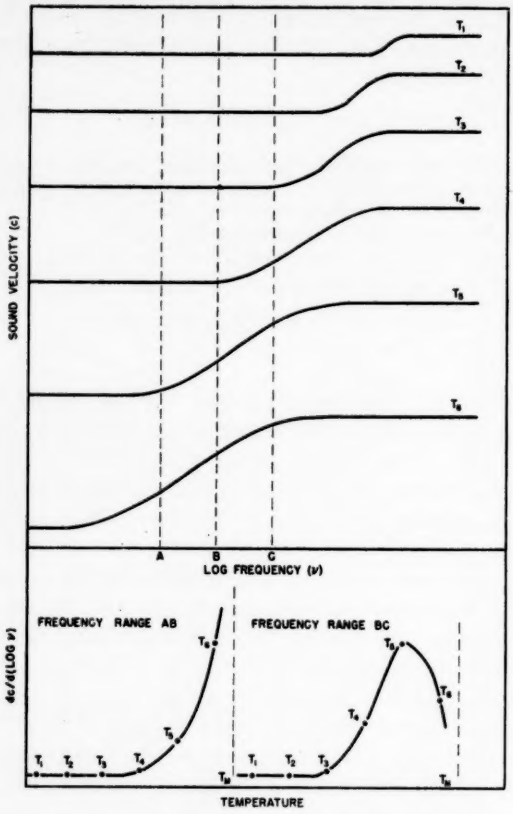


FIG. 1. Top diagram: Schematic representation of the expected change in the shape of the full dispersion curve as the critical temperature is approached. Bottom left: The average slope of the experimental velocity—log frequency curve plotted against temperature assuming that the experimental frequency range covers the interval *AB*. Bottom right: The same curve plotted for the case where the experimental frequency range covers the interval *BC*.

potential barriers regulating the process. In particular, if small density or pressure changes are imposed upon the medium, there will be a relatively large change in the amount of clustering or inhomogeneity. As the temperature is raised above the critical region the imposed pressure changes will have less effect on the structure of the medium, and sufficiently above the critical temperature, the single phase can be regarded as a very dense gas.

Consider now the effect of suddenly applying a small increment of pressure to the system in the critical region. The immediate effect will be a compression of the system, though in general the new spatial distribution of the atoms will not correspond to that of lowest energy. Hence, immediately after the compression, the atoms will start re-arranging themselves by the processes suggested in the foregoing paragraph so as to reach the new equilibrium distribution. However, owing to the extremely weak inter-atomic forces involved and the cooperative nature of the changes, some time will be required for attaining equilibrium, and consequently, the density of the medium can be said to be lagging the applied pressure variation. In just the same way, the density will lag the sinusoidally varying pressure imposed by the transducer and, if the time lag is sufficient, appreciable attenuation of the acoustic wave will occur.

Well away from the critical region, the density changes will be established immediately with respect to the timescale represented by the acoustic wave. In the critical region, the time lag of the density can become conceivably of the order of the period of the acoustic wave or even much longer. For example, hysteresis effects in the density can be observed for several hours in "static" experiments.[5] Consequently, the acoustic attenuation will be markedly increased in the critical region. This picture is complicated, however, owing to the fact that there will be a wide diversity of cluster sizes present, and therefore there will be a wide range of local relaxation times associated with the attainment of over-all equilibrium. The simplification has to be made that the density relaxation of the medium can be represented by a single mean relaxation frequency. Thus, we may predict that, as the critical region is approached from either direction, the mean relaxation time will become longer and the spread of local relaxation times will become wider.

From these considerations an attempt has been made in Fig. 1 (top diagram) to predict the qualitative variation of the velocity with frequency as the critical temperature is approached. At temperatures well away from the critical point the magnitude of the dispersion is relatively small and is confined to a narrow frequency range. Approaching the critical temperature the dispersion in the sound velocity will become greater and will extend over a wider frequency range and at the same time the mean dispersion frequency will become progressively lower. Near the critical temperature it is likely that the dispersion will cover a frequency range of many orders of magnitude. Unfortunately, experimental difficulties associated with the use of a double crystal interferometer for investigating such a system allowed the measurements to be made over a frequency range of at most only one order of magnitude. Using Fig. 1, we can predict the results to be expected with such a limited frequency range. Two experimental ranges *AB*, *BC* are represented in the figure, and it is seen that to within the limits of experimental error it is possible that the velocity-log frequency curves will approximate to straight lines over the measured frequency range. Thus, as the critical temperature is approached, only a small part of the full dispersion curve is seen at one time as it moves past the "window" representing the experimental frequency range. The slope of the measured velocity-frequency curve can therefore vary in different ways depending on the relative position of the "window." Two types of predicted variation are given in the bottom left and bottom right of Fig. 1 corresponding to the frequency ranges *AB*, *BC*, the temperature $T_M$ representing the temperature of meniscus disappear-

[5] O. Maass, Chem. Revs. **23**, 17 (1938).

ance. For the frequency range $AB$ the temperature of maximum dispersion (and accordingly attenuation) will roughly coincide with $T_M$, whereas for the range $BC$, the maximum will be displaced from $T_M$. These considerations will be compared with the experimental results later.

## TECHNIQUE OF MEASUREMENT

In view of the preceding discussion, a relatively large total dispersion could be anticipated, though over the experimental frequency range the observed change in velocity may be expected to amount to only a few percent. The factors affecting the accuracy of the measurements must therefore be carefully considered.

All the records were obtained as the upper crystal moved away from the lower one starting at a separation of about a millimeter. A few degrees away from the critical temperature the attenuation was relatively small, and the record covered a crystal separation of up to a centimeter, a large number of very sharp and unambiguous peaks thus being obtained. The separation between peaks several wavelengths apart was measured over various parts of the record and the reproducibility of the wavelength measurements was usually to within ±0.2 percent. The frequency measurements being more accurate by an order of magnitude the resulting error in the velocity measurements was thus of the order of ±0.2 percent.

As the critical temperature was approached, the resonance peaks tended to broaden, and at the same time the increased attenuation allowed measurements to be made over a smaller number of peaks only. In addition, the trace had superimposed on it small fluctuations due to the small signal-to-noise ratio obtaining under the critical conditions. These factors gave rise to a larger error in the wavelength measurements and two methods of measuring were tried. In the first the separation between the points of maximum amplitude was measured, while in the second the distances between the points of contact of the peaks with their envelope were determined. Both methods were found to give comparable values of the velocity and measurement error. In the worst cases the error in the velocity was estimated to be ±0.7 percent.

In addition to the errors of measurement just described it is possible that other systematic sources of error may be present. First, it has been noted recently by some observers working with double crystal interferometers that the peak separation progressively alters as the crystal separation increases so that the wavelength measurements will vary according to the part of the record from which they were taken. It has been claimed that errors of a few tenths of a percent may arise in this way. However, no evidence for any progressive or systematic variation in the wavelength measurements could be found in our experiments with a crystal separation of up to a centimeter.

Theoretically, there is another possible cause for a gradual progressive change in the wavelength as the crystals separate. It has long been known that in a system near its critical point density gradients may be set up which can persist for several hours even when the system is gently stirred. Recent work in this laboratory using tracer techniques has demonstrated this effect very convincingly.[6] These density gradients are a consequence of the gravitational effect of the pressure head of fluid on the lower layers and the extremely high compressibility of the system at the critical temperature. The density gradients become more marked the greater the vertical height of the bomb. Hence the system as a whole cannot be described by a unique point in the $PVT$ diagram, and in particular, it is to be expected that the density and compressibility will vary with vertical distance in the bomb. Consequently there should also be a progressive change in the sound velocity with distance (height). However, it must be concluded that as no such variation was observed, the effect must be smaller than the experimental errors. This is quite understandable, since owing to the large attenuation under these conditions only a few resonance peaks could be obtained corresponding to a change in crystal separation of one or two millimeters compared with the length of the bomb of about 7 cm. Further, all the measurements were confined to a region near the bottom of the bomb where the density gradients are nowhere near as great as in the center of the bomb in the region of the meniscus.

A further difficulty appeared in certain cases when the envelopes to the recorded resonance peaks were of complex shape instead of smoothly decreasing curves represented by hyperbolic functions. This effect, in general, was more serious in the critical region and for the higher frequencies and introduced in many cases a further difficulty in the measuring of the wavelengths. It is probable that the main origin of these superimposed intensity fluctuations lay in the pick-up of an additional signal of the same frequency as the acoustic signal though differing in phase. This additional signal could originate from another acoustic path in the interferometer or by electromagnetic pick-up from currents running in conductors supposedly at earth potential.†

For these reasons, accurate attenuation measurements were impossible without extreme precautions being taken. Attenuation measurements have accordingly been made only on the traces obtained at the fundamental frequency, as these traces were the only ones that presented suitably consistent envelopes. The value of the attenuation was determined using the same

[6] M. A. Weinberger and W. G. Schneider (to be published).

† Dr. E. Shaw has formulated the behavior of a double crystal interferometer under such conditions and has been able to predict traces which reproduce in a convincing manner many of the details of those found experimentally. In particular, the analysis shows how, under the conditions pertaining to the critical region, the experimental trace can be so misleading as to make the measured wavelength longer by a factor of 2. This error was made in some of the earlier publications from this laboratory. See J. Chem. Phys. **20**, 759 (1952).

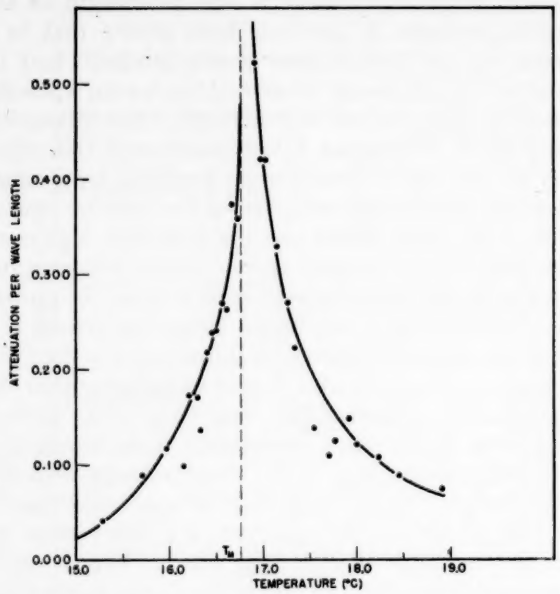


FIG. 2. Curve showing the variation of attenuation in xenon at 250 kc/sec as a function of temperature. Below $T_M$ the measurements refer to the liquid phase.

approximate method described in the earlier papers, that is,

$$\mu=-\frac{2}{n}\log_e\frac{A_n}{A_0}\text{ per wavelength,}$$

where $A_0$, $A_n$ are the amplitudes of the first peak and the $n$th peak, respectively, the amplitudes being measured from the peak to the mean level of the adjacent troughs.

In performing the measurements, the thermostat was set at a temperature known to $\pm 0.002$°C, and after several hours had elapsed, traces were obtained at the fundamental frequency and at as many of the harmonics as possible. The temperature of the bath was then altered and the procedure repeated; the order of the temperature settings chosen was randomized, and at each temperature sufficient time to reach equilibrium was allowed before readings were commenced. As the critical region was approached, it became more and more difficult to detect any acoustic signal at the higher frequencies and over an appreciable temperature range traces could only be obtained at the frequencies 250, 750, and 1250 kc/sec. This occurred in spite of the fact that the attenuation did not increase with frequency to any large extent. Consequently, in the region of greatest interest, the frequency range over which measurements could be made was severely restricted.

## EXPERIMENTAL RESULTS

### (a) Attenuation

A curve showing semiquantitatively the behavior of the attenuation at the fundamental frequency is given in Fig. 2. It shows that, as observed previously for sulfur hexafluoride, the attenuation is increased by a very large factor as the critical temperature is approached. For reasons discussed above the traces were not sufficiently accurate to enable any quantitative study of the variation of attenuation with frequency and within the limits of experimental error, no theoretically significant variation could be discerned.

Since xenon was used for the experiments, internal relaxational modes cannot be responsible for the high attenuation. There are two other possibilities: (1) the structural relaxation already discussed, and (2) attenuation due to scattering of the acoustic wave. It is difficult to form an estimate of the possible magnitude of the latter. If scattering is occurring then presumably it is due to density inhomogeneties (clusters). Because of the vanishingly small heat of vaporization and high compressibility of the system, the clusters will almost certainly partake of the motion of the sound wave and can hardly be thought of as rigid scattering centers, as postulated in classical scattering theory. For the moment, however, assuming that an approximation to rigid scattering centers holds to a certain extent, an estimate of attenuation by scattering using classical theory gives a value for $\mu$, which is orders of magnitude lower than those measured in the experiments.

Perhaps a better estimate of the effect of scattering can be made using an equation given by Liebermann in connection with the scattering due to temperature

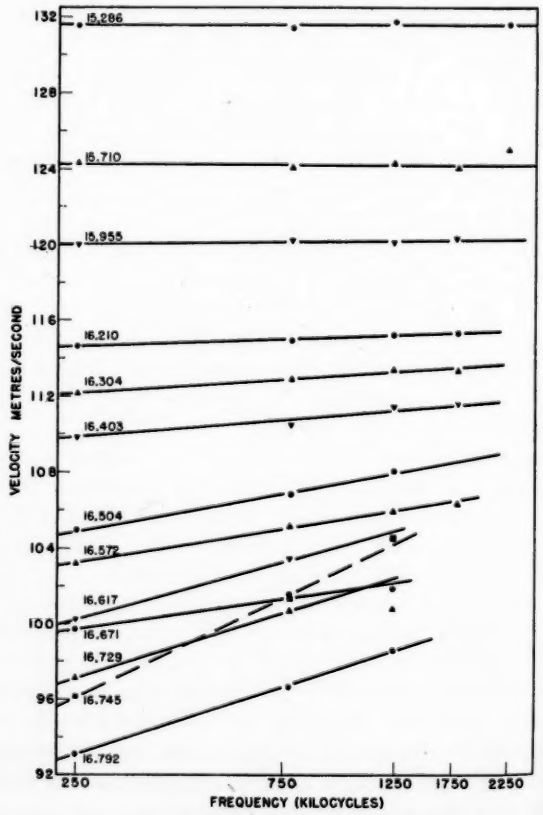


FIG. 3. The experimental values of the velocity plotted against frequency at different temperatures, all in the liquid phase.

inhomogeneities in the ocean.[7] Physically, this problem is more closely related to the critical region than the above theory since the clusters can be regarded as density (or temperature) fluctuations. Liebermann deduces the equation

$$\mu=\frac{4\pi^2}{\lambda^2}\left(\left(\frac{\Delta c}{c}\right)^2\right)\frac{a}{1+(4\pi^2/\lambda^2)\cdot a^2}\text{ per wavelength,}$$

where $\Delta c$ is the mean deviation of the velocity $c$ in the inhomogeneities of average radius $a$. Supposing that $\lambda\sim10^{-2}$, $(\Delta c/c)\sim10^{-2}$ (which would imply relatively large temperature fluctuations as can be seen by interpolating Fig. 5 in the critical region), then this equation gives a maximum value of approximately $10^{-2}$ for $\mu$ when $a$ is of the order of $10^{-3}$. Hence on the basis of the above rough calculations as well as a consideration of the molecular processes that would be involved, attenuation by scattering does not appear to be of sufficient magnitude to explain entirely the enormous increase close to the critical point. It seems almost certain that the high attenuation is due to structural relaxation processes.

### (b) Sound Velocity

The results of the velocity measurements are shown in Figs. 3 and 4, the velocity being plotted against the log of the frequency for various temperatures. Figure 3 represents the results for temperatures below the critical point, i.e., in the liquid phase, while Fig. 4 gives the results for the supercritical phase. It is seen that as the temperature approaches the critical point from either direction the slopes of the curves increase in accordance

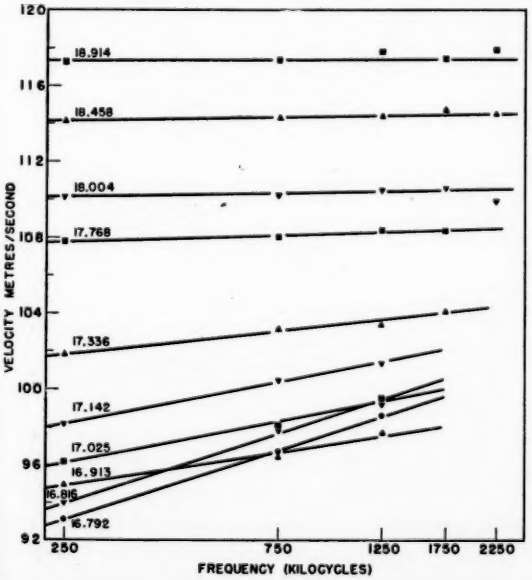


FIG. 4. The experimental values of the velocity plotted against frequency at different temperatures, all in the supercritical phase.

[7] L. Liebermann, J. Acoust. Soc. Am. **23**, 563 (1951).

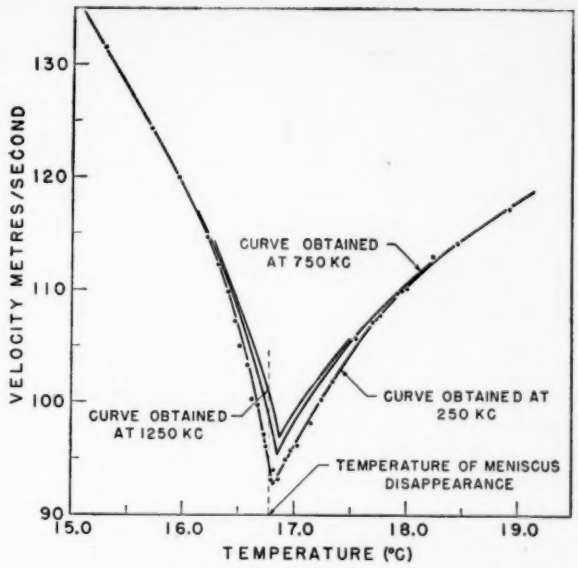


FIG. 5. The velocity plotted as a function of temperature at three frequencies. To avoid confusion, the experimental points for the curves at 750 kc/sec and 1250 kc/sec are not shown.

with the predictions made earlier. However, to within the limits of experimental error there is no evidence that the slopes pass through a maximum before reaching the critical temperature and consequently, it must be concluded that the frequency range remains well within the dispersive region right up to the critical point.

The velocities are plotted as a function of temperature in Fig. 5, and the increasing dispersion as the critical temperature is approached is again evident. Another feature to be noted is that, although the velocity curve exhibits a sharp cusp at the critical temperature, there does not appear any tendency towards a finite discontinuity or for it to suddenly drop to zero. Further, the results show that at 250 kc/sec at least, the temperature of minimum velocity (and also maximum absorption) is displaced slightly from the temperature of meniscus disappearance. However, this effect may be due to the fact that the measurements were made in an unstirred system.

## DISCUSSION

On the basis of the nature of sound propagation one may ascribe to a system in the critical region a characteristic visco-elastic behavior. To represent the complex relaxational mechanisms taking place in the critical state as proposed above, recourse may be had to the familiar mechanical analogy of the "spring and dashpot."[8–10] When subjected to a force the behavior of the system as regards the instantaneous and relaxational compressibilities can be compared to that of the spring

[8] J. M. Burgers, First Report on Viscosity and Plasticity, Amsterdam, 1935.

[9] Markham, Beyer, and Lindsay, Revs. Modern Phys. **23**, 353 (1951).

[10] T. Alfrey, *Mechanical Behaviour of High Polymers* (Interscience Publishers, Inc., New York, 1948).

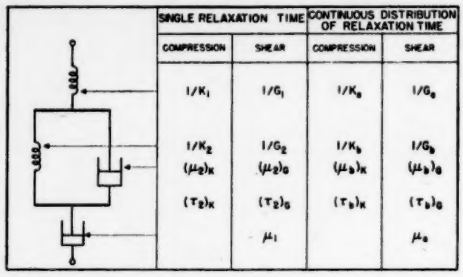


FIG. 6. Terminology and spring and dashpot model used as a mechanical analogy to describe the visco-elastic behavior of xenon in the critical state.

and dashpot model shown in Fig. 6. The lower dashpot represents the irreversible fluidity, or flow, of the medium while the remainder of the system represents the reversible processes. To represent the critical state more closely the spectrum of relaxation times could be represented by a whole series of parallel combinations of springs and dashpots. However, to begin with, only the system with one parallel combination will be considered.

Frenkel[11] has generalized the theory of elasticity so as to include relaxational behavior. He shows that the Lamé coefficients $L$, $M$, are then given by (for the case of sinusoidal variation of the applied force with frequency $\omega$)

$$L=K_1+\frac{K_2}{1+[1/i\omega(\tau_2)_K]} \tag{1}$$

and

$$M^{-1}=\frac{1}{G_1 i\omega\tau_1}+\frac{1}{G_1+G_2\{1-1/[1+i\omega(\tau_2)_G]\}}, \tag{2}$$

where $K_1$, $K_2$ are termed the ordinary and deviation adiabatic bulk moduli; $G_1$, $G_2$ are termed the ordinary and deviation shear moduli; $\tau_1$ is the Maxwell relaxation time of the fluid and equals $\mu_1/G_1$, where $\mu_1$ is the ordinary coefficient of viscosity; $(\tau_2)_K$, $(\tau_2)_G$ are the relaxation times corresponding to structural changes brought about by compression and shear, respectively. Further,

$$\left.\begin{aligned}(\mu_2)_K&=(\tau_2)_K\cdot K_2\\ \text{and}\qquad\qquad&\\ (\mu_2)_G&=(\tau_2)_G\cdot G_2\end{aligned}\right\}, \tag{3}$$

where $(\mu_2)_K$ and $(\mu_2)_G$ are deviation viscosity coefficients (also variously called compressional, dilational, or volume viscosity coefficients).

The velocity $c$ of longitudinal waves in the medium is given by

$$c^2\rho=L+2M, \tag{4}$$

where $\rho$ is the density of the medium.

In the general case the expression for the real part of (4) is intractable, and consequently two limiting cases will be considered. First, if all reversible fluidity is absent (that is, no relaxational processes present), then $(\tau_2)_K=(\tau_2)_G=0$ and the expression for the velocity is

$$c^2\rho=K_1+2G_1[\omega^2\tau_1^2/(1+\omega^2\tau_1^2)]. \tag{5a}$$

In the second case, that of the absence of irreversible fluidity, $\mu_1$ or $\tau_1$ is put equal to infinity. Further, the simplifying assumption is made that $(\tau_2)_K\simeq(\tau_2)_G$. This seems quite a reasonable approximation as the relaxation mechanisms for shear or for compression can be assumed to be due basically to the same molecular processes. The velocity is then given by

$$c^2\rho=(K_1+2G_1)+(K_2+2G_2)\cdot[\omega^2\tau_2^2/(1+\omega^2\tau_2^2)]. \tag{5b}$$

Equations (5a) and (5b) both apply to the case of a single relaxation time. Alfrey[10] has shown that a compound spring and dashpot system representing a continuous spectrum of relaxation times can be reduced effectively to the simple system used above by making suitable changes to the definitions of the various coefficients. The new coefficients are given in Fig. 6, and assuming that the shear motion can be considered separately from that brought about by compressive forces, Alfrey derives the following expressions:
$1/G_1$ is replaced by $1/G_a$ where

$$1/G_a=\int_0^{t_1} d\tau/G(\tau); \tag{6a}$$

$1/G_2$ is replaced by $1/G_b$ where

$$1/G_b=\int_{t_1}^{t_2} d\tau/G(\tau); \tag{6b}$$

$\mu_1$ is replaced by $\mu_a$ where

$$1/\mu_a=\int_{t_2}^{\infty} d\tau/\tau G(\tau)+1/\mu_1; \tag{6c}$$

and $\tau_2$ is replaced by $\tau_b$ where

$$\tau_b=\frac{\int_{t_1}^{t_2}\tau\cdot d\tau/G(\tau)}{\int_{t_1}^{t_2} d\tau/G(\tau)}. \tag{6d}$$

In these formulas $G(\tau)$ represents the distribution of $G$ as a function of $\tau$. The limits of integration $t_1$ and $t_2$ are set by the limits of the experimental timescale and consequently, in the experiments described here, $t_1\simeq 1/f_1$ and $t_2\simeq 1/f_2$, where $f_1$ and $f_2$ are the upper and lower frequency limits of the velocity measurements. For a continuous distribution of relaxation times extending over several orders of magnitude, $G(\tau)$ can be regarded as approximately constant over the experimental time-

[11] J. Frenkel, *Kinetic Theory of Liquids* (Oxford University Press, London, 1946).

scale. Then in particular, (6d) becomes

$$\tau_b = t_m, \tag{7}$$

where $t_m = (t_1+t_2)/2$. Presumably, similar expressions would also hold for the case of compressive forces. The important conclusion from these equations is that if the temperature is varied, $G(\tau)$ varies but $\tau_b$ will vary only very slightly and will remain approximately equal to $t_m$ as long as the spectrum of relaxation times embraces the experimental timescale. This latter condition appears to be fulfilled near the critical region as was noted above.

Thus for the case of a spectrum of relaxation times, Eqs. (5a) and (5b) still hold if $K_1$, $K_2$, $G_1$, $G_2$, and $\tau_2$ are replaced by $K_a$, $K_b$, $G_a$, $G_b$, and $\tau_b$, respectively. That is, when there is no reversible fluidity,

$$c^2\rho = K_a + 2G_a \cdot \frac{\omega^2\tau_1^2}{1+\omega^2\tau_1^2}, \tag{8a}$$

and when there is no irreversible fluidity,

$$c^2\rho = (K_a+2G_a) + (K_b+2G_b)\frac{\omega^2\tau_b^2}{1+\omega^2\tau_b^2}. \tag{8b}$$

These two equations have exactly the same mathematical form but with different coefficients and, as will be described, it is possible to determine $\tau$ from the experimental data for temperatures approaching the critical point. If the velocity dispersion is due mainly to irreversible fluidity, then the measured $\tau$ should behave roughly as $\tau_1 (= \mu_1/G_1)$ and would possibly vary rapidly with temperature near the critical point. If, on the other hand, the dispersion is due mainly to structural relaxation, the measured $\tau$ should change very little with temperature and, furthermore, should be of the order of $t_m$.

If the velocity is known at three different frequencies, then $\tau$ can be obtained very easily. If $c_1$, $c_2$, $c_3$ are the velocities measured at frequencies $\omega_1$, $\omega_2$, $\omega_3$, then the coefficients in either of Eqs. (8) can be eliminated to yield the equation

$$\frac{c_3^2-c_1^2}{c_2^2-c_1^2} = \frac{\omega_3^2\tau^2/(1+\omega_3^2\tau^2) - \omega_1^2\tau^2/(1+\omega_1^2\tau^2)}{\omega_2^2\tau^2/(1+\omega_2^2\tau^2) - \omega_1^2\tau^2/(1+\omega_1^2\tau^2)}.$$

Letting the left-hand side be represented by $\psi$ and remembering that $\omega_2 = 3\omega_1$ and $\omega_3 = 5\omega_1$, then

$$\tau = \frac{1}{\omega_1}\left[\frac{\psi-3}{27-25\psi}\right]^{\frac{1}{2}}. \tag{9}$$

Using relation (9), $\tau$ was calculated over a range of temperatures both above and below the critical temperature. The results are given in Table I, and it is clear that over an appreciable range of temperature the experimental results for $\tau$ remain relatively constant. Also, from the upper and lower frequency limits a rough estimate of $t_m$ may be made; it was approximately $8\times10^{-7}$ sec. Thus, the experiments have shown that the apparent relaxation time remains constant and approximately equal to the experimental timescale over a relatively wide range of temperature. It therefore appears probable from these observations that structure relaxation processes are mainly responsible for the velocity dispersion observed in the critical region. Further, there is a spectrum of relaxation times present which can possibly extend over several orders of magnitude. It seems highly unlikely that such results could be obtained as a result of irreversible fluidity alone although this possibility, on the basis of the present experimental data, cannot be definitely included.

TABLE I. The relaxation time $\tau$ at various temperatures as obtained from the experimental results.

| Below critical point | | Above critical point | |
|---|---|---|---|
| Temp. °C | $\times10^7$ sec | Temp. °C | $\times10^7$ sec |
| 16.50 | 1.82 | 16.90 | 2.29 |
| 16.55 | 1.74 | 16.95 | 2.20 |
| 16.60 | 1.90 | 17.00 | 2.29 |
| 16.65 | 2.02 | 17.05 | 2.29 |
| 16.70 | 2.20 | 17.10 | 2.33 |
| 16.75 | 2.31 | 17.15 | 2.50 |
| 16.80 | 2.37 | 17.20 | 2.70 |

## CONCLUSIONS

The present measurements on the dispersion of the sound velocity in the critical region of xenon appear to indicate that visco-elastic relaxation of the structure of the medium is mainly responsible for the high attenuation due to viscous flow; or scattering may also be present though its effect appears to be of second order importance only. Oscillating disk experiments have shown that in fact the low frequency viscosity coefficient continuously decreases as the system changes from the liquid phase to the supercritical phase.[12] As no dispersion is observed well below the critical temperature, it seems reasonable to suppose that viscosity does not play an important role in the critical region. This might not be true, though, in the case of the critical solution temperatures of binary liquid systems where it is known that the viscosity coefficient goes through a sharp maximum at the critical temperature. Further experiments are needed over an extremely wide frequency range and, in particular, attention should be paid to low frequency investigations.

[12] S. N. Naldrett and O. Maass, Can. J. Research **18B**, 322 (1940).

# Crystalline Field in Chrome Alum*†

W. H. KLEINER
*Massachusetts Institute of Technology, Cambridge, Massachusetts*
(Received June 5, 1952)

A calculation is made to test the detailed applicability of the crystalline field approximation for describing magnetic properties of chrome alum.

The theoretical susceptibility formula of Schlapp and Penney represents the experimental susceptibility as a function of temperature reasonably well provided the parameter $Dq$, which gives a measure of the interaction between the crystalline field and the paramagnetic ion, is arbitrarily chosen to give the best fit. Here $Dq$ is calculated; a model of the surroundings of the $Cr^{+++}$ ion is used to determine the crystalline field. The calculated $Dq$ is in poor agreement with experimental values, from which it is inferred that the interaction between the $Cr^{+++}$ ion and its surroundings is so strong that the crystalline field approximation is inadequate to give detailed agreement with experiment. The results are expected to apply to other hydrated paramagnetic salts of the iron group.

## 1. INTRODUCTION

THE concept of the crystalline field has been extensively applied in theories of spectra,[1–5] of paramagnetism,[6] and of heat capacity[7] in hydrated salts of transition group elements ever since Bethe[8] gave his comprehensive treatment based on symmetry. The full implication of the concept has, however, not been used in these applications. The usual theories leave undetermined certain parameters which can in principle be determined theoretically within the framework of the crystalline field approximation, but which are generally fixed by comparison with experiment. In this paper we describe a calculation which tests in more detail the validity of using the crystalline field approximation in a hydrated iron group salt, chrome alum.

A quantum-mechanical calculation of the effect of a crystalline field on a paramagnetic ion of the iron transition group was made by Schlapp and Penney[9] to determine theoretically the magnetic susceptibility of certain hydrated iron group salts. They determined the effect on the energy levels of the $Cr^{+++}$ ion due to a crystalline field of cubic symmetry. From the resulting energy level system they obtained the formula

$$\chi=\frac{15N\beta^2}{3kT}\left(1-\frac{2\lambda}{5Q}\right)^2 \qquad (1)$$

for the magnetic susceptibility according to Van Vleck's theory;[10] $N$ is the number of paramagnetic ions per mole, $\beta$ the Bohr magneton, $k$ the Boltzmann constant, $\lambda$ the spin-orbit coupling parameter (see Appendix 3). Given the magnetic susceptibility $\chi$ as a function of temperature $T$, $Q$ ($Dq$ in their notation) can be determined from Eq. (1), since the other quantities, whose dependence on $T$ and $Q$ may be disregarded, are known. The published measurements of $\chi$ for hydrated salts containing the $Cr^{+++}$ ion yield[11] $Q=3730$ cm$^{-1}$ (chrome alum) and $Q=1600$ cm$^{-1}$ ($K_3Cr(SCN)_6\cdot 4H_2O$). There is some uncertainty in these values because of the difficulty of measuring $\chi$ accurately enough to determine $Q$ accurately from (1). $Q$ has been determined more accurately from extensive measurement of $\chi$ in other hydrated salts containing other iron group paramagnetic ions, in particular $Ni^{++}$. In these other measurements $Q$ falls in the range $1000<Q<2000$ cm$^{-1}$. There is reason to believe[12] that $Q$ is relatively independent of the salt and of the iron group ion, so that we may reasonably expect $Q$ to fall in the range $1000<Q<2000$ cm$^{-1}$ for chrome alum. Unfortunately, the optical absorption spectrum[3,13] has not been sufficiently correlated with the theoretical energy level structure to provide an experimental determination of $Q$. The microwave absorption spectrum[14,15] agrees well with the theoretical energy level structure which depends on $Q$ and on other parameters which are at present somewhat uncertain.[5] However, since the dependence on these other parameters is slight, a satisfactorily precise value of $Q$ can be inferred from the spectrum with only a rough knowledge of the other parameters. Weiss[14] finds roughly $Q=1000$ cm$^{-1}$.

Each paramagnetic $Cr^{+++}$ ion in a chrome alum[16,16a,17] is surrounded by an octahedron of water molecules as nearest neighbors. The $H_2O-Cr^{+++}$ distance[18] is about

* This paper is based on a thesis submitted in partial fulfillment of the requirements for the degree of Doctor of Philosophy at the Massachusetts Institute of Technology.

† Supported by the ONR.

[1] F. H. Spedding, Phys. Rev. **58**, 255 (1940).
[2] J. H. Van Vleck, J. Phys. Chem. **41**, 67 (1937).
[3] J. H. Van Vleck, J. Chem. Phys. **8**, 787 (1940).
[4] C. Kittel and J. M. Luttinger, Phys. Rev. **73**, 162 (1948).
[5] A. Abragam and H. M. L. Pryce, Proc. Roy. Soc. (London) **205A**, 135 (1951).
[6] J. H. Van Vleck, J. Chem. Phys. **7**, 61 (1939).
[7] B. Bleaney, Proc. Roy. Soc. (London) **204A**, 216 (1950).
[8] H. A. Bethe, Ann. Physik **3**, 133 (1929).
[9] R. Schlapp and W. G. Penney, Phys. Rev. **42**, 666 (1932).
[10] J. H. Van Vleck, *The Theory of Electric and Magnetic Susceptibilities* (Oxford University Press, London, 1932).
[11] R. B. Janes, Phys. Rev. **48**, 78 (1935).
[12] J. H. Van Vleck, J. Chem. Phys. **7**, 72 (1939). See p. 82.
[13] D. L. Kraus and G. C. Nutting, J. Chem. Phys. **9**, 133 (1941).
[14] P. R. Weiss, Phys. Rev. **73**, 470 (1948).
[15] B. Bleaney, Proc. Roy. Soc. **204A**, 203 (1950).
[16] H. Lipson and C. A. Beevers, Proc. Roy. Soc. (London) **148A**, 664 (1935).
[16a] H. Lipson, Proc. Roy. Soc. (London) **151A**, 347 (1935).
[17] J. Eisenstein, Revs. Modern Phys. **24**, 74 (1952).
[18] This distance is an extrapolation from aluminum alums. A diffraction determination of the structure of chrome alums is

3.73 atomic units (unit of length $= a_0 = 0.529$A). The nearest neighbor of the $Cr \cdot 6H_2O^{+++}$ complex is a water molecule associated with the monovalent ion of the alum at a distance[16a] of about 4.73 from one of the waters of the complex. Other neighbors appear to be at least 5.0 distant from the complex. As far as paramagnetic properties are concerned, we assume that it is adequate to treat each $Cr \cdot 6H_2O^{+++}$ complex as an isolated unit. This would be a poor approximation if, e.g., one were interested in calculating the equilibrium configuration of the complex, for it is unstable in the free state. On the other hand, the direct effect on the $Cr^{+++}$ ion of the neighbors of the complex is expected to be small.[6]

How good an approximation is it to assume further that gross paramagnetic effects of the $Cr \cdot 6H_2O^{+++}$ complexes can be treated adequately by considering only each $Cr^{+++}$ ion and the electrostatic influence on it of its waters of hydration? When this approximation, called the crystalline field approximation, is used, the parameter $Q$ is given theoretically by (13), derived in Sec. 3, and is proportional to the mean value with respect to the $3d$ radial wave function $r^{-1}P(r)$ of free $Cr^{+++}$, of a radial coefficient $V_4(r)$ in the spherical harmonic expansion of the potential energy $V(\mathbf{r})$ of an electron in the field of the water molecules. Equation (13) results from using the wave function for all the electrons of the free $Cr^{+++}$ ion (including the angular dependences) in finding the average value of the potential energy of the $Cr^{+++}$ ion in the electric field of the octahedron of water molecules; when the angular dependences have been eliminated, only the radial part of the $Cr^{+++}$ $3d$ wave function and the $g$ part $V_4(r)$ of the expansion of the potential energy $V(\mathbf{r})$ remain in the formula for $Q$. The potential energy of a $Cr^{+++}$ electron associated with the presence of the chromium nucleus and other chromium electrons is not included in $V(\mathbf{r})$. This energy, assumed already to have been dealt with in the theory of the free ion, has no direct bearing on $Q$. Fine structure effects, important in paramagnetic alums for the theory of magnetic susceptibility at low temperature and for the theory of microwave absorption spectra, and generally treated by means of the crystalline field approximation, will be ignored in the calculation in this paper.

Let us consider the potential energy of a $Cr^{+++}$ electron in the field of the octahedron of water molecules, and let us suppose that the ten electrons of each water molecule form a spherically symmetrical charge distribution about the oxygen nucleus. With only one water molecule present and the effects of the protons neglected, the potential energy at a great distance from the $O^{--}$ is Coulombic corresponding to a charge $-2e$; it increases as the $O^{--}$ is approached until a maximum is reached on a spherical surface about the oxygen center which encloses no net charge; still nearer the oxygen nucleus the potential energy changes sign, finally approaching negative infinity at the oxygen nucleus. The average potential energy, obtained by taking the expectation value of this potential energy with respect to a $Cr^{+++}$ wave function, can be either positive or negative, depending on the form of the wave function. When all six waters are present, the potential energy is a superposition of such one-ion potential energies; there are then six regions near the oxygen nuclei where the potential energy is negative; the average potential energy, found in the same way as before, can again be either positive or negative. The theoretical formula (13) for $Q$ clearly is closely related to the average potential energy discussed above; it differs essentially in that it involves $V_4(r)$ instead of $V(\mathbf{r})$ and only the radial part of the wave function in the expectation value. Figure 2, which will be discussed in more detail later, illustrates how $V_4(r)$ assumes both positive and negative values and how the sign of $Q$ depends on the radial wave function.

## 2. MODEL FOR THE $Cr \cdot 6H_2O^{+++}$ COMPLEX

We here discuss the model used in the evaluation of $Q$ of Eq. (13). For the $Cr^{+++}$ $3d$ radial wave function $r^{-1}P(r)$ we choose the Hartree (without exchange) free $Cr^{++}$ $3d$ function of Mooney.[19] Each water molecule of the $Cr \cdot 6H_2O^{+++}$ complex is assumed to consist of a spherically symmetrical $O^{--}$ ion whose center is on a coordinate axis a distance $R$ from the origin together with two hydrogens the positions and effects of which will be considered presently. The potential energy of an electron in the field of one of the $O^{--}$ ions is given in atomic units (unit of energy $= 109737$ cm$^{-1}$) by

$$U(t) = 2 \cdot 2t^{-1}$$
$$-2 \cdot \tfrac{1}{3} e^{-at}(a^3t^2 + 6a^2t + 18a + 24t^{-1}), \qquad (2)$$

where $t$ is the distance from the oxygen nucleus, and $a = 3.85$. $U(t)$ is obtained by integrating Poisson's equation in which the charge density corresponds to $O^{--}$ wave functions approximated by the atomic shielding constant method of Slater.[20] The first line of (2) is the potential energy of a point charge equal to the total charge ($-2e$ esu) of the $O^{--}$ ion. The second line of Eq. (2) is associated with the fact that the $n=2$ shell $2s^22p^6$ of $O^{--}$ is a distributed charge; if it were somehow concentrated at the oxygen nucleus, the second line would be absent. The similar contribution[21] to (2) from the $n=1$ shell of $O^{--}$ is suppressed; the charge of the $n=1$ shell is concentrated sufficiently close to the oxygen

desirable. An elucidation of the phase transformation occurring in $NH_4Cr(SO_4)_2 \cdot 12H_2O$ at 80°K would be of particular interest, since the optical and microwave absorption spectra have been investigated, and an anomaly found in the latter. See references 13 and 15; A. F. Kip (private communication).

[19] R. L. Mooney, Phys. Rev. **55**, 557 (1939).

[20] J. C. Slater, Phys. Rev. **36** (2), 57 (1930). By comparing a Slater function for $O^-$ with the corresponding free ion Hartree function (with exchange), we are led to expect that the Slater function for $O^{--}$ decreases more rapidly with $r$ at large $r$ than would the corresponding Hartree function, if it were available.

[21] The contribution to (2) from the $n=1$ shell $1s^2$ of $O^{--}$ is $-2e^{-at}(a-2t^{-1})$ where $a=14.4$.

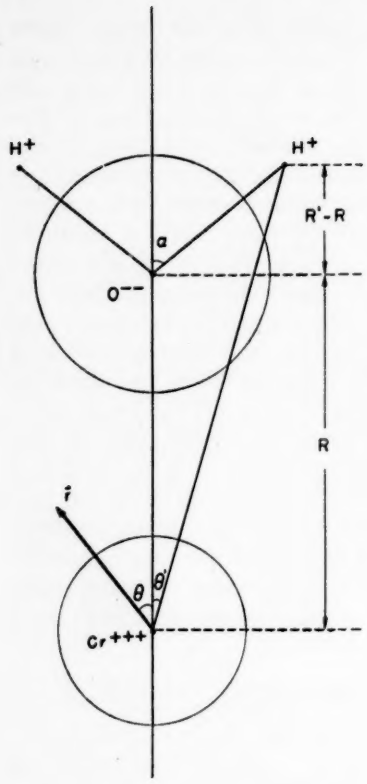


FIG. 1. Nuclear configuration of a free water molecule ($2\alpha=105°$, $R'-R=1.10$ atomic units). The water molecule is shown oriented with respect to a $Cr^{+++}$ ion as expected in the $Cr\cdot 6H_2O^{+++}$ complex. In aluminum alums $R=3.73$.

nucleus so that the effect of this contribution may be neglected in the evaluation of $Q$. The potential energy of the octahedron of $O^{--}$ ions is then obtained by a spacial sum of potential energies of the type (2).

Now let us consider the hydrogen part of a water molecule. The nuclear configuration[22] of a free water molecule is shown in Fig. 1; the experimentally determined parameters are given in the caption. In order to maintain the cubic symmetry of the crystalline potential energy, we represent the hydrogens by a uniform ring charge obtained by averaging the proton charge $2e$ of Fig. 1 about the $H_2O-Cr^{+++}$ axis. The plane of the ring charge is $R'-R$ distant from the $O^{--}$ center. The dipole moment of a water molecule depends only on $R'-R$, and is assumed to point radially outward, since the electric field of the $Cr^{+++}$ ion tends to orient it this way. The potential energy due to the hydrogens of the $Cr\cdot 6H_2O^{+++}$ complex is then represented by the potential energy of an octahedron of such ring charges.

### 3. DERIVATION OF THE FORMULA FOR $Q$

In this section a derivation of (13) for $Q$ is outlined. The Hamiltonian $\mathcal{H}_0$ for the motion of the electrons of the free $Cr^{+++}$ ion is perturbed by the addition of

$$\mathcal{H}_1=\sum_j V(\mathbf{r}_j), \tag{3}$$

when the free ion is placed in the center of the octahedron of water molecules to form the $Cr\cdot 6H_2O^{+++}$ complex. The subscript $j$ denotes the $j$th electron, and the summation is over the 21 electrons of $Cr^{+++}$. $V(\mathbf{r})$, the crystalline potential energy, is the electrostatic potential energy of an electron at the point $\mathbf{r}$ in the field of the octahedron of water molecules, and may be expanded as

$$V(\mathbf{r})=\sum_{k=0}^{\infty} V_k(r)S_k(\theta,\phi), \tag{4}$$

where the $S_k(\theta,\phi)$ are spherical harmonics having cubic symmetry. $S_k=0$ for $k$ odd and $k=2$. We choose[23] $S_0=1$ and

$$S_4=Y_4^0+(5/14)^{\frac{1}{2}}(Y_4^4+Y_4^{-4}) =(15/4\pi^{\frac{1}{2}})r^{-4}(x^4+y^4+z^4-(3/5)r^4). \tag{5}$$

$\mathcal{H}_1$ may be expanded analogously,

$$\mathcal{H}_1=\sum_{k=0}^{\infty}\mathcal{H}_{1k}, \quad \text{where} \quad \mathcal{H}_{1k}=\sum_j V_k(r_j)S_k(\theta_j,\phi_j). \tag{6}$$

An eigenfunction $\Psi^{(0)}$ of the unperturbed Hamiltonian $\mathcal{H}_0$ is expanded[24] as a linear combination of determinants of order 21 whose elements are normalized one-electron wave functions of the form

$$r^{-1}R_{nl}(r)Y_l^{m_l}(\theta,\phi)\chi_{m_s}(\sigma) \tag{7}$$

depending on both space and spin coordinates and on the quantum numbers[25] $nlm_lm_s$. Nuclear terms, except the nuclear Coulomb energy $-\sum_j Ze^2/r_j$, and relativistic terms, including energies associated with electron spin, are neglected in $\mathcal{H}_0$, since they lead only to fine structure effects. $\mathcal{H}_0$ then commutes with the total orbital and total spin angular momenta $\mathbf{L}=\sum_j \mathbf{l}_j$ and $\mathbf{S}=\sum_j \mathbf{s}_j$, and each $\Psi^{(0)}$ may be labeled by the set of quantum numbers[26] $LSM_LM_S$.

To solve the problem of the ion in the crystalline field, the matrix

$$(\epsilon' L'S'M_L'M_S'|\mathcal{H}_0+\mathcal{H}_1|\epsilon LSM_LM_S) \tag{8}$$

must be diagonalized. $\epsilon$ and $\epsilon'$ are eigenvalues of $\mathcal{H}_0$. Each element of the matrix

$$(\epsilon' L'S'M_L'M_S'|\mathcal{H}_1|\epsilon LSM_LM_S) \tag{9}$$

can be expressed as a linear combination of one-electron matrix elements of the type

$$(n'l'm_l'm_s'|V(\mathbf{r})|nlm_lm_s). \tag{10}$$

In the expansion of each $\Psi^{(0)}$ each coefficient depends on the configuration of its determinant. For free $Cr^{+++}$ the expansion is assumed (see Appendix 1) to converge

[22] N. V. Sidgwick, *The Chemical Elements and Their Compounds* (Oxford University Press, London, 1950), Vol. II, p. 864.

[23] The $Y_l^m(\theta,\phi)=\Theta_l^m(\theta)\Phi_m(\phi)$ are the usual normalized spherical harmonics, angular parts of solutions of Schrödinger's equation for one electron in a central field. See, e.g., E. U. Condon and G. H. Shortley, *The Theory of Atomic Spectra* (Cambridge University Press, Cambridge, 1951), p. 50.

[24] D. R. Hartree, Reports of Progress in Physics **11**, 113 (1946–1947).

[25] See reference 23, Chapter 6.

[26] See reference 23, Chapter 7.

rapidly enough so that the configurations higher than the ground configuration $3d^3$ may be neglected when only states near the ground state are of interest, as here. The diagonalization of (8) has been carried out in this one-configuration approximation by Finkelstein and Van Vleck[27] with a special assumption for the crystalline field in connection with the theory of the optical Zeeman effect in chrome alum.[3] In this approximation the core ($1s^2 2s^2 2p^6 3s^2 3p^6$) contribution and the $\mathcal{H}_{10}$ contribution to (9) may be regarded as having the trivial effect of displacing the origin of energy for the energy levels of the free ion. The remaining contribution to (9) comes from the $3d$ electrons outside the core and involves only matrix elements of the type (10) with $n'=n=3$ and $l'=l=2$. When (4) is introduced into (10), terms associated with $k>4$ vanish on account of selection rules[28] for angular momenta.

Thus, in the one-configuration approximation, (9) may be replaced by the matrix

$$(\epsilon' L' S' M_L' M_S' | \mathcal{H}_{14} | \epsilon L S M_L M_S) \tag{11}$$

in which the core contributions, which, incidentally, vanish in this particular case, are neglected. The matrix elements of (11) may be expressed as a linear combination of elements of the matrix

$$(32 m_l' m_s' | V_4(r) S_4(\theta, \phi) | 32 m_l m_s) = 14\pi^{\frac{1}{2}} (2 m_l' | S_4(\theta, \phi) | 2 m_l) \delta_{m_s' m_s} Q. \tag{12}$$

The nonvanishing elements of the matrix

$$14\pi^{\frac{1}{2}} (2 m_l' | S_4(\theta, \phi) | 2 m_l)$$

are 5 for $m_l' = -m_l = \pm 2$ and 1, $-4$, and 6 for the diagonal elements $m_l = \pm 2$, $\pm 1$, and 0, respectively, and we have

$$Q = (14\pi^{\frac{1}{2}})^{-1} \int_0^\infty P^2(r) V_4(r) dr, \tag{13}$$

where $r^{-1}P(r) = r^{-1}R_{32}(r)$ is a normalized $3d$ radial wave function for $Cr^{+++}$. From (12) it is evident that each term of an element of (11) has $Q$ as a factor, so that in the one-configuration approximation the matrix (11) and, effectively, the matrix (9) have $Q$ as a factor. $Q$ may be interpreted as a measure of the interaction between the $Cr^{+++}$ ion and the crystalline field.

For

$$V_4(r) = (4\pi^{\frac{1}{2}}/15) r^4 D \tag{14}$$

with $D$ a constant, the special case assumed by Finkelstein and Van Vleck,[27] (13) reduces to

$$Q = D(2/105) \int_0^\infty P^2(r) r^4 dr \tag{15}$$

which is $Dq$ in their notation, and which is the empirically determined constant in the paramagnetic susceptibility theory of Schlapp and Penney.[9] The assumption (14), as may be seen from (5), corresponds to a crystalline potential energy with the $k=4$ component $D(x^4+y^4+z^4 - (3/5)r^4)$ having its source at infinite distance and having a vanishing Laplacian.

[27] R. Finkelstein and J. H. Van Vleck, J. Chem. Phys. **8**, 790 (1940).

[28] See, e.g., reference 23, p. 176.

### 4. THE CALCULATION

Using the model of the $Cr \cdot 6H_2O^{+++}$ complex of Sec. 2 we evaluate $Q$ defined by (13). From the model of the octahedron of water molecules described in Sec. 2, $V(\mathbf{r})$ of (4) is given by

$$V(\mathbf{r}) = V^{O^{--}}(\mathbf{r}) + V^H(\mathbf{r}) \tag{16}$$

where, from (2), the potential energy due to the $O^{--}$ ions is, in atomic units

$$V^{O^{--}}(\mathbf{r}) = \sum_{i=1}^{6} U(|\mathbf{r} - \mathbf{r}_i|) \tag{17}$$

and $V^H(\mathbf{r})$ is the potential energy due to the octahedron of ring charges representing the protons. The $\mathbf{r}_i$, $i=1, 2, \cdots, 6$, denote the positions of the oxygen centers and the $\mathbf{r}_i'$, which will be used presently, denote the projections of the ring charges on the corresponding $Cr^{+++}-O^{--}$ axes; $|\mathbf{r}| = R$, $|\mathbf{r}'| = R'$. The $V_4(r)$ associated with (16) is

$$V_4(r) = V_4^{O^{--}}(r) + V_4^H(r) \tag{18}$$

where

$$(14\pi^{\frac{1}{2}})^{-1} V_4^H(r) = -2 \cdot \tfrac{1}{3} \cos^4\theta' (1 - 3\tan^2\theta' + \tfrac{3}{8}\tan^4\theta') f(r, R' \sec\theta') \tag{19}$$

with $f(r, r') = (r^4/r'^5)$ for $r<r'$ and $(r'^4/r^5)$ for $r>r'$. The meaning of $\theta'$ is shown in Fig. 1. (19) can be derived by using the Legendre polynomial expansion theorem for $|\mathbf{r} - \mathbf{r}'|^{-1}$. When the ring charges are projected into an octahedron of point charges, (19) reduces to $(14\pi^{\frac{1}{2}})^{-1} V_4^H(r) = -2 \cdot \frac{1}{3} f(r, R')$. There is a similar term $+2 \cdot \frac{1}{3} f(r, R)$ in $(14\pi^{\frac{1}{2}})^{-1} V_4^{O^{--}}(r)$ corresponding to the first line in (2). The two terms together may be interpreted as a finite point dipole, the remaining part of $(14\pi^{\frac{1}{2}})^{-1} V_4^{O^{--}}(r)$ acting as a "correction" associated with the $O^{--}$ negative charge being a distributed instead of a point charge. This latter part, associated with the second line in (2), has a complicated form which is of no particular physical interest, and will not be given here[29] explicitly.

In order to evaluate analytically the integrals involved in (13), the Mooney $3d$ function $P(r)$ was

[29] From (17) and (2) one sees that expansions about $\mathbf{r}=0$ in terms of Legendre polynomials are required for functions of the type $|\mathbf{r} - \mathbf{r}'|^{N-1} \exp -a|\mathbf{r} - \mathbf{r}'|$, $N=0$, 1, 2, and 3. The radial coefficients in these expansions for $N \neq 0$ may be obtained from the $N=0$ expansion given by G. N. Watson, *A Treatise of the Theory of Bessel Functions* (The Macmillan Company, New York, 1945), second edition, Sec. 11.41, Eq. (11). See also C. A. Coulson, Proc. Cambridge Phil. Soc. **33**, 104 (1937); these coefficients involve Bessel and Hankel functions of imaginary argument and half-odd integer order.

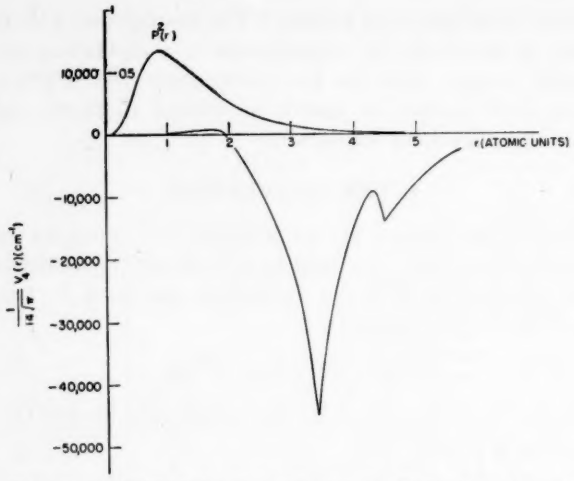


FIG. 2. $(1/14\pi^{\frac{1}{2}})^{-1}V_4(r)$ *vs* $r$. The $O^{--}-Cr^{+++}$ internuclear distance here is 3.4 atomic units. The protons are represented by a single point charge $2e$ a distance 1.10 atomic units farther out corresponding to the free molecule nuclear configuration. $P^2(r)$ of the $Cr^{++}$ $3d$ radial wave function of Mooney (see reference 19) is also plotted.

expressed analytically[30] in atomic units as

$$r^{-3}P(r)=49.26e^{-5.576r}+7.198e^{-2.795r}+0.7989e^{-1.540r} \quad (20)$$

where the normalization is $\int_0^\infty P^2(r)dr=1$. $P(r)$ of (20) differs from Mooney's function (when normalized) by less than 1 percent for $r>0.3$, the domain of importance for the evaluation of $Q$. Although the computation was done analytically,[31] in retrospect it appears to the author that it might have been accomplished more simply using primarily numerical methods.[32]

## 5. RESULTS AND DISCUSSION

The calculation yields $Q=-550$ cm$^{-1}$ when the parameters are chosen as in Fig. 1 as compared with the experimental value $1000<Q_{\text{exp}}<2000$ cm$^{-1}$. When $Q$ is regarded as composed of contributions from a finite dipole and from a correction charge (see Sec. 4), the former contributes 1000 cm$^{-1}$, the latter $-1500$ cm$^{-1}$. As the chromium-oxygen internuclear distance $R$ is increased with $R'-R$ kept constant, the magnitude of each of these contributions decreases, the latter more rapidly, thus increasing $Q$; on the other hand, since the only positive contribution is decreasing, one cannot hope to obtain agreement with $Q_{\text{exp}}$. If one were justified in neglecting the large correction contribution,[33] the calculated $Q$, corresponding to a water molecule in the $Cr\cdot 6H_2O^{+++}$ complex with a dipole moment three times as large as the free molecule moment $1.86\times10^{-18}$ esu, would agree well with the lower limit of $Q_{\text{exp}}$. $Q$ could be even further improved[34] by increasing the dipole moment even more, although $Q$ is not nearly so sensitive to the positions of the hydrogens as it is to the distribution of the ten electrons of the water molecule. The increase of the dipole moment of $H_2O$ in the complex is consistent with what one expects from a consideration of the structure of the complex based simply on electrostatic interaction among the parts of the complex; this will be discussed presently. Figure 2 shows a plot of $(14\pi^{\frac{1}{2}})^{-1}V_4(r)$. Near the chromium nucleus $V(\mathbf{r})$ approximately satisfies Laplace's equation so that in that region $V_4(r)$, given by (14), is proportional to $r^4$, and is small for small values of $r$; at greater distances from the chromium nucleus, where $r^4$ becomes appreciable, $V(\mathbf{r})$ no longer satisfies Laplace's equation even approximately.

One may ask whether the poor agreement found between the calculated $Q$ and $Q_{\text{exp}}$ comes from a poor choice of a model for the surroundings of the $Cr^{+++}$ ion. To answer this let us first consider whether our model is reasonable from an electrostatic viewpoint,[35] and then let us see what sort of changes in the model lead to agreement between the calculated $Q$ and $Q_{\text{exp}}$.

Although the nuclear configuration of our model, the water molecule of Fig. 1, is that of a free molecule, the dipole moment is three times too large. Thus, distributing the ten electrons about the oxygen nucleus so as to have spherical symmetry makes a poor model for a free molecule, the polarizing effect of the protons having been neglected. On the other hand, in the $Cr\cdot 6H_2O^{+++}$ complex the $Cr^{+++}$ polarizes the waters so as to increase their dipole moments. In fact, the electric field of the $Cr^{+++}$ at an oxygen nucleus approximately cancels the electric field of the protons of the corresponding water molecule, so that at least within a certain volume around the oxygen nucleus, one may expect roughly a spherical electron distribution in accordance with our model.

The $Cr^{+++}$ also repels the protons, tending to further increase the dipole moment. However, the remaining five water molecules exert an electric field on the sixth which tends to decrease the dipole moment. This field is roughly proportional to the dipole moment and thus provides an equilibrium mechanism for the polarization of the water molecules. Unfortunately, the positions of the nuclei, particularly the protons, are not known from diffraction study, even for the homologous aluminum alums (see reference 16), so that one cannot be very sure about the electric field near an oxygen due to the $Cr^{+++}$ ion, the protons, the other

[30] J. C. Slater, Phys. Rev. **42**, 33 (1932).

[31] Methods of the type used in the computation are discussed by M. P. Barnett and C. A. Coulson, Trans. Roy. Soc. (London) **243A**, 221 (1952).

[32] S. O. Lundquist and P. O. Löwdin, Arkiv. Fysik **3**, 147 (1951).

[33] In a similar calculation Van Vleck, reference 12, p. 81, found that the free water molecule dipole moment yielded a $Q$ in good agreement with $Q_{\text{exp}}$. This calculation differs from the one above in that besides omitting the correction contribution, the dipole is assumed to be a point dipole, the form of $V_4(r)$ is not changed at $r=R$, and the $3d$ wave function is for $Ti^{+++}$ rather than for $Cr^{+++}$. A hydrogenic $3d$ function with effective nuclear charge 6.39 yields the same expectation value of $r^4$ as does the Mooney $3d$ function for $Cr^{++}$.

[34] Increasing $\alpha$ (see Fig. 1) keeping $R$ and $R'$ fixed corresponds to a change in the model of the water molecule which increases $Q$.

[35] Before the advent of quantum mechanics the theory of molecular structure was based largely on electrostatics (see, e.g., P. Debye, *Polar Molecules* (Dover Publications, New York, 1945), and references contained therein) and achieved a certain amount of success. Its relative simplicity makes it still useful for obtaining insight into molecular problems.

waters, and the surroundings of the complex. Nevertheless, our model is much more reasonable in the complex than for a free water molecule.

For the $V_4(r)$ of Fig. 2 it would be possible, according to (13), to obtain a $Q$ in fair agreement with $Q_{exp}$ if the $Cr^{+++}$ $3d$ function $P(r)$ were suitably but arbitrarily chosen (an extreme example would be a $\delta$-function at the point where $(14\pi^{\frac{1}{2}})^{-1}V_4(r)$ has its maximum value). $P^2(r)$ for the Mooney function is also plotted in Fig. 2. The corresponding integrand of (13) is shown in Fig. 3. It is clear how the negative contribution in the vicinity of the oxygen nucleus causes the violent disagreement between the resulting calculated $Q$ and the $Q_{exp}$. The situation might be partly remedied by arbitrarily requiring $P(r)$ to vanish for $r>2.0$, so as to eliminate the negative contribution; at the same time $P^2(r)$ would be increased about 20 percent in the region $0<r<2.0$ because of the new normalization. A perturbed $3d$ function of the required sort could conceivably arise as a molecular orbital when the detailed interaction between the chromium ion and the waters is taken into account, for one would expect the Pauli exclusion principle to keep chromium electrons out of the oxygen closed shells. Even with a function of this sort, $Q$ would be less than 200 $cm^{-1}$. The closer one comes to the chromium nucleus the less one expects the chromium wave functions to be changed from the free ion functions by an external influence. In particular, the form of the $3d$ wave function will not be changed appreciably for $r<1.25$, and $\int_0^{1.25} P^2(r)dr$ is already 0.5, so that any reasonable perturbed $3d$ orbital will be inadequate to obtain agreement with $Q_{exp}$; we are thus justified in using Mooney's $3d$ function for $Cr^{++}$ instead of a corresponding Hartree function for $Cr^{+++}$.

Let us see if we can obtain agreement by altering the $O^{--}$ electron distribution from the previously assumed spherical distribution. The positive part of $(14\pi^{\frac{1}{2}})^{-1}V_4(r)$, and consequently the integrand of (13), can be increased by concentrating more oxygen negative charge nearer the chromium nucleus. One may expect this physically since the charge $3e$ of the $Cr^{+++}$ ion attracts an oxygen electron more, relative to the opposite proton attraction, the closer the latter comes to the chromium ion, at least until it penetrates the shells of the chromium ion where the exclusion principle operates. A crude estimate of this obtained by calculating the effect on $(14\pi^{\frac{1}{2}})^{-1}V_4(r)$ of moving the oxygen nucleus and $1s^2$ shell together toward the protons as much as 0.3 a.u. indicates that we cannot expect the integral of the positive part of the integrand of (13) to be more than about 750 $cm^{-1}$. Such a displacement, associated with a polarization of the $O^{--}$ ion, yields an additional contribution to the water molecule dipole moment.

It thus appears that no reasonable change of the model of the surroundings of the $Cr^{+++}$ ion in the complex will yield a satisfactory $Q$, and that even a fairly arbitrary alteration of the $Cr^{+++}$ $3d$ radial wave function doesn't eliminate the discrepancy. The implication that the crystalline field approximation is inadequate for obtaining detailed agreement with magnetic susceptibility data in chrome alum may be extended. One may expect that the crystalline field approximation will also be inadequate for obtaining detailed agreement with observed microwave and optical absorption spectra in chrome alum, and that the same is true for other paramagnetic salts in the iron group in which the paramagnetic ions have surroundings similar to those in chrome alum.‡

$Q$ for the $Ni^{++}$ ion in the $Ni\cdot 6H_2O^{++}$ octahedral complex analogous to the $Cr\cdot 6H_2O^{+++}$ complex is also given by (13), assuming the one-configuration approximation (see Sec. 3) is valid. The $Ni^{++}$ free ion $3d$ Hartree radial wave function is more compact than the corresponding $Cr^{+++}$ function. The nickel-oxygen internuclear distance[36] $R$ in $NiSO_4\cdot 6H_2O$, e.g., is the same within 5 percent as the chromium-oxygen internuclear distance in the alum. The arguments and conclusions about the crystalline field approximation carry through for the $Ni\cdot 6H_2O^{++}$ complex as for the $Cr\cdot 6H_2O^{+++}$ complex. For $NiSO_4\cdot 6H_2O$, $Q_{exp}=1328$ $cm^{-1}$, and the susceptibility measurement[37] appears to be of high precision, so that the lack of precise experimental determinations of $Q$ for the $Cr^{+++}$ ion in a hydrated salt does not represent a weak point in the evidence for the inapplicability of the crystalline field approximation in the iron group.

That the theory of paramagnetism based on the crystalline field approximation gives good agreement with experiment when the parameters such a $Q$ are fixed experimentally, but appears to give such poor agreement when one attempts to refine the theory on the basis of a

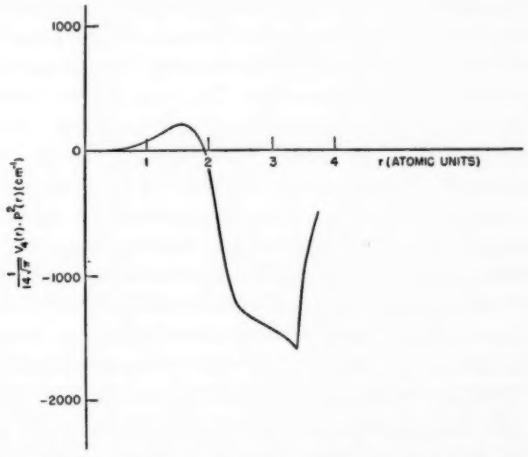


FIG. 3. $(1/14\pi^{\frac{1}{2}})^{-1}V_4(r)\cdot P^2(r)$ *vs* $r$, where $r^{-1}P(r)$ is the $Cr^{++}$ $3d$ radial wave function of Mooney (see reference 19).

‡ G. H. Wannier, private communication. Dr. Wannier proposes that an explanation of the large hyperfine splitting in the microwave absorption spectra of certain hydrated iron group salts may be given more naturally in terms of contributions from electrons wandering into the paramagnetic ion from other parts of the complex than in terms of the ground states of the free ion being simply perturbed by a crystalline field of cubic symmetry, as proposed by Abragam, see reference 5. Wannier's proposal is consistent with our conclusion about the inadequacy of the crystalline field approximation.

[36] R. W. G. Wyckoff, *Crystal Structures* (Interscience Publishers, Inc., New York, 1951), Vol. II, (X, f 14).

[37] K. S. Krishnan and A. Mookherji, Trans. Roy. Soc. (London) **237A**, 135 (1938).

crystalline field, suggests that the crystalline field approximation contains aspects in common with a more satisfactory foundation for the theory. It suggests that the usual form of the theory of paramagnetism based on a crystalline field and having undetermined parameters depends essentially only on the symmetry of the surroundings of the ion, which symmetry is, indeed, embodied in the crystalline field. If this is true, one may ask when it is valid to use the crystalline field to study properties other than those depending purely on symmetry. The answer to this question may be expected within the larger framework of molecular theory in which a $Cr^{+++}$ electron interacts with the $O^{--}$ electrons individually instead of as a group represented by a static charge distribution. In a molecular treatment integrals other than $Q$, which are neglected in the crystalline field approximation, may be expected to be important.

The author is deeply indebted to Professor J. C. Slater for directing this research and for many stimulating discussions. A large part of the numerical computation was performed by Mrs. Patricia Halpern.

## APPENDIX

### 1. Effects of Higher Configurations

The effect of configurations higher than the ground $3d^3$ configurations of free $Cr^{+++}$ is neglected in the derivation of (13). The ground level which results when the crystalline field is applied (spin interactions being neglected) is a $^4\Gamma_2$ (notation of Bethe) arising from the ground term $^4F$ of the free ion, the only $^4\Gamma_2$ arising from terms of the $3d^3$ configuration. The next higher term of the free ion which is connected by nonvanishing matrix elements of the perturbed Hamiltonian $\mathcal{H}_0+\mathcal{H}_1$ (see Sec. 3) with the ground $^4\Gamma_2$ is the $3d^2(^3F)4s\ ^4F$, some $10^5$ $cm^{-1}$ above the $3d^3\ ^4F$. Other configurations with the parent $3d^2(^3F)$ are at least as high. Promoting another $3d$ electron requires considerably more energy. The splittings and displacements of terms within the $3d^3$ configuration which result when the crystalline field is applied are of the order of $10^4$ $cm^{-1}$,[27] corresponding to $Q=1500$ $cm^{-1}$. Although the multiplet structure within the $3d^3$ configuration is well-destroyed, one may still expect that higher configurations, such as the $3d^2(^3F)4s$, will have only a second-order effect on the $3d^3$ configuration, particularly on the ground level.

The same approximation of neglecting effects from configurations higher than the $3d^3$ configuration is made in the derivation of (1). In this derivation second-order perturbation contributions to the energy of the ground $^4\Gamma_2$ arise from the cross terms in the square of the matrix elements of the magnetic energy $\beta\mathbf{H}\cdot(\mathbf{L}+2\mathbf{S})$ plus other energies, such as the spin-orbit interaction energy; the cross terms vanish whenever the matrix element of the magnetic energy alone vanishes, thus in particular, whenever the matrix element is nondiagonal in $L$ or $S$.

### 2. Fine Structure Effects

Terms in the Hamiltonian involving spin and the noncubic component of the crystalline potential energy split the ground level $^4\Gamma_2$ of the $Cr^{+++}$ ion in the $Cr\cdot 6H_2O^{+++}$ complex in the absence of an external magnetic field.[5] These terms do not alter (1) provided the matrix of the Hamiltonian effective in the $2S+1$ dimensional spin manifold of this level has a vanishing trace. For example, the effective Hamiltonian $-(\delta/2)[S_z^2-\frac{1}{3}S(S+1)]$, corresponding to a splitting $\delta$ arising from a small noncubic (axial) crystalline potential energy together with the spin-orbit interaction energy, has a vanishing trace.

The $^4\Gamma_2$ splits into four levels when a magnetic field is applied. When the splitting $\delta$ is present, these have a complicated dependence on the magnitude and direction of the magnetic field, as observed in microwave absorption spectra.[14,15] This complication is reflected in the magnetic susceptibility only at sufficiently low temperature where (1) is no longer valid.

### 3. Spin-Orbit Coupling Parameter $\lambda$

We give here arguments for the validity of assuming that the dependence of the spin-orbit coupling parameter $\lambda$ on the crystalline field is negligible. If it were not, values of $Q$ derived from (1) would not be reliable unless the dependence of $\lambda$ on the crystalline field were known.

The form $\lambda\mathbf{L}\cdot\mathbf{S}$ is not a rigorous expression for the spin-orbit interaction energy. However, if one neglects the value of the commutator§ $[\mathbf{P}_{ij}, \mathbf{L}]$, where $\mathbf{P}_{ij}$, given in Gaussian units by

$$\mathbf{P}_{ij}=(2m^2c^2)^{-1}\nabla_i W(\mathbf{r}_i)\times\mathbf{p}_i\delta_{ij}+\mathbf{A}_{LSij}, \tag{A1}$$

enters in the spin-orbit interaction Hamiltonian[38]

$$\mathcal{H}_{LS}=\sum_{i,j}\mathbf{P}_{ij}\cdot\mathbf{s}_i, \tag{A2}$$

then $\mathcal{H}_{LS}$ may be expressed as

$$\mathcal{H}_{LS}=\lambda\mathbf{L}\cdot\mathbf{S} \tag{A3}$$

for matrix elements with respect to the eigenfunctions of $\mathcal{H}_0+\mathcal{H}_1$ (see Sec. 3) provided these eigenfunctions may be considered to arise from only one term of the free ion in the process of diagonalizing $\mathcal{H}_0+\mathcal{H}_1$; this provision is satisfied for the $^4\Gamma_2$ ground level of $Cr^{+++}$ in the $Cr\cdot 6H_2O^{+++}$ complex. The first term of (A1) is associated with the potential energy $W(\mathbf{r})$ of an electron arising from sources outside of the electron system, and $\mathbf{A}_{LSij}$ is associated with the mutual interaction among the electrons and satisfies $[\mathbf{A}_{LSij}, \mathbf{L}]=0$; $\mathbf{p}_i$ is the momentum, $\mathbf{s}_i$ the spin angular momentum of the $i$th electron. When (A3) holds, one can show that $\lambda$ may be associated with a contribution $\lambda_0$ valid for the free ion and a contribution $\lambda_1$ associated with the presence of the crystalline potential energy of cubic symmetry:

§ The commutator $[\mathbf{P}_{ij}, \mathbf{L}]$ vanishes identically in the case of the free ion.

[38] G. Breit, Phys. Rev. 34, 553 (1929).

$\lambda=\lambda_0+\lambda_1$, and that $\lambda_0/\lambda_1\sim10^{-4}$, showing that the free ion value of $\lambda_0$ determined from optical spectroscopic data is a good approximation to $\lambda$ for the $Cr^{+++}$ ion in the $Cr\cdot6H_2O^{+++}$ complex.

There is experimental evidence for the lack of dependence of $\lambda$ on the crystalline field. The fact that so many successes have been scored in the susceptibility theory using free ion $\lambda$ values lends general support to the assumption. More specifically, Krishnan, Mookherji, and Bose[39] deduce $\lambda=-330$ cm$^{-1}$ from the anisotropies of $NiSeO_4\cdot6H_2O$ measured at two temperatures by using Schlapp and Penney's susceptibility formula, compared to the spectroscopic value $\lambda=-335$ cm$^{-1}$.

[39] Krishnan, Mookherji, and Bose, Trans. Roy. Soc. (London) **238A**, 125 (1939). See also B. C. Guha, Proc. Roy. Soc. (London) **206A**, 365 (1951).

THE JOURNAL OF CHEMICAL PHYSICS VOLUME 20, NUMBER 11 NOVEMBER, 1952

# The Infrared Spectrum of $SO_2F_2$

W. D. PERKINS* AND M. KENT WILSON
*Mallinckrodt Chemical Laboratory, Harvard University, Cambridge, Massachusetts*

(Received June 30, 1952)

The infrared spectrum of sulfuryl fluoride has been investigated between 240 cm$^{-1}$ and 4000 cm$^{-1}$ with a prism spectrometer. Seven of the nine fundamentals have been observed and assigned to their appropriate symmetry species. Ten additional bands have been assigned as combinations or overtones. A partial force constant calculation has been made.

## INTRODUCTION

THE vibrational spectrum of the slightly aspherical top, sulfuryl fluoride, has not previously been reported. Both electron diffraction measurements[1] and the microwave spectrum[2] indicate that the molecule possesses $C_{2v}$ symmetry, but the microwave data yield a value for the S—O distance, $1.37_0\pm0.01$A, which is 0.06A shorter than that reported from the electron diffraction investigation. The value of 1.37A is the shortest S—O bond distance that has yet been reported. If this shortening of the S—O bond in $SO_2F_2$ is real and is taken as a consequence of an increase in importance of a triple bond resonance structure it is to be expected that the stretching force constant and the stretching frequency for the S—O bond will be larger in $SO_2F_2$ than in other sulfur oxygen compounds. The results of the present investigation indicate that this is the case.

## EXPERIMENTAL

Sulfuryl fluoride was prepared by passing a slow stream of $SO_2$ over $AgF_2$ at room temperature:[3]

$$SO_2+2AgF_2\rightarrow2AgF+SO_2F_2.$$

The product, collected in a trap cooled in liquid nitrogen, contained sulfur dioxide and silicon tetrafluoride as its chief impurities. The latter contaminant was removed by reaction with $H_2O$, while the $SO_2$ was removed by fractional distillation in vacuum at $-110$°C. These procedures were repeated until the infrared spectrum remained unchanged.

The infrared spectrum of the gas was observed between 400 cm$^{-1}$ and 4000 cm$^{-1}$ in 4.0 cm cells with a Perkin-Elmer Model 12C spectrometer equipped with $CaF_2$, NaCl, and KBr prisms. The region between 240 cm$^{-1}$ and 400 cm$^{-1}$ was investigated with a modified Perkin-Elmer Model 12B Spectrometer equipped with a thallium bromoiodide prism.[4]†

The observed spectrum from 240 cm$^{-1}$ to 4000 cm$^{-1}$ is presented in Fig. 1, while the positions of the absorption maxima and the observed P—R spacings are given in Table I.

## ASSIGNMENT OF FREQUENCIES

The general form of the nine normal vibrations for $SO_2F_2$ on the assumption of $C_{2v}$ symmetry is indicated in Fig. 2. The four totally symmetric ($A_1$) vibrations loosely may be described as bending and stretching motions involving the $SF_2$ and $SO_2$ subgroups. Species $A_2$ contains only the torsional vibration. The two modes of $B_1$ symmetry are the asymmetrical S—O stretch and a rocking motion. Species $B_2$ contains the asymmetrical S—F stretch and the remaining rocking vibration. Of these nine normal vibrations only the torsional mode is forbidden in the infrared. All first overtones are infrared active while only those binary combinations arising from $b_1\times b_2=A_2$ and $a_1\times a_2=A_2$ are forbidden in the *IR*. Since $SO_2F_2$ is very nearly a spherical top all of the bands show a well-defined *PQR* structure and, thus, band contour is no help in making the assignment.

On the basis of their relatively high intensities the bands at 1502, 1269, 885, 848, and those near 550 cm$^{-1}$ may be chosen as fundamentals. The band at 767 cm$^{-1}$, although less intense, cannot be explained in terms of

* Present address: Shell Oil Company, Inc., Martinez, California.
[1] D. P. Stevenson and H. Russell, J. Am. Chem. Soc. **61**, 3264 (1939).
[2] R. M. Fristrom, J. Chem. Phys. **20**, 1 (1952).
[3] H. J. Emeleus and J. F. Wood, J. Chem. Soc. 2183 (1948).
[4] Lord, MacDonald and Miller, J. Opt. Soc. Am. **42**, 149 (1952).
† The authors are indebted to Professor Richard C. Lord for making this instrument available.

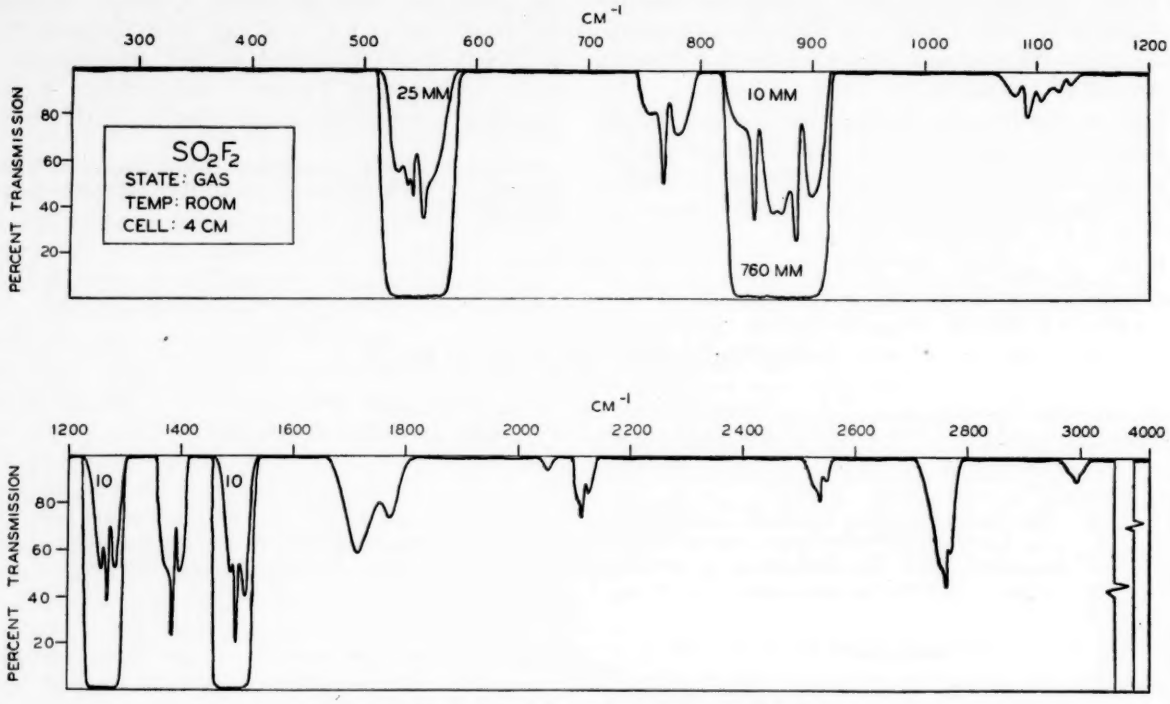


FIG. 1. The infrared absorption spectrum of $SO_2F_2$.

the foregoing frequencies, and so must be presumed to be either a fundamental or to contain an unobserved fundamental.

By comparison with the S—O stretching frequencies in $SO_2$ [5] and $SO_2Cl_2$ [6] the bands at 1269 $cm^{-1}$ and 1502 $cm^{-1}$ may be assigned to $\nu_1(A_1)$ and $\nu_6(B_1)$, respectively. From a consideration of the stretching frequencies in $SF_6$,[7] the bands at 885 $cm^{-1}$ and 848 $cm^{-1}$ must be assigned to the two S—F stretching motions, and by analogy with $SOF_2$ [8] where the $SF_2$ asymmetric stretch

TABLE I. Observed frequencies and band assignments for $SO_2F_2$.

| $\nu$ ($cm^{-1}$) | P—R spacing ($cm^{-1}$) | Assignment | $\Delta$[a] ($cm^{-1}$) |
|---|---|---|---|
| ([b]) | | $\nu_4(A_1)$ | |
| (385)[c] | | $\nu_5(A_2)$ | |
| 539 | | $\nu_9(B_2)$ | |
| 544 | | $\nu_3(A_1)$ | |
| 553 | | $\nu_7(B_1)$ | |
| 767 | 26 | $2\nu_5(A_1)$ | |
| 848 | 29 | $\nu_2(A_1)$ | |
| 885 | 26 | $\nu_8(B_2)$ | |
| 1091 | | $2\nu_3(A_1)$ or $\nu_3+\nu_7(B_1)$ | |
| 1269 | 26 | $\nu_1(A_1)$ | |
| 1389 | 19 | $\nu_2+\nu_3(A_1)$ or $\nu_3+\nu_7(B_1)$ | 3 or 2 |
| 1502 | 26 | $\nu_6(B_1)$ | |
| 1716[d] | | $2\nu_2(A_1)$ or $\nu_2+\nu_8(B_2)$ | |
| 1772 | | $2\nu_5(A_1)$ | 2 |
| 2051 | | $\nu_3+\nu_6(B_1)$ or $\nu_6+\nu_7(A_1)$ | 3 or 10 |
| 2115 | 31 | $\nu_1+\nu_2(A_1)$ | 2 |
| 2536 | | $2\nu_1(A_1)$ | 2 |
| 2762 | | $\nu_1+\nu_6(B_1)$ | 9 |
| 2993 | | $2\nu_6(A_1)$ | 11 |

[a] Difference between calculated and observed frequencies.
[b] Estimated to be near 300 $cm^{-1}$.
[c] Estimated from band at 767 $cm^{-1}$.
[d] Position less reliable than other bands as it is overlaid by water vapor.

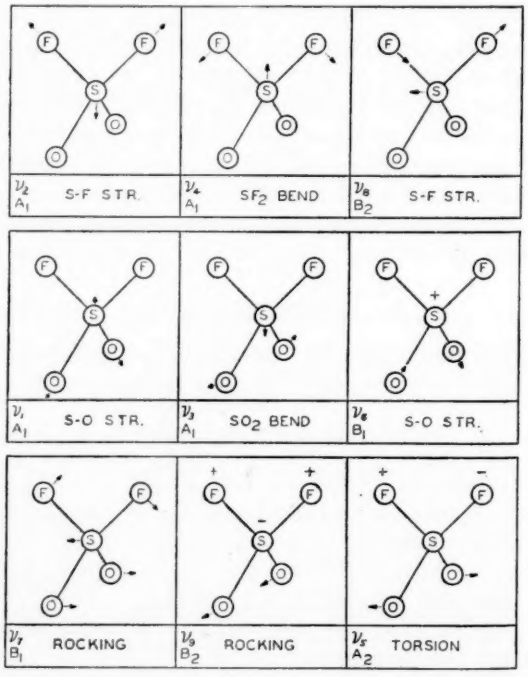


FIG. 2. The general form of the normal modes for $SO_2F_2$.

[5] G. Herzberg, *Infrared and Raman Spectra of Polyatomic Molecules* (D. Van Nostrand Company, Inc., New York, 1945).
[6] R. Vogel-Hogler, Acta Physica Austriaca **1**, 323 (1948).
[7] R. T. Langemann and E. A. Jones, J. Chem. Phys. **19**, 534 (1951).
[8] T. Wu, *Vibrational Spectra and Structure of Polyatomic Molecules* (J. W. Edwards, Ann Arbor, Michigan, 1946).

occurs at a higher frequency than the symmetric stretch, the 885 $cm^{-1}$ band is assigned as $\nu_8(B_2)$ and the band at 848 $cm^{-1}$ as $\nu_2(A_1)$.

This leaves yet unassigned the two bending modes, the two rocking modes, and the torsional vibration, and available for assignment, the band at 767 $cm^{-1}$ and those near 550 $cm^{-1}$. Figure 3 is a reproduction of the original spectrometer record for this region, and in Fig. 4 these data are replotted as percent transmission. The latter figure suggests that there are three bands contributing to the observed absorption. The peak at 553 $cm^{-1}$ is obviously a $Q$ branch, and, in view of the shape of the other bands in the spectrum, the peaks at 539 $cm^{-1}$ and 544 $cm^{-1}$ seem too sharp to be explained as P or R branches. Furthermore, it is difficult to reconcile an interpretation based upon only two bands with the requirement that the P−R spacing be about 26 $cm^{-1}$ as observed for other bands of this molecule. Accordingly, in Fig. 4 there is suggested a possible resolution into three bands of the required shape and P−R spacing which, when added together, will reproduce the essential features of the observed absorption.

The close proximity of these three bands at once imposes severe limitations on the possible assignments which can be made, for in general three energy levels so close together would exhibit Fermi resonance[9] unless they belong to different symmetry species.

It can be shown that the triply degenerate $F_2$ vibrations of a tetrahedral molecule go over to $A_1+B_1+B_2$ for a molecule of $C_{2v}$ symmetry. Since $SO_2F_2$ is nearly

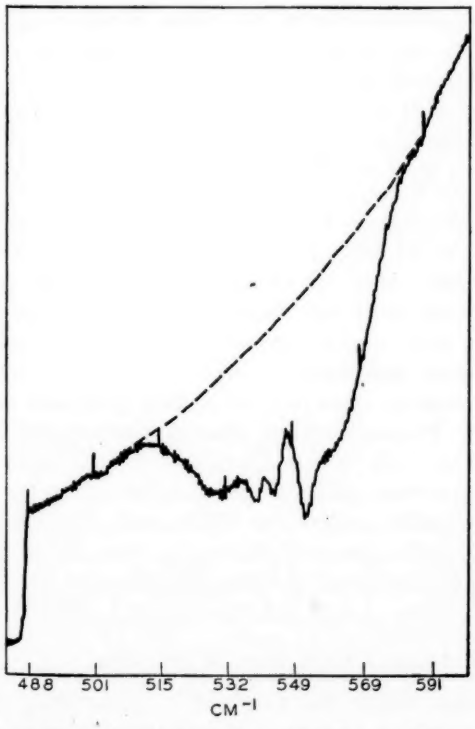


FIG. 3. The infrared absorption of $SO_2F_2$ near 550 $cm^{-1}$.

[9] See reference 5, pp. 215–217.

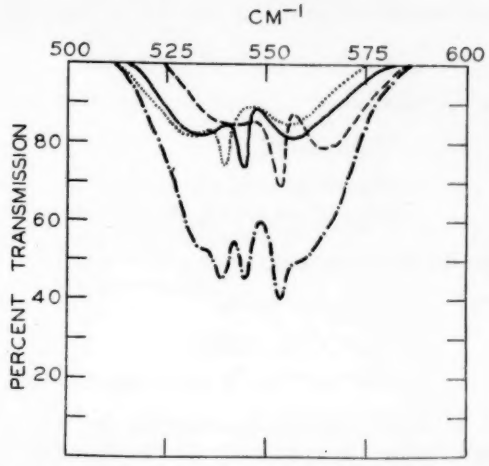


FIG. 4. Suggested resolution of the $SO_2F_2$ absorption near 550 $cm^{-1}$ into three bands. The data of Fig. 3 have been replotted as percent transmission.

tetrahedral in form, the splitting of these frequencies may be small. On this basis the absorption near 550 $cm^{-1}$ is assigned to three vibrations belonging to species $A_1$, $B_1$, and $B_2$. In molecules of similar symmetry the $B_1$, and $B_2$ vibrations are farthest apart and the $B_1$ vibration has the higher frequency. Therefore, a probable assignment is $\nu_9(B_2)=539$ $cm^{-1}$, $\nu_3(A_1)=544$ $cm^{-1}$, and $\nu_9(B_1)=553$ $cm^{-1}$.

The absorption at 767 $cm^{-1}$ cannot be explained as a combination or overtone band involving any of the frequencies thus far assigned and it is much too high in frequency to be the unobserved bending vibration, $\nu_4(A_1)$. Although the fundamental of the torsional frequency, $\nu_5(A_2)$, is forbidden in the infrared, the first overtone is allowed. The vibrations in $SO_2F_2$ occur at higher frequencies than the corresponding modes in $SO_2Cl_2$. Since the torsional frequency in $SO_2Cl_2$ occurs at 280 $cm^{-1}$, this vibration in $SO_2F_2$ may be estimated to lie between 300 and 400 $cm^{-1}$, probably closer to the higher value. It then seems reasonable to make the assignment: $\nu_5(A_2)\sim385$ $cm^{-1}$; $2\nu_5=767$ $cm^{-1}$. This leaves only $\nu_4(A_1)$ as unassigned. Since the fundamental of this vibration was not observed and it apparently does not occur as an overtone or combination band its frequency is undetermined. However, this vibration is the lowest fundamental in $CF_2Cl_2$ and $CF_2Br_2$ and on this basis may be assumed to be near 300 $cm^{-1}$ in $SO_2F_2$.

The complete interpretation of the observed spectrum in terms of the above assignment is contained in Table I.

## CALCULATION OF FORCE CONSTANTS

Force constants have been calculated for the $A_2$, $B_1$, and $B_2$ species using the $FG$ matrix method of Wilson[10] and the most general potential function. Because of the large number of matrix elements and the paucity of data from related molecules, no calculations were attempted for the $A_1$ species.

[10] E. B. Wilson, Jr., J. Chem. Phys. 7, 1047 (1939); 9, 76 (1941).

The $F$ matrix elements are, for the $A_2$ vibration,

$$F_{11}=f_\alpha-f_{\alpha\alpha}{}^d-f_{\alpha\alpha}{}^r-f_{\alpha\alpha}{}';$$

for the $B_1$ vibrations,

$$F_{11}=f_r-f_{rr}$$
$$F_{12}=\sqrt{2}(f_{r\alpha}-f_{r\alpha}{}')$$
$$F_{22}=f_\alpha+f_{\alpha\alpha}{}^r-f_{\alpha\alpha}{}^d-f_{\alpha\alpha}{}';$$

and for the $B_2$ vibrations,

$$F_{11}=f_d-f_{dd}$$
$$F_{12}=\sqrt{2}(f_{d\alpha}-f_{d\alpha}{}')$$
$$F_{22}=f_\alpha+f_{\alpha\alpha}{}^d-f_{\alpha\alpha}{}^r-f_{\alpha\alpha}{}'.$$

The $G$ matrix elements, obtained by use of the Decius[11] Tables are as follows: for the $A_2$ vibration,

$$G_{11}=\frac{\mu_F}{d^2\sin^2\alpha}(1-\cos\theta)+\frac{\mu_0}{r^2\sin^2\alpha}(1-\cos\varphi);$$

for the $B_1$ vibrations,

$$G_{11}=\mu_O+\mu_S(1-\cos\theta),$$

$$G_{12}=\sqrt{2}\mu_S(1-\cos\theta)\left[\frac{\cos\alpha}{r\sin\alpha}-\frac{1}{d\sin\alpha}\right],$$

$$G_{22}=\frac{\mu_F}{d^2\sin^2\alpha}(1-\cos\theta)+\frac{\mu_O}{r^2\sin^2\alpha}(2\sin^2\alpha-[1-\cos\varphi])$$
$$+2\mu_S(1-\cos\theta)\left[\frac{\cos\alpha}{r\sin\alpha}-\frac{1}{d\sin\alpha}\right]^2;$$

and for the $B_2$ vibrations,

$$G_{11}=\mu_F+\mu_S(1-\cos\varphi),$$

$$G_{12}=\sqrt{2}\mu_S(1-\cos\varphi)\left[\frac{\cos\alpha}{d\sin\alpha}-\frac{1}{r\sin\alpha}\right],$$

$$G_{22}=\frac{\mu_O}{r^2\sin^2\alpha}(1-\cos\varphi)+\frac{\mu_F}{d^2\sin^2\alpha}(2\sin^2\alpha-[1-\cos\theta])$$
$$+2\mu_S(1-\cos\varphi)\left[\frac{\cos\alpha}{d\sin\alpha}-\frac{1}{r\sin\alpha}\right]^2.$$

In the above expressions $\mu_F$, $\mu_S$, and $\mu_O$ are the reciprocals of the masses of the F, S, and O atoms, respectively; $d$ is the S−F bond distance (1.57A), $r$ is the S−O bond distance (1.37A), $\alpha$ is the O−S−F angle (107°4′), $\varphi$ is the F−S−F bond angle (92°47′), and $\theta$ is the O−S−O bond angle (129°38′).[2]

The determinental equation for the $A_2$ species can be solved to yield a unique value for the $F$ element, but for both $B$ species the $F_{11}$ and $F_{22}$ matrix elements can be obtained only as a function of $F_{12}$. The choice of $F_{12}$ is somewhat arbitrary. Value of $F_{12}$ lower than 0.06 give imaginary solutions for $F_{11}$ and $F_{22}$ in the $B_2$ species, but for the $B_1$ species $F_{12}$ may be as low as −2.0 and still yield real values for $F_{11}$ and $F_{22}$. However, it is doubtful that $F_{12}$ could be negative for in the extensively investigated halomethanes a positive value for $F_{12}$ was always encountered.[12–14] Accordingly in Table II only positive values of $F_{12}$ are considered in calculating the elements of the $F$ matrices.

[11] J. C. Decius, J. Chem. Phys. **16**, 1025 (1948).

TABLE II. Numerical values of the $F$ matrix elements for $SO_2F_2$.[a]

| | | | |
|---|---|---|---|
| $A_2$ | | $F_{11}=1.14$ | |
| $B_1$ | $F_{12}$ | $F_{11}$ | $F_{22}$ |
| | 0.00 | 11.06 | 1.72 |
| | 0.25 | 11.41 | 1.67 |
| | 0.50 | 11.73 | 1.64 |
| | 0.75 | 12.03 | 1.62 |
| | 1.00 | 12.32 | 1.62 |
| $B_2$ | $F_{12}$ | $F_{11}$ | $F_{22}$ |
| | 0.00 | imag. | imag. |
| | 0.07[b] | 3.75 | 3.11 |
| | 0.25 | 4.64 | 2.52 |
| | 0.50 | 5.16 | 2.30 |
| | 0.75 | 5.55 | 2.20 |
| | 1.00 | 5.86 | 2.17 |

[a] The following units are employed: $F$=millidyne A. $F_{12}$=millidynes. $F_{11}$=millidynes/A. $F_{22}$=millidyne A.
[b] Values of $F_{12}$ less than 0.07 gave imaginary values for $F_{11}$ and $F_{22}$.

Because of the uncertainty in the value of the $F_{12}$ matrix elements for both the $B_1$ and $B_2$ species a definite value cannot be obtained for the S−O bond stretching constant. However, some information can be obtained from a consideration of the range of values given in Table II in conjunction with a comparison of the magnitude of the asymmetric S−O stretching frequencies in $SO_2$ and $SO_2F_2$. In $SO_2$ this frequency occurs at 1361 $cm^{-1}$,[5] while in $SO_2F_2$ it is increased to 1502 $cm^{-1}$. Also it is to be noted that even for small positive values of $F_{12}$ the $F_{11}$ element is greater than $11.0\times10^5$ dynes/cm as compared to $9.97\times10^5$ dynes/cm for $SO_2$.[15] These data must be considered at best only suggestive of an abnormally short S−O bond in $SO_2F_2$ and further conclusions as to the length of the S−O bond must await a more complete experimental treatment of $SO_2F_2$ and related molecules.

The authors wish to express their gratitude to Professor E. Bright Wilson, Jr., for his helpful discussions in connection with this problem and to Dr. Santiago R. Polo for setting up the $F$ and $G$ matrices and for many other helpful suggestions. We wish to thank the Mallinckrodt Chemical Works for financial assistance covering a portion of this investigation and the American Academy of Arts and Sciences for a grant-in-aid.

[12] J. C. Decius, J. Chem. Phys. **16**, 214 (1948).
[13] E. L. Pace, J. Chem. Phys. **18**, 881 (1950).
[14] Decker, Meister, and Cleveland, J. Chem. Phys. **19**, 784 (1951).
[15] See reference 5, p. 170.

# On the Solution of the Poisson-Boltzmann Equation with Application to the Theory of Thermal Explosions

P. L. CHAMBRÉ
*Department of Mathematics, University of California, Berkeley, California*
(Received April 28, 1952)

The theory of thermal explosions originally proposed by Frank-Kamenetzky has been the subject of a number of investigations. The critical condition of inflammability requires the solution of the nonlinear Poisson-Boltzmann differential equation. For the case of a reaction vessel of cylindrical or spherical shape the solution was obtained by previous investigators by numerical integration of the equation. It is shown, however, in the following that the solutions can be obtained in terms of known functions.

IN the theory of thermal explosion it is postulated that the critical condition for inflammability is reached when the amount of heat developed by the chemical reaction is just equal to the amount lost to the surroundings. The mathematical models which have been developed to date fall basically into the following categories.

In one model the gas contained in a vessel is assumed well mixed but loses heat through a fictitious "thermal boundary layer." This process of heat transfer is described by the introduction of an empirical heat transfer coefficient the magnitude of which cannot be predicted *a priori*. The thermal balance for critical ignition is reached when the amount of heat generated by the chemical reaction is just equal to the amount of heat lost due to this fictitious conduction process.[1]

The second model, with which this paper is concerned, avoids the use of the concept of the coefficient of heat transfer. As first proposed by Frank-Kamenetzky[2] the loss of heat to the vessel walls, which must be in balance with the chemical heat liberation, takes place entirely by conduction inside the gas volume. For this limiting case of pure conduction the theory should yield the explosion limits from the kinetics of the reaction, the heat of reaction, the thermal conductivity of the gaseous mixture, and the form and dimensions of the vessel. The limitation of the assumption of molecular conduction through the gas, in view of the possibility of mixing of the gas due to convection currents, has been investigated.[3]

The appropriate equation for the thermal balance between the heat generated by the chemical reaction and that conducted away can be written as

$$\lambda\nabla^2 T = -QW, \tag{1}$$

where $T$ is the gas temperature, $Q$ the heat of reaction, $\lambda$ the thermal conductivity, $W$ the reaction velocity, and $\nabla^2$ the Laplacian operator. It is assumed that the reaction is monomolecular and that its velocity follows the Arrhenius law, so that

$$W = ca\exp(-E/RT), \tag{2}$$

where $c$ is the concentration of the reactant, $a$ the frequency factor, and $E$ the energy of activation of the reaction. Hence

$$\nabla^2 T = -(Q/\lambda)ca\exp(-E/RT). \tag{3}$$

We desire the solution of this equation subject to certain boundary conditions. The values of the parameters at which such a solution becomes impossible is taken as a condition of inflammation. The following simplification is made in Eq. (3). As first shown by Todes[4] the maximum temperature increment $(T-T_0)$ before the explosion is of order $RT_0^2/E$, where $T_0$ is the temperature of the walls of the vessel. If the exponent in the term $\exp(-E/RT)$ is expanded in a series of powers $(T-T_0)/T_0$ and powers higher than the first are neglected, there results

$$-\frac{E}{RT} = -\frac{E}{RT_0}\left[\frac{1}{1+(T-T_0/T_0)}\right] \cong -\frac{E}{RT_0}\left[1-\frac{T-T_0}{T_0}\right].$$

It is worthwhile to note, since the expansion is valid only for values of $T/T_0$ close to unity, that Todes' criterion implies $RT_0/E \ll 1$. With

$$\theta = (E/RT_0^2)(T-T_0), \tag{4}$$

Eq. (3) becomes

$$\nabla^2\theta = -\left[\frac{Q}{\lambda}\frac{E}{RT_0^2}ca\exp(-E/RT_0)\right]\exp(\theta). \tag{5}$$

Since the theory is applied to geometries where the conduction process depends on only one space coordinate, say $x$, the Laplacian operator can be made dimensionless by replacing the space coordinate $x$ by $z=x/r$, where $r$ is the significant geometric dimension of the vessel. There results then finally the Poisson-Boltzmann equation

$$\frac{d^2\theta}{dz^2} + \frac{k}{z}\frac{d\theta}{dz} = -\delta\exp(\theta), \tag{6}$$

[1] N. Semenoff, Z. Physik **48**, 571 (1928).
[2] D. A. Frank-Kamenetzky, Acta Physicochimica U.R.S.S. **10**, 365 (1939).
[3] G. Barsky and J. Zeldowitsch, Compt. Rend. Acad. Sci. U.S.S.R. **21**, 114 (1938).
[4] O. M. Todes, dissertation (unpublished).

where

$$\delta=\left[\frac{Q}{\lambda}\frac{E}{RT_0{}^2}r^2ca\exp(-E/RT_0)\right]. \tag{7}$$

Equation (6) has been applied to the determination of explosion limits in an (a) infinite plane-parallel vessel ($k=0$), (b) cylindrical vessel of length very much greater than its radius ($k=1$), (c) spherical vessel ($k=2$). The appropriate boundary conditions are:

at center of vessel,

$$z=0,\quad d\theta/dz=0 \text{ due to symmetry;} \tag{8a}$$

at walls of vessel,

$$z=1,\quad \theta=0. \tag{8b}$$

Subject to these conditions one requires the maximum value of the parameter $\delta$, for which a solution of Eq. (6) is possible. Frank-Kamenetzky has stated that the analytical solution of Eq. (6) is possible only for $k=0$, which he has obtained[5] (a similar opinion is held by Harris).[6] He numerically integrates the equation for $k=1, 2$. In the following we shall show, however, that an analytical solution for $k=1$ in terms of quadratures is possible and that for $k=2$ the solution of the equation can be obtained in terms of a known tabulated function.

Introducing the variables[7]

$$\eta=z^2\exp(\theta);\quad \omega=zd\theta/dz, \tag{9}$$

Eq. (6) becomes with $k=1$

$$d\omega/d\eta=-\delta/(2+\omega). \tag{10}$$

The general integral is

$$\omega^2+4\omega+D=-2\delta\eta. \tag{11}$$

Owing to the boundary condition at the center, $D=0$. Introducing again the original variables, we have

$$z^2\left(\frac{d\theta}{dz}\right)^2+4z\frac{d\theta}{dz}=-2\delta z^2\exp(\theta). \tag{12}$$

However, from Eq. (6)

$$2z^2\frac{d^2\theta}{dz^2}+2z\frac{d\theta}{dz}=-2\delta z^2\exp(\theta).$$

Eliminating the common term, there results

$$\frac{d^2\theta}{dz^2}-\frac{1}{z}\frac{d\theta}{dz}-\frac{1}{2}\left(\frac{d\theta}{dz}\right)^2=0. \tag{13}$$

The solution of this equation is

$$\theta=A-2\ln(Bz^2+1). \tag{14}$$

Since the original differential equation is of second order and we have assigned already one constant of integration through boundary condition (8a), there exists a relationship between $A$ and $B$ which is determined by substitution of Eq. (14) into Eq. (6). There results

$$A=\ln\left(\frac{8B}{\delta}\right), \tag{15}$$

so that

$$\theta=\ln\left[\frac{8B/\delta}{(Bz^2+1)^2}\right]. \tag{16}$$

The remaining boundary condition (8b) yields

$$\frac{8B/\delta}{(B+1)^2}=1. \tag{17}$$

The maximum value of $\delta$ for which a solution is possible is

$$\delta_{\text{crit}}=2;\quad B=1. \tag{18}$$

Hence the critical temperature distribution is given by

$$\theta_{\text{crit}}=\ln\left[\frac{4}{(z^2+1)^2}\right]. \tag{19}$$

The maximum dimensionless temperature is

$$\theta_{\text{max, crit}}=\ln 4. \tag{20}$$

The critical parameter values determined by numerical integration check these values closely.

It is shown next that the differential Eq. (6) for $k=2$ has a solution in terms of a known tabulated function. Numerical integrations for $k=2$ have been given by Frank-Kamenetzky[5] and Harris,[6] and by O. K. Rice.[8]

With $k=2$, Eq. (6) can be written as

$$\frac{1}{z^2}\frac{d}{dz}\left(z^2\frac{d\theta}{dz}\right)=-\delta\exp(\theta). \tag{21}$$

We introduce the new variables

$$\psi=\theta_0-\theta;\quad \eta=z[\delta\exp(\theta_0)]^{\frac{1}{2}}, \tag{22}$$

where $\theta_0$ is the as yet unknown dimensionless temperature at the center of the vessel. Equation (21) becomes

$$\frac{1}{\eta^2}\frac{d}{d\eta}\left(\eta^2\frac{d\psi}{d\eta}\right)=\exp(-\psi), \tag{23}$$

while the boundary conditions Eqs. (8a) and (8b) transform into

$$\eta=0;\qquad \psi=\frac{d\psi}{d\eta}=0 \tag{24}$$

$$\eta=[\delta\exp(\theta_0)]^{\frac{1}{2}};\quad \psi=\theta_0. \tag{25}$$

[5] D. A. Frank-Kamenetzky, Acta Physicochimica U.R.S.S. **16**, 357 (1942).
[6] E. J. Harris, Proc. Roy. Soc. (London) **A175**, 254 (1940).
[7] H. Lemke and J. Reine, Angew. Math. **142**, 118 (1913).
[8] O. K. Rice, J. Chem. Phys. **8**, 727 (1940).

Equation (23), subject to the conditions of Eq. (24) is of importance in certain astrophysical problems. The equation represents the model of an isothermal gas sphere in gravitational equilibrium.[9] The solution has been extensively studied, and the isothermal function $\psi$ and its derivative $d\psi/d\eta$ have been tabulated[10] as functions of their argument $\eta$. In order to find the maximum value of the parameter $\delta$ we utilize Eq. (25), which can be written as

$$\delta=\eta^2\exp(-\psi). \tag{26}$$

[9] S. Chandrasekhar, *An Introduction to the Study of Stellar Structure* (University of Chicago Press, Chicago, 1939).
[10] S. Chandrasekhar and G. W. Wares, Astrophys. J. **109**, 551 (1949).

The extremum of $\delta$ is subject to the condition that

$$\eta\frac{d\psi}{d\eta}=2. \tag{27}$$

From the tables the values of $\eta$ and $\psi$ which satisfy Eq. (27) are found to be $\eta=4.07$, $\psi=1.61$. With these values the magnitudes of the critical ignition parameters are readily computed as

$$\theta_{\max,\,\mathrm{crit}}=1.61\,;\quad \delta_{\mathrm{crit}}=3.32. \tag{28}$$

One can establish with help of certain properties of the solution of Eq. (23) that the critical ignition parameters given by Eq. (28) have indeed the largest possible values. The writer is pleased to acknowledge valuable discussion with Dr. R. M. Lakness.

THE JOURNAL OF CHEMICAL PHYSICS VOLUME 20, NUMBER 11 NOVEMBER, 1952

# Diffusional Processes in the Growth of Aerosol Particles*

H. L. Frisch† and F. C. Collins
*Department of Chemistry, Polytechnic Institute of Brooklyn, Brooklyn, New York*
(Received May 14, 1952)

Various theoretical problems encountered in the diffusional growth process of aerosol particles have been investigated. Fick's differential law with a modified boundary condition has been shown to be approximately valid even where the mean free path of the diffusing molecules is long compared to the radius of the aerosol droplet. A new method has been developed for handling the case of a plurality of competing sinks in the diffusion field. The contribution of a time-dependent uniform source function to the flux into the sinks has been calculated by a method which enables account to be taken of the transient in concentration due to the diffusion process. Such a time-dependent source function representing a change in the number of molecules available for diffusion, will arise because of temperature changes in the diffusion field in the aerosol growth problem.

## INTRODUCTION

In aerosol systems, the primary growth process is assumed to consist in the condensation of single molecules which diffuse from the supersaturated vapor to pre-existing nuclei. In the case of aerosols, as distinguished from hydrosols, the mean free path of the diffusing molecules may be much longer than the radius of the growing droplet, particularly in the initial stages of the process. Here, the applicability of boundary conditions used to solve Fick's second law is not at all obvious. This is because Fick's law and the boundary conditions used in solving it are derived from Taylor's expansions[1] in which, in the limiting case of small mean free path or diffusional jump length, higher order terms may be neglected. The general applicability of Fick's second law for spherically symmetric jump diffusion has been previously discussed.[2] It has been shown that for jumps of all lengths, Fick's law is applicable for times larger than $\nu^{-1}$, where $\nu$ is the collision frequency for molecules of the diffusing species. In the present instance, it is further necessary to establish that the approximate boundary condition used to solve Fick's law yields solutions which converge to correct values of the flux within times shorter than the experimental observation times in the aerosol growth problem.

The growth of aerosol and hydrosol particles is distinguished from most diffusional problems by the presence in the diffusion field of a homogeneous and random distribution of competing sinks around any sink selected for study. This competition leads to depletion and final disappearance of the supersaturation of the medium supplying the molecules, a most significant effect in the growth of colloid particles. This problem has been treated by Reiss and La Mer[3] and by Reiss[4] using two different methods. In this paper, the problem

* "The research reported in this paper has been sponsored by the Geophysics Research Division of Air Force Cambridge Research Center under Contract No. AF19(122)-412."
† Present address: Department of Physics, Syracuse University, Syracuse, New York.
[1] A. Einstein, *Theory of Brownian Movement* (E. P. Dutton and Company, Inc., New York, 1926), p. 14.
[2] F. C. Collins and G. E. Kimball, Ind. Eng. Chem. **41**, 2551 (1949).
[3] H. Reiss and V. K. La Mer, J. Chem. Phys. **18**, 1 (1950).
[4] H. Reiss, J. Chem. Phys. **19**, 482 (1951).

is solved directly using assumptions which lead to a simpler formulation. It turns out that the resulting computations are considerably simpler than those obtained in the previous treatments.

Most colloid growth problems are characterized by a time dependence of the concentration of molecules available for diffusion toward the several sinks because of changes in the supersaturation due to temperature variation or chemical reaction. This variation in the supersaturation due to external factors may be described by a suitable source function, $Q(t)$. In many cases, the contribution of the source function is small compared to the depletion of the concentration arising from the competition of the plurality of sinks, earlier discussed. The problem is solved in general for the case of an arbitrary source function $Q(t)$, and an estimate is made of the error committed in neglecting this source function in the calculation of the flux.

## APPLICABILITY OF FICK'S LAW AND DERIVATION OF AN APPROPRIATE BOUNDARY CONDITION

In the case of radially symmetric diffusion, Fick's Second Law assumes the form:

$$\frac{\partial c}{\partial t}=D\left[\frac{\partial^2 c}{\partial r^2}+\frac{2}{r}\frac{\partial c}{\partial r}\right], \tag{1}$$

where $c$ is the concentration; $t$, the time; $D$, the diffusion constant; and $r$, the distance from the origin. The boundary condition

$$c(R, t)=0, \tag{2}$$

where $R$ is the radius of the sink was proposed by Smoluchowski.[5] It is unsatisfactory in two respects:

(a) It presupposes that all molecules colliding with the sink are absorbed by it, while in reality a small liquid droplet always exerts an appreciable vapor pressure, and

(b) The flux derived by using this boundary condition becomes infinite in the neighborhood of the starting point in time.

It becomes desirable therefore to define an absorption probability $\alpha<1$ for the sink in order to account for the vapor molecules reflected or evaporated from it. The boundary condition satisfied at the surface of such a sink is obtained by independently calculating the flux of vapor molecules which are absorbed by the sink. In the case of systems in which the diffusional jump length is much less than the radius of the sink, it has been previously shown[6,7] that this leads to the boundary condition

$$\left(\frac{\partial c}{\partial r}\right)_R=\frac{\alpha}{\rho}c(R, t), \tag{3}$$

where

$$\rho=\frac{\int_0^\infty s^2\varphi(s)ds}{\int_0^\infty s\varphi(s)ds}=\frac{\langle s^2\rangle}{\langle s\rangle}. \tag{4}$$

It will now be shown that both Eq. (1) and an equation of the form of Eq. (3) are valid in case of diffusion with long free path. In a previous paper,[1] the following integro-differential equation was found to govern the diffusion process in the case of a spherically uniform distribution of the diffusing material and a spherically uniform jump length density function:

$$\frac{\partial c(r, t)}{\partial t}=-\nu c(r, t)+\nu\int_0^\infty dr_0\int_{|r-r_0|}^{r+r_0}\frac{r_0}{2rs}c(r_0, t)\varphi(s)ds, \tag{5}$$

where $\nu$ is the mean jumping frequency and $r_0$ is the original distance from the origin of a molecule jumping into a volume element at a distance $r$ from the origin. Expanding $c(r_0, t)$ in Eq. (1) in a Taylor's series and carrying out the indicated integrations, one obtains the series

$$\frac{\partial c(r, t)}{\partial t}=\nu\left[\frac{1}{3}\frac{\langle s^2\rangle}{r}\frac{\partial c(r, t)}{\partial r}+\frac{1}{6}\langle s^2\rangle\frac{\partial^2 c(r, t)}{\partial r^2}+\cdots\right]. \tag{6}$$

If the function $c(r, t)$ is well-behaved, terms of order higher than the second may be neglected[8] and Fick's law (Eq. (1)) obtained upon equating

$$D=\tfrac{1}{6}\nu\langle s^2\rangle. \tag{7}$$

The condition that the neglect of the higher order terms in Eq. (6) introduce only a negligible error is that

$$t\gg\nu^{-1}=\langle s^2\rangle/6D,$$

which is usually of the order of $10^{-7}$ to $10^{-6}$ second in aerosol systems. Since this time involves a fraction of only 0.001 or less of the time ordinarily required for the growth of a stable droplet, the interval when Eq. (5) is not well represented by Eq. (1) will introduce only a minor error since neither Eq. (5) nor Eq. (1) will involve singularities at the starting point in time in the physical situation.

It may be here mentioned that the "jumps" above discussed can be taken essentially as the path of the molecule between successive collisions. The persistence of velocity upon collision, however, causes the jump density function $\varphi(s)$ to be no longer spherically uniform but to depend upon the direction of the jump immediately preceding the jump under consideration in the manner of a Markov process. However, as is well

[5] M. V. Smoluchowski, Ann. Physik **48**, 1103 (1915).
[6] F. C. Collins and G. E. Kimball, J. Colloid Sci. **4**, 425 (1949).
[7] F. C. Collins, J. Colloid Sci. **5**, 499 (1950).

[8] Frank and v. Mises, *Differentialgleichungen der Physik* (Rosenberg, 1943), Vol. II, p. 594 ff.

known,[9] this effect can be accounted for by multiplying $\langle s^2\rangle$ by a correction factor slightly greater than unity. For convenience in this discussion, it will be assumed that this correction factor has been already incorporated in $\langle s^2\rangle$ and in the other moments of $\varphi(s)$.

Let us now seek an appropriate boundary condition for use in solving Eq. (1) for the special case of the existence of a spherically symmetric sink of radius $R$, where $R$ is much smaller than the mean jump length $\langle s\rangle$. The total flux of molecules impinging on the sink at any time $t$ is first required. The probability that a molecule suffer its preceding collision in $dv$ at a distance $r_0$ from the origin, impinge on the sink of radius $R$ on its next jump of distance $s\geq s_c$, is readily calculated. The geometry of the situation is illustrated in Fig. 1. The distance between the volume element $dv$ and the face of the sink is given by

$$s_c=r_0\cos\theta-(R^2-r_0^2\sin^2\theta)^{\frac{1}{2}}, \tag{8}$$

where the solid angle intercepted by the sink is $2\pi\sin\theta$, with $0\leq\theta\leq\sin^{-1}R$. The total flux of molecules impinging on the sink of radius $R$ is

$$\Phi_T=+\nu\int_R^\infty\int_0^{\sin^{-1}R/r_0}\int_{r_0\cos\theta-(R^2-r_0^2\sin^2\theta)^{\frac{1}{2}}}^\infty \times\frac{2\pi\sin\theta}{4\pi}c(r_0,t)\varphi(s)dsd\theta dr_0. \tag{9}$$

Since $R\leq\langle s\rangle$ only a small error is committed by simplifying Eq. (9) by substituting for the spherical sink, a disk of area $\pi R^2$ tangent to a sphere of radius $r_0-R$ concentric with the volume element $dv$. Then Eq. (9) becomes, after interchanging the order of integration and integrating over $\theta$,

$$\Phi_T(t)=\nu\pi R^2\int_R^\infty\int_{r_0-R}^\infty c(r_0,t)\varphi(s)dsdr_0. \tag{10}$$

Integrating Eq. (10) over $s$, we find

$$\Phi_T(t)=\nu\pi R^2\langle s\rangle\int_R^\infty c(r_0,t)\psi(r_0-R)dr_0, \tag{11}$$

where $\psi(z)$ is so defined that

$$\psi(z)=\frac{1}{\langle s\rangle}\int_z^\infty\varphi(s)ds. \tag{11'}$$

From the initial postulates, it follows that $\psi(+\infty)=0$ and $\psi(0)=1/\langle s\rangle$. The effective flux $\Phi(t)$ of molecules lost by the diffusion field to the sink at $r=R$ is $\alpha\Phi_T(t)$. Since the diffusion flow is continuous for $r>R$, $t>0$ this flux $\Phi(t)$ must be identical with the flux obtained by integrating Eq. (10) with respect to $r$ over a sphere of radius $\rho$ as $\rho\to R+0$.

$$\Phi(t)=\lim_{\rho\to R+0}4\pi\rho^2D\left(\frac{\partial c(r,t)}{\partial r}\right)_\rho$$

$$=\tfrac{2}{3}\langle s^2\rangle\nu\pi R^2\left(\frac{\partial c}{\partial r}\right)_R=4\pi R^2D\left(\frac{\partial c}{\partial r}\right)_R. \tag{12}$$

Thus, at the boundary, $r=R$, of the sink, $c(r,t)$ must satisfy

$$\gamma\left(\frac{\partial c}{\partial r}\right)=\int_R^\infty c(r_0,t)\psi(r_0-R)dr_0, \tag{13}$$

where

$$\gamma=\frac{2\langle s^2\rangle}{3\alpha\langle s\rangle}=\rho/\alpha' \tag{14}$$

with

$$\rho=\langle s^2\rangle/\langle s\rangle$$
$$\alpha'=\tfrac{3}{2}\alpha. \tag{15}$$

Fick's diffusion equation (1) will now be solved with the derived boundary condition Eq. (13). The initial concentration will be assumed constant:

$$c(r,0)=a,\quad r>R. \tag{16}$$

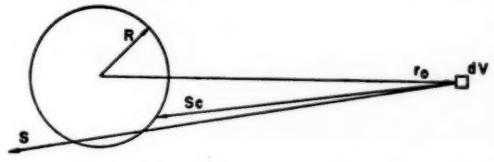


FIG. 1. Diffusion into small spherical sink.

At long distances from the origin

$$c(r,t)\to a\quad r\to+\infty,\quad t>0. \tag{17}$$

Let the Laplace transform of $c(r,t)$ be

$$L\{c(r,t)\}=\int_0^\infty e^{-pt}c(r,t)dt=\bar{c}(r,p).$$

Then $\bar{c}(r,p)$ satisfies the transforms of Eqs. (1) and (17) and is easily found to be given by

$$\bar{c}(r,p)=\frac{a}{p}-\frac{A}{r}e^{-qr}, \tag{18}$$

where

$$q=(p/D)^{\frac{1}{2}}.$$

The constant $A$ is determined by substituting Eq. (18) into the transform of Eq. (13) keeping in mind that $\psi(r_0-R)$ is independent of the time. The transform of Eq. (13) is

$$\gamma\left(\frac{\partial\bar{c}}{\partial r}\right)_R=\int_R^\infty\bar{c}(r_0,p)\psi(r_0-R)dr_0. \tag{19}$$

Substituting for $\bar{c}(r,p)$, the function given by Eq. (18),

[9] J. H. Jeans, *Kinetic Theory of Gases* (Cambridge University Press, Cambridge, 1948), p. 204.

we find that $A$ satisfies

$$A\left\{\frac{\gamma e^{-qR}}{R^2}+\frac{\gamma q e^{-qR}}{R}+\int_R^\infty \frac{e^{-qr_0}}{r_0}\psi(r_0-R)dr_0\right\} =\frac{a}{P}\int_R^\infty \psi(r_0-R)dr_0; \quad (20)$$

but

$$\int_R^\infty \psi(r_0-R)dr_0=\int_0^\infty \psi(\rho)d\rho \quad (21)$$

on substituting $r_0-R=\rho$. From Eq. (11′)

$$\psi(\rho)=\frac{1}{\langle s\rangle}\int_\rho^\infty \varphi(s)ds. \quad (22)$$

Hence,

$$\int_0^\infty \psi(\rho)d\rho=\frac{1}{\langle s\rangle}\int_0^\infty d\rho\left\{\int_\rho^\infty \varphi(s)ds\right\}. \quad (23)$$

Integrating this last expression by parts, we find

$$\frac{1}{\langle s\rangle}\int_0^\infty d\rho\left\{\int_\rho^\infty \varphi(s)ds\right\}=-\frac{1}{\langle s\rangle}\rho\int_0^\infty \varphi(s)ds\Big]_{\rho=0}^{\rho=\infty} +\frac{1}{\langle s\rangle}\int_0^\infty \rho\varphi(\rho)d\rho=1. \quad (24)$$

Therefore, Eq. (20) simplifies to

$$A\left\{\frac{\gamma e^{-qR}}{R^2}+\frac{\gamma q e^{-qR}}{R}+\int_R^\infty \frac{e^{-qr_0}}{r_0}\psi(r_0-R)dr_0\right\}=\frac{a}{P}. \quad (25)$$

Since $e^{-qr_0}/r_0$ and $\psi(r_0-R)$ are continuous and $e^{-qr_0}/r_0$ is a monotone decreasing function in the interval $[R,+\infty]$ we can apply the Second Mean Value Theorem[10] to the integral

$$\int_R^\infty \frac{e^{-qr_0}}{r_0}\psi(r_0-R)dr_0.$$

If $R\leq R+\delta\leq\infty$, then

$$\int_R^\infty \frac{e^{-qr_0}}{r_0}\psi(r_0-R)dr_0=\frac{e^{-qR}}{R}\int_R^{R+\delta}\psi(r_0-R)dr_0 =\frac{e^{-qR}}{R}\int_0^\delta \psi(z)dz=\frac{e^{-qR}}{R}I(\delta), \quad (26)$$

and $A$ is found to be

$$A=\frac{aRe^{qR}}{P\gamma[q+(1/R+I(\delta)/\gamma)]}. \quad (27)$$

$\bar{c}(r,p)$ is thus determined.

[10] J. F. Sokolnikoff, *Advanced Calculus* (McGraw-Hill Book Company, Inc., New York, 1939), p. 115.

Taking the inverse transform of $\bar{c}(r,p)$ yields the following expression:

$$\frac{c(r,t)}{a}=1-\frac{R-\beta}{rI(\delta)}\left\{\operatorname{erfc}\left[\frac{r-R}{2(Dt)^{\frac{1}{2}}}\right] -\exp\left[\frac{r-R}{\beta}+\frac{Dt}{\beta^2}\right]\operatorname{erfc}\left[\frac{r-R}{2(Dt)^{\frac{1}{2}}}+\frac{(Dt)^{\frac{1}{2}}}{\beta}\right]\right\}, \quad (28)$$

where $\beta=R\gamma/[\gamma+RI(\delta)]$ and $\gamma=\rho/\alpha'$.

Equation (28) assumes a limiting form if the jump length density function $\varphi(s)$ falls off rapidly for jumps of length $s$ greater than the mean free length $\langle s\rangle$. This is the case in gases. If we assume statistical equilibrium and "molecular chaos," then the path length distribution is given approximately by

$$F_0(l)=\frac{1}{\langle l\rangle}\exp -l/\langle l\rangle, \quad (29)$$

where $\langle l\rangle$ is the mean free length. As previously remarked, after correction for persistence of velocity, $\langle l\rangle\approx\langle s\rangle$. Then

$$\int_0^\delta \varphi(s)ds\approx 1 \quad \delta\gtrsim\langle s\rangle. \quad (30)$$

Then if the limits are interchanged in the double integral,

$$I(\delta)=\int_0^\delta \psi(z)dz=\int_0^\delta \frac{dz}{\langle s\rangle}\int_z^\infty \varphi(s)ds =\int_0^\delta \varphi(s)ds\int_0^s \frac{dz}{\langle s\rangle}+\int_\delta^\infty \varphi(s)ds\int_0^\delta \frac{dz}{\langle s\rangle} =\int_0^\delta \frac{s}{\langle s\rangle}\varphi(s)ds+\int_\delta^\infty \frac{\delta}{\langle s\rangle}\varphi(s)ds\approx 1. \quad (31)$$

If now Eq. (28) is compared with the solution $u(r,t)$ obtained by the boundary condition, Eq. (3), previously derived for diffusion with short mean jump length, it will be seen that they are identical. Further, it may be readily shown that, no matter the value of $I(\delta)$, for sufficiently large values of the time

$$\left|\frac{u(r,t)-c(r,t)}{a}\right|<\frac{|M|}{t^{\frac{1}{2}}}\quad |M|\leq 1. \quad (32)$$

In the remainder of this paper, Eq. (3) will be used as the limiting boundary condition for the case of long mean jump length.

## THE EFFECT OF THE PRESENCE OF A PLURALITY OF SINKS IN THE DIFFUSION FIELD ON THE FLUX

A complication in the theory of growth of aerosols by diffusion is that the diffusion flow is not directed only

towards one droplet but towards a large number of them. Hence the effective flux is smaller than the flux that would be observed if there were but one droplet in the diffusion field.

Let $M+1$ such droplets be distributed at random in $V$, the volume of the diffusion field. In the present treatment, it will be assumed that all droplets have the same radius $R$ which is constant with time. The essential features of the derivation, however, remain valid when the latter restriction is lifted. Let us consider a small finite volume $\delta V$ at a distance $r$ from the center of an arbitrarily selected droplet, which will be later referred to as the "reference sink." As diagrammatically illustrated in Fig. 2, the volume $\delta V$ contains $m(r, t)\delta V = \delta M$ droplets, where $m(r, t)$ is defined by

$$\lim_{\delta V \to 0} \frac{\delta M}{\delta V} = m(r, t). \tag{33}$$

In the aerosol system, a purely random distribution of the droplets may be assumed and

$$m = M/V = \text{constant}. \tag{34}$$

The rate of change of concentration of vapor molecules inside $\delta V$, relative to their availability for diffusion to the reference sink, will be denoted by $\delta V \partial c/\partial t$.

This change in concentration is due to:

(a) The flow through the surface, $\delta S$, of the volume, $\delta V$, due to the existence of the sink at $r=0$. This is equal to $D\nabla^2 c \cdot \delta V$.

(b) The absorption at any of the $\delta M$ sinks in $\delta V$. Let this be denoted by $f\delta V$.

By the principle of conservation of mass in $\delta V$ we have

$$\delta V \partial c/\partial t = D\nabla^2 c \delta V - f\delta V. \tag{35}$$

Canceling $\delta V$ on both sides of Eq. (35) we obtain an equation independent of the size of the volume element $\delta V$.

$$\partial c/\partial t = D\nabla^2 c - f. \tag{36}$$

The following assumptions are now made: (a) the sinks act independently of each other, (b) the diffusion field flow lines surrounding the $j$th sink are not disturbed by the presence of the other homogeneously distributed sinks, and (c) the absorption probability of each sink is the same. Then if a vapor molecule is present in the volume element $\delta V$, the probability that it diffuse to the $j$th sink and be captured there is merely $\Phi_j(t) = \Phi(t)$. Here $\Phi(t)$ is the effective flux to the reference sink. These assumptions may be assumed to be fulfilled in the case of monodispersed colloid systems.

Now, $f$, the rate of change of molecules in the volume element, $\delta V$, relative to their availability for flow toward the reference sink at the origin may be explicitly calculated. This is the *a priori* probability that a molecule diffuse into the $j$th sink, $\Phi_j(t)/a$, times the effective concentration relative to the reference sink, $c(r, t)$. For all $\delta M$ sinks in $\delta V$ we must multiply this number by $m$, the number concentration of independent, homogeneously distributed droplets in $\delta V$. Thus we finally obtain

$$f = m\Phi(t)\frac{c(r, t)}{a}. \tag{37}$$

Substitution of Eq. (37) into Eq. (36) yields a modified form of Fick's law:

$$\frac{\partial c}{\partial t} = D\nabla^2 c - \frac{m}{a}\Phi(t)c, \tag{38}$$

where

$$\Phi(t) = 4\pi R^2 D(\partial c/\partial r)_R.$$

In the future, the ratio $m/a$ will be denoted by $\eta$. The analogous equation for $u(r, t)$, the concentration in the presence of the reference sink alone is given by Fick's law

FIG. 2. Competition among sinks for the diffusing molecules.

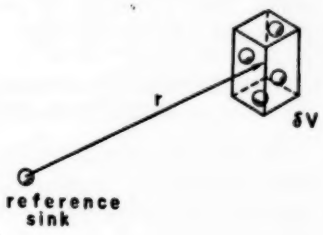


$$\frac{\partial u}{\partial t} = D\nabla^2 u \quad R < r < \infty\,;\ t > 0,$$
$$\Phi_0 = 4\pi R^2 D\left(\frac{\partial u}{\partial r}\right)_R. \tag{39}$$

Let us define

$$c(r, t) = u(r, t)\exp\left[-\eta\int_0^t \Phi(\tau)d\tau\right]. \tag{40}$$

Equation (40) is a solution of Eq. (38), and possesses the further property that, when $\eta \to 0$, $c(r, t) \to u(r, t)$ as it must, since $u(r, t)$ is a solution of Eq. (39). By differentiating Eq. (40) with respect to $r$, evaluating at $r=R$, and substituting the result in $\Phi(t)$, the following integral equation for the flux $\Phi(t)$ is obtained:

$$\Phi(t) = \Phi_0(t)\exp\left(-\eta\int_0^t \Phi(\tau)d\tau\right). \tag{41}$$

Differentiating Eq. (41) with respect to time, we obtain

$$\frac{d\Phi}{dt} - \Phi\frac{d\ln\Phi_0}{dt} = -\eta\Phi^2$$

where at $t=0$, $\Phi=\Phi_0$. If we now let $z=1/\Phi(t)$, the following differential equation in $z$ is obtained:

$$\frac{dz}{dt}+\left[\frac{d\ln\Phi_0}{dt}\right]z=\eta. \tag{42}$$

By rearranging the solution of Eq. (42), we can solve for $\Phi(t)$ explicitly in terms of $\Phi_0(t)$:

$$\Phi(t)=\frac{\Phi_0(t)}{1+\eta\int_0^t\Phi_0(\tau)d\tau}. \tag{43}$$

Equation (43) possesses the important property that

$$\operatorname*{Lim}_{t\to\infty}\Phi(t)=0$$

corresponding to the disappearance of the supersaturation due to the competition of the multiplicity of the sinks. This property, of course, follows from the exponential form of Eq. (40).

## THE EFFECT OF A TIME-DEPENDENT SOURCE FUNCTION UPON THE FLUX

In the diffusional growth of colloid particles, the concentration of molecules effectively available for diffusion may vary during the process due to variation of the supersaturation arising from temperature changes or a homogeneous chemical reaction. This variation may be described by a source function, $Q(t)$, and Eq. (1) assumes the form

$$\frac{\partial c}{\partial t}=D\left[\frac{\partial^2 c}{\partial r^2}+\frac{2}{r}\frac{\partial c}{\partial r}\right]+Q(t) \tag{44}$$

in the region $R<r<\infty$ for $t>0$. As before, the initial concentration is taken to be a constant, $a$. The boundary conditions are

$$c(r,t)\to a+\int_0^t Q(\tau)dt \quad \text{as} \quad r\to+\infty, \tag{45}$$

while, at the surface of the sink of radius $R$, Eq. (3) holds:

$$\gamma\left(\frac{\partial c}{\partial r}\right)_R=c(R,t), \quad t>0. \tag{46}$$

We will now assume $Q(t)$ possesses a Laplace transform,

$$L\{Q(t)\}=\int_0^\infty e^{-pt}Q(t)dt=\bar{Q}(p). \tag{47}$$

The transforms of Eq. (44) and (45), (46), and (16) are

$$p\bar{c}-a-\bar{Q}(p)=D\left(\frac{\partial^2\bar{c}}{\partial r^2}\right)+\frac{2D}{r}\frac{\partial\bar{c}}{\partial r}, \tag{48}$$

$$\operatorname*{Lim}_{r\to\infty}\bar{c}(r,p)=\frac{a}{P}+\frac{\bar{Q}(p)}{P}, \tag{49}$$

and

$$\gamma\left(\frac{\partial\bar{c}}{\partial r}\right)_R=\bar{c}(R,p), \tag{50}$$

respectively. The solution is easily found to be

$$\bar{c}(r,p)=\frac{a+\bar{Q}(p)}{p}-\frac{Rae^{-q(r-R)}}{r\gamma p[q+1/\beta]}-\frac{\bar{Q}(p)Re^{-q(r-R)}}{r\gamma p[q+1/\beta]} \tag{51}$$

in which $q=(p/D)^{\frac{1}{2}}$ and $\beta=R\gamma/(R+\gamma)$. The inverse transform of Eq. (51) is

$$c(r,t)=a\left\{1-\frac{R-\beta}{r}F(r-R;t;\beta)\right\}+\int_0^t Q(\tau)\left\{1-\frac{R-\beta}{r}F(r-R;t-\tau;\beta)\right\}dt, \tag{52}$$

where

$$F(r-R;t;\beta)=\operatorname{erfc}\frac{r-R}{2(Dt)^{\frac{1}{2}}}-\exp\left[\frac{r-R}{\beta}+\frac{Dt}{\beta^2}\right]\times\operatorname{erfc}\left[\frac{r-R}{2(Dt)^{\frac{1}{2}}}+\frac{(Dt)^{\frac{1}{2}}}{\beta}\right].$$

Comparing $c(r,t)$, given by Eq. (52), with the solution of the sourceless problem, $u(r,t)$, given by Eq. (28), we see that

$$c(r,t)=u(r,t)+\int_0^t Q(\tau)\left\{\frac{u(r,t-\tau)}{a}\right\}dt, \tag{53}$$

whence

$$|c(r,t)-u(r,t)|\leqslant\left|\int_0^t Q(\tau)d\tau\right|, \quad \text{since} \quad \left|\frac{u(r,t)}{a}\right|\leqslant 1.$$

The last inequality gives a measure of the error committed in neglecting the source function, $Q(t)$.

The flux, $\Phi_s(t)$, in the presence of the source is readily obtained in terms of the sourceless flux, $\Phi_0(t)$, from Eq. (53) and is

$$\Phi_s(t)=\Phi_0(t)+\int_0^t\frac{Q(\tau)}{a}\Phi_0(t-\tau)d\tau. \tag{54}$$

Equation (54) may be solved in principle if $Q(t)$ is given explicitly.

The solution, Eq. (52), may be modified to account for the presence of a plurality of sinks in the diffusion field as follows:

The total rate of production of molecules produced in the volume element, $\delta V$, by the source is $Q(t)\delta V$. However only a fraction of these molecules are effectively available for diffusion to the "reference sink." This number is $Q_M\delta V$ and is by the previous argument

$$Q_M(t)=Q(t)\exp\left(-\eta\int_0^t\Phi(\tau)d\tau\right). \tag{55}$$

Introducing Eq. (55) into Eq. (36) yields

$$\frac{\partial c}{\partial t}=D\nabla^2c+Q(t)\exp\left[-\eta\int_0^t\Phi(\tau)d\tau\right]-\eta\Phi c. \tag{56}$$

Equation (56) is again solved by the substitution

$$c(r,t)=w(r,t)\exp\left(-\eta\int_0^t\Phi(\tau)d\tau\right), \tag{40}$$

where $w(r,t)$ satisfies Eq. (44). Then in analogy with Eqs. (40) to (43), we obtain for the flux in the presence of both a source function and a plurality of competing sinks

$$\Phi_{sc}=\frac{\Phi_s(t)}{1+\eta\int_0^t\Phi_s(\tau)dt}, \tag{57}$$

where $\Phi_s$ is given by Eq. (54).

## CONCLUSION

It has been shown that Fick's Second Law may be used to describe the diffusion of vapor to droplets of condensate even when the radius of these droplets is smaller than the mean free path of the vapor molecules. A boundary condition has been derived for the above case of long mean jump length which allows for the vapor pressure exerted by the liquid droplets, in such a manner that the flux of the diffusing molecules remains finite at the start of the process. The limiting form of this boundary condition exhibits a linear relation between the gradient of the concentration and the concentration at the boundary and is applicable whenever the diffusional jump length probability distribution function falls off sufficiently rapidly with distance. This condition is fulfilled in the case of gaseous diffusion.

The depletion of the supersaturation due to the competition of the many droplets for the vapor molecules becomes marked during the latter portion of the growth process. The effective flux in the presence of a plurality of sinks has been shown to bear a simple relation to the flux in the absence of the competing sinks and to be readily calculable, given the concentration of droplets and the initial concentration of vapor molecules.

Homogeneous variation of the supersaturation due to external factors such as a homogeneous chemical reaction or a time-dependent variation of the temperature serves merely to add a linear term of simple form to the calculated flux. The magnitude of this term is readily evaluated and it may be neglected in many problems where the source function contributes but little compared with the primary diffusion process.

The study of the growth process in the formation of aerosols requires account to be taken of the effect of the moving boundary of the droplet on the diffusion process.[3,11] The application of the present study to the calculation of the droplet boundary radius as a function of time will be the subject of a subsequent paper.

---

[11] H. L. Frisch, Z. Elektrochem. **56**, 324 (1952).

# Nuclear Quadrupole Coupling Constants and Molecular Vibrations

JULES DUCHESNE
*Institut d'Astrophysique, University of Liège, Cointe-Sclessin, Belgium*
(Received August 1, 1952)

The nuclear quadrupole coupling constants may be expected to change with vibrational quantum number. The observations of various workers on some molecules are discussed and the experimental results are interpreted in terms of theory.

IN a recent paper,[1] the present author has drawn attention to the great interest attached to the study of the variations of the nuclear quadrupole coupling constants with the vibrational quantum number, and has predicted that even in the lower states the effect would be significant. This statement was indeed a direct consequence of a theoretical analysis in which he discussed the general problem of the dependence of the distribution of the electronic density in a molecule on the normal modes of vibrations. It was shown, in particular, that, in order to interpret properly the intensities of the absorption infrared bands, the formal charges carried by the atoms must sometimes be drastically changed with the vibrational state of the molecule.[2]

In their experimental study of the $K^{39}Cl^{35}$ molecule by the molecular beam electrical resonance method, Fabricand, Carlson, Lee, and Rabi[3] have just determined, with great accuracy, the nuclear quadrupole interactions for several vibrational states. Their values are reproduced in Table I. The results obtained clearly indicate a not inconsiderable increase of $(eqQ)_{Cl}$ with $v$. This is in accord with the author's general predictions. It is, therefore, worthwhile to try to analyze this new fact in more detail along the lines suggested by the theory.[2] As the averaging of $q$ over each vibrational state determines $(eqQ)_{Cl}$, the mean value of the internuclear distance for each $v$ state has to be computed. These values may be deduced from the rotational constants $B_e=3856.352$ mc/sec and $\alpha_e=23.680$ mc/sec, as obtained from molecular beam techniques.[3] For $v=0$, 1, 2, 3, the internuclear distances are found to be 2.670, 2.679, 2.687, 2.695A, respectively. This corresponds to results obtained by Stitch, Honig, and Townes[4] for $B_v$ from their microwave spectroscopic work. It, therefore, appears that a change in the internuclear distance of 0.025A alters $(eqQ)_{Cl}$ by a factor of five. However, the absolute $(eqQ)_{Cl}$ value is very small compared with the one characterizing a covalently bonded chlorine atom ($\sim -75$ mc/sec). From this, it may be deduced that for $v=0$ the KCl bond is essentially ionic and that the fraction of covalent character is approximately one-thousandth. For $v=3$, $(eqQ)_{Cl}$ amounts to one two-hundredth of the normal value and this would mean that the fraction of covalent structure, which has also to be increased by a factor of five from $v=0$ to $v=3$, becomes 1/200. The coupling constant appears to be linear with the internuclear distance for small $v$, and if it can be assumed that it also remains so, far from the equilibrium position, it can be shown that for a stretching of the bond by about 2.5A there is the same proportion of ionic and covalent structures. Consequently, at 5.17A (equilibrium distance=2.67A), the potential curves of the ionic and covalent states are presumed to cross one another, and the molecule dissociates into atoms. It is also to be pointed out that the charge bound to the K and Cl atoms changes by 0.5 percent for an extension of 0.025A. This is not surprising as it has been established that greater variations occur in other cases.[2] It is, therefore, to be expected that further work in this field may reveal even more rapid changes with the internuclear distances than those which have been discovered thus far. It was also predicted[1] that $(eqQ)$ does not only depend on the valency vibrations, but also on the other types of fundamental vibrations and, in particular, on the bending modes appearing in polyatomic molecules. A very recent paper by Tetenbaum[5] shows that the coupling constant in the first excited bending mode of BrCN is smaller by about 1 part in 250 than in the ground state. This result gives much support to the prediction.

$K^+$, which as well as $Cl^-$ has an argon-like structure at the equilibrium position of the molecule, may now be considered. It may be seen from the table that the nuclear quadrupole interaction for $K^+$ is 5.656 mc/sec for $v=0$ and only decreases by a very small amount with $v$. In this connection, it is to be recalled that to form the covalent KCl bond the potassium $s$ electron and the chlorine $3p_x$ must be paired and that when the bond length is increased the bonding becomes more covalent. But in this process $K^+$ tends to go into K with the addition of an $s$ orbital which is spherically symmetric. Therefore, this change in the status of $K^+$, which does not contribute to a change in $q$, accounts for the practically constant value of $(eqQ)$. It is to be noticed that the slight decrease observed is possibly due to the fact that the distortion of the ionic shells decreases when

[1] J. Duchesne, communication sent to the "Colloque sur l'optique et les microondes" Milan, June, 1952; Nuovo cimento, Supplement XI (to be published).
[2] J. Duchesne, J. Chem. Phys. **18**, 1120 (1950); Bull. Acad. Roy. Sci. Belg. **38**, 197 (1952).
[3] Fabricand, Carlson, Lee, and Rabi, Phys. Rev. **86**, 607 (1952).
[4] Stitch, Honig, and Townes, Phys. Rev. **86**, 607 (1952).
[5] S. J. Tetenbaum, Phys. Rev. **86**, 440 (1952).

the internuclear distance is increasing. The dipole moment of KCl is also to be taken into consideration. The observed value in the state $v=0$ is $10.61D$,[3] whereas the computed one is $12.8D$. This would indicate that for $v=0$ the molecule is only 83-percent ionic. Because more than 99-percent ionic structure are present, according to the considerations developed above, there is strong evidence that the use of the dipole moment for direct computation of ionic character gives a poor approximation when the polarization of the shells is neglected.

The influence of the vibrations on the nuclear quadrupole coupling constant was manifested, though less directly, in another way. It has been shown[6] that in $CH_3X$ (X=halogen), $(eqQ)_X$ is greater than it is in the corresponding isotopic molecule $CD_3X$, and that the discrepancy amounts to 0.72 mc/sec in the chlorinated derivative. The polarity of the CCl bond and the hybridization character of the chlorine orbital decrease as the CCl bond is lengthened from $CD_3X$ to $CH_3X$. In spite of the very small increase in the bond length the coupling constant should be greatly increased on account of these factors. The similarity of this behavior with KCl shows that whether the bond is stretched by vibrational excitation or by a change in the zero-point energy, due to isotopic substitution, no qualitative difference appears in the results. However, for the same expansion in both molecules a much greater variation of $(eqQ)_{Cl}$ appears in $CH_3Cl$ than in KCl. This statement results from the fact that a change of the order of magnitude of one-thousandth A in the CCl internuclear distance of $CH_3Cl$ with respect to $CD_3Cl$ alters $(eqQ)_{Cl}$ by 0.72 mc/sec, whereas in KCl a change of 0.025A only alters $(eqQ)_{Cl}$ by 0.3 mc/sec. If this is real, it must be accepted that the ionic character of the CCl bond in $CH_3Cl$ decreases much more rapidly with the increase of the internuclear distance than it does in KCl. Of course,

[6] J. W. Simmons and J. H. Goldstein, J. Chem. Phys. **20**, 122 (1952).

TABLE I.

| | $v=0$ | 1 | 2 | 3 |
|---|---|---|---|---|
| $(eqQ)_K$ mc/sec | −5.656 | −5.622 | −5.571 | −5.511 |
| $(eqQ)_{Cl}$ mc/sec | >0.070 | −0.080 | −0.240 | −0.380 |

the variations of $(eqQ)_{Cl}$ in $CH_3Cl$ with the vibrational CCl state would have to be determined experimentally in order to clear up completely the question.

The work of Dehmelt and Krüger[7] on $C_2H_2Cl_2$ and of Dean and Pound[8] on benzene derivatives shows that thermal motions which appear in the solid state cause a decrease of the nuclear quadrupole coupling constant when the temperature is increased. This is just the opposite effect to the one discussed above. It must, therefore, be supposed that the effect observed by these authors is due to the fact that at low temperatures the thermal motions overbalance the $eqQ$ vibrational increase so that the net effect is a decrease with temperature. In the case of benzene derivatives it may be that the low frequency out-of-plane vibrations of the $B_{2g}$ class play a particularly important role as an intramolecular effect.

A result of general interest is that the recent experiments on the nuclear quadrupole coupling constants demonstrate that the charge distribution in a molecule is largely under the dependence of the molecular vibrations. This is in agreement with the premises on which the author's theory of molecular reactivity rests.[2] The experimental work must be extended to include polyatomic molecules, and specifically investigations must be made with regard to the dependence of $(eqQ)$ upon the symmetry of the vibrations.

Further treatment of the present subject and related ones are contemplated.

[7] H. G. Dehmelt and H. Krüger, Z. Physik **129**, 401 (1951).
[8] C. Dean and R. V. Pound, J. Chem. Phys. **20**, 195 (1952).

# Intermolecular Forces in Acetone and Methyl Alcohol

VERNON MYERS
*The Pennsylvania State College, State College, Pennsylvania*
(Received August 13, 1952)

The long-range intermolecular forces between acetone molecules and between methyl alcohol molecules are computed from optical dispersion data and dipole moments, and the short-range repulsive forces are estimated from second virial coefficients. The experimental second virial coefficients for $(CH_3)_2CO$ and $CH_3OH$ are those of Lambert and his co-workers (Proc. Roy. Soc. (London) **196A**, 113 (1949)).

## ACETONE

THE dipole moment for acetone is $2.74\cdot10^{-18}$ esu.[1] The optical dispersion data may be represented by[2]

$$n-1=\frac{15.089\cdot10^{27}}{14069\cdot10^{27}-\nu^2}. \quad (1)$$

Equation (1) yields a static polarizability of $6.32\cdot10^{-24}$ cm$^3$, an oscillator strength of 13.9 and a resonance energy of 15.8 ev. Table I shows the results for the potential

$$V=-7.51\cdot10^{-12}(R^{-3}+R^{-5})f(\theta_1,\theta_2,\phi)-(853\cdot10^{-12}R^{-6}+1930\cdot10^{-12}R^{-8})\text{ erg},\quad R>4.35\text{A}; \quad (2)$$

$$V=\infty,\quad R<4.35\text{A}.$$

The term in $R^{-5}$ is included to account approximately for dipole-quadrupole interactions[3,4] and $f(\theta_1,\theta_2,\phi)$ is the angular function for two interacting dipoles. $R$ is the distance between the molecular centers in angstrom units.

The effect of an exponential repulsion

$$V=3.3\cdot10^{-7}e^{-R/0.28}-7.51\cdot10^{-12}(R^{-3}+R^{-5})f(\theta_1,\theta_2,\phi)-(853\cdot10^{-12}R^{-6}+1930\cdot10^{-12}R^{-8})\text{ erg} \quad (3)$$

is given in Table II.

TABLE I. A comparison of the experimental and theoretical second virial coefficients for acetone on the basis of the hard sphere model.

| Temp. °K | Experimental virial cm³/mole | Theoretical virial cm³/mole | Percent difference |
|---|---|---|---|
| 323 | −1550 | −1640 | −5.8 |
| 353 | −1175 | −1170 | 0.4 |
| 383 | −850 | −860 | −1.2 |

TABLE II. A comparison of the experimental and theoretical second virial coefficients for acetone on the basis of an exponential repulsion.

| Temp. °K | Experimental virial cm³/mole | Theoretical virial cm³/mole | Percent difference |
|---|---|---|---|
| 323 | −1550 | −1620 | −4.5 |
| 353 | −1175 | −1180 | −0.4 |
| 383 | −850 | −910 | −7.1 |

TABLE III. A comparison of the experimental and theoretical second virial coefficients for methyl alcohol on the basis of the hard sphere model.

| Temp. °K | Experimental virial cm³/mole | Theoretical virial cm³/mole | Percent difference |
|---|---|---|---|
| 333 | −1250 | −1290 | −3.2 |
| 363 | −875 | −870 | 0.6 |
| 393 | −625 | −640 | −2.4 |

TABLE IV. A comparison of the experimental and theoretical second virial coefficients for methyl alcohol on the basis on an exponential repulsion.

| Temp. °K | Experimental virial cm³/mole | Theoretical virial cm³/mole | Percent difference |
|---|---|---|---|
| 333 | −1250 | −1250 | 0.0 |
| 363 | −875 | −870 | 0.6 |
| 393 | −625 | −660 | −5.6 |

## METHYL ALCOHOL

The dipole moment is taken to be $1.70\cdot10^{-18}$ esu.[5] Ramaswamy[6] found

$$n-1=\frac{5.7567\cdot10^{27}}{11462\cdot10^{27}-\nu^2}. \quad (4)$$

There results a static polarizability of $3.23\cdot10^{-24}$ cm$^3$, an oscillator strength of 5.8 and a resonance energy of 14 ev. Table III gives the comparison with experiment for the potential

$$V=-2.89\cdot10^{-12}(R^{-3}+R^{-5})f(\theta_1,\theta_2,\phi)-(194\cdot10^{-12}R^{-6}+496\cdot10^{-12}R^{-8})\text{ erg},\quad R>3.28\text{A}; \quad (5)$$

$$V=\infty,\quad R<3.28\text{A}.$$

Table IV gives the results for the potential

$$V=1.1\cdot10^{-8}e^{-R/0.28}-2.89\cdot10^{-12}(R^{-3}+R^{-5})f(\theta_1,\theta_2,\phi)-(194\cdot10^{-12}R^{-6}+496\cdot10^{-12}R^{-8})\text{ erg}. \quad (6)$$

The quantum correction[4] is negligible for $(CH_3)_2CO$ and $CH_3OH$ because of the large sizes of these molecules.

[1] O. Fuchs and H. L. Donle, Z. Physik. Chem. **22B**, 1 (1933).
[2] H. Lowery, Proc. Roy. Soc. (London) **133A**, 188 (1931).
[3] H. Margenau and V. Myers, Phys. Rev. **66**, 307 (1944).
[4] V. Myers, J. Chem. Phys. **18**, 1442 (1950).
[5] J. D. Stranathan, J. Chem. Phys. **6**, 395 (1938).
[6] K. L. Ramaswamy, Proc. Indian Acad. Sci. **4A**, 675 (1936).

# Letters to the Editor

*THIS section will accept reports of new work, provided these are terse and contain few figures, and especially few half-tone cuts. The Editorial Board will not hold itself responsible for opinions expressed by the correspondents. Contributions to this section should not exceed 600 words in length and must reach the office of the Editor not later than the 15th of the second month preceding that of the issue in which the Letter is to appear. No proof will be sent to the authors. A publication charge of $10.00 per Letter is made which, when honored, will entitle the Institution to 100 free reprints.*

## The Influence of a Direct-Current Electric Field on the Adhesion Tension

Z. LÁSZLÓ
*Budapest, Hungary*
(Received September 19, 1952)

OUR experimental set-up is shown in Fig. 1. Two nickel cylinders (a) and (b) are fixed in coaxial position by an insulating spacer (c). The axis of the cylinders are brought exactly in horizontal position. A few drops of liquid (e) are introduced between the two cylinders. Through the tubing (d) a pressure (p) is applied that will cause the surface of the liquid to form a flat surface on the left opening of the apparatus. (Marked on Fig. 1 in a dotted line.) The correct setting is checked in the following manner: the illuminated image of a slit (f) is projected on the plane perpendicular to the axis of the cylinders and the reflected image is observed with a microscope. Correct adjustment of the air pressure is indicated by the fact that the image on both the metal and liquid surfaces comes to fall into one straight line. From the distance between the cylinders and from the value of the pressure (p), the surface tension ($\gamma_1$) of the liquid is readily calculated.

The procedure is essentially identical with that used by Ferguson and Kennedy.[1] The authors used one glass capillary tubing in order to determine $\gamma_1$. The modification introduced by us makes it possible to determine the value of $\gamma_1$ also in the presence of an electric field, for which purpose a potential difference is applied between the two cylinders. When the electric field is being switched on, the liquid column does not alter its position, i.e., by a displacement in the horizontal interspace of the two cylindrical electrodes (where there is no electrical potential gradient in axial direction, no change of either the mechanical or electrical energy will take place). Thus, there is no disturbing effect caused by ponderomotoric forces.

We ascertained first by our tests that a 5000-cycle 600-volt field has no influence at all on ethyl, methyl, isopropyl, isoamyl, isobutyl alcohols, on acetone, on carbon tetrachloride, and on benzene. This corresponds with previous test results and theoretical considerations[2] which have led to the conclusion that $\Delta\gamma_1$ is too small to be observed.

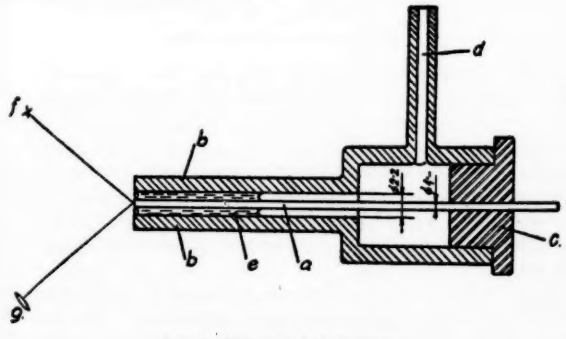


FIG. 1. Diagram of apparatus.

When a dc potential of about 250 volts is connected between the two cylinders, it was found that it was no longer possible to obtain a flat liquid surface by adjusting the pressure. The positive electrode becomes entirely covered with liquid before we could succeed in flattening the liquid surface by regulating the air pressure. This holds for both cases whether the outer electrode or the inner electrode is made positive. This phenomenon can only be explained by assuming that the adhesion tension ($\gamma_2$) is altered under the action of the electric field in such a manner that the value of $\gamma_2$ becomes greater on the positive electrode than on the negative electrode. From the observation that the positive electrode becomes covered with liquid at a smaller pressure (p) than without electric field, it follows that for the liquids which behave thus the adhesion tension increases compared with that existing for the field-free condition.

Through the influence of dc field no change of $\gamma_2$ could be observed for carbon tetrachloride and benzene.

Our experimental set-up is well suited to demonstrate the change of $\gamma_2$ in the presence of a dc electric field. The apparatus, however, does not provide means for a qualitative estimation of the test results. The change of $\gamma_2$ in a dc electric field is the consequence of the orientation of the polar molecules in the field.

[1] Ferguson and Kennedy, Proc. Phys. Soc. (London) **44**, 511 (1932).
[2] I. Bikerman, J. phys. et radium **9**, 386 (1928).

## The Thermal *Trans-Cis* Isomerization of Dideuteroethylene*

B. S. RABINOVITCH, JOHN E. DOUGLAS, AND F. S. LOONEY
*Department of Chemistry and Chemical Engineering, University of Washington, Seattle 5, Washington*
(Received September 15, 1952)

THERMAL *cis-trans* isomerization reactions of substituted olefins have been interpreted[1] as unimolecular reactions proceeding either via a high energy, singlet mechanism, displaying normal frequency factor, or by a low energy, triplet mechanism, characterized by a small frequency factor. The terms "singlet" and "triplet" refer to the $N$ and $T$ states of ethylene and the analysis of the electronic states of ethylene given by Mulliken.[2] We employ his notation. The isomerization of *trans*-ethylene, $d_2$ proceeds via the singlet mechanism in the absence of effective collisional perturbations, since the spin-orbit interaction connecting the singlet and triplet states of ethylene is very small.[1] The activation energy $E$ for this reaction may thus be identified with the height of the lowest singlet state ($N'$) for perpendicular ($\phi=\pi/2$) ethylene.

We have studied the isomerization of *trans*-ethylene, $d_2$ in quartz vessels over the pressure range 9–310 mm and in the temperature interval 450–550°C. *Cis-trans* ratios were obtained by infrared analysis, with the use of empirical calibration curves constructed from synthetic mixtures made from pure *cis*- and *trans*-ethylene, $d_2$. Exchange and polymerization is negligible at low pressures. Since the equilibrium ratio of *cis*- and *trans*-ethylene, $d_2$ is essentially 50:50,[3] the specific rates of forward and reverse reactions have been assumed equal. In the low pressure region, the kinetic constants are $A=3\times10^{12}$ sec$^{-1}$, $E=61.3\pm1.2$ kcal. At higher pressures both $A$ and $E$ decline, but these data are complicated by attendant increase in the extent of polymerization and sensitization of isomerization by decomposition of higher weight product. We believe from packed bulb studies that the effect of heterogeneous reaction at low pressure is minor.

Calculation of the rate of isomerization due to quantum mechanical tunneling[4] using a harmonic potential corresponding to a torsion frequency[5] of 1027 cm$^{-1}$ shows that this process is negligible.

The data thus indicate that the energy at the top of the singlet barrier is 61.3 kcal (2.66 ev). This quantity may be used to assist in the calibration of the parameters in the semitheoretical calculations that have been made for ethylene.[2b,6] In particular, in the

calculations of Parr and Crawford for the two-electron problem, a value of the screening constant $Z$ less than 3.18 formally corresponds to our result.

A crude estimate of the height of the $Z'$ state ($\phi=\pi/2$) may be made. On the assumption of harmonic torsional potential functions for the *cis*- and *trans*-configurations of the ground state, which in the absence of interaction would cross at 95 kcal, the $Z'$ state would lie at approximately 129 kcal (5.6 ev).

The energy required to "open the double bond" in ethylene has sometimes been deduced by methods which are erroneous in principle, e.g., as $D(C=C)-D(C-C)$ where $D(C-C)$ is for ethane, or from heats of hydrogenation, where $D(CH_3CH_2-H)$ is equated to $D(\dot{C}H_2CH_2-H)$. The above measured activation energy corresponds to this quantity for one of the two possible "opening" processes of interest in thermal reactions; namely, $C_2H_4 \rightarrow C_2H_4(N')-61.3$ kcal. Then $D(\dot{C}H_2CH_2-H \rightarrow C_2H_4(N')+H) = 100.5$ kcal.[7] Unfortunately, the necessary data for transformation to the perpendicular triplet state of ethylene are not available; its energy is something less than 61 kcal.

Finally, by specification of a value for $D(CH_2-H)$ ($CH_2$ produced in the ground state) some carbon-carbon bond dissociation energies may be indicated. $D(CH_2-H)$ has been given recently as 89.4 kcal[8] and <87 kcal;[9] the latter is more probably correct. We use here $D(CH_2-H)=<87$ kcal and obtain

$$D[\dot{C}H_2-\dot{C}H_2(N')](sp^2-sp^2)=<60.5 \text{ kcal},$$
$$D(CH_3-\dot{C}H_2)(sp^3-sp^2)=<74 \text{ kcal},$$
$$D(CH_3-CH_3)(sp^3-sp^3)=84.4 \text{ kcal}.[7]$$

$D(CH_2=CH_2)$ is of course known independently of L(C) if $D(CH_2-H)$ is known. The value used above corresponds to $D(CH_2=CH_2)=<122$ kcal.

A full report, together with some results on the rate of the reverse isomerization of pure *cis*-ethylene, $d_2$ will be presented later.

We thank Professor D. F. Eggers, Jr., for valuable discussions on the vibrations of ethylene.

* This work was sppported by the ONR.

[1] Magee, Shand, and Eyring, J. Am. Chem. Soc. **63**, 677 (1941); see also H. McConnell, J. Chem. Phys. **20**, 1043 (1952).
[2] (a) R. S. Mulliken, Phys. Rev. **41**, 751 (1932); (b) R. S. Mulliken and C. C. J. Roothaan, Chem. Revs. **41**, 219 (1947).
[3] N. R. Larson and B. S. Rabinovitch, unpublished results.
[4] D. M. Dennison and G. E. Uhlenbeck, Phys. Rev. **41**, 313 (1931).
[5] R. L. Arnett and B. L. Crawford, Jr., J. Chem. Phys. **18**, 118 (1950).
[6] R. G. Parr and B. L. Crawford, Jr., J. Chem. Phys. **16**, 526 (1948).
[7] Necessary thermochemical data are taken from J. S. Roberts and H. A. Skinner, Trans. Faraday Soc. **45**, 339 (1949).
[8] D. P. Stevenson, J. Chem. Phys. **18**, 1347 (1950); $D(CH_3-H)$ taken as 102 kcal.
[9] K. J. Laidler and E. J. Casey, J. Chem. Phys. **17**, 1087 (1949).

## The Sodium Photosensitized Isomerization of *Cis*-Butene-2*

W. MacF. Smith
*Department of Chemistry, Queen's University, Kingston, Ontario, Canada*
(Received September 3, 1952)

BUTENE-2 has a high cross section for the quenching of sodium atoms in the $3^2P$ state.[1] The energy given up by the excited sodium atom in the quenching collision is 48.3 kilocalories per gram atom, and the site of reception of the energy in an unsaturated molecule is probably the double bond.[1,2] The highest energy of activation recorded for thermal *cis-trans* isomerization of ethylene derivatives is about 46 kilocalories per gram molecule.[3] The fact that the energy donated to a butene molecule during the quenching collision is of the order of magnitude of the energy of activation for *cis-trans* isomerizations suggested that a study of the reactions of *cis*-butene-2 photosensitized by sodium in the $3^2P$ state might yield information about the distribution of energy required for isomerization.

We have investigated the sodium photosensitized reactions of *cis*-butene-2 in a quartz reaction vessel about 10 cm long and 200 cm³ in volume. The vessel, containing sodium had plane windows at both ends and was housed in a furnace fitted with windows which permitted the irradiating beam, originating in an Osira sodium lamp and filtered through a Corning filter No. 3480, to pass through the reaction vessel and out of the furnace. Weston photronic cells were used to measure roughly the intensity of the radiation, and it was estimated that the rate of absorption of radiation by the contents of the vessel under the conditions of our experiments was in excess of $2\times10^{17}$ quanta per minute. At the pressures of butene used about 90 percent of the sodium atoms excited by absorption undergo quenching collisions with butene.[1] Consequently, the rate at which butene molecules were energized through quenching collisions was in excess of $1.8\times10^{17}$ molecules per minute. Absorption measurements were carried out throughout the series of runs and indicated the presence of a reproducible concentration of sodium vapor in the reaction vessel at all times.

Runs of twelve hours duration were carried out with and without irradiation. The pressure of the butene was either 2 or 3 cm Hg, and the temperature of the reaction vessel (and sodium) was 170°C. The products were analyzed with a Perkin-Elmer infrared spectrometer through the cooperation of Dr. R. N. Jones of the Pure Chemistry Branch of the National Research Council of Canada. Differences in *cis*-butene-2 content of about 2 percent could be detected. The infrared absorption curves of the products were indistinguishable from the curve of the reactant (research grade *cis*-butene-2 of the Phillips Petroleum Company). It appears that isomerization was occurring to less than 2 percent, if at all. This conclusion, along with the above mentioned measurements on the absorption of radiation in the reaction vessel indicates that the quantum yield is less than 0.016. It may, of course, be much less than this.

These results show that the energy made available to the butene molecule by excited sodium atoms in the $3^2P$ state is inadequate to lead to *cis-trans* isomerization with high quantum yield. This may be due to the fact that the energy of activation for the "adiabatic" mechanism for isomerization[4] is in excess of the energy given up by the sodium in a quenching collision. The results are also consistent with an energy of activation several kilocalories less than the energy yielded by the excited sodium atom if there is rapid flow of energy away from the site of reception, which is doubtlessly the double bond, since the probability of localization of sufficient energy in the appropriate tortional vibration of the double bond before collisional deactivation occurs would then be very small.

* Assisted by a grant from the National Research Council of Canada.
[1] R. G. W. Norrish and W. MacF. Smith, Proc. Roy. Soc. (London) **A176**, 295 (1940).
[2] K. J. Laidler, J. Chem. Phys. **10**, 34 (1942).
[3] Glasstone, Laidler, and Eyring, *The Theory of Rate Processes* (McGraw-Hill Book Company, Inc., New York, 1941) p. 323.
[4] Magee, Shand, and Eyring, J. Am. Chem. Soc. **63**, 677 (1941).

## The Flame Emission Spectrum of HBr*

B. W. Bullock, C. E. Feazel, P. Gloersen, and S. Silverman
*Applied Physics Laboratory, The Johns Hopkins University, Silver Spring, Maryland*
(Received September 8, 1952)

THE emission spectrum of HBr has been observed in the hydrogen-bromine flame in the fundamental region at about 2600 cm$^{-1}$. The gases were premixed by passing hydrogen through boiling bromine, with a hydrogen by-pass to permit moderately accurate gas ratio control. The flame was ignited by means of a spark and sustained on a 50-mesh platinum gauze of about 2 cm in diameter. Sapphire viewing windows were mounted 3 mm from the flame proper to reduce the effects of absorption by cool outer regions.

A Perkin-Elmer Model 83 monochromator with LiF optics and a PbTe detector was used in these experiments. The intensity was such that, with a Baird 450-cycle phase sensitive amplifier,

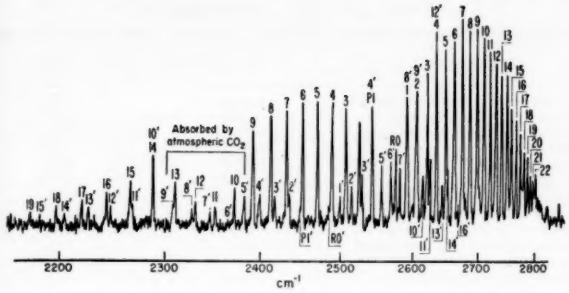


FIG. 1. The emission spectrum of HBr at approximately 1450°K.

it was possible to use an effective slit width as small as 1.6 $cm^{-1}$. Under these conditions, the $R$ branch of the 1−0 band was observed out to $J=22$ with indications of a band head at $J=25$. The $P$ branch was observed out to $J=20$. In addition, a number of lines of the 2−1 band in both $P$ and $R$ branches were observed. A typical spectrum is shown in Fig. 1.

Various empirical temperature determinations on a flame burning under approximately stoichiometric conditions indicate that equilibrium between the rotational and vibrational modes of excitation exists in the region of the flame *ca* 7 mm (0.02 sec) beyond the gauze. The 2−1 lines are sufficiently free from self-absorption to permit a rotational temperature to be estimated since the distribution is Boltzmann-like in character. The temperature so determined is 1430°K compared with about 1500°K for the theoretical temperature as determined by Anderson.[1] A self-absorption correction, obtained graphically from one and two path observations (using a plane mirror behind the flame to attain the second traversal), was applied to the 1−0 lines. The resultant distribution of intensities was again Boltzmann in character, and the temperature so determined was 1360°K. Using the iso-intensity method,[2,3] the average temperature for the 1−0 band was 1390°K. All of the above temperatures are estimated to be consistent to within about 5 percent.

The vibrational temperature was estimated to be 1400°K±125° using the transition probability values of Crawford and Dinsmore.[4] As a check the rotational temperature determined from the 1−0 band of HCl, present in the flame due to a 0.3 percent chlorine impurity in the bromine, was found to be 1550°K, again to a 5 percent accuracy. No self-absorption correction was needed for this latter determination due to the low intensity of the HCl impurity spectrum.

Further work is in progress both in absorption and emission of the $H_2+Br_2 \rightleftarrows 2HBr$ reaction and will be reported on in greater detail at a later date.

* This work was supported by the U. S. Navy Bureau of Ordnance under Contract NOrd-7386.

[1] R. C. Anderson, "Temperature and concentration changes in the reaction of hydrogen and bromine in various gas mixtures," Section T, Report No. CF-1350, September, 1949, Defense Research Laboratory, The University of Texas.

[2] G. H. Dieke and H. M. Crosswhite, "The ultraviolet bands of OH fundamental data," Bumblebee Series, Report No. 87, November, 1948, The Johns Hopkins University.

[3] K. E. Shuler, J. Chem. Phys. **18**, 1466 (1950).

[4] B. L. Crawford and H. L. Dinsmore, J. Chem. Phys. **18**, 983 (1950).

## A Note on the Classification of Normal Vibrations of Molecules

YONEZO MORINO AND KŌZO KUCHITSU
*Department of Chemistry, Faculty of Science, Tokyo University, Bunkyo-ku, Tokyo, Japan*
(Received September 9, 1952)

IN order to indicate the essential features of normal vibrations of molecules, it is customary to classify the frequencies as stretching, deformation, rocking, wagging, etc. In fact, such a classification has been made empirically according to their wave numbers, but the rules for them are not exactly defined. At once it may be thought that when a certain frequency has the largest amplitude of displacement in an internal coordinate, this frequency may be called the characteristic frequency of the coordinate, irrespective of finite displacements of the others. It can, however, be easily shown that this definition does not always come up to our expectation. In Table I are shown the ratios of the amplitudes of displacements of the internal coordinates, $\Delta R$(C=C), $\Delta r$(C−F), and $r\Delta\beta$($\angle$C−C−Cl) of $CF_2=CF_2$ molecule, all of which are calculated by the use of the matrix elements $L_{ik}$, given in our recent article.[1] The largest amplitudes are designated by black type letters. Although the vibrations of $A_g$ and $B_{2u}$ groups satisfy the above definition, either of the two normal vibrations in $B_{1g}$ group has larger amplitude in $r\Delta\beta$; therefore, according to this definition, both of them must be assigned to rocking vibration, and we have no C−F stretching vibration in this symmetry class. Further, for $B_{2u}$ group, the vibration $\nu_8$, which has the frequency 1186 $cm^{-1}$ and is obviously to be assigned to the C−F stretching frequency, has almost the same amplitude in $r\Delta\beta$ as that in $\Delta r$(C−F). Accordingly, it would be better to look for another standard for the definition of the characteristic frequencies.

TABLE I. The assignment of the vibrations and the ratios of the displacements of the internal coordinates of $CF_2=CF_2$ molecule.

| | $\nu$obd ($cm^{-1}$) | Assignment | $\Delta r$(C=C) | $\Delta r$(C−F) | $r\Delta\beta$(C−C−Cl) |
|---|---|---|---|---|---|
| $A_g$ | $\nu_1$ 1872 | C=C stretching | **0.404** | −0.126 | −0.172 |
| | $\nu_2$ 778 | C−F stretching | 0.052 | **0.099** | −0.038 |
| | $\nu_3$ 394 | $CF_2$ deformation | −0.018 | −0.011 | **0.106** |
| $B_{1g}$ | $\nu_4$ 1340 | C−F stretching | ··· | −0.203 | **0.481** |
| | $\nu_5$ 544 | $CF_2$ rocking | ··· | 0.038 | **0.228** |
| $B_{2u}$ | $\nu_6$ 1335 | C−F stretching | ··· | **−0.206** | 0.091 |
| | $\nu_7$ 245 | $CF_2$ rocking | ··· | −0.002 | **0.131** |
| $B_{3u}$ | $\nu_8$ 1186 | C−F stretching | ··· | **−0.159** | **0.140** |
| | $\nu_9$ 558 | $CF_2$ deformation | ··· | 0.021 | **0.151** |

Recently Torkington[2] and Thomas[3] discussed the distribution of potential energy in the internal coordinates for each normal mode of vibration. The potential energy of the whole molecule for a given normal vibration $X_k$, may be expressed as

$$V=\tfrac{1}{2}\sum_{i,j} F_{ij}R_iR_j=\tfrac{1}{2}X_k^2\sum_{i,j} L_{ik}L_{jk}F_{ij},$$

where the $L_{ik}$'s are the elements of the transformation matrix: $\mathbf{R}=\mathbf{LX}$. If the largest term in this expression is $L_{ik}^2F_i^2$, this frequency is to be called the $R_i$ characteristic frequency; and particularly, if $R_i$ corresponds to a change of a bond distance, it is called the $R_i$ stretching frequency; and, if it corresponds to a change of a bond angle, it is called the $\alpha_i$ deformation or rocking

TABLE II. Potential energy terms $L_{ik}L_{jk}F_{ij}$ for each normal vibration of $CF_2=CF_2$ molecule.

$A_g$

$\nu_1$(C=C stretching)

| | $R_1$ | $R_2$ | $R_3$ |
|---|---|---|---|
| $R_1$ | **1.896** | | |
| $R_2$ | −0.129 | 0.485 | |
| $R_3$ | −0.084 | −0.056 | 0.219 |

$\nu_2$(C−F stretching)

| $R_1$ | $R_2$ | $R_3$ |
|---|---|---|
| 0.032 | | |
| 0.013 | **0.298** | |
| −0.002 | 0.010 | 0.022 |

$\nu_3$($CF_2$ deformation)

| | $R_1$ | $R_2$ | $R_3$ |
|---|---|---|---|
| $R_1$ | 0.004 | | |
| $R_2$ | 0.000 | 0.004 | |
| $R_3$ | 0.002 | −0.003 | **0.083** |

$B_{1g}$

$\nu_4$(C−F stretching)

| | $R_4$ | $R_5$ |
|---|---|---|
| $R_4$ | **0.990** | |
| $R_5$ | −0.118 | 0.456 |

$\nu_5$($CF_2$ rocking)

| $R_4$ | $R_5$ |
|---|---|
| 0.034 | |
| 0.010 | **0.103** |

$B_{2u}$

$\nu_6$(C−F stretching)

| | $R_6$ | $R_7$ |
|---|---|---|
| $R_6$ | **1.024** | |
| $R_7$ | −0.023 | 0.018 |

$\nu_7$($CF_2$ rocking)

| $R_6$ | $R_7$ |
|---|---|
| 0.000 | |
| −0.000 | **0.034** |

$B_{3u}$

$\nu_8$(C−F stretching)

| | $R_8$ | $R_9$ |
|---|---|---|
| $R_8$ | **0.774** | |
| $R_9$ | −0.057 | 0.144 |

$\nu_9$($CF_2$ deformation)

| $R_8$ | $R_9$ |
|---|---|
| 0.013 | |
| 0.008 | **0.168** |

frequency according to the symmetry of the group, to which the $R_i$ belongs. In Table II each term of the potential energy $L_{ik}L_{jk}F_{ij}$ is listed for every normal vibration, where the largest term is marked by black type letters. It is easily seen that the difficulties mentioned above are all overcome by this definition, i.e., $\nu_4$ and $\nu_8$ have the largest terms in the bond distance $\Delta r$(C−F), corresponding to $\nu_5$ and $\nu_9$ in the angle $r\Delta\beta$, just as we expected.

Of course, there might be a case when two terms $L_{ik}^2$, in the potential energy expression have the largest but almost the same magnitude, or when a cross term $L_{ik}L_{jk}F_{ij}(i\neq j)$ is the largest. In such a case we may say that the vibration is a characteristic frequency of the group to which the $R_i$ and $R_j$ belong. Fortunately, in $C_2F_4$ molecule there appear no such cases, and hence the usual classification can be applied to this molecule.

It was shown that in the case of vinylidene difluoride $CF_2=CH_2$ this rule provided the usual classification without any modification. I. Nakagawa[4] also showed that this rule clears up the difficulties in the case of the skeleton vibrations of monochloroacetylchloride.

[1] Morino, Kuchitsu, and Shimanouchi, J. Chem. Phys. **20**, 726 (1952).
[2] P. Torkington, J. Chem. Phys. **17**, 347 (1949).
[3] J. O. Thomas, J. Chem. Phys. **19**, 1162 (1951).
[4] I. Nakagawa, J. Chem. Soc. (Japan) (to be published).

## On the Infrared Spectrum of Methyl Chloroform

PUTCHA VENKATESWARLU
*Department of Physics, Duke University, Durham, North Carolina*
*And*
*Spectroscopy Laboratory, Massachusetts Institute of Technology, Cambridge, Massachusetts*
(Received May 7, 1952)

THE infrared spectrum of methyl chloroform ($CH_3CCl_3$) obtained with a Perkin-Elmer infrared spectrometer using LiF, NaCl, and KBr prisms was discussed[1] by the author sometime ago. Later El-Sabban, Meister, and Cleveland,[2] and Smith, Brown, Nielsen, Smith, and Liang[3] published their Raman and infrared work on methyl chloroform. Our infrared data[1] agree very well with the data of Smith *et al.* but not with the data of El-Sabban *et al.* This is probably because the data of El-Sabban *et al.* were obtained only with a KBr prism and their spectrum[2] in the region 600–5000 cm$^{-1}$ has small resolution compared to the spectra given in our earlier paper[1] and that given by Smith *et al.*[3] However, El-Sabban *et al.* included in their paper the then unpublished data of Smith *et al.* and gave the assignments.

The band envelopes of the infrared bands (parallel as well as some of the perpendicular type bands) of methyl chloroform are expected in general to show peaks corresponding to the *P*, *Q*, and *R* branches. This was discussed to some extent in our earlier paper.[1] Although El-Sabban *et al.* mentioned that some of the bands obtained by Smith *et al.* may be due to rotational structure, they in their assignments[2] did not take into consideration the very probable existence of the *P*, *Q*, and *R* peaks. Thus, in many cases they assigned three different vibrations to the three peaks, which in our opinion correspond to the *P*, *Q*, and *R* branches of a single vibrational band. For example, the *P*, *Q*, *R* peaks of the vibrational band $\nu_7(e)$ at 3014 cm$^{-1}$ (our value) were assigned by them to three different vibrations $\nu_2+\nu_6+\nu_8'$, $\nu_7$, and $3\nu_3'$, respectively, and those of the vibrational band $\nu_1(a_1)$ at 2954 cm$^{-1}$ to $(\nu_1+\nu_{10}')-\nu_{10}''$, $\nu_1$, and $\nu_3''+\nu_4+\nu_8'$, respectively. Although El-Sabban *et al.* in the following letter still appear to feel partly convinced about their assignments, it is extremely unlikely that these *P* and *R* peaks could be due to overtones and combinations while the central peak is due to a fundamental and while these have the right separation and the right relative intensities.

The infrared spectrum of the gaseous methyl chloroform has recently been recorded with a modified Perkin-Elmer 12-B instrument using a KRS-5 prism at the Spectroscopy Laboratory, Massachusetts Institute of Technology. Path lengths of 6, 80, 160, and 240 cm with varying pressures were used. Methyl chloroform obtained from the Chemistry Department of Harvard University was twice distilled before using. Two bands were obtained in the region 400−250 cm$^{-1}$. One of them is a strong band at 345 cm$^{-1}$, which has been observed by many investigators[1–4] in the Raman effect and by Smith *et al.* in the infrared for the liquid. The other band, which is very weak, is at 381 cm$^{-1}$. This band could be observed only with the path lengths 80–160 cm and a pressure of 100 mm, whereas the strong band could be observed with a 6-cm cell.

TABLE I. Fundamentals of $CH_3CCl_3$.

| Description | Designation | $\nu_{vac}$ in cm$^{-1}$ |
|---|---|---|
| Symmetric C−H stretching | $\nu_1(a_1)$ | 2951 |
| Symmetric $CH_3$ deformation | $\nu_2(a_1)$ | 1386 |
| Symmetric C−C stretching | $\nu_3(a_1)$ | 867,[1] 1009,[2] or 1075[3] |
| Symmetric C−Cl stretching | $\nu_4(a_1)$ | 526 |
| Symmetric $CCl_3$ deformation | $\nu_5(a_1)$ | 345 |
| Torsion | $\nu_6(a_2)$ | |
| Degenerate C−H stretching | $\nu_7(e)$ | 3014 |
| Degenerate $CH_3$ deformation | $\nu_8(e)$ | 1457 |
| Degenerate $CH_3$ rocking | $\nu_9(e)$ | 1088 |
| Degenerate C−Cl stretching | $\nu_{10}(e)$ | 724 |
| Degenerate $CCl_3$ deformation | $\nu_{11}(e)$ | 381 or 301 |
| Degenerate $CCl_3$ rocking | $\nu_{12}(e)$ | 241 |

Because of these results and because of the now available polarization data[2–4] the assignment of the fundamentals given in the earlier paper has to be slightly modified. The vibrational assignments of the fundamentals is given in Table I. The frequency of the degenerate $CCl_3$ deformation vibration might be 381 cm$^{-1}$, which is now obtained as a weak band in the infrared, or 301 cm$^{-1}$, which was obtained by Smith *et al.* as a weak Raman line. Similarly, the frequency of the C−C stretching vibration is still uncertain.[1–3] However, El-Sabban *et al.* feel quite strongly in the following letter[5] that the value 867 cm$^{-1}$ (Table I and reference 1) is too low for the C−C stretching vibration in $CH_3CCl_3$, but they do not discuss why in both $C_2D_6$ and $CH_3CF_3$ it is of the order of 850 cm$^{-1}$. Further work, probably with high resolving grating instruments, may give a definite answer about the frequency of this vibration.

I would like to express my thanks to Mr. H. Shreepathi Rao for his kind help in the experimental part of the work.

[1] P. Venkateswarlu, J. Chem. Phys. **19**, 298 (1951).
[2] El-Sabban, Meister, and Cleveland, J. Chem. Phys. **19**, 855 (1951).
[3] Smith, Brown, Nielsen, Smith, and Liang, J. Chem. Phys. **20**, 473 (1952).
M. Zaffar Ullah, unpublished work done at the Spectroscopy Laboratory, Massachusetts Institute of Technology.
[5] El-Sabban, Meister, and Cleveland, J. Chem. Phys. **20**, 1810 (1952).

## Vibrational Assignments for 1,1,1-Trichloroethane*

M. ZAKI EL-SABBAN, ARNOLD G. MEISTER, AND FORREST F. CLEVELAND
*Spectroscopy Laboratory, Department of Physics, Illinois Institute of Technology, Chicago 16, Illinois*
(Received May 19, 1952)

IN the preceding letter,[1] Venkateswarlu points out that some of the infrared bands, assigned in our previous paper[2] as overtone or combination bands, may be *P*, *Q*, and *R* branches of a single band. This, of course, may be true, as we stated in our paper. On the other hand, unless our assignment of the fundamentals can be shown to be incorrect (and Venkateswarlu's new assignment of these is the same as ours, except that he admits two other possibilities for $\nu_3$ and one other possibility for $\nu_{11}$), one cannot arbitrarily rule out the possibility that the allowed overtones and combination frequencies (mostly binary) may contribute to the intensities of the observed bands in question.

Our normal coordinate treatment indicates that, unless the potential constants are unreasonably different from their values in similar molecules, the C−C stretching frequency cannot be as low as 867 cm$^{-1}$ without changing the other $A_1$ frequencies to values so different from the observed values as to be unacceptable.

TABLE I. Variation of the central bond stretching frequency with the mass of the substituents for substituted ethanes, ethylenes, and acetylenes.

| Molecule | C−C | Molecule | C=C | Molecule | C≡C |
|---|---|---|---|---|---|
| $H_3C-CH_3$ | 993[a] | $H_2C=CH_2$ | 1623 | $HC\equiv CH$ | 1974 |
| $D_3C-CD_3$ | 852 | $D_2C=CD_2$ | 1515 | $DC\equiv CH$ | 1851 |
| $H_3C-CF_3$ | 831 | $H_2C=CF_2$ | 1728[b] | $DC\equiv CD$ | 1762 |
| $F_3C-CF_3$ | 809 | $F_2C=CCl_2$ | 1739 | $IC\equiv CI$ | 2113 |
| $Cl_3C-CCl_3$ | 975 | $F_2C=CF_2$ | 1872[b] | $H_3CC\equiv CH$ | 2124 |
| $H_3C-CCl_3$ | 1010 | $Cl_2C=CCl_2$ | 1571 | $H_3CC\equiv CCl$ | 2263 |
| $Br_3C-CBr_3$ | 1028[c] | $H_2C=C(CH_3)_2$ | 1638 | $H_3CC\equiv CBr$ | 2230 |
| | | $(CH_3)_2C=C(CH_3)_2$ | 1676 | $H_3CC\equiv CI$ | 2197 |

[a] Wave number in $cm^{-1}$.
[b] Value for the gaseous state.
[c] Calculated value.

The principal potential constant involved is that for the C−C bond. For this, Stitt's value of 4.50 md/A for ethane was used. That this is the correct value for this constant is indicated by the value of 1.55A obtained very recently[3] for the C−C bond distance in this molecule by a microwave investigation. Since this is the normal ethane value for the C−C bond length, one would expect the potential constant also to be the same as for ethane. Consequently, it appears that Venkateswarlu's value of 867 $cm^{-1}$ should be dropped as one of the possibilities for $\nu_3$.

It is not safe to suppose that the C−C stretching frequency will necessarily be low because of the greater mass of the $CCl_3$ group. Table I, for example, gives values of the central bond stretching frequency for several of the more carefully investigated molecules, not only for the C−C bond but also for the C=C and C≡C bonds. Examination of this table shows that there is no definite trend of frequency with mass. In fact, the frequency for the higher masses is, for each of the three types of central bond, often greater than for the parent compound itself. It seems clear, then, that it is dangerous to assign a frequency of this type on the assumption that an increased mass means a decreased frequency. A careful normal coordinate treatment appears to be essential for a reliable assignment of this frequency for the substituted ethanes.

If the weak infrared band found at 381 $cm^{-1}$ by Venkateswarlu does correspond to the fundamental $\nu_{11}$ (as seems probable), this provides an interesting confirmation of our deduction[2] that this band should appear higher than the $A_1$ frequency at 343 $cm^{-1}$, rather than lower (at 301 $cm^{-1}$) as in the assignment of Smith *et al.*[4] Since the 381 value was for the gas, the corresponding liquid value would normally appear at about 371 $cm^{-1}$, which is to be compared with our calculated value of 363 $cm^{-1}$, obtained with potential constants adjusted to fit frequencies for the liquid.

* Supported in part by Office of Ordnance Research, contract DA-11-022-ORD-464.

[1] Putcha Venkateswarlu, J. Chem. Phys. **20**, 1810 (1952).
[2] El-Sabban, Meister, and Cleveland, J. Chem. Phys. **19**, 855 (1951).
[3] Ghosh, Trambarulo, and Gordy, J. Chem. Phys. **20**, 605 (1952).
[4] Smith, Brown, Nielsen, Smith, and Liang, J. Chem. Phys. **20**, 473 (1952).

## The Stability of the Acetyl Radical

A. J. C. NICHOLSON
*Chemical Physics Section, Division of Industrial Chemistry, Commonwealth Scientific and Industrial Research Organization, Melbourne, Australia*
(Received August 20, 1952)

IN a recent paper on the photolysis of acetone in the presence of iodine, Pitts and Blacet[1] observed that the low yield of carbon monoxide at 177°C indicates that the acetyl radical is stable at this temperature. McDowell and Thomas[2] reached the same conclusion from a study of the oxidation of acetaldehyde. This seems difficult to reconcile with the fact that the quantum yield of carbon monoxide in the uninhibited photolysis is 1 at temperatures as low as 100°C. Pitts and Blacet suggest that "it now seems evident that from 100–177°C the acetyl radical dissociates readily only in the presence of relatively large quantities of free radicals, whereas in the absence of such free radicals it is quite stable over that temperature range." A simpler explanation of this anomaly is available. If the reaction

$$CH_3\cdot CO \rightarrow CH_3 + CO \qquad (A)$$

has an activation energy of about 18 kcal/mole (Gorin,[3] Herr and Noyes,[4] Marcotte and Noyes[5]) and a pre-exponential factor of $10^{12}$ $sec^{-1}$, then at 127°C, the rate of removal of $CH_3\cdot CO$ by (A) $\simeq 1.4\times 10^{2}[CH_3\cdot CO]$ mole $cc^{-1}$ $sec^{-1}$. Suppose 3 mm of iodine ($1.14\times 10^{-7}$ mole $cc^{-1}$) are present, and the reaction

$$CH_3\cdot CO + I_2 \rightarrow CH_3\cdot CO\cdot I + I \qquad (B)$$

occurs with a pre-exponential factor of $10^{14}$ cc $mole^{-1}$ $sec^{-1}$ and an activation energy of zero. Then the rate of removal of $CH_3\cdot CO$ by (B) $\simeq 1.14\times 10^{7}[CH_3\cdot CO]$ mole $cc^{-1}$ $sec^{-1}$.

Thus, although acetyl radicals are "unstable" in the uninhibited photolysis, their reaction with iodine is so much faster than their natural decay that they all disappear by (B) in the inhibited photolysis. At 177°C the rate of (A) would increase by a factor of 10, so (B) would still be overwhelmingly predominant. Essentially similar arguments would apply to the reaction of acetyl radicals with oxygen discussed by McDowell and Thomas.[2]

The numerical values chosen, particularly for (B), are only rough estimates. It could be argued, by analogy with hydrogen abstraction reactions, that (B) has a steric factor as low as $10^{-3}$. Alternatively, if the activation energy of (B) was 5 kcal/mole, its rate would be reduced by a factor of 1000. Unless both these effects operated together (B) would still be the faster reaction. The point of the calculation is merely to emphasize that it is meaningless to compare the "stabilities" of free radicals in different systems unless all the rate constants of the reactions in which the radicals disappear are known.

[1] J. N. Pitts, Jr., and F. E. Blacet, J. Am. Chem. Soc. **74**, 455 (1952).
[2] C. A. McDowell and J. H. Thomas, J. Chem. Soc. 2217 (1949).
[3] E. Gorin, J. Chem. Phys. **7**, 256 (1939).
[4] H. S. Herr and W. A. Noyes, Jr., J. Am. Chem. Soc. **62**, 2052 (1940).
[5] F. B. Marcotte and W. A. Noyes, Jr., J. Am. Chem. Soc. **74**, 783 (1952).

## On the Internuclear Distance and Dipole Moment of the LiF Molecule*

J. W. TRISCHKA
*Syracuse University, Syracuse, New York*
(Received August 25, 1952)

THE internuclear distance $r$ and the dipole moment $\mu$ of the LiF molecule have never been measured experimentally. However, theoretical predictions of these quantities have been made by Rittner;[1] and the quantity $\mu^2 A$, where $A$ is the moment of inertia, has been obtained by the electric resonance method of molecular beam spectroscopy.[2] Rittner's calculations make use of the experimental binding energy and a classical theory of this energy which is "in the spirit of the Born-Mayer lattice theory." The electrostatic terms in the binding energy are obtained with the aid of a classical molecular model in which the molecule is assumed to be composed of two mutually polarized ions. It is the purpose of the present note to obtain estimates of $\mu$ and $r$ from the experimentally determined value of $\mu^2 A$ and from formulas derived with the use of the above mentioned model.

Let $f$ be defined by $f=\mu/er$, where $e$ is the electronic charge. If $m$ is the reduced mass of the molecule, then $A=mr^2$. From the two preceding statements it follows that

$$r=(\mu^2 A/e^2 f^2 m)^{\frac{1}{4}}. \qquad (1)$$

The theoretical expression for $f$ is now introduced:[1,3]

$$f=1-[r^3(\alpha_1+\alpha_2)+4\alpha_1\alpha_2]/(r^6-4\alpha_1\alpha_2), \qquad (2)$$

where $\alpha_1$ and $\alpha_2$ are the polarizabilities of the ions. When Pauling's values[4] of the polarizabilities are used, the simultaneous solution of (1) and (2) gives for LiF, $r=1.65\times 10^{-8}$ cm. From (3) and the definition of $f$, the value $\mu=6.0\times 10^{-18}$ esu cm is found.

To test the validity of the above procedure, calculations were

TABLE I. Comparison of calculated and experimental values of internuclear distances and dipole moments.

| Molecule | Exptl $r$, $10^{-8}$ cm | Calc $r$, $10^{-8}$ cm | Exptl $\mu$, $10^{-18}$ esu cm | Calc $\mu$, $10^{-18}$ esu cm |
|---|---|---|---|---|
| LiF | ... | 1.65 | ... | 6.0[a] |
| KF[b] | 2.55 | 2.22 | 7.3 | 10.7 |
| KCl[c] | 2.67 | 2.79 | 10.6 | 9.2 |
| CsF[d] | 2.35 | 2.39 | 7.9 | 7.3 |
| CsCl[e,f] | 2.90 | 2.99 | 10.5 | 9.3 |

[a] From the calculated value of $r$.
[b] L. Grabner and V. Hughes, Phys. Rev. **79**, 819 (1950).
[c] Fabricand, Carlson, Lee, and Rabi, Phys. Rev. **86**, 607 (1952).
[d] J. W. Trischka, Phys. Rev. **76**, 1365 (1949).
[e] R. G. Luce and J. W. Trischka, Phys. Rev. **83**, 851 (1951).
[f] Stitch, Honig, and Townes, Phys. Rev. **86**, 813 (1952).

made for those alkali halides for which the values of $\mu^2A$, $\mu$, and $r$ have been measured. The results of these calculations are shown in Table I. Attention is called first to the internuclear distances. With the exception of the distance for KF, the calculated values are larger than the experimental values. Thus, it appears that (2) usually gives too small a value of $f$. This conclusion is re-enforced when the experimental values of $\mu$ are compared with the calculated values obtained by the use of (2) and the experimental internuclear distances. Again, KF is an exception. For the other molecules the experimental values of $\mu$ are larger than the calculated values. Hence, the use of the classical polarized-ion model leads in these cases to an underestimation of $f$. If LiF behaves as do the majority of the molecules in Table I, then the present estimation method gives too large a value of the internuclear distance. Therefore, the value of $r$ given above is likely to constitute an upper bound.

A lower bound may be set for the value of $r$ with a high degree of certainty. From (2) it is clear that $f<1$, and this is confirmed by all experimental measurements on the alkali halides. Hence, from (1) it can be concluded that for LiF $r>1.44\times10^{-8}$ cm.

Rittner's value of $r$, $1.53\times10^{-8}$ cm, is consistent with the results presented here.

* Supported in part by ONR.
[1] E. S. Rittner, J. Chem. Phys. **19**, 1030 (1951).
[2] J. C. Swartz and J. W. Trischka, Phys. Rev. **86**, 606 (1952).
[3] P. Debye, *Polar Molecules* (Dover Publications, New York, 1945), p. 61.
[4] L. Pauling, Proc. Roy. Soc. (London) **A114**, 191 (1927).

## London Dispersion Forces between Unlike Molecules*

JAMES F. HORNIG AND JOSEPH O. HIRSCHFELDER
*University of Wisconsin Naval Research Laboratory, Madison, Wisconsin*
(Received August 21, 1952)

FOLLOWING the method of Margenau,[1] we have derived an expression for the London dispersion forces between unlike nonpolar molecules. This is a simple generalization of Margenau's result for the interaction between two like nonpolar molecules. If the dispersion curves for substances $a$ and $b$ can be represented in terms of the resonant frequencies $\nu_a$ and $\nu_b$ respectively, and if the polarizabilities of the two molecular species are $\alpha_a$ and $\alpha_b$ respectively, then the interaction energy between the unlike molecules is given by:

$$\varphi_{ab}=-\frac{3h}{2}\frac{\alpha_a\alpha_b\nu_a\nu_b}{\nu_a+\nu_b}\frac{1}{R^6}-\frac{45h^2\alpha_a\alpha_b\nu_a\nu_b}{8e^2}\left[\frac{\alpha_a\nu_a}{2\nu_a+\nu_b}+\frac{\alpha_b\nu_b}{\nu_a+\nu_b}\right]\frac{1}{R^8}$$
$$-\frac{315h^3}{16e^4}\frac{\alpha_a^2\alpha_b^2\nu_a^2\nu_b^2}{\nu_a+\nu_b}\frac{1}{R^{10}}+\cdots. \quad (1)$$

The terms in the inverse eighth and inverse tenth powers of the separation, $R$, are higher order corrections to the simple London formula. Since $h\nu_a$ is usually nearly equal to the ionizational potential, Eq. (1) is convenient for estimating the long-range energy of interaction between the unlike molecules.

Each molecule is represented by a three-dimensional isotropic harmonic oscillator, and the energy of interaction is calculated by the second-order perturbation method. Such a model seems quite artificial, and its use can only be justified on the basis of previous successful applications and upon the validity of the correspondence principle. First of all, Margenau has shown that his result for like molecules gives excellent values in the two cases where detailed accurate quantum-mechanical calculations have been carried out: the interaction of two hydrogen or two helium atoms. Secondly, Mulliken[2] has observed that frequently the dispersion curves for index of refraction *versus* frequency can be represented by a single resonance frequency. This suggests that only a single transition plays an important role in charge transfer processes. Van Vleck[3] has noted the success of the oscillator model for describing such dispersion phenomena, but remarks that the reasons for its success are not yet fully understood.

In general, one would expect that the third-order perturbation would contribute a term in the dispersion energy which varies as $1/R^9$. However, this term is zero for the simple harmonic oscillator wave function used.

* This work was carried out under Contract NOrd 9938 with the Navy Bureau of Ordnance.
[1] H. Margenau, J. Chem. Phys. **6**, 896 (1938).
[2] R. S. Mulliken, J. Chem. Phys. **7**, 14, 20 (1938).
[3] J. H. Van Vleck, J. Chem. Phys. **5**, 556 (1937).

## Preliminary Analysis of the Pure-Rotational Spectrum of Methyl Amine*

DAVID R. LIDE, JR.
*Mallinckrodt Chemical Laboratory, Harvard University, Cambridge, Massachusetts*
(Received September 17, 1952)

A NUMBER of microwave absorption lines of methyl amine have been reported by Hershberger and Turkevich.[1] The spectrum of this compound has been reinvestigated with a Stark modulation spectrograph, and about sixty-five lines have been measured in the 18,000- to 27,000-mc region. Three of these lines have distinctive Stark effects which suggest that they correspond to transitions in the over-all rotation. On the assumption that the molecule can be regarded in the first approximation as a rigid rotor, an analysis of the Stark effects has led to the following tentative assignments:

| | |
|---|---|
| 23,340.92 mc | $5_{1,4}\rightarrow4_{2,2}$ |
| 23,449.90 | $5_{2,3}\rightarrow6_{1,5}$ |
| 36,452.60 | $5_{1,5}\rightarrow4_{2,3}$. |

These transitions are active from the component of dipole moment along the large axis of inertia. While their Stark effects are essentially second order at low values of $E^2M^2$, the near degeneracy of the $4_{2,2}-4_{2,3}$ levels and of the $5_{2,3}-5_{2,4}$ levels, which can interact through the dipole component along the small inertial axis, leads to strong deviations from the second-order dependence at high field strengths. Rotational constants have been determined from these three assigned transitions, and the Stark effects have been calculated in detail by the theory of Golden and Wilson.[2] The two components of the dipole moment, which are the only adjustable parameters in this calculation, were determined by fitting the Stark effect of the $5_{1,4}\rightarrow4_{2,2}$ transition. A comparison of experimental and predicted Stark effects, which is shown in Fig. 1,[3] lends strong support to these assignments. In regions where no points are reported near the predicted curves, the presence of other lines prevented measurements from being made.

The rotational constants obtained from the above assignment (on the assumption of a rigid rotor) are $a=105{,}976$ mc, $b=22{,}604$ mc, and $c=21{,}723$ mc. These constants yield a value of 22,163 mc for the parameter $\frac{1}{2}(b+c)$, which agrees closely with the infrared determination[3] of 22,135 mc. Furthermore, the observation of Stark lobes from the forbidden $5_{1,4}\rightarrow4_{2,2}$ transition, which becomes permitted in the presence of the field, gives an independent loca-

tion of the $4_{2,3}$ level which agrees within 0.20 mc with the energy calculated from the rotational constants. The components of dipole moment obtained by fitting the Stark effects are $\mu_a=0.304$ and $\mu_c=1.232$ debye units. This gives a total dipole moment of 1.27 debye units, in good agreement with the results of dielectric constant measurements. The dipole makes an angle of 76° 8 min with the $a$ principal axis; if the nitrogen valence angles are assumed to be the same as in $NH_3$, it is found that this dipole moment falls about 5° from the axis of the pyramid formed by the three nitrogen bonds.

While the above assignment is supported by the self-consistency of the data, it has not been possible to assign other rotational transitions. The next transitions which are predicted in the accessible frequency region involve $J$ values in the neighborhood of ten, and there are no lines within 1000 mc of these predicted frequencies which can reasonably be assigned to them. A possible explanation for this difficulty is that the interaction of the torsional oscillation with the other vibrational modes results in unusually large centrifugal distortion shifts of the levels. If this is the case, the self-consistency of the Stark effects of the three assigned lines should still be expected, since the levels involved in the perturbations do not have widely differing quantum numbers. However, it is apparent that the rotational constants given above may be off by a considerable amount as a result of the nonrigidity of the molecule. The question can probably be settled by a study of the lines of very low $J$ value, all of which fall above 40,000 mc.

Qualitative considerations make it clear that only a small fraction of the observed spectrum can be due to pure-rotational transitions. About twenty lines with first-order Stark effects form a well-defined series beginning around 27,000 mc and running to low frequencies. The similarity of this series to the one found in methyl alcohol[4] suggests that it involves a transition between sublevels which are split by tunneling through the potential barrier to internal rotation. Although no regularities have been recognized in the remaining lines, it seems probable that they arise from transitions of this same type.

We are grateful to Professor E. Bright Wilson, Jr., and Dr. Daniel Kivelson for several discussions on the effects of nonrigidity upon the rotational spectrum.

* The research reported in this paper was made possible by support extended Harvard University by the ONR under ONR Contract N5ori-76, T.O.V.

[1] W. D. Hershberger and J. Turkevich, Phys. Rev. **71**, 554 (1947).
[2] S. Golden and E. B. Wilson, Jr., J. Chem. Phys. **17**, 439 (1949).
[3] R. G. Owens and E. F. Barker, J. Chem. Phys. **8**, 229 (1940).
[4] Hughes, Good, and Coles, Phys. Rev. **84**, 418 (1951).

## Effect of Pressure on the Melting Point of Teflon Tetrafluoroethylene Resin

P. L. McGeer and H. C. Duus
*Polychemicals Department, E. I. du Pont de Nemours and Company, Wilmington, Delaware*
(Received September 8, 1952)

RECENT measurements in this laboratory have shown the crystalline melting point of Teflon tetrafluoroethylene resin increases considerably on applying external pressure. From this pressure dependence of the melting point plus a knowledge of the change in volume at the transition, the latent heat of fusion of the material can be calculated by the Clausius-Clapeyron equation

$$dP/dT=\Delta S/\Delta V=L/T\Delta V. \quad (1)$$

A piezometer was used to follow the specific volume temperature curve of a sample of coagulated dispersion Teflon tetrafluoroethylene resin at three pressures. Constant pressure from a pneumatic cylinder was maintained on a piston which rested on the sample. Changes in sample length with temperature were followed by means of a dial gauge attached to the piston.

Two of the specific volume *vs* temperature curves obtained by these measurements are shown in Fig. 1, both of which show

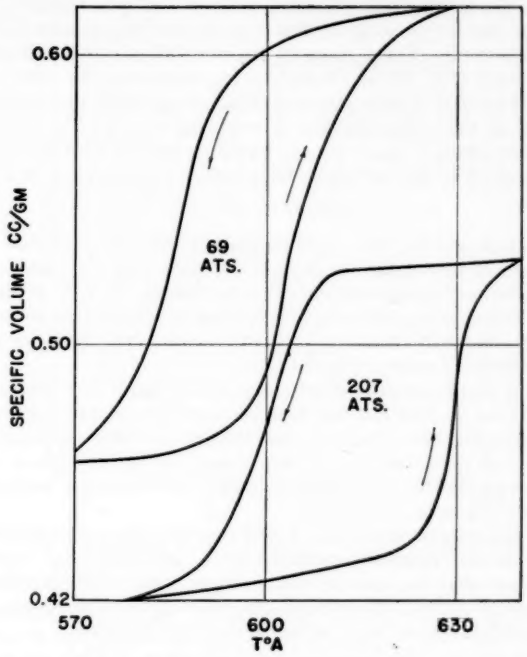


FIG. 1. Specific volume *versus* temperature at two pressures.

marked discontinuities at the melting point. The mid-points of these discontinuities on the warming curves are taken as the true average melting temperatures. The hysteresis shown by the cooling curves is due, presumably, to supercooling.

The transition temperatures obtained are 608°K at 69 atmos, 629°K at 207 atmos, and 692°K at 615 atmos. If the transition temperature is plotted as a function of pressure, a straight line is obtained which can be represented by the equation

$$T_m=a+bP, \quad (2)$$

where $a=597$°K and $b=0.154$°C/atmos.

At atmospheric pressure, the melting point by this equation is 597°K or 324°C. Since this value corresponds to an average melting point for all the crystallites, it is considered to be in good agreement with the 327°C value previously reported by Hanford and Joyce.[1] Their value, obtained by a method which depends on optical transmittivity, corresponds to the disappearance of the last crystallites. Substituting (2) in (1) and solving for $L$ gives

$$L/0.0242=P\Delta V+a/b\Delta V. \quad (3)$$

The factor 0.0242 is required to convert the units cc atmospheres/g on the right-hand side of the equation to calories/g, the conventional units used to express heats of transition. The volume changes obtained from Fig. 1 are 0.143 cc/g at 69 atmos and 0.085 cc/g at 207 atmos. Using these values, the latent heats of fusion of 14.6 cal/g at 69 atmos and 8.4 cal/g at 207 atmos were obtained from Eq. (3).

The corresponding entropies of fusion are 0.0240 cal/g/degree and 0.0134 cal/g/degree. The lowering of the entropy of fusion by 0.0106 cal/g/degree in going to the higher temperature and pressure is presumed to have been due to a change in the degree of crystallinity of the sample between the time it was first melted at 69 atmos pressure and the time it was remelted at 207 atmos pressure.

It is necessary to consider, however, the effect of temperature and pressure on the entropy of fusion. The dependence of entropy on pressure is given by the Maxwell relationship

$$(\partial S/\partial P)_T=-(\partial V/\partial T)_P. \quad (4)$$

The quantity $(\partial V/\partial T)_P$ can be estimated for the solid and the melt from the specific volume-temperature curves above and

below the melting point. For the solid $(\partial V/\partial T)_P$ is 0.00038 cc/g/degree and for the melt 0.00080 cc/g/degree. The decrease in $S$ on increasing the pressure from 69 atmos to 207 atmos is $-0.00038\times0.0242\times(207-69)=-0.00127$ cal/g/degree for the solid, and $0.0008\times0.0242\times(207-69)=-0.00268$ cal/g/degree for the liquid. Thus, at the higher pressure it would be expected that, due to pressure alone, $S_{(\text{solid})}\rightarrow S_{(\text{liquid})}$ would be smaller by 0.00141 cal/g/degree. The effect of higher temperature is given by the relation

$$(\partial S/\partial T)_P=C_P/T. \quad (5)$$

Although specific heat data are not available for Teflon, for all normal substances $C_P$ (liquid) is greater than $C_P$ (solid), and the effect of temperature alone is to increase the entropy of fusion. The effects of pressure and temperature on the entropy of fusion oppose each other and are apparently far too small to account for the difference observed in this study.

It is significant that despite apparent changes in crystallinity $dP/dT=1/b$. This fact has been confirmed by other experiments not reported here. It means that changes in $L$ due to changes in degree of crystallinity are compensated for by changes in $\Delta V$, and suggests that both these quantities are constants multiplied by the degree of crystallinity.

It has been assumed that Teflon can, to a first approximation, be regarded thermodynamically as a one-component system. The fact that the melting occurs over a range of several degrees means, of course, that the system really is multicomponent and that the calculated heats of fusion are average values.

[1] W. E. Hanford and R. M. Joyce, J. Am. Chem. Soc. **68**, 2082 (1946).

## Absorption by Pyrimidines of Plane Polarized Ultraviolet Light

L. E. Lyons
*Sir William Ramsay and Ralph Forster Laboratories, University College, London, England*
(Received September 15, 1952)

POLARIZATION properties of absorption bands have been determined and used to assign certain electronic transitions concerned in ultraviolet spectra of single crystals of 2-amino-4-chloro-6-methyl-pyrimidine, *P*, and 2-chloro-4, 6-dimethyl-pyrimidine, *Q*.

The ultraviolet spectra of pyrimidines above 2000A generally contain three characteristic band systems[1] which may be called *I*, *II*, and *III*. The weakest system, *I*, occurs usually at the lowest frequency, but in the spectra of some derivatives it is hidden under *II*, as is the case with *P*; however, *I* and *II* are separate for *Q*.

Analogy with benzene indicates that *II* and *III* are $\pi-\pi$ transitions corresponding to the 2600 and 2000A systems in the hydrocarbon; however, *I*, by reason of its disappearance in acidic solutions, belongs to the class of transitions which is called by Kasha[2] $n-\pi$, and which originates in nonbonding nitrogen orbitals.

Crystals of *P* were grown from the melt and also by sublimation, and their orientations were determined optically with the use of known x-ray data.[3] It was shown for *II* that the vibration of the absorbed electric vector occurred in the molecular $(xy)$ plane (as was known[4]), and further that of the two directions in that plane one was favored. This conclusion is in agreement with the group theoretical prediction which says that *II*, forbidden in molecules possessing group $D_{6h}$ symmetry, becomes electronically allowed when the symmetry is lowered to $C_{2v}$, and in this case only one polarization is effective.

Thus, in the usual notation,[5] the transition *II* may be assigned $A_1-B_1$, with polarization $x$ parallel to the line joining the two nitrogen atoms.

Although the crystal structure of *Q* does not appear to be known, some interesting conclusions may be derived from a study of its spectrum in polarized light. The variation of the spectrum with changing orientation of the crystal showed that *I* and *III* behaved similarly to one another but differently from *II*. But it is known[6] that for hexamethyl benzene the analog of *III* is polarized in the molecular plane. Now, if the similar behavior of *III* and *I* does indicate similar polarizations, as seems probable, then it follows that both *III* and *I* are polarized chiefly $y$, since they have been shown not to be polarized $x$ (the polarization of *II*).

TABLE I. Proposed assignments and polarizations.

| Transition | | λ(A) | ε | Upper electronic state | Polarization |
|---|---|---|---|---|---|
| *Q* | *I* | 2850 | 400 | $\pi$? | $y$ |
| Benzene | *II* | 2550 | 250 | $B_{2u}$ | $x, y$ |
| *P* | | 2930 | 4500 | $B_1$ | $x$ |
| *Q* | *II* | 2490 | 4500 | $B_1$ | $x$ |
| Benzene | *III* | 1980 | 8000 | $E_{2g}$ or $B_{1u}$ | $x, y$ |
| *P* | *III* | 2500 | 8000 | $A_1$[a] | $y$ |
| *Q* | *III* | 2200 | 8000 | $A_1$[a] | $y$ |

[a] If electronically allowed; otherwise $B_1$, in which case $B_{1u}$ is not a possible benzene assignment.

Thus the vibronic assignment of *III* which is deduced is $A_1-A_1$. These conclusions, which are to be regarded as tentative (in view of the assumptions necessarily made), are summarized in the table, where also there is given the correlation with the benzene transitions.

A further point of interest follows from the association of $y$ polarization with *I*. Considering the operation of reflection in the $xy$ plane, the ground electronic state is symmetric and the $y$ vector is also symmetric; for an allowed electronic transition, therefore, the upper electronic state must also be symmetric. One of two conclusions follows: either the transition is electronically forbidden (but Sponer's work[7] on pyridine suggests it is allowed) and is thus probably made allowed by the action of vibrations antisymmetric with regard to reflection in the $xy$ plane; or else the upper state does not contain one electron in a (normally unoccupied) $\pi$-molecular orbital, which is necessarily antisymmetric to such a reflection.

[1] R. Andrisano and G. Modena, Gazz. chim. ital. **81**, 405 (1951).
[2] M. Kasha, Disc. Faraday Soc., No. 9, 14 (1950).
[3] C. J. B. Clews and W. Cochran, Acta Cryst. **1**, 4 (1948).
[4] W. E. Seeds, Disc. Faraday Soc., No. 9, 394 (1950).
[5] Eyring, Walter, and Kimball, *Quantum Chemistry* (John Wiley and Sons, Inc., New York, 1944).
[6] D. P. Craig and L. E. Lyons, Nature **169**, 1102 (1952).
[7] H. Sponer, Revs. Modern Phys. **16**, 224 (1944).

## Dissociation Energies of C—Br Bonds in the Bromo-Naphthalenes, 9-Bromo-Phenanthrene, and 9-Bromo-Anthracene

M. Ladacki
*Chemistry Department, Manchester University, Manchester, England*
AND
M. Szwarc
*College of Forestry, State University of New York, Syracuse, New York*
(Received August 20, 1952)

WILLIAMS and one of us[1] reported an investigation of the pyrolysis of bromobenzene carried out in the presence of an excess of toluene. They showed that the molecule of bromobenzene splits initially into a bromine atom and a phenyl radical

$$\text{Ph}\cdot\text{Br}\rightarrow\text{Ph}\cdot+\text{Br}; \quad (1)$$

and the kinetic studies demonstrated that reaction (1) is a homogeneous, first-order gas reaction, its activation energy being estimated at 70.9 kcal/mole, corresponding to the frequency factor of $2\times10^{13}$ sec$^{-1}$. On the assumption that the recombination process does not require any activation energy, the observed activation energy may be identified with the C—Br bond dis-

TABLE I.

| Bromobenzene | | β-Bromonaphthalene | | α-Bromonaphthalene | | 9-Bromophenanthrene | | 9-Bromoanthracene | |
|---|---|---|---|---|---|---|---|---|---|
| $T$ (°K) | $10^3k$ (sec$^{-1}$) | $T$ (°K) | $10^3k$ (sec$^{-1}$) | $T$ (°K) | $10^3k$ (sec$^{-1}$) | $T$ (°K) | $10^3k$ (sec$^{-1}$) | $T$ (°K) | $10^3k$ (sec$^{-1}$) |
| 1023 | 1.89 | 1022 | 2.13 | 1014 | 2.32 | 1002 | 2.02 | 964 | 2.63 |
| 1028 | 2.37[a] | 1024 | 2.52 | 1019 | 4.28[a] | 1009 | 2.96 | 975 | 3.18 |
| 1040 | 3.93 | 1027 | 2.87 | 1024 | 3.31 | 1011 | 3.49 | 982 | 5.49[a] |
| 1046 | 4.50[a] | 1038 | 4.30[a] | 1029 | 5.64[a] | 1016 | 4.12[a] | 983 | 4.59 |
| 1054 | 6.04 | 1042 | 4.06 | 1030 | 3.55 | 1031 | 4.99 | 985 | 5.31 |
| 1055 | 6.32 | 1048 | 4.61 | 1031 | 4.91 | 1031 | 5.51 | 988 | 4.93 |
| 1061 | 6.34 | 1049 | 5.35 | 1033 | 5.36 | 1036 | 7.41 | 988 | 5.61 |
| 1077 | 12.9[a] | 1050 | 5.65 | 1034 | 4.83 | 1037 | 5.70 | 992 | 5.36 |
| 1085 | 16.3 | 1052 | 5.46 | 1037 | 5.12 | 1043 | 7.98 | 998 | 7.99 |
| 1093 | 19.5 | 1059 | 6.12 | 1041 | 6.85 | 1057 | 13.0 | 1011 | 12.3 |
| 1110 | 32.2 | 1059 | 7.91 | 1044 | 6.85 | 1059 | 13.4 | 1015 | 13.1 |
| 1127 | 51.9 | 1070 | 10.9 | 1046 | 7.55 | 1069 | 21.7 | 1018 | 14.3 |
| | | 1071 | 9.88 | 1048 | 7.96 | 1078 | 27.0[a] | 1018 | 15.8[a] |
| | | 1073 | 9.87 | 1052 | 8.04 | 1083 | 27.3 | 1032 | 19.8 |
| | | 1074 | 10.5 | 1053 | 8.00 | 1087 | 32.2 | 1048 | 37.7 |
| | | 1078 | 13.3 | 1054 | 7.84 | 1103 | 49.0 | 1050 | 37.8 |
| | | 1083 | 16.3 | 1061 | 13.2 | 1114 | 60.5 | 1053 | 48.5 |
| | | 1091 | 19.1[a] | 1065 | 12.4 | 1115 | 75.1 | 1055 | 50.2 |
| | | 1096 | 20.4 | 1076 | 15.9 | 1123 | 89.7 | 1059 | 53.8 |
| | | 1100 | 27.2 | 1080 | 23.3 | 1125 | 91.7 | 1062 | 49.1 |
| | | 1106 | 30.1 | 1081 | 23.2[a] | | | 1062 | 54.8 |
| | | 1107 | 32.6 | 1084 | 19.6 | | | | |
| | | 1113 | 37.0 | 1085 | 27.0 | | | | |
| | | 1118 | 42.2 | 1086 | 21.9 | | | | |
| | | 1121 | 45.3 | 1091 | 28.9 | | | | |
| | | 1122 | 43.8 | 1093 | 26.7 | | | | |
| | | 1124 | 49.8 | 1094 | 32.7 | | | | |
| | | 1133 | 65.9 | 1100 | 39.9 | | | | |
| | | | | 1104 | 43.0 | | | | |
| | | | | 1108 | 50.1 | | | | |
| | | | | 1119 | 73.5 | | | | |
| | | | | 1121 | 75.0 | | | | |
| | | | | 1125 | 79.8 | | | | |
| | | | | 1133 | 90.2 | | | | |
| | | | | 1133 | 97.6 | | | | |

[a] Runs carried out in a packed reaction vessel (surface increased by a factor of 12). These runs were omitted when calculating the activation energies.

sociation energy, i.e.,

$$D(Ph-Br) = 70.9 \text{ kcal/mole.}$$

We have now extended these studies to other aromatic bromo-derivatives, namely: β-bromonaphthalene, α-bromonaphthalene, 9-bromophenanthrene, and 9-bromoanthracene, and for the sake of completeness we also reinvestigated the pyrolysis of bromobenzene. It has been found that all these compounds decompose initially into bromine atoms and the respective aromatic radicals, and that the kinetics of the pyrolyses are analogous to that of bromobenzene. The results obtained are summarized in Table I. Plots of the log's of the unimolecular rate constants against the reciprocal of temperature are given in Figs. 1–5. The activation energies and frequency factors were computed by the least square method, and the results thus obtained are given in Table II (the results quoted for bromobenzene are those obtained by Szwarc and Williams[1]).

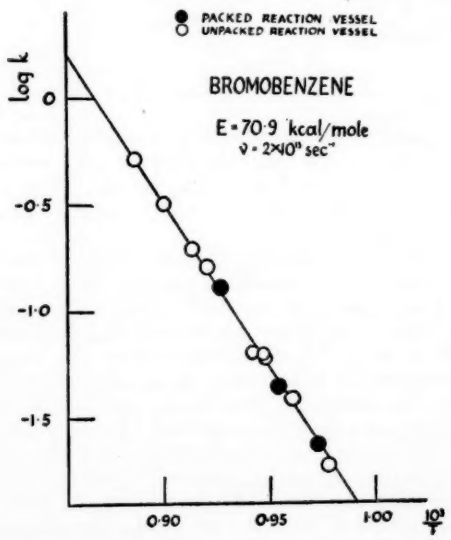


FIG. 1. Logarithm of the reaction constant plotted against the inverse temperature. Bromobenzene.

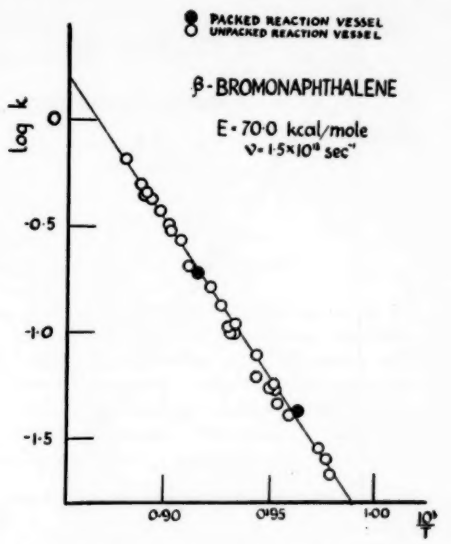


FIG. 2. Logarithm of the reaction constant plotted against the inverse temperature. β-Bromonaphthalene.

Inspection of Table II strongly suggests that a constant frequency factor may be attributed to the whole series (see in this connection a note by Szwarc and Williams[2]), and we assumed for it a value of $1.5\times10^{13}$ sec$^{-1}$. On this basis the activation energies given in the last column of Table II were obtained,* and we believe that these values give the correct trend in the respective C—Br bond dissociation energies.

There are two conclusions which one might draw from the values given in the last column of Table II: (1) It appears that the increasing size of the π-electron system has no appreciable effect on the C—Br bond dissociation energy (compare bromobenzene with β-bromonaphthalene, and α-bromonaphthalene with 9-bromophenanthrene). This suggests that the conjugation between the bromine atom and the π-electron system of the aromatic

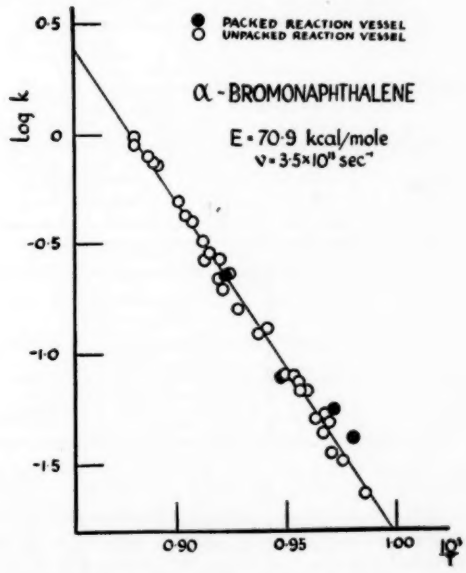


FIG. 3. Logarithm of the reaction constant plotted against the inverse temperature. α-Bromonaphthalene.

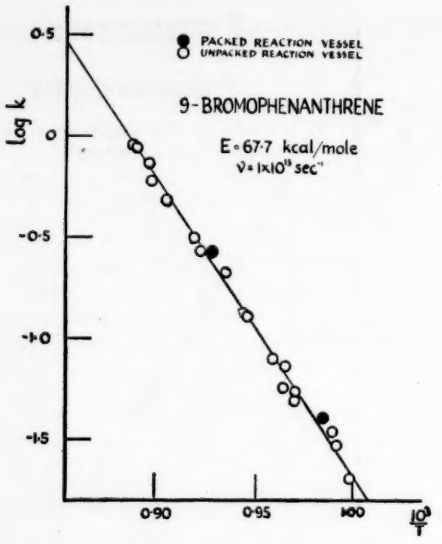


FIG. 4. Logarithm of the reaction constant plotted against the inverse temperature. 9-Bromophenanthrene.

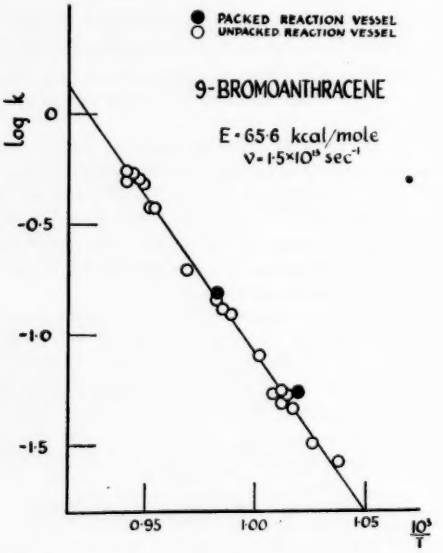


FIG. 5. Logarithm of the reaction constant plotted against the inverse temperature. 9-Bromoanthracene.

| COMPOUND | EXPERIMENTAL | | | ASSUMING CONSTANT ν (ν = 1·5×10¹³ sec⁻¹) |
|---|---|---|---|---|
| | E kcal/mole | ν sec⁻¹ | $10^5 k_{100°A}$ sec⁻¹ | E kcal/mole |
| | 70·9 | 2 × 10¹³ | 0·93 | 70·3 |
| | 70·0 | 1·5 × 10¹³ | 1·02 | 70·0 |
| | 70·9 | 3·5 × 10¹³ | 1·51 | 69·2 |
| | 67·7 | 1 × 10¹³ | 1·95 | 68·5 |
| | 65·6 | 1·5 × 10¹³ | 8·32 | 65·6 |

TABLE II.

molecule is small, and that the $\sigma$-electron of the radical interacts only weakly with $\pi$-electrons. (2) The observed decrease in the C—Br bond dissociation energies seems to be due to "ortho" effects, being the greatest in 9-bromoanthracene where two benzene rings are fused in ortho position to the bromine atom. This conclusion is supported by the independent evidence on the effect of substituents on the C—Br bond dissociation energy in substituted bromobenzenes (unpublished results by Williams).

A detailed report of this work will be published later.

[1] M. Szwarc and D. Williams, J. Chem. Phys. **20**, 1171 (1952).
[2] M. Szwarc and D. Williams, Nature (to be published).
* By assuming a slightly different value for the frequency factor we would obtain different values for the $E$'s, but the trend in the $E$'s would remain unaltered.

## Inhibition of the Gelation of Gelatin by Autoclaved Gelatin

RICHARD J. GOLDBERG
*Department of Chemistry, University of Wisconsin, Madison, Wisconsin*
(Received August 20, 1952)

PREVIOUS studies on the inhibition of the gelation of gelatin by such substances as thyocyanate, urea, acetyltryptophanate, etc., have indicated that these inhibitors are not suitable in a gelatin system which is to be used as a "blood substitute." We wish to report a case of inhibition which is sufficiently promising to warrant further research along these lines.

The theory of molecular distributions in condensation polymers[1–3] is applied here to the gelatin problem employing a heterogeneous initial mixture.[4] A starting mixture consisting of $N_1, N_2, \cdots, N_f$ molecules with one, two, $\cdots$, $f$ reactive sites, respectively, yields the distribution

$$m(n_1 \cdots n_f) = (\Sigma k N_k) p^{\Sigma n_k - 1}(1-p)^{\Sigma k n_k - 2\Sigma n_k + 2} \times \frac{(\Sigma k n_k - \Sigma n_k)!}{(\Sigma k n_k - 2\Sigma n_k + 2)!} \prod_{k=1}^{f} \left[\frac{k N_k}{\Sigma k N_k} \frac{1}{n_k!}\right], \quad (1)$$

for the number of aggregates $m(n_1 \cdots n_f)$ containing $n_1, \cdots, n_f$ molecules with one, $\cdots$, $f$ sites, respectively, as a function of the fraction $p$, of gelatin sites which have reacted. The sums go over all $k$ values from one to $f$. The gel point of the system occurs at

$$p_{gel} = 1/(\bar{f}-1),$$

$$\bar{f} = \sum_{k=1}^{f} k^2 N_k / \sum_{k=1}^{f} k N_k. \quad (2)$$

Since $p$ cannot exceed unity we may write

$$\bar{f} \geqslant 2, \quad (3)$$

and, consequently,

$$N_1 \leqslant \sum_{k=2}^{f} k N_k (k-2). \quad (4)$$

If the number of molecules in the system with one reactive site exceeds the sum on the right side of Eq. (4), then gelation cannot occur. Further, if the average valence of the system $\bar{f}$ is made progressively smaller, gelation becomes progressively more difficult.

These theoretical considerations have led this writer to search for univalent gelatin molecules, which could be added to the special Knox gelatin solution used clinically as a "blood substitute." This special Knox gelatin solution is 6 percent protein at a $p$H of about 7 in physiological saline and has previously been autoclaved for 20 minutes at 15 pounds pressure (designated as $P$-20). We have used it as the starting material for further autoclaving under the same conditions. After a total autoclaving time of 500 minutes, samples (designated as $P$-500) were mixed with the starting material in various proportions. Gel points of these systems were obtained by the Gordon and Ferry method.[5] They are compared with the gel points for mixtures of $P$-20 and physiological saline in Table I. These data indicate that the $P$-500 gelatin has a tendency to inhibit the gelation of $P$-20

TABLE I.

| Mixture | | Gel point °C | |
|---|---|---|---|
| *P*-20 ml | *P*-500 or saline added ml | *P*-500 added | Saline added |
| 1.00 | 4.00 | 17.5 | 20.1 |
| 0.90 | 4.10 | 16.5 | 19.3 |
| 0.80 | 4.20 | 15.6 | 18.2 |
| 0.70 | 4.30 | 14.3 | 16.6 |
| 0.60 | 4.40 | 13.0 | <0.5 |
| 0.50 | 4.50 | 11.8 | ... |
| 0.40 | 4.60 | 9.8 | ... |
| 0.30 | 4.70 | 4.9 | ... |
| 0.20 | 4.80 | <0.5 | ... |

gelatin. We surmise that the *P*-500 gelatin molecules are being incorporated into the aggregates as the theory predicts. The gel point decreases as the ratio of *P*-500 to *P*-20 increases without changing the concentration of gelatin. This decrease is in qualitative agreement with the decrease in $\hat{f}$. The fact that the *P*-20, *P*-500 mixtures continue to gel, while those without *P*-500 do not, indicates that the *P*-500 contains molecules of more than one reactive site which are needed to produce gelation. Consequently, we have not obtained the ideal substance in *P*-500. Further investigation of these kinds of mixtures is indicated.

The author is deeply grateful to Dr. W. H. Stockmayer for the opportunity to examine his manuscript describing a similar distribution in advance of its publication. We wish to acknowledge the support of this work by the National Science Foundation, Contract NSF-G22.

[1] P. J. Flory, J. Am. Chem. Soc. **63**, 3083, 3091, 3096 (1941).
[2] W. H. Stockmayer, J. Chem. Phys. **11**, 45 (1943).
[3] W. H. Stockmayer, J. Polymer Sci. **9**, 69 (1952).
[4] Scatchard, Oncley, Williams, and Brown, J. Am. Chem. Soc. **66**, 1980 (1944).
[5] R. S. Gordon and J. D. Ferry, Federation Proc. **5**, 136 (1946).

## Isotope Enrichment by the Photoexcitation of Specific Isotopes*

C. C. McDONALD AND H. E. GUNNING
*Department of Chemistry, Illinois Institute of Technology, Chicago 16, Illinois*
(Received September 12, 1952)

THE possibility of separating the isotopes of mercury through the photoexcitation of specific isotopes was first suggested apparently by Mrowzowski,[1] during the course of his classic studies of the hyperfine structure of the 2537A resonance line of mercury. The experimental work was done by Zuber,[2] who irradiated oxygen and oxygen-nitrogen mixtures, both saturated with mercury vapor, with the $\gamma$-group from the 2537A line under static conditions. The $\gamma$-group, which consists essentially of the 0.0 mA and +11.5 mA hyperfine components, originating from Hg-200 and Hg-202, respectively, was isolated by passing the collimated radiation of a cooled mercury-in-quartz arc through a Mrowzowski magnetic filter.[3] Zuber decomposed the mercuric oxide formed and obtained an estimate of the ratio Hg(200, 202)/Hg(198, 199, 201, 204) in the resulting mercury by resonance absorption. No significant change in the ratio was found using pure oxygen as substrate; however, for the oxygen-nitrogen mixtures a marked enhancement of the ratio over that for normal mercury was obtained.

In the present investigation, some preliminary results of which are reported here, a flow system was used. Dried air, presaturated with mercury vapor at 25°C, was allowed to flow through a long quartz tube which was irradiated near the downstream end. The source consisted of an NBS-Meggers Hg-198 electrodeless discharge tube, fashioned of Vycor No. 7910 glass, coupled with a 200-megacycle oscillator.

To obtain the data below, six 10-hour flow runs were made at an air pressure of 8 mm in the reaction zone. The source was operated at approximately 150°C. At the end of the exposures the mercuric oxide, which deposited upstream from the irradiated zone, was first freed of mercury by prolonged evacuation. The oxide was then decomposed thermally, and the mercury formed was frozen with liquid nitrogen into an evacuated sample tube provided with a breakseal. The isotopic composition of the mercury as determined on a mass spectrometer is given in Table I below.

TABLE I. Isotopic composition of mercury in mercuric oxide formed in the photosensitized air reaction, using a hot Hg-198 source.

| Isotope | Isotopic composition | |
|---|---|---|
| | Natural Hg[4] | Hg from HgO |
| Hg-196 | 0.15 | 0.013 ±0.009 |
| Hg-198 | 10.1 | 0.158 ±0.012 |
| Hg-199 | 17.0 | 10.71 ±0.09 |
| Hg-200 | 23.3 | 18.17 ±0.06 |
| Hg-201 | 13.2 | 24.62 ±0.15 |
| Hg-202 | 29.6 | 14.34 ±0.09 |
| Hg-204 | 6.7 | 31.99 ±0.10 |

The results shown in Table I are of considerable interest. In the first place by running the lamp hot, the −10.4 mA component normally emitted has been almost completely removed presumably by self-reversal, as shown by the large reduction in the Hg-198 present in the oxide. Furthermore, the reversed emission line is quite broad, with the red end of the fringes largely coinciding with the +21.5 mA component as shown by the enrichments at Hg-204 and Hg-201.

Detailed papers on these studies using Hg-198 and Hg-202 sources will be submitted to this journal in the near future.

The authors would like to thank Dr. R. F. Hibbs, Superintendent of the Assay Laboratory, Carbide and Carbon Chemicals Division, Union Carbide and Carbon Corporation, Oak Ridge, Tennessee for performing the isotope analyses. The authors are also indebted to Dr. R. B. Bernstein of this department for many helpful discussions.

* This work was supported by the AEC under Contract AT(11-1)-43.
[1] S. Mrowzowski, Z. Physik **78**, 826 (1932).
[2] K. Zuber, Helv. Phys. Acta **8**, 487 (1935); Helv. Phys. Acta **9**, 285 (1936); Nature **136**, 796 (1935).
[3] S. Mrowzowski, Bull. Acad. Pol. **I**, 464 (1930).
[4] A. O. Nier, Phys. Rev. **52**, 933 (1937).

## Some Effects of Cobalt Gamma-Radiation on Aqueous Benzene Solutions*

THOMAS J. SWORSKI
*Chemistry Division, Oak Ridge National Laboratory, Oak Ridge, Tennessee*
(Received August 29, 1952)

THE chemical action of ionizing radiation on aqueous solutions of benzene has been demonstrated by Stein and Weiss[1] to result in phenol formation. The author has found that hydrogen peroxide, determined by a spectrophotometric technique previously reported,[2] is also a principal product. The presence of benzene or phenol does not interfere in this determination.

Carr[3] has suggested a direct estimation of phenol production by using its ultraviolet absorption at 270 m$\mu$. This method is unsatisfactory in oxygen-free solutions because of interference by other products of irradiation such as diphenyl.

A spectrophotometric determination of phenol was developed using the difference in absorption of unbuffered and alkaline phenol solutions at 290 m$\mu$ as shown in Fig. 1. This method minimizes interference due to those products of irradiation which have no appreciable difference in ultraviolet absorption spectra of unbuffered and alkaline solutions. The alkaline sample consisted of 5 ml of irradiated solution to which was added 3 ml of 0.1*N* NaOH, and the mixture diluted with distilled water to 10 ml (dilution = 2). The unbuffered sample consisted of 5 ml of irradiated solution diluted with distilled water to 10 ml. The optical densities for alkaline sample ($D_{AS}$) and unbuffered sample ($D_{US}$)

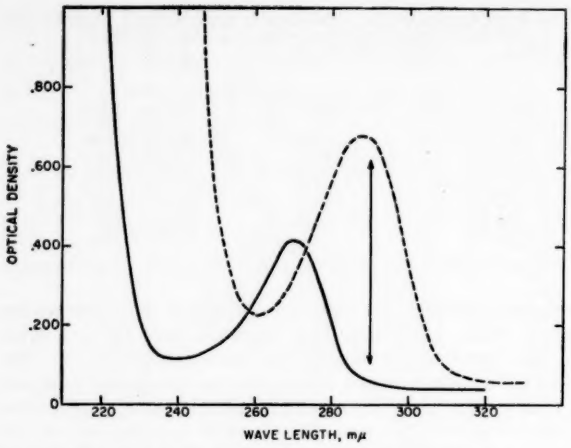


FIG. 1. Ultraviolet absorption spectra of aqueous phenol solutions: —— 240 micromoles/liter; - - - - 240 micromoles/liter in 0.03$N$ NaOH.

were measured at 290 mμ on a Beckman Model D.U. spectrophotometer in the same 1-cm cell, using for comparison the intensity with no cell in the optical path. Using the nonirradiated solution, optical densities for the alkaline blank ($D_{AB}$) and unbuffered blank ($D_{UB}$) were similarly obtained. The concentration of phenol in the irradiated solution was calculated using:

$$\text{Micromoles/Liter} = 397[(D_{AS}-D_{US})-(D_{AB}-D_{UB})]\ \text{(dilution)}.$$

The constant was evaluated by use of a standard phenol solution[4] which was found to have a molar extinction coefficient at 270 mμ of 1495.

Hydrogen peroxide has been measured by Lefort[5] by using its increased ultraviolet absorption in alkaline solutions. Use of standard phenol and hydrogen peroxide solutions by the author has shown that hydrogen peroxide, in amounts produced with phenol, does not appreciably interfere in the phenol determination. Hydrogen peroxide does induce a slow increase of the optical density of the alkaline sample ($D_{AS}$). The optical density must be followed as a function of time and extrapolated to zero time of alkalinity.

The radiation exposures were made in a cobalt gamma-ray source[6] using closed vessels with no air space. Determination of the rate of energy absorption in solution was based upon a measured yield of 15.5 $Fe^{++}$ oxidized per 100 ev absorbed in solution.[2]

In Fig. 2, hydrogen peroxide formation in air-saturated aqueous benzene solution is compared with hydrogen peroxide formation in air-saturated water. The enhancement of the initial rate of hydrogen peroxide formation by benzene is similar to the effect of hydrogen.[2,7] It is interesting to note that the sharp break in the rate of phenol production, as shown in Fig. 2 and as previously reported,[1] occurs simultaneously with the onset of hydrogen peroxide disappearance.

A detailed study of this system is being continued in an attempt to elucidate the mechanism of phenol and hydrogen peroxide formation.

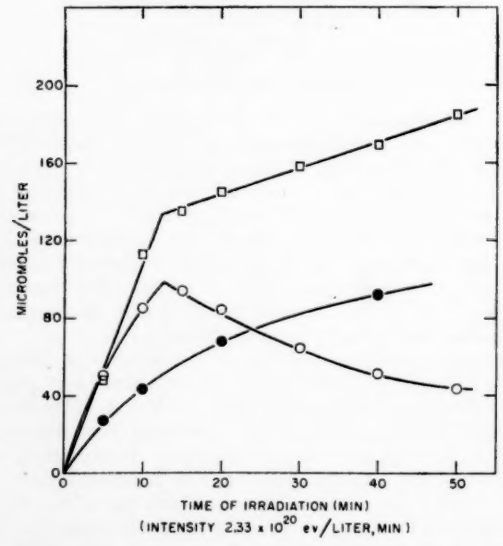


FIG. 2. Comparison of hydrogen peroxide and phenol production: □ phenol and ○ hydrogen peroxide in air-saturated benzene solution; ● hydrogen peroxide in air-saturated water.

* This work was performed for the AEC.

[1] G. Stein and J. Weiss, J. Chem. Soc., 3245 (1949).
[2] C. J. Hochanadel, J. Phys. Chem. **56**, 587 (1952).
[3] M. E. J. Carr, Nature **167**, 363 (1951).
[4] Snell, *Colorimetric Methods of Analysis* (1937), Vol. II, p. 352.
[5] Marc Lefort, J. chim. phys. **48**, 339 (1951).
[6] J. A. Ghormley and C. J. Hochanadel, Rev. Sci. Instr. **22**, 473 (1951).
[7] W. J. Toulis, UCRL-583, February 10, 1950.

## An Interpretation of the Visible and Near-Infrared Spectra of $NpO_2^+$ and $PuO_2^{++}$ Ions

D. M. GRUEN
*Chemistry Division, Argonne National Laboratory, Chicago, Illinois*

(Received August 28, 1952)

THE spectra of these isoelectronic ions are remarkably similar, the chief difference between them being the displacement toward shorter wavelengths of the $PuO_2^{++}$ [1] spectrum as compared with the $NpO_2^+$ [2] spectrum.

The assumption made here is that the spectra are essentially "rare-earth" like, the various bands arising from electronic transitions between the terms of the $5f^2$ configuration. The treatment is similar to that given by Bethe and Spedding[3] and by Spedding[4] for the ions $Pr^{+++}$ and $Tm^{+++}$.

The electrostatic terms of the $5f^2$ configuration of the ThIII emission spectrum[5,6] were multiplied by the constant factor $[(94-58)+(93-58)]/[2(90-58)]=1.11$ to correct for the increase in nuclear charge in going from Th to Np and Pu. The

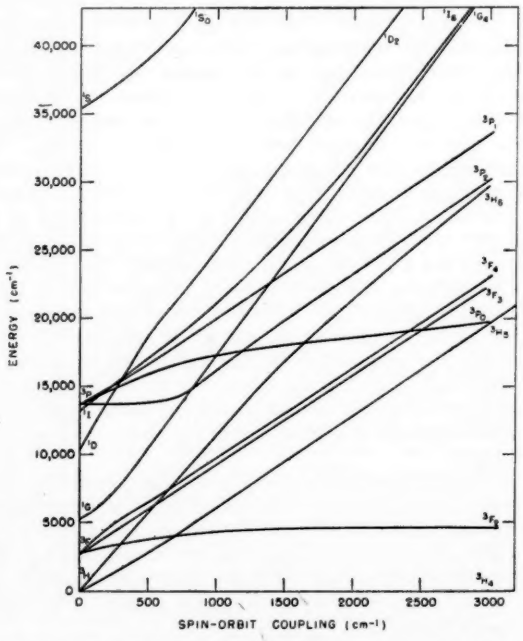


FIG. 1. Energy levels of the $5f^2$ configuration as a function of spin-orbit coupling.

TABLE I. The configuration $5f^2$.

| Classification | | | Spin-orbit coupling ($cm^{-1}$) | | | | | |
|---|---|---|---|---|---|---|---|---|
| | | | 1100 | 1100 | 1100 | 950 | ($PuO_2^{++}$) | ($NpO_2^{+}$) |
| *LS* | *jj* | *J* | *LS* | *jj* | *I* | *I* | *O* | *O* |
| $^3H$ | (5/2, 5/2) | 4 | 0 | 0 | 0 | 0 | | |
| $^3F$ | (5/2, 5/2) | 2 | 5161 | 5588 | 4230 | 4100 | | |
| $^3H$ | (7/2, 5/2) | 5 | 5500 | 6423 | 6500 | 5550 | | |
| $^3F$ | (7/2, 5/2) | 3 | 8461 | 9384 | 9800 | 8800 | 10,131 | 9070 |
| $^3F$ | (7/2, 5/2) | 4 | 12,861 | 9706 | 10,300 | 9200 | 10,471 | 9708 |
| $^3H$ | (7/2, 7/2) | 6 | 12,100 | 16,040 | 12,460 | 10,600 | 12,004 | 10,172 |
| $^3P$ | (7/2, 7/2) | 2 | 21,517 | 24,879 | 16,650 | 15,600 | 16,000 | 15,873 |
| $^3P$ | (5/2, 5/2) | 0 | 18,217 | 21,787 | 17,200 | 16,950 | 17,730 | 16,835 |
| $^1G$ | (7/2, 7/2) | 4 | 11,930 | 17,854 | 18,150 | 16,400 | 19,230 | 16,207 |
| $^3P$ | (7/2, 5/2) | 1 | 19,317 | 20,240 | 20,550 | 19,450 | 19,801 | |
| $^1I$ | (7/2, 5/2) | 6 | 20,020 | 17,926 | 21,800 | 20,550 | 20,790 | 21,008 |
| $^1D$ | (7/2, 5/2) | 2 | 17,024 | 16,280 | 26,100 | 24,250 | | |
| $^1S$ | (7/2, 7/2) | 0 | 41,995 | 40,763 | 45,450 | 44,000 | | |

value 58 was chosen as the screening constant on the basis of magnetic susceptibility measurements.[7] Figure 1 shows the energy levels of the $5f^2$ configuration as a function of spin-orbit coupling, with the level $^3H_4$ as the zero of energy. The energy levels were calculated by simultaneously diagonalizing the matrices of the electrostatic and spin-orbit interactions (intermediate coupiing).

Best agreement between calculated and observed levels was obtained for spin-orbit coupling values of 950 $cm^{-1}$ for $NpO_2^+$ and 1100 $cm^{-1}$ for $PuO_2^{++}$. These values are not unreasonable in view of the fact that the spin-orbit coupling which increases approximately as $Z_{eff}^4$ in an isoelectronic series, is 517 $cm^{-1}$ in ThIII.[6] In Table I are given the classification of the levels in the *LS* and *jj* coupling schemes, and their energies in *LS* and *jj* coupling for spin-orbit coupling, 1100 $cm^{-1}$. The columns labeled *I* and *O* are for the intermediate coupling cases and for the observed spectra, respectively.

Work is in progress on the low temperature behavior of these spectra.

[1] Connick, Kasha, McVey, and Sheline, Paper 4.20, "The Transuranium Elements," Vol. 14B of the NNES (McGraw-Hill Book Company, Inc., New York, 1949). See also unpublished work of J. C. Hindman.
[2] R. Sjoblom and J. C. Hindman, J. Am. Chem. Soc. **73**, 1744 (1951).
[3] H. Bethe and F. H. Spedding, Phys. Rev. **52**, 454 (1937).
[4] F. H. Spedding, Phys. Rev. **58**, 255 (1940).
[5] P. F. A. Klinkenberg, Physica **16**, 618 (1950).
[6] G. Racah, Physica **16**, 651 (1950).
[7] Dawson, Mandleberg, and Davies, J. Chem. Soc. **1951**, 2047.

## Heat Conduction and Isotherms of Adsorbed Helium on Silica Gel*

DAVID WHITE, CHIEN CHOU, AND H. L. JOHNSTON
*Department of Chemistry, The Ohio State University, Columbus 10, Ohio*
(Received August 20, 1952)

DURING the experiments on the thermal conductivity of bulk liquid helium II, it was noted that equilibrium with the surroundings was very rapidly attained when helium gas, just below the condensation pressure, was present in the capillary. In view of the anomalous properties of adsorbed helium reported by Long and Meyer[1,2] an attempt was made to determine whether the unsaturated film below the λ-point temperature also exhibited an anomalous heat conduction.

The apparatus consisted of a tube 2 mm in diameter and 12 cm long, filled with powdered silica gel, along which temperature drops were measured, as a function of energy input for different amounts of adsorbed helium at a series of temperatures below the λ-point. It was found that for equilibrium pressures below 95–97 percent of the saturation pressure $P_0$, and at any temperature, equilibrium was never attained. The temperature of the powder-filled tube constantly rose. Since the energy input was of the order of $1\times10^{-6}$ watt, it was estimated that the thermal conductivity of the system was less than $1\times10^{-4}$ cal/deg/cm². In fact the thermal conductivity appeared to be smaller than when the tube was devoid of powder, as in the earlier experiments. Above $P/P_0=0.97$ it was found that the thermal conductivity was much improved and of the order of 0.1–0.5 cal/deg/cm².

Since the results were not in agreement with what had been reported by Long and Meyer,[2] who observed superfluidity for values of $P/P_0$ as low as 0.26, an attempt was made to resolve this inconsistency by measuring the isotherms of helium adsorbed on silica gel above and below the λ-point temperature. The results are shown in Fig. 1. The data above and below the λ-point can all be fitted to the same curve, indicating that there is no tendency to build up a Rollin film below the λ-point as in the case of the ferric oxide experiments.[1] Furthermore, the isotherms do not exhibit the usual S-shape characteristic of multilayer adsorption on silica gel. Application of the Langmuir theory of monomolecular adsorption gives good agreement with the data and leads to a value of $V_m$, the volume for a complete monolayer, of 335 cc/g of silica gel. The surface area of the silica gel determined by the adsorption of nitrogen at 77°K is 806 $m^2$/g. Thus, the $V_m/m^2$ for helium on silica gel is 0.41 cc. This is about twice the value calculated from the liquid density. Although this would mean that the helium is under considerable pressure, this value is much smaller than reported for ferric oxide[1] ($V_m=0.9$ cc/$m^2$) or glass and oxygen[3,4] ($V_m=0.57$ cc/$m^2$). On the other hand, one can also fit the data to the B.E.T. multilayer theory below $P/P_0\sim0.4$. The isotherm would correspond to a type IV in which capillary condensation takes place. A value of $V_m/m^2=0.22$ is obtained, the value expected if the packing on the surface is that of bulk liquid helium. At saturation the total number of layers would be approximately four.

The absence of multilayer adsorption in the case of helium on silica gel or capillary condensation could account for the absence of superfluidity in the adsorbed layer. In the former case the adsorbed molecules would be strongly bound to the surface. In the latter case the binding energy of the higher layers built up in

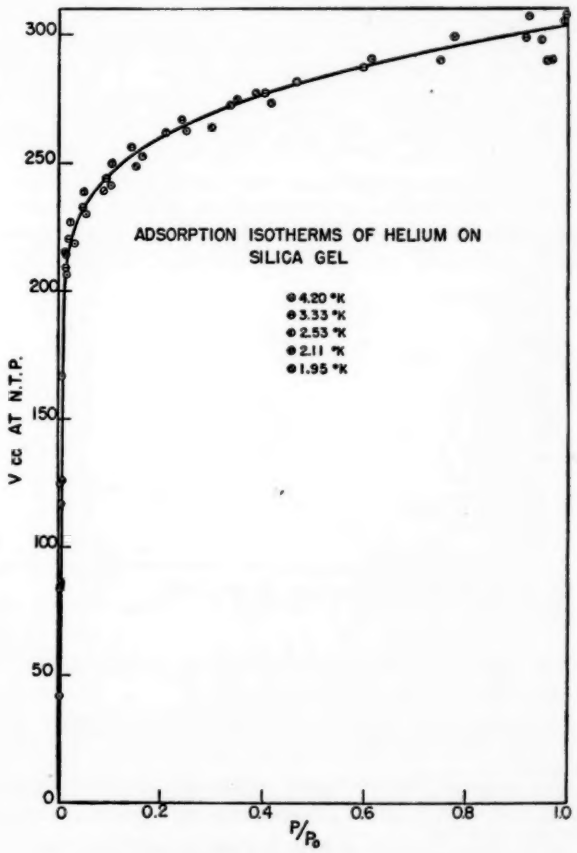


FIG. 1.

the capillaries would be considerably larger than that corresponding to normal liquefaction. Thus, superfluidity could occur when the capillaries are overflowing. This, of course, would lead to the very low thermal conductivities observed. This would also account for the similarity of the isotherms above and below the λ-point. The reason for the behavior of helium on silica gel is not quite clear since practically all other adsorbates exhibit simple multilayer adsorption.

Perhaps it is of interest to note here the importance of the adsorbed layer in bulk helium transfer velocity experiments where the rate depends on the perimeter of the vessel. For vessels in which the adsorbed helium can become superfluid in the pores, one would expect an increased rate due to the fact that the true perimeter is much larger than the measured one. For materials which behave like silica gel where the helium must fill the capillaries before superfluidity occurs, the true perimeter should more closely approximate the measured one.

* This work was supported in part by the ONR under contract with The Ohio State University Research Foundation.

[1] E. A. Long and L. Meyer, Phys. Rev. **76**, 440 (1949).
[2] E. A. Long and L. Meyer, Phys. Rev. **79**, 1031 (1950).
[3] J. Schweers, thesis, Leiden (1941).
[4] Schaeffer, Smith, and Wendell, J. Am. Chem. Soc. **71**, 863 (1949).
[5] S. Brunauer, *The Adsorption of Gases and Vapors* (Princeton University Press, Princeton, New Jersey, 1943), p. 172.

## Integrated Absorption for Vibration-Rotation Bands of $CO_2$*

D. Weber, R. J. Holm,† and S. S. Penner
*Jet Propulsion Laboratory, California Institute of Technology, Pasadena, California*
(Received August 20, 1952)

Quantitative infrared intensity measurements have been carried out for some of the more intense vibration-rotation bands of $CO_2$. Experimental studies were performed by use of the extrapolation procedure of Wilson and Wells[1] using helium as pressurizing agent and total pressures up to 700 psia. For the weaker bands, the self-broadening technique of Penner and Weber[2] was employed. The results of the present studies are summarized in Table I, where they are contrasted with data obtained by other investigators. Reference to the numerical values listed in Table I shows satisfactory agreement between the experimentally determined values.

Table I. Integrated intensities for vibration-rotation bands of $CO_2$.

| Band center ($cm^{-1}$) | Thorndike[a] (1947) | Eggers and Crawford[b] (1951) | Present study (±20%) |
|---|---|---|---|
| 5109 | | | 0.43 |
| 4984 | | | 1.0 |
| 4861 | | | 0.27 |
| 3716 | | 39.0 | 42 |
| 3609 | | 27.0 | 29 |
| 2349 | 2867 | 2693 | 2700 |
| 2137 | | | |
| 2094 | | | 0.15 |
| 2077 | | 0.14 (*P* and *Q*) | |
| 2077 | | 0.05 (*Q* only) | |
| 1933 | | 0.005 | 0.083 |
| 1886 | | | |
| 721 | | | |
| 668 | | | |
| 667 | 187 | 161 | 170 |
| 648 | | | |
| 618 | | | |

[a] A. M. Thorndike, J. Chem. Phys. **15**, 868 (1947).
[b] D. F. Eggers, Jr., and B. L. Crawford, Jr., J. Chem. Phys. **19**, 1556 (1951).

* This paper presents the results of one phase of research carried out at the Jet Propulsion Laboratory, California Institute of Technology, under contract No. DA-04-495-ORD 18, sponsored by the U. S. Army Ordnance Department.
† Lt. Colonel, U.S.M.C. This paper contains part of a thesis submitted by R. J. Holm to the graduate school of the California Institute of Technology, in partial fulfillment of requirements for the degree of Aeronautical Engineer, June 1952.
[1] E. B. Wilson, Jr., and A. J. Wells, J. Chem. Phys. **14**, 578 (1946).
[2] S. S. Penner and D. Weber, J. Chem. Phys. **19**, 817 (1951).

## Vibrational Frequencies of Phosphine-*d* and Phosphine-$d_2$*

Ralph E. Weston, Jr., and Marshall H. Sirvetz
*Departments of Chemistry and Physics, Brookhaven National Laboratory, Upton, Long Island, New York*
(Received August 20, 1952)

In connection with the microwave spectroscopy of phosphine-*d* and phosphine-$d_2$, it was necessary to know the vibrational frequencies of these molecules. It was not possible to obtain all of these experimentally because the isotopic species were not separated, and as a result there was an overlapping of infrared absorption bands from different species. Therefore, the method used was to calculate the fundamental frequencies using a suitable model and to compare these with the absorption bands which could be observed and assigned.

(*1*) *Calculation of frequencies:* Reasonable agreement between calculated and observed frequencies for $PH_3$ and $PD_3$ was found assuming either a valence force field, or valence forces together with an additional force resulting from interaction between changes in bond angles.[1] The significance of this latter method has been discussed in terms of a change in bond hybridization in certain vibrational modes.[2] Results of these calculations are compared with observed values in Table I; the force constants used are given in Table II. It is seen that frequencies for $PD_3$ can be calculated from force constants of $PH_3$ with an error of about one percent.

Because of the rather improved over-all agreement provided by the modified valence force model, the additional term in the potential energy was retained in the calculations for $PH_2D$ and $PHD_2$. Salant and Rosenthal[3] have given expressions for the frequencies of pyramidal $XY_2Y'$ molecules, using the most general force field. However, it was found more convenient to obtain the secular equation for the modified valence force model using suitable symmetry coordinates.[4] The secular equation factors into a second-order and a fourth-order matrix; the latter may be conveniently expanded using the procedure described by Fettis.[5] The frequencies obtained, together with their symmetry species, are listed in Table I. Using the noncrossing rule for vibrations of the same symmetry species, frequencies of $PH_2D$ and $PHD_2$ may be correlated with those of $PH_3$.

(*2*) *Observed frequencies:* Phosphine containing deuterium was prepared by equilibration of ordinary phosphine with mixtures of ordinary and heavy water.[6] A Baird recording infrared spectrophotometer with rock salt prism was used to obtain spectra. The assignment of observed absorption bands to the various isotopic species was made difficult by the inability to work with pure samples. The bands could be assigned, however, in a fairly unambiguous way by noting changes in intensity with deuterium

Table I. Vibrational frequencies of isotopic phosphine species.

| | $\nu_1$ | $\nu_2$ | $\nu_3$ | $\nu_4$ | In $cm^{-1}$ |
|---|---|---|---|---|---|
| $PH_3$ | 2323 ($a_1$) | 991 ($a_1$) | 2328 ($e$) | 1121 ($e$) | Obs[a] |
| | 2334 | 1031 | 2342 | 1055 | Calc[b] |
| | 2322 | 991 | 2328 | 1121 | Calc[c] |
| $PH_2D$ | 1700 | 892 | — | 1097 | Obs |
| | 1672 ($a'$) | 888 ($a'$) | 2325 ($a'$) | 1096 ($a'$) | Calc[c] |
| | | | 2329 ($a''$) | 969 ($a''$) | |
| $PHD_2$ | — | — | 2320 | 980, 906 | Obs |
| | 1669 ($a'$) | 761 ($a'$) | 2327 ($a'$) | 909 ($a'$) | Calc[c] |
| | | | 1675 ($a''$) | 978 ($a''$) | |
| $PD_3$ | 1694 ($a_1$) | 730 ($a_1$) | (1658)[d] ($e$) | 806 ($e$) | Obs[e] |
| | 1671 | 721 | 1671 | 799 | Calc[b] |
| | 1667 | 721 | 1675 | 799 | Calc[e] |

[a] V. M. McConaghie and H. H. Nielsen, Proc. Natl. Acad. Sci. U. S. **34**, 455 (1948). Note that other authors (see references 2 and 3) have used an apparently incorrect value of $\nu_3 = 2421\ cm^{-1}$.
[b] Using mean of $k_1$ and $k_\delta/l^2$ from $PH_3$ and $PD_3$.
[c] Using $k_1$, $k_\delta/l^2$, and $k_\delta'/l^2$ from $PH_3$. Calculations use $\angle H-P-H = 93°\ 20'$ obtained from microwave spectra.
[d] Computed from other frequencies using product rule.
[e] E. Lee and C. K. Wu, Trans. Faraday Soc. (London) **35**, 1366 (1939).

TABLE II. Force constants in $10^5$ dynes $cm^{-1}$.

| | | From $\nu_1$ and $\nu_2$ | | From $\nu_3$ and $\nu_4$ |
|---|---|---|---|---|
| $PH_3$ | $k_1$ | 3.113 | | 3.110 |
| | $k_\delta/l^2$ | 0.292 | | 0.356 |
| | $k_{\delta'}/l^2$ | | −0.0213 | |
| $PD_3$ | $k_1$ | 3.215 | | (3.050) |
| | $k_\delta/l^2$ | 0.299 | | (0.362) |
| | $k_{\delta'}/l^2$ | | (−0.0210) | |

content and by partially balancing out masking bands with a suitable sample in the reference cell.

Phosphine containing about one percent deuterium showed a weak line resulting from $PH_2D$ at 1700±10 $cm^{-1}$, in addition to bands due to $PH_3$. A mixture of $PH_2D$ and $PH_3$ run against various pressures of $PH_3$ in the reference cell exhibited lines at 1700±10, 1097±5, and 892±5 $cm^{-1}$. Phosphine containing about 99 percent deuterium showed weak lines at 2320±10, 980±5, and 906±5 $cm^{-1}$. A sample containing 80 percent deuterium was run against the nearly pure $PD_3$ in the reference cell, and an additional band was found at 775–780 $cm^{-1}$; however, this may be due to rotational structure of $\nu_2$ and $\nu_4$ of $PD_3$.

Considering the agreement between observed and calculated frequencies for $PH_3$ and $PD_3$, and the agreement for $PH_2D$ and $PHD_2$ where frequencies are observed, it seems safe to state that the maximum deviation is about one percent. Thus, the modified valence force field is well suited to calculations for phosphine.

We wish to thank Miss Jean Snover for carrying out computations involved in the solution of the secular equations.

* Research carried out under the auspices of the U. S. AEC.

[1] G. Herzberg, *Infrared and Raman Spectra of Polyatomic Molecules* (D. Van Nostrand Company, Inc., New York, 1945), pp. 175, 187.

[2] Heath, Linnet, and Wheatley, Trans. Faraday Soc. (London) **46**, 137 (1950), and preceding papers in this series.

[3] E. O. Salant and J. E. Rosenthal, Phys. Rev. **42**, 812 (1932); J. E. Rosenthal, Phys. Rev. **45**, 426 (1934).

[4] See reference 1, p. 154.

[5] H. E. Fettis, Quart. Appl. Math. **8**, 206 (1950).

[6] R. E. Weston, Jr., and J. Bigeleisen, J. Chem. Phys. (to be published).

## Search for Weak Absorption Bands of Benzonitrile in the Near Ultraviolet

ROBERT C. HIRT AND FRANK T. KING
*Stamford Research Laboratories, American Cyanamid Company, Stamford, Connecticut*

(Received September 12, 1952)

WEAK absorption bands of benzonitrile (phenyl cyanide) in iso-octane solution are shown between 33,500 and 34,800 $cm^{-1}$ ($\epsilon$=6 to 15) in an A.P.I. curve.[1] A weak band near 33,000 $cm^{-1}$ ($\epsilon$=15) was shown as an "*n*-band" by Platt in the paper on iso-conjugate spectra.[2] Recently McConnell[3] mentioned a "shoulder" band at 33,000 $cm^{-1}$ ($\epsilon\approx1$) which displayed a "blue-shift" in more polar solvents, with, however, the comment that it might arise from vibrational structure of a stronger band or from an impurity in the samples used.

Since such a band had *not* been observed in the vapor spectra[4,5] nor in various samples in solution examined in these Laboratories, it was decided to search thoroughly the ultraviolet region near 33,000 $cm^{-1}$ using highly purified samples.

Eastman Kodak benzonitrile was successively steam distilled, distilled under reduced pressure, crystallized twice, and finally distilled again under reduced pressure, to end with about 10 percent of the starting material. The purity of the final product was 99.75-mole percent, determined cryoscopically.[6] Most of the residual impurity was water, by Karl Fischer titration.

Spectra were obtained using a Cary automatic recording spectrophotometer, Model 11, No. 67, operated at minimum scanning speed of 1 A/sec and with slit widths of 0.025 to 0.04 mm in the region below 36,500 $cm^{-1}$. Pure liquid benzonitrile was examined in fused quartz cells of 100-, 50-, and 10-mm light path length, and in micrometer Baly cells.[7] The use of the latter with lengths from 2 mm to less than 0.01 mm permitted the spectrum of liquid benzonitrile to be obtained over the familiar bands near 36,500 $cm^{-1}$. A matched empty cell was used in the comparison beam. Spectra were also obtained in cyclohexane solution and in 95 percent ethyl alcohol solution (with pure solvent in the comparison cell) using a variety of cell lengths and concentrations (up to 30 g/100 ml). Data for pure liquid benzonitrile and cyclohexane solutions are shown in Figs. 1 and 2. The divergence between the curves for pure liquid and *c*-hexane solution is similar to that observed by Pitts[8] for pure liquid and iso-octane solution of benzene.

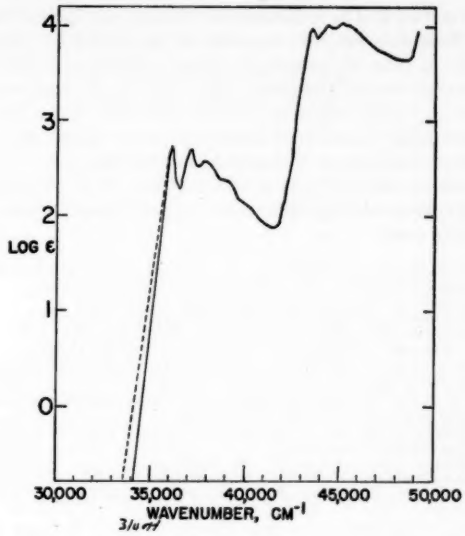


FIG. 1. Major bands of benzonitrile. - - - - pure liquid; —— cyclohexane solution.

No indication of a band or inflection was found near 33,000 $cm^{-1}$. The intensity at this point is 0.01, which is a factor of 100 lower than that of the reported bands.[1–3] Thus the bands reported in this region must have been due to impurities.

In the spectra obtained using 50 or 100 mm of undiluted benzonitrile, a definite shoulder band was observed at 31,900 $cm^{-1}$ and a suggestion of another near 31,000 $cm^{-1}$.[9] These are shown

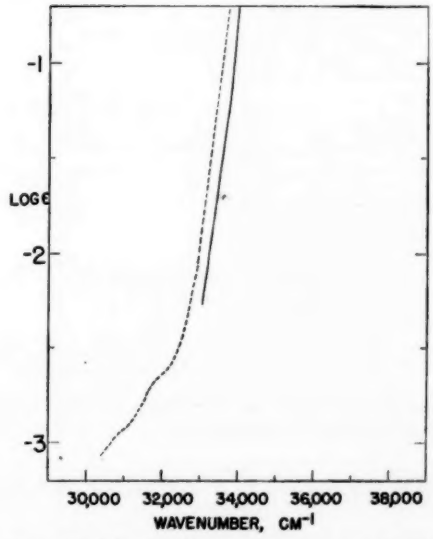


FIG. 2. Weak bands of benzonitrile. - - - - pure liquid; —— cyclohexane solution.

in detail in Fig. 2. The intensities are 0.0021 and 0.0012 from the curve. These are in the range for a singlet-triplet transition, analogous to that of benzene.[8,10] These weak bands are on the higher energy side of the phosphorescence bands reported up to 27,000 $cm^{-1}$.[11] This would be roughly 4000 $cm^{-1}$ from these very weak absorption bands, which seems rather large. New phosphorescence measurements would be interesting.

We wish to thank Dr. D. J. Berets, Mr. E. F. Williams, and Dr. D. L. Swanson for their work in purifying the samples of benzonitrile used.

[1] American Petroleum Institute, Project 44, Catalog of Ultraviolet Spectrograms, Curve No. 227, from Socony-Vacuum Company.
[2] J. R. Platt, J. Chem. Phys. **19**, 101 (1951), Fig. 14.
[3] H. McConnell, J. Chem. Phys. **20**, 700 (1952), reference 17.
[4] A. D. Walsh, Proc. Roy. Soc. (London) **A191**, 32 (1947).
[5] R. C. Hirt and J. P. Howe, J. Chem. Phys. **16**, 480 (1948).
[6] We are grateful for this measurement to Dr. C. R. Witschonke, Anal. Chem. **24**, 350 (1952).
[7] R. C. Hirt and F. T. King, Anal. Chem. (to be published).
[8] A. Pitts, J. Chem. Phys. **18**, 1416 (1950).
[9] The possibility cannot be eliminated, of course, that these weak bands are due to a residual impurity.
[10] H. Shull, J. Chem. Phys. **17**, 295 (1949).
[11] J. Von Kowalski, Z. Physik. **12**, 956 (1911); and G. N. Lewis and M. Kasha, J. Am. Chem. Soc. **66**, 2100 (1944), Table II.

## Light Scattering of Multicomponent Macromolecular Systems

JACOB JOSEPH BLUM AND MANUEL F. MORALES
*Naval Medical Research Institute, Bethesda, Maryland*
(Received July 21, 1952)

BY using the method of molecular distribution functions, Zimm[1] has developed the theory of light scattering by a solution of one macromolecular component. Recently, several authors[2–4] have derived the proper thermodynamic form for the light-scattering equation and have applied it to multicomponent solutions of small molecules. In our studies of muscle proteins[5] we have found it useful to follow Stockmayer's[4] suggestion, *viz.*, to extend Zimm's[1] treatment to multicomponent systems. Using the same notation, method, and assumptions as Zimm,[3] and bearing in mind the thermodynamic form prescribed by Stockmayer[4] (Eq. (2.16)), we obtain the (excess over solvent) intensity of light scattered by unit volume of a solution of $z$ macromolecular components:

$$\frac{I(\theta)}{k'}=\sum_{i=1}^{i=z} N_i n_i^2 P_i(\theta)\left\{\frac{\partial \nu}{\partial(n_i N_i)}\right\}^2 + \sum_{i=1}^{i=z}\sum_{j=1}^{j=z} N_i N_j n_i^2 n_j^2 P_i(\theta) P_j(\theta) X_{ij} \times\left\{\frac{\partial \nu}{\partial(n_i N_i)}\right\}\left\{\frac{\partial \nu}{\partial(n_j N_j)}\right\}. \quad (1)$$

Introducing the weight concentrations $c_i=(M_i/N_0)N_i$ and the functions $A_2^{(ij)}=-N_0 n_i n_j X_{ij}/2M_iM_j$, we obtain from (1)

$$\frac{I(\theta)}{N_0 k'}=\sum_{i=1}^{i=z}\frac{M_i P_i(\theta)}{(M_i/n_i)^2}\left\{\frac{\partial \nu}{\partial(n_i N_i)}\right\}^2 c_i - 2\sum_{i=1}^{i=z}\sum_{j=1}^{j=z} A_2^{(ij)}\frac{M_i M_j P_i(\theta) P_j(\theta)}{(M_i M_j/n_i n_j)} \times\left\{\frac{\partial \nu}{\partial(n_i N_i)}\right\}\left\{\frac{\partial \nu}{\partial(n_j N_j)}\right\} c_i c_j. \quad (2)$$

If it can be assumed that the derivatives $(\partial\nu/\partial c_i)$ are the same for all $i$, then (2) simplifies further to

$$\frac{I(\theta)}{k}=\sum_{i=1}^{i=z} M_i P_i(\theta) c_i - 2\sum_{i=1}^{i=z}\sum_{j=1}^{j=z} A_2^{(ij)} M_i M_j P_i(\theta) P_j(\theta) c_i c_j, \quad (3)$$

where $k=k'N_0(\partial\nu/\partial c_i)^2$. In terms of the weight fractions $x_i$ and total weight concentration $c$, the linear approximation to the reciprocal of (3) is

$$\frac{kc}{I(\theta)}=\frac{1}{\sum_{i=1}^{i=z} M_i P_i(\theta) x_i}+2\frac{\sum_{i=1}^{i=z}\sum_{j=1}^{j=z} A_2^{(ij)} M_i M_j P_i(\theta) P_j(\theta) x_i x_j}{(\sum_{i=1}^{i=z} M_i P_i(\theta) x_i)^2} c. \quad (4)$$

If the $ii$, $ij$, and $jj$ interactions all have the same sign, say $\epsilon=\pm 1$, and we assume that $A_2^{(ii)}A_2^{(jj)}=[A_2^{(ij)}]^2$, then the coefficient of $2c$ in Eq. (4) may be written as

$$\epsilon(\sum_{i=1}^{i=z}(A_2^{(ij)})^{\frac{1}{2}} M_i P_i(\theta) x_i/\sum_{i=1}^{i=z} M_i P_i(\theta) x_i)^2 \equiv \epsilon(\langle\sqrt{A_2^{(ii)}}\rangle)^2,$$

and Eq. (4) becomes

$$[kc/I(\theta)]=[1/\sum_{i=1}^{i=z} M_i P_i(\theta) x_i]+2\epsilon[\langle\sqrt{A_2^{(ii)}}\rangle]^2 c. \quad (5)$$

Equation (5) is the generalization of Zimm's[3] Eq. (16). When $P_i(\theta)=1$, for all $i$, it reduces to Stockmayer's[4] Eq. (3.14).

[1] B. H. Zimm, J. Chem. Phys. **16**, 1093 (1948).
[2] H. C. Brinkman and J. J. Hermans, J. Chem. Phys. **17**, 574 (1949).
[3] J. G. Kirkwood and R. J. Goldberg, J. Chem. Phys. **18**, 54 (1950).
[4] W. H. Stockmayer, J. Chem. Phys. **18**, 58 (1950).
[5] To be published elsewhere.

## The Raman and Infrared Spectra of $CF_3Br$ and $CF_3I$

WALTER F. EDGELL AND C. E. MAY
*Chemistry Department, Purdue University, Lafayette, Indiana*
(Received August 27, 1952)

WE have been engaged in a study of the Raman and infrared spectra of certain molecules containing the trifluoromethyl group. Recently several reports[1–3] on the infrared spectra of $CF_3Br$ and $CF_3I$ have appeared in which the lowest fundamental frequencies have been estimated from combination bands or vibrational calculations.[4] Since these estimated fundamentals differ in part among these reports and in part from our observations, it seems worthwhile to indicate our results at this time.

The $CF_3Br$ used in this work was a commercial sample, while the $CF_3I$ was prepared by the reaction of iodine with silver trifluoroacetate.[5] Both were dried and then purified by distillation through a 50-plate column.

The Raman spectra were obtained on the liquids at −100°C and −40°C, respectively, with an Applied Research Laboratories Raman spectrograph. The source was a low pressure Hg arc operated so that no filters were required to reduce the general background. Exposures varied from three to nine hours when Tri-X Panchromatic film was used with slit widths of 150 microns. It was found convenient to reduce the rate of decomposition of $CF_3I$ by using a Wratten 2A filter. Only lines interpreted as fundamentals appeared, and they are found in Table I.

The infrared spectra were obtained from the gas phase at various pressures using a Perkin-Elmer, Model 21 infrared spectrometer and $CaF_2$, NaCl, and KBr optics. The bands reported earlier[1] at 711, 1114, and 1246 for $CF_3I$ and at 470 and 830 $cm^{-1}$ for $CF_3Br$ were not found. Otherwise our infrared spectra are in essential

TABLE I. Fundamental vibrational frequencies.

| | $CF_3Br$ | | $CF_3I$ | |
|---|---|---|---|---|
| Assignment | Raman[a] | ir[b] | Raman[a] | ir[b] |
| *E* rock | 305 | | 265 | |
| *A* CX stretch | 352 | | 286 | |
| *E* $CF_3$ def | 548 | 550 | 537 | 540 |
| *A* $CF_3$ def | 760 | 761 | 741 | 740 |
| *A* CF stretch | 1067 | 1085 | 1056 | 1073 |
| *E* CF stretch | 1188 | 1206 | 1168 | 1185 |

[a] For the liquid state.
[b] For the vapor state.

agreement with those reported earlier.[1-3] (Small differences in wavelength exist for some of the bands.) The values for the fundamental bands directly observed are found in Table I.

The assignment of the fundamentals is found in Table I. It is supported by results for other molecules containing the $CF_3$ group.[6] These results confirm the values of 348 and 284 $cm^{-1}$ for the lowest $A_1$ fundamentals of $CF_3Br$ and $CF_3I$ (which we interpret as being substantially the C—Br or C—I stretching vibration) found by Plyler and Acquista[1] in KRS-5 region of the infrared spectra and obtained by Polo and Wilson[3] from their interpretation of the combination and overtone bands. In addition these results give the first observation of the lowest type $E$ fundamental and confirm the value estimated by McGee, Cleveland, and Miller[2] and by Polo and Wilson.[3]

A more complete report of this work will appear in the near future. Support of this research by the AEC is gratefully acknowledged.

[1] E. K. Plyler and N. Acquista, J. Research Natl. Bur. Standards **48**, 92 (1952).
[2] McGee, Cleveland, and Miller, J. Chem. Phys. **20**, 1044 (1952).
[3] S. R. Polo and M. K. Wilson, J. Chem. Phys. **20**, 1183 (1952).
[4] B. I. Stepanov, Compt. rend. acad. sci. U.S.S.R. **45**, 56 (1944).
[5] R. N. Hazeldine, J. Chem. Soc. **1951**, 584.
[6] Walter F. Edgell and co-workers (to be published).

## Effect of Nuclear Substituents on the $C^{14}$ Isotope Effect in the Saponification of Carboxyl-Labeled Ethyl Benzoates* at 25°C

GUS A. ROPP AND VERNON F. RAAEN
*Chemistry Division, Oak Ridge National Laboratory, Oak Ridge, Tennessee*
(Received September 9, 1952)

THE effect of varying the group $R$ on the isotope effect[1] $(k_{14}/k_{12})$ for the reaction,

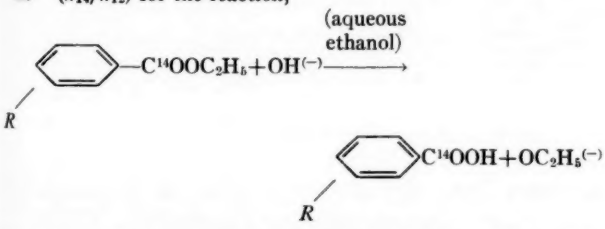


has been evaluated. For each substituent this ratio of the specific rate constants for the reaction of the two isotopic species was measured as the ratio, $S_3/S_{100}$, of the specific activity of the product acid produced at 3-percent reaction to the specific activity of that produced at 100-percent reaction.[2]

Results are presented in Table I. The several values of $k_{14}/k_{12}$ reported for each ester in the second row of the table represent the results of repeating the isotope effect determinations with individually purified samples of the same ester.

Further work is in progress to extend the series and also to investigate the effect of changing temperature, solvent, concentration, etc., on the $k_{14}/k_{12}$ ratio for a given ester. The method described above is particularly well-suited to the latter type of studies since $S_{100}$ cancels out and a simple relation holds:

$$\frac{(k_{14}/k_{12})\text{ condition } A}{(k_{14}/k_{12})\text{ condition } B}=\frac{(S_3)_A}{(S_3)_B}.$$

The experimentally found variation of $k_{14}/k_{12}$ with the type of substituent suggests that the isotope effect may be greatest in the saponification of those esters in which the largest contributions to the normal state are made by resonance forms of the type:

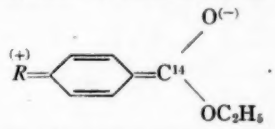


The degree of double bond character of the bond between the ring and the labeled carbon might be considered to be a measure of the tightness of bonding[3] of this labeled atom. It is hoped that further experimental work now in progress will indicate more definitely the relationship between the substituent type and the ratio, $k_{14}/k_{12}$.

* This paper is based upon work performed under Contract Number W-7405-eng-26 for the AEC at the Oak Ridge National Laboratory, Tennessee.
[1] Cf. W. H. Stevens and R. Attree, Can. J. Research **27B**, 807 (1949).
[2] A detailed account of the method has been submitted for publication elsewhere. A somewhat similar method has been used previously; see Lindsay, McElcheran, and Thode, J. Chem. Phys. **17**, 589 (1949).
[3] J. Bigeleisen, J. Chem. Phys. **17**, 675 (1949); according to the theory the isotope effect should be greater, the tighter the bonding of the labeled atom in the normal molecule.

TABLE I.

| Nuclear substituent | *Para* methoxy | *Para* chloro | *Para* methyl | None | *Meta* chloro | *Meta* nitro |
|---|---|---|---|---|---|---|
| $k_{14}/k_{12}$ | 0.916 | 0.922 | 0.929 | 0.928 | 0.932 | 0.937 |
| | 0.915 | 0.926 | 0.927 | 0.930 | | |
| | | 0.927 | 0.928 | 0.928 | 0.933 | 0.937 |
| $k_{14}/k_{12}$ average | 0.916 | 0.925 | 0.928 | 0.929 | 0.933 | 0.937 |

## Some Examples of Weak Detonations

S. G. REED, JR.
*Naval Ordnance Laboratory, White Oak, Silver Spring, Maryland*
(Received August 26, 1952)

IN chemical detonation processes, a weak detonation (in the sense of Courant and Friedrichs[1]) is known to be possible only under very unusual circumstances. The chemical reactions are touched off by the increase of temperature in a compression, and only if the reaction achieves a high rate at a relatively low temperature can the compression be diminished quickly and sufficiently for a weak detonation to occur.[2] The unburned material

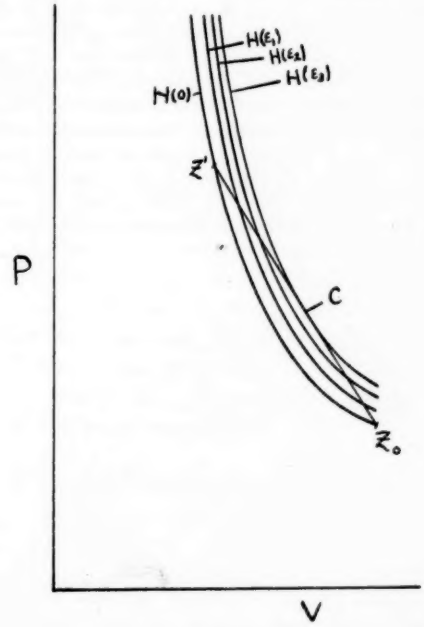


FIG. 1.

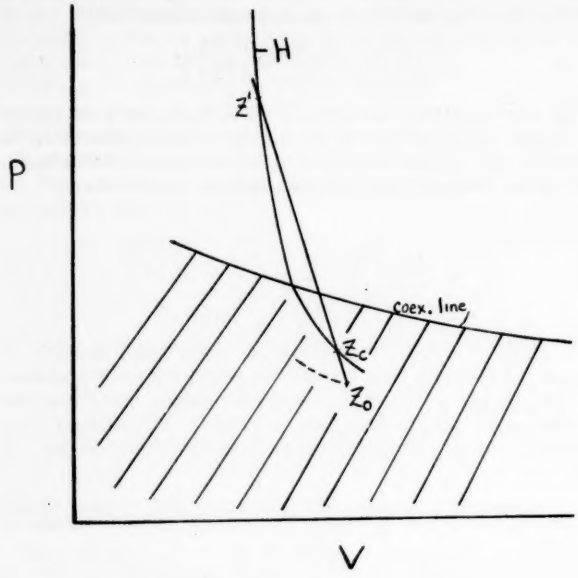


FIG. 2.

is assumed stable, i.e., the reaction rate before compression is effectively zero.

The purpose of this note is to point out that some irreversible condensation processes occurring in supersonic nozzle flow[3] can be regarded as examples of weak detonations. In these processes a sudden condensation of metastable supersaturated material takes place, induced by an expansion. The rate of condensation increases as long as the temperature falls. The processes are stable.

Figure 1 is an adaptation of the Hugoniot diagram used in the Zeldovich-von Neumann detonation analysis[4] to the "condensation shock" of water vapor contained in air.[5] The curves marked $H(\epsilon)$ are Hugoniot curves[1] for which the energy zero changes by a fraction $\epsilon \gtrless 0$ owing to condensation. The water vapor content is assumed small, so that only its function in liberating heat to the air is considered.[5]

The two sets of intersections of the straight line $\mathbf{Z_0Z'}$ passing through the upstream point $Z_0$ and the curves $H(\epsilon)$ approach distinct limits as $\epsilon \to 0$. The weak detonations on the lower branch $\mathbf{Z_0C}$ approach $Z_0$, and the strong detonations on the upper branch approach $Z'$, the ordinary shock solution without change of energy zero. Condensation processes belong to the set approaching $Z_0$, and chemical detonations are associated with those approaching $Z'$, as is appropriate to their physical mechanism. The point of tangency $C$, determinate for a fixed slope of $\mathbf{Z_0Z'}$ and fixed $\epsilon$, corresponds to a Chapman-Jouguet process. It is reached as the limit of exothermic processes starting both from $Z^0$ and from $Z'$ along fixed $\mathbf{Z_0Z'}$. As a verification of Jouguet's rule, the flow downstream of the condensation shock is observed to be supersonic.[6]

Figure 2 depicts the situation for irreversible condensation of pure steam or nitrogen in supersonic flow. There is here only one Hugoniot curve, for equilibrium conditions downstream, which is convex and bends sharply at the coexistence line, as can be shown by an extension of Bethe's discussion.[7] $Z_0$ is located as it would be for supersaturation along a metastable gas isentrope, part of which is shown dotted. The solution $Z_c$, appropriate to the observed downstream mixture of phases, lies in the shaded coexistence region and clearly corresponds to a weak detonation. It is noteworthy that the slope of the saturated isentrope along which the flow presumably continues downstream from $Z_c$ is less steep than the metastable isentrope at $Z_0$;[8] in chemical detonations, or for the condensation of water vapor in air, it is just the other way around. In other words, sound speed jumps down for the condensation of steam or nitrogen but jumps up for the chemical detonations or water vapor condensation in air.

I am indebted to Dr. R. J. Seeger for raising the question of the relation of condensation and detonation, and to Dr. K. F. Herzfeld, Dr. W. Heybey, and Dr. Z. I. Slawsky for profitable conversations.[9] A detailed paper in collaboration with Dr. W. Heybey is in preparation.

[1] R. Courant and K. O. Friedrichs, *Supersonic Flow and Shock Waves* (Interscience Publishers, Inc., New York, 1948), Sec. 84.

[2] Y. B. Zeldovich, *Theory of Combustion and Detonation of Gases* (Academy of Sciences, U.S.S.R., 1944); K. O. Friedrichs, NavOrd Report 79-46 (1946).

[3] See, for example, P. Wegener, Phys. Rev. **76**, 6 (1949), and Kl. Oswatitisch, Z.A.M.M. **22**, 13 (1942) (water vapor in air); C. Robb, Can. J. Research **A19**, 67, 87 (1941) (steam); H. T. Nagamatsu and P. D. Arthur, GALCIT Report (1952) (nitrogen, no shocklike gradients).

[4] J. von Neumann, OSRD Report 549 (1942); also see Zeldovich, reference 2.

[5] To this approximation the equation of the Hugoniot curves in Fig. 1 is $(\gamma+1/\gamma-1)(pv-p_0v_0)-pv_0+p_0v=2eh_0$, where $\gamma$ is the ratio of specific heats of air and $h_0$ is the stagnation enthalpy.

[6] That the condensation shock solution should approach $Z_0$ as $\epsilon \to 0$ had been pointed out independently by Dr. W. Heybey of this laboratory in unpublished notes.

[7] H. A. Bethe, OSRD Report 545 (1942); H. Weyl, Comm. Appl. Math. **2**, 103 (1949).

[8] S. G. Reed, Jr., J. Chem. Phys. **20**, 539 (1952).

[9] It has come to my attention that Dr. J. M. Burgers in his address at the dedication of the NOL Aeroballistic Facilities, 1949, had suggested that the condensation shock might perhaps be compared to a weak detonation.

## Erratum: Kinetics of Solidification of Supercooled Liquid Mercury Droplets

[J. Chem. Phys. **20**, 411 (1952)]

DAVID TURNBULL
*General Electric Research Laboratory, Schenectady, New York*

ON Page 411, footnote 2, for "catalytic acid": read "catalytic aid." On Page 424, Eq. (26) should read

$$X=1-\exp\{-m[1-\exp(-kt)]\}. \qquad (26)$$